FLECHT SEASET Program

NRC/EPRI/Westinghouse Report No.5

NUREG/CR-1370

NP-1382

WCAP-9658

PWR FLECHT SEASET 21-ROD BUNDLE FLOW BLOCKAGE TASK TASK PLAN REPORT

March 1980

1205580004096 1 ANR2
US NRC
NRR DIV OF SITE SFTY & ENVIRN
DEPUTY DIVISION DIRECTOR
P-202
WASHINGTON DC 20555

Program Jointly Sponsored by USNRC, EPRI and

Westinghouse Under Contract Number

NRC-04-77-127 and EPRI RP959-1

8007240339

FLECHT SEASET Program
NRC/EPRI/Westinghouse Report No. 5
NUREG/CR-1370
NP-1382
WCAP-9658

PWR FLECHT SEASET
21-ROD BUNDLE FLOW BLOCKAGE TASK
TASK PLAN REPORT

March 1980

L. E. Hochreiter
R. A. Basel
R. J. Dennis
N. Lee
H. W. Massie, Jr.
M. J. Loftus
E. R. Rosal
M. M. Valkovic

prepared for

United States Nuclear Regulatory Commission
Washington, D.C. 20555

Electric Power Research Institute
3412 Hillview Avenue
Palo Alto, California 94303

and

Westinghouse Electric Corporation
Nuclear Energy Systems
P.O. Box 355
Pittsburgh, Pennsylvania 15230

by

Westinghouse Electric Corporation

under

Contract No. NRC-04-77-127, EPRI Project No. RP959-1

Program Management Group
NRC - L. H. Sullivan
EPRI - K. H. Sun
Westinghouse - L. Chajson

NOTICE

This report was prepared as an account of work sponsored by the United States Nuclear Regulatory Commission, the Electric Power Research Institute, Inc., and the Westinghouse Electric Corporation. Neither the United States government nor any agency thereof, nor the Institute nor members thereof, nor the Westinghouse Electric Corporation, nor any of their employes, makes any warranty, express or implied, or assumes any legal liability or responsibility for any third party's use or the results of such use of any information, apparatus, product, or process disclosed in this report or represents that its use by such third party would not infringe privately owned rights.

ABSTRACT

This report presents a descriptive plan of tests for the 21-Rod Bundle Flow Blockage Task of the Full-Length Emergency Cooling Heat Transfer Separate Effects and Systems Effects Test Program (FLECHT SEASET). This task will consist of forced and gravity reflooding tests utilizing electrical heater rods to simulate PWR nuclear core fuel rod arrays. All tests will be performed with a cosine axial power profile. These tests are planned to be used to determine effects of various flow blockage configurations (shapes and distributions) on reflooding behavior, to aid in development/assessment of computational models in predicting reflooding behavior of flow blockage configurations, and to screen flow blockage configurations for future 161-rod flow blockage bundle tests.

ACKNOWLEDGMENTS

The authors acknowledge the efforts of those individuals who formulated the blockage strategy contained herein. The work of the following Westinghouse Nuclear Energy Systems contributors is hereby acknowledged:

PWR PROJECTS
H. J. Fix
L. Chajson

SAFEGUARDS DEVELOPMENT
R. P. Vijuk
K. Beatty
D. H. Dixon
C. E. Dodge
A. Tong
D. P. Kitzmiller

THERMAL HYDRAULIC METHODS
J. E. Olhoeft

FACILITIES ENGINEERING
L. R. Katz
C. E. Conway
B. R. Sinwell
W. D. Humbel

TEST OPERATIONS
C. E. Fuchs
P. F. Orangio
F. L. Lilly
A. C. Toth
H. F. Andrew
R. V. Rulis
R. J. Priddy
D. C. Kalo

NUCLEAR FUEL DIVISION
D. L. Burman
A. H. Wenzel
T. K. Engel

The work of the following members of the Program Management Group, their colleagues, and their consultants is hereby acknowledged:

EPRI - K. H. Sun, R. B. Duffey
NRC-RSR - E. Davidson, L. B. Thompson, M. L. Picklesimer, H. Sullivan
NRC-NRR - W. Hodges, D. A. Powers
EG&G - G. Wilson
NUS Corporation - D. A. Prelewicz

GLOSSARY

This glossary explains definitions, acronyms, and symbols included in the text which follows.

Analysis -- the examination of data to determine, if possible, the basic physical processes that occur and the interrelation of the processes. Where possible, physical processes will be identified from the data and will be related to first principles.

Average fluid conditions -- average thermodynamic properties (for example, enthalpy, quality, temperature, pressure) and average thermal-hydraulic parameters (for example, void fraction, mass flow rate) which are derived from appropriately reduced data for a specified volume or a specified cross-sectional area

Axial peaking factor -- ratio of the peak-to-average power for a given power profile

Blocked -- a situation in which the flow area in the rod bundle or single tube is purposely obstructed at selected locations so as to restrict the flow

Bottom of core recovery (BOCR) -- a condition at the end of the refill period in which the lower plenum is filled with injected ECC water as the water is about to flood the core

Bundle -- a number of heater rods, including spares, which are assembled into a matrix with CRG-type rods, using necessary support hardware to meet the Task Plan design requirements

Carr out -- same as carryover

Carryout rate fraction -- the fraction of the inlet flooding flow rate which flows out the rod bundle exit by upflowing steam

Carryover -- the process in which the liquid is carried in a two-phase mixture out of a control volume, that is, the test bundle

Computational methods -- the procedure of reducing, analyzing, and evaluating data or mathematical expressions, either by hand calculations or by digital computer codes

Computer code -- a set of specific instructions in computer language to perform the desired mathematical operations utilizing appropriate models and correlations

Computer data acquisition system (CDAS) -- the system which controls the test and records data for later reduction and analysis

Computer tape -- magnetic tapes that store FLECHT SEASET data

Core rod geometry (CRG) -- a nominal rod-to-rod pitch of 12.6 mm (0.496 inch) and outside nominal diameter of 9.50 mm (0.374 inch) representative of various nuclear fuel vendors' new fuel assembly geometries (commonly referred to as the 17 x 17 or 16 x 16 assemblies)

Correlation -- a set of mathematical expressions, based on physical principles and experimental data but resting primarily on experimental data, which describes the thermal-hydraulic behavior of a system

Cosine axial power profile -- the axial power distribution of the heater rods in the CRG bundle that contains the maximum (peak) linear power at the midplane of the active heated rod length. This axial power profile will be used on all FLECHT SEASET tests as a fixed parameter.

Data -- recorded information, regardless of form or characteristic, of a scientific or technical nature. It may, for example, document research, experimental, developmental, or engineering work, or be usable or used to define a design or process or to procure, produce, support, maintain, or operate material. The data may be graphic or pictorial delineations in media such as drawings or photographs, text in specifications or related performance or design type documents, or computer printouts. Examples of data include research and engineering data, engineering drawings and associated lists, specifications, standards, process sheets, manuals, technical reports, catalog item identifications and related information, computer

programs, computer codes, computer data bases, and computer software documentation. The term data does not include financial, administrative, cost and pricing, and management information or other information incidental to contract administration.

Data validation -- a procedure used to ensure that the data generated from a test meet the specified test conditions, and that the instrumentation was functioning properly during the test

Design and procurement -- the design of the system, including the specification (consistent with the appropriate Task Plan) of the material, component, and/or system of interest; and the necessary purchasing function to receive the material, component, and/or system on the test site. This does not preclude Contractor from constructing components and systems on the test site to meet requirements of the Task Plan.

ECC -- emergency core cooling

Entrainment -- the process by which liquid, typically in droplet form, is carried in a flowing stream of gas or two-phase mixture

Evaluation -- the process of comparing the data with similar data, other data sets, existing models and correlations, or computer codes to arrive at general trends, consistency, and other qualitative descriptions of the results

Fallback -- the process whereby the liquid in a two-phase mixture flows countercurrent to the gas phase

FLECHT -- Full-Length Emergency Core Heat Transfer test program

FLECHT SEASET -- Full-Length Emergency Core Heat Transfer - Systems Effects and Separate Effects Tests

FLECHT SET -- Full-Length Emergency Core Heat Transfer - Systems Effects Tests

Heat transfer mechanisms -- the process of conduction, convection, radiation, or phase changes (for example, vaporization, condensation, boiling) in a control volume or a system

Hypothetical -- conjectured or supposed. It is understood that this program is concerned with study of physical phenomena associated with reactor accidents that have an extremely low probability and are therefore termed hypothetical.

Loss-of-coolant accident -- a break in the pressure boundary integrity resulting in loss of core cooling water

Model -- a set of mathematical expressions generated from physical laws to represent the thermal-hydraulic behavior of a system. A model rests mainly on physical principles.

PMG -- Program Management Group

Pressurized water reactor (PWR) -- a nuclear reactor type in which the system pressure exceeds saturation pressure, thus preventing gross vapor formation under normal operating conditions

Reduce data -- convert data from the measured signals to engineering units. In some cases the data are manipulated in a simple fashion to calculate quantities such as flows.

Separation -- the process whereby the liquid in a two-phase mixture is separated and detached from the gas phase

Silicon-controlled rectifier (SCR) -- a rectifier control system used to supply dc current to the bundle heater rods

Spacer grids -- the metal matrix assembly (egg crate design) used to support and space the heater rods in a bundle array

Test section -- lower plenum, bundle, and upper plenum

Test site -- the location of the test facilities where tests will be conducted

Transducer -- the devices used in experimental systems that sense the physical quantities, such as temperature, pressure, pressure difference, or power, and transform them into electrical outputs, such as volts

Unblocked -- the situation in which the flow area in the rod bundle or a single tube is not purposely obstructed

TABLE OF CONTENTS

Section	Title	Page
1	SUMMARY	1-1
2	BACKGROUND	2-1
3	TASK OBJECTIVES	3-1
4	BLOCKAGE SHAPES AND TEST CONFIGURATIONS	4-1
	4-1. General	4-1
	4-2. Blockage Shapes	4-1
	4-3. Blockage Shape cf Beta Phase Burst	4-3
	4-4. Review of Available Test Programs	4-3
	4-5. Hydrodynamic Aspects	4-5
	4-6. Conclusion	4-15
	4-7. Blockage Shape of Alpha Phase Burst	4-15
	4-8. Blockage Configurations	4-33
	4-9. Blockage Configurations To Be Tested	4-33
	4-10. Noncoplanar Blockage Distribution	4-34
	4-11. Method for Burst Location Determination	4-35
	4-12. Input Data	4-39
	4-13. Relationships Between Different Configurations	4-40
	4-14. Concentric Versus Nonconcentric Sleeve Shapes	4-40
	4-15. Coplanar Versus Noncoplanar Sleeve Arrangements	4-43
	4-16. Relationship Between 21-Rod and 161-Rod Bundles	4-43
5	INITIAL CONDITIONS AND RANGE OF CONDITIONS	5-1
6	TEST FACILITY DESCRIPTION	6-1
	6-1. Facility Design and Layout	6-1

TABLE OF CONTENTS (cont)

Section		Title	Page
	6-2.	Facility Component Description	6-5
	6-3.	Test Section	6-5
	6-4.	Test Bundle	6-6
	6-5.	Carryover Vessel	6-6
	6-6.	Entrainment Separator	6-6
	6-7.	Exhaust Line Piping and Components	6-21
	6-8.	Coolant Injection System	6-21
	6-9.	Downcomer	6-23
	6-10.	Boiler	6-23
	6-11.	Steam Injection System	6-23
	6-12.	Facility Operation	6-24
	6-13.	Blockage Sleeves and Changeover	6-25
	6-14.	Hydraulic Characteristics Tests	6-27
7		TEST FACILITY INSTRUMENTATION	7-1
	7-1.	General	7-1
	7-2.	Bundle Instrumentation	7-2
	7-3.	Heater Rod Thermocouples	7-2
	7-4.	Steam Probe Instrumentation	7-7
	7-5.	Blockage Sleeve Instrumentation	7-10
	7-6.	Differential Pressure Measurements	7-11
	7-7.	Power Measurements	7-11
	7-8.	Upper Plenum	7-12
	7-9.	Lower Plenum	7-12
	7-10.	Housing	7-12
	7-11.	Loop Instrumentation	7-14
	7-12.	Data Acquisition and Processing System	7-19
	7-13.	Computer Data Acquisition System	7-23
	7-14.	Fluke Data Logger	7-24
	7-15.	Multiple Pen Strip Chart Recorders	7-24
	7-16.	Data Validation Criteria and Procedures	7-24

TABLE OF CONTENTS (cont)

Section	Title	Page
8	TEST MATRIX	8-1
	8-1. Introduction	8-1
	8-2. Shakedown Test Matrix	8-1
	8-3. Bench Tests	8-1
	8-4. Steam Probe Check	8-1
	8-5. Thermocouple Wiring Connection Checks	8-2
	8-6. Forced Reflood Configuration Testing	8-2
	8-7. Heater Rod Power Connection Check	8-2
	8-8. Instrumented Heater Rod Radial Location and Corresponding Thermocouple Checks	8-2
	8-9. Heater Rod, Blockage Sleeve, and Steam Probe Axial Location Checks	8-2
	8-10. Test Section Differential Pressure Cell Axial Locations, Steam Separator Collection Tank and Carryover Tank Volume, and Level Transmitter Checks	8-3
	8-11. Pressure Control Valve Operation, Exhaust Orifice Plate Flow, and Differential Pressure Cell Zero Shift Checks	8-3
	8-12. Turbine Flowmeter Calibration and Flow Control Valve Operation Checks	8-3
	8-13. Carryover Tank, Steam Separator Tank, and Connecting Piping Heatup Checks	8-4
	8-14. Hydraulic Characteristics Shakedown Tests	8-4
	8-15. Low-Power and Low-Temperature Test, Forced Reflood Configuration	8-4
	8-16. Test Facility Special Single-Phase Testing	8-4
	8-17. Steam Cooling Shakedown Test	8-4

TABLE OF CONTENTS (cont)

Section			Title	Page
		8-18.	Gravity Reflood Configuration Testing	8-5
		8-19.	High-Range Turbine Flowmeter Flow Checks	8-5
		8-20.	Bidirectional Turbine Meter Flow Checks	8-6
		8-21.	Low-Power and Low-Temperature Test, Gravity Reflood Configuration	8-6
	8-22.		Hydraulic Characteristics Test Matrix	8-6
	8-23.		Test Matrix	8-11
		8-24.	Steam Cooling	8-11
		8-25.	Constant Flooding Rate	8-11
		8-26.	Pressure Effects	8-13
		8-27.	Coolant Subcooling Effects	8-13
		8-28.	Radial Power Distribution	8-13
		8-29.	Variable Flooding Rate	8-13
		8-30.	Repeat Tests	8-16
		8-31.	Gravity Reflood	8-16
9	DATA REDUCTION, ANALYSIS, AND EVALUATION PLANS			9-1
	9-1.		Data Reduction	9-1
	9-2.		Data Analysis and Evaluation	9-1
	9-3.		Mechanistic Data Analysis	9-15
	9-4.		Statistical Data Evaluation	9-17
	9-5.		Hydraulic Characteristics Test Data Reduction and Analysis Plan	9-23
10	TASK SCHEDULE			10-1
Appendix A	COBRA CODE			A-1
Appendix B	COMPARISON OF THEORETICAL FLOW SEPARATION LENGTH WITH EXPERIMENTAL DATA			B-1

TABLE OF CONTENTS (cont)

Section	Title	Page
Appendix C	DESCRIPTION OF COFARR PROGRAM	C-1
Appendix D	COFARR LISTING AND SAMPLE OUTPUT	D-1
Appendix E	VENDOR INPUTS AND COMMENTS	E-1
Appendix F	WORK SCOPE	F-1
Appendix G	FACILITY DRAWINGS	G-1
Appendix H	BUNDLE INSTRUMENTATION PLAN	H-1
Appendix I	CALCULATIONAL MODEL OF STEAM PROBE	I-1
Appendix J	BLOCKAGE SLEEVE EFFECT ON HEATER ROD TEMPERATURE	J-1
Appendix K	BLOCKAGE SLEEVE ATTACHMENT AND INSTRUMENTATION TEST	K-1
Appendix L	FLECHT SEASET RUN SPECIFICATION AND VALIDATION SHEET	L-1
Appendix M	DATA REDUCTION AND ANALYSIS COMPUTER PROGRAMS	M-1

LIST OF ILLUSTRATIONS

Figure	Title	Page
4-1	Swelling of Fuel Rods in TREAT Experiment FRF-2	4-6
4-2	Blockage Shape of Beta Phase Burst	4-8
4-3	C_{Dform}/C_{Dtot} Versus d/L	4-10
4-4	Flow Separation Schematic Diagram	4-12
4-5	Simulated Sleeve Shapes	4-14
4-6	Blockage Arrangements for COBRA	4-16
4-7	Flow Rate Change in Center Channel (COBRA)	4-17
4-8	Flow Rate Change in Most Blocked Subchannel (COBRA)	4-18
4-9	ORNL Multirod Burst Test Burst Shapes After Test	4-23
4-10	German Out-of-Pile Test Results	4-24
4-11	Sequence of Swelling and Burst of Alpha Phase Zircaloy	4-26
4-12	Shape of Nonconcentric Sleeve	4-30
4-13	Nonconcentric Sleeve Dimensions	4-31
4-14	Procedure for Determining Sleeve Numbers on Each Axial Increment	4-38
4-15	Strain Data From ORNL Rod Burst Tests and German In-Pile Tests	4-41
4-16	21-Rod Islands in 161-Rod Bundle	4-45
5-1	Cosine Axial Power Profile	5-5
6-1	Schematic Diagram -- FLECHT SEASET 21-Rod Bundle Flow Diagram	6-3
6-2	21-Rod Test Housing Assembly	6-7
6-3	21-Rod Bundle Test Low Mass Housing	6-9
6-4	21-Rod Bundle Test Section Cross Section	6-11
6-5	Heater Rod Details	6-13
6-6	21-Rod Test Bundle (3 sheets)	6-15
6-7	21-Rod Upper Plenum Baffle	6-22
6-8	Blockage Sleeves	6-26
7-1	FLECHT SEASET Computer Hardware Interface for 21-Rod Bundle Flow Blockage Task	7-3
7-2	21-Rod Bundle Flow Blockage Task Instrumentation Summary	7-5
7-3	Proposed Steam Probe Design for 21-Rod Bundle Flow Blockage Task	7-8
7-4	21-Rod Bundle Flow Blockage Task Steam Probe Summary	7-9
7-5	Upper and Lower Plenum Thermocouple Location for 21-Rod Flow Blockage Task	7-13

LIST OF ILLUSTRATIONS (cont)

Figure	Title	Page
7-6	21-Rod Bundle Flow Blockage Task Instrumentation Schematic Diagram (2 sheets)	7-15
8-1	Test-Simulated Boundaries of Predicted Upper Plenum Pressures During Reflood	8-12
8-2	Predicted Flooding Rate During Core Reflood of a Westinghouse PWR Dry Containment Plant	8-14
8-3	Predicted Flooding Rate During Core Reflood of a Westinghouse Ice Condenser Plant	8-15
8-4	Variable Stepped Flow Simulation of Predicted Core Reflood of a Westinghouse PWR Dry Containment Plant (Two Steps)	8-17
9-1	Flow Logic of Computer Codes	9-2
9-2	FLECHT SEASET Data Reduction Flow Chart	9-3
9-3	Sample Distribution Plots	9-20
9-4	Sample Frequency Distribution Plots at Different Elevations for a Given Time	9-21
9-5	Grid Location/Pressure Measurement Relationships	9-25
10-1	Task Schedule for FLECHT SEASET 21-Rod Blocked Bundle Task	10-3

LIST OF TABLES

Table	Title	Page
2-1	Comparison of PWR Vendors' Fuel Rod Geometries (Old and New)	2-4
3-1	Blockage Shapes and Configurations To Be Tested in 21-Rod Bundle	3-2
4-1	ORNL Beta Phase Burst Test Results	4-4
4-2	Fuel Rod Dimensional Changes in TREAT Experiment	4-7
4-3	Alpha Phase Burst of Single Rod in ORNL Tests	4-19
4-4	ORNL Alpha Phase Multirod Burst Test Data	4-21
4-5	KFK In-Pile Burst Test Results	4-27
4-6	ORNL In-Pile Burst Test Results	4-28
5-1	Basic Data To Be Obtained for 21-Rod Bundle Flow Blockage Task	5-2
5-2	Reference and Range of Test Conditions for 21-Rod Bundle Flow Blockage Task	5-4
6-1	Thermophysical Properties of Heater Rod Materials	6-12
7-1	21-Rod Bundle Flow Blockage Task Heater Rod Instrumentation Axial and Azimuthal Distribution	7-6
7-2	Bundle Instrumentation for 21-Rod Bundle Flow Blockage Task	7-20
7-3	Operable Heater Rod Thermocouples Required for Data Validation	7-26
8-1	Test Matrix for 21-Rod Bundle Flow Blockage Task	8-7
9-1	Data Reduction and Analysis Computer Codes for Flow Blockage Task	9-4
9-2	Information Derived From Basic Flow Blockage Task Data	9-11
10-1	Major Milestones for FLECHT SEASET 21-Rod Blocked Bundle Task	10-2

SECTION 1
SUMMARY

As part of the NRC/EPRI/Westinghouse FLECHT SEASET reflood heat transfer and hydraulic program,[1] a series of forced flow and gravity feed reflooding tests with flow blockage will be conducted on a 21-rod bundle whose dimensions are typical of current PWR fuel rod arrays. The purpose of these tests will be to screen various fuel rod flow blockage configurations which are postulated to occur in a hypothetical loss-of-coolant accident (LOCA), to determine which configuration provides the least favorable heat transfer characteristics. This blockage configuration will subsequently be placed in the larger 161-rod bundle to evaluate the additional effect of flow bypass. The 21-rod bundle will also be utilized to develop a blockage heat transfer analysis method. This analysis method will be assessed through comparison and analysis of the 161-rod blocked bundle data.

This document describes the data requirements, instrumentation plan, test facility, test matrix, and data reduction and analysis plans for Task 3.2.2, 21-Rod Bundle Flow Blockage Task, in the FLECHT SEASET program. This task replaces the Single Tube, Flow Blockage and Heat Transfer Task (as described in the FLECHT SEASET Program Plan).[1]

In this particular test program, a new FLECHT facility will be built to accept a 21-rod bundle whose dimensions are typical of the PWR fuel rod array sizes currently in use by PWR and PWR fuel vendors. This test facility will be very similar to the facility in the 161-rod unblocked bundle task,[2] except that flow areas will be scaled appropriately. Sufficient instrumentation will be installed in the test facility to perform mass and energy balances from the data. The instrumentation plan has also been developed such that local thermal-hydraulic parameters can be calculated from the experimental data. The thermal-hydraulic phenomena occurring during these tests will be identified and analyzed.

---

1. Conway, C. E., et al., "PWR FLECHT Separate Effects and Systems Effects Test (SEASET) Program Plan," NRC/EPRI/Westinghouse-1, December 1977.
2. Hochreiter, L. E., et al., "PWR FLECHT SEASET Unblocked Bundle, Forced and Gravity Reflood Task: Task Plan Report," NRC/EPRI/Westinghouse-3, March 1978.

SECTION 2
BACKGROUND

The flow blockage tasks in the FLECHT SEASET program are intended to provide sufficient data and resulting analysis such that the existing Appendix K flow blockage (steam cooling requirements used in PWR safety analyses) can be reassessed and replaced by a suitably conservative but physically correct safety analysis model.

Appendix K of 10CFR50.46 requires that any effect of fuel rod flow blockage must be explicitly accounted for in safety analysis calculations when the core flooding rate drops below 2.54 cm/sec (1 in./sec). The rule also requires that a pure steam cooling calculation must also be performed in this case. To comply with this requirement, PWR vendors have developed semiempirical methods of treating fuel rod flow blockage and steam cooling. Experimental data on single-rod and multirod burst test behavior have been correlated into a burst criterion which yields a worst planar blockage given the burst temperature and internal rod pressure of the average power rod in the hot assembly. The test data used to establish this burst criterion indicate that the rod burst is random and noncoplanar, and is distributed over the axial length of the hot zone. When calculating the flow redistribution due to flow blockage, PWR vendors used multichannel codes to obtain the blocked channel flow.

Simpler models developed by Gambill[1] have also been used for flow redistribution calculations. In its ECCS evaluation model, Westinghouse modeled noncoplanar blockage as a series of planar blockages distributed axially over the region of interest, with each plane representing a given percentage blockage. The flow distribution effect was then calculated from a series of proprietary THINC-IV[2] computer runs and correlated into a simple expression for flow redistribution. The hot assembly was used as the unit cell in these calculations so that the individual

1. Gambill, W. R., "Estimate of Effect of Localized Flow Blockages on PWR Clad Temperatures During Reflood," CONF-730304-4, 1972.

2. Chelemer, H., et al., "An Improved Thermal-Hydraulic Analysis Method for Rod Bundle Cores," Nucl. Sci. Eng. 41, 219-229 (1977).

subchannel flow redistribution effects generated by the noncoplanar blockage at a given plane are averaged and each subchannel has the same flow reduction. However, it should be remembered that the percentage blockage simulated in these calculations was derived by examination of noncoplanar multirod burst data.

The resulting flow redistribution is then used to calculate a hot assembly enthalpy rise as part of the steam cooling calculation. The resulting fluid sink temperature and a radial conduction fuel rod model is then used to predict the clad peak temperature. Again, the flow redistribution or blockage effects and the steam cooling calculation is only used when the core flooding rate drops below 2.54 cm/sec (1 in./sec). Above 2.54 cm/sec (1 in./sec), the unblocked FLECHT heat transfer data are used.

The purpose of the flow blockage task will be to provide sufficient experimental data such that a heat transfer model for low flooding rates, with flow blockage, can be developed to replace the current steam cooling calculation.

A review of flow blockage literature[1-4] indicates that there are four primary heat transfer effects which need to be examined for both forced and gravity reflooding:

-- Flow redistribution effects due to blockage and their effect on the enthalpy rise of the steam behind the blockage. Bypass of steam flow will result in increased superheating of the remaining steam flow behind the blockage region. The higher the steam temperature, the lower the rod heat flux and resulting heat transfer coefficient behind the blockage.

---

1. Gambill, W. R., "Estimate of Effect of Localized Flow Blockages on PWR Clad Temperatures During Reflood," CONF-730304-4, 1972.

2. Davis, P. R., "Experimental Studies of the Effect of Flow Restrictions in a Small Rod Bundle Under Emergency Core Coolant Injection Conditions," Nucl. Technol. 11, 551-556 (1971).

3. Rowe, D. S., et al., "Experimental Study of Flow and Pressure in Rod Bundle Subchannels Containing Blockages," BNWL-1771, September 1973.

4. Hall, P. C., and Duffey, R. B., "A Method of Calculating the Effect of Clad Ballooning on Loss-of-Coolant Accident Temperature Transients," Nucl. Sci. Eng. 58, 1-20 (1975).

-- Effect of blockage downstream of the blockage zone and the resulting mixing of the steam and droplet breakup behind the blockage. The breakup of the entrained water droplets will increase the liquid surface area so that the drops will become a more effective heat sink for the steam. The breakup should desuperheat the steam; this would result in greater rod heat transfer behind the blockage zone in the wake of the blockage.

-- The heat transfer effects in the immediate blockage zone due to drop impact, breakup, and mixing, as well as the increased steam velocity due to blockage flow area changes. The drop breakup is a localized effect primarily caused by the blockage geometry; it will influence the amount of steam cooling which can occur farther downstream of the blockage.

-- Effect of blockage on the upstream region of the blockage zone due to steam bypass, droplet velocities, and sizes

In simpler terms, the flow blockage heat transfer effects are a combination of two key thermal-hydraulic phenomena:

-- A flow bypass effect, which reduces the mass flow in the blocked region and consequently decreases the heat transfer

-- A flow blockage effect, which can cause flow acceleration, droplet breakup, improved mixing, steam desuperheating, and establishment of new boundary layers, which consequently increases the heat transfer

These two effects are dependent on blockage geometry; they counteract each other such that it is not evident which effect dominates over a range of flow conditions.

It is expected that the tests planned in the 21-rod bundle task will provide sufficient data for the analysis of the preceding flow blockage effects. A better assessment of flow bypass effects on heat transfer will be made in the 161-rod blocked bundle task (to be performed later).

The tests planned under the 21-rod bundle flow blockage task will utilize a new core rod geometry (CRG)[1] that is typified by the Westinghouse 17 x 17 fuel rod design (table 2-1). This CRG is representative of all current vendors' PWR fuel assembly geometries.

TABLE 2-1

COMPARISON OF PWR VENDORS' FUEL ROD GEOMETRIES (OLD AND NEW)

Vendor	Dimension	
	Rod Diameter [mm (in.)]	Rod Pitch [mm (in.)]
NEW FUEL ASSEMBLIES (CRG)		
Westinghouse	9.5 (0.374)	12.6 (0.496)
Babcock & Wilcox	9.63 (0.379)	12.8 (0.502)
Combustion Engineering	9.7 (0.382)	12.9 (0.506)
OLD FUEL ASSEMBLIES		
Westinghouse	10.7 (0.422)	14.3 (0.563)
Babcock & Wilcox	10.9 (0.430)	14.4 (0.568)
Combustion Engineering	11.2 (0.440)	14.7 (0.580)

The tests performed in this task are classified as separate effects tests. In this case, the bundle is isolated from the system and the thermal-hydraulic conditions are prescribed at the bundle entrance and exit. Within the bundle, the dimensions are full scale (compared to a PWR) with the exception of overall radial dimension. The low mass housing used in this test series is designed to minimize the wall effects. Examination of the housing performance for the skewed axial profile FLECHT tests[2] indicates that it does simulate this radial boundary condition and that only the rods immediately adjacent to the housing are affected by the housing presence. To preserve proper thermal scaling of the FLECHT facility

1. The CRG is defined in this program as a nominal rod-to-rod pitch of 12.6 mm (0.496 in) and outside nominal diameter of 9.5 mm (0.374 in.), representative of various nuclear fuel vendors' new fuel assembly geometries and commonly referred to as the 17 x 17 or 16 x 16 assemblies.
2. Rosal, E. R., et al., "FLECHT Low Flooding Rate Skewed Test Series Data Report," WCAP-9108, May 1977.

with respect to a PWR, the power to flow area ratio is made to be nearly the same as that of a PWR fuel assembly. In this fashion, the steam vapor superheat, entrainment, and fluid flow behavior should be similar to that in a PWR bundle environment for the same boundary conditions.

SECTION 3
TASK OBJECTIVES

The objectives of the 21-rod bundle heat transfer tests are threefold:

-- To obtain, evaluate, and analyze thermal hydraulic data using 21-rod bundles to determine the effects of flow blockage geometry variation on the reflood heat transfer

-- To guide the selection of a blockage shape for use in the large blocked bundle task (Task 3.2.3)[1]

-- To develop an analytical or empirical method for use in analyzing the blocked bundle heat transfer data

To achieve these objectives, the fuel rod burst and blockage literature and test programs have been studied to find the most representative blockage shapes, which would be candidates for testing in the 21-rod bundle test facility. The shapes which have been chosen and the basis for the choice is given in section 4. Many different shapes and distributions of the blockage sleeves are possible; these combinations have been reduced to a total of seven test series in the 21-rod bundle through engineering judgment, examination of postulated flow blockage effects (section 2), and examination of the existing flow blockage model or method of calculation suggested by Hall and Duffey.[2] The seven 21-rod bundle test series are listed in table 3-1 with an explanation of the different effects which are expected to be observed from the experiments. The exact geometric description of each shape is given in section 4.

1. Conway, C. E., et al., "PWR FLECHT Separate Effects and System Effects Test (SEASET) Program Plan," NRC/EPRI/Westinghouse-1, December 1977.

2. Hall, P. C., and Duffey, R. B., "A Method of Calculating the Effect of Clad Ballooning on Loss-of-Coolant Accident Temperature Transients," Nucl. Sci. Eng. 58, 1-20 (1975).

TABLE 3-1

BLOCKAGE SHAPES AND CONFIGURATIONS TO BE TESTED IN 21-ROD BUNDLE

Test Series	Configuration Description	Comments
1	No blockage on the rods	This configuration will serve as a reference.
2	Short concentric sleeve, coplanar blockage on all rods	Coplanar is easiest to analyze, no flow bypass effects, maximum flow area effect at one axial plane.
3	Short concentric sleeve, coplanar blockage on center nine rods	This series increases the complexity of series 1 by adding some bypass effect. Use COBRA-IV to calculate bypass.
4	Short concentric sleeve, noncoplanar blockage on all sleeves	This test series examines a different blockage distribution and is comparable to series 2. COBRA-IV will be used to calculate flow.
5	Long nonconcentric blockage sleeve, noncoplanar blockage on all sleeves	This test series will permit a one-to-one comparison with series 4 in which all rods are blocked. Comparison of series 4 and 5 with unblocked data should indicate the worst shape.
6	Short, concentric, coplanar blockage on center nine rods, 90% blockage	This test series increases the flow bypass effect relative to series 3.
7	Test series 4 or 5 with increased blockage sleeve strain, whichever series provided the worst shape	This test series increases the blockage effect relative to series 4 or 5, whichever series provided the worst shape.

As shown in table 3-1, the majority of the tests will use a noncoplanar blockage sleeve distribution. This type of distribution will be employed since most of the out-of-pile and in-pile data indicate that burst occurs in a noncoplanar fashion. The sleeves for all test series will be smooth, and no attempt will be made to simulate the burst opening in the clad. Reflood tests will be conducted with no blockage in the same facility at the same thermal-hydraulic conditions, to serve as a basis to evaluate the flow blockage heat transfer.

Rod bundle instrumentation factors, such as heater rod thermocouple location and instrumented rods, will be nearly the same for each blockage shape or configuration. The instrumentation in the test facility loop, housing, flow system, and controls will be identical for all test series. Through replicate tests at the same conditions in the same facility, the local heat transfer on a given blocked rod can be compared to that on an unblocked rod, to obtain the effect of the flow blockage. Comparisons of this fashion, on a one-to-one basis with unblocked data, will allow the determination of which shape or distribution results in the poorest heat transfer relative to the unblocked geometry. If no measurable difference is observed, then the blockage shape which appears most common in the out-of-pile or in-pile burst tests will be used in the 161-rod blocked bundle. Also, some consideration will be given to installation and testing problems when choosing a shape in this fashion.

To help ascertain both the hydraulic and the heat transfer effect of the flow blockage shapes relative to the unblocked bundle, single-phase hydraulic tests, steam cooling, forced reflooding, and gravity reflooding tests will be performed on each blockage configuration. The hydraulic tests will be used to characterize the bundle in a hydraulic fashion by measuring the blockage region loss coefficient, grid loss coefficients, and the 21-rod bundle friction factor. These hydraulic parameters will then be input to a COBRA-IV[1] model of the 21-rod bundle test facility. The COBRA-IV code (appendix A) will then be used to calculate the single-phase flow redistribution in and around the blockage zone for each configuration. In this fashion, the measured local heat transfer can be associated with a calculated local flow (single-phase) from COBRA; this should help to explain the heat transfer behavior.

1. Wheeler, C. L., et al., "COBRA-IV: An Interim Version of COBRA for Thermal-Hydraulic Analysis of Rod Bundle Nuclear Fuel Elements and Cores," BNWL-1962, March 1976.

The COBRA-IV calculations to be performed will be single-phase steam flow redistribution calculations. Although the flow during reflooding is two-phase for most of the test time, the flow regime which will exist at the quench front is highly dispersed flow. A typical void fraction above the quench front for the low flooding rate test conditions given in section 9 is 0.95. Therefore, steam flow is in the continuous phase and the relatively few droplets do not affect the macroscopic (subchannel average) steam flow and/or flow redistribution. Sample calculations have been performed and reported in the FLECHT SEASET program plan on the single-phase flow redistribution effect on droplets. It was shown that, except for the extremely small drops, the liquid phase does not redistribute with the steam flow. The drops have sufficient inertia to continue their flight through the blockage zone without any significant deviations.

Single-phase steam cooling tests will also be conducted and will serve as a reference heat transfer environment which can be compared to both unblocked single-phase steam cooling data and two-phase reflooding heat transfer data. In this manner, both the single- and two-phase effects of the blockage on the local rod heat transfer can be evaluated. Similarly, the gravity-driven reflood tests will again permit one-to-one comparison with the unblocked gravity reflood tests in the 21-rod bundle test facility for each blockage shape and/or configuration.

Most of the tests in the 21-rod bundle test matrix will be constant forced flooding reflood tests. The test conditions represent typical safety evaluation model assumptions and initial conditions. The forced flooding tests will be used primarily to help develop a blockage model or method of analysis through comparisons with identical unblocked forced reflooding tests and the associated COBRA-IV flow redistribution analysis. The data analysis emphasis in these experiments will be on calculation of the fluid conditions at each instrumented bundle axial plane, to help develop a model and a mechanistic explanation of the flow blockage effect in the bundle. The model or experimental method of predicting blockage heat transfer will then be evaluated in the larger 161-rod bundle test, where ample flow bypass can occur.

SECTION 4
BLOCKAGE SHAPES AND TEST CONFIGURATIONS

4-1. GENERAL

The high internal pressure and temperature of fuel rods during a postulated PWR LOCA are expected to cause the fuel rods to swell and burst. The resulting rod deformation would reduce the fluid flow area in the rod array. The shape of the rod swelling and burst is referred to as a blockage shape. This flow area reduction (or flow blockage) is governed by the shapes and spatial distribution of blockage. Therefore blockage shapes and their spatial distribution must be chosen properly to simulate the thermal-hydraulic conditions of the fluid flow in the blocked rod array. The number of selected blockage shapes should be minimized to make blockage tests feasible, but it must be sufficient to address the important effects of the flow blockage on heat transfer. The spatial blockage distribution must also be chosen to represent typical situations and/or to provide fundamental understandings of blockage effects on the local heat transfer.

The results of several single-rod and multirod burst tests are available. These results were used to define the blockage shapes to be simulated in the task. Discussions with NRC and EPRI were also considered in the choice of blockage shape. The blockage shapes so determined will be simulated by stainless steel sleeves which can be attached to rods to effect flow blockage. Each rod will have a sleeve to simulate the state of rod swelling and burst.

Further, a preliminary approach to better utilize the 21-rod bundle results in the design of the 161-rod bundle was also discussed. It is desirable to have a geometric similarity between the 21-rod and 161-rod bundle. This similarity is expected to provide a better basis for a data analysis and the understanding of bypass effects.

4-2. BLOCKAGE SHAPES

Several out-of-pile and in-pile burst tests have been executed to aid in the understanding of rod burst phenomena during a LOCA. Out-of-pile tests have

employed several heating methods to simulate rod heatup during a reflooding period. The heating methods include a stiff internal heater rod (continuous rigid heating element) method, external radiation heatup, and direct resistance heating. But the external radiation heating and direct resistance heatup are believed to distort the thermal response of the clad during its deformation.[1] The internal heater rod may reduce the clad temperature nonuniformity which is expected in the real situation of stacked fuel pellets. Although an out-of-pile test method is not ideal, the tests have led most experimenters to agree that an internal heater method is most representative of the real situation. Therefore the results from the tests using internal heater rod methods are reviewed here to provide a basis for defining blockage shape. Very limited in-pile test results have also been reviewed.

The available results from several rod burst tests show that there are two distinctive rod swelling patterns, depending on the burst temperature. This is due to the existence of two phases of Zircaloy, whose material properties are quite different from each other. Zircaloy is in the alpha phase at temperatures of less than about 830°C (1529°F) and in mixed phase of alpha and beta types between 830°C and 970°C (1529°F and 1779°F).[2] Above 970°C (1779°F) Zircaloy is in the beta phase. Alpha phase Zircaloy has an anisotropic strain property. Therefore, deformation of alpha phase Zircaloy is very sensitive to minor temperature irregularity in both circumferential and axial directions. This anisotropic property causes rod bowing, in addition to swelling and burst. Although the burst phenomenon in the mixed phase is not well understood, this burst range can be treated essentially as alpha phase burst because of the nonisotropic property of alpha phase. Beta phase Zircaloy has an isotropic strain property which causes more or less uniform clad swelling. Thus, the property of alpha phase Zircaloy is different from that of beta phase Zircaloy. This difference gives a quite different clad swelling phenomenon for each phase. Therefore, two typical blockage shapes representing alpha and beta phase swelling were chosen to be simulated in tests.

---

1. Picklesimer, M. L., Presentation at the PMG meeting for FLECHT SEASET, April 1978.

2. Chapman, R. H., "Significant Results From Single-Rod and Multirod Burst Tests in Steam With Transient Heating," paper presented at Fifth Water Reactor Safety Research Information Meeting, Germantown, MD, November 7-10, 1977.

SECTION 4
BLOCKAGE SHAPES AND TEST CONFIGURATIONS

4-1. GENERAL

The high internal pressure and temperature of fuel rods during a postulated PWR LOCA are expected to cause the fuel rods to swell and burst. The resulting rod deformation would reduce the fluid flow area in the rod array. The shape of the rod swelling and burst is referred to as a blockage shape. This flow area reduction (or flow blockage) is governed by the shapes and spatial distribution of blockage. Therefore blockage shapes and their spatial distribution must be chosen properly to simulate the thermal-hydraulic conditions of the fluid flow in the blocked rod array. The number of selected blockage shapes should be minimized to make blockage tests feasible, but it must be sufficient to address the important effects of the flow blockage on heat transfer. The spatial blockage distribution must also be chosen to represent typical situations and/or to provide fundamental understandings of blockage effects on the local heat transfer.

The results of several single-rod and multirod burst tests are available. These results were used to define the blockage shapes to be simulated in the task. Discussions with NRC and EPRI were also considered in the choice of blockage shape. The blockage shapes so determined will be simulated by stainless steel sleeves which can be attached to rods to effect flow blockage. Each rod will have a sleeve to simulate the state of rod swelling and burst.

Further, a preliminary approach to better utilize the 21-rod bundle results in the design of the 161-rod bundle was also discussed. It is desirable to have a geometric similarity between the 21-rod and 161-rod bundle. This similarity is expected to provide a better basis for a data analysis and the understanding of bypass effects.

4-2. BLOCKAGE SHAPES

Several out-of-pile and in-pile burst tests have been executed to aid in the understanding of rod burst phenomena during a LOCA. Out-of-pile tests have

employed several heating methods to simulate rod heatup during a reflooding period. The heating methods include a stiff internal heater rod (continuous rigid heating element) method, external radiation heatup, and direct resistance heating. But the external radiation heating and direct resistance heatup are believed to distort the thermal response of the clad during its deformation.[1] The internal heater rod may reduce the clad temperature nonuniformity which is expected in the real situation of stacked fuel pellets. Although an out-of-pile test method is not ideal, the tests have led most experimenters to agree that an internal heater method is most representative of the real situation. Therefore the results from the tests using internal heater rod methods are reviewed here to provide a basis for defining blockage shape. Very limited in-pile test results have also been reviewed.

The available results from several rod burst tests show that there are two distinctive rod swelling patterns, depending on the burst temperature. This is due to the existence of two phases of Zircaloy, whose material properties are quite different from each other. Zircaloy is in the alpha phase at temperatures of less than about 830°C (1529°F) and in mixed phase of alpha and beta types between 830°C and 970°C (1529°F and 1779°F).[2] Above 970°C (1779°F) Zircaloy is in the beta phase. Alpha phase Zircaloy has an anisotropic strain property. Therefore, deformation of alpha phase Zircaloy is very sensitive to minor temperature irregularity in both circumferential and axial directions. This anisotropic property causes rod bowing, in addition to swelling and burst. Although the burst phenomenon in the mixed phase is not well understood, this burst range can be treated essentially as alpha phase burst because of the nonisotropic property of alpha phase. Beta phase Zircaloy has an isotropic strain property which causes more or less uniform clad swelling. Thus, the property of alpha phase Zircaloy is different from that of beta phase Zircaloy. This difference gives a quite different clad swelling phenomenon for each phase. Therefore, two typical blockage shapes representing alpha and beta phase swelling were chosen to be simulated in tests.

---

1. Picklesimer, M. L., Presentation at the PMG meeting for FLECHT SEASET, April 1978.

2. Chapman, R. H., "Significant Results From Single-Rod and Multirod Burst Tests in Steam With Transient Heating," paper presented at Fifth Water Reactor Safety Research Information Meeting, Germantown, MD, November 7-10, 1977.

4-3. Blockage Shape of Beta Phase Burst

Several tests which have been conducted in beta phase were briefly reviewed and the most probable burst shape was chosen. Hydrodynamic aspects of the fluid flow around blockages were also considered, to pinpoint important factors in the blockage tests. Based on the hydrodynamic arguments, a sleeve shape which is shorter than the observed one was chosen and recommended for use as a blockage simulation of beta phase bursts.

4-4. Review of Available Test Programs -- The data of the beta phase burst tests at Oak Ridge National Laboratory (ORNL)[1-8] are summarized in table 4-1. These single-rod tests showed wide variation in maximum strains. Also, it was observed that the bulge was localized, with high baseline strain. Pictures of the test rods after burst show that the axial length of the localized swelling was about four times the rod diameter, and this local bulge was continued by gradually diminishing swellings on both sides of the bulge. These gradual tails resulted in a long blockage shape whose axial length was the same as that of the test rod. An

---

1. Chapman, R. H., "Multirod Burst Test Program Quarterly Progress Report, October-December 1975," ORNL/NUREG/TM-10, May 1976.

2. Chapman, R. H., "Multirod Burst Test Program Quarterly Progress Report, January-March 1976," ORNL/NUREG/TM-36, September 1976.

3. Chapman, R. H., "Multirod Burst Test Program Quarterly Progress Report, April-June 1976," ORNL/NUREG/TM-74, January 1977.

4. Chapman, R. H., "Multirod Burst Test Program Quarterly Progress Report, October-December 1976," ORNL/NUREG/TM-95, April 1977.

5. Chapman, R. H., "Multirod Burst Test Program Quarterly Progress Report, January-March 1977," ORNL/NUREG/TM-108, May 1977.

6. Chapman, R. H., "Multirod Burst Test Program Quarterly Progress Report, April-June 1977," ORNL/NUREG/TM-135, November 1977.

7. Chapman, R. H., "Some Preliminary Results of Single-Rod and Multirod Tests with Internal Heaters," presentation at NRC Fuel Cladding Review Meeting, January 18, 1978.

8. Chapman, R. H., "Significant Results From Single-Rod and Multirod Burst Tests in Steam With Transient Heating," paper presented at Fifth Water Reactor Safety Research Information Meeting, Germantown, MD, November 7-10, 1977.

TABLE 4-1

ORNL BETA PHASE BURST TEST RESULTS

Test	ε_{max} (a) (%)	ε_1 (a) (%)	$\varepsilon_1/\varepsilon_{max}$	ε_2 (a) (%)	$\varepsilon_2/\varepsilon_{max}$
PS-18	24	18	0.75	14	0.58
PS-19	30	19	0.63	12	0.40
SR-2	45	33	0.73	21	0.47
SR-3	42	35	0.83	30	0.71
SR-4	17	11	0.65	8	0.47
SR-8	45	38	0.84	27	0.60
SR-13	70	63	0.90	47	0.67
SR-17	52	46	0.88	40	0.77
SR-20	58	46	0.79	40	0.69
SR-21	58	44	0.76	30	0.52
SR-22	53	44	0.83	36	0.68
SR-23	38	31	0.82	25	0.66
SR-24	66	58	0.88	47	0.71
SR-25	78	65	0.83	50	0.64

a. ε_{max}, ε_1, and ε_2 are defined as follows:

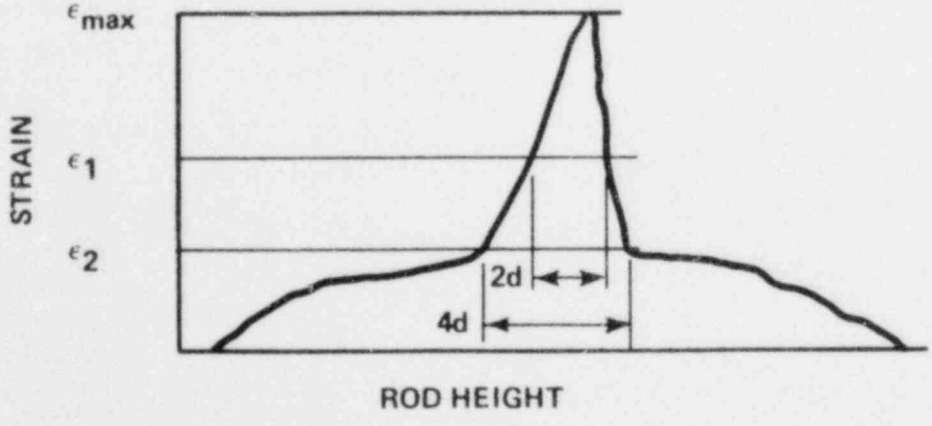

in-pile test[1] conducted at the Transient Reactor Test Facility (TREAT) by ORNL showed rod diameter increases as shown in figure 4-1. The strain values are given in table 4-2.

The above two test series show that all heated clad suffered some degree of strain. German tests[2] showed that grids acted as an excellent heat sink and prevented clad swelling at the grid points. Therefore it can be concluded that blockage length could be of the order of the grid span. But it must be noted that rod swelling near the grid has less than 5 percent strain. In the beta phase burst, more or less uniform circumferential temperature and isotropic strain give rise to relatively uniform and concentric clad swelling around the test heater rod. Further, the accompanying burst is small. Therefore the blockage can be seen as symmetrical. From the above observations, the blockage shape is visualized as symmetrical laterally and long axially with a short bulge at the center of the blockage. The maximum possible swelling length can be taken at about 50 times the original rod diameter (based on the Westinghouse PWR grid span). A schematic sketch for this shape is shown in figure 4-2. The center portion (4d) of the blockage shape is shown to be composed of two superimposed shapes, a short local bulge (2d long) and the appreciable strain increase (over 4d long) which has been observed experimentally from strain information.

Maximum strains for beta bursts are in the range of 20 to 80 percent. Actual simulation strain must be determined by also considering the alpha phase burst strain for comparison.

4-5. Hydrodynamic Aspects -- Although the physical shape of clad swelling is long (as noted above), it is difficult to simulate the long shape in blockage tests. The difficulties are mainly associated with the following four aspects:

-- Manufacturing
-- Attaching sleeve to and detaching from rod

---

1. Lorenz, R. A., et al., "Final Report on the First Fuel Rod Failure Transient Test of a Zircaloy-Clad Fuel Rod Cluster in TREAT," ORNL-4635, March 1971.

2. Wiehr, K., et al., "Fuel Rod Behavior in the Refill and Flooding Phase of a Loss-of-Coolant Accident," CONF-771252-5, December 1977.

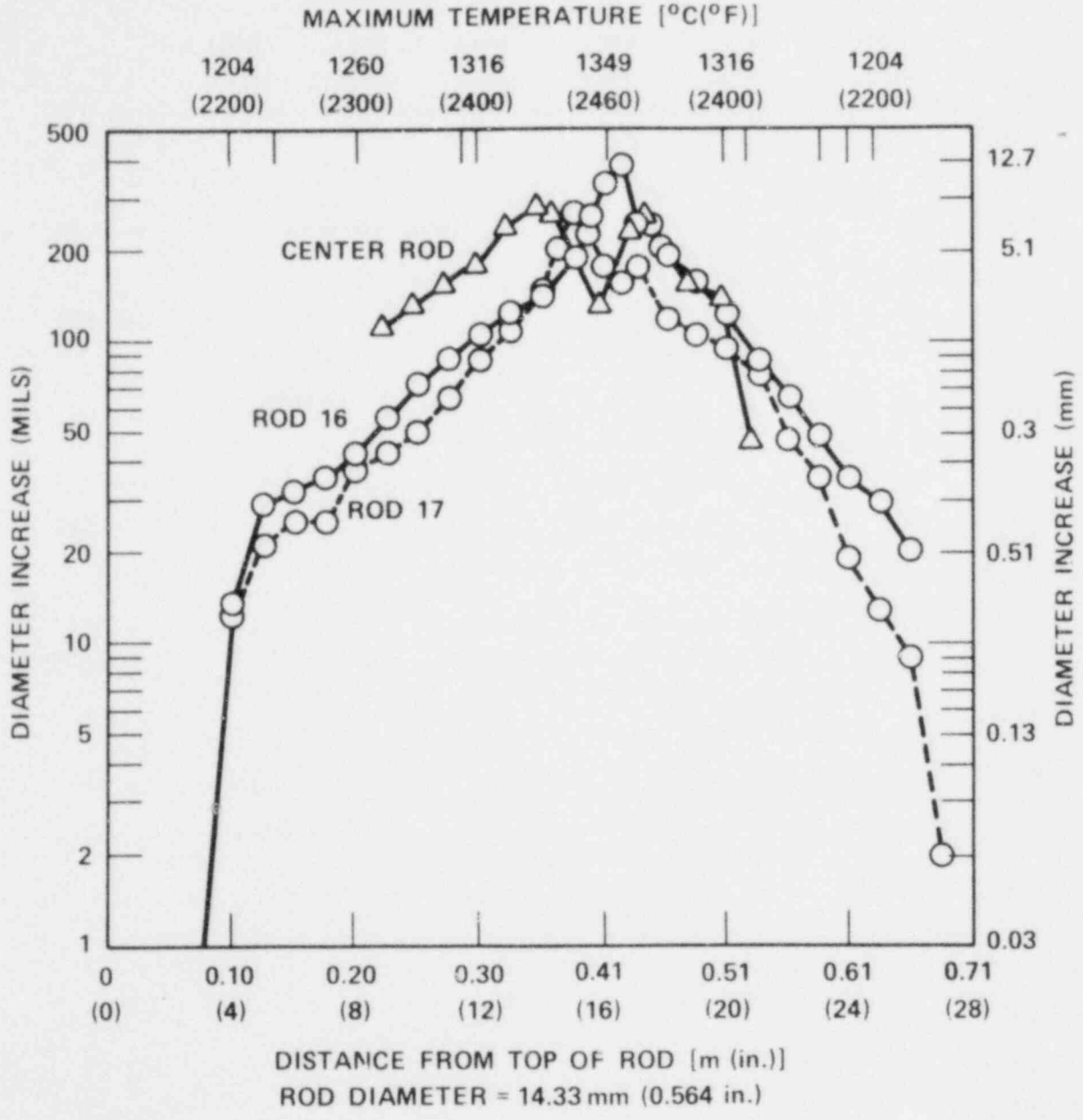

Figure 4-1. Swelling of Fuel Rods in TREAT Experiment FRF-2

TABLE 4-2

FUEL ROD DIMENSIONAL CHANGES IN TREAT EXPERIMENT

Rod Identification	Diameter Increase, Rupture-to-Back (%)	Diameter Increase, Viewed by Center Rod (%)	Increase in Rod Length [mm(in.)]	Volume Increase From Swelling [cm^3(in^3)]
Center (58-3)	51	57	2.3 (0.09)	42 (2.6)
11	50	48	8.1 (0.32)	29 (1.8)
12	62	74	8.6 (0.34)	33 (2.0)
13	52	55	7.1 (0.28)	33 (2.0)
16	77	75	9.4 (0.37)	40 (2.4)
17	57	53	8.1 (0.32)	29 (1.8)
18	63	63	7.1 (0.28)	35 (2.1)

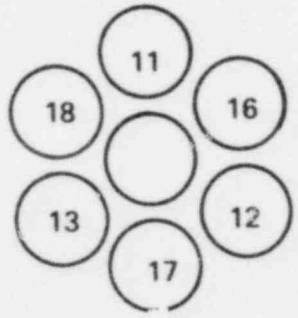

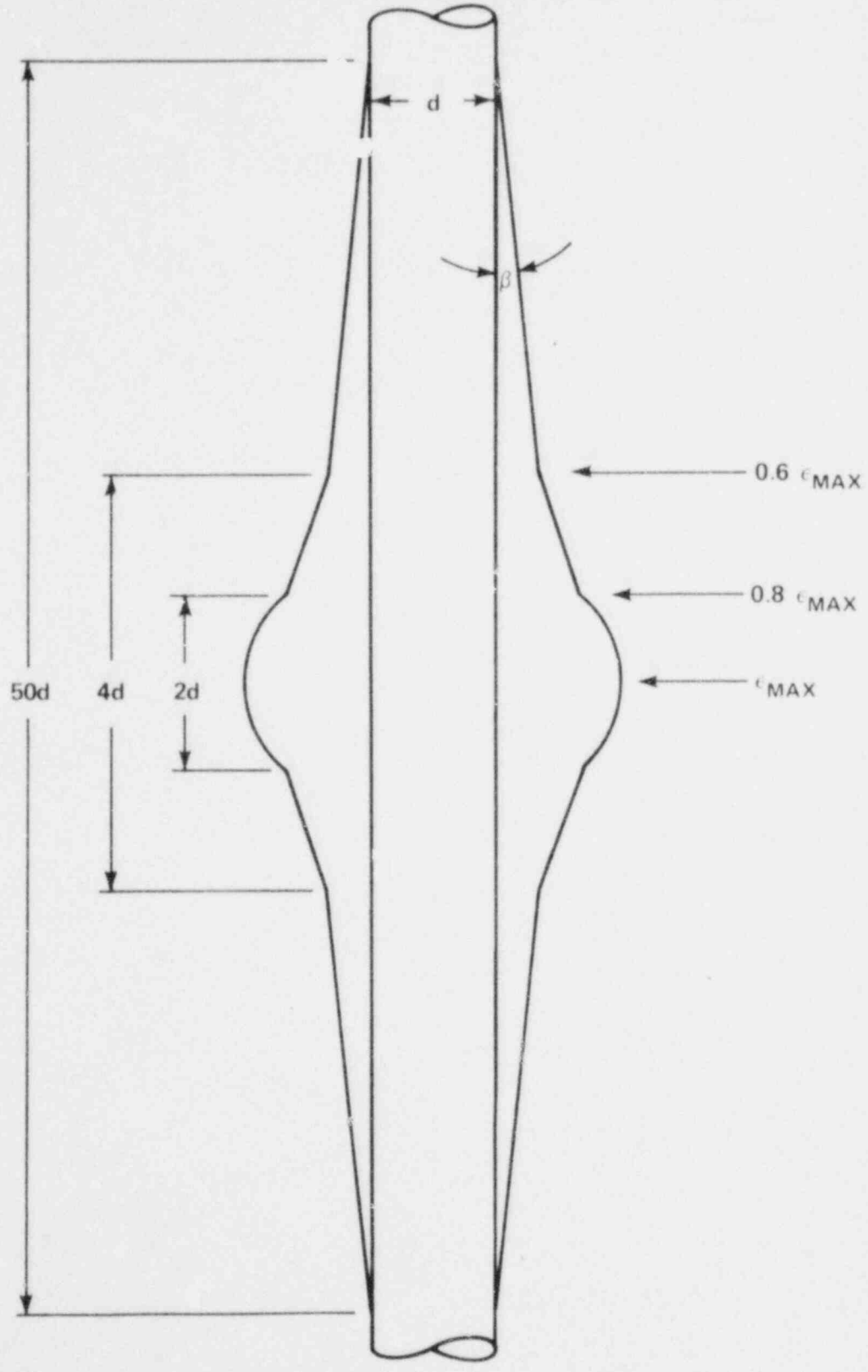

Figure 4-2. Blockage Shape of Beta Phase Burst

-- Instrumentation
-- Data analysis

Therefore a compromise is required to avoid these problems without jeopardizing the blockage tests objective, which is understanding heat transfer at and downstream of blockage. Blockage effects on fluid flow can be classified into two areas: change in flow behavior (flow separation, turbulence intensity) around the blockage, and flow diversion out of the blocked channel. The most important phenomenon to be simulated in the blockage test is the local flow characteristics around the blockage.

A dispersed flow should be considered during a reflood phase to illustrate the flow around the blockage. The interaction between the solid walls and the droplets upstream of the maximum blockage can be accounted for by keeping the same lateral cross-sectional area of blockage. Downstream of the blockage, fluid separation from the wall is mainly governed by the steam flow itself, because there is a high-quality two-phase flow at the blockage when a quench front is far below the blockage. Also, the downstream mixing is strongly affected by steam flow. Therefore, single-phase flow characteristics with respect to blockage will be considered to determine blockage shapes.

As shown in figure 4-2, the long sleeve tails have very small approaching angles (β = 0.27 degree when ϵ_{max} = 36 percent). Schlichting[1] compared form drag to total drag for aerofoils (figure 4-3). For d/L = 0.05 (equivalent to an approaching angle of about 3 degrees), the form drag is about 5 percent of total drag. Thus, if the angle is less than 3 degrees, the flow can be assumed to be essentially straight. Therefore the effect of long sleeve tails on the fluid flow is negligible; only the fluid flow around the local bulge portion is important to characterization of the heat transfer. Flow may be separated immediately downstream of blockage, resulting in an increase of turbulence at this point. Flow separation and reattachment are strongly dependent on the local geometry. Thus, it is necessary to simulate the local geometry in the region of flow separation and to estimate the extent of the separation zone.

---

1. Schlichting, H., Boundary-Layer Theory, 6th edition, McGraw-Hill, New York, 1968.

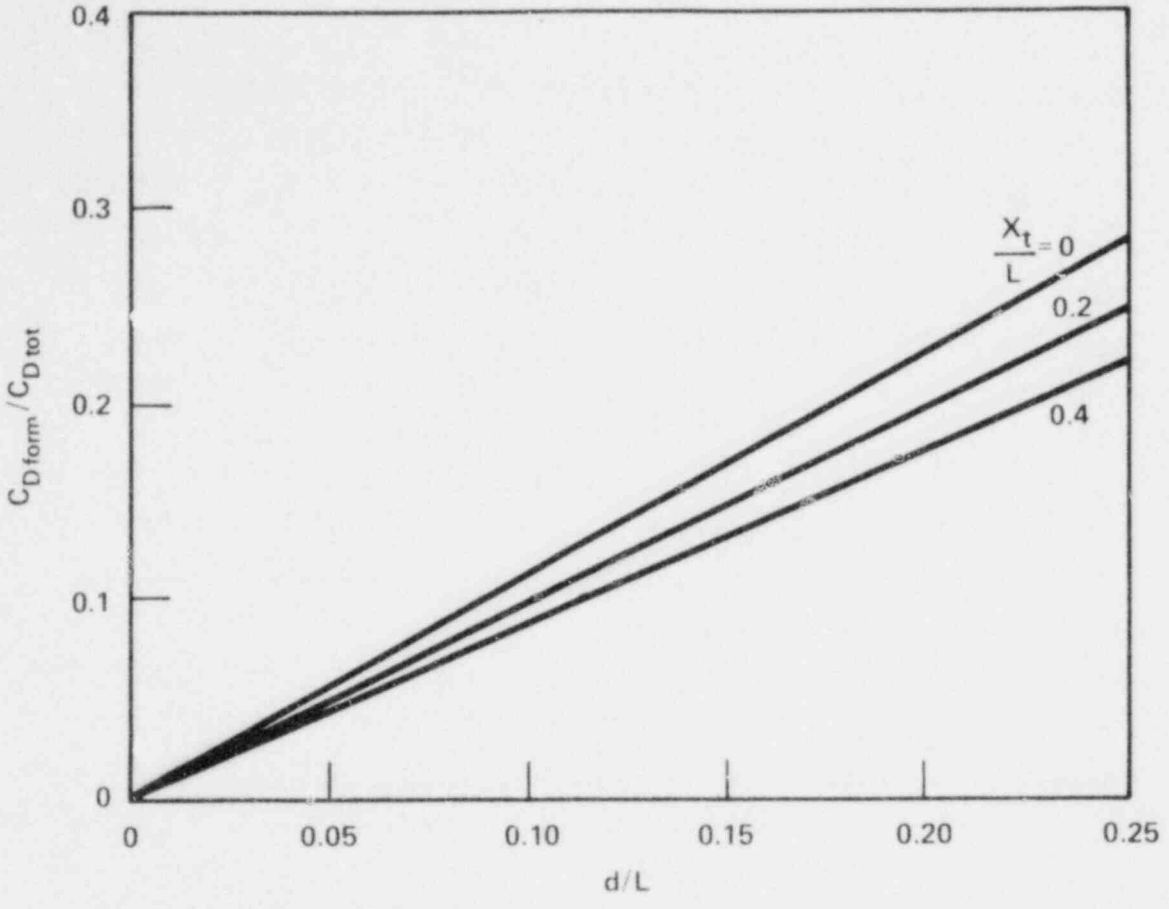

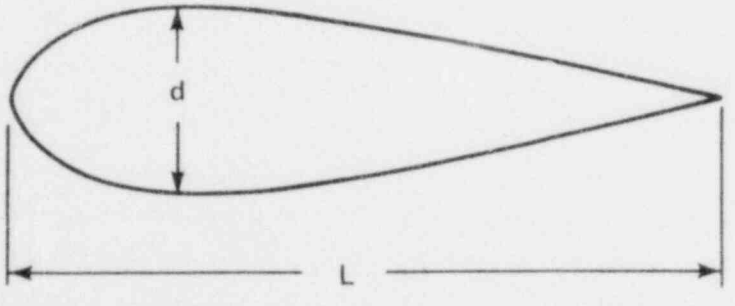

X_t: TRANSITION BETWEEN LAMINAR AND TURBULENT FLOW IN A BOUNDARY LAYER FLOW

Figure 4-3. C_{Dform}/C_{Dtot} Versus d/L

The diversion section of blockage is shown schematically in figure 4-4a. The separation zone can be idealized (figure 4-4b) to determine the point of reattachment. Abramovich[1] analyzed a free jet like that in figure 4-4b and showed that the turbulent boundary layer spreads linearly with α equal to approximately 9 degrees during the initial period of the jet, which extends up to about four or five times the jet gap. This analysis was based on the boundary layer similarity, continuity, and momentum equations. It must be noted that the spread angle was derived for the case of a turbulent jet in an unbounded space.

Assuming that the divergence downstream of blockage can be viewed as an unbounded space for the jet, a rough estimate of the reattachment point can be obtained as a function of channel geometries. Since the spread angle (α) can be taken as 9 degrees based on the assumption, the relation between h and χ is simply

$$\chi = h/\tan 9^{o} = 6.3\ h \qquad (4\text{-}1)$$

where χ is the reattachment distance from the step and h is the step height.

Equation (4-1) was compared with experimental data and proved to be a reasonable estimate of the reattachment point (appendix B). Therefore if the blockage geometry between $\chi = 0$ and $\chi = 6.3$ h is maintained, it can be said that the flow separation effect can be simulated.

The remaining concerns of the local flow downstream of the blockage are the turbulence intensity decay pattern after the flow reattachment in the downstream and upstream flow pattern of blockage. The blockage observed in several multirod burst tests has a gradual strain change portion superimposed by a relatively abrupt strain change. The approaching angle of the gradual change portion is generally less than 1 degree. Since Schlichting showed that, if a diverging angle was less than 3 degrees, the flow was essentially the same as a straight flow, the gradual portion can be neglected without affecting the turbulence intensity decay pattern. Also, if the abrupt strain change portion is simulated, it can be seen that the upstream flow pattern will not change significantly.

---

1. Abramovich, G. N., The Theory of Turbulent Jets, MIT Press, Cambridge, MA, 1963.

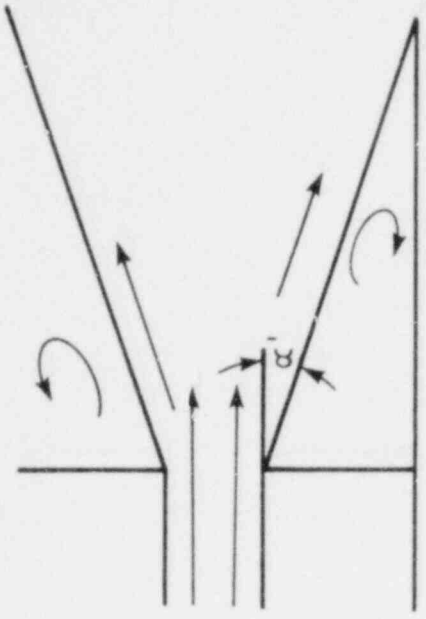

(B)

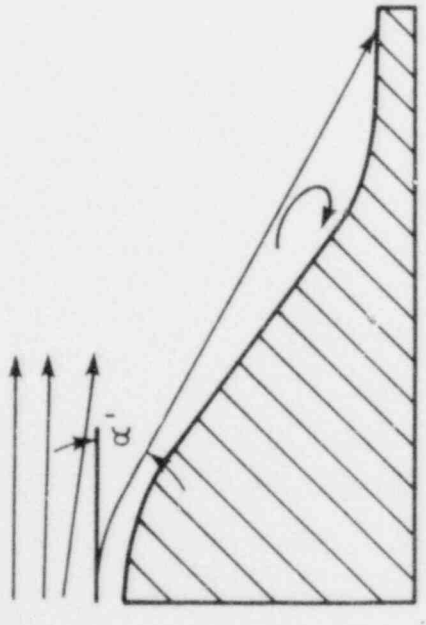

(A)

Figure 4-4. Flow Separation Schematic Diagram

Based on above discussions, the blockage shape may be chosen in the following way:

(1) Take a physical simulation of sleeve.

(2) Draw a straight line at an angle of 3 degrees (this value is arbitrarily chosen to provide a conservatism to the calculated 9 degrees) with respect to the axial direction from the tip of the maximum strain to define the downstream portion of the sleeve.

(3) Determine the upstream portion to make the sleeve symmetrical with respect to the downstream strain planes.

The short sleeve thus simulated maintains blockage geometry in the region of flow separation downstream of the maximum strain (the axial length of the zone is determined by equation (4-1)). Since the ends of the resulting sleeve lie on the gradual change portion of the long sleeve, the turbulence decay pattern thereafter and the flow pattern upstream of the blockage are not expected to be altered considerably.

The blockage shape thus determined is shown in figure 4-5a. But since the sleeve to simulate this blockage shape will be made of material with a finite thickness, some simplification of the resulting shape without much distortion is worthwhile in view of the required efforts and cost. It is also necessary to modify the end portion of the blockage to avoid abrupt flow streamline change. The center portion of the blockage (4d long) can be modified to a cosine curve with a minimal alteration of the resulting curve. Further, the tail section of the sleeve can be modified to a straight line by grinding off the thickness at the ends of the sleeve. This simplified sleeve is not considered much different in hydrodynamic effects from the observed blockage shape. The simplified shape considering the material thickness (0.5 mm (0.02 in.)) is shown in figure 4-5b.

Since a relatively short sleeve is to be used in the FLECHT SEASET tests, the effect of cross flow out of a subchannel was investigated for both long and short sleeves. The COBRA-IV code was used to calculate the flow redistribution effects

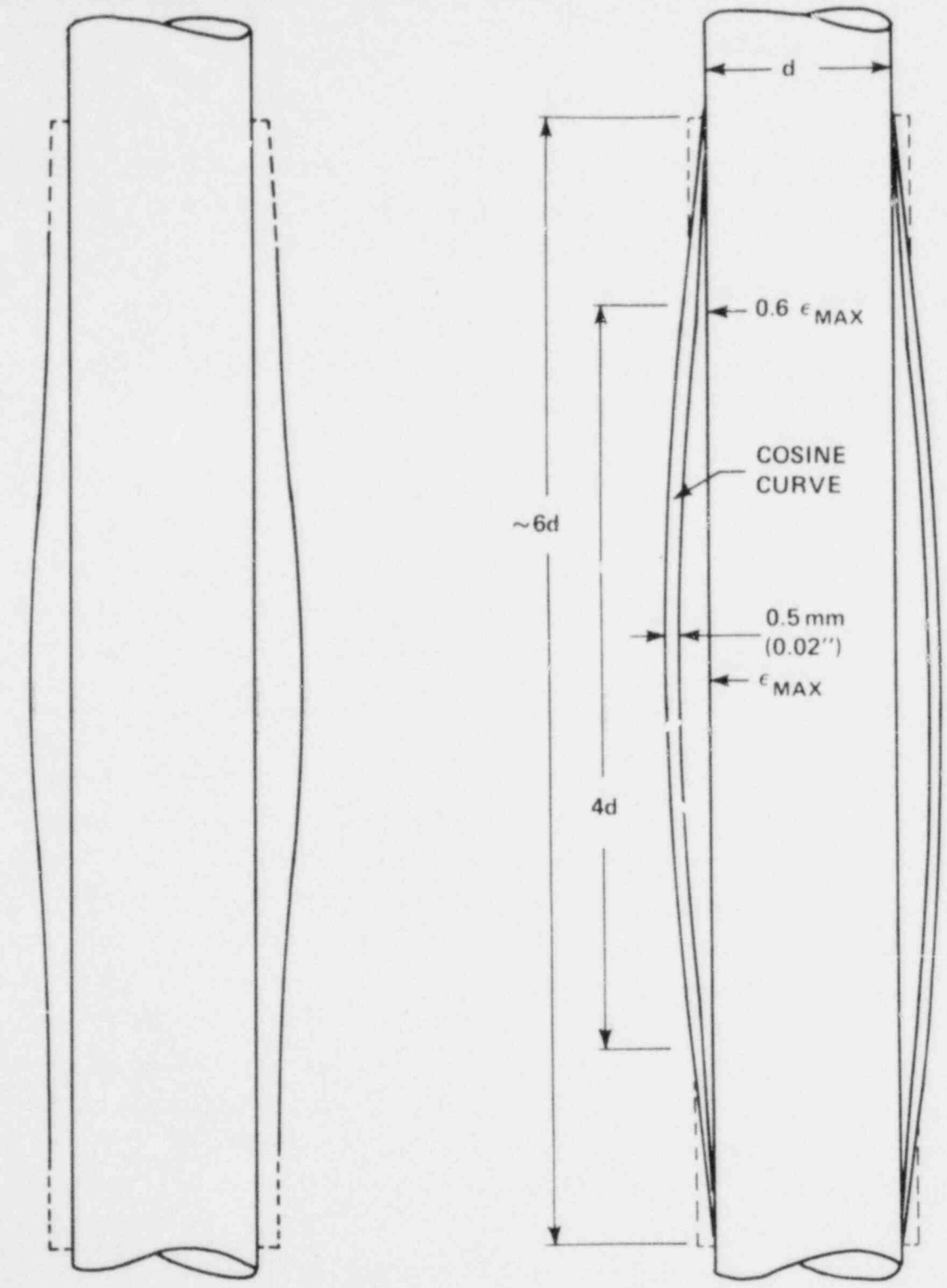

(A) BASED ON FIGURE 4-2

(B) MODIFIED SLEEVE SHAPE

Figure 4-5. Simulated Sleeve Shapes

caused by the different blockage sleeve lengths. The sleeve model in the calculations was a symmetrical concentric sleeve with a strain of 32.6 percent. Both a single sleeve and a coplanar four-sleeve blockage were studied in the 21-rod bundle (figures 4-6a and 4-6b). A slightly superheated steam at 275.8 kPa (40 psia) was used as fluid; the Reynolds number was about 13,300. Figures 4-7 and 4-8 show the calculated flow rates in the channels which are most affected by blockages. Since the sleeve wall thickness is 0.5 mm (0.02 in.), the maximum length the sleeve could have is about 20 to 24 times the heater rod diameter. (At this point the sleeve wall thickness would equal the strain.) Therefore flow diversion effects due to sleeves of L/d=18 were also calculated and compared in figures 4-7 and 4-8.

The calculations show that the longer sleeves (L/d = 18, L/d = 50) have lower local flow rates in the blocked channels than the shorter one (L/d = 6). This flow diversion effect is due to the flow leaving the blocked subchannel sooner with the longer sleeves. If the flows are integrated in the most blocked subchannel of the coplanar four-sleeve blockage up to the blockage throat, the longer sleeves have 4 and 16 percent flow diversion effects for L/d = 18 and L/d = 50, respectively.

4-6. Conclusion -- Based on the above arguments, the sleeve shape to simulate beta phase blockage in FLECHT SEASET is recommended to be a short one (L/d = 6), as depicted in figure 4-5b. This sleeve shape is expected to correctly simulate flow separation, flow reattachment, and turbulence intensity reduction after the wake due to flow separation.

4-7. Blockage Shape of Alpha Phase Burst

Several burst tests have studied the behavior and shape of clad swelling. The most extensive is the ORNL program, in which a series of single-rod burst tests preceded multirod burst tests. So far three bundle (4 x 4) tests have been completed. The ORNL single-rod alpha phase burst results are summarized in table 4-3. The maximum circumferential strains observed in the tests were about 25 percent with $\pm$5 percent variations.

Three ORNL multirod burst tests were designed for burst in the alpha phase. However, only the first bundle data are available now; the data are summarized in

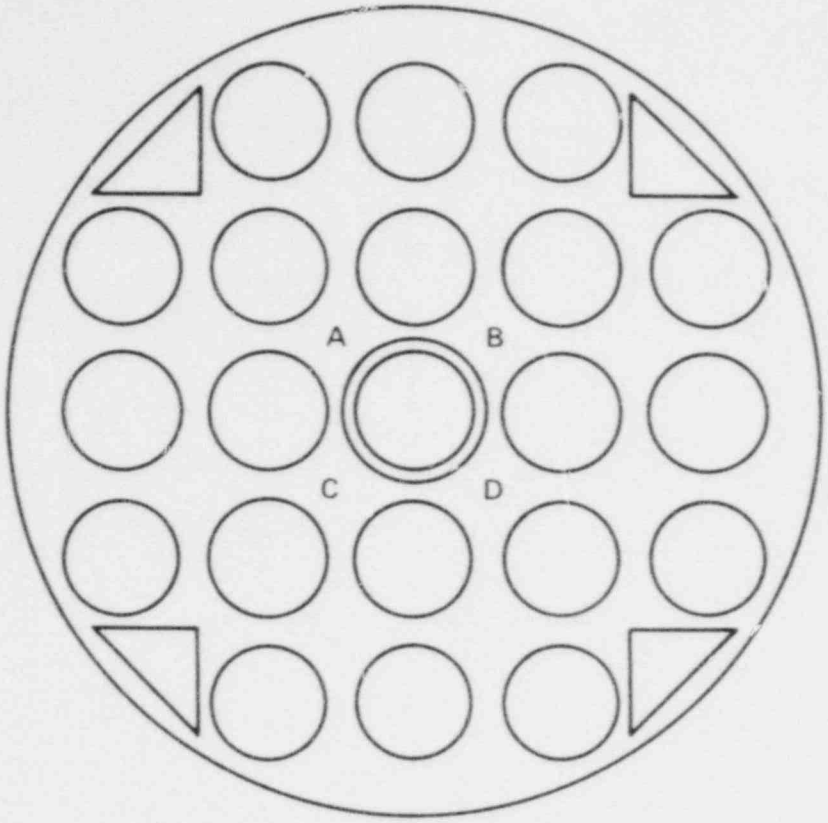

A, B, C, D: BLOCKED CHANNELS

(A) SINGLE-SLEEVE BLOCKAGE

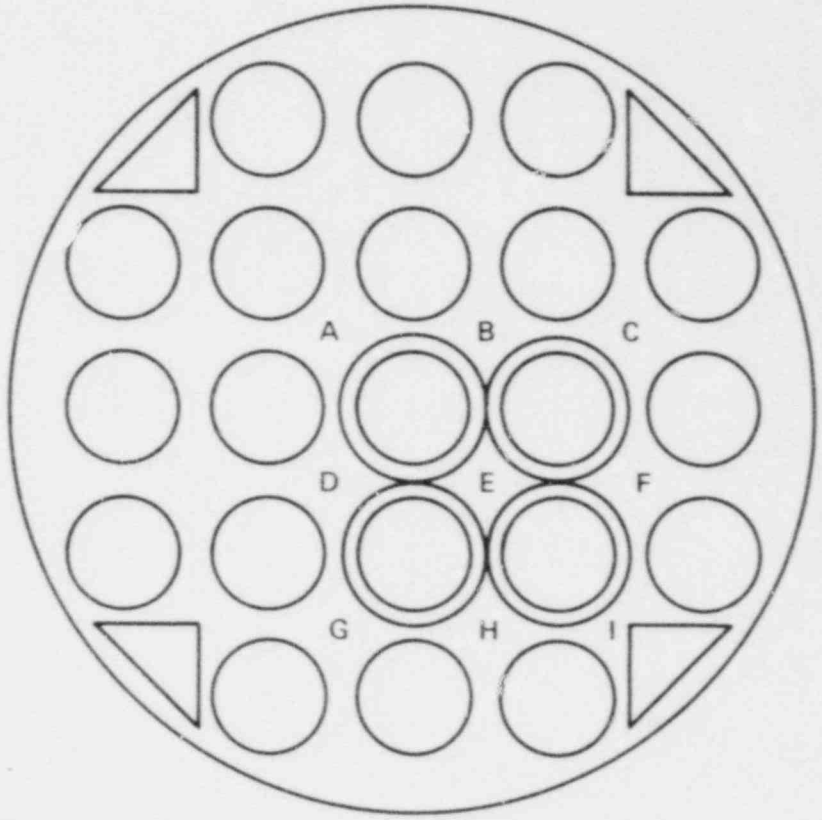

A, B, C, D, F, G, H, I: BLOCKED CHANNELS
E: MOST BLOCKED CHANNEL

(B) FOUR-SLEEVE COPLANAR BLOCKAGE

Figure 4-6. Blockage Arrangements for COBRA

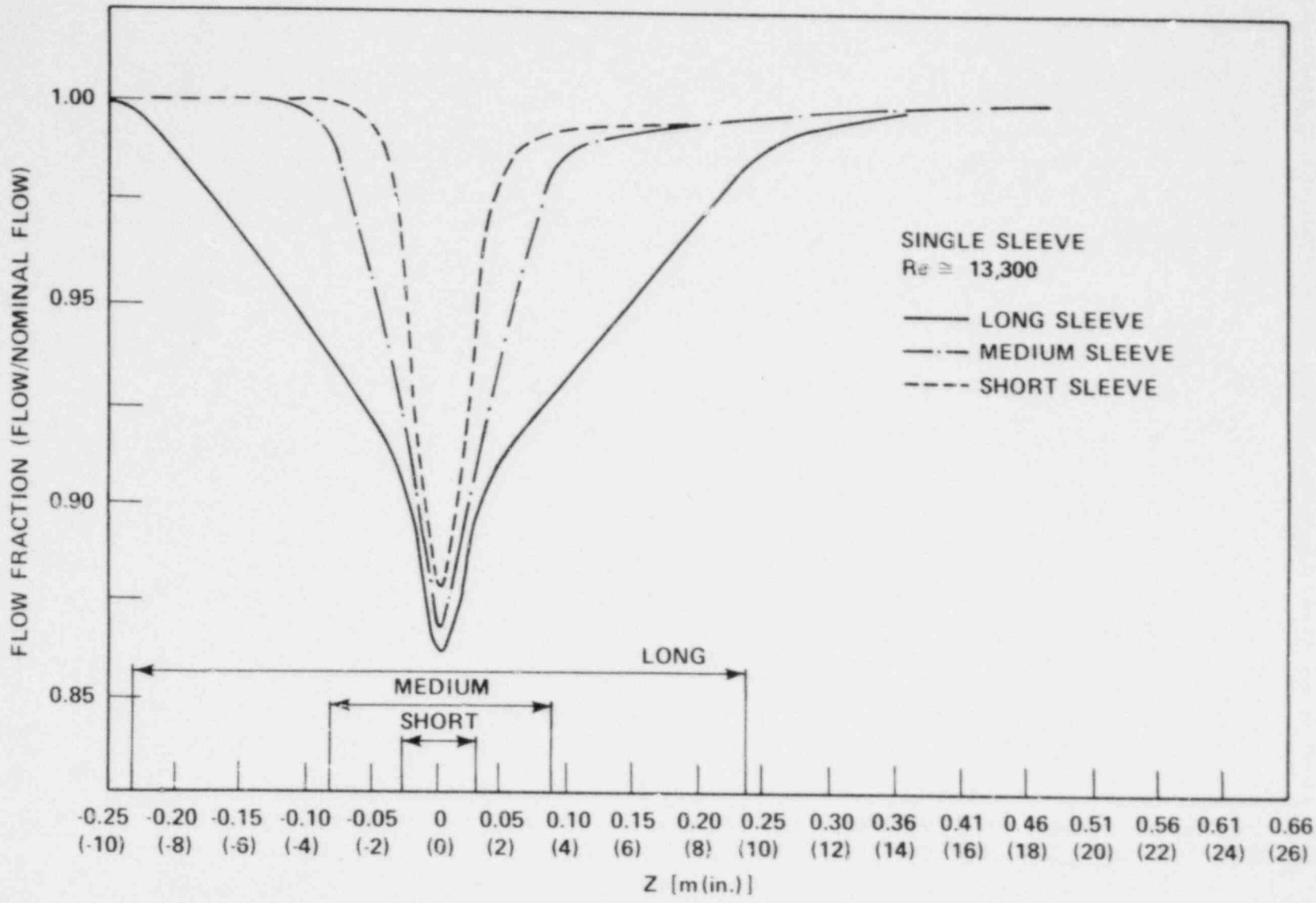

Figure 4-7. Flow Rate Change in Center Channel (COBRA)

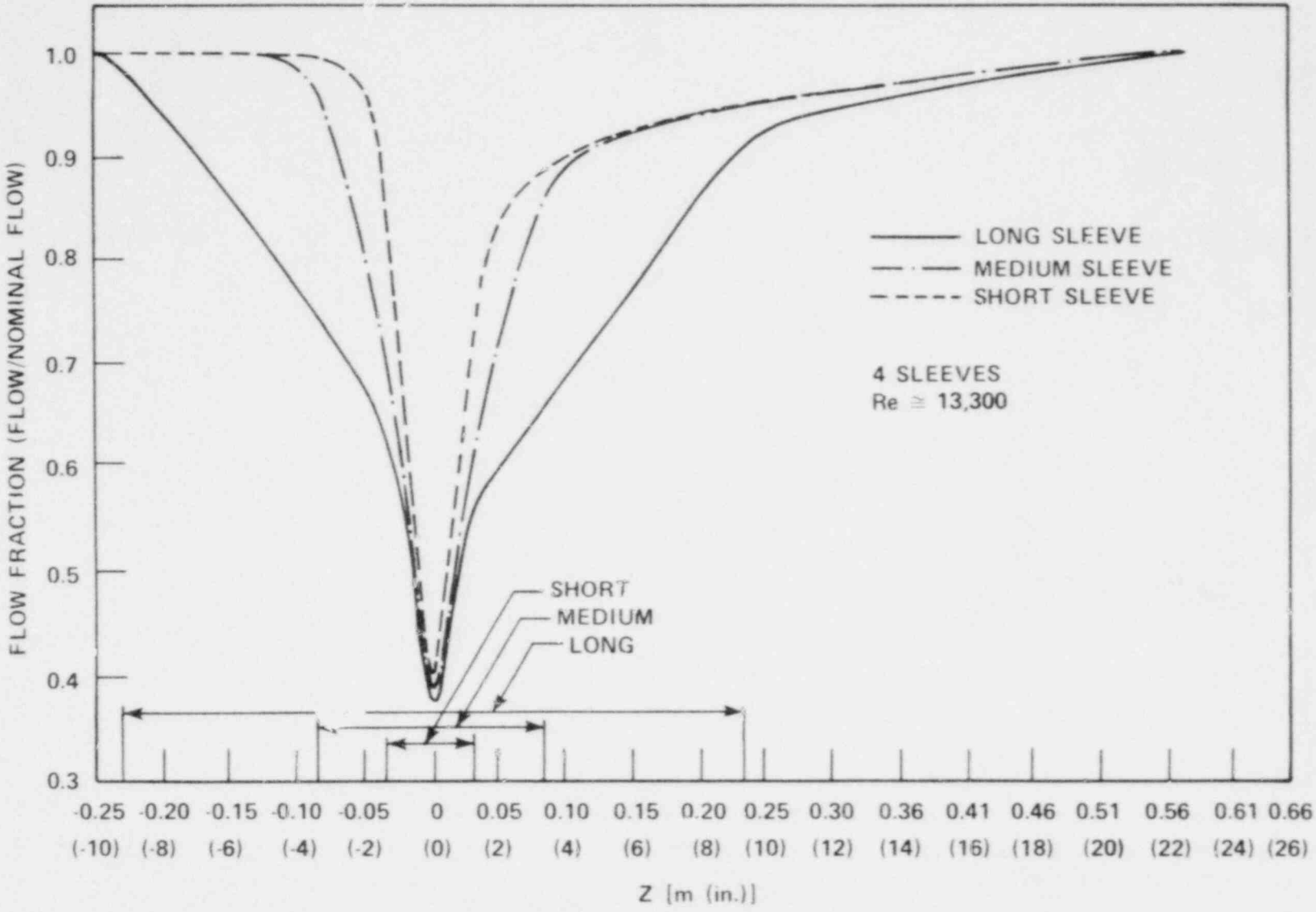

Figure 4-8. Flow Rate Change in Most Blocked Subchannel (COBRA)

TABLE 4-3

ALPHA PHASE BURST OF SINGLE ROD IN ORNL TESTS[a]

Test	Axial Length at Indicated Strain [cm(in.)]		Maximum Strain (%)
	10% Strain	20% Strain	
PS-8	26 (10)	3 (1.2)	20
PS-9	33 (13)	17 (6.7)	25
PS-10	17 (6.7)	2 (0.79)	20
PS-12	32 (13)	0 (0)	18
PS-14	24 (9.4)	9 (3.5)	25
PS-15	24 (9.4)	0 (0)	17
PS-17	10 (3.9)	4 (1.6)	25
SR-5	13 (5.1)	5 (2.0)	26
SR-7	16 (6.3)	3 (1.2)	20

a. Unswelled rod diameter = 1.09 cm (0.429 in.)

table 4-4. The maximum strains are between 32 and 59 percent, depending on the test conditions (such as system pressure and heatup rates). A few sample burst shapes are shown in figure 4-9.

Chapman[1] found from the ORNL tests that circumferential and axial temperature gradients caused nonuniform deformations in alpha phase Zircaloy bursts. That is, initial temperature gradients existed both axially and circumferentially. As the clad deformed, the initial gradients were modified; the deformations were very sensitive to even small temperature gradients.

A series of out-of-pile tests has also been conducted at the Nuclear Research Center Karlsruhe of West Germany (KFK). Wiehr, et al.,[2] ran a 5 x 5 full-length burst test in which rods were burst in the range of 600°C to 800°C (1112°F to 1472°F). The observed maximum strains were in the range of 8 to 32 percent. The resulting axial strain distributions are shown in figure 4-10. KFK also ran single-rod burst tests and observed strains of about 30 percent. From another series of tests, Wiehr and Schmidt reported the results of a preliminary test with a shortened fuel rod simulator which had an internal heater rod.[3] They observed the following interesting facts:

-- Initial rod internal pressure of 7MPa (1015 psi) gave a circumferential strain of 36 percent. The higher the internal pressure, the lower was the strain.

-- In case of pronounced differential circumferential temperatures, the rupture point was always located on the hotter side of the clad, which, in most cases, was axially straight or slightly concave, with maximum weakening of the wall thickness.

---

1. Chapman, R. H., "Significant Results From Single-Rod and Multirod Burst Test in Steam With Transient Heating," paper presented at Fifth Water Reactor Safety Research Information Meeting, Germantown, MD, November 7-10, 1977.

2. Wiehr, K., et al., "Fuel Rod Behavior in the Refill and Flooding Phase of a Loss-of-Coolant Accident," CONF-771252-5, December 1977.

3. Wiehr, K., and Schmidt, H., "Out-of-Pile Experiments on Ballooning of Zircaloy Fuel Rod Claddings: Test Results With Shortened Fuel Rod Simulators," KFK-2345, October 1977.

TABLE 4-4

ORNL ALPHA PHASE MULTIROD BURST TEST DATA[a]

Rod Number	Maximum Strain (%)	Strain (%)	Axial Length [cm(in.)]	Comment
1	36	27	5 (2.0)	Two long 15% strain side swellings
		20	12.5 (4.9)	
		10	20 (7.9)	
2	32	27	7.5 (3.0)	Long 25% and short 18% strain side bulges
		20	14 (5.5)	
		10	19.5 (7.7)	
3				Leak during the test and burst at 918°C (1681°F)
4	37	27	3 (1.2)	Long 15% strain side bulge
		20	7 (2.8)	
		10	16 (6.3)	
5	45	27	10 (3.9)	Long 43% strain swelling at the side of the main bulge
		20	16 (6.3)	
		10	19.5 (7.7)	
6	42	27	6 (2.4)	Side swelling of 15% strain
		20	21 (8.3)	
		10	43 (17)	
7	38	27	6 (2.4)	Long 10% strain side bulge
		20	11 (4.3)	
		10	18 (7.1)	
8	42	27	10 (3.9)	Relatively short 10% strain side bulge
		20	21 (8.3)	
		10	50 (20)	

a. Rod diameter = 1.09 cm (0.429 in.)
Burst temperature = 843°C-858°C (1550°F-1578°)

TABLE 4-4 (cont)

ORNL ALPHA PHASE MULTIROD BURST TEST DATA[a]

Rod Number	Maximum Strain (%)	Strain (%)	Axial Length [cm(in.)]	Comment
9	48	27	14 (5.5)	Numbers are for the
		20	19 (7.4)	largest swelling. There
		10	50 (20)	were two other signi-
				ficant bulges on the rod.
10	44	27	11 (4.3)	Two other 20% strain
		20	22 (8.7)	swellings
		10	50 (20)	
11	52	27	11 (4.3)	Another 10% strain
		20	17 (6.7)	swelling
		10	50 (20)	
12	38	27	6 (2.4)	Another 20% strain
		20	11 (4.3)	swelling
		10	48 (19)	
13	59	27	5.5 (2.2)	Several other high-
		20	17.5 (6.9)	strain swellings
		10	50 (20)	(10%-37%)
14	42	27	11 (4.3)	Two side bulges (28%
		20	17 (6.7)	strain) and one small
		10	50 (20)	bulge (13% strain)
15	39	27	10 (3.9)	Another long 20% strain
		20	13 (5.1)	swelling
		10	50 (20)	
16	38	27	9 (3.5)	Side swellings (10% and
		20	14.5 (5.7)	20% strain)
		10	47 (19)	

a. Rod diameter = 1.09 cm(0.429 in.)
Burst temperature = 843°C-858°C (1550°F-1578°F)

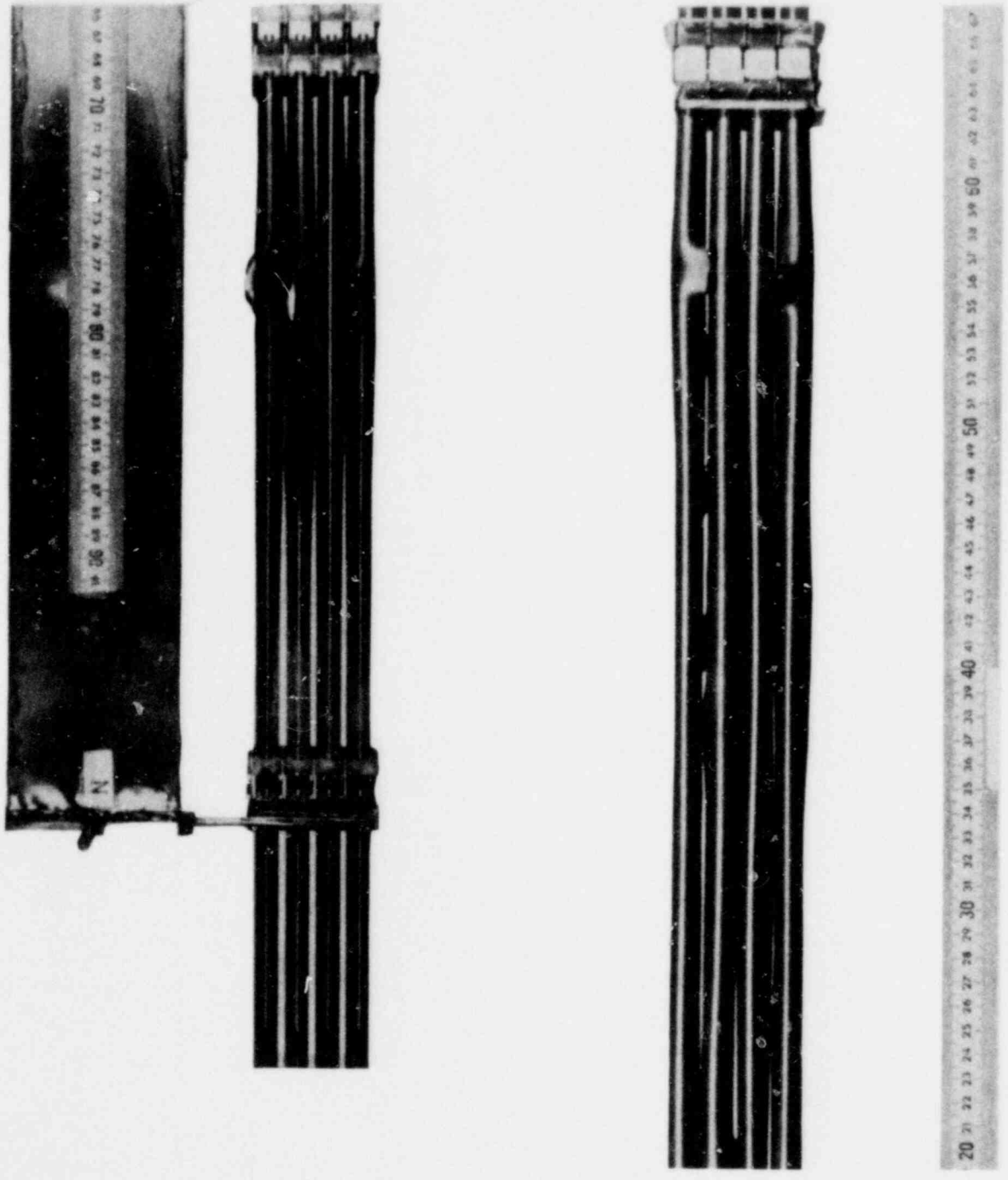

BUNDLE 1

BUNDLE 2

Figure 4-9. ORNL Multirod Burst Test Burst Shapes After Test

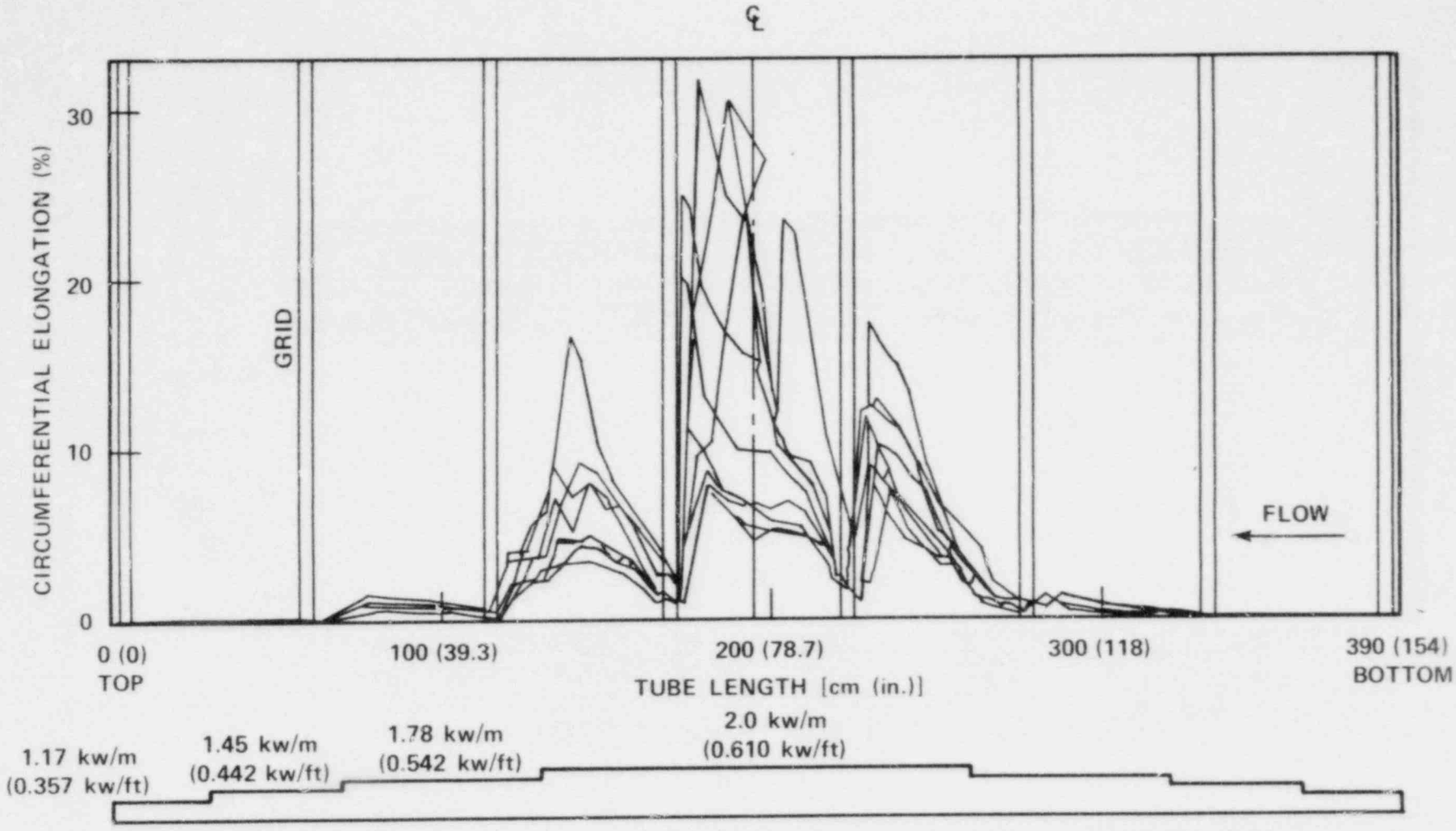

Figure 4-10. German Out-of-Pile Test Results

-- The hotter side was not lifted off the heat source, whereas the opposite colder side was, but without any measurable reduction in wall thickness.

-- When the clad began to lift off the heat source, all temperature-measuring points on a circumferential line within a segment with an angle of approximately 300 degrees showed the following temperature transient: first the temperature rise slowed and reached a maximum temperature, then the temperature began to drop. The temperature in the remaining angular segment of 60 degrees, where the clad eventually ruptured, showed a different behavior: temperature did not drop but continued to rise, and finally reached its maximum value at the time of rupture.

Observations of the results of single- and multirod burst tests using internal heater rods were well summarized by Picklesimer[1,2] as follows: while the opposite side of the clad hot point swells, the hot point side remains straight or bends slightly toward the heating element inside. Then a balloon starts to grow at the hot point and eventually bursts to leave lips. A schematic sequence of burst is shown in figure 4-11. Therefore, the flow blockage in the alpha phase burst is mainly due to the cold side swelling, which is long axially and nonsymmetrical radially. The burst lips are expected to work as fins to enhance heat transfer there, and are not a significant contribution to the flow restriction because they have small cross-sectional area.

There are very limited in-pile test results. KFK ran a series of in-pile single-rod burst tests using 500 mm (19.7 in.) long Zircaloy tubes.[3] These tests showed maximum strains of 30 to 43 percent. Axial strain distribution profiles were comparable to those obtained from the out-of-pile tests discussed above. The strain data of this in-pile test are summarized in table 4-5. ORNL ran an in-pile burst test on a seven-rod bundle in TREAT. The length of the rods was 686 mm (27 in.). The strain results of this test are summarized in table 4-6. The observed

---

1. Picklesimer, M. L., presentation at the PMG meeting for FLECHT SEASET, April 1978.
2. Picklesimer, M. L., "Configurations of Ballooned Cladding Recommended for FLECHT SEASET Test Bundles," personal communication to E. H. Davidson of USNRC, RSR, April 17, 1978.
3. Telephone conversations between Mr. Karb (KFK) and L. E. Hochreiter (Westinghouse), March 31, 1978, and April 5, 1978, on KFK in-pile tests.

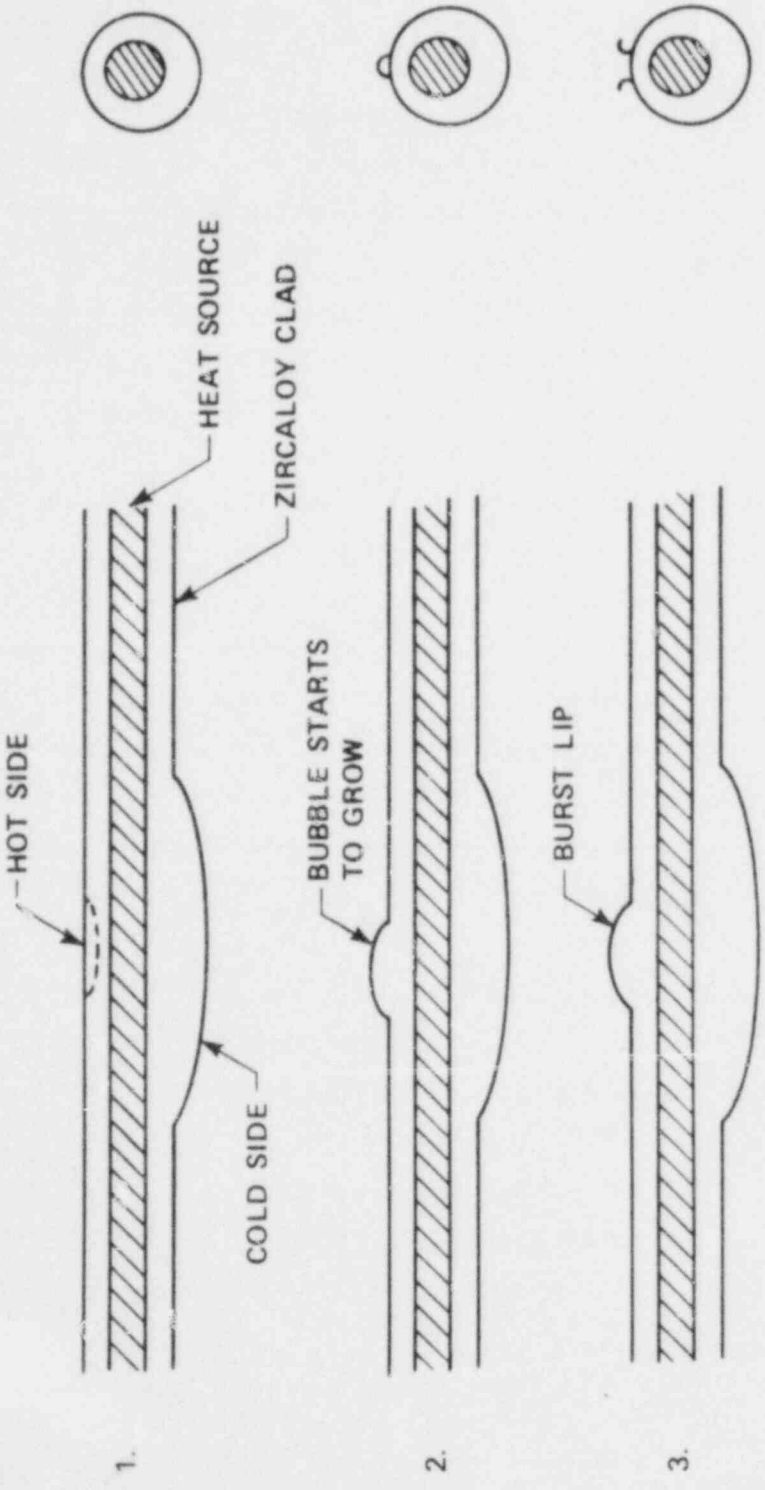

Figure 4-11. Sequence of Swelling and Burst of Alpha Phase Zircaloy

TABLE 4-5

KFK IN-PILE BURST TEST RESULTS[a]

Test	Maximum Strain (%)	Strain (%)	Clad Length [cm(in.)]	Burst Temperature [°C(°F)]	Burst Pressure [Pa(psi)]
A2.1	43	10	27.3 (10.7)	820 (1508)	88×10^5 (1276)
		15	16.9 (6.65)		
		20	10.8 (4.25)		
B1.6	40	10	45.5 (17.9)	875 (1608)	80×10^5 (1160)
		15	20.5 (8.07)		
		20	9.5 (3.7)		
		25	6.5 (2.6)		
B3.1	30	10	27 (11)	825 (1518)	79×10^5 (1146)
		15	15.4 (6.06)		
		20	11 (4.3)		
		25	5 (2.0)		

a. Active Zircaloy tube length = 500 mm (19.7 in.)
Tube diameter = 1.07 cm (0.421 in.)

maximum strains were in the range of 26 to 42 percent, depending on the test conditions. Axial strain distribution patterns were similar to the out-of-pile test results.

From the observations of the in-pile and out-of-pile rod burst tests discussed above, it can be concluded that the blockage shape at the maximum strain zone is relatively long axially and nonsymmetrical radially. To represent the swelling shape quantitatively and mechanistically, the characteristic axial dimensions of the swelling were chosen from the discussed data as follows:

TABLE 4-6

ORNL IN-PILE BURST TEST RESULTS[a]

Rod	Maximum Strain (%)	Strain (%)	Axial Length [cm(in.)]	Burst Temperature [°C(°F)]
4-1	35	>10 >25	6.35 (2.5) 1.3 (0.5)	799 (1470)
4-2	42	>10 >25	9.1 (3.6) 2.5 (1.0)	816 (1500)
R	36	>10 >25	10 (4.0) 1.5 (0.6)	743 (1370)
L	36	>10 >25	15 (6.0) 2.5 (1.0)	877 (1610)
H	26	>10 >25	10 (4.0) 0 (0)	893 (1640)
I	35	>10 >25	10 (4.0) 1.5 (0.6)	827 (1520)
C	40	N/A[c]	N/A[c]	810 (1490)

a. Seven-rod cluster, triangular spacing:

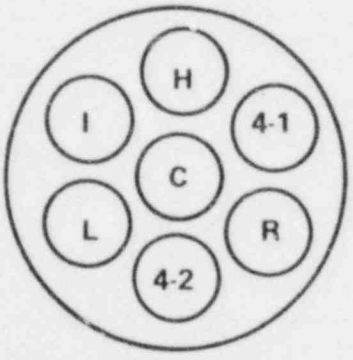

b. Rod length = 686 mm (27 in.)
Tube diameter = 1.43 cm (0.564 in.)

c. Not available

-- Axial length with an appreciable strain - 40d
-- Axial length with a strain greater than 43 percent of maximum strain - 10d
-- Axial length with a strain greater than 75 percent of maximum strain - 5d

Here d is the rod diameter and the specific strain values were chosen for a rough matching with the observed data.

The rod length with swellings is about 40 to 50 times the rod diameter. However, this long swelling is hard to simulate physically in tests. Considering that the material thickness of the sleeve is 0.5 mm (0.020 in.), it is calculated that the practical sleeve length is about 20 times the rod diameter. This axial length is sufficient to simulate hydraulic conditions at the blockage zone according to the arguments given in paragraphs 4-3 through 4-6.

One possible sleeve shape can be chosen (figure 4-12). This shape is chosen to have a nonconcentric portion at the center and to be symmetrical with respect to the maximum strain plane. It will allow systematic determinations of the sleeve geometry dimensions with a provided maximum strain. This shape also allows flexibility in changing maximum strain.

Quantitatively, the general dimensions of this sleeve can be defined by the following relations, using the notations shown in figure 4-13:[1]

For $0 \leq Z \leq Z_1$,

$$h = R^2 - Z^2 + h_{max} - R \qquad (4\text{-}2)$$

where $$R = \frac{Z_1^2 + (h_{max} - h_1)^2}{2\,(h_{max} - h_1)}$$

For $Z_1 \leq Z \leq Z_2$,

1. Only the symmetrical half of the sleeve is defined here.

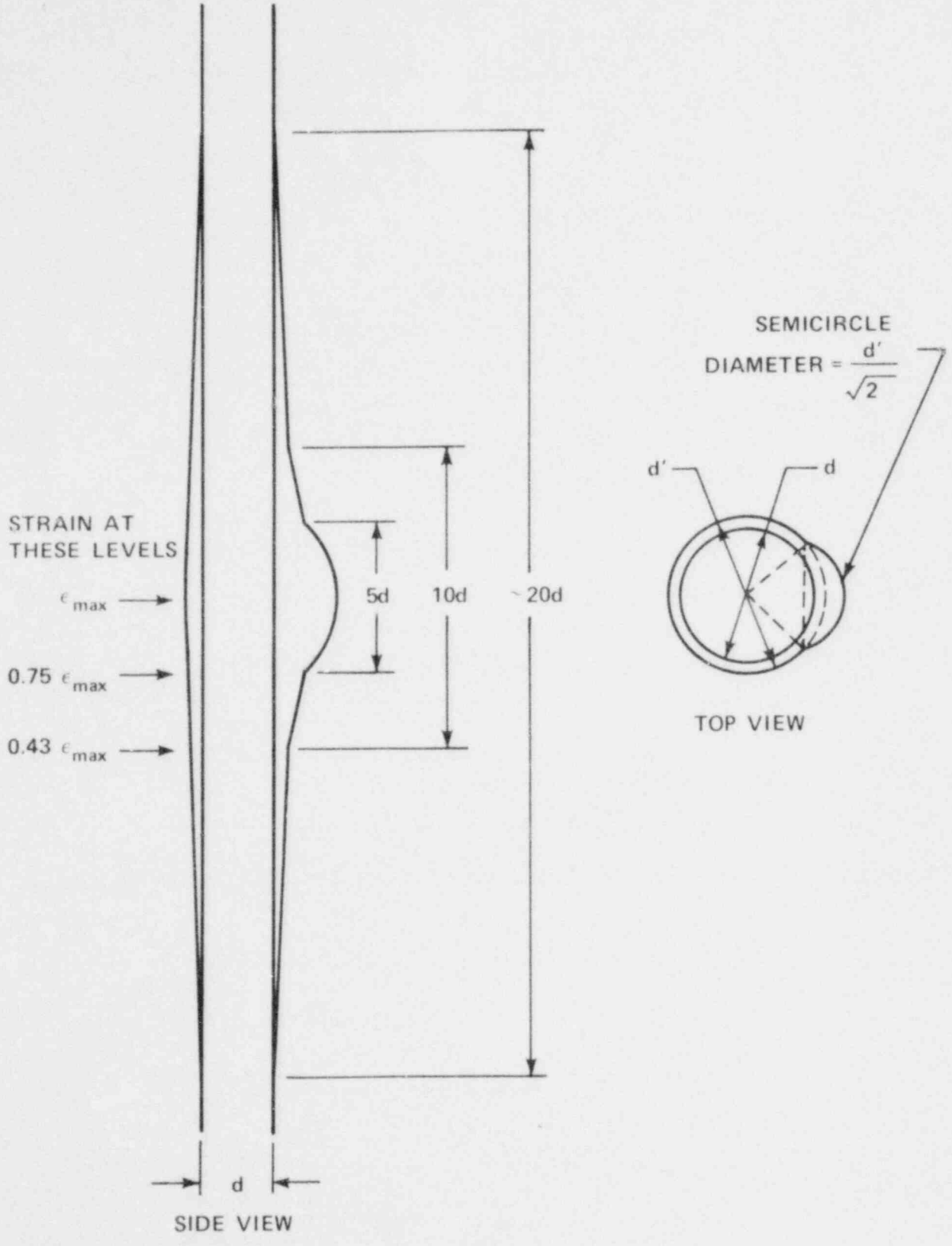

Figure 4-12. Shape of Nonconcentric Sleeve

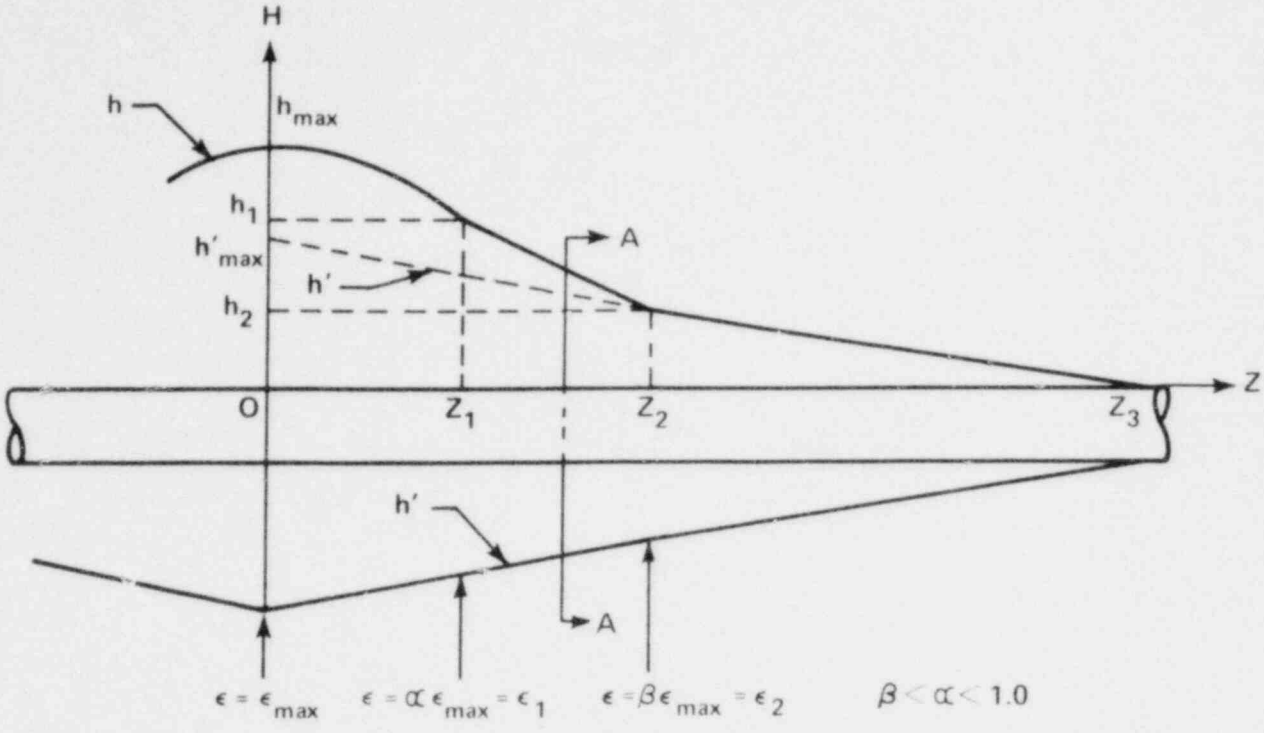

(A) SIDE VIEW SHOWING MAXIMUM SWELLING

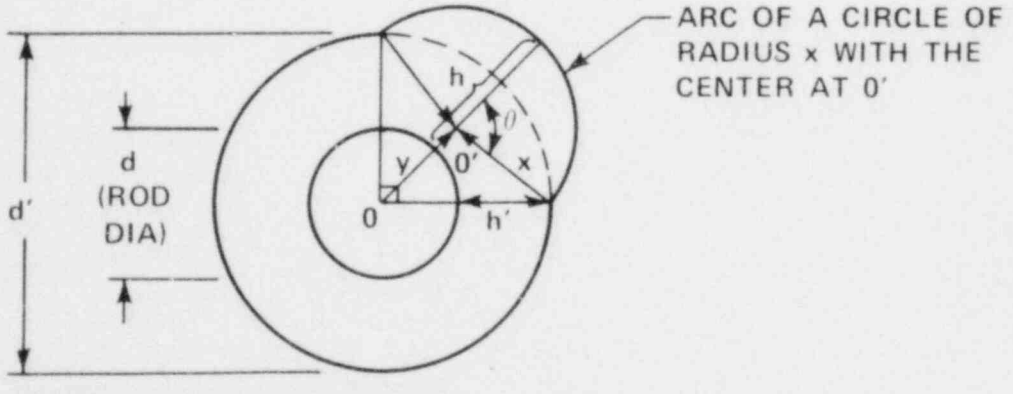

(B) CROSS SECTIONAL VIEW (A-A)

Figure 4-13. Nonconcentric Sleeve Dimensions

$$h = \left(\frac{h_2 - h_1}{Z_2 - Z_1} \right) (Z - Z_2) + h_2 \qquad (4\text{-}3)$$

For $Z_2 \leq Z \leq Z_3$,

$$h = -\left(\frac{h_2}{Z_3 - Z_2} \right) (Z - Z_3) \qquad (4\text{-}4)$$

For $0 \leq Z \leq Z_2$,

$$h' = -\left(\frac{h_{max} - h_2}{Z_2} \right) Z + h'_{max} \qquad (4\text{-}5)$$

For $Z_2 \leq Z \leq Z_3$,

$$h' = h \qquad (4\text{-}6)$$

At $Z = 0$,

$$\theta = \frac{\pi}{2}$$

$$\varepsilon = \varepsilon_{max}$$

At $Z = Z_1$,

$$\varepsilon = \varepsilon_1 = \alpha \varepsilon_{max}$$

At $Z = Z_2$,

$$\varepsilon = \varepsilon_2 = \beta \varepsilon_{max}$$

For the sleeve shown in figure 4-12, the general parameters in the above defining equations are given as

Z_1 = 23.75 mm (0.935 in.)
Z_2 = 47.5 mm (1.870 in.)
Z_3 = 95 mm (3.74 in.)

$\alpha = 0.75$

$\beta = 0.43$

The sleeve geometry can be determined completely using the above definitions and a few geometric relations if the maximum strain of the sleeve is known.

4-8. BLOCKAGE CONFIGURATIONS

The 21-rod bundle task will examine the reflooding phenomenon in simple blockage configurations, to obtain a fundamental understanding of the heat transfer change effected by blockage and to select a worst blockage shape in terms of heat transfer. This selected shape will be used in a separate large bundle test with ample bypass. The effects of blockage on heat transfer are due to flow bypassing the blockage zone and local flow behavior in and downstream of the blockage. Bypass flow is expected to reduce heat transfer in the blocked region because of reduction of fluid flow, but the geometry blockage itself may increase heat transfer as a result of increased turbulence and droplet disintegration. These two heat transfer effects are counteracting; for a clear understanding it is necessary to determine which effect can dominate under which thermal-hydraulic conditions. Therefore, this test series will study these effects to determine the relative importance of flow bypass and local blockage geometry on reflood heat transfer. Blockage arrangements in the bundle and relevant information are discussed in paragraphs 4-9 through 4-15.

4-9. Blockage Configurations To Be Tested

The following seven blockage configurations are planned for testing:

(1) Unblocked
(2) Concentric sleeve, 32.6 percent strain, coplanar on all rods
(3) Concentric sleeve, 32.6 percent strain, coplanar on nine rods
(4) Concentric sleeve, 32.6 percent strain, noncoplanar on all rods
(5) Nonconcentric sleeve, 36 percent strain, noncoplanar on all rods
(6) Concentric sleeve, coplanar on nine rods with maximum blockage of 90 percent (tentative)
(7) Worst sleeve, more strain, noncoplanar on all rods

The unblocked test is required as a reference test. The next three configurations (tests 2, 3, and 4) employ concentric sleeves which represent the blockage shape resulting from a high-temperature beta phase burst of Zircaloy clad. The coplanar sleeve location was chosen because of its geometric simplicity, which is advantageous for data analysis. A configuration with sleeves on all rods (test 2) is designed to study blockage effect without bypass. The configuration in test 3 is expected to show the effect of a partial bypass of fluid flow. Test 4 is a noncoplanar test to simulate a prototypical blockage distribution. The method of distributing sleeves in a noncoplanar way is discussed in paragraphs 4-10 through 4-12.

Test configuration 5 uses long nonsymmetrical sleeves on 21 rods. The results of this test will be compared to those of test 4 to help determine the effect of sleeve shape and geometry on reflood heat transfer. These comparisons are expected to help choose a blockage shape. This chosen shape will be used in the 161-rod bundle test.

By tentative agreement, test configuration 6 will test coplanar concentric sleeve distribution with a higher blockage; however, this could be changed depending on the future German FEBA test.[1] A worst sleeve shape based on the tests up to configuration 5 will be tested in configuration 7 with higher strain.

4-10. Noncoplanar Blockage Distribution

A noncoplanar blockage test configuration requires a method to axially distribute blockage in a noncoplanar fashion. The following paragraphs describe the method of distributing the blockage sleeves on the heater rods. The objective is to locate blockage sleeves in the bundle in such a manner that the statistics of the location coincide with the expected deformation and bursts of a PWR. The basis of this approach is the following statement from the ORNL multirod burst test results: "Posttest deformation measurements showed excellent correlation with the axial temperature distribution, with deformation being extremely sensitive to small temperature variations."[2]

---

1. Ihle, P., and Rust, K., "FEBA - Flooding Experiments With Blocked Arrays - Influence of Blockage Shape," Trans. Am. Nucl. Soc. 31, 398-400 (1979).

2. Chapman, R. H., "Significant Results From Single-Rod and Multirod Burst Tests in Steam With Transient Heating," paper presented at Fifth Water Reactor Safety Research Information Meeting, Germantown, MD, November 7-10, 1977.

Burman and Olson[1] have studied temperature distributions on rods in a bundle. Their method can be employed to determine the statistics of burst locations in the bundle.

The burst locations so determined were selected without considering the grid effect on burst location which was observed in the German REBEKA tests.[2] It was found that rod burst locations were shifted toward the fluid flow direction because of enhanced heat transfer downstream of the grids.

Incorporation of this hydraulic effect on burst location requires knowledge of the time of rod burst. Rod bursts during blowdown are expected to occur at locations shifted downward, because of the downward fluid flow at the time. Burst at the end of blowdown may not be affected by fluid flow because there is virtually no fluid flow. During the refill and reflood phases, rod bursts would occur at locations shifted upward.

Rods in a PWR can burst at any phase of a LOCA transient, depending on power distribution, operating life, type of break, material strength uncertainties, and the like. Therefore, the hydraulic effect can be incorporated into the determination of burst locations in several ways. On the other hand, the most interesting phenomenon in the present study is local heat transfer under a typical blockage distribution; such a situation can be achieved without considering any hydraulic effect. This case is considered to be most typical when bursts occur during all three phases: blowdown, refill, and reflood.

4-11. Method for Burst Location Determination -- It is assumed that all rods to be deformed have the same or similar temperature distribution. The ORNL multirod burst tests showed that there were no interactions among rods during burst, so it may be assumed that each rod in a bundle bursts independently. Then the characteristics of one rod may be used to infer the behavior of the rod bundle.

---

1. Burman, D. L., and Olson, C. A., "Temperature and Cladding Burst Distributions in a PWR Core During LOCA," paper presented at the Specialists Meeting on the Behavior of Water Reactor Fuel Elements Under Accident Conditions, Spatind (Nord-Torpa), Norway, September 13-16, 1976.

2. Wiehr, K., et al., "Fuel Rod Behavior in the Refill and Flooding Phase of a Loss-of-Coolant Accident," CONF-771252-5, December 1977.

A rod is divided into several sections with the same interval. Burman and Olson computed the probability that a certain section (say, the i-th increment) of a fuel rod is at the highest temperature in the rod as follows:

$$\int_0^{\infty} \left\{ \frac{1}{\sigma_T\sqrt{2\pi}} \exp\left[\frac{(\mu_i - T)^2}{2\sigma_T{}^2}\right] \prod_{j\neq i}^{j=1,N} \frac{1}{\sigma_T\sqrt{2\pi}} \int_0^{T} \exp\left[\frac{-(\mu_i - t)^2}{2\sigma_T{}^2}\right] dt \right\} dT \qquad (4\text{-}7)$$

Here σ_T and μ_i are the standard deviation of local temperature and the mean temperature at the i-th increment, respectively. It can be seen that these two characteristics (σ_T and μ_i) must be known to compute the local probability of highest temperature. As ORNL showed, this highest-temperature location can be interpreted as the burst location.

The mean temperature distribution required in equation (4-7) is the axial mean temperature of a nuclear fuel rod at the time of rod burst. The standard deviation of local temperature is included to account for the local temperature fluctuation. Burman and Olson assumed that the fluctuation is normally distributed.

The local temperature can be divided into two components:

$$T_{local} = \bar{T}_{local} + T'_{local}$$

where $\bar{T}_{local}$ and T'_{local} are the mean and variation of local temperature, respectively. The mean temperature is obtained from the axial mean temperature distribution. The local temperature variation is a function of the following several effects:

-- Manufacturing effect

- Initial fuel pellet density
- Fuel pellet diameter
- Fuel enrichment
- Manufacturing variables which affect fuel densification
- Clad local ovality
- Fuel pellet chemical bonding

-- In-pile effect

- Fuel pellet radial offset within clad
- Fuel pellet cracking
- Fuel densification

Specific values of these inputs are discussed in paragraph 4-12. However, burst probabilities at each increment of rod can be computed by equation (4-7) with the inputs of σ_T and μ_i.

Westinghouse has developed a statistical method for the distribution of sleeves in a 161-rod bundle according to the above calculated probability distribution. However, this method cannot be applied directly to the 21-rod bundle, because of the small sample number. Therefore, a different method was developed for the small bundle. The method used for the 21-rod bundle maintains the principle of the previous statistical arguments and can be applied to the large bundle to remove the slight dependency of the axial blockage distribution on sample random numbers.

Multiplying the probabilities by the total rod number gives theoretical burst numbers at the corresponding axial increments. These numbers are usually not integers. Therefore, for practical purpose, these numbers are transformed to integers to satisfy the requirement that the total burst number is the same as the total rod number. These integer numbers indicate how many sleeves should be located at specific axial increments. This procedure is shown schematically in figure 4-14. An increment (i-th) is then selected at random. Since it is known from the above calculation that N_i rods have bursts at this increment, N_i rods are selected at random. Each of these selected rods has a sleeve on the i-th increment. Then another increment and corresponding rods are selected at random. This procedure is repeated until all the axial increments where bursts occur have been considered.

A computer program has been written to execute this procedure for selection of sleeve locations. This program, called COFARR (Coolant Flow Area Reduction), can calculate subchannel blockage with given input strain information on the blockage sleeve. The program is explained in appendix C, and a sample case result is shown in appendix D.

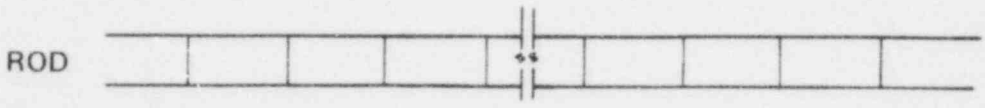

INCREMENT NUMBER	1	2	3		L-1	L
BURST PROBABILITY [EQ. (4-7)]	P_1	P_2	P_3		P_{L-1}	P_L
$N P_i$	X_1	X_2	X_3		X_{L-1}	X_L
SLEEVE NUMBER AT THE i-th INCREMENT	n_1	n_2	n_3		n_{L-1}	n_L

$\left(\sum_{L=1}^{L} n_i = N \right)$ N: TOTAL ROD NUMBER

Figure 4-14. Procedure for Determining Sleeve Numbers on Each Axial Increment

4-12. Input Data -- The mean temperature distribution at time of burst and local temperature fluctuation data are required to compute burst probability according to equation (4-7). Further strain information is required to compute actual blockage distribution and subchannel area.

Relevant information on mean temperature distribution and local temperature fluctuation are summarized in appendix E. From these available data, bounding axial blockage distributions can be determined to decide the test range of blockage distribution. For this purpose, one must remember that an axial blockage distribution can be adjusted by either mean temperature or local temperature uncertainty. The larger the local temperature standard deviation, the flatter is the blockage distribution. The flatter the mean temperature, the flatter is the resulting blocking distribution.

Appendix E shows that the most peaked mean temperature distribution is obtained by either Westinghouse or Babcock & Wilcox plants, and clad rupture is calculated to occur for Babcock & Wilcox and Westinghouse plants during and at the end of blowdown, respectively. Therefore, it is expected that the Westinghouse plant has the most peaked axial blockage distribution. Calculations for Combustion Engineering and Exxon plants show a flatter mean temperature distribution. The maximum local temperature distribution standard deviation is taken at the time of the accident. Therefore, the bounding cases for noncoplanar distributions are as follows:

-- For peaked axial blockage distribution

Mean temperature: Westinghouse (figure E-1)
Standard deviation of local temperature fluctuation: 6.7°C (12°F)

-- For flatter axial blockage distribution

Mean temperature: Combustion Engineering (figure E-4)
Standard deviation of local temperature fluctuation: 13.4°C (24°F)

Strain data are required to finalize the sleeve shapes discussed in this chapter. A real blockage distribution can be calculated by COFARR with input sleeve strain data.

It is expected that rod bursts in a bundle will show a range of strain and shape sizes; however, a single size strain is suggested for all rods in the present tests for simplicity of both experimental setup and data analysis. The effect of different sleeve sizes will be indirectly addressed by tests with a higher-strain sleeve.

Strain data are available from various rod burst tests. The results of the ORNL multirod burst tests are plotted in figure 4-15, along with the German in-pile test results. In the ORNL in-pile test, strains ranging from 26 to 42 percent were observed. The German out-of-pile test showed relatively low strain, ranging from 8 to 32 percent.

The most representative strain value is considered to be about 36 percent, with a standard deviation of 8 percent, assuming that strains are distributed normally. Of course, these numbers are rough estimates. Therefore, a strain of 36 percent is planned as a reference case for tests which use nonconcentric sleeves. The strain relation between the concentric and nonconcentric sleeves is discussed in paragraphs 4-13 through 4-15.

4-13. Relationships Between Different Configurations

Several configurations and sleeve shapes will be employed in this series, as explained above. The results obtained from these tests will be used to develop a blockage shape in terms of heat transfer and to get a better understanding of heat transfer as affected by blocked geometry. There are bases of comparison between different test conditions for these purposes.

Two distinct pairs of test configurations are significant: concentric versus nonconcentric sleeve shapes and coplanar versus noncoplanar sleeve arrangements.

4-14. Concentric Versus Nonconcentric Sleeve Shapes -- As noted above, the 21-rod test results will be used to determine a blockage shape which gives poorer heat transfer. This selected sleeve will be used in the large bundle tests. To select the sleeve shape, it is necessary to establish a certain basis of comparison. This comparison basis will also govern the sleeve distributions in the bundle.

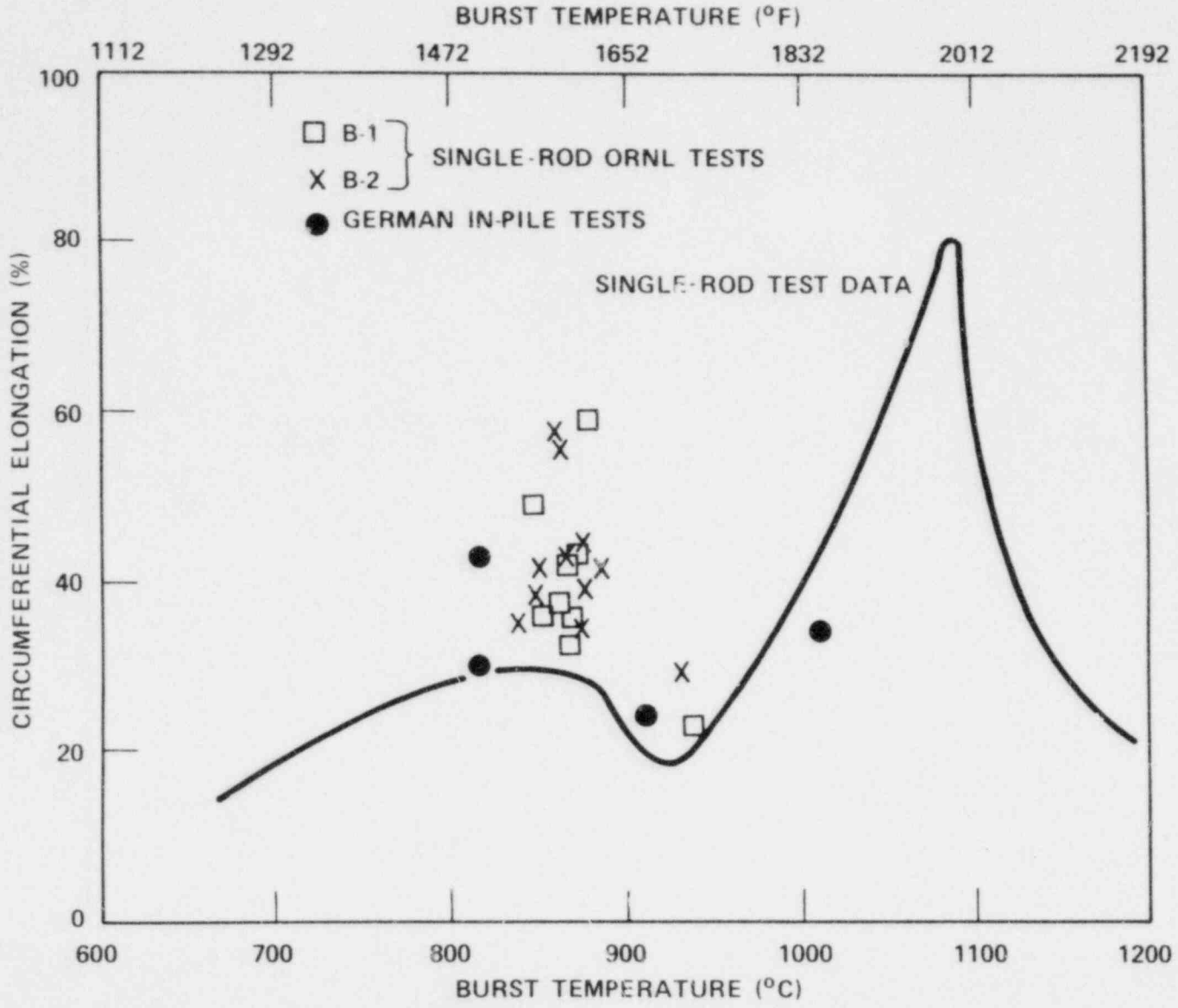

Figure 4-15. Strain Data From ORNL Rod Burst Tests and German In-Pile Tests

16,047-28

The planned blockage configurations allow one set of sleeve comparisons: test configurations 1 and 4 versus test configurations 1 and 5.

Two parameters introduced by the multiplicity of blockage sleeve in a bundle are sleeve locations and maximum bundle average blockage. Sleeve locations govern the environment factor (N_E) in the tentative modeling scheme:

$$\frac{h_B}{h_O} = \left(\frac{G_B}{G_O}\right)^m N_e N_E \tag{4-8}$$

where h and G are the heat transfer rate and fluid flow rate, respectively; m is a constant factor; and N_e is the shape factor. Subscripts B and O represent blocked and unblocked bundles, respectively.

The total blockage test provides the heat transfer rate, which can be modeled as

$$(h_B)_{c \text{ or } n} = h_O \left[\left(\frac{G_B}{G_O}\right)^m N_e N_E\right]_{c \text{ or } n} \tag{4-9}$$

where c and n denote concentric and nonconcentric sleeves, respectively.

G_O and m should be known, and G_B can be calculated by COBRA for each subchannel. It should be noted that G_B/G_O is not equal to one for a non-coplanar blockage distribution without bypass, in contrast to the coplanar case. The flow rate in each subchannel (G_B) and N_E are determined by sleeve distribution. Therefore it is necessary to have the same sleeve (not blockage) distribution for both shapes to have a common basis for comparison.

The maximum average blockage is also governed by sleeve locations. Keeping this blockage at the same value for the two sleeve shapes disturbs sleeve locations; this is not desirable from the viewpoint of model development.

It must be noted again that this total blockage case has no bypass flow area. Fluid is forced through the blocked zone. Therefore $(h_B)_n$ and $(h_B)_c$ obtained from the tests cannot be compared directly. Any flow depletion in the blocked subchannel

which can be expected for the case with bypass flow area should be accounted for, to make the rates comparable. One possible way is to modify the experimental heat transfer rates, as follows:

$$(h_B^*)_{n \text{ or } c} = \left[h_B \left(\frac{\bar{G}_B}{G_O} \right)^m \right]_{n \text{ or } c} = \left[\left(\frac{\bar{G}_B}{G_O} \right)^m \left(\frac{G_B}{G_O} \right)^m N_e N_E \right]_{n \text{ or } c} \qquad (4\text{-}10)$$

where G_B is the average flow rate in the blocked zone when there is a sufficient bypass flow area. Then it is possible to compare $(h_B^*)_n$ to $(h_B^*)_c$, to determine which gives lower heat transfer.

4-15. Coplanar Versus Noncoplanar Sleeve Arrangements -- When coplanar and noncoplanar sleeve test results are compared, one parameter must be kept constant. The parameter may be either sleeve strain or overall pressure drop. However, keeping the pressure drop constant is difficult, because the total pressure drop is expected to be small and it is difficult to predict such a small pressure drop with good accuracy. Keeping the strain constant is straightforward. It is also a sensible way to study heat transfer phenomena, with the degree of noncoplanarity as a parameter. The coplanar arrangement is a special case in which the noncoplanarity (or local temperature uncertainty) is zero.

4-16. RELATIONSHIP BETWEEN 21-ROD AND 161-ROD BUNDLES

It is desirable to relate the 21-rod bundle to the 161-rod bundle, because the relationship may improve understanding of the data from both bundle tests. Also, a bypass effect which cannot be explored satisfactorily in the small bundle can be studied in the large bundle through a relationship between the two bundles. Therefore, an attempt was made to establish a physical relationship between the two tests.

Aside from the size, a basic difference between the two bundles is that only the large bundle has thimbles. This difference makes it difficult to provide similarity between the bundles; however, an adequate similarity can be achieved by noting that a blockage at the highest axial location does not significantly affect the flow

field of a blocked zone at lower elevation. Thus, a rod with blockage at the highest elevation can be treated as a thimble in the region local to a blockage at a lower elevation.

A set, or island, of 21 rods in the large bundle which are arranged in the same way as the 21-rod bundle can be selected. Although such a 21-rod island may have one or two thimbles, it is better to select an island with only one thimble to minimize the thimble effect. Then there are one-to-one correspondences between the rods in the 21-rod bundle and those in the island. Therefore it is possible to distribute sleeves for the rods of the island in the same way as in the 21-rod bundle to preserve the physical resemblance of blockage distribution. But since a thimble does not burst, it cannot have a sleeve. This difference can be minimized if the rod which corresponds to the thimble has a sleeve at the highest axial position; such a blockage will not affect the flow field in the blocked region significantly.

One way to build such an island in the large bundle is to select 21 rods arranged in the 21-rod bundle pattern with a thimble at the center of the rod group. This method of island selection is shown in figure 4-16.

A restriction must be imposed in the selection of sleeve locations for the 21-rod bundle, to use the sleeve distributions in building the large bundle according to the method discussed above. Since a thimble is at the center of the island, the sleeve must be located on the center rod at the highest axial position within the blocked zone.

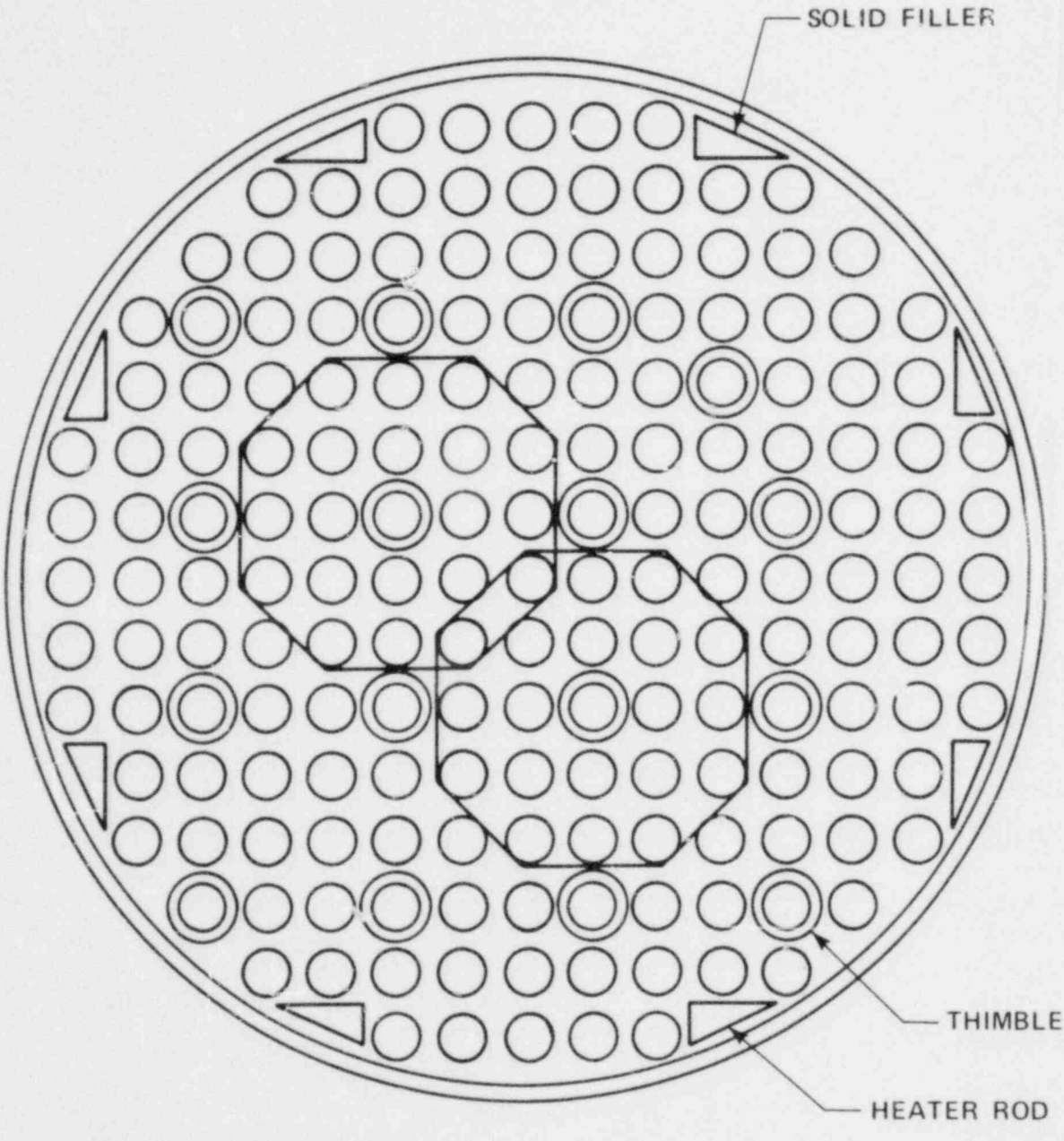

Figure 4-16. 21-Rod Islands in 161-Rod Bundle

SECTION 5
INITIAL CONDITIONS AND RANGE OF CONDITIONS

Data requirements for the 21-rod flow blockage task are determined by the task objectives, as presented in section 3 of this report, and by contract commitments, as presented in the work scope (appendix F). To meet task objectives, the heater rod bundle and test facility system instrumentation must be designed to provide sufficient data for calculating the following:

-- Mass and energy balances around each loop component

-- Global and local thermal-hydraulic conditions to develop models based on experimental data which can be used to interpret reflooding phenomena, and to identify flow and heat transfer regimes during reflood

-- Heat transfer and mass entrainment data for formulating empirical correlations

Table 5-1 summarizes the basic data to be obtained and the instrumentation that will allow the above calculations to be made and hence achieve task objectives and task work scope. A more detailed description of bundle and system instrumentation is presented in section 7 of this report.

The resulting data and analysis from this task will be used to determine differences in flow blockage configurations and for screening blockage configurations for future 161-rod flow blockage reflood experiments. The 161-rod flow blockage experiments will provide data which could be used to remove the steam cooling requirement imposed by the Appendix K rule for reflooding rates below 2.54 cm/sec (1 in./sec) and to replace it with a more realistic design requirement. Parameter studies will subsequently be performed around the reference initial conditions for a worst case analyzed for a hypothetical loss-of-coolant accident of a Westinghouse standard 17 x 17 four-loop plant.[1]

1. Johnson, W. J., et al., "Westinghouse ECCS Four-Loop Plant (17x17) Sensitivity Studies," WCAP-8566, July 1975.

TABLE 5-1

BASIC DATA TO BE OBTAINED FOR 21-ROD BUNDLE FLOW BLOCKAGE TASK

Desired Data	Instrumentation	Location
Clad temperatures	Heater rod thermocouples	Inside surface of heater cladding at various axial and radial bundle elevations
Fluid temperatures	Fluid thermocouples and shielded steam probes	Test section plenums, in bundle at various elevations
Inlet flow rate	Turbine meter	Injection line
Inlet enthalpy	Fluid thermocouple and pressure transducer	Injection line and accumulator
System pressure	Pressure transducer	Test section upper plenum
System pressure drops	Differential pressure transducer	Across various loop components
Bundle exit steam mass rate	Orifice plate flowmeter	Exhaust line
Bundle exit liquid mass rate	Differential pressure transducer	Carryover tank and steam separator tank
Mass storage (void fraction distributions)	Differential pressure transducer	At each 0.3 m (1 ft) increment along the rod bundle heated length
System temperatures	Thermocouples	Accumulator, carryover tank, and steam separator piping
Rod bundle power	Wattmeter transducer	Input power lines
Blockage sleeve temperatures	Sleeve thermocouples	Embedded at point of maximum strain in blockage sleeve
Housing temperatures	Wall thermocouple	Outside housing surface at various elevations
Bundle exit steam temperature	Aspirating steam probe	Exhaust line, on either side of steam separator

The currently intended test reference initial conditions are listed in table 5-2. These specific conditions were derived from the following reference assumptions:

-- The core hot assembly is simulated in terms of peak power [kw/m (kw/ft)] and initial temperature at the time of core recovery.

-- Decay power is ANS + 20%, as specified by Appendix K.

-- The initial rod clad temperature is primarily dependent on the full-power linear heating rate at the time of core recovery. For the period from 30 seconds to core recovery, typical results yield an initial clad temperature in the hot assembly of 871°C (1600°F).

-- Coolant temperatures will be selected to maintain a constant subcooling to facilitate the determination of parametric effects.

-- Coolant will be injected directly into the test section lower plenum for the forced flooding rate tests, and into the bottom of the downcomer for the gravity reflood scoping tests. Injection into the bottom of the downcomer is used for better test facility pressure control. (In previous gravity reflood experiments,[1] injection into the top of the simulated downcomer resulted in severe flow oscillation in the test section. This phenomenon was believed to be due to condensation effects associated with downcomer piping. The condensation-induced oscillations were reduced by injection into the bottom of the downcomer.)

-- Upper plenum pressure at the end of blowdown is approximately 0.14 MPa (20 psia) for an ice condenser plant, and about 0.28 MPa (40 psia) for a dry containment plant.

-- The tests will be performed with a uniform radial power profile.

-- The axial power shape built into the heater rod will be the modified cosine with a power peak-to-average ratio of 1.66 (figure 5-1).

---

1. Waring, J. P., and Hochreiter, L. E., "PWR FLECHT SET Phase B-1 Evaluation Report," WCAP-8583, August 1975.

TABLE 5-2

REFERENCE AND RANGE OF TEST CONDITIONS FOR
21-ROD BUNDLE FLOW BLOCKAGE TASK

Parameter	Initial Condition	Range of Conditions
Initial clad temperature	871°C (1600°F)	260°C - 871°C (500°F - 1600°F)
Peak power	2.30 kw/m (0.7 kw/ft)	0.88 - 2.30 kw/m (0.27 - 0.7 kw/ft)
Upper plenum pressure	0.28 MPa (40 psia)	0.14 - 0.28 MPa (20 - 40 psia)
Flooding rate:		
-- Constant	25.4 mm/sec (1 in./sec)	10.2 - 152 mm/sec (0.4 - 6 in./sec)
-- Variable in steps	-	152 to 20 mm/sec (6.0 to 0.8 in./sec)
Injection rate (gravity reflood) - variable in steps	-	0.82 to 0.09 kg/sec (1.8 to 0.2 lb/sec)
Coolant ΔT subcooling	78°C (140°F)	3°C-78°C (5°F-140°F)

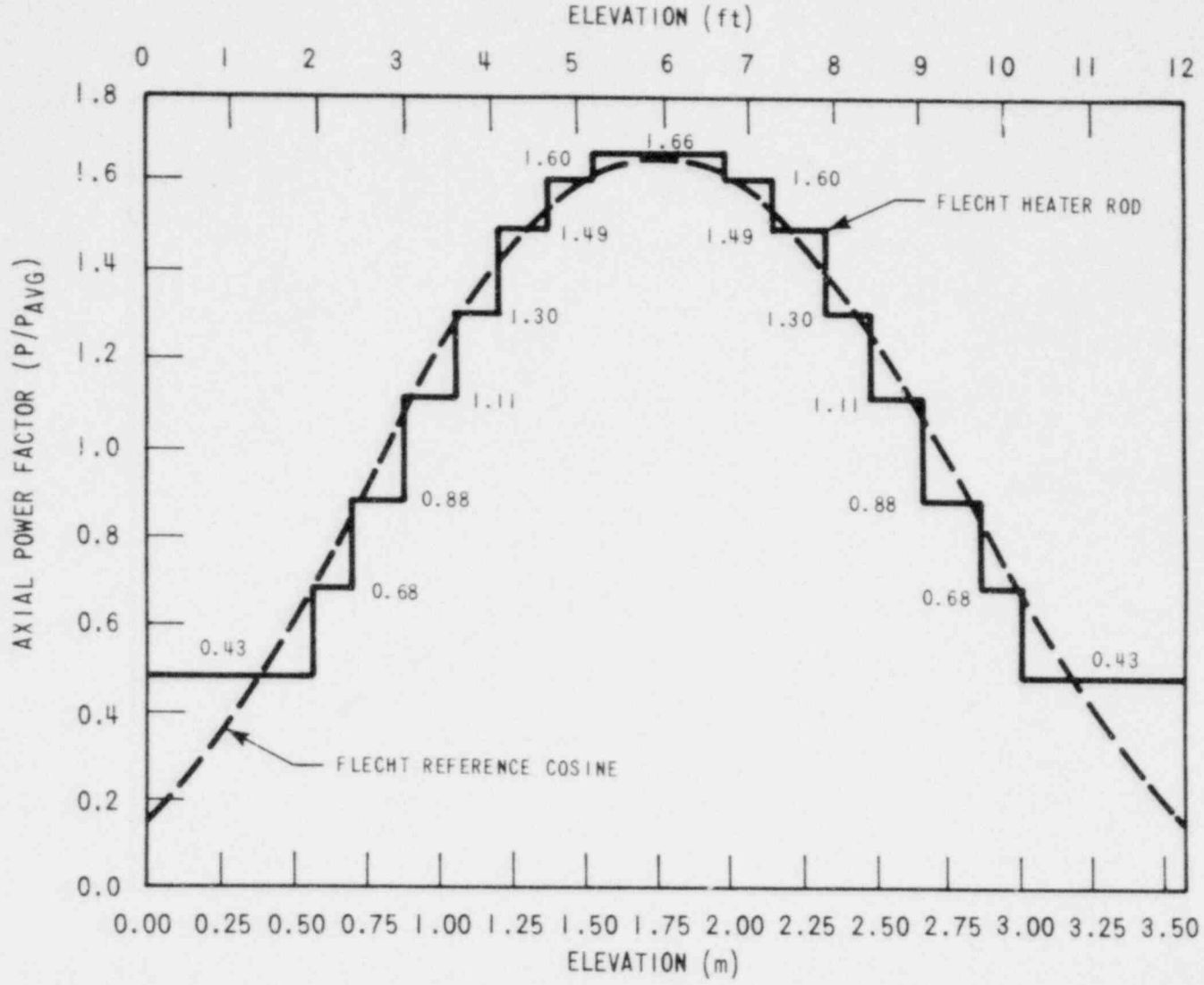

Figure 5-1. Cosine Axial Power Profile

The use of the 1.66 axial power profile will allow comparisons with the large 161-rod unblocked and blocked bundle tests such that the bundle sizes are the primary difference among these tests.

The ranges of initial test conditions are listed in table 5-2. The specific tests to be conducted in this series are presented in section 8 of this report.

SECTION 6
TEST FACILITY DESCRIPTION

6-1. FACILITY DESIGN AND LAYOUT

A new facility will be designed and built for conducting the 21-rod bundle flow blockage tests.

The test facility will be designed to the following basic requirements (figure 6-1):

-- The facility will be capable of performing reflood heat transfer tests with a 21-rod bundle utilizing 0.95 cm (0.374 in.) OD heater rods (see table 2-1).

-- The facility will be capable of performing forced flooding, steam cooling, and gravity reflood tests similar to those performed in the unblocked bundle facility,[1] and also capable of performing hydraulic characteristics tests.

-- All loop components and piping except the housing will be designed for 0.525 MPa (75 psia) and 371°C (700°F) service. The housing will be designed for 0.525 MPa (75 psia) and 816°C (1500°F) service. The materials will be carbon steel.

-- The upper and lower plenums, carryover tank, and steam separator tanks will have the same volume to flow area ratio as the unblocked bundle facility.[1]

-- The downcomer and crossover pipe flow area will be scaled down from the unblocked bundle flow area[1] to the 21-rod bundle flow area.

-- The test section will be designed to facilitate disassembling the bundle for changing blockage configurations.

---

1. Hochreiter, L. E., et al., "PWR FLECHT SEASET Unblocked Bundle, Forced and Gravity Reflood Task: Task Plan Report," NRC/EPRI/Westinghouse-3, March 1978.

The test facility will utilize certain existing equipment: the silicon-controlled rectifiers and circuit breakers for the bundle power supply, the computer front end for data acquisition, a water supply accumulator to supply flow, and a separator steam injection system to supply steam cooling flow. The remaining facility hardware and equipment will be new and includes the test section, test bundles, carryover vessel, entrainment separator, exhaust line piping, coolant injection system, downcomer, and electric boiler. Appendix G contains applicable drawings for the test facility (in addition to those contained in this section and section 7).

During operation, coolant flow from the 0.379 m^3 (100 gal) capacity water supply accumulator will enter the test section housing through a series of hand valves or automatically through a pneumatically operated control valve and a series of solenoid valves. Coolant flow will be measured by a turbine meter located in the injection line. Test section pressure will initially be established by a steam boiler connected to the upper plenum of the test section. During the experimental run, the boiler will be valved out of the system and pressure maintained by a pneumatically operated control valve located in the exhaust line. Liquid effluent leaving the test section will be separated in the upper plenum and collected in a close-coupled carryover tank. An entrainment separator located in the exhaust line will be used to separate any remaining entrained liquid in the vapor. Dry steam flow leaving the separator will be measured by an orifice meter before it is exhausted to the atmosphere. Additional system features include the following, as previously developed in the skewed power profile test series:[1]

-- Axial test section differential pressure (DP) cells installed every 0.30 m (1 ft) for accurate mass accumulation and void fraction measurements

-- Two steam probes located in the test section outlet pipe

-- A V-ball control valve to improve system pressure control

The facility will be modified during the test series to conduct gravity reflood tests (figure 6-1). The modifications consist of connecting a downcomer to the lower plenum, moving the injection line from the lower plenum to the bottom of the

1. Rosal, E. R., et al., "FLECHT Low Flooding Rate Skewed Test Series Data Report," WCAP-9108, May 1977.

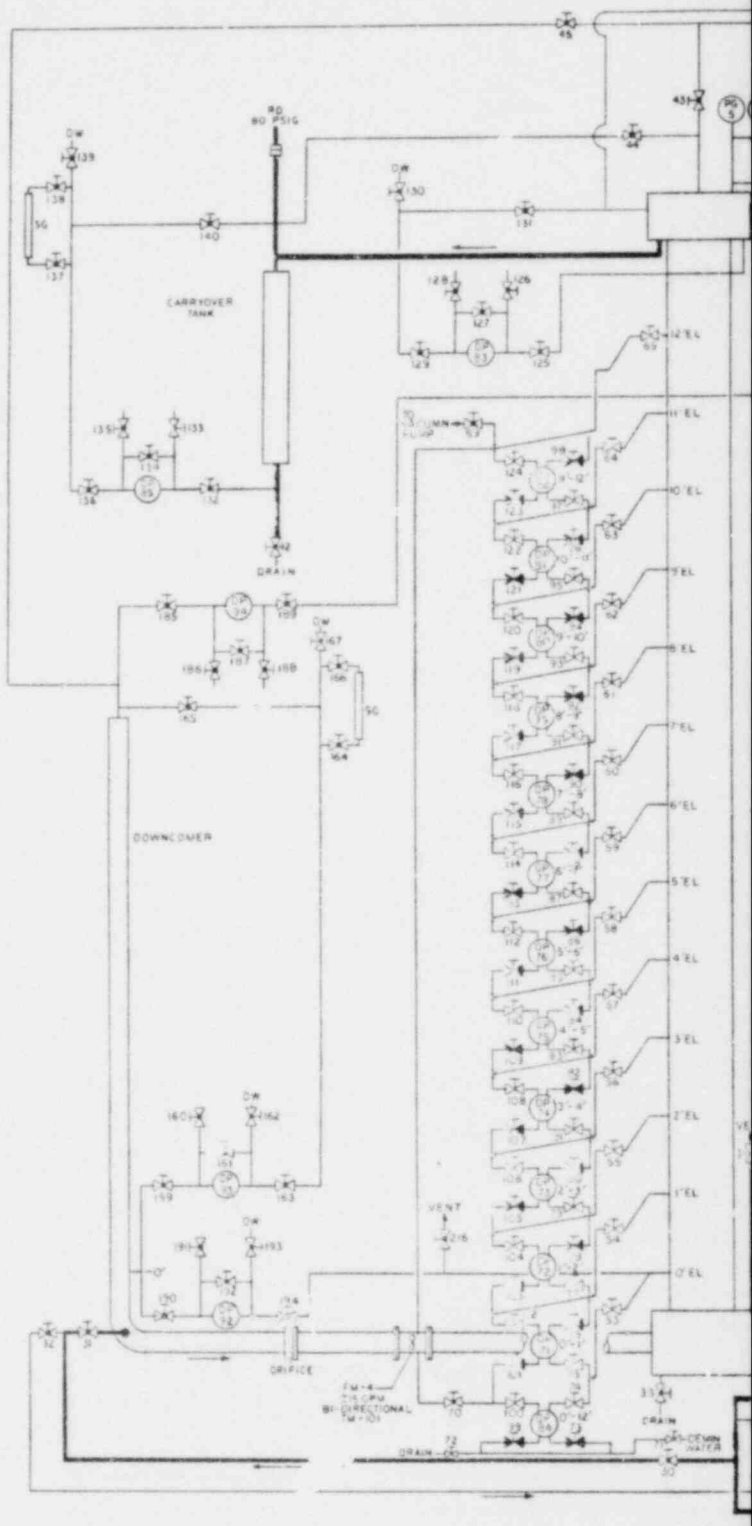
90 PSIG
DW
139
138
5G
137
140
DW
130
131
CARRYOVER TANK
128
127
126
129
125
12'EL
135
133
134
132
DRAIN
11'EL
10'EL
9'EL
8'EL
7'EL
6'EL
5'EL
4'EL
3'EL
2'EL
1'EL
0'EL
DOWNCOMER
DW
167
166
5G
164
160
DW
162
159
163
VENT
216
DW
193
191
192
194
ORIFICE
FM-4 DISCHARGE BI-DIRECTIONAL METER
DRAIN
DRAIN

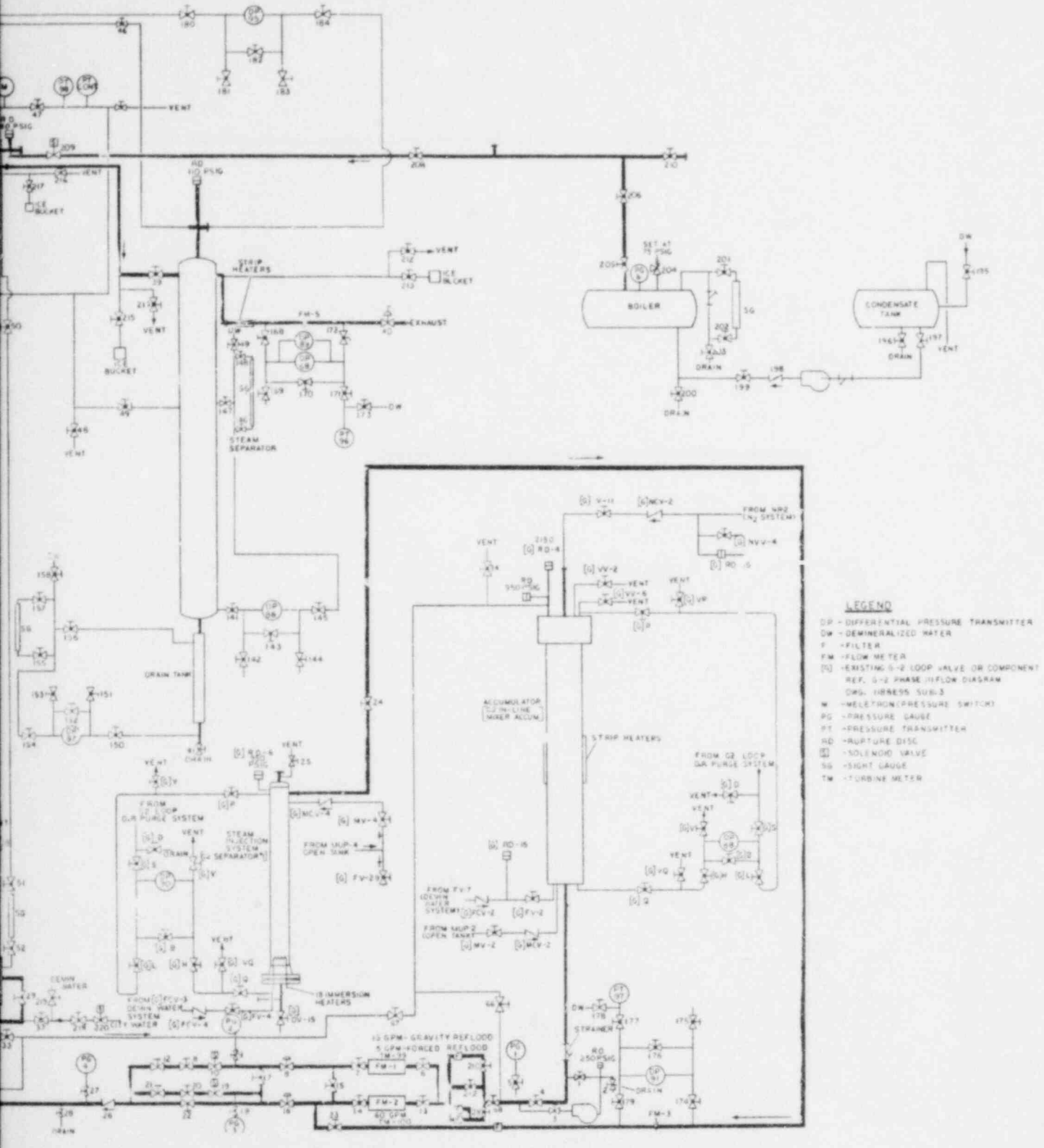

Figure 6-1 Schematic Diagram - FLECHT SEASET 21-Rod Bundle Flow Diagram (Drawing No. 1541E68)

downcomer,[1] utilizing a gate valve between the test section outlet pipe and the inlet flange to the entrainment separator to simulate hot leg resistances, venting the top of the downcomer to the entrainment separator, and installing additional instrumentation and differential pressure cells. Reflood flow into the test section and any reverse flow out of the test section will be measured by a bidirectional turbine meter located in the downcomer crossover leg.

6-2. FACILITY COMPONENT DESCRIPTION

The various components of the test facility are described in the following paragraphs.

6-3. Test Section

The low mass housing, together with the lower and upper plenums, constitutes the test section (figure 6-2). The low mass housing (figure 6-3) is a cylindrical vessel with inside diameter of 6.825 cm (2.687 in.) and 0.399 cm (0.157 in.) wall, constructed of 304 stainless steel rated for 0.551 MPa (80 psi) at 816°C (1500°F). The wall thickness was chosen so that the housing will absorb, and hence release, the minimum amount of heat as compared with the rod bundle. The inside diameter of the housing was made as close to the rod bundle outer dimensions as possible to minimize excess flow area. The excess flow area is further minimized by solid triangular fillers (figure 6-4). The housing will also have differential pressure cell pressure taps located every 0.30 m (1 ft) to measure liquid level in the housing. To help eliminate thermal buckling and distortion, the section will be supported from the upper plenum to permit the housing to freely expand downwards.

---

1. In previous gravity reflood experiments,[2] injection into the top of the simulated downcomer resulted in severe flow oscillation in the test section. This phenomenon was believed to be due to condensation effects which were reduced by injection into the bottom of the downcomer.

2. Waring, J. P., and Hochreiter, L. E., "PWR FLECHT SET Phase B-1 Evaluation Report," WCAP-8583, August 1975.

6-4. Test Bundle

A cross section of the test bundle is shown in figure 6-4. The bundle is composed of 21 instrumented heater rods and four solid triangular fillers. Details of the heater rods are shown in figure 6-5. The thermophysical properties of the heater rod materials are listed in table 6-1. The triangular fillers are split and pin-connected to each other between grids, and welded to the grids to maintain the proper grid location and accommodate thermal growth. In addition to reducing the amount of excess flow area in the housing, the fillers will also support test bundle instrumentation leads. The excess flow area is 7.8 percent with the fillers.

6-5. Carryover Vessel

The function of the carryover vessel is to collect liquid overflow from the test section. The carryover vessel is a dual-diameter vessel which provides sufficient capacity for high flow rate tests and also accurate measurement for low flow rate tests. The vessel shell is a 6.35 cm (2.5 in.) diameter schedule 40 and 7.62 cm (3 in.) diameter schedule 40 carbon steel pipe. The small-diameter vessel is 2.23 m (88 in.) long and the large-diameter pipe is 2.16 m (85 in.) long. The vessel is close coupled to the upper plenum via a stainless steel flexible hose as shown in figure 6-6.

6-6. Entrainment Separator

Located in the exhaust line, the separator (figure 6-6) is designed to remove any remaining water droplets exhausting from the test section, so that a meaningful single-phase flow measurement can be obtained by an orifice section downstream of the separator. The vessel shell is 15.24 cm (6 in.) schedule 40 carbon steel pipe and the vessel volume is 0.0284 m^3 (1.004 ft^3). The separator utilizes centrifugal action to force the heavier moisture against the wall, where it drains to the bottom. The water is collected in a separator drain tank directly connected to the bottom of the separator. The drain tank shell is a 3.81 cm (1.5 in.) carbon steel pipe and the volume is 0.011 m^3 (0.065 ft^3).

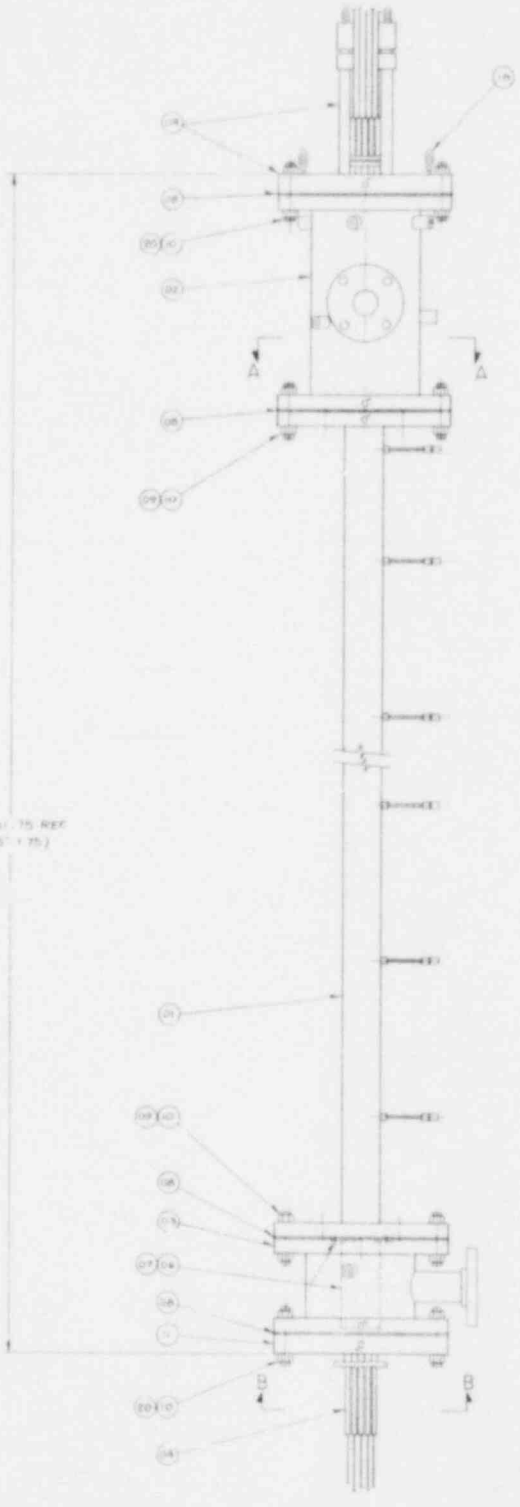
A
A
B
B
(A) .75 REF
(A) + .75

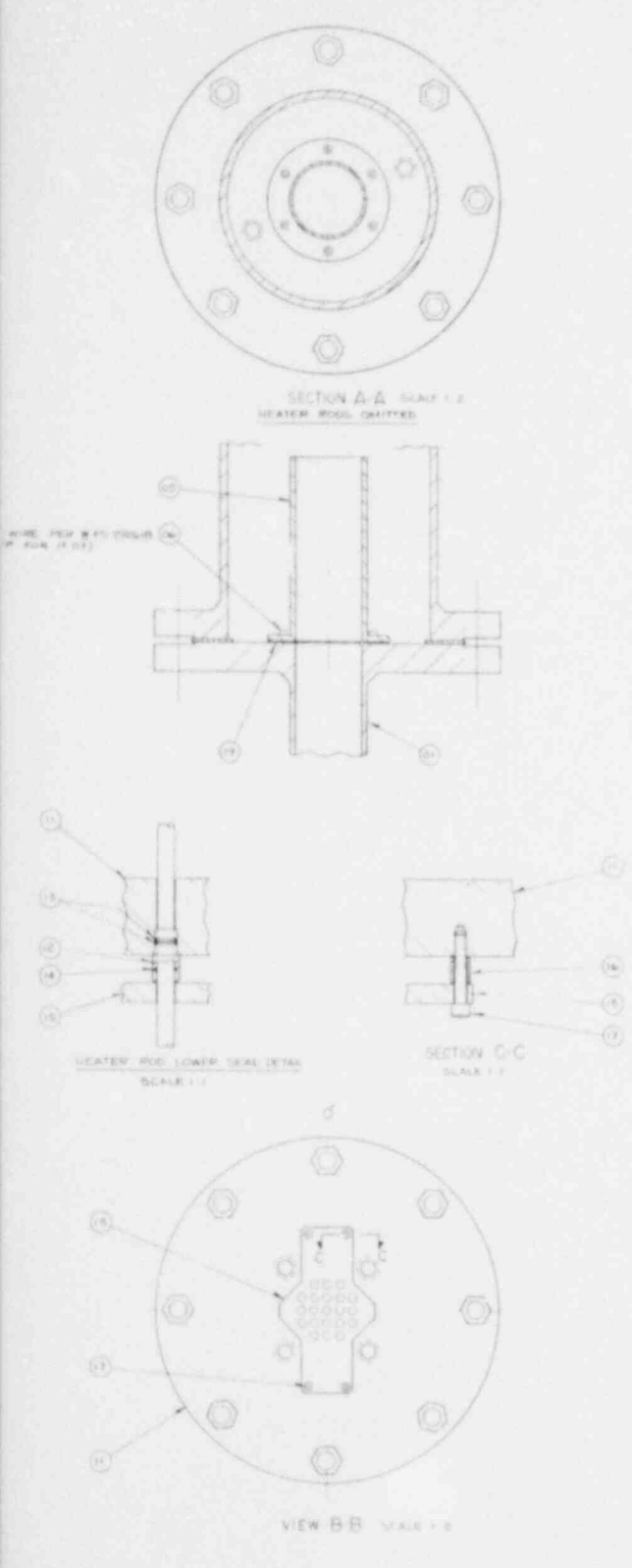

BILL OF MATERIAL

ITEM	QTY	PART NAME	DRAWING OR SPEC.	MATERIAL	WEIGHT LB.
01	1	HOUSING	1453E62G01		
02	1	UPPER PLENUM	1453E62G02		
03	1	LOWER PLENUM	1453E62G03		
04	1	BUNDLE ASSY	1460E63G01		
05	1	UPPER EXTENSION SLEEVE	1460E59G01		
06	12	250-20 UNC-2A x 1.62 LG. HX CAP SCR.			
07	1	LOWER EXTENSION SLEEVE	1460E59G02		
08	4	GASKET .8" SQ. x .19			
09	16	STUD .750-10 x 4.50		C STL	
10	16	NUT HEX .750-10		C STL	
11	1	SEAL A	1460E60G01		
12	1	SLEEVE	1460E57G03		
13	42	O-RING .604 I.D. x .051	SPECIAL	E 692-90	
14	21	O-RING .391 I.D. x .040	S 209	E 692-90	
15	1	PLATE	1460E59G02		
16	4	SPACER	1460E57G03		
17	4	250-20 UNC-2A x .38 LG. HX CAP SCR.			
18	2	EYE BOLT .375-16		SS 3	
19	1	GASKET .06 THK		DURABLA	
20	16	STUD .750-10 x 5.0		C STL	

A - FLEXITALLIC GASKET CO., CAMDEN, N.J.
B - PARKER SEALS, LEXINGTON, KY.
C - SHORTEN A 1.50 LG. SCR. TO 1.38 (4)
D - REID TOOL SUPPLY CO. MUSKEGON HEIGHTS, MICH.
E - MAKE GASKET USING 1.05 AS TEMPLATE

Figure 6-2. 21-Rod Test Housing Assembly (Drawing No. 1460E65)

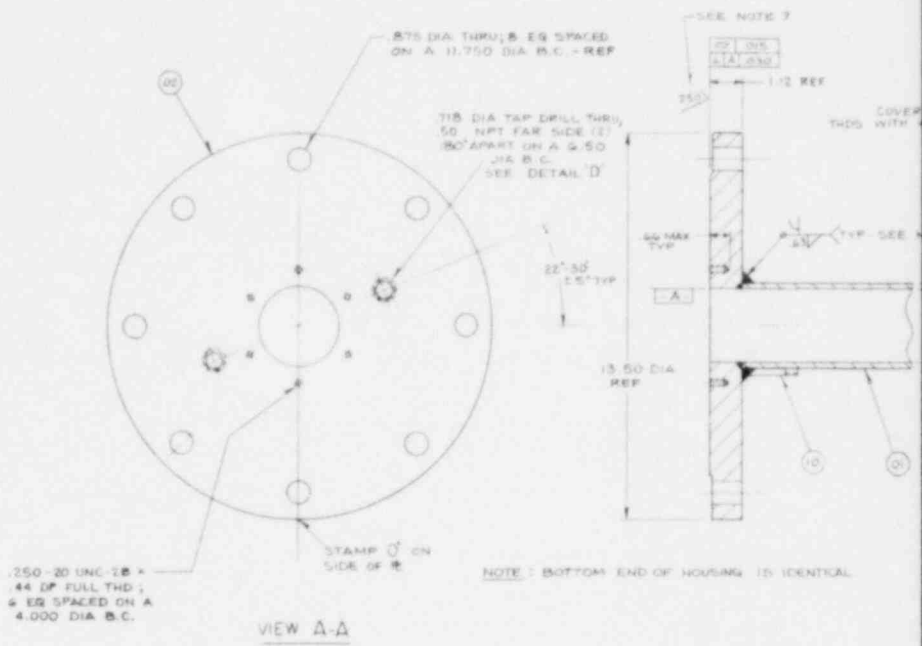
.875 DIA THRU; 8 EQ SPACED ON A 11.750 DIA B.C. - REF
.718 DIA TAP DRILL THRU, 50 NPT FAR SIDE (2) 180° APART ON A 9.50 DIA B.C. SEE DETAIL 'D'
SEE NOTE 7
1.12 REF
22°-30' ±5° TYP
13.50 DIA REF
TYP - SEE
.250-20 UNC-2B x .44 DP FULL THD ; 4 EQ SPACED ON A 4.000 DIA B.C.
STAMP ♂ ON SIDE OF ⌖
NOTE : BOTTOM END OF HOUSING IS IDENTICAL

VIEW A-A

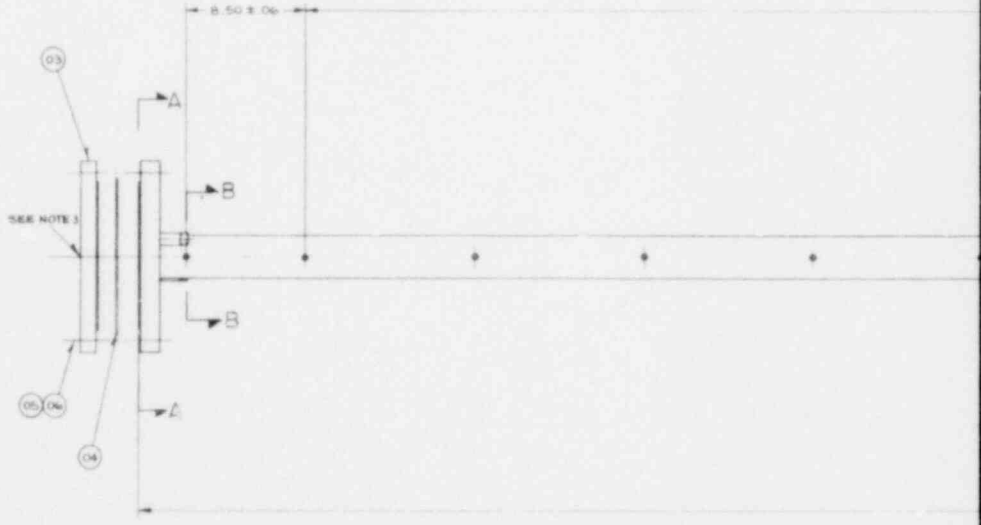
8.50 ± .06
SEE NOTE 3
A
B
B
C

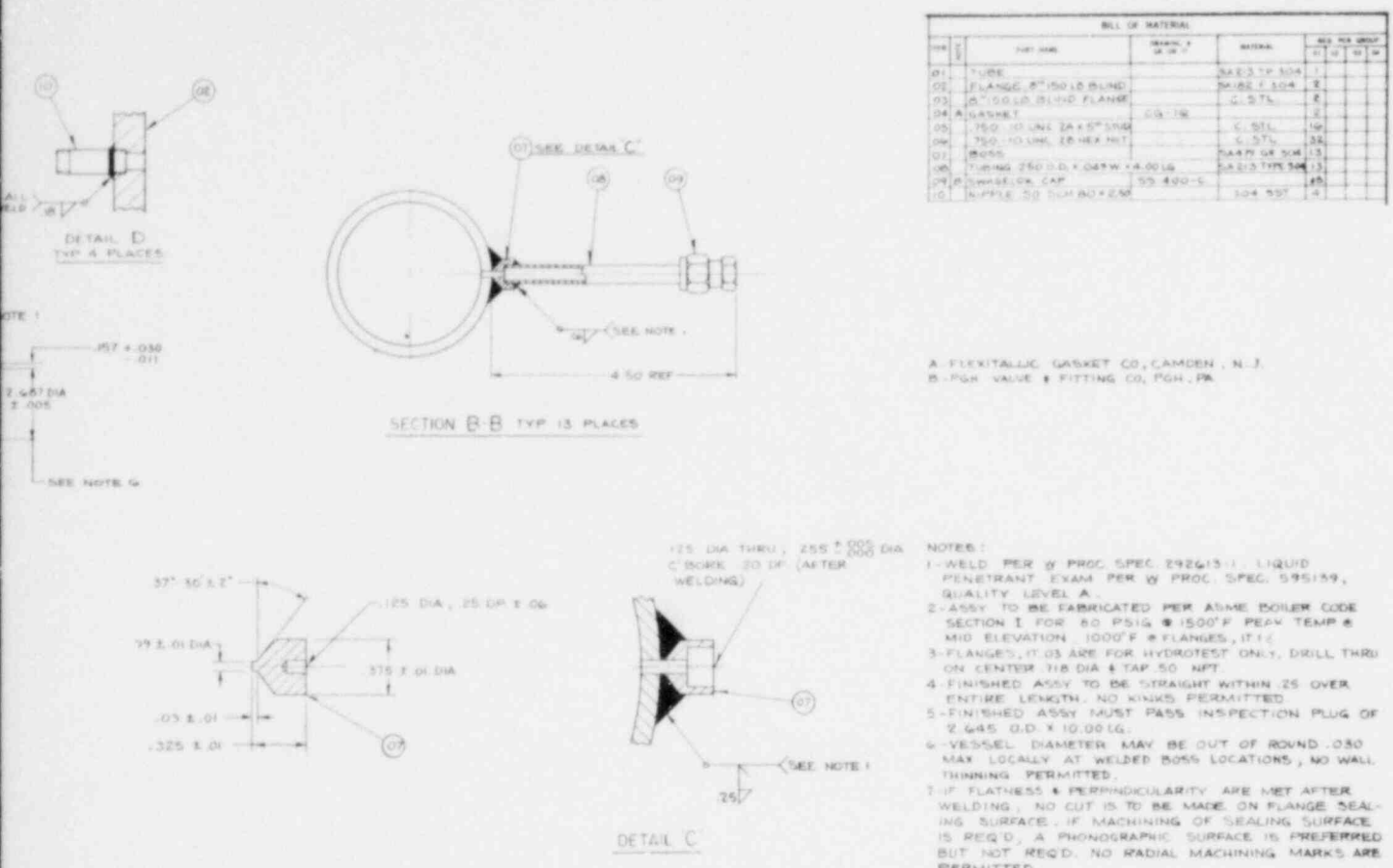

Figure 6-3. 21-Rod Bundle Test Low Mass Housing (Drawing No. 1453E60)

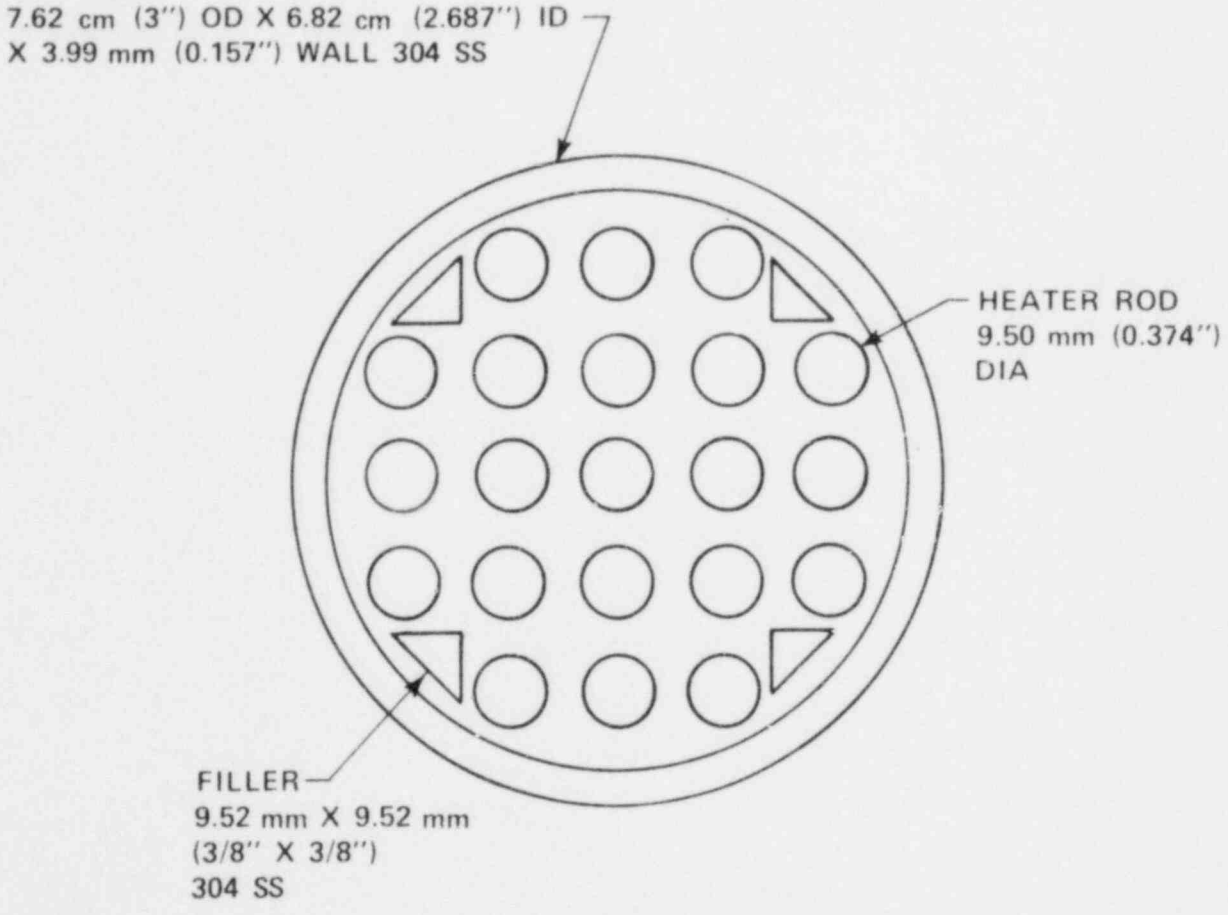

Figure 6-4. 21-Rod Bundle Test Section Cross Section

TABLE 6-1

THERMOPHYSICAL PROPERTIES OF HEATER ROD MATERIALS

Material	Density [kg/m^3 (lbm/ft^3)]	Specific Heat [J/kg-^oC (Btu/lbm-^oF)]	Thermal Conductivity [W/m-^oC (Btu/hr-ft-^oF)]
Kanthal	2898.70 (180.96)	456.36 + 0.45674 T for T $\leq$ 649^oC (0.109 + 0.000059 T for T $\leq$ 1200^oF) 4161.68 - 3.843 T for 649^oC < T < 871^oC (0.994 - 0.00051 T for 1200^oF < T < 1600^oF) 664.86 + 0.0904 T for $\geq$ 871^oC (0.1588 + 0.000012 T for T $\geq$ 1600^oF	16.784 + 0.0134 T (9.7 + 0.0043 T)
Boron nitride	2212.15 (138.1)	2017.74 - 1396.26$e^{-0.00245\ T}$ [0.48193-0.333492$e^{-0.0013611\ T}$]	25.571 - 0.00276 T (14.7778 - 0.0008889 T)
Stainless steel	8025.25 (501.0)	443.8 + 0.2888 T for T < 315^oC (0.106 + 3.833 x 10^{-5} T for T < 599.25^oF) 484.4 + 0.1668 T for T $\geq$ 315^oC (0.1157 + 2.2143 x 10^{-5} T for T $\geq$ 599.25^oF)	14.535 + 0.01308 T (8.4 + 0.0042 T)

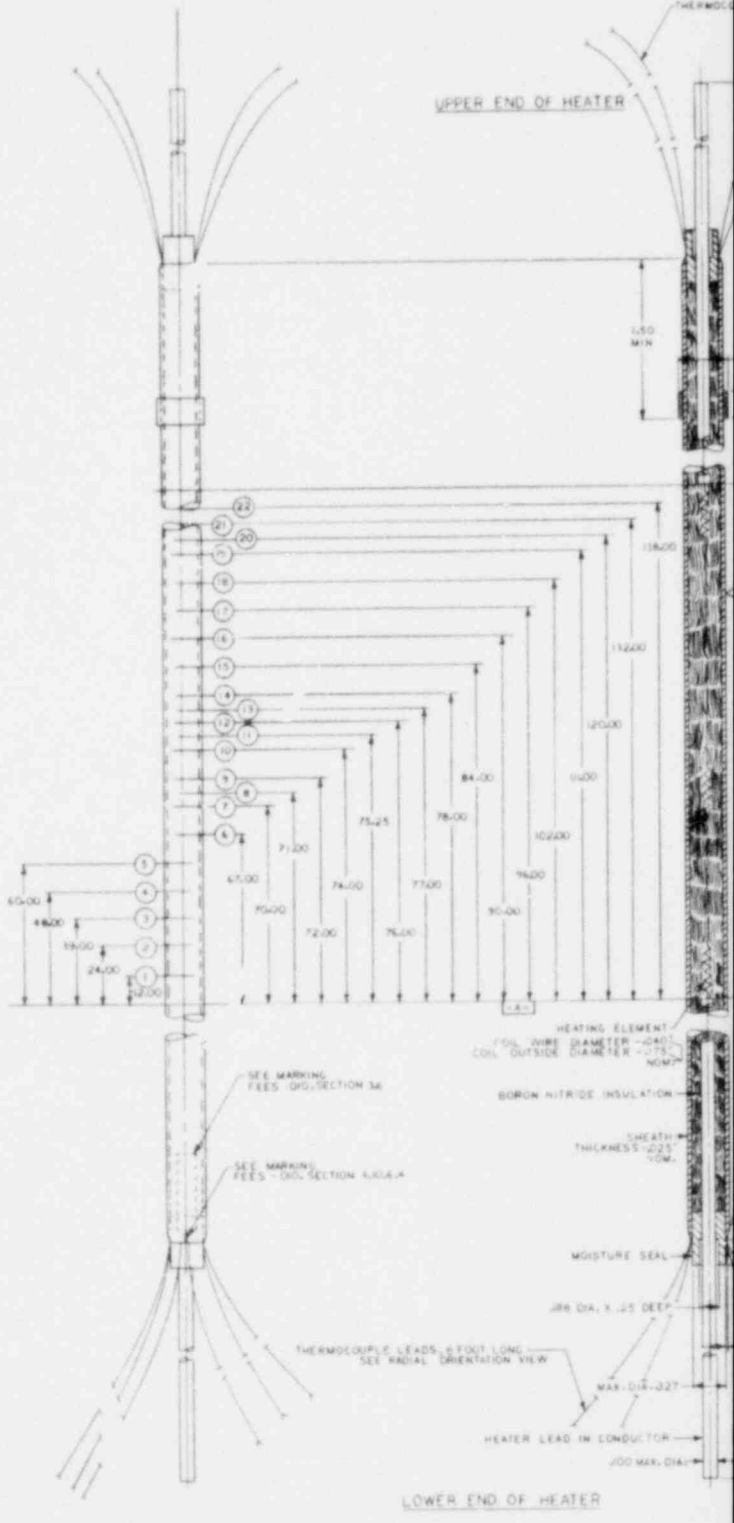
UPPER END OF HEATER
.150 MIN
22
21
20
19
18
17
16
15
14
13
12
11
10
9
8
7
6
5
4
3
2
1
138.00
132.00
120.00
114.00
102.00
96.00
90.00
84.00
78.00
75.25
77.00
74.00
72.00
71.00
67.00
60.00
48.00
36.00
24.00
12.00
A
HEATING ELEMENT
COIL WIRE DIAMETER -040"
COIL OUTSIDE DIAMETER -175"
NOM.
BORON NITRIDE INSULATION
SHEATH
THICKNESS -025"
NOM.
MOISTURE SEAL
.188 DIA. X .25 DEEP
THERMOCOUPLE LEADS, 6 FOOT LONG
SEE RADIAL ORIENTATION VIEW
MAX. DIA. .327
HEATER LEAD IN CONDUCTOR
.100 MAX. DIA.
SEE MARKING
FEES - DFG. SECTION 3K
SEE MARKING
FEES - DFG. SECTION 4.10.6.4
LOWER END OF HEATER

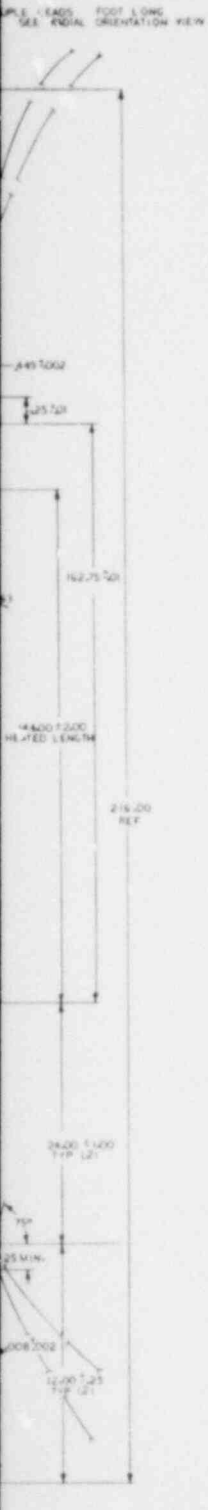

420 V - BKW		
DOUBLE ENDED ROD		
GROUP NO	T/C REQUIRED	
	LOWER END	UPPER END
2 B	9,10,12,14	———
2 C	9,10,12,14	15,16,17,18
4 B	1,3,5,6,12,14	19,21
13 B	2,4,7,8	15,17,18,20
14	8,10,11,13	16,18,20,22

NOTES

1-THIS DWG IS NOT INTENDED TO BE A COMPLETE FABRICATION DWG. THIS DWG IS TO BE USED IN CONJUNCTION WITH ORDERING DATA INCLUDED WITH CE SPECIFICATION FEES-010.

2-REMOVE ALL BURRS AND SHARP EDGES.

3-SURFACE ROUGHNESS 63 UNLESS OTHERWISE NOTED.

4-ULTRASONIC INSPECT PER ASME BOILER AND PRESSURE VESSEL CODE, SECTION III, CLASS 2 COMPONENTS. CALIBRATION STANDARDS AND DEFECT ACCEPTANCE CRITERIA ARE AS FOLLOWS:

(A) CALIBRATION DEFECT STANDARDS:
DEPTH - .0025 IN.
LENGTH - .050 IN.
WIDTH - .0025 IN.

(B) ACCEPTANCE CRITERIA:
DEFECT IN SHEATH MUST BE LESS THAN THE CALIBRATION DEFECT STANDARDS.

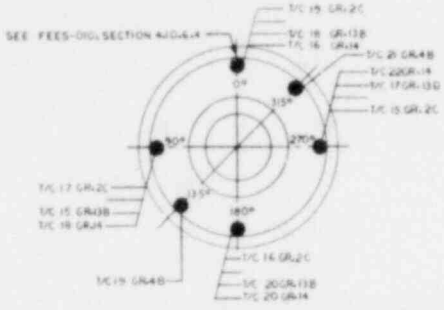

AZIMUTHAL ORIENTATION OF THERMOCOUPLES AS VIEWED FROM BOTTOM END OF ROD

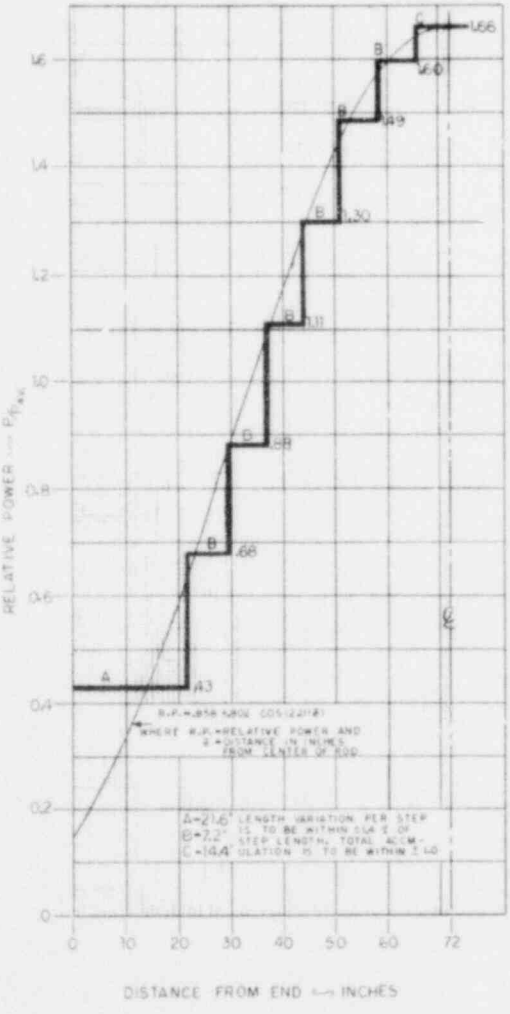

NOTE

1-CIRCLED ① THRU ㉒ ARE THERMOCOUPLES (.025 MIN. 304 STAINLESS STEEL SHEATH, TYPE K PREMIUM GRADE INSULATED JUNCTIONS ANNEALED OVER ENTIRE LENGTH) TOLERANCE ON ALL T/C DIMENSIONS TO BE ±1% AS MEASURED FROM DATUM A.

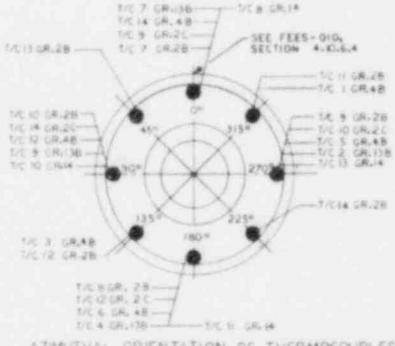

AZIMUTHAL ORIENTATION OF THERMOCOUPLES AS VIEWED FROM BOTTOM END OF ROD

Figure 6-5. Heater Rod Details (Drawing No. 1460E39)

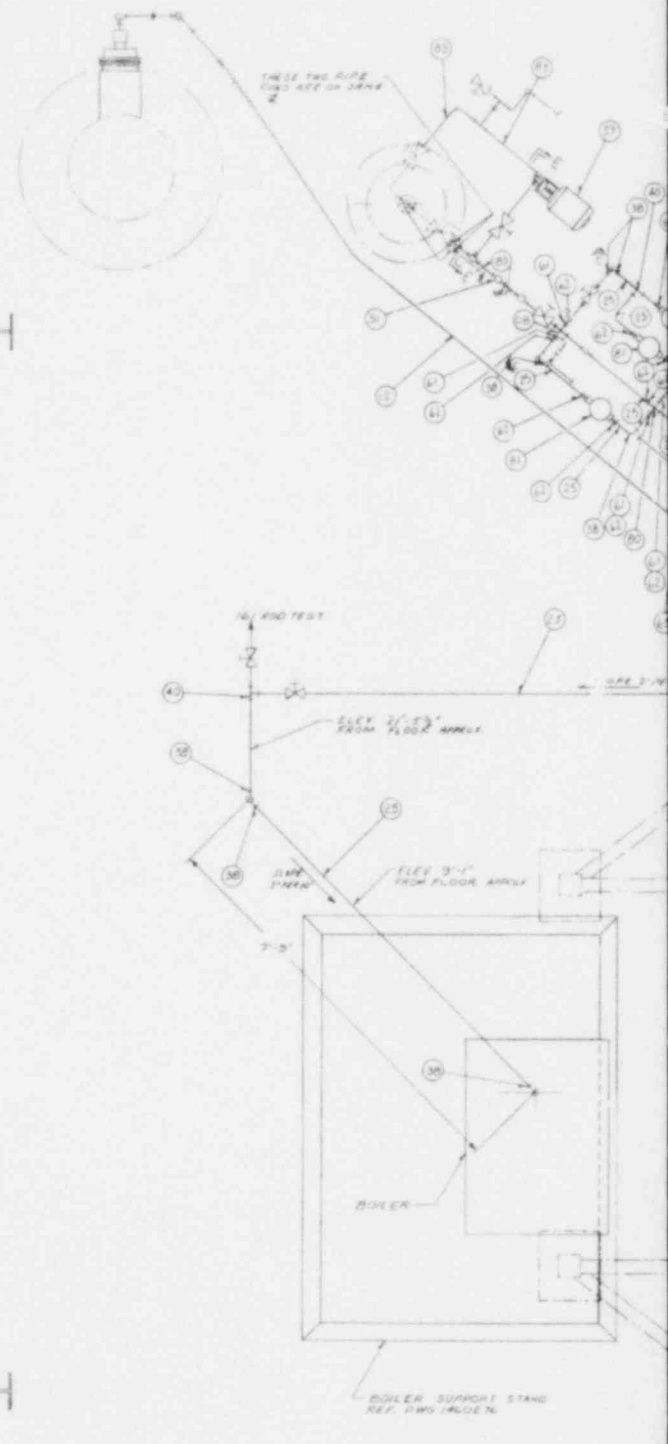
THESE TWO PIPE LINES ARE ON SAME
FLEX 3/4" FROM FLOOR APPROX
FLEX 3'-1" FROM FLOOR APPROX
7'-9"
BOILER
BOILER SUPPORT STAND
REF. DWG (ADDED)

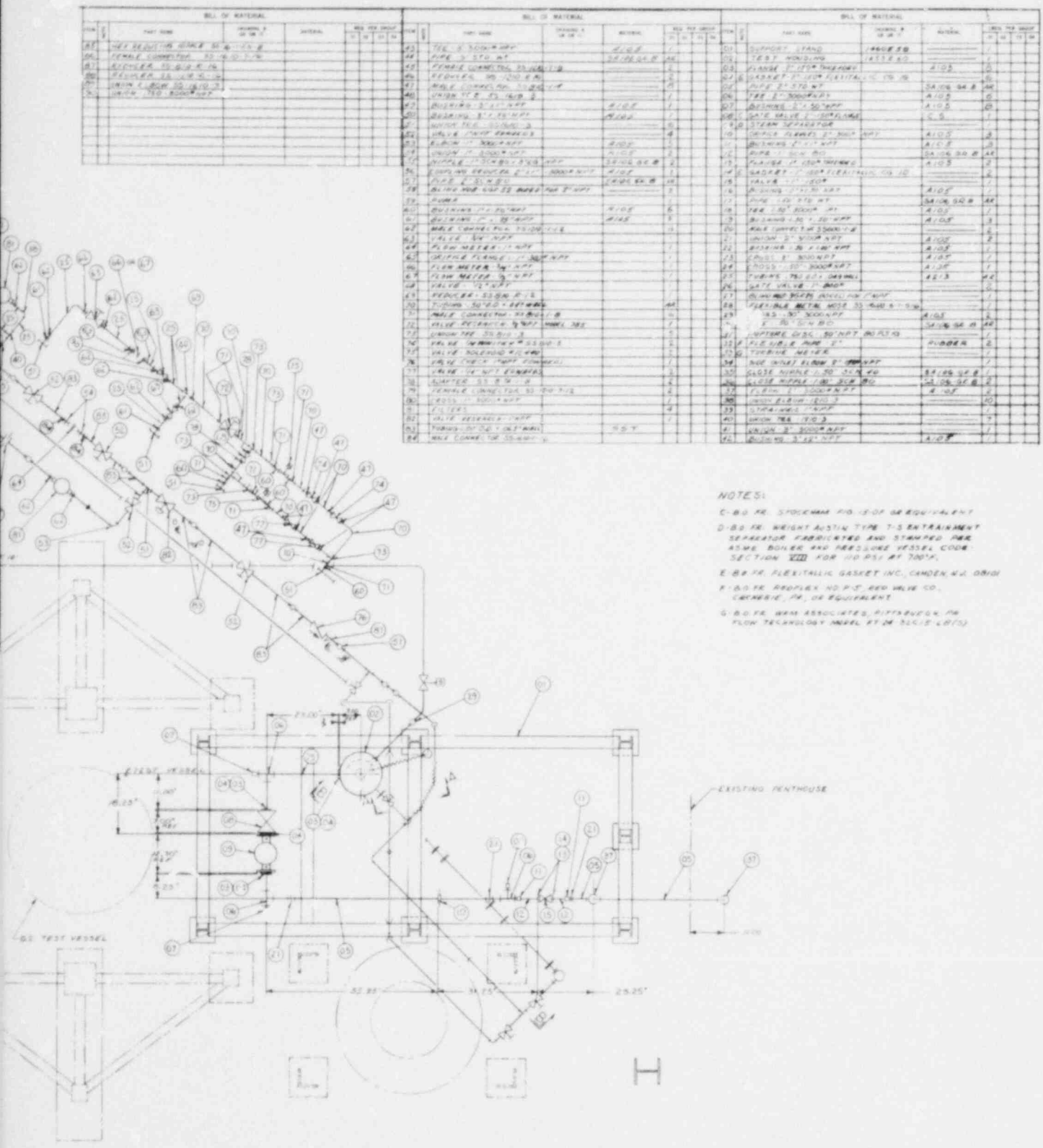

Figure 6-6. 21-Rod Test Bundle
(sheet 1 of 3)
(Drawing No. 1460E76)

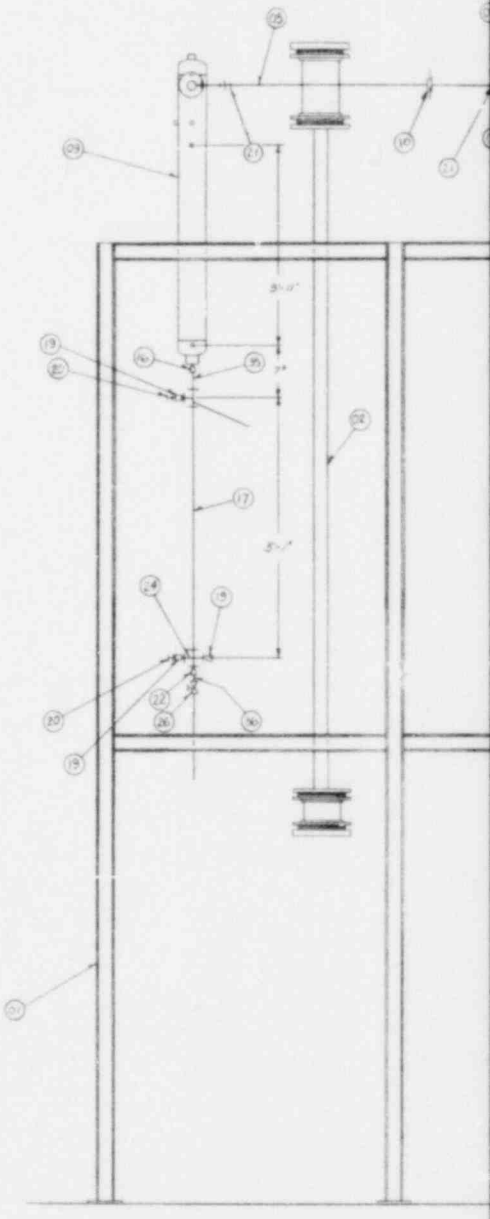

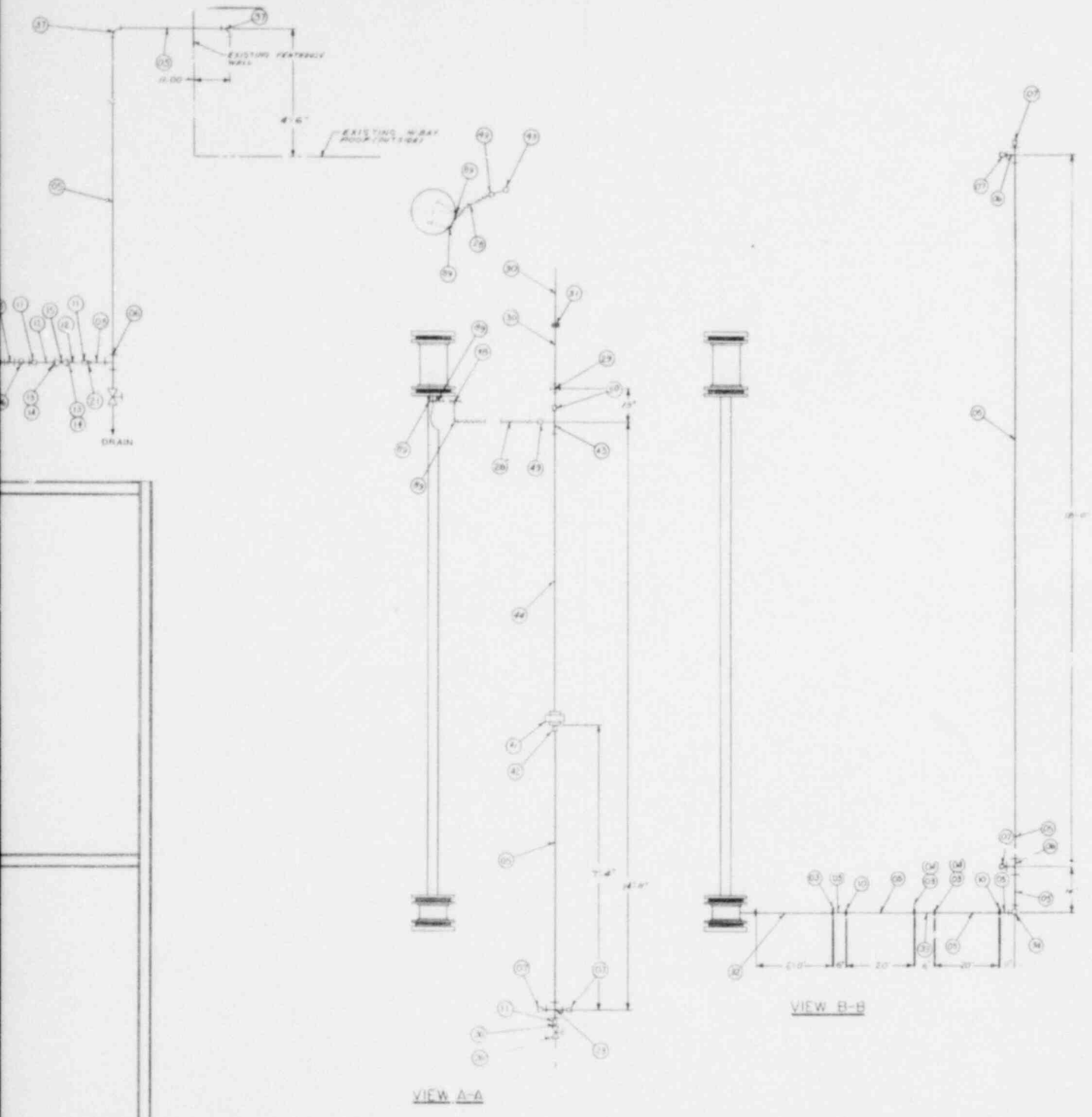

Figure 6-6. 21-Rod Test Bundle
(sheet 2 of 3)
(Drawing No. 1460E76)

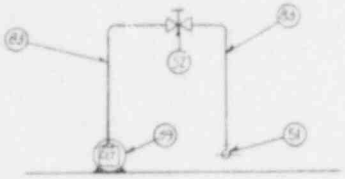

VIEW E-E

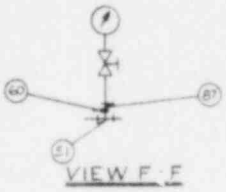

VIEW F-F

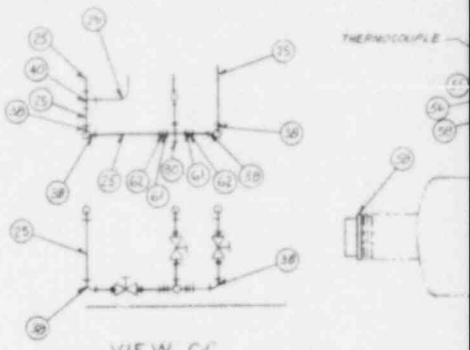

VIEW C C

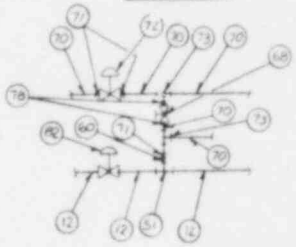

VIEW D D

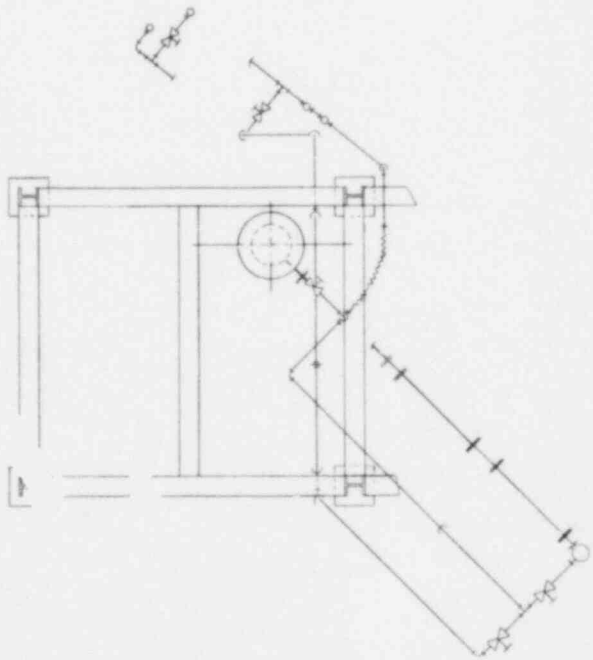

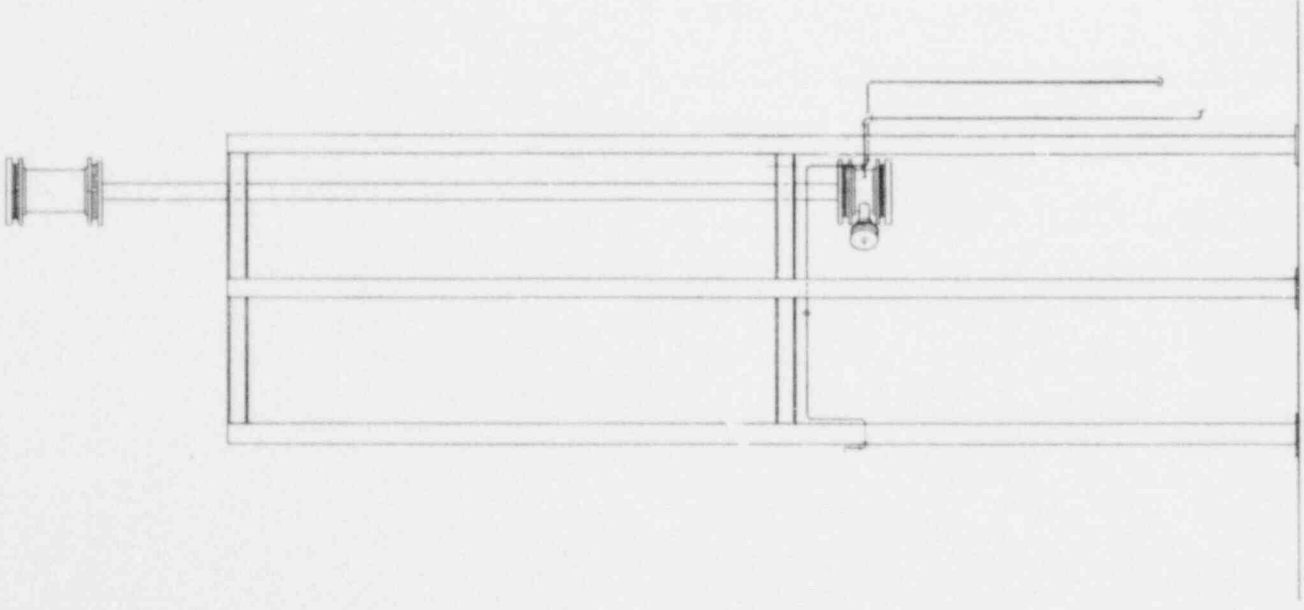

Figure 6-6. 21-Rod Test Bundle
(sheet 3 of 3)
(Drawing No. 1460E76)

6-7. Exhaust Line Piping and Components

Test section effluent discharges to the atmosphere through 5.08 cm (2 in.) exhaust line piping. A nozzle penetration on the upper plenum provides the attaching point for the exhaust line piping. Sandwiched between the two mating flanges is a plate which serves as a structural attachment for an internal baffle pipe assembly (upper plenum baffle, figure 6-7). This baffle serves to improve the liquid carryout separation and minimize liquid entrainment in the exhaust vapor. After passing through the upper plenum baffle pipe, the exhaust vapor passes through a 90-degree elbow and a straight run of pipe into the entrainment separator.

Dry steam leaving the separator passes through a 90-degree elbow and along a straight run of heated pipe to an orifice flange assembly utilized to measure flow rate. Clamp-on strip heaters on the pipe are used to heat the pipe to 260°C (500°F) to assure single-phase steam flow through the orifice. Steam then exhausts to the atmosphere through a pressure control valve. The control valve is an air-operated V-ball control valve of the type used successfully on the skewed FLECHT test series[1] to minimize the pressure oscillations during a test run. Aspirating steam probes are located in each of the two 90-degree elbows to measure the temperature of the exhaust steam. A full-bore gate valve installed at the entrainment separator inlet flange will be employed to simulate the hot leg resistances for the gravity reflood tests.

6-8. Coolant Injection System

This system provides reflood water to quench the rod bundle during testing. In brief, coolant injection water is supplied by the 0.379 m^3 (100-gal) accumulator through a series of valves and turbine meters. Nitrogen overpressure on the accumulator provides the necessary driving head to attain the required injection rates.

Constant or stepped injection flow is accomplished by the proper sequencing of solenoid valves, which are located in a piping manifold arrangement, as shown in figure 6-1. Programmed flow to the test section is controlled by means of a

1. Rosal, E. R., et al., "FLECHT Low Flooding Rate Skewed Test Series Data Report," WCAP-9108, May 1977.

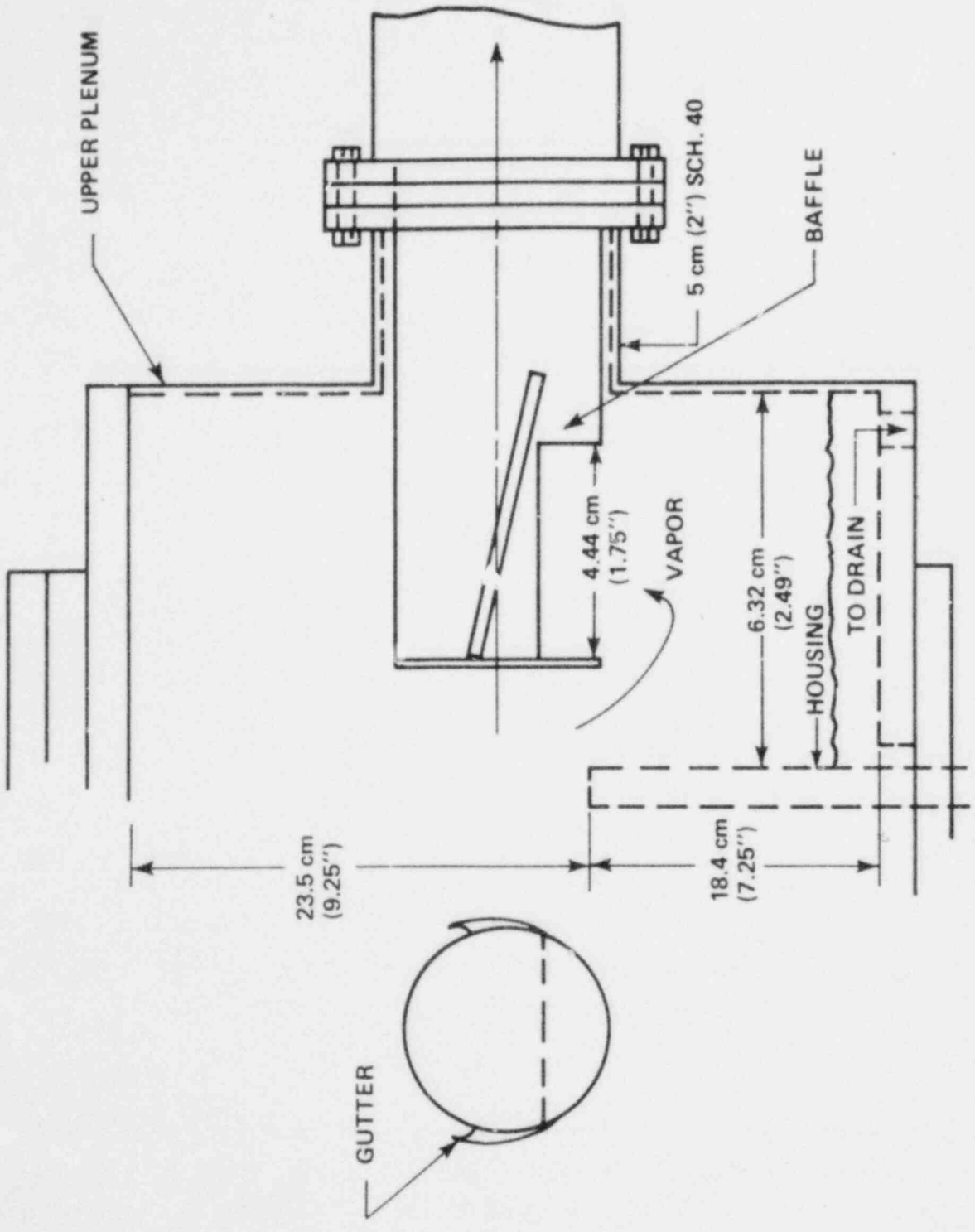

Figure 6-7. 21-Rod Bundle Upper Plenum Baffle

pneumatic valve which operates off a demand signal from the computer, with feedback from the turbine meter. Two turbine meters are used for flow rate measurement, one with a range of 1.58×10^{-5} to 31.54×10^{-5} m^3/sec (0.25 to 5.0 gal/min) for forced flooding tests and one with a range of 1.58×10^{-5} to 94.62×10^{-5} m^3/sec (0.25 to 15 gal/min) for gravity reflood tests.

A full flow bidirectional turbine meter with a range of 3.15×10^{-5} to 94.62×10^{-5} m^3/sec (0.5 to 15 gal/min) will be installed in the downcomer crossover leg during gravity reflood tests to measure flow into the test section and any reverse flow from the test section to the downcomer.

6-9. Downcomer

The downcomer will be connected to the test section lower plenum for the gravity reflood tests, as shown in figure 6-6. The downcomer is fabricated from 5.08 cm (2 in.) schedule 40 pipe, a 90-degree long radius elbow and a flexible rubber pipe. The rubber pipe connects the downcomer to the lower plenum and allows for downward thermal expansion of the test section. The horizontal crossover run of the downcomer is 221 cm (7.25 ft) long and the vertical run is approximately 610 cm (20 ft). A nozzle located in the elbow of the downcomer will be used to inject the coolant water from the accumulator. The bidirectional turbine meter will be located in the crossover pipe.

6-10. Boiler

The boiler is a Reimers Electric steam boiler with a steam capacity of approximately 15.7×10^{-3} kg/sec (125 lb/hr) at $100^{\circ}C$ ($212^{\circ}F$). The boiler is used to pressurize the facility and for pretest facility heatup. This is accomplished by valving the boiler into the upper plenum of the test section.

6-11. Steam Injection System

This system provides saturated steam to the rod bundle during steam cooling tests. The steam injection system is composed of a large-volume tank with immersible electric heaters capable of providing steam flow in the range of approximately 0.0045 kg/sec (0.01 lb/sec) to 0.045 kg/sec (0.10 lb/sec).

6-12. FACILITY OPERATION

The facility operation will be similar to that detailed in WCAP-9108.[1] The following general procedure will be used to conduct a typical reflood test:

(1) Fill accumulator with water and heat to desired coolant temperature, 53°C (127°F) nominal.

(2) Turn on boiler and bring the pressure up to 0.62 MPa (75 psig) nominal gage pressure.

(3) Steam heat the carryover vessel, entrainment separator, separator drain tank, test section plenum, and test section outlet piping (located before the entrainment separator) while they are empty to slightly above the saturation temperature corresponding to the test run pressure. The exhaust line between the separator and exhaust orifice is electrically heated to 260°C (500°F) nominal; the test section lower plenum is heated to the temperature of the coolant in the accumulator.

(4) Pressurize the test section, carryover vessel, and exhaust line components to the specified test run pressure by valving in the boiler and setting the exhaust line control valve to the specified pressure.

(5) Scan all instrumentation channels by the computer to check for defective instrumentation. The differential pressure and static pressure cell zero readings are taken and entered into the computer calibration file. These zero readings are compared with the component calibration zero reading. The straight-line conversion to engineering units is changed to the new zero when the raw data are converted to engineering units. This zero shift process accounts for errors due to transducer zero shifts and compensates for level reference legs, enabling the engineering units to start with an empty reading.

---

1. Rosal, E. R., et al., "FLECHT Low Flooding Rate Skewed Test Series Data Report," WCAP-9108, May 1977.

(6) Apply power to the test bundle at a peak rate of 1.31 kw/m (0.4 kw/ft) and allow rods to heat up. When the temperature in any two designated bundle thermocouples reaches the desired test flood temperature, 871°C (1600°F), the computer automatically initiates flood and controls power decay. The exhaust control valve regulates the system pressure at the preset value by releasing steam to the atmosphere.

(7) Ascertain that all designated rods have quenched (indicated by the computer printout of bundle quench).

(8) Cut power from heaters, terminate coolant injection, and depressurize the entire system.

(9) Drain and weigh water from all components.

During the test series, the facility will be modified to conduct gravity reflood tests. The same procedure will be used to conduct these tests with the following exception: after flood is initiated, the flooding rate will be adjusted if necessary to ensure that the level in the downcomer does not exceed the 4.88 m (16 ft) elevation. This is necessary to avoid condensation, which affects the pressure transient of the facility (see paragraph 6-1).

6-13. BLOCKAGE SLEEVES AND CHANGEOVER

Two basic blockage sleeve shapes will be tested: concentric short sleeves and nonconcentric long sleeves. The blockage sleeves will be fabricated by hydroforming circular-cross-section stainless steel tubing. The tube wall thickness will be approximately 0.076 cm (0.030 in.). Provisions will be made to instrument the sleeves with a thermocouple. The blockage sleeves will be spot-welded to the heater rod. This sleeve attachment method was tested in a single-rod test facility to verify its adequacy under reflood conditions (see paragraph 7-5). Figure 6-8 shows the two sleeve shapes.

The test facility is designed to make six bundle changeovers for the seven bundle configurations previously described (paragraph 4-9). After completion of the test

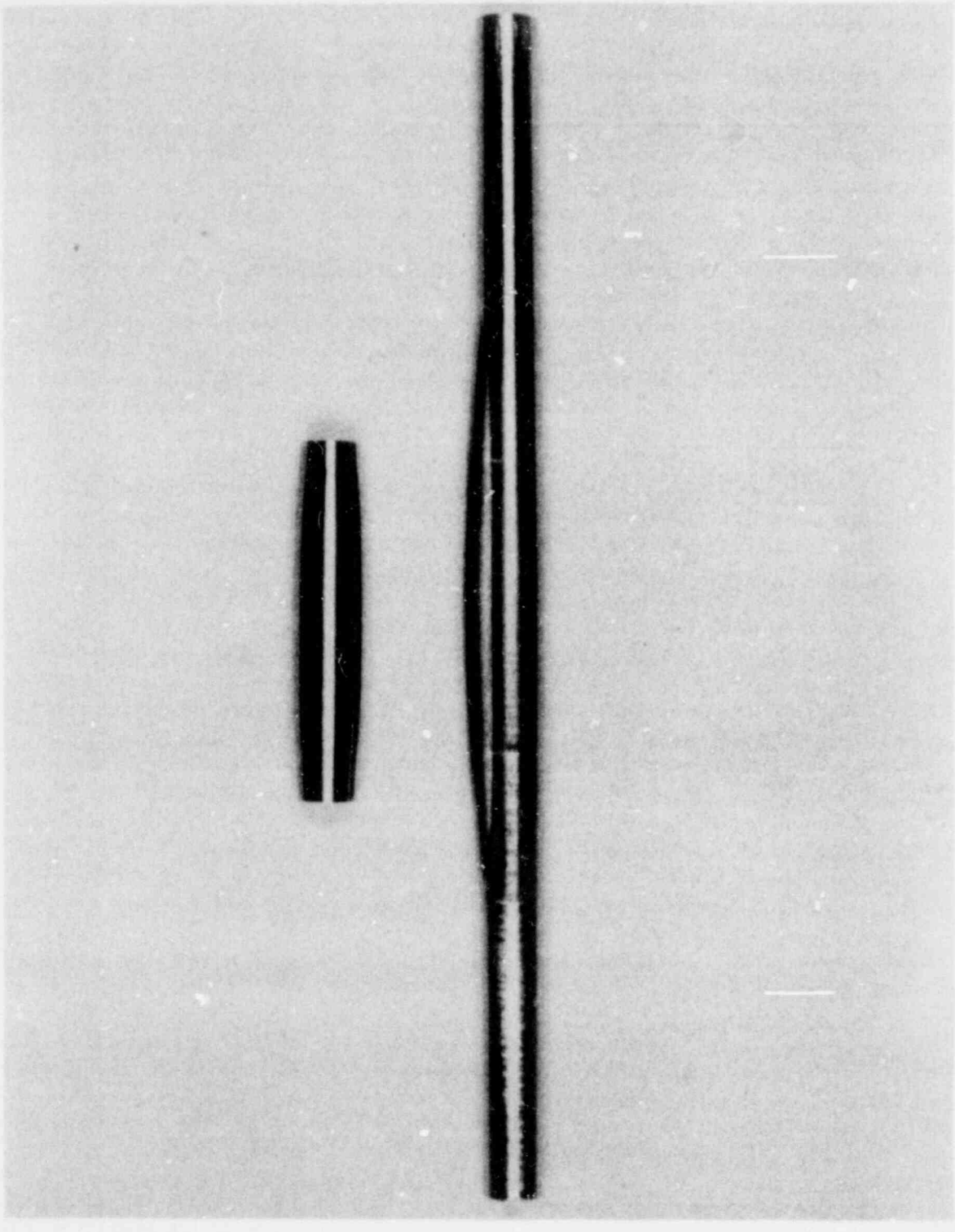

Figure 6-8. Blockage Sleeves

matrix (see tables 8-1 and 8-2), the bundle will be replaced with a newly assembled bundle with the proper blockage configuration and the test matrix will be repeated. Bundles for future blockage configurations will be made in a series or parallel effort during the testing period, depending on manpower availability. Sufficient hardware, such as grids and fillers, will be available for three bundles.

6-14. HYDRAULIC CHARACTERISTICS TESTS

Single-phase (water) hydraulic characteristic tests will be performed on the seven bundle configurations listed in paragraph 4-9, with the test bundle installed in the test vessel prior to conducting the heat transfer tests.

The purpose of these tests is to obtain loss coefficients for bundle grids, blockage geometries, and friction factors for ranges and conditions applicable to reflooding in the 21-rod bundle heat transfer facility. This information will be used as input to development of an analytical or experimental method of bundle blockage heat transfer, such as a COBRA-IV model.

Flow will be supplied by the pressurized water supply accumulator over a range of 6.30×10^{-4} to 37.8×10^{-4} m^3/sec (10 to 60 gal/min). Flow will pass once through the test vessel to the entrainment separator and to drain. Test vessel pressures and differential pressures will be measured with differential pressure cells and the flow rate will be measured with a 3.154×10^{-4} to 3.785×10^{-3} m^3/sec (5 to 60 gal/min) turbine meter.

SECTION 7
TEST FACILITY INSTRUMENTATION

7-1. GENERAL

The data recorded in this task will consist of temperature, power, flow, fluid level, and static pressure. The temperature data will be measured by type K (Chromel-Alumel) thermocouples using 66°C (150°F) reference junctions. The thermocouple locations are divided into two groups: test section bundle and loop. Bundle thermocouples consist of heater rod thermocouples, steam probes, and blockage sleeve thermocouples. The heater rod thermocouples will be monitored by the Computer Data Acquisition System (CDAS) for temperature at time of flood, overtemperature, and bundle quench temperature. The loop thermocouples measure fluid, vessel wall, and piping wall temperature.

Power input to the bundle heater rods will be measured by Hall-effect watt transducers. These watt transducers produce a direct current electrical output proportional to the power input. The voltage and current input to the watt transducer is scaled down by transformers so that the range of the watt transducer matches the bundle power. The scaling factor of the transformers will be accounted for when the raw data (millivolts) are converted to engineering units.

Injection flow will be measured by two turbine meters: one for forced flooding tests and one for gravity reflood tests. Gravity feed flow into or out of the bundle will be measured by a bidirectional turbine meter located in the crossover leg. The turbine meter will be connected to a preamplifier and flow rate monitor for conversion of turbine blade pulses into flow rate in engineering units. The turbine meter flow rate monitor analog signal is proportional to the speed and direction of flow in the downcomer crossover leg. Calibration of the turbine meter by the manufacturer provides for data conversion to volumetric flows for the turbine meter analog signal.

The system pressure measurements will be both static and differential. The pressure transducers will be balanced bridge strain gage devices. The differential pressure readings will measure level in the vessels and the bundle and pressure drops across selected horizontal pipes.

Standard thermocouple calibration table entries and the corresponding coefficients will be used to compute the temperature value. All other channel calibration files will be straight-line interpolations of calibration data. The slope intercept and zero for the least-squares fit of a straight line to the equipment calibration data are computed for each channel and entered into its calibration file. The software uses this straight-line formula to convert millivolts to engineering units. Figure 7-1 presents a schematic diagram of the computer hardware interface.

7-2. BUNDLE INSTRUMENTATION

The bundle instrumentation consists of heater rod thermocouples, steam probes, blockage sleeve thermocouples, differential pressure cells, power measurements, and plenum fluid thermocouples.

The exact locations of the heater rod thermocouples, steam probes, and blockage sleeve thermocouples for the first four bundles are shown in appendix H. Minor modifications to this bundle instrumentation plan are expected for subsequent bundles, depending on the test data obtained.

7-3. Heater Rod Thermocouples

All 21 heater rods in this task are instrumented with eight thermocouples each, for a total of 168. All 168 thermocouples will be connected to the computer. The placement of the heater rod thermocouples was based on the following (see appendix H):

- Achieving an axial distribution both in the blockage zone (inner 3x3 array of nine rods) and outside the blockage zone (outer 12 rods) the same as in the unblocked bundle task

- Achieving a radial distribution such that rods both in the blockage zone and outside of the blockage zone are instrumented

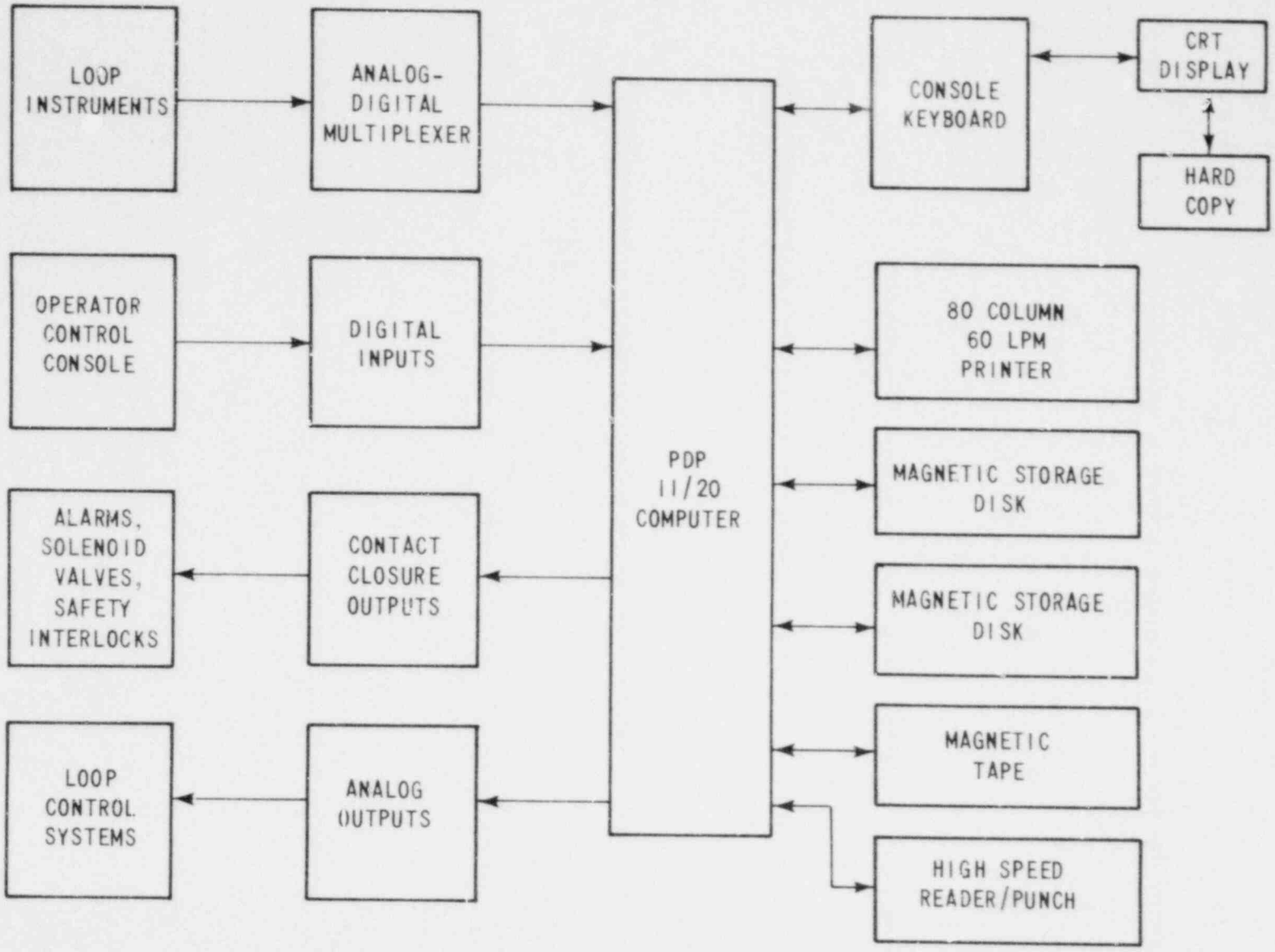

Figure 7-1. FLECHT SEASET Computer Hardware Interface for 21-Rod Bundle Flow Blockage Task

-- Achieving an azimuthal orientation such that the heater rod thermocouple is "directed" toward the blocked subchannel instead of toward an adjacent heater rod

-- Achieving a sufficient number of thermocouples upstream and downstream of the blockage zone to determine the axial effects of blockage sleeves

Figure 7-2 shows the number of thermocouples per elevation for all 21 rods and for the center 3 x 3 array of nine rods.

Heater rods in the 21-rod bundle task will be manufactured with five different thermocouple groupings, as shown in table 7-1. Also shown is the relative azimuthal orientation of the thermocouples. Groups 2b and 2c, which are very similar to group 2 in the unblocked bundle task,[1] cover the blockage zone of 1.778 m (70 in.) to 2.134 m (84 in.) very thoroughly. Groups 4b and 13b, which are similar to groups 4 and 13, respectively, in the unblocked bundle task, provide fairly uniform axial coverage from 0.3 m (1 ft) to 3.0 m (10 ft). Group 14 rods provide temperature measurements in both the blockage zone and the high-temperature zone at 2.13 m (7 ft) to 3.0 m (10 ft) The axial and azimuthal locations of heater rod thermocouples are shown in figures H-3 through H-26.

Groups 2b and 4b will have eight and six thermocouple leads, respectively, coming out the bottom end of the rod. Groups 2c, 13b, and 14 will each have four leads coming out both ends of the rod. Running leads out the bottom end of the rod will prevent thermocouple leads passing through the high-temperature zone and introducing temperature measurement errors.[2] Thermocouples at the 1.98 m (78 in.) elevation and below have their leads coming out the bottom end of the rod.

1. Hochreiter, L. E., et al., "PWR FLECHT SEASET Unblocked Bundle, Forced and Gravity Reflood Task: Task Plan Report," NRC/EPRI/Westinghouse-3, March 1978.

2. Roberts, M. J., and Kollie, T. G., "Derivation and Testing of a Model to Calculate Electrical Shunting and Leakage Errors in Sheathed Thermocouples," Rev. Sci. Instrum. 48, 1179-1191 (1977).

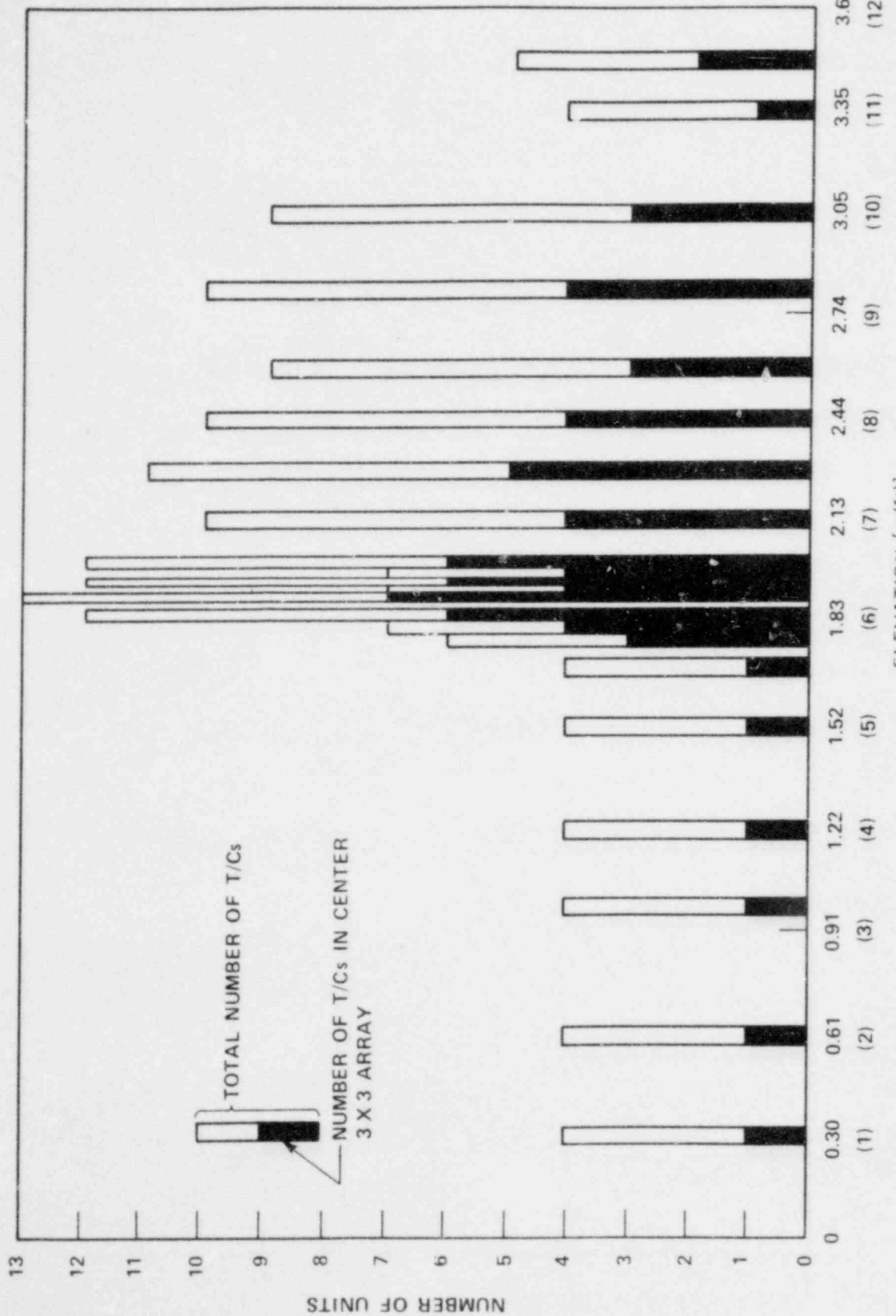

Figure 7-2. 21-Rod Bundle Flow Blockage Task Instrumentation Summary

TABLE 7-1

21-ROD BUNDLE FLOW BLOCKAGE TASK HEATER ROD INSTRUMENTATION
AXIAL AND AZIMUTHAL DISTRIBUTION

Elevation [m (in.)]	Group 2c	Group 2b	Group 4b	Group 13b	Group 14
0.30 (12)			315°		
0.61 (24)				270°	
0.99 (39)			135°		
1.22 (48)				180°	
1.52 (60)			270°		
1.70 (67)			180°		
1.78 (70)		0°		0°	
1.80 (71)		180°			0°
1.83 (72)	0°	270°		90°	
1.88 (74)	270°	90°			90°
1.91 (75.25)		315°			180°
1.93 (76)	180°	135°	90°		
1.96 (77)		45°			270°
1.98 (78)	90°	225°	0°		
2.13 (84)	270°			90°	
2.29 (90)	180°				0°
2.44 (96)	90°			270°	
2.59 (102)				0°	90°
2.82 (111)	0°		135°		
3.05 (120)				180°	180°
3.35 (132)			315°		
3.51 (138)					270°

7-4. Steam Probe Instrumentation

Steam temperature data required for data analysis and evaluation efforts will be measured by means of a steam probe specifically designed in the 21-rod bundle task. These steam probes will provide data for evaluation of the following:

- Mass and energy balances
- Nonequilibrium vapor properties
- Radial and axial fluid temperature variation
- Effect of flow blockage sleeves

Unlike the steam probe in the unblocked bundle task, which was located within a thimble tube and aspirated steam to the atmosphere, this steam probe is enclosed within a 0.238 cm (0.09375 in.) hollow tube and relies on the frictional pressure drop across a 0.635 cm (0.25 in.) length to drive steam flow. The proposed design is shown in figure 7-3. A 0.81 mm (0.032 in.) thermocouple is enclosed within a 0.238 cm (0.09375 in.) OD hollow tube of 0.015 cm (0.006 in.) wall thickness. The two flow holes spaced 0.635 cm (0.25 in.) apart, are diametrically opposed. The thermocouple junction is located midway between the two flow holes thereby providing radiation shielding and protection from water droplets. Best-estimate calculations have been performed on the expected behavior of the steam probe; the results are shown in appendix I. This steam probe will be placed in the unblocked bundle test facility adjacent to the thimble-type aspirating steam probe for shakedown and evaluation of the design.

There will be 26 steam probes in the 21-rod bundle facility, including one steam probe located in the periphery of the bundle for determining any cold wall effects. These steam probes will be located at elevations where heater rod temperatures are being measured and, for the most part, in identical subchannels (see figures H-3 through H-26). The steam probe will be attached to the nearest grid and centered in the subchannel. The thermocouple lead for each steam probe will lie on the top or bottom of the grid and run to the corner filler, and subsequently lie in "scallops" in the filler to exit at the top of the bundle.

Figure 7-4 shows the axial distribution of steam probes for both the center four subchannels and the outer eight subchannels. The steam probes at 0.99 m (39 in.), 3.35 m (132 in.) and 3.51 m (138 in.) are placed in the center of the bundle without

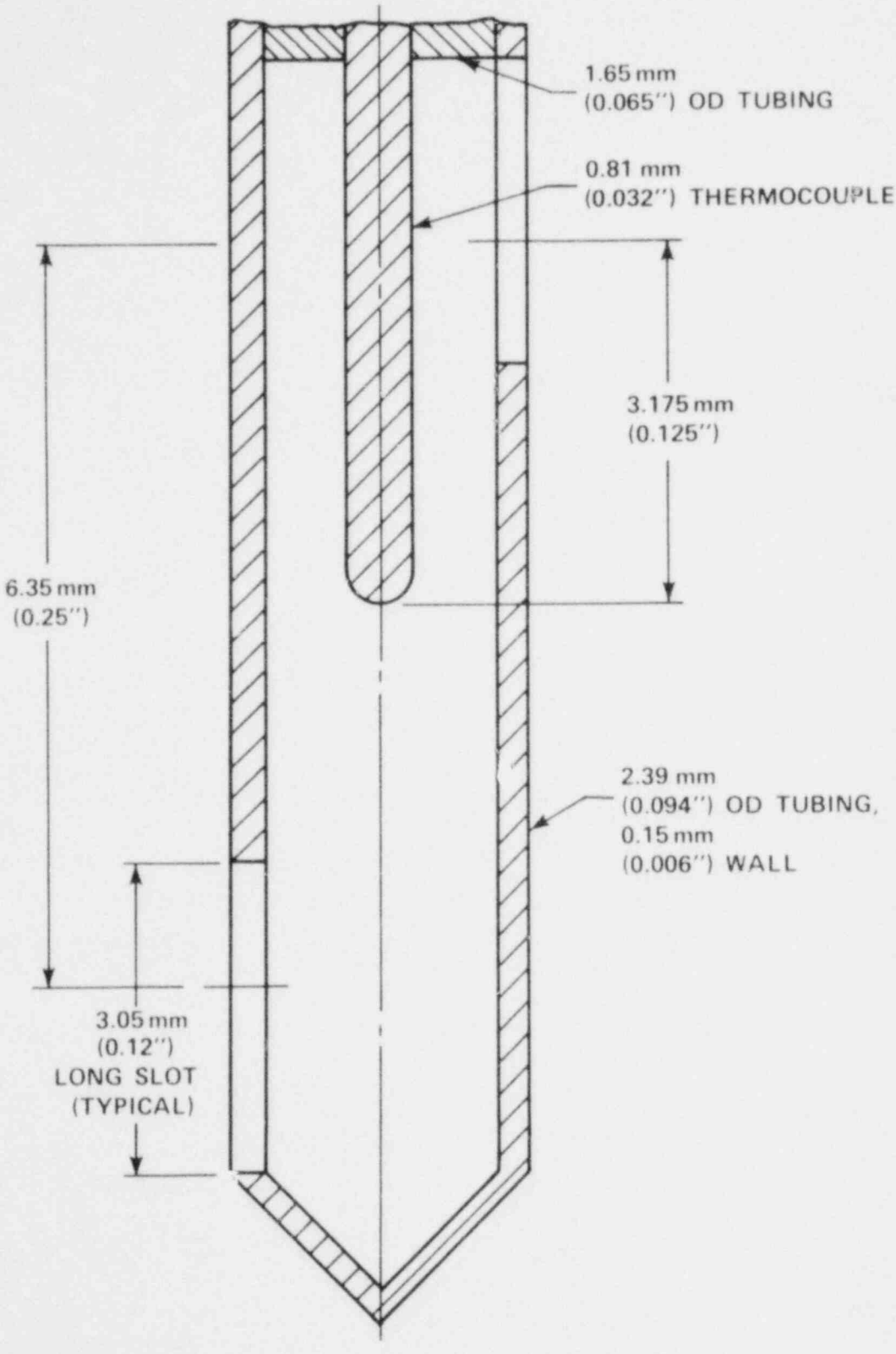

Figure 7-3. Proposed Steam Probe Design for 21-Rod Bundle Flow Blockage Task

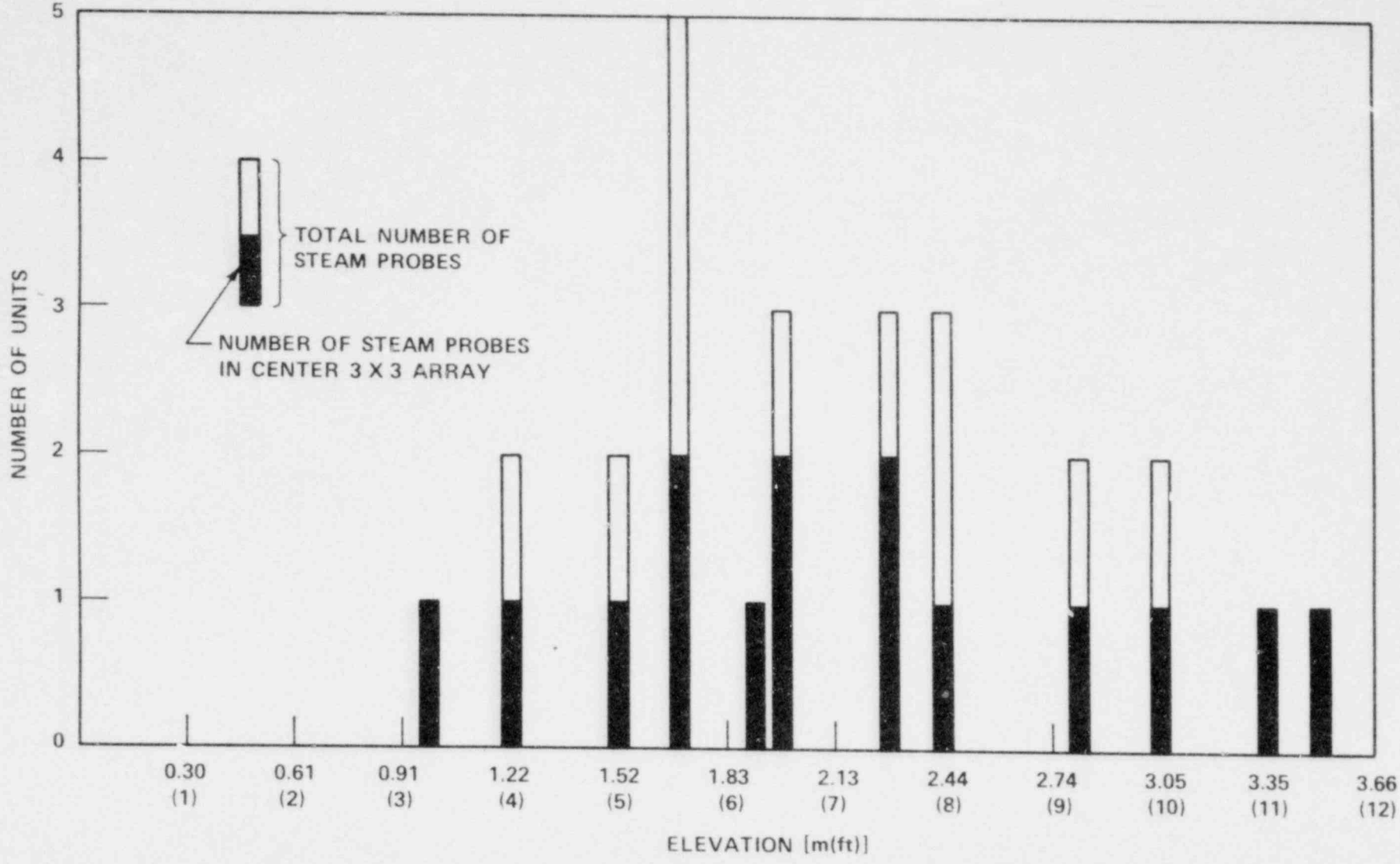

Figure 7-4. 21-Rod Bundle Flow Blockage Task Steam Probe Summary

16,047-34

redundancy. It is expected that these elevations will quench relatively rapidly and will be of limited use later in the test, as demonstrated by the FLECHT skewed power profile tests.[1] Steam probe redundancy begins at 1.22 m (48 in.) and continues through 3.05 m (120 in.), with the exception of the 1.91 m (75.25 in.) and 2.59 m (102 in.) elevations. Steam probes are concentrated immediately upstream and downstream of the blockage zone to determine axial and radial effects of blockage on steam temperature.

7-5. Blockage Sleeve Instrumentation

The placement of blockage sleeves on the heater rod to simulate prototypical subchannel flow blockage adds a thermal resistance to the heater rod. Since this thermal resistance is a function of the sleeve temperature, it is necessary to measure the temperature of the blockage sleeve so that the heat transfer to the coolant can be determined. Also, it is desirable to know the quench temperature and quench time of the sleeve (see appendix J).

A 0.81 mm (0.032 in.) diameter thermocouple will be embedded in the blockage sleeve at the point of maximum strain. The thermocouple lead will run downstream of the blockage sleeve in the flow subchannel to the periphery of the bundle and out of the top of the bundle.

The azimuthal orientation of the blockage sleeve thermocouple (see figures H-27 and H-28) will be essentially identical to that of the heater rod thermocouple at that elevation, so that the rod heat flux and sleeve thermal resistance can both be determined for a given subchannel.

The blockage sleeve attachment and thermocouple concept were evaluated in a single-rod test. A blockage sleeve with an embedded thermocouple was attached to a heater rod and subsequently cycled in a single-rod test. The sleeve and rod temperatures were recorded throughout the heatup and quench cycle.

The heater rod and blockage sleeve were subjected to an adiabatic heatup cycle until a specified clad temperature was reached, at which time flood was initiated with room-temperature water. The power during the heatup cycle was 2.3 kw/m

1. Lilly, G. P., et al., "PWR FLECHT Skewed Profile Low Flooding Rate Test Series Evaluation Report," WCAP-9183, November 1977.

(0.7 kw/ft), subsequently reduced to 1.8 kw/m (0.55 kw/ft) at time of flood. After 180 seconds, the power was reduced to 1.4 kw/m (0.42 kw/ft) until such time that all thermocouples indicated quench. The sequence of testing is shown below:

Number of Cycles	Initial Clad Temperature at Time of Flood [°C (°F)]	Flooding Rate [cm/sec (in./sec)]
1-2	538 (1000)	3.8 (1.5)
3-12	1093 (2000)	3.8 (1.5)
13-22	1093 (2000)	2.0 (0.8)

Test results are presented in appendix K.

A short mockup of the 21-rod bundle will be built to assess the bundle instrumentation (steam probes and blockage sleeve thermocouples) routing techniques and bundle building steps. This mockup will be approximately 1.78 m (70 in.) long and will be made of 0.95 cm (0.375 in.) diameter tubing. Three grid spans will be incorporated in the mockup.

7-6. Differential Pressure Measurements

Differential pressure measurements are made every 0.30 m (1 ft) along the length of the bundle to determine mass accumulation in the bundle. Differential pressure transmitters [$\pm 3.7 \times 10^3$ Pa ($\pm$ 15 inches wg)] are utilized to obtain an accurate mass accumulation measurement representative of an average across the bundle. An additional cell measures the overall pressure drop from the bottom to the top of the heated length.

These transmitters will also be used to measure the frictional and form losses across the grid, rods, and blockage sleeves in hydraulic characteristics tests, which will be performed prior to the single-phase steam and heat transfer tests. These pressure transmitters are accurate to $\pm$0.20 percent of full scale.

7-7. Power Measurements

Two instrumentation channels are devoted to measurement of power into the bundle. One is used as a primary measurement from which power is controlled by

the computer software. One independent power measurement will be used for data reduction purposes.

7-8. Upper Plenum

The upper plenum (figure 7-5) is an important component of the FLECHT loop. The upper plenum is utilized to separate the liquid and steam phases in close proximity to the test section so that accurate mass and energy balances can be accomplished. A differential pressure cell connected between the top and bottom of the upper plenum is used to measure liquid accumulation within this component. Liquid will collect at the bottom of the upper plenum before draining into the carryover tank. System pressure is controlled from a transducer located in the upper plenum for constant flooding rate tests. Another transducer is connected to the computer for system pressure data acquisition.

Two upper plenum thermocouples are designed to measure the fluid temperature at upper plenum exit and in the upper plenum extension. These thermocouples should indicate the location and presence of liquid in the upper plenum and housing extension. An aspirating steam probe located in the upper plenum at the bundle exit is utilized to measure vapor nonequilibrium temperature. Provisions will also be made in the upper plenum to insert endoscopes.

7-9. Lower Plenum

The only instrumentation found in the lower plenum (figure 7-5) is a fluid thermocouple, which will be used to measure inlet subcooling as water floods the bundle. Two fluid thermocouples located in the injection line will be utilized as a backup to the lower plenum fluid thermocouples.

7-10. Housing

Housing wall temperatures will be measured to compute housing heat release as part of the overall mass and energy balance analysis. Housing wall temperature measurements will also be used to evaluate bowing effects.

A total of 38 thermocouples, distributed axially and azimuthally on the housing, will be recorded by the computer.

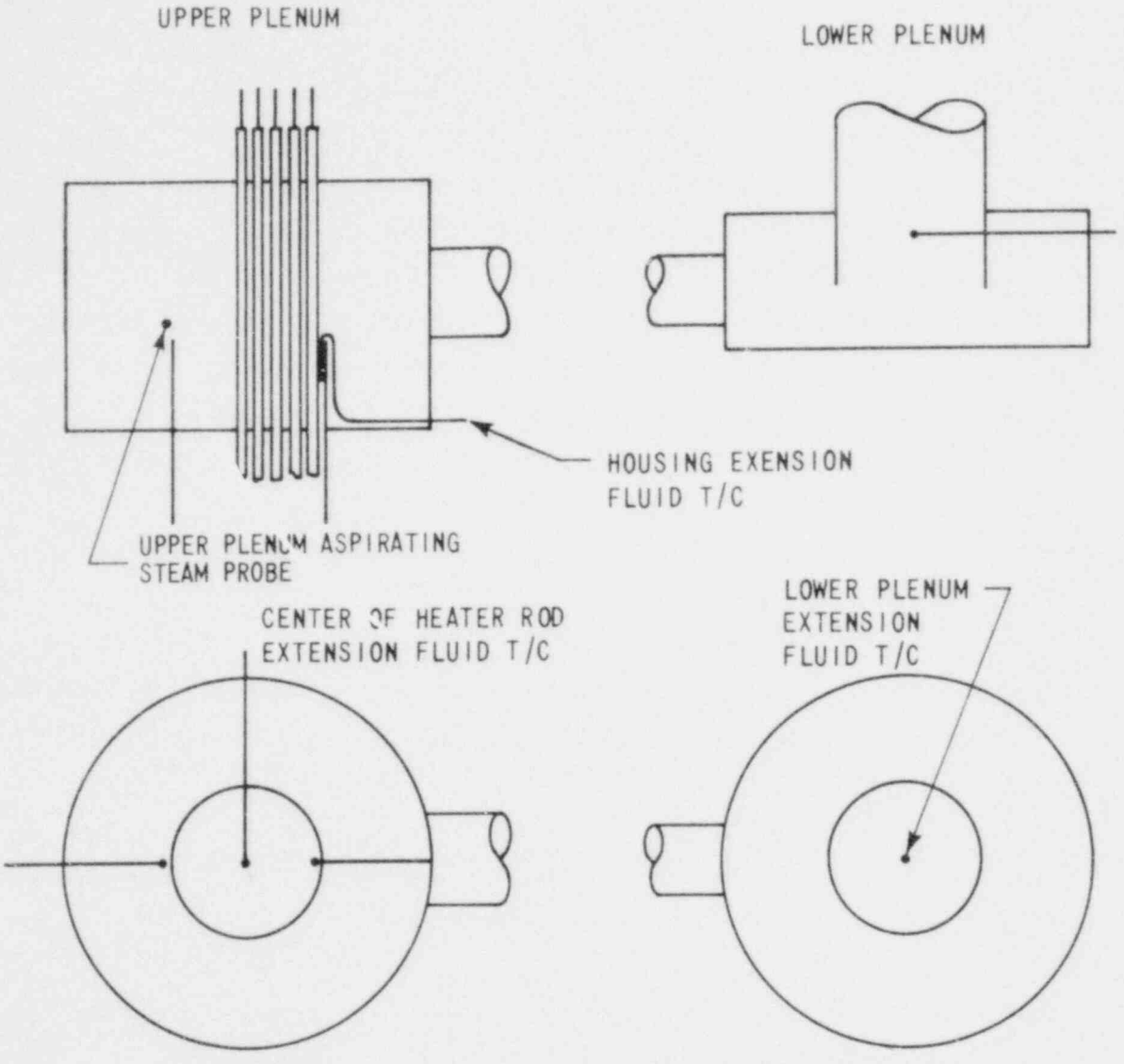

Figure 7-5. Upper and Lower Plenum Thermocouple Location for 21-Rod Flow Blockage Task

7-11. LOOP INSTRUMENTATION

Thirty-eight computer channels have been assigned to the collection of temperature, flow, and pressure data throughout the loop, exclusive of the instrumentation found in the upper and lower plenum, bundle, and housing (figure 7-6). This instrumentation includes 14 fluid thermocouples, 3 turbine meters, 1. differential pressure cells, and 3 pressure cells.

The 14 fluid thermocouples are placed in the water and steam supply systems, the exhaust line, the carryover tank, the steam separator, the steam separator drain tank, the crossover leg (gravity reflood tests), and the downcomer (gravity reflood tests). The fluid thermocouples are utilized to measure the temperature of either stored or injected flow. Two of these thermocouples are utilized in aspirating steam probes placed in the elbows of the exhaust line on either side of the steam separator. These steam probes are designed to measure vapor nonequilibrium in the test section exit and the desuperheating effect of the steam separator. The design of this steam probe is similar to that used in the unblocked bundle test series.(1)

The seven wall thermocouples to be monitored by the computer have been placed on the carryover tank, steam separator, steam separator drain tank, and exhaust line. This instrumentation is utilized to control the heatup period such that component wall temperatures are at T_{SAT} + 11.1°C (T_{SAT} + 20°F). This instrumentation is also used to estimate the heat release from the fluid to the loop components during the test.

The three turbine meters are utilized to measure the flow rate of injected water in both the forced flooding and gravity reflooding tests. One turbine meter is used to measure the injected flow for the forced flooding tests, and two turbine meters, one in the injection line and one in the crossover leg, are used to measure flow for the gravity reflooding tests. The turbine meter in the crossover leg is bidirectional, to measure both forward and reverse flow into and out of the test section. A turbine

1. Hochreiter, L. E., et al., "PWR FLECHT SEASET Unblocked Bundle, Forced and Gravity Reflood Task: Task Plan Report," NRC/EPRI/Westinghouse-3, March 1978.

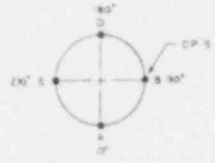
90°
D
DP 5
270° E
S 90°
A
OF

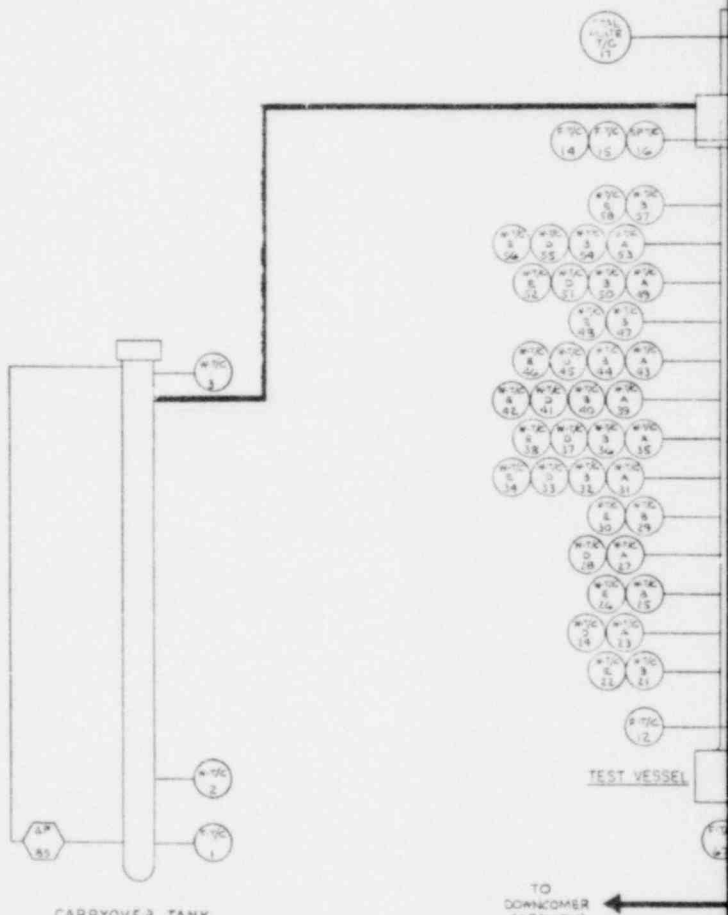
TEST VESSEL
CARRYOVER TANK
TO
DOWNCOMER
(GRAVITY)

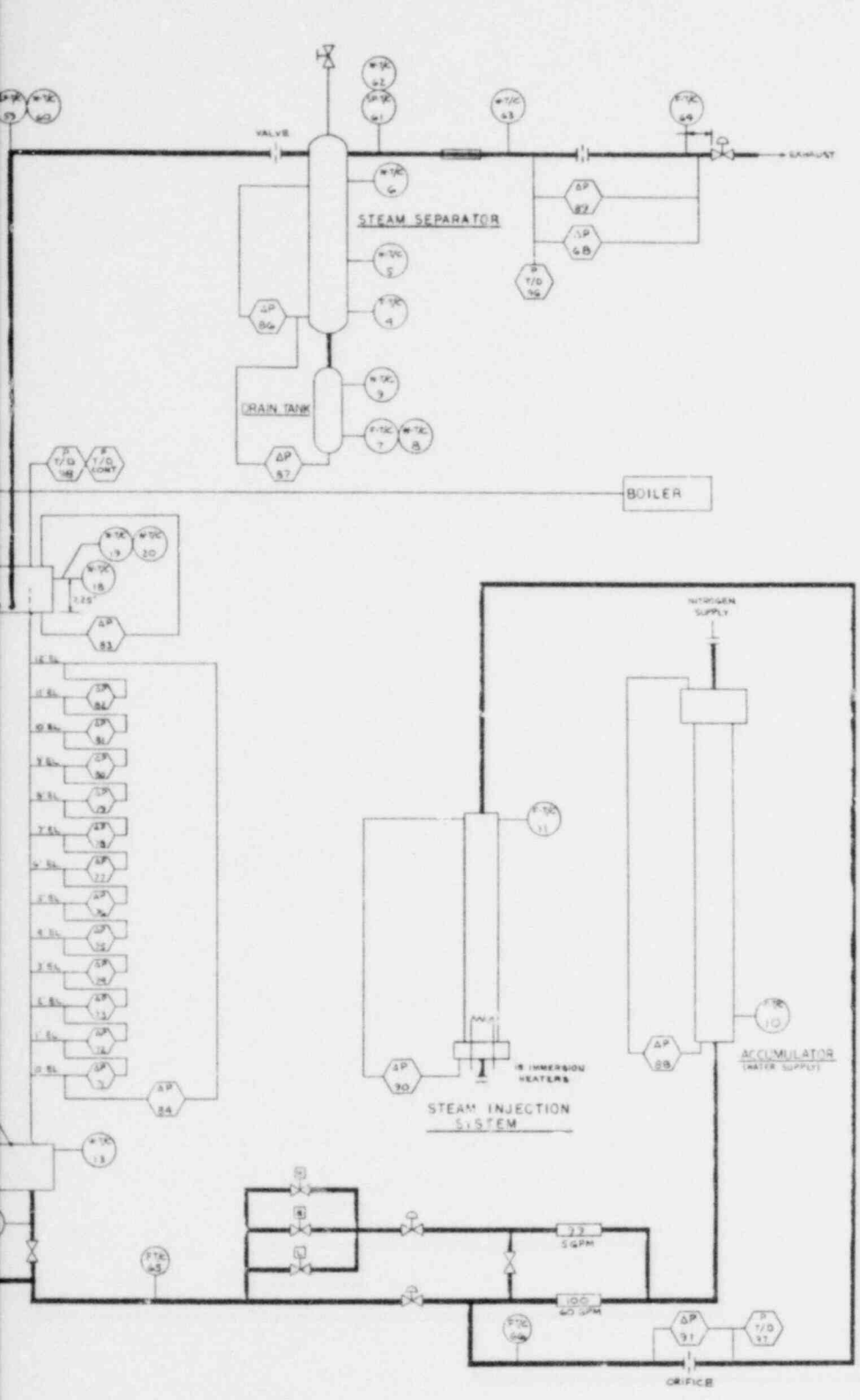

LOOP NO.	DESCRIPTION	COMP CHAN	FLUKE CHAN	T.E. CHAN
1	CARRYOVER TANK EL FLUID T/C	300	35	
2	" " EL WALL T/C	301	31	
3	" " EL WALL T/C	302	32	
4	STEAM SEPARATOR EL FLUID T/C	303		
5	" " EL WALL T/C	304		
6	" " EL WALL T/C	305	33	
7	DRAIN TANK EL FLUID T/C	306		
8	" " EL WALL T/C	307	36	
9	" " EL FLUID T/C	308		
10	ACCUMULATOR EL FLUID T/C	309	37	
11	STEAM INJECTION SYSTEM EL FLUID T/C	310	45	
12	LOWER PLENUM FLUID T/C	311		
13	" " WALL T/C	312	39	
14	UPPER PLENUM #1 FLUID T/C	313		
15	" " #2 FLUID T/C	314		
16	" " STEAM PROBE T/C	315		
17	" " SEAL PLATE T/C	316		
18	" " 90° WALL T/C	317		
19	" " 180° WALL T/C	318	30	
20	" " 270° WALL T/C	319		
21	0 FT 90° HOUSING WALL T/C	320		
22	1 FT 0°	321		
23	" 90°	322		
24	" 180°	323		
25	" 270°	324		
26	2 FT 0°	325		
27	" 90°	326		
28	" 180°	327		
29	" 270°	328		
30	3 FT 0°	329		
31	" 90°	330		
32	" 180°	331		
33	" 270°	332		
34	4 FT 0°	333		
35	" 90°	334		
36	" 180°	335		
37	" 270°	336		
38	5 FT 0°	337		
39	" 90°	338		
40	" 180°	339		
41	" 270°	340		
42	6 FT 0°	341		
43	" 90°	342		
44	" 180°	343		
45	" 270°	344		
46	7 FT 0°	345		
47	" 90°	346		
48	" 180°	347		
49	" 270°	348		
50	8 FT 0°	349		
51	" 90°	350		
52	" 180°	351		
53	" 270°	352		
54	9 FT 0°	353		
55	" 90°	354		
56	" 180°	355		
57	" 270°	356		
58	10 FT 0°	357		
59	ELBOW SETN UPPER PLENUM W/STM SEP STM PROBE T/C	358		
60	" " " " WALL T/C	359	34	
61	ELBOW SETN STM SEP/EXHAUST LINE STM PROBE T/C	360		
62	" " " " WALL T/C	361		
63	EXHAUST LINE BEFORE ORIFICE PLATE WALL T/C	362		
64	" " FLOW VALVE FLUID T/C	363		
65	INJECTION LINE TO LOWER PLENUM FLUID T/C	364		
66	S.I. SYSTEM ORIFICE FLUID T/C	365	40	
67	INJECTION LINE TO LOWER PLENUM FLUID T/C	366	38	
68	EXHAUST ORIFICE ΔP - LOW RANGE	367		
69				
70				
71	0 TO 1 FT HOUSING ΔP	368	0	
72	1 TO 2 FT	369	1	
73	2 TO 3 FT	370	2	
74	3 TO 4 FT	371	3	
75	4 TO 5 FT	372	4	
76	5 TO 6 FT	373	5	
77	6 TO 7 FT	374	6	
78	7 TO 8 FT	375	7	
79	8 TO 9 FT	376	8	
80	9 TO 10 FT	377	9	
81	10 TO 11 FT	378	10	
82	11 TO 12 FT	379		
83	UPPER PLENUM ΔP	380	6	
84	OVERALL HOUSING ΔP	381	3	10" H2O
85	CARRYOVER TANK ΔP	382	4	0-5 PSI
86	STEAM SEPARATOR ΔP	383	5	
87	STEAM LINE	384	6	0-100
88	ACCUMULATOR ΔP	385	7	0-5 PSI
89	EXHAUST ORIFICE ΔP LOW RANGE	386	8	0-10
90	S.I. SYS ΔP LEVEL DURING COOLING TEST	387	9	
91	S.I. SYS ORIFICE ΔP STEAM COOLING	388	10	
92				
93				0-5K
94				
95				
96	EXHAUST LINE ORIFICE PRESS	389		
97	S.I. LINE AFTER FIX ORIFICE PRESS	390		
98	UPPER PLENUM PRESS	391		0-100 PSIG
99	TURBINE METER 1 GPM	392		0-1 GPM
100	40 GPM	393		0-40 GPM
101		394		0-100 GPM

Figure 7-6. 21-Rod Bundle Flow Blockage Task Instrumentation Schematic Diagram (sheet 1 of 2) (Drawing No. 1460E40)

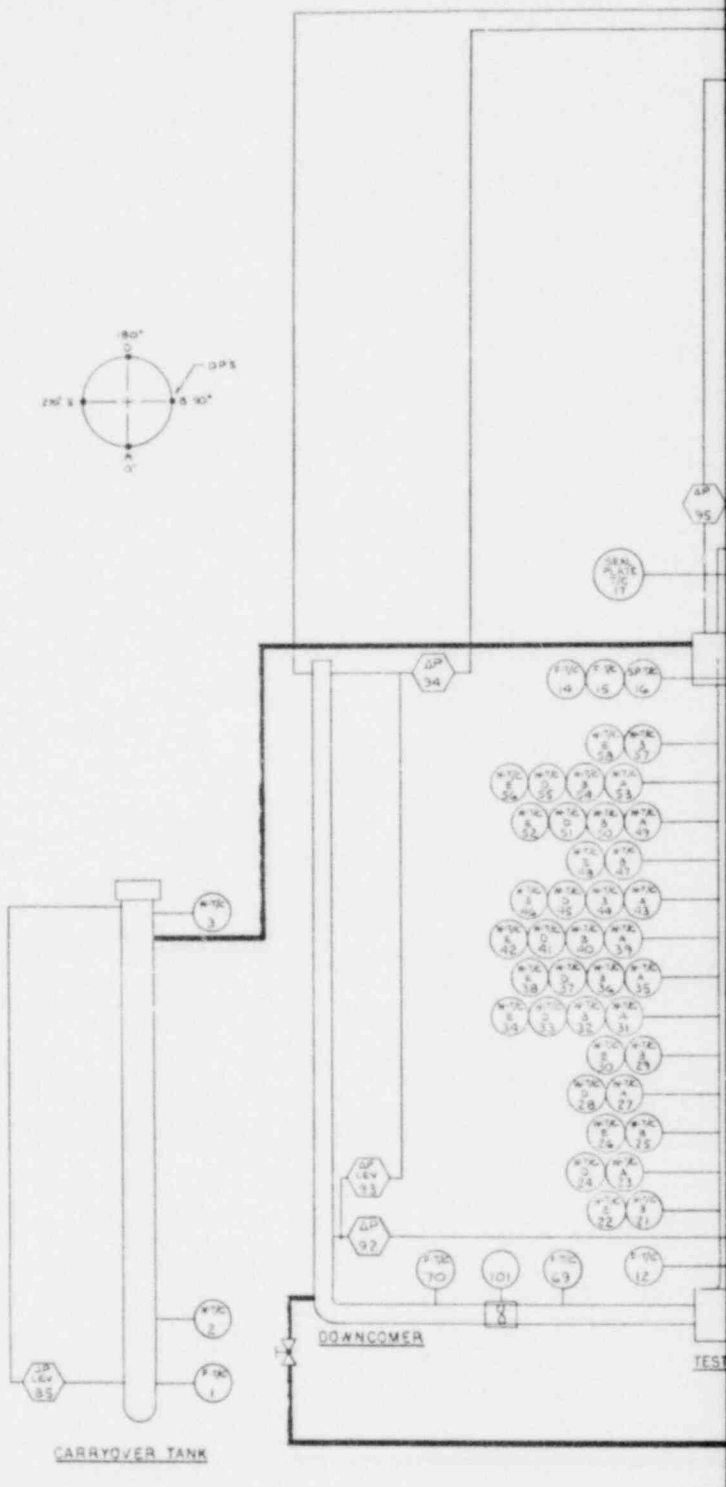
180°
270°
90°
0°
DP'S
DOWNCOMER
CARRYOVER TANK

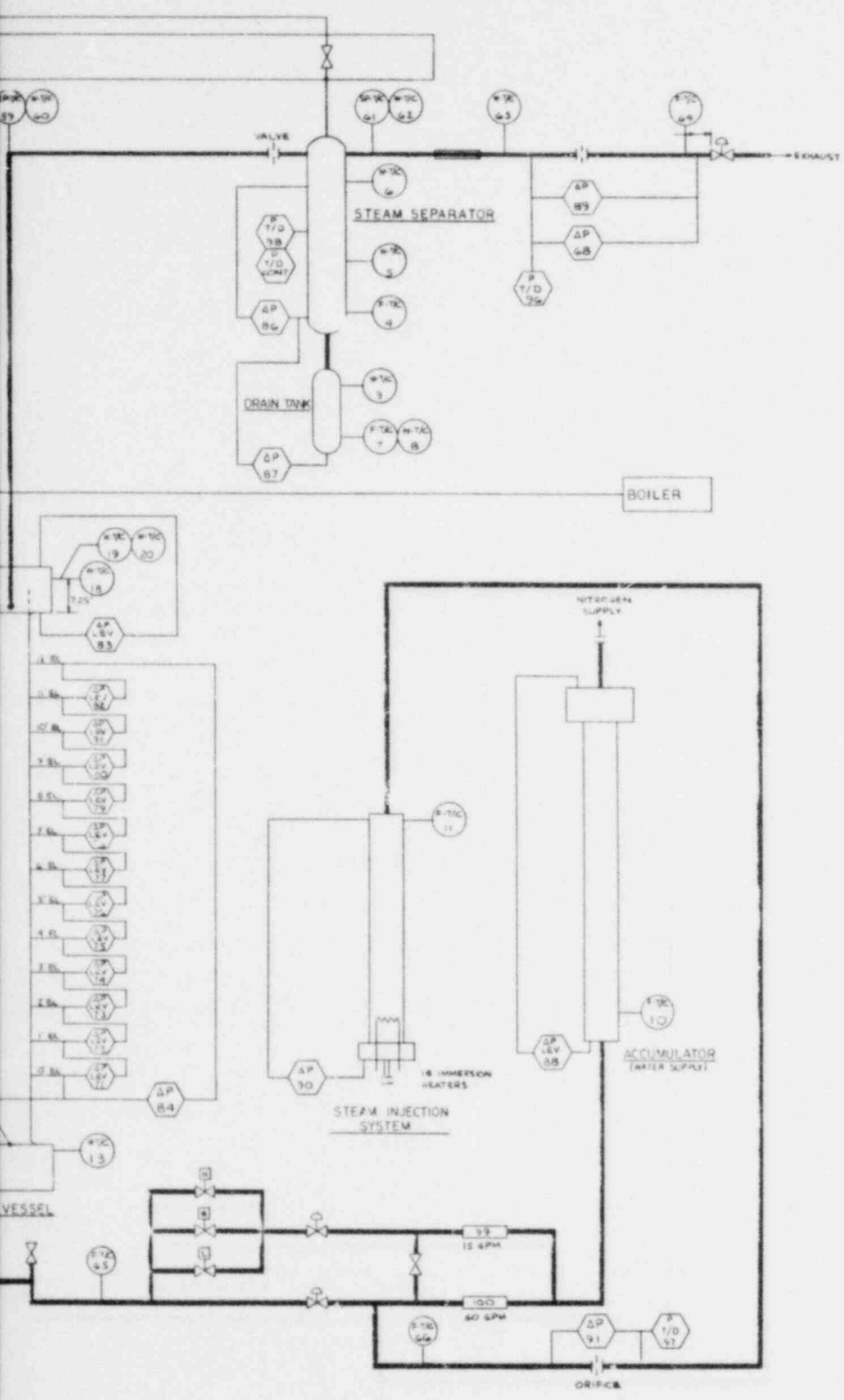

LOOP & D #	DESCRIPTION	COMP CH	FLUKE CH	T I CH
1	CARRYOVER TANK EL FLUID T/C	300	15	
2	" EL WALL T/C	301	31	
3	" EL WALL T/C	302	12	
4	STEAM SEPARATOR EL FLUID T/C	303		
5	" EL WALL T/C	304		
6	" EL WALL T/C	305	23	
7	DRAIN TANK EL FLUID T/C	306		
8	" EL WALL T/C	307	36	
9	" EL WALL T/C	308		
10	ACCUMULATOR EL FLUID T/C	309	37	
11	STEAM IN SYS EL FLUID T/C	310	46	
12	LOWER PLENUM FLUID T/C	311		
13	" WALL T/C	312	39	
14	UPPER PLENUM #1 FLUID T/C	313		
15	" #2 FLUID T/C	314		
16	" STEAM PROBE T/C	315		
17	" SEAL PLATE T/C	316		
18	" 90° WALL T/C	317		
19	" 90° WALL T/C	318	20	
20	" 220° WALL T/C	319		
21	0 FT 90° HOUSING WALL T/C	320		
22	" 1.25"	321		
23	1 FT 0°	322		
24	" 90°	323		
25	" 180°	324		
26	1 FT 0°	325		
27	" 90°	326		
28	" 180°	327		
29	2 FT 0°	328		
30	" 90°	329		
31	" 180°	330		
32	3 FT 0°	331		
33	" 90°	332		
34	" 180°	333		
35	4 FT 0°	334		
36	" 90°	335		
37	" 180°	336		
38	5 FT 0°	337		
39	" 90°	338		
40	" 180°	339		
41	6 FT 0°	340		
42	" 90°	341		
43	" 180°	342		
44	7 FT 0°	343		
45	" 90°	344		
46	" 180°	345		
47	8 FT 0°	346		
48	" 90°	347		
49	" 180°	348		
50	9 FT 0°	349		
51	" 90°	350		
52	" 180°	351		
53	10 FT 0°	352		
54	" 90°	353		
55	" 180°	354		
56	11 FT 0°	355		
57	" 90°	356		
58	" 180°	357		
59	SLOW DETN UPPER PLENUM/STM SEP STM PROBE T/C	358		
60	" EXIT T/C	359	34	
61	SLOW DETN STM SEP/EXHAUST LINE STM PROBE T/C	360		
62	" EXIT T/C	361		
63	EXHAUST LINE BEFORE ORIFICE PLATE WALL T/C	362		
64	" FLUID T/C	363		
65	INJECTION LINE TO LOWER PLENUM FLUID T/C	364		
66	C.C.S.S. ORIFICE FLUID T/C	365		
67		366		
68	EXHAUST ORIFICE ΔP HIGH RANGE	367		
69	DOWNCOMER LINE AFTER TURBO PROBE FLUID T/C	368	41	
70	" ORIFICE	369		
71	0 TO 1 FT HOUSING ΔP	370	0	
72	1 TO 2 FT	371		
73	2 TO 3 FT	372	1	
74	3 TO 4 FT	373	2	
75	4 TO 5 FT	374	3	
76	5 TO 6 FT	375	4	
77	6 TO 7 FT	376	5	
78	7 TO 8 FT	377	6	
79	8 TO 9 FT	378	7	
80	9 TO 10 FT	379	8	
81	10 TO 11 FT	380	9	
82	11 TO 12 FT	381	10	
83	UPPER PLENUM ΔP	382		
84	OVERALL HOUSING ΔP	383	13	C 100
85	CARRYOVER TANK ΔP	384	14	C 84
86	STEAM SEPARATOR ΔP	385	15	
87	DRAIN TANK ΔP	386	16	C LOW
88	ACCUMULATOR ΔP	387	17	C HIGH
89	EXHAUST ORIFICE ΔP LOW RANGE	388	18	C 50
90	C.C.S.S. ΔP LOOP SYSTEM CALIBRATION TEST	389	19	
91	C.C.S.S. ORIFICE ΔP STEAM COOLING	390	20	
92	DOWNCOMER/D FT EL ΔP	391	21	
93	" LOOP ΔP	392	22	C 84
94	STEAM SEPARATOR ΔP	393	23	
95	UPPER PLENUM/STEAM SEPARATOR ΔP	394	24	
96	EXHAUST LINE ORIFICE PRESS	395		
97	C.C.S.S. LINE AFTER THE ORIFICE PRESS	396		
98	STEAM SEPARATOR PRESS	397		C 96
99	TURBINE METER 1 GPM	398		C 98
100	" 60 GPM	399		C 94
101	BI DIRECTIONAL TURBOPROBE	400		C GEN

Figure 7-6. 21-Rod Bundle Flow Blockage Task Instrumentation Schematic Diagram (sheet 2 of 2) (Drawing No. 1460E41)

meter is also required to measure the high flow in the hydraulic characteristics tests; however, this turbine meter will replace the gravity reflooding injection line turbine meter. Together, these turbine meters require three computer channels.

The 11 differential pressure cells are used to measure injected flow or separated water accumulation. The accumulator tank has a differential pressure cell which can be utilized as a backup to or a check on the injection line turbine meters. The steam supply system for the steam cooling test utilizes an orifice plate coupled with a differential pressure cell, fluid thermocouple, and pressure cell to measure the injected steam flow. The three storage tanks on the downstream side of bundle, the carryover tank, the steam separator, and the steam separator drain tank, are each instrumented with differential pressure cells to measure liquid accumulation. The exit steam flow is measured downstream of the steam separator utilizing an orifice plate, differential pressure cell, fluid thermocouple, and pressure cell. Four additional differential pressure cells are utilized in the gravity reflood tests to measure mass accumulated in the downcomer, and to measure differential pressures between the downcomer and bundle, between the upper plenum and steam separator, and between the top of the downcomer and the steam separator.

The three loop pressure cells are utilized to measure the absolute pressure at the orifice plates on the bundle inlet and outlet, and at the steam separator in the gravity reflood tests.

The loop instrumentation has been set up to provide redundant measurements and eliminate computer channel reassignments between forced flooding tests and gravity reflood tests, as previously required in unblocked bundle tests. This instrumentation design will allow for efficient facility turnaround for conducting the tests.

7-12. DATA ACQUISITION AND PROCESSING SYSTEM

Three types of recording systems will monitor the instrumentation on the FLECHT facility. Figure 7-6, sheets 1 and 2, are the facility instrumentation schematic diagrams which can be used in conjunction with table 7-2 to locate and identify all

TABLE 7-2

BUNDLE INSTRUMENTATION FOR 21-ROD BUNDLE FLOW BLOCKAGE TASK

Instrumentation	Number of Channels Used		
	CDAS	Fluke	Strip Chart Recorders
Rod Bundle			
Heater rod thermocouples	168	-	4
Blockage sleeve thermocouples[a]	13	-	-
Steam probes	26	-	-
Differential pressure cells	13	13	1
Power			
Primary	1	-	1
Independent	1	-	-
Housing			
Wall thermocouples	38	-	- -
Upper Plenum			
Pressure	1	-	1
Differential pressure cell	1	1	-
Fluid thermocouples	2	-	-
Wall thermocouples	4	1	-
Steam probe	1	-	-

a. All blocked bundle

TABLE 7-2 (cont)

BUNDLE INSTRUMENTATION FOR 21-ROD BUNDLE FLOW BLOCKAGE TASK

Instrumentation	Number of Channels Used		
	CDAS	Fluke	Strip Chart Recorders
Lower Plenum			
Fluid thermocouples	1	1	-
Wall thermocouples	1	-	-
Loop			
Water supply system			
Fluid thermocouples	3	3	1
Wall thermocouples	-	-	-
Flow meters:			
Turbine meter	2	2	2
Accumulator differential pressure cell	1	-	1
Steam supply system			
Fluid thermocouples	2	-	-
Wall thermocouples	-	1	-
Differential pressure cell	2	-	-
Pressure cell	1	-	-
Exhaust system			
Steam probe	2	-	-
Fluid thermocouples	4	2	-

TABLE 7-2 (cont)

BUNDLE INSTRUMENTATION FOR 21-ROD BUNDLE FLOW BLOCKAGE TASK

Instrumentation	Number of Channels Used		
	CDAS	Fluke	Strip Chart Recorders
Wall thermocouples	7	8	-
Pressure	1	-	-
Differential pressure cells:			
Tank levels	3	-	2
Orifice plate ΔP	1	-	1
Gravity reflood test (additional)			
Differential pressure cells:			
Downcomer/bundle	1	-	-
Downcomer level	1	-	1
Upper plenum/steam separator	1	-	-
Downcomer/steam separator	1	-	-
Bidirectional turbine meter	1	-	-
Crossover leg			
Fluid thermocouple	2	-	-
Downcomer wall thermocouple	-	-	-
Crossover pipe wall	-	1	-
Steam separator pressure	1	-	-
Injection line fluid thermocouple	1	-	-
Total channels	309	33	15

the facility instrumentation monitored by the various data acquisition systems. The data acquisition consists of a PDP-11 computer, a Fluke data logger, and Texas Instruments strip chart pen recorders.

7-13. Computer Data Acquisition System (CDAS)

The CDAS, the primary data collecting system used on the FLECHT facility, consists of a PDP-11 computer and associated equipment. The system can record 309 channels of analog input data representing bundle and system temperatures, bundle power, flows, and absolute and differential pressures. The computer is capable of storing approximately 2500 data scans for each of the 309 analog input channels.

Typically, each data channel can be recorded once every second until flood, then once every half second for 200 seconds, and then back to once every second thereafter to a maximum of 2500 data points.

The computer software has the following features:

-- A calibration file to convert raw data into engineering units

-- A preliminary data reduction program which transfers the raw data stored on disk to a magnetic tape, in a format which is compatible for entry into a Control Data Corporation 7600 computer

-- A program called FLOOK which reduces raw data into engineering units; a program called FVALID which prints out key data used in validating FLECHT SEASET runs; and a PLOT program, which plots up to four data channels on a single graph. All three programs are utilized to quickly understand and evaluate test runs.

In addition to its role as a data acquisition system, the computer also plays a key role in the performance of an experimental run. Important control functions include initiation and control of reflood flow and power decay as well as termination of bundle power in the event of an overtemperature condition. Table 7-2 lists the instrumentation recorded on the CDAS.

7-14. Fluke Data Logger

The Fluke data logger has 60 channels of analog input for monitoring loop heatup and aiding in equipment troubleshooting. The Fluke records key facility vessel and fluid temperatures, displaying temperature directly in ^{o}F. This makes the task of monitoring loop heatup more efficient. The Fluke also records millivolt data from the test section differential pressure cells, allowing the operator to keep a check on their operation and repeatability. The Fluke is further used to trouble-shoot problems with loop equipment in a quick and convenient manner. Table 7-2 lists channels monitored on the Fluke.

7-15. Multiple Pen Strip Chart Recorders

Four Texas Instruments strip chart recorders are used to record bundle power; selected bundle thermocouples; reflood line turbine meter flows; accumulator, separator drain tank, housing, and carryover tank levels; and exhaust orifice differential pressure. These recorders give the loop operators and test directors immediate information on test progress and warning in the event of system anomalies. The strip charts give an analog recording of critical data channels as a backup to the computer. Strip charts are also needed during the heatup phase of the facility when the computer is not available. Table 7-2 lists the channels associated with the strip chart recorders.

7-16. DATA VALIDATION CRITERIA AND PROCEDURES

The data validation process is initiated when all instrumentation is checked for proper operation prior to the actual running of a test. A reading from each channel is recorded and compared to the expected value for that channel. In this manner, an abnormal reading will indicate a problem in that channel and corrective actions will be taken before the actual test is run. This channel verification procedure will increase the probability that all instrumentation will work properly once a test is under way.

If some instrumentation fails just prior to or during a test but the remaining instrumentation is sufficient to calculate overall mass balances, void fraction in the test section, some heat transfer coefficients, fluid temperatures, and carryout fraction, then the run may still be considered valid. If the instrumentation is not

sufficient for these calculations, the run is considered invalid and will be repeated. When too many rod bundle and/or fluid thermocouples fail in critical locations, serious consideration will be given to discontinuing testing and repairing or replacing the affected channels. In any event, an attempt will be made to repair any failure before another test is performed.

The following criteria are used to determine if sufficient instrumentation exists for conducting a valid test:

-- The number of heater rod thermocouples required to be functioning properly for a valid test at each elevation are specified in table 7-3.

-- For flooding rates above 38.1 mm/sec (1.5 in./sec), the upper plenum differential pressure cell is required to be functioning properly for a valid test. Of the 12 bundle differential pressure cells, no more than one can fail for the test to be valid.

-- Sufficient blockage sleeve thermocouples are required to be functional for a valid test.

-- Of the test section steam probes, 10 have been selected at the 1.70 (two each), 1.98 (two each), 2.29 (two each), 2.44 (two each), 2.82, and 3.05 m (67, 78, 90, 96, 111, and 120 in.) elevations along with the two exit steam probes as required to be functional for a valid test.

-- The upper plenum pressure transducer is required to be functioning properly for all tests except the gravity reflood tests. The steam separator pressure transducer is required to be functional for gravity reflood tests.

-- For a valid test, one lower plenum and one upper plenum fluid thermocouple are also required to be functional.

-- It is required, for the test section bundle power supply, that the one independent power meter be functioning properly for a valid test. Also, this power measurement must be within the accuracy range specified for a test.

TABLE 7-3

OPERABLE HEATER ROD THERMOCOUPLES REQUIRED FOR DATA VALIDATION

Elevation [m (in.)]	Number of Operable Thermocouples Required at Each Elevation/Center 3x3 Rod Array
0.305 (12)	2
0.61 (24)	2
0.99 (39)	2
1.22 (48)	2
1.52 (60)	2
1.70 (67)	2
1.78 (70)	3/1
1.80 (71)	4/2
1.83 (72)	6/3
1.88 (74)	7/4
1.91 (75.25)	4/2
1.93 (76)	6/3
1.955 (77)	4/3
1.98 (78)	6/3
2.13 (84)	5/2
2.19 (90)	7/3
2.44 (96)	5/2
2.59 (102)	5/1
2.82 (111)	5/2
3.05 (120)	5/1
3.35 (132)	2
3.51 (138)	2

-- Four loop fluid thermocouples are required for a valid test, as follows:

(1) Carryover tank - 0 m (0 ft) elevation
(2) Steam separator drain tank - 0 m (0 ft) elevation
(3) Exhaust orifice
(4) Accumulator fluid thermocouple

-- Four additional loop wall thermocouples are required for a valid test, as follows:

(1) Upper plenum
(2) Carryover tank - 0 m (0 ft) elevation
(3) Steam separator drain tank - 0 m (0 ft) elevation
(4) Test section hot leg

-- The injection line turbine meter must be functioning properly for a valid test.

-- Three liquid level measurements are required for a valid test, as follows:

(1) Carryover tank
(2) Steam separator
(3) Accumulator

-- At the exhaust orifice, both the orifice differential pressure measurement and the static pressure measurement upstream of the orifice are required to be functional.

-- For the gravity reflood tests, the additional instrumentation required to be functioning is as follows:

(1) Downcomer level differential pressure cell
(2) Bidirectional turbine meter
(3) Injection line turbine meters
(4) Steam separator pressure transducer
(5) Upper plenum/steam separator differential pressure cell
(6) Downcomer/steam separator differential pressure cell

-- For the single-phase steam heat transfer tests, the orifice differential pressure measurement, the static pressure measurement, and the fluid temperature measurement on the steam injection system are required to be functional.

A run specification and validation sheet will be completed (appendix L). This sheet specifies the initial test conditions and the validation requirements for each FLECHT SEASET 21-rod bundle test. It also provides space for comments on run conditions, causes for terminating and invalidating a run, instrumentation failures, preliminary selected thermocouple data, and drained water weights from collection tanks and the test section.

Once the instrumentation has checked out satisfactorily and the test has been run, the data for each channel are scrutinized to see if the system behaved as expected. Abnormal behavior of a data channel is investigated to determine if it is due to equipment malfunction or to a physical phenomenon. These procedures, along with periodic equipment calibrations, are designed to assure that the data recorded are accurate and reliable.

Another aspect of data validation is considered once the instrumentation reliability has been determined. The actual test conditions are compared to the parameters specified by the test matrix to see if the run satisfies the test matrix. The facility conditions before initiation of reflood are compared to the expected values for such parameters as bundle power, system pressure, average vessel wall temperature, and hottest thermocouple at the start of reflood. The injection flow is checked against what has been specified and the system pressure is reviewed to see if the system pressure control worked properly.

After the instrumentation is functionally checked and the test parameters and performance compared with the test matrix, the final validation is performed during data analysis. In the process of analysis, a system mass and energy balance is computed. These calculations determine if the data are within the specified accuracy and whether the instrumentation is adequate for analyzing what has happened in the system.

SECTION 8
TEST MATRIX

8-1. INTRODUCTION

Paragraphs 8-2 through 8-21 of this section describe the bench tests and single-phase, forced reflood and gravity reflood shakedown tests required to ensure that the FLECHT SEASET 21-rod bundle test loop will operate properly and perform tests specified in the test matrix. The test matrix (paragraphs 8-22 and 8-23) is designed to meet the task objectives and fulfill the data requirements discussed in sections 3 and 5.

8-2. SHAKEDOWN TEST MATRIX

Prior to conducting the reflood tests outlined in paragraph 8-23, a series of shakedown tests will be run on the test facility. These shakedown tests will be conducted not only on separate facility components prior to final assembly (bench tests), but also on the completely assembled test facility.

The purpose of the shakedown tests is to ensure that the instrumentation, control, and data acquisition systems are working properly so that useful and valid data can be obtained during the reflood experiments. Some of the shakedown tests are also intended to verify and adjust control procedures. A brief summary of each shakedown test follows.

8-3. Bench Tests

The following list of tests outlines the portion of the shakedown test matrix that will be conducted on various facility components prior to final assembly of the test facility.

8-4. Steam Probe Check - This test is intended to compare the self-aspirating steam probe measurements with those from the steam probe in the unblocked bundle facility. The self-aspirating thimble tube steam probe will be placed

adjacent to the thimble tube steam probe; it will subsequently be operational for all tests in the test matrix.[1]

8-5. Thermocouple Wiring Connection Checks - The purpose of this test is to check the continuity of each thermocouple wiring connection from the patch board to the computer. If any deviation is observed, the circuit will be checked, repaired, and retested.

8-6. Forced Reflood Configuration Testing

The following list of tests outlines another portion of the shakedown test matrix. It covers those shakedown tests conducted on the completely assembled test facility in the forced reflood configuration.

8-7. Heater Rod Power Connection Check - This test is intended to check the continuity of each heater rod power connection at the fuse panel. If any abnormal reading is observed, the circuit will be checked, repaired, and retested.

8-8. Instrumented Heater Rod Radial Location and Corresponding Thermocouple Checks - This test is intended to check the following items:

-- For each instrumented heater rod, all corresponding thermocouples are checked for correct computer channel hookup and proper data recording.

-- During the above check, radial power connections between the fuse panel and the appropriate heater rod are confirmed.

-- The output polarity of each thermocouple at the computer is also checked.

8-9. Heater Rod, Blockage Sleeve, and Steam Probe Thermocouple Axial Location Checks - This test is intended to check the following items:

-- For each bundle thermocouple elevation, all corresponding heater rod, blockage sleeve, and steam probe thermocouples are checked for appropriate computer channel axial hookup and proper recording of data.

1. Hochreiter, L. E., et al., "PWR FLECHT SEASET Unblocked Bundle, Forced and Gravity Reflood Task: Task Plan Report," NRC/EPRI/Westinghouse-3, March 1978.

-- In completing the above check, each heater rod, blockage sleeve, and steam probe thermocouple elevation is confirmed.

8-10. Test Section Differential Pressure Cell Axial Locations, Steam Separator Collection Tank and Carryover Tank Volume, and Level Transmitter Checks - This test is intended to check the following items:

-- Test section differential pressure cells are checked for appropriate computer channel axial hookup.

-- Test section control volumes are established in 30.5 cm (1 ft) increments.

-- The lower plenum volume is checked.

-- The steam separator collection tank and the carryover tank volumes are determined.

-- The steam separator collection tank and the carryover tank level transmitters, along with the test section differential pressure cells, are checked for proper operation.

8-11. Pressure Control Valve Operation, Exhaust Orifice Plate Flow, and Differential Pressure Cell Zero Shift Checks - This test is intended to check the following items:

-- The test section, tank, and orifice differential pressure cells zero readings and zero shifts are checked.

-- The response of the pressure control valve to sudden changes in flow is also checked.

8-12. Turbine Flowmeter Calibration and Flow Control Valve Operation Checks - This test is intended to check the following items:

-- A spot check of turbine meter calibration (for agreement with the full flow range calibrations performed prior to the shakedown tests) is conducted.

-- The flowmeters are checked for appropriate computer channel hookup.

-- Flow control valve response to a continuously variable flooding signal is also checked.

8-13. Carryover Tank, Steam Separator Tank, and Connecting Piping Heatup Checks - This test is intended to evaluate the pretest heatup of the test facility tanks and connecting piping. The heatup of this portion of the test facility is achieved by circulating slightly superheated steam through the facility. Loop thermocouple temperatures are reviewed to determine temperature uniformity of the tanks and piping walls both before and after the steam is injected. The time needed for heating the facility components to the required temperatures is also determined from this test.

8-14. Hydraulic Characteristics Shakedown Test - This shakedown test, a trial run for the complete test facility in the hydraulic characteristics test configuration, is intended to check the following items:

-- A spot check of the turbine meter calibration for agreement with full flow range calibrations performed prior to the shakedown test is conducted.

-- Flow control valve response to step change in the flowrate is checked.

8-15. Low-Power and Low-Temperature Test, Forced Reflood Configuration - This shakedown test, a trial run for the complete test facility in the forced reflood configuration, is conducted according to normal procedures (paragraph 6-12), with care taken to meet all requirements for a valid run (paragraph 7-16). Test conditions are a nominal 0.28 MPa (40 psia) run having low power [1.31 kw/m (0.4 kw/ft)] and low initial clad temperature [(260°C (500°F)].

8-16. Test Facility Special Single-Phase Testing - The shakedown tests outlined in the following paragraphs will employ only single-phase steam flow through the facility in the forced reflood configuration.

8-17. Steam Cooling Shakedown Test - This unpowered shakedown test will be used to examine and adjust control procedures in preparation for the steam cooling

tests described in paragraph 8-22. The following items are specific goals of this steam cooling shakedown test:

-- Pressure control valve response to the initial steam injection into the lower plenum at about 0.31 MPa (45 psia) pressure is observed.

-- The value of the lower plenum pressure is determined, in order to achieve a 0.28 MPa (40 psia) upper plenum setpoint pressure when steady flow conditions have been established.

-- The magnitude of pressure oscillations are studied to determine how well automatic controls can maintain a 0.28 MPa (40 psia) static pressure in the upper plenum with the high steam flow velocity.

-- After the test has been completed, any control adjustments needed to improve the results are determined.

The operation of the steam probes is also checked in this test by comparison with the upper plenum aspirating steam probe.

8-18. Gravity Reflood Configuration Testing

Gravity reflood modifications and testing will be scheduled after completion of the forced reflood testing. The shakedown tests listed below will be conducted on the completely assembled facility after it has been modified for the gravity reflood configuration (paragraph 6-1).

8-19. High-Range Turbine Flowmeter Flow Checks - With the facility modified for the gravity reflood testing, this shakedown test is intended to check the following items:

-- The flowmeters are checked for appropriate computer channel hookup.

-- A spot check of the new high-range turbine meter calibration is made for agreement with the full flow range calibrations conducted prior to the shakedown tests.

8-20. Bidirectional Turbine Meter Flow Checks - With the facility in the gravity reflood configuration, this shakedown test is intended to be a functional check of the bidirectional turbine meter calibration for agreement with its full flow range calibrations. This test is conducted in two phases: the first with the turbine meter oriented in its forward direction and the second with the turbine meter turned 3.14 radians (180 degrees) to check the reverse flow measurements of the instrument. The turbine meter instrumentation is also reviewed for appropriate computer channel hookup.

8-21. Low-Power and Low-Temperature Test, Gravity Reflood Configuration - This shakedown test, a trial run for the complete test facility in the gravity reflood configuration, is conducted according to normal procedures (paragraph 6-12), with care taken to meet all requirements for a valid run (paragraph 7-16). Test conditions are a nominal 0.28 MPa (40 psia) run having low power [1.64 kw/m (0.5 kw/ft)] and low initial clad temperature [457°C (855°F)].

8-22. HYDRAULIC CHARACTERISTICS TEST MATRIX

To evaluate the pressure losses associated with the rod friction, grids, and blockage sleeves, isothermal hydraulic (water) tests will be conducted for the seven blockage configurations prior to conducting the heat transfer tests. These hydraulic tests will be conducted at a Reynolds number in the same range as that expected in the heat transfer tests. The expected range of Reynolds numbers is 2,000 to 15,000, which when simulated by 21.1°C (70°F) water provides flows from 28.4 l/min (7.5 gal/min) to 208.2 l/min (55 gal/min), respectively. This range of Reynolds numbers is based on the assumption that approximately half of the injection water is evaporated into steam. These Reynolds numbers envelop flooding rates from 10.1 mm/sec (0.4 in./sec) to 38.1 mm/sec (1.5 in./sec). Although the text matrix shown in table 8-1 includes a test at 152 mm/sec (6 in./sec), which corresponds to a Reynolds number of approximately 50,000, it is expected that the pressure loss coefficients will not vary significantly for Reynolds numbers greater than 10,000. The following six flowrates will be run for the seven blockage configurations: 37.9, 75.7, 113.6, 151.4, 189.3 and 227.1 l/min (10, 20, 30, 40, 50 and 60 gal/min).

Test No.	Pressure [MPa (psia)]
1	0.276 (40)
2	0.276 (40)
3	0.276 (40)
4	0.276 (40)
5	0.276 (40)
6	0.276 (40)
7	0.276 (40)
8	0.276 (40)
9	0.276 (40)
10	0.136 (20)
11	0.138 (20)
12	0.138 (20)
13	0.276 (40)
14	0.276 (40)
15	0.276 (40)

TABLE 8-1

TEST MATRIX FOR 21-ROD BUNDLE FLOW BLOCKAGE TASK

Rod Initial Temperature [°C(°F)]	Rod Peak Power [kw/m (kw/ft)]	Flow Rate [kg/sec (lb/sec)]	Inlet Subcooling [°C (°F)]	Parameter	Test Series
131 (267)	0.043 (0.013)	0.013 (0.03)	0	Steam	1
131 (267)	0.088 (0.027)	0.027 (0.06)	0	cooling	
131 (267)	0.111 (0.034)	0.033 (0.075)	0	test	
		Flooding Rate [mm/sec (in./sec)]			
871 (1600)	0.884 (0.27)	10.1 (0.4)	78 (140)		
871 (1600)	1.31 (0.4)	16.2 (0.6)	78 (140)	Constant	2
871 (1600)	2.3 (0.7)	20.3 (0.8)	78 (140)	flooding	(reference)
871 (1600)	2.3 (0.7)	25.4 (1.0)	78 (140)	rate	
871 (1600)	2.3 (0.7)	38.1 (1.5)	78 (140)	tests	
871 (1600)	2.3 (0.7)	152.0 (6.0)	78 (140)		
871 (1600)	0.884 (0.27)	10.1 (0.4)	78 (140)	Pressure	3
871 (1600)	1.31 (0.4)	16.2 (0.6)	78 (140)	effect	
871 (1600)	2.3 (0.7)	25.4 (1.0)	78 (140)	tests	
871 (1600)	2.3 (0.7)	25.4 (1.0)	3 (5)	Subcooling	4
871 (1600)	2.3 (0.7)	152.4 (6) (5 sec) 20.3 (0.8) (onward)	78 (140)	Variable stepped flow	5
871 (1600)	2.3 (0.7)	25.4 (1.0)	78 (140)	Repeat test	6

Test No.	Pressure [MPa (psia)]
16	0.276 (40)
17	0.138 (20)

TABLE 8-1 (cont)

TEST MATRIX FOR 21-ROD BUNDLE FLOW BLOCKAGE TASK

Rod Initial Temperature [^{o}C(^{o}F)]	Rod Peak Power [kw/m (kw/ft)]	Flow Rate [kg/sec (lb/sec)]	Inlet Subcooling [^{o}C (^{o}F)]	Parameter	Test Series
871 (1600)	2.3 (0.7)	0.816 (1.8) (14 sec) 0.095 (0.21) (onward)	78 (140)	Gravity Reflood	7
871 (1600)	2.3 (0.7)	0.816 (1.8) (14 sec) 0.095 (0.21) (onward)	78 (140)		

8-23. TEST MATRIX

A test matrix was designed to satisfy the objectives in this task (section 3) and is presented in table 8-1. This test matrix is based on a planned comparison of results from the unblocked[1] and blocked bundle tests. Each of the bundle configurations listed in paragraph 4-9 will be subjected to the same test conditions tabulated in table 8-1.

The test parameters are centered on two containment pressures, representing the range applicable to PWR plants (figure 8-1). Within these containment pressures, initial clad temperature, peak power, flooding rate (or injection rates for gravity reflood tests), and inlet subcooling are varied to determine reflood behavior (maximum clad temperature, turnaround time, quench time, and mass effluent) and heat transfer capability on a comparable basis with previous FLECHT rod geometries. This test matrix has parameter effects similar to those in the previous FLECHT cosine power tests.

8-24. Steam Cooling

Data from these tests will be used to provide the basis for addressing the appendix K steam cooling penalty.

These tests will be conducted at an outlet Reynolds number which corresponds to the steam phase Reynolds number of the constant flooding rate test numbers 5, 7, and 8 (table 8-1). The temperature of the outlet steam must be limited to 205°C (400°F) to prevent failure of the upper seals of the heater rods (made of polyurethane).

8-25. Constant Flooding Rate

Data from these tests will be used to examine the effects of flooding rates on heat transfer and entrainment. These tests will be used as base for comparisons with other test series and to study effects of various flooding rates at reference conditions such as pressure, rod initial clad temperature, and inlet subcooling.

---

1. Hochreiter, L. E., et al., "PWR FLECHT SEASET Unblocked Bundle, Forced and Gravity Reflood Task: Task Plan Report," NRC/EPRI/Westinghouse-3, March 1978.

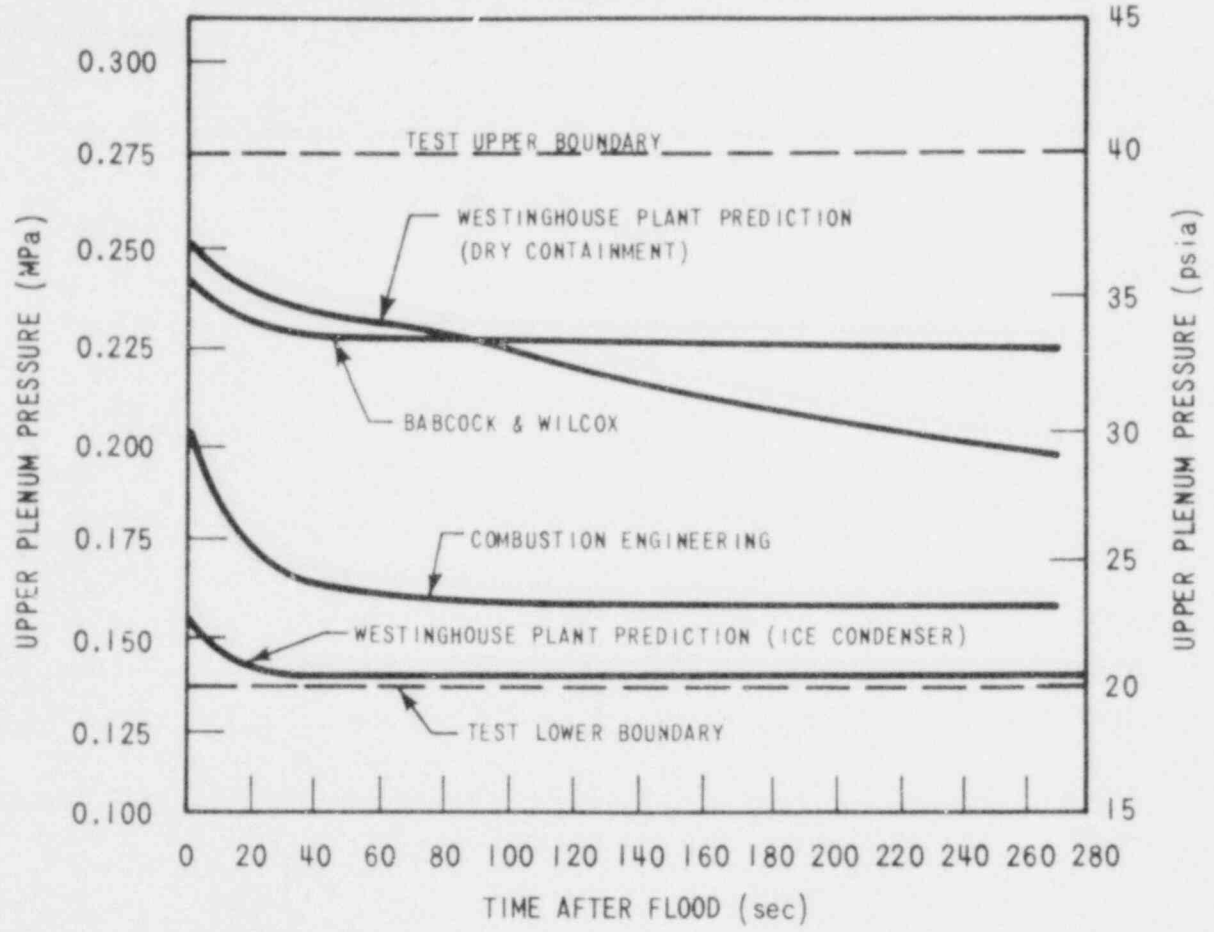

Figure 8-1. Test-Simulated Boundaries of Predicted Upper Plenum Pressures During Reflood

However, for tests 4 and 5, the peak power has been reduced to 0.88 kw/m (0.27 kw/ft) and 1.31 kw/m (0.4 kw/ft), respectively, because unblocked bundle testing and calculations showed that peak clad temperatures above 1232°C (2250°F) could be reached for the test bundle if the rod peak power were 2.30 kw/m (0.7 kw/ft). These elevated temperatures would reduce the life of the rod bundle.

8-26. Pressure Effects

The parametric effect of pressure on heat transfer and entrainment at 0.138 MPa (20 psia) at reference conditions will be studied by comparing the results of test 12 of this series with the results of test 7 (table 8-1). These data will also be used to determine the effect of decreasing flooding rates on heat transfer and entrainment at low pressures (tests 10 through 12).

8-27. Coolant Subcooling Effects

Data from these tests will be used to examine the effects of coolant subcooling at 0.276 MPa (40 psia) by comparing results of test 13 and test 7. It would also be desirable to perform the test with the coolant at saturation temperature (no subcooling). However, this would cause cavitation across the injection line and flowmeters, thereby impeding proper flooding rate measurements and, consequently, mass balance calculations.

8-28. Radial Power Distribution

All tests will be conducted with a uniform radial power distribution.

8-29. Variable Flooding Rate

The flooding rate predicted by plant analysis[1,2] is constantly changing, as shown in figure 8-2 for a dry containment plant and figure 8-3 for an ice condenser

1. Cadek, F. F., et al., "PWR Full Length Emergency Cooling Heat Transfer (FLECHT)," WCAP-7665, April 1971.

2. Cadek, F. F., et al., "PWR FLECHT Final Report Supplement," WCAP-7931, October 1972.

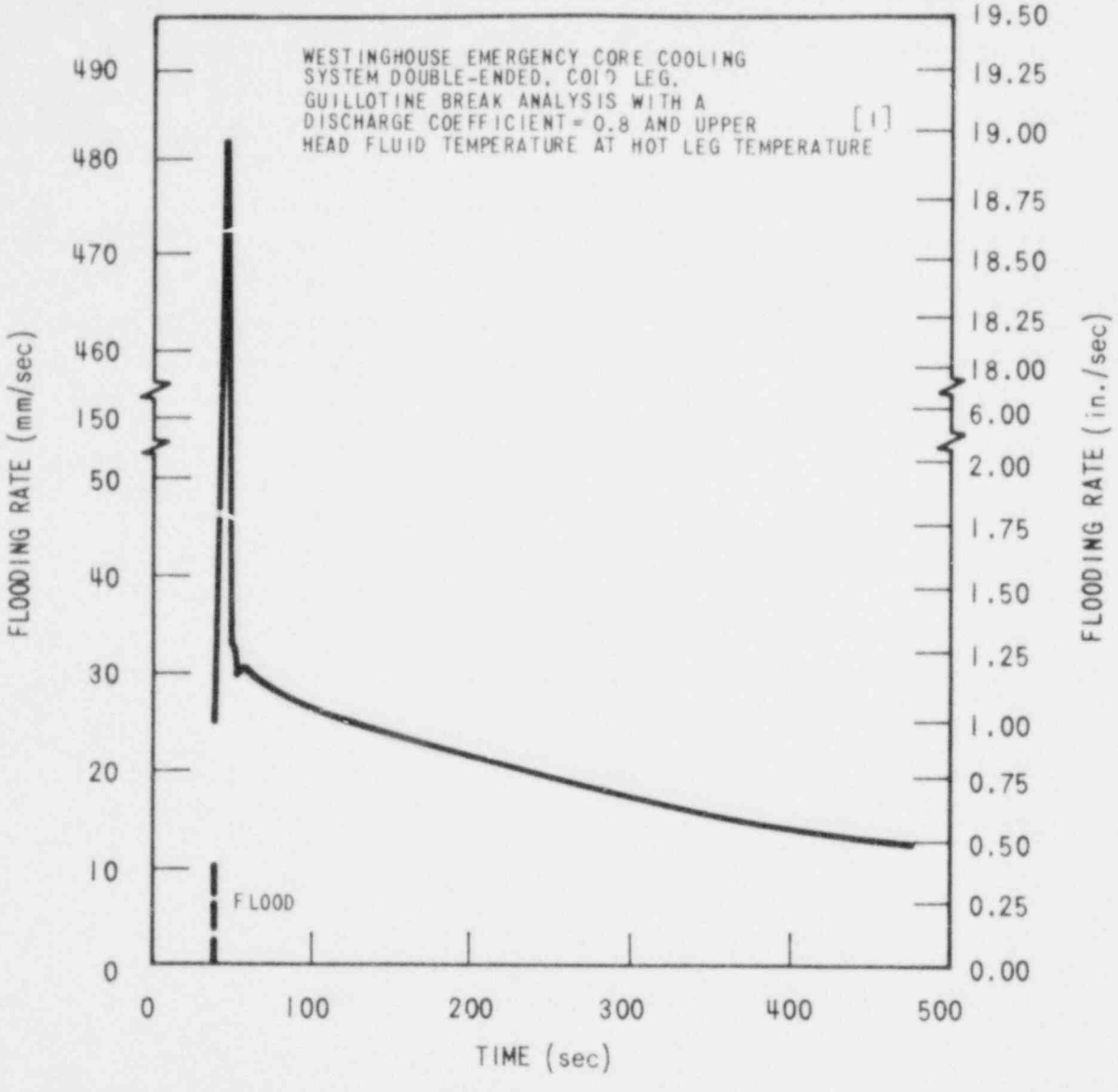

1. BECK, H. S. AND KEMPER, R. M., "WESTINGHOUSE ECCS – FOUR-LOOP PLANT (17 x 17) SENSITIVITY STUDIES WITH UPPER HEAD FLUID TEMPERATURES AT T_{HOT}," WCAP-8365-A, MAY 1977.

Figure 8-2. Predicted Flooding Rate During Core Reflood of a Westinghouse PWR Dry Containment Plant

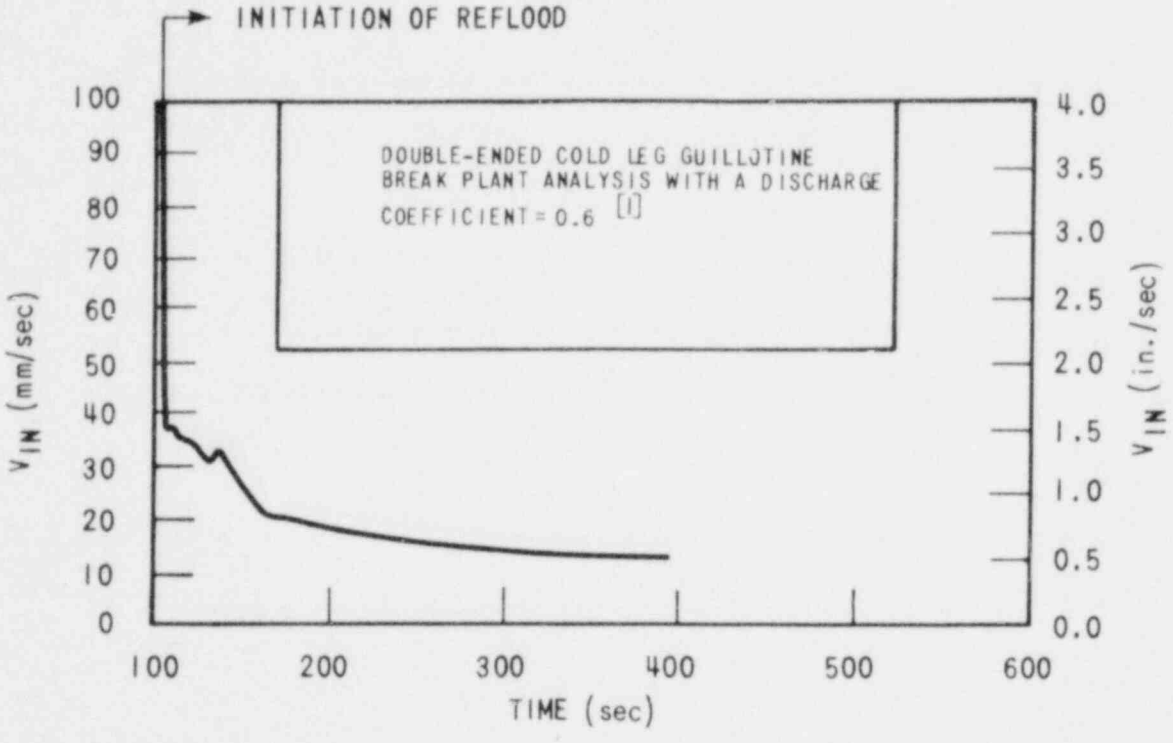

1. SEQUOYAH NUCLEAR POWER PLANT, FSAR AMENDMENT 50, JANUARY 31, 1978

Figure 8-3. Predicted Flooding Rate During Core Reflood of a Westinghouse Ice Condenser Plant

plant. Test 14 has variable stepped flow (figure 8-4), to facilitate data analysis and to enable comparison to unblocked bundle tests having similar initial conditions.

8-30. Repeat Tests

Statistical analysis will be performed on the results of these tests to determine the repeatability and validity of the heat transfer coefficient and entrainment data within the test matrix. Test 15 is planned to be run near the end of the test program. Comparison of the results of test 15 with an identical test (test 7) conducted earlier is expected to show that use of the bundle and its instrumentation does not influence recorded data from one run to the next.[1,2]

8-31. Gravity Reflood

The effects of gravity reflooding on heat transfer and entrainment at two different pressures will be studied in this series. Tests 16 and 17 will be conducted to evaluate the difference in heat transfer, mass storage in the bundle, and entrainment between gravity and forced flooding.

---

1. Lilly, G. P., et al., "PWR FLECHT Cosine Low Flooding Rate Test Series Evaluation Report," WCAP-8838, March 1977.

2. Lilly, G. P., et al., "PWR FLECHT Skewed Profile Low Flooding Rate Test Series Evaluation Report," WCAP-9183, November 1977.

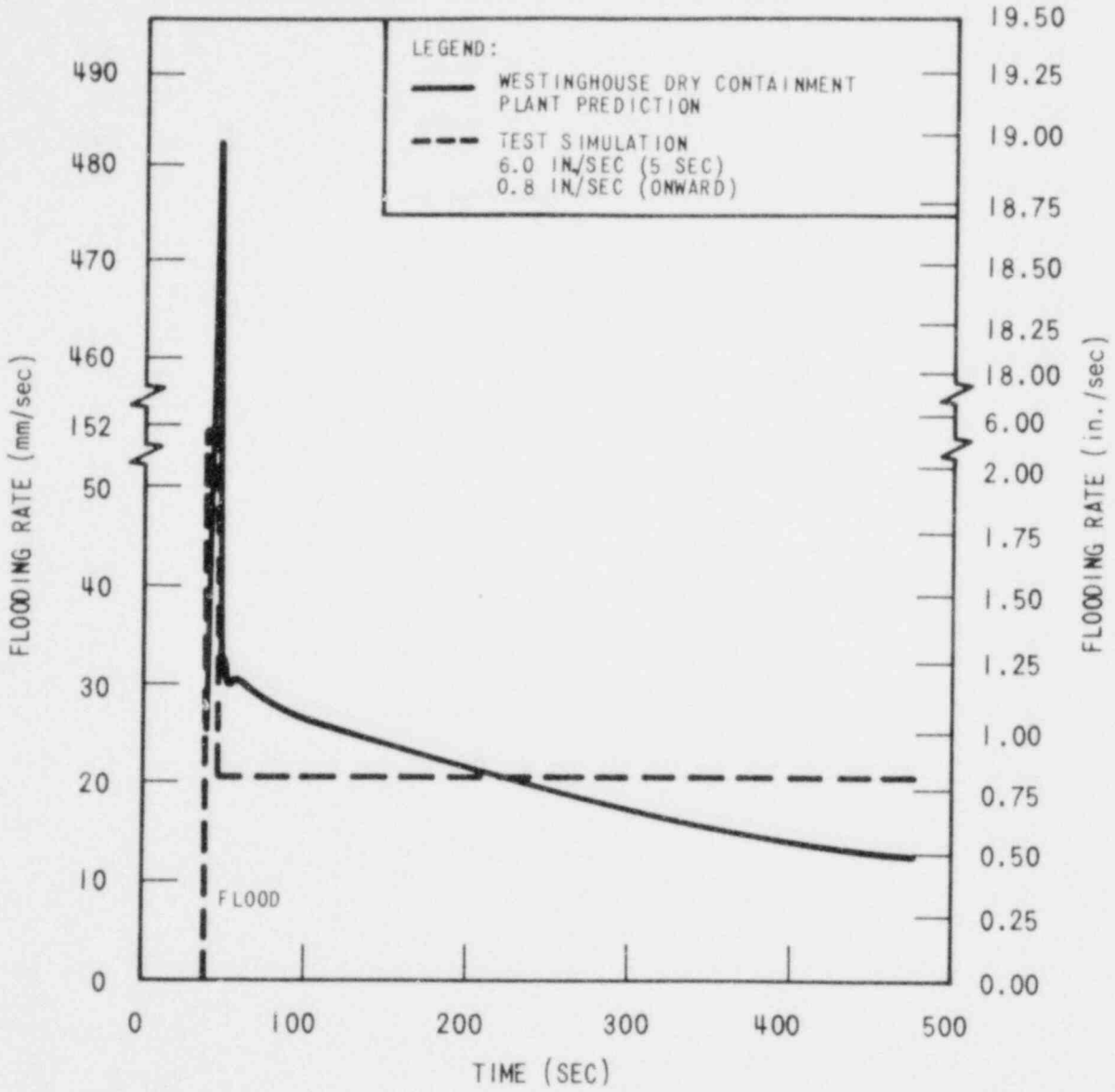

Figure 8-4. Variable Stepped Flow Simulation of Predicted Core Reflood of a Westinghouse PWR Dry Containment Plant (Two Steps)

SECTION 9
DATA REDUCTION, ANALYSIS, AND EVALUATION PLANS

9-1. DATA REDUCTION

The data to be analyzed in detail will be recorded on the PDP-11/20 computer at the Forest Hills, PA, test site, and then transferred to magnetic tape. The magnetic tape will then be processed at the Westinghouse Nuclear Center (Monroeville, PA) through a series of data reduction and analysis programs to obtain the necessary data. The flow logic of the computer codes, which is identical to that in the unblocked bundle facility, is shown in figures 9-1 and 9-2. The different data reduction stages needed first to validate the test and then to evaluate the data are also shown. In this fashion only test data which are judged to be valid are fully reduced. The catalog tape for all tests, whether valid or invalid, is saved. Table 9-1 briefly describes the main function and the output for each data reduction and analysis code. New codes (for either data reduction or analysis) used in this task will be discussed in either the data or the evaluation reports. Detail of each of the codes listed in table 9-1 are discussed in appendix M.

All data reduction and analysis codes are written in English engineering units. This system will be maintained and results of the calculations will be converted to metric units for presentation in reports.

9-2. DATA ANALYSIS AND EVALUATION

The data for this task will be evaluated and analyzed by procedures similar to those used for the unblocked bundle data.[1] As part of the data evaluation process, the single parameter trends in temperature rise, turnaround time, and quench time will be compared to see if trends found in these new data are consistent with previous FLECHT data. The data trends will be investigated for each test parameter

1. Hochreiter, L. E., et al., "PWR FLECHT SEASET Unblocked Bundle, Forced and Gravity Reflood Task: Task Plan Report," NRC/EPRI/Westinghouse-3, March 1978.

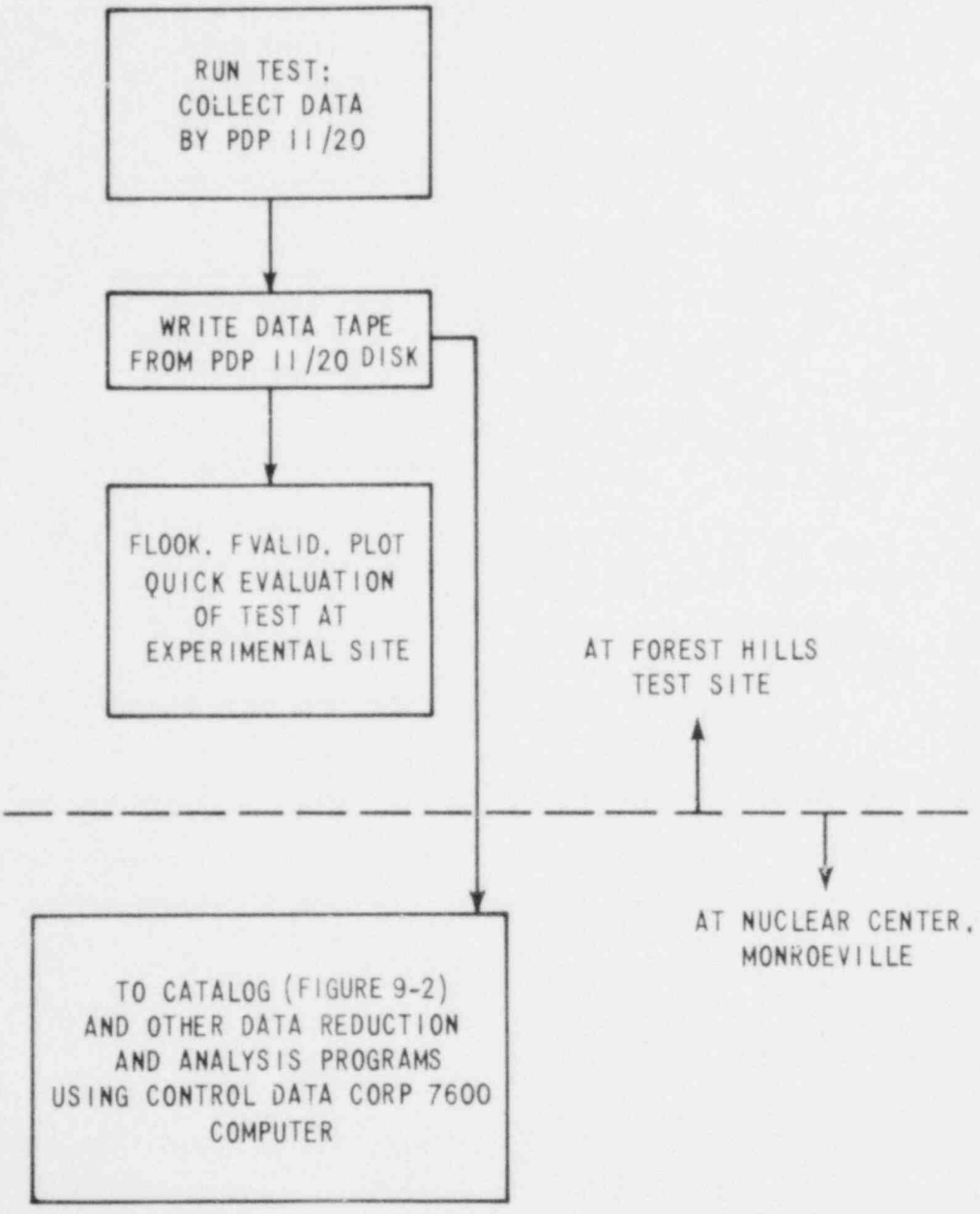

Figure 9-1. Flow Logic of Computer Codes

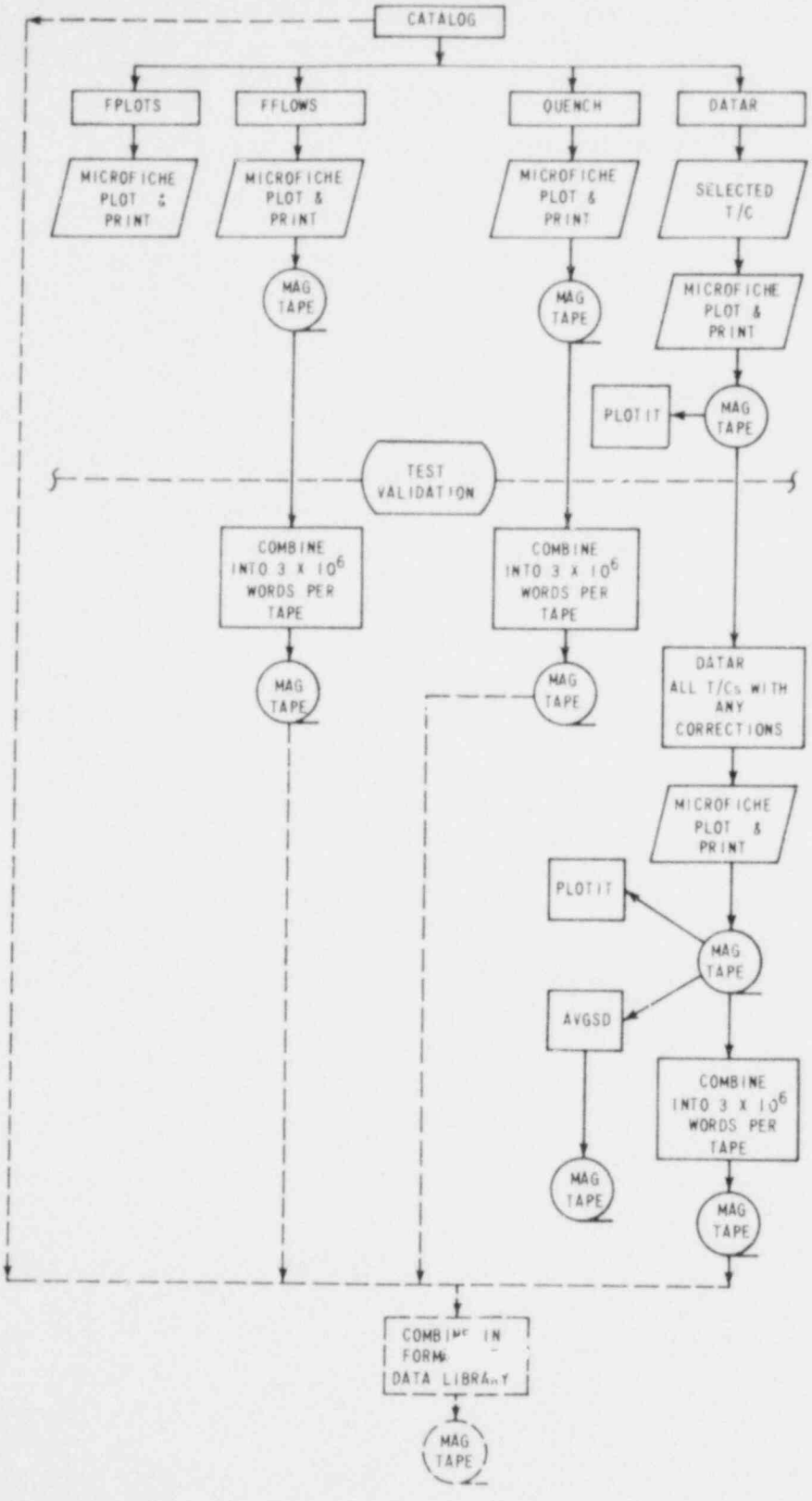

Figure 9-2. FLECHT SEASET Data Reduction Flow Chart

TABLE 9-1

DATA REDUCTION AND ANALYSIS

COMPUTER CODES FOR FLOW BLOCKAGE TASK

Data Reduction Code	Main Function	Output	Units	
			Metric	English Engineering
CATALOG	Lists each data channel as a function of run time	Tables of data and time in engineering units:		
		Time	sec	sec
		Temperature	^{o}C	^{o}F
		Pressure	MPa	psia
		Differential pressure	MPa	psig
		Flow	m^3/sec	gal/min
		Power	kw	kw
FPLOTS	Plots each data channel as a function of time	Same as CATALOG	Same as CATALOG	Same as CATALOG
FFLOWS	Calculates overall mass balances, mass accumulation, and bundle exit rates	Two-phase pressure drop	MPa	psid
		Void fraction	-	-
		Two-phase density	kg/m^3	lbm/ft^3
		Two-phase mass	kg	lbm
		Two-phase frictional pressure drop	MPa	psid
		Mass stored in bundle based on		
		a) Overall differential pressure cells 0-3.66 m (0- 144 in.)	kg	lbm
		b) Sum of incremental differential pressure cells $\sum_{i=0}^{144} \Delta P_i$	kg	lbm

TABLE 9-1 (cont)

DATA REDUCTION AND ANALYSIS
COMPUTER CODES FOR FLOW BLOCKAGE TASK

Data Reduction Code	Main Function	Output	Units	
			Metric	English Engineering
FFLOWS (cont)		Mass difference	kg	lbm
		Two-phase steam velocity	m/sec	ft/sec
		Time	sec	sec
		Accumulator mass loss	kg	lbm
		Mass injected		
		Total	kg	lbm
		Rate	kg/sec	lbm/sec
		Mass stored		
		Total	kg	lbm
		Rate	kg/sec	lbm/sec
		Mass out		
		Total	kg	lbm
		Rate	kg/sec	lbm/sec
		Mass difference		
		Total	kg	lbm
		Rate	kg/sec	lbm/sec
		Carryout fraction:		
		(a) Based on mass stored		
		Total	-	-
		Rate	-	-
		(b) Based on mass out		
		Total	-	-
		Rate	-	-

TABLE 9-1 (cont)

DATA REDUCTION AND ANALYSIS
COMPUTER CODES FOR FLOW BLOCKAGE TASK

Data Reduction Code	Main Function	Output	Units	
			Metric	English Engineering
FFLOWS (cont)		Test section mass		
		Total	kg	lbm
		Rate	kg/sec	lbm/sec
		Carryover tank mass		
		Total	kg	lbm
		Rate	kg/sec	lbm/sec
		Steam separator mass		
		Total	kg	lbm
		Rate	kg/sec	lbm/sec
		Exhaust orifice mass		
		Total	kg	lbm
		Rate	kg/sec	lbm/sec
		Overall mass balance	kg	lbm
		Lower bound quality	-	-
		Upper bound quality	-	-
		Mass leaving each differential pressure increment	kg	lbm
QUENCH	Determines time-temperature history for each rod thermocouple	Initial temperature	^{o}C	^{o}F
		Turnaround temperature	^{o}C	^{o}F
		Turnaround time	sec	sec
		Temperature rise	^{o}C	^{o}F
		Quench time	sec	sec
		Quench temperature	^{o}C	^{o}F

TABLE 9-1 (cont)

DATA REDUCTION AND ANALYSIS
COMPUTER CODES FOR FLOW BLOCKAGE TASK

Data Reduction Code	Main Function	Output	Units	
			Metric	English Engineering
DATAR	Calculates local surface temperature, heat flux, and heat transfer coefficients for each rod thermocouple	Measured temperature Calculated surface temperature Heat flux Heat transfer coefficient	^{o}C ^{o}C W/m^2 $W/m^2-^{o}C$	^{o}F ^{o}F $Btu/hr-ft^2$ $Btu/hr-ft^2-^{o}F$
PLOTIT	Plots DATAR variables versus time	Plots of DATAR output	Same as DATAR	Same as DATAR
AVGSD	Statistical analysis of DATAR output	Mean, one standard deviation, maximum and minimum for rod temperature heat transfer coefficient and heat flux in specified bundle zones	Same as DATAR	Same as DATAR
FLEMB	Calculates local conditions and other quantities relevant to heat transfer	Mass flow Quality Enthalpy Vapor Reynolds number Nusselt number Radiative heat flux to vapor Void fraction Wall temperature Vapor temperature Hot rod heat flux Total integrated heat flow	kg/sec - J/kg - - W/m^2 - ^{o}C ^{o}C W/m^2 J	lbm/sec - Btu/lbm - - $Btu/hr-ft^2$ - ^{o}F ^{o}F Btu/ft^2-hr Btu

TABLE 9-1 (cont)

DATA REDUCTION AND ANALYSIS

COMPUTER CODES FOR FLOW BLOCKAGE TASK

Data Reduction Code	Main Function	Output	Units	
			Metric	English Engineering
ALLTURN (Z-Zq)	Calculates heat transfer coefficient based on distance above the quench front	Heat transfer coefficient	$W/m^2-{}^oC$	$Btu/hr-ft^2-{}^oF$
		as a function of elevation	m	ft
		for a given time	sec	sec
HEAT-II	Calculates components of heat transfer to entrained liquid and steam	Droplet diameter	m	ft
		Droplet number density	$drops/m^3$	$drops/ft^3$
		Droplet velocity	m/sec	ft/sec
		Vapor velocity	m/sec	ft/sec
		Slip ratio	-	-
		Void fraction	-	-
		Droplet Reynolds number	-	-
		Droplet Weber number	-	-
		Rod heat flux	W/m^2	Btu/ft^2-hr
		Surface-to-surface radiation heat flux	W/m^2	Btu/ft^2-hr
		Wall-to-vapor radiation heat flux	W/m^2	Btu/ft^2-hr
		Wall-to-droplet radiation heat flux	W/m^2	Btu/ft^2-hr
		Wall-to-vapor convective heat flux	W/m^2	Btu/ft^2-hr
		Vapor-to-droplet radiation heat flux	W/m^2	Btu/ft^2-hr
		Heat transfer coefficient	$W/m^2-{}^oC$	$Btu/hr-ft^2-{}^oF$
		Nusselt number	-	-
		Quality	-	-
		Steam temperature	^oC	^oF
		Wall temperature	^oC	^oF

TABLE 9-1 (cont)

DATA REDUCTION AND ANALYSIS
COMPUTER CODES FOR FLOW BLOCKAGE TASK

Data Reduction Code	Main Function	Output	Units	
			Metric	English Engineering
HEAT-II (cont)		Normalized surface-to-surface radiation heat flux	-	-
		Normalized wall-to-droplet radiation heat flux	-	-
		Normalized wall-to-vapor radiation heat flux	-	-
		Normalized wall-to-vapor convective heat flux	-	-
		Vapor Reynolds number	-	-
		Optical thickness	mm	in.

such as pressure, flooding rate, power, initial clad temperature, and subcooling. In addition, heat transfer, clad temperature, and total mass carryout will be compared for each test parameter.

The special tests, such as the gravity reflood tests, will be examined separately to determine the effect of each test variation on the heat transfer, clad temperature, and total mass entrainment. In this fashion, qualitative statements can be made on the effect of each test parameter.

The entrainment and bundle void fraction data, also obtained from the experiments, will be compared to the semiempirical entrainment model developed in WCAP-8838.[1] The model proposed by Sun and Duffey[2] will also be compared with the mass effluent data and the entrainment model given in WCAP-8838. Entrainment criteria such as superficial velocity or critical void fraction will also be investigated and compared with criteria in the literature.

In addition, the data will be analyzed to investigate heat transfer mechanisms occurring during reflood. The analytical methods developed in WCAP-9183[3] will be used to perform a mass and energy balance on the test bundle.

The bundle thermal-hydraulic parameters which will be calculated from the bundle mass and energy balance are given in table 9-2. Using these quantities, the measured wall heat flux will be divided into the individual heat transfer mechanisms using the HEAT-II computer code described in appendix M. The HEAT-II program will give the radiation-to-vapor wall heat flux component, radiation to drops, radiation to other surfaces, and the resulting convective wall heat flux component. This approach will enable quantification of the different reflooding heat transfer mechanisms, which in turn will allow others to verify or develop mechanistic

---

1. Lilly, G. P., et al., "PWR FLECHT Cosine Low Flooding Rate Test Series Evaluation Report," WCAP-8838, March 1977.

2. Sun, K. H., and Duffey, R. B., "A Generalized Theory for Predicting Mass Effluence During Reactor Reflooding," Nucl. Tech. 43, 22-27 (1979).

3. Lilly, G. P., et al., "PWR FLECHT Skewed Profile Low Flooding Rate Test Series Evaluation Report," WCAP-9183, November 1977.

TABLE 9-2

INFORMATION DERIVED FROM BASIC FLOW BLOCKAGE TASK DATA

Derived Thermal-Hydraulic Quantity	Method Used - Code	Location
Rod surface heat flux	Inverse conduction code - DATAR	At each rod thermocouple elevation
Heat transfer coefficient	Heat flux and rod surface and saturation temperatures - DATAR	At each rod thermocouple elevation
Bundle rod heat release rate	Bundle energy balance - FLEMB	Rod bundle heated length
Fluid mass storage rate	Test section mass balance - FFLOWS	Rod bundle
Effluent rate	Test section mass balance - FFLOWS	Exhaust orifice, carryover, and steam separator tank
Quench front velocity	Rod thermocouple quench data - QUENCH	Rod bundle heated length
Bundle axial void fraction	Momentum balance using different pressure readings corrected for frictional losses - FFLOWS	Rod bundle heated length

TABLE 9-2 (cont)

INFORMATION DERIVED FROM BASIC FLOW BLOCKAGE TASK DATA

Derived Thermal-Hydraulic Quantity	Method Used - Code	Location
Blockage sleeve heat flux	Rod surface heat flux and blockage sleeve temperature	At each instrumented sleeve location
Carryout fraction	Mass balance around test section - FFLOWS	Injection rates, mass storage, and exhaust liquid and steam measurements
Liquid entrainment rate	Mass balance around test section - FFLOWS	Carryover and steam separator collection tanks
Nonequilibrium quality	Mass and energy balance	Rod bundle at each steam probe location
Equilibrium quality	Mass and energy balance	Rod bundle at each steam probe location
Exit quality	From test section exit liquid and steam flow measurements - FFLOWS	Test section exhaust
Heat flow to droplets	From axial quality changes, mass flows, and two-phase flow temperatures - HEAT-II	Rod bundle at each steam probe location

TABLE 9-2 (cont)

INFORMATION DERIVED FROM BASIC FLOW BLOCKAGE TASK DATA

Derived Thermal-Hydraulic Quantity	Method Used - Code	Location
Convective heat flux to steam	From axial quality changes, mass flows, and two-phase flow temperatures - HEAT-II	Rod bundle at each steam probe location
Radiative heat flux to drops	From axial quality changes, mass flows, and two-phase flow temperatures - HEAT-II	Rod bundle at each steam probe location
Radiative heat flux to steam	From axial quality changes, mass flows, and two-phase flow temperatures - HEAT-II	Rod bundle at each steam probe location

reflood heat transfer models. The analyzed data will also be compared with existing heat transfer correlations or models, and improved models will be proposed if possible. The resulting information will be presented in tabular form to enable correlation of the data in various ways.

The effect of different subchannel blockage configurations will be obtained by direct comparison between the uniformly blocked tests and the unblocked bundle data. The instrumentation layout of both bundles will allow direct comparison of the transient wall temperature, FLECHT heat transfer coefficient, wall heat flux, and vapor temperature at several locations within and downstream of the blockage zone. These data can then be plotted against the test parameters (such as flooding rate and pressure) to determine whether any heat transfer decrease occurs over the test parameter range investigated.

In addition, zones of either improved or degraded heat transfer downstream of the blockage region will be mapped out and normalized to the unblocked bundle data.

For the bypass flow blockage tests, additional comparisons will be available with both the unblocked and uniformly blocked tests. Comparisons of these data will allow assessment of the flow redistribution effect on the heat transfer, both in the blockage wake and in the flow bypass region. Comparisons will indicate the relative importance of the flow bypass effect compared to the droplet breakup effect as a function of the different test parameters.

For the uniformly blocked tests, the data will be analyzed in the manner described above. Because, in this case, the flow in the bundle will be one-dimensional, the mass and energy balances described above are applicable. For the case of flow redistribution, the data will be analyzed in a more approximate manner, since the flow will not be one-dimensional. The single-phase flow field will be calculated with the COBRA-IV code or other appropriate analyses to obtain the redistribution effects in the bundle. This calculation will be used with the measured data to estimate the local quality on the different sides of the bundle and the quality behavior downstream of the blockage zone. These calculations will be less accurate than the one-dimensional calculations, since the flow behavior will only be estimated by means of COBRA-IV. The flow behavior and the local fluid conditions calculated in this manner will be compared to similar calculations for the

unblocked tests and the tests with uniform flow blockage. Thus, by comparing the fluid conditions such as quality, vapor Reynolds number, T_{wall}, T_{vapor}, and the wall heat flux, the effect of the flow blockage on the rod heat transfer can be examined.

9-3. MECHANISTIC DATA ANALYSIS

During the course of experimentation in the 21-rod bundle task, a mechanistic model for flow blockage will be developed which will subsequently be assessed in the 161-rod bundle task.

At the present time, the easiest and most direct approach for analysis and correlation of the data appears to be a modification of an existing FLECHT-type correlation to account for both flow blockage effects and flow bypass.

As previously discussed in the program plan,[1] an expression for the heat transfer downstream of a single blocked rod can be written, using the method of Hall and Duffey,[2] as

$$h_B = h_o\left(\frac{G_B}{G_o}\right)^m N_e \qquad (9\text{-}1)$$

where

G_B = single-phase flow rate, which can be obtained from a subchannel analysis code like COBRA-IV

N_e = empirical blockage factor, which accounts for the effects of droplet atomization, increased turbulence, local flow

1. Conway, C. E., et al., "PWR FLECHT Separate Effects and Systems Effects Test (SEASET) Program Plan," NRC/EPRI/Westinghouse-1, December 1977.

2. Hall, P. C., and Duffey, R. B., "A Method of Calculating the Effect of Clad Ballooning on Loss-of-Coolant Accident Temperature Transients," Nucl. Sci. Eng. 58, 1-20 (1975).

acceleration, and slip between vapor and droplet caused by single-rod blockage. It is expected to be a function of the blockage shape.

G_o = unblocked single-phase flow rate from COBRA-IV

h_o = unblocked heat transfer coefficient

m = exponent of the flow, depending on the convective heat transfer, using a Dittus-Boelter correlation (typically m = 0.8)

Quantification of N_e can be obtained by analysis of the 21-rod bundle experiment for the different blockage shapes tested. In reality, the above equation becomes the defining equation for N_e. The blocked test series with no bypass would yield data to determine N_e, since $(G_B/G_o)^m$ is equal to 1.

Although the single balloon blockage effect is expected to affect the local heat transfer downstream, the interaction effects of blockages on adjacent rods will also affect the heat transfer downstream of any individual rod. This interaction effect is caused by the noncoplanar blockage, which will promote subchannel crossflow, increased turbulence intensity, slip, and mixing between adjacent subchannels which could have more or less blockage than the particular channel being examined. The effect of other channel blockage on a particular channel is called the environmental effect and may be characterized by N_E. Therefore, the heat transfer downstream of a blocked rod surrounded by other blocked rods can be expressed as

$$\frac{h_B}{h_o} = \left(\frac{G_B}{G_o}\right)^m N_e N_E \qquad (9\text{-}2)$$

where N_E accounts for the blockage environment. In equation (9-2), as in equation (9-1), it should be noted that G_B is a single-phase flow rate and m is taken from a single-phase correlation. G_B can be conservatively obtained from a subchannel analysis code like COBRA and m is also obtainable from the literature for single-phase flow (for example m = 0.8). Equation (9-2) then becomes the defining relationship

for N_E. The value of N_E, which again is empirical, will be obtained through comparisons with the unblocked data and determination of G_B/G_o using the single-phase COBRA-IV calculations. It is expected that N_E will be a function of the flow properties, initial flooding rate, distance downstream of the blockage, and the blockage distribution. The resulting expression or models for N_e and N_E will be compared with the 161-rod blocked bundle data, where ample flow bypass will be allowed.

The capability of a model such as that given in equation (9-2) to predict behavior in the large-bundle blockage experiments with bypass may determine the need for additional 21-rod bundle tests to better define N_E.

9-4. STATISTICAL DATA EVALUATION

When test data are presented in support of a safety analysis model, the data are normally screened, evaluated, and examined to determine whether bias exists in the data which would indicate a particular correlation with one or more parameters. The hot rod unblocked FLECHT data[1] have been examined in this manner and it has been found that distributions of the hot rod heat transfer data can be generated from individual rods. The rod-to-rod variations are due to radial position within the bundle; this could reflect local subchannel heat transfer effects, rod manufacturing and instrumentation differences, and test repeatability uncertainties. Other effects which could cause bias in the data are normally eliminated by selecting the hot rods. These other factors include different power rods, housing effects, and proximity of any failed rods. The methods used to select the hot rods in previous FLECHT tests are discussed in the FLECHT cosine[2] and skewed power[1] evaluation reports.

Flow blockage is another parameter which can promote bias and variation in the data which should be greater than other variations within the data. To properly

1. Lilly, G. P., et al., "PWR FLECHT Skewed Profile Low Flooding Rate Test Series Evaluation Report," WCAP-9183, November 1977.

2. Lilly, G. P., et al., "PWR FLECHT Cosine Low Flooding Rate Test Series Evaluation Report," WCAP-8838, March 1977.

assess either a heat transfer benefit or a penalty due to flow blockage, the blockage effect must be separable from these other variations.

The proposed statistical approach will establish the distributions of the unblocked heat transfer data and the blocked heat transfer data on a common basis, so that the effect of blockage can be obtained. Data means, standard deviations, and frequency distributions will be compared at each elevation as a function of time to ascertain the additional variation introduced by the blockage.

Each effect which could cause variation between a blocked rod in the blocked bundle and an unblocked rod in the unblocked bundle must be examined to establish the true effect of blockage. Those effects which can create variance in the FLECHT data are as follows:

-- Uncertainty in the calculated heat transfer due to manufacturing differences and the measured heater rod temperature and power[1]

-- Variation due to radial position within the bundle, which can result in local heat transfer being different from channel to channel

-- Uncertainty of establishing repeatable test conditions

-- Variation between the two bundles used

-- Variation caused by the noncoplanar blockage on the local heat transfer in the bundle

To screen out the first four effects, suitable instrumentation and repeat tests will be necessary for both the unblocked bundle tests and the blocked bundle tests. This necessity has been examined in the unblocked test series and will be considered in the blocked bundle task plan.

The instrumentation plan for the 21-rod bundle has been designed to provide data for examining the above five reasons for data variance. Similar instrumentation

1. Rosal, E. R., et al., "FLECHT Low Flooding Rate Skewed Test Series Data Report," WCAP-9108, May 1977.

locations exist in the 21-rod bundle and in the unblocked bundle. There is ample instrumentation at different radial locations to obtain any radial variation. In addition, the azimuthal location of the thermocouples is also being specified in the 21-rod bundle, again to determine sources of data variance. Tests have been shown to be repeatable in previous FLECHT test series, and repeat tests within each test series of the 21-rod bundle are planned. The bundle- to-bundle variation can be examined by comparing the data at elevations below the blockage zone for similar tests with different bundles. In these comparisons, two sources of variance would be present: bundle-to-bundle difference and test-to-test difference. Since the facility loop design, controls, and associated instrumentation are the same for all test series, the test-to-test variance should be quantified by the repeat tests in each test series. Therefore, the additional variance due to bundle-to-bundle effects should be separable if it is significant.

By performing the heater rod error analysis described in WCAP-9108, appendix B, the uncertainty due to rod manufacturing effects, power measurements, and thermocouple error can be calculated. The repeat tests to be conducted in each test series will give the uncertainty due to fixing the bundle test conditions. It is expected that the slight differences in actual test conditions between the paired blocked and unblocked tests can be accounted for by adjusting the unblocked data by deterministic methods or using the results of unblocked tests. The bundle-to-bundle variation between the blocked bundle and the unblocked bundle will be obtained by comparing the thermocouple variation for "identical tests" at elevations away from the blockage plane, for example, at 1.2 m (4 ft).

Since these uncertainties can be determined, the resulting unknown variations which would exist in the heat transfer data would be the rod-to-rod heat transfer variation for the unblocked data and the local effect of blockage for the blocked bundle test. Statistical tests will be performed on the data to identify the parent population distribution from the data sample distribution. These resulting distributions will then be compared, as shown in figure 9-3. Such curves will be generated at different elevations for different times of interest so that the effect of the blockage on the heat transfer can be evaluated. One such elevation dependence curve is shown schematically in figure 9-4. To generate the distributions for the heat transfer data, some data pooling may be necessary, or additional assumptions on normality of the parent distributions may be required. Instrumentation has

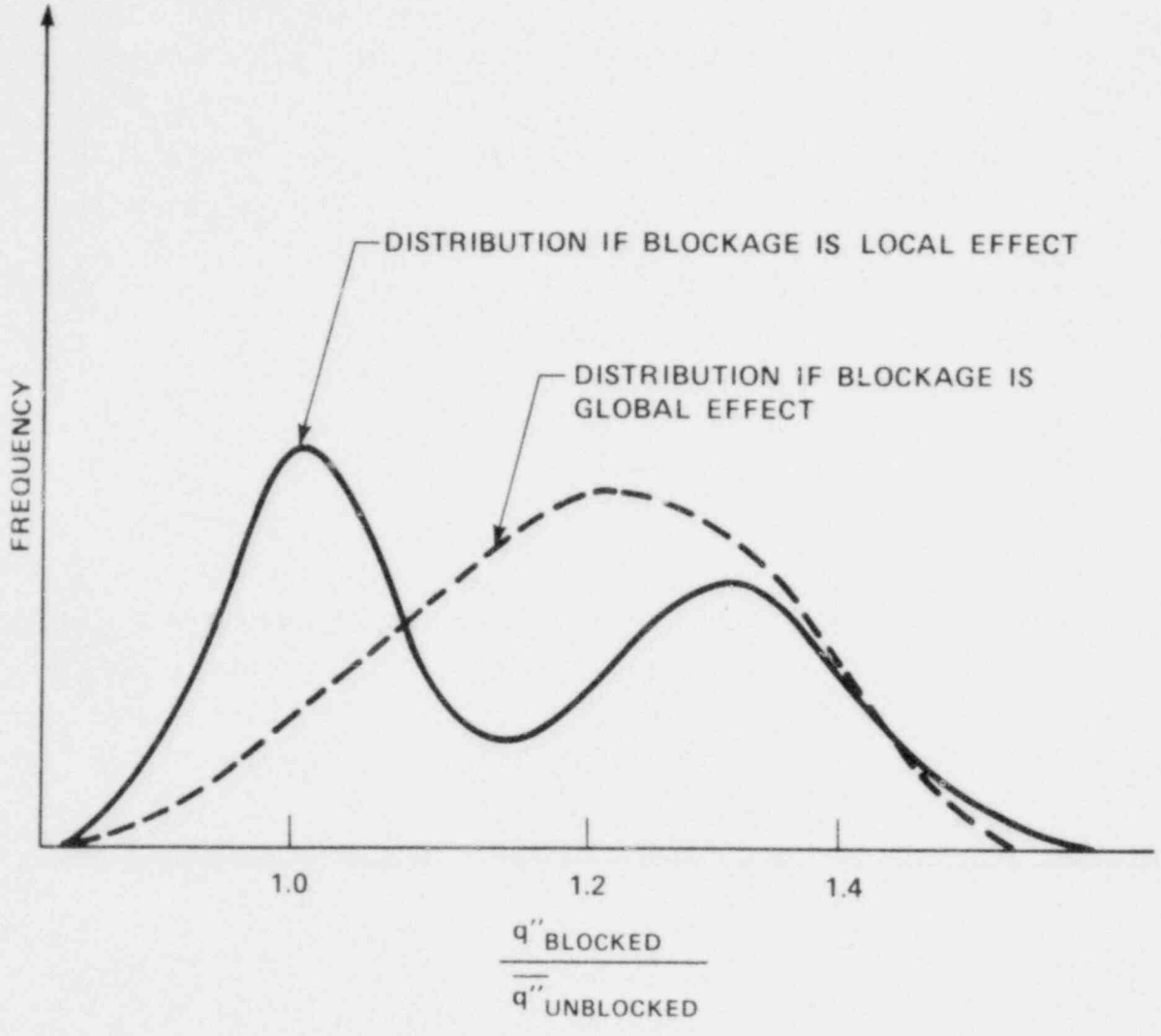

Figure 9-3. Sample Distribution Plots

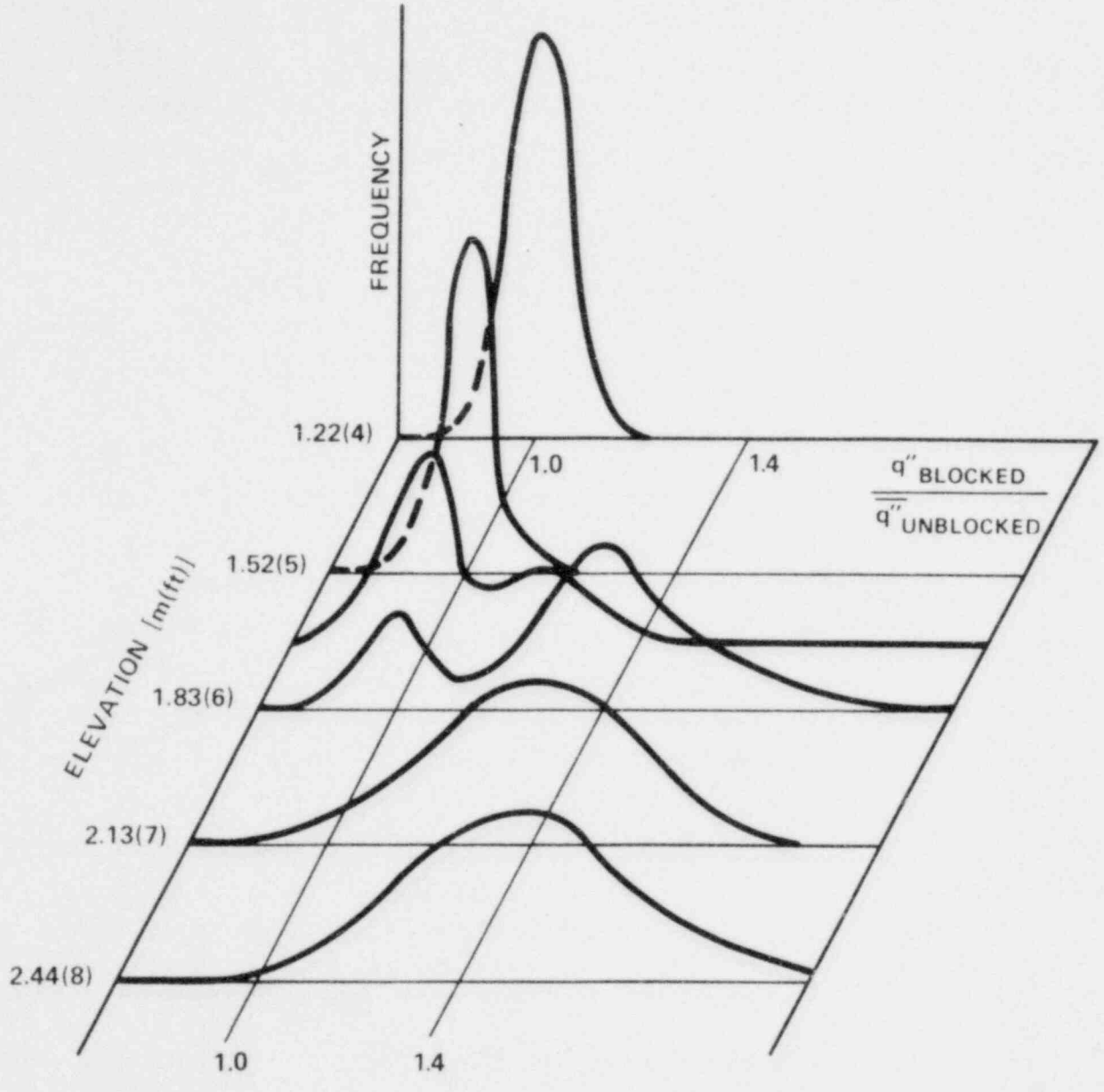

Figure 9-4. Sample Frequency Distribution Plots at Different Elevations for a Given Time

been planned and provided in the bundle so that these assumptions can be confirmed for a few tests, and then applied for other tests.

Similar comparisons will also be performed with the blocked tests with bypass. In this case, results of the blocked tests with bypass and the blocked tests without bypass will be compared to assess the effects of bypass on the blocked heat transfer. The bypass test results will also be compared to the unblocked test results to obtain the total effect of the flow blockage with bypass relative to the unblocked geometry.

The end result of this data evaluation will be the assessment of the effect of blockage, both with and without flow bypass, relative to the unblocked data, with the only variations in the data caused by rod position, flow blockage at different rod positions, and flow bypass. Comparison of the generated frequency distribution plots should indicate the variations of the data means and the relative position of the tails of the frequency distributions. If the data indicate that the means for the unblocked data with and without bypass are greater than those for the unblocked data, and that the distribution tails are within the distribution tails of the unblocked data, then clearly flow blockage is not a penalty relative to unblocked FLECHT data, since no negative variance has been introduced into the data by the blockage. If the frequency distributions indicate that the means of the blocked data with and without bypass are greater than those of the unblocked data, but the tails of the blockage distribution data yield lower heat transfer than the tails of the unblocked data, then these data will be investigated more closely to see if there is a thermal-hydraulic explanation for this trend. If a thermal-hydraulic explanation can be found, then this particular effect would be included in a model for flow blockage.

In summary, the combination of the statistical data evaluation and the deterministic data analysis should provide sufficient tools to explain the effect of the flow blockage on the resulting bundle heat transfer from a mechanistic viewpoint. If the resulting blocked bundle heat transfer is observed to always be a heat transfer benefit relative to the unblocked data, the proposed analytical methods should be able to explain why. If the blockage heat transfer is found to be a penalty relative to the unblocked heat transfer, the proposed analytical methods should provide the explanation of why a penalty results.

9-5. HYDRAULIC CHARACTERISTICS TEST DATA REDUCTION AND ANALYSIS PLAN

As previously described, the static pressure differential will be measured over 0.30 m (1 ft) increments utilizing a $\pm$ 3.7 x 10^3 Pa ($\pm$ 15 in.'wg) differential pressure transmitter. The pressure measurements are made from just below the first grid at the 0 m (0 ft) elevation to just below the eighth grid at the 3.57 m (11.7 ft) elevation. The pressure losses due to friction, support grids, and blockage sleeves can be determined by evaluating the mechanical energy equation between any two points, as follows:

$$\Delta P_{LOST} = (P_a - P_b) + \frac{\rho}{2g_c} (V_a^2 - V_b^2) + \frac{\rho g}{g_c} (Z_a - Z_b)$$

where

P_a = measured static pressure at upstream point

P_b = measured static pressure at downstream point

$\Delta P_{LOST} = \frac{K\rho V^2}{2g_c}$, where V is the velocity in the unblocked portion of the bundle

Therefore, since the gravity head can be neglected because of the pressure of a reference leg,

$$K \frac{\rho V^2}{2g_c} = (P_a - P_b) + \frac{\rho}{2g_c} (V_a^2 - V_b^2)$$

$$K = \frac{(P_a - P_b) + \frac{\rho}{2g_c} (V_a^2 - V_b^2)}{\frac{\rho V^2}{2g_c}}$$

where

$$K = \begin{cases} \frac{fL}{D_h}, \text{ for frictional losses} \\ K_{grid}, \text{ for grid losses} \\ \frac{fL}{D_h} + K_{blockage}, \text{ for blockage sleeve losses} \end{cases}$$

The friction factor for the heater rods can be determined by evaluating the data between grid locations. As shown by figure 9-5, the differential pressure measurement between 0.61 m (2 ft) and 0.91 m (3 ft), between 2.74 m (9 ft) and 3.05 m (10 ft), and between 3.35 m (11 ft) and 3.57 m (11.7 ft) will allow evaluation of the friction factor. The velocity between grid locations along the tube bundle is assumed constant. The above relationship for the frictional losses reduces to the following:

$$\frac{fL}{D_h} = \frac{\Delta P_{a-b}}{\frac{\rho V^2}{2g_c}}$$

The grid loss coefficient in combination with the rod friction can be determined by evaluating the data across the support grids. As shown by figure 9-5, the differential pressure measurement between 0.30 m (1 ft) and 0.61 m (2 ft), between 0.91 m (3 ft) and 1.22 m (4 ft), between 2.44 m (8 ft) and 2.74 m (9 ft) and between 3.05 m (10 ft) and 3.35 m (11 ft) will allow evaluation of the grid loss coefficient. The velocity is assumed to be the same at the grid entrance and exit. The grid loss coefficient will be corrected for the inherent rod friction, as shown below:

$$K_{grid} = \frac{\Delta P_{a-b}}{\frac{\rho V^2}{2g_c}} - \frac{fL}{D_h}$$

The blockage sleeve loss coefficient can be determined by evaluating the data across the blockage zone for a test configuration with blockage sleeves. Figure 9-5

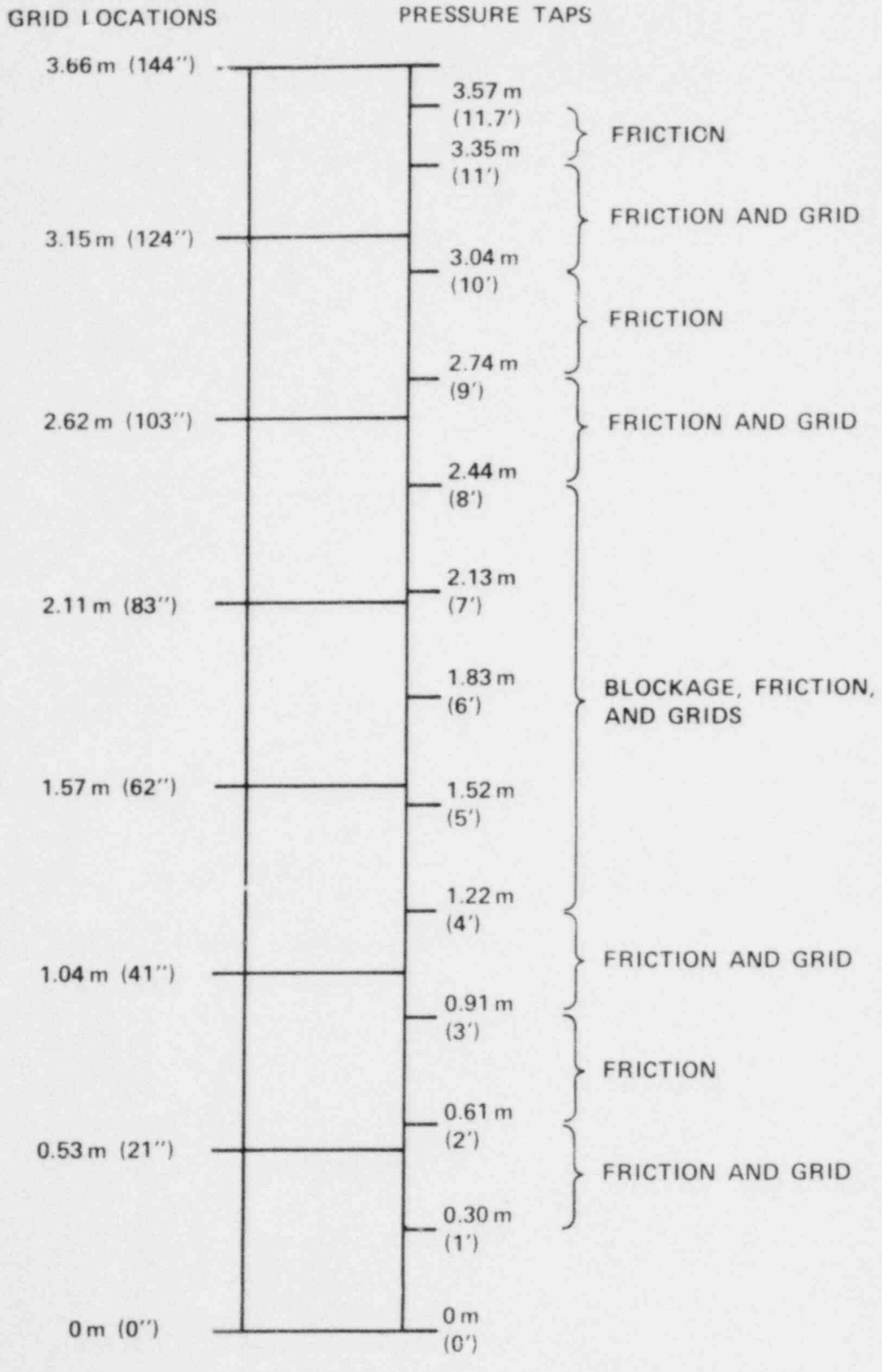

Figure 9-5. Grid Location/Pressure Measurement Relationships

shows that the differential pressure measurement between 1.22 m (4 ft) and 2.44 m (8 ft) will allow evaluation of the blockage sleeve coefficient. Although this 1.22 m (4 ft) span includes two grids and 1.22 m (4 ft) of frictional losses, the velocity can be assumed constant at each of the respective pressure measurement locations. The blockage sleeve loss coefficient will be corrected for the rod friction and grid as shown below:

$$K_{sleeve} = \frac{\Delta P_{a-b}}{\frac{\rho V^2}{2g_c}} - \frac{fL}{D_h} - K_{grid}$$

The measured values for the friction factor, grid loss coefficient, and blockage sleeve loss coefficient will subsequently be compared to values available in the literature.

SECTION 10
TASK SCHEDULE

Figure 10-1 presents a revised schedule for the 21-rod bundle task based on a work hiatus from February 1, 1979, to August 16, 1979. The seven test series are planned for completion by March 15, 1981, and a blockage sleeve shape decision will be made for the 161-rod bundle task by April 15, 1981. At that point, the computer "front end" for the 21-rod bundle facilities will be converted for use in the 161-rod bundle testing facility. Table 10-1 describes the major milestones presented in figure 10-1.

A draft data report for the seven test series will be completed by July 15, 1981; a draft data analysis and evaluation report will be completed by October 15, 1981. In addition, Westinghouse will publish informal letter data reports after each test series, to provide early information to the PMG and its consultants for review and comment.

TABLE 10-1

MAJOR MILESTONES FOR FLECHT SEASET 21-ROD BLOCKED BUNDLE TASK

Milestone No.	Milestone	Months After Contract Start Date[a]	Calendar Date
F1	Initiate test planning and facility design	9	4/1/78A[b]
F2	Issue draft task plan for review	16.5	11/15/78A
F3	Initiate work hiatus	19	2/1/79A
F4	End hiatus and restart work	25.5	8/16/79A
F5	Initiate continuation of facility construction	26.5	9/17/79A
F6	Complete facility construction and initiate shakedown	30	1/1/80
F7	Complete all test series	44.5	3/15/81
F8	Select blockage sleeves for 161-rod bundle	45.5	4/15/81
F9	Complete draft data summary report	48.5	7/15/81
F10	Complete draft data analysis and evaluation report	51.5	10/15/81

a. 7/1/77
b. A - actual date

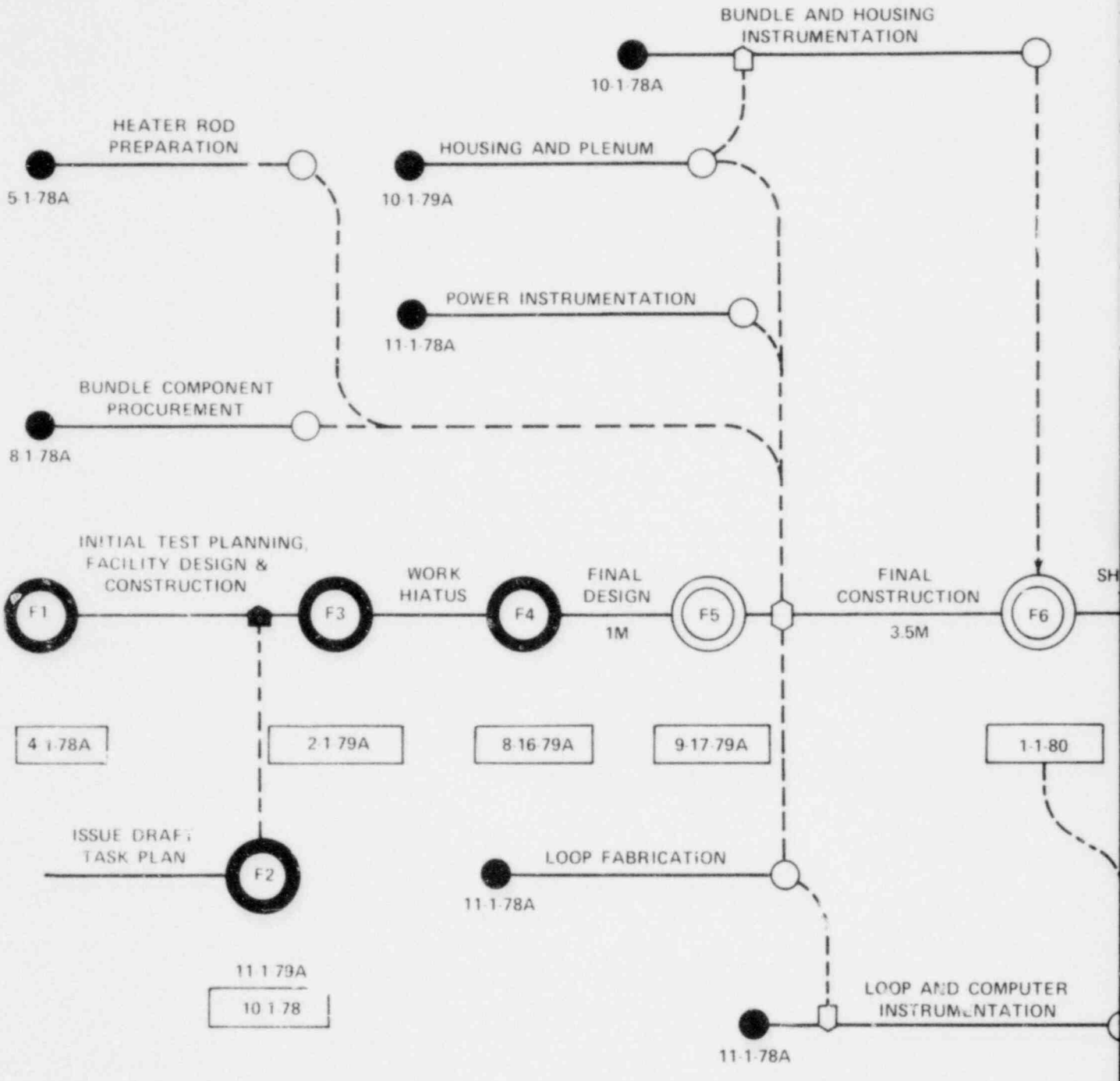
BUNDLE AND HOUSING INSTRUMENTATION
10-1-78A
HEATER ROD PREPARATION
5-1-78A
HOUSING AND PLENUM
10-1-79A
POWER INSTRUMENTATION
11-1-78A
BUNDLE COMPONENT PROCUREMENT
8-1-78A
INITIAL TEST PLANNING, FACILITY DESIGN & CONSTRUCTION
F1
F3
WORK HIATUS
F4
FINAL DESIGN
1M
F5
FINAL CONSTRUCTION
3.5M
F6
SH
4-1-78A
2-1-79A
8-16-79A
9-17-79A
1-1-80
ISSUE DRAFT TASK PLAN
F2
LOOP FABRICATION
11-1-78A
11-1-79A
10-1-78
LOOP AND COMPUTER INSTRUMENTATION
11-1-78A

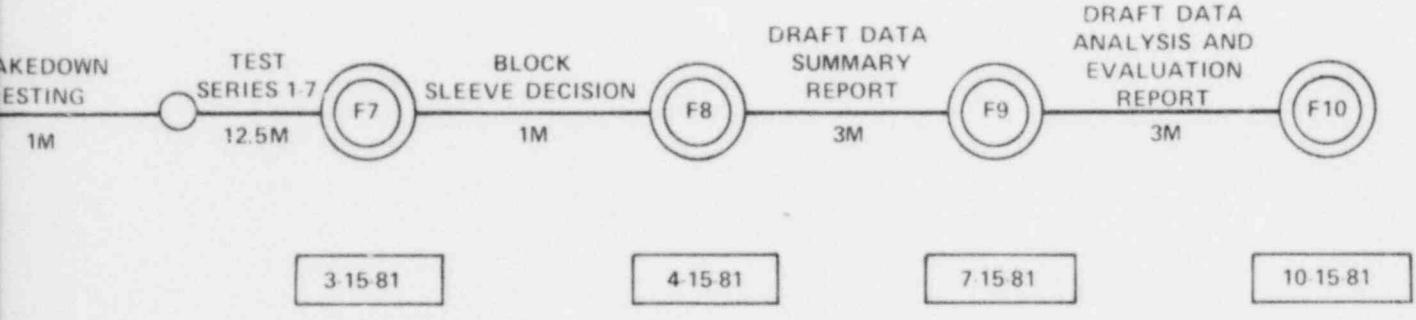

Figure 10-1. Task Schedule for FLECHT SEASET 21-Rod Blocked Bundle Task

APPENDIX A
COBRA CODE

A-1. CODE DESCRIPTION AND INPUT PARAMETERS

Westinghouse has proposed to use the COBRA-IV subchannel computer code[1] to predict the local flow redistribution effects in both the 21-rod and large bundle flow blockage heat transfer tests. The COBRA-IV code is identical to the previously reported COBRA-IIIC code,[2] except that COBRA-IV can handle a wider range of thermal-hydraulic problems (table A-1[3]). Existing COBRA-IIIC and COBRA-IV comparisons with flow blockage and flow redistribution data have been reviewed to investigate COBRA's applicability for the FLECHT SEASET flow blockage program.

The COBRA code (either COBRA-IIIC or COBRA-IV) solves the following conservations for the subchannel flow in a rod bundle:

-- Continuity

$$A \frac{\partial \rho}{\partial t} + \frac{\partial m}{\partial \chi} + [DC]^T w = 0$$

-- Energy

$$A \frac{\partial (\rho h)}{\partial t} + \frac{\partial (mh)}{\partial \chi} + [DC]^T h^* w = q'$$

-- Axial momentum

$$\frac{\partial m}{\partial t} + \frac{\partial mu}{\partial \chi} + [DC]^T u^* w + A \frac{\partial p}{\partial \chi} = F$$

1. Wheeler, C. L., et al., "COBRA-IV: An Interim Version of COBRA for Thermal-Hydraulic Analysis of Rod Bundle Nuclear Fuel Elements and Cores," BNWL-1962, March 1976.
2. Rowe, D. S., "COBRA-IIIC: Digital Computer Program for Steady-State and Transient Thermal-Hydraulic Analysis of Rod Bundle Nuclear Fuel Elements," BNWL-1695, March 1973.
3. Stewart, C. W., et al., "COBRA-IV: The Model and the Method," BNWL-2214, July 1977.

TABLE A-1

COBRA DEVELOPMENT CHRONOLOGY

Capability or Model	COBRA Version (Publication and Date)				
	I BNWL-371 3/67	II BNWL-1229 2/70	III BNWL-B-82 7/71	IIIC BNWL-1695 3/73	IV-1 BNWL-1962 5/76
Flow solution - steady state					
Forward march	x	x			
Inlet flow/exit pressure boundary conditions			x	x	x
Pressure drop boundary conditions					x
Flow solution - transient					
Full implicit				x	x
Explicit arbitrary flow field and boundary conditions					x
Single-phase flow					
Nonuniform channel friction		x	x	x	x
Hot wall friction correction				x	x
Laminar friction correction					x
Two-phase flow					
1D slip flow	x	x	x	x	x
Subcooled voids		x	x	x	x
Turbulent mixing					
Single-phase	x	x	x	x	x
Two-phase models		x	x	x	x

TABLE A-1 (cont)

COBRA DEVELOPMENT CHRONOLOGY

Capability or Model	COBRA Version (Publication and Date)				
	I BNWL-371 3/67	II BNWL-1229 2/70	III BNWL-B-82 7/71	IIIC BNWL-1695 3/73	IV-1 BNWL-1962 5/76
Crossflow model					
Pressure-resistance only	x	x	x		
Transient momentum equation				x	x
Forced diversion				x	x
Lateral momentum flux					x
Equation of state					
Reference pressure	x	x	x	x	x
Superheated steam properties					x
Geometry					
Variable gap and area		x	x	x	x
Grid spacers		x	x	x	x
Blocked crossflow (transient)					x
Wire wrap spacer				x	x
Fluid energy solution					
Spatially explicit	x	x	x	x	
Spatially implicit					x
Heat conduction - fuel rods					
Specified axial and radial heat flux	x	x	x	x	x
CHF correlations				x	x
Transient fuel rod model finite difference				x	

TABLE A-1 (cont)

COBRA DEVELOPMENT CHRONOLOGY

Capability or Model	COBRA Version (Publication and Date)				
	I BNWL- 371 3/67	II BNWL- 1229 2/70	III BNWL- B-82 7/71	IIIC BNWL- 1695 3/73	IV-1 BNWL- 1962 5/76
Orthogonal collocation					x
Axial conduction					x
Temperature-dependent conductivity					x
Axial fuel zones					x
Boiling curve package					x
Heat conduction - fluid					
Radial conduction		x	x	x	x
Axial conduction					x

-- Transverse momentum

$$\frac{\partial w}{\partial t} + \frac{\partial u^* w}{\partial \chi} + \frac{\partial V_y w}{\partial y} - [DC]\, p = C$$

where

χ	=	channel axial direction
y	=	lateral direction
t	=	time
A	=	subchannel flow area
ρ	=	density
m	=	flow rate
h	=	subchannel enthalpy
w	=	diversion crossflow between adjacent subchannels per unit length
u	=	axial subchannel velocity
V_y	=	lateral velocity in subchannel
p	=	subchannel pressure
$[DC]$	=	difference operator for subchannels
$[DC]^T$	=	transpose of difference operator
q'	=	heat transfer from all sources
F	=	axial friction and gravity force
C	=	lateral friction force
$*$	=	convected quantity

These balance equations are based on several assumptions, summarized in table A-2.[1] The derivation of the equations used in COBRA-IIIC or COBRA-IV can be found in BNWL-2214.[2]

To solve this system of equations, several empirical models must be provided to yield a closed form of the conservation equations, which can then be numerically

---

1. Wheeler, C. L., et al., "COBRA-IV: An Interim Version of COBRA for Thermal-Hydraulic Analysis of Rod Bundle Nuclear Fuel Elements and Cores," BNWL-1962, March 1976.

2. Stewart, C. W., et al., "COBRA-IV: The Model and the Method," BNWL-2214, July 1977.

TABLE A-2

MAJOR ASSUMPTIONS AND RESTRICTIONS

Assumption or Restriction	Equations Involved	Effects
Common to both numerical algorithms:		
Thermal equilibrium	All	Requires equal phase temperatures
Geometry constant in time	All	Restricts problems that can be addressed
Lateral turbulence model based on equal mass exchange	All	$w'_{ij} = w'_{ji}$
No turbulent mixing between axial nodes	All	$u' = 0$
Fluid properties a function of h and the reference pressure	All	Thermal expansion is included but compressibility (due to local pressure changes) is not.
$\delta p/\delta t$ neglected in the energy equation	Energy	No sonic propagation
Negligible heat generation within the fluid	Energy	
Changes in kinetic energy assumed small	Energy	Only mechanisms for internal energy change are heat transfer, convection, and turbulent mixing.
Viscous dissipation neglected	Energy	
Work against the gravity field neglected	Energy	
Gravitational acceleration the only body force	Momentum	Electromagnetic forces not considered

TABLE A-2 (cont)

MAJOR ASSUMPTIONS AND RESTRICTIONS

Assumption or Restriction	Equations Involved	Effects
Transverse body force neglected	Transverse momentum	No lateral buoyancy effects (restricts only when flow channel not vertical)
Surface tension contributions neglected	Momentum	Requires equal phase pressures
Fluid drag forces represented by wall friction and form drag	Momentum	Fluid-fluid shear neglected (turbulent momentum exchange modeled, however)
Two of the six terms in the transverse momentum equation neglected	Transverse momentum	Allows arbitrary lateral coupling of channels
Flow area varying linearly between axial locations	All	No step area changes
For the explicit method:		
Homogeneous fluid	Momentum and energy	Equal phase velocities, that is $u_g = u_l$ $V_g = V_l$
Courant restriction	All	Maximum time step limited to $\Delta t \leq \Delta x/u$
For the implicit method:		
Specified axial slip an option; however, transverse slip neglected	Momentum and energy	$u_g \neq u_l$, $V_g = V_l$
No reverse flow	All	Stability

solved. Those parameters which affect isothermal single-phase flow redistribution are as follows:

-- Axial friction factor

The friction factor correlation is assumed to be of the form

$$f = a(Re)^b + C$$

where a, b, and C are specified constants that depend on the subchannel roughness and geometry. This is typically provided from experimental data on rod bundles, such as that given by Tong.[1]

-- Spacer loss coefficient

The pressure drop from spacers is lumped into an effective loss coefficient which may be defined in terms of all-liquid flow as

$$\Delta p = \frac{K}{2\rho} \left(\frac{m}{A}\right)^2$$

Grid loss coefficient data are provided either from experiments or from calculational schemes such as those of Rehme[2] or Kays and London,[3] which are based on some experimental data for similar geometries.

-- Turbulent crossflow and mixing

There are several available expressions for specifying the turbulent crossflow in COBRA-IIIC or IV:

---

1. Tong, L. S., "Pressure Drop Performance of a Rod Bundle," in Heat Transfer in Rod Bundles, pp 57-69, American Society of Mechanical Engineers, New York, 1968.

2. Rehme, K., "Pressure Drop Correlations for Fuel Element Spacers," Nucl. Technol. 17, 15-23 (1973).

3. Kays, W. M., and London, A. L., Compact Heat Exchangers, 2nd edition, McGraw-Hill, New York, 1964.

$$W'_k = \beta S_k \bar{G}$$

$$W'_k = a (Re)^b S_k \bar{G}$$

$$W'_k = a (Re)^b \bar{D} \bar{G}$$

$$W'_k = a (Re)^b \left(\frac{S_k}{Z}\right) \bar{D} \bar{G}$$

where

W'_k = turbulent (fluctuating) crossflow per unit length

$$Re = \frac{\bar{G} \bar{D}}{\mu}$$

$$\bar{D} = \frac{4(A_{i(k)} + A_{j(k)})}{PW_{i(k)} + PW_{j(k)}}$$

$$\bar{G} = \frac{\dot{m}_{i(k)} + \dot{m}_{j(k)}}{A_{i(k)} + A_{j(k)}}$$

$$\bar{\mu} = 1/2 (\mu_{i(k)} + \mu_{j(k)})$$

S = subchannel gap spacing

Z = centroid-to-centroid distance between adjacent channels

and a and b are user input constants. Since there are no unique and definitive mixing correlations, the COBRA code allows the user to specify the relationship of his choice.

In addition to the above three parameters, the crossflow resistance, K_{ij}, and the crossflow momentum parameter, s/ℓ (S is the rod gap and ℓ is the distance between subchannels over which the lateral acceleration occurs), are required. Also, the method of assigning the velocity and enthalpy of the crossflow must be decided. With respect to the crossflow resistance, K_{ij}, numerical studies by BNWL[1] indicated that this parameter would not influence the crossflow velocity

1. Rowe, D. S., et al., "An Experimental Study of Flow and Pressure in Rod Bundle Subchannels Containing Blockages," BNWL-1771, September 1973.

and flow redistribution to any measurable degree. This same effect was found in THINC-IV subchannel program.[1] The value chosen for the ratio S/ℓ is typically 0.5. BNWL studies[2] which varied this parameter also showed no measurable effect on the flow redistribution.

It should also be noted that the range of variation of S/ℓ is rather small. BNWL also examined the effects of different methods of calculating the value of the velocity and enthalpy for the crossflow, and found that the donor cell approach was the most suitable. The donor cell method means that the subchannel which is gaining flow or energy gains it from the adjacent cell (donor cell) at that cell's average velocity and enthalpy. This approach, the same as used in several other subchannel codes, has been found acceptable.[1,3]

A-2. COMPARISONS BETWEEN COBRA PREDICTIONS AND DATA

BNWL has compared the COBRA-IIIC and COBRA-IV code versions with a substantial amount of rod bundle flow redistribution data. In particular, BNWL has conducted several hydraulic flow blockage experiments in which local subchannel velocity values were measured both upstream of, within, and downstream of the flow blockage zone. These experiments and COBRA comparisons, and the basis for adjusting the three empirical models indicated above are discussed below.

Rowe, et al.,[4] first tested the COBRA-IIIC calculational ability using a two-dimensional 1x4 blockage subchannel geometry (figure A-1). The test section is shown in figure A-2 and the blockage shape details are given in figure A-3. Both plate and tapered sleeve coplanar blockage were tested in this experiment. Both

---

1. Chelemer, H., et al., "THINC-IV: An Improved Program for Thermal-Hydraulic Analysis of Rod Bundle Cores," WCAP-7956, June 1973.

2. Rowe, D. S., "COBRA-IIIC: Digital Computer Program for Steady-State and Transient Thermal-Hydraulic Analysis of Rod Bundle Nuclear Fuel Elements," BNWL-1695, March 1973.

3. Welch, J. E., et al., "The MAC Method - A Computing Technique for Solving Viscous, Incompressible, Transient Fluid-Flow Problems Involving Free Surfaces," LA-3425, November 1965.

4. Rowe, D. S., et al., "An Experiment Study of Flow and Pressure in Rod Bundle Subchannels Containing Blockages," BNWL-1771, September 1973.

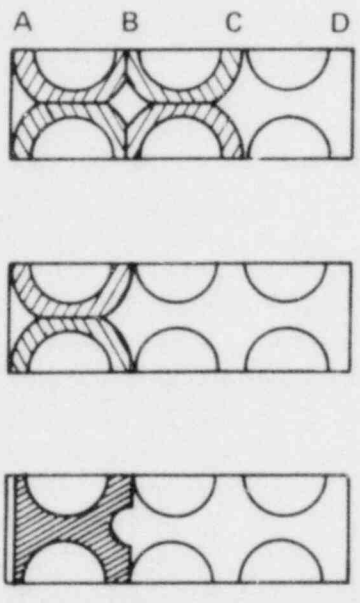

		SUBCHANNEL AREA FACTORS			
		A	B	C	D
I	SLEEVE	0.23	0.09	0.46	1.0
II	SLEEVE	0.23	0.46	1	1
IV	PLATE	0.23	0.46	1	1

Figure A-1. 1x4 Channel Cross Section Tested

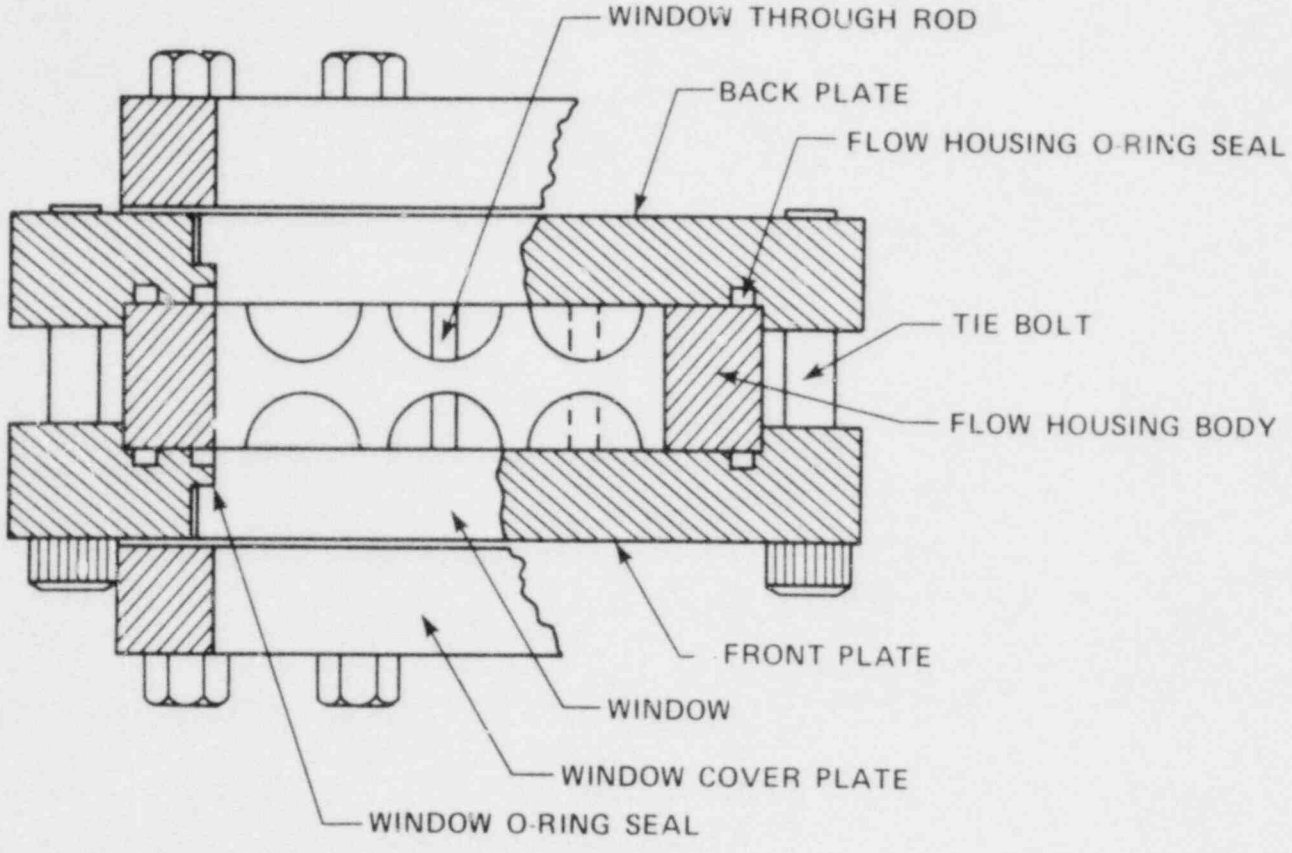

Figure A-2. Test Section Construction Details

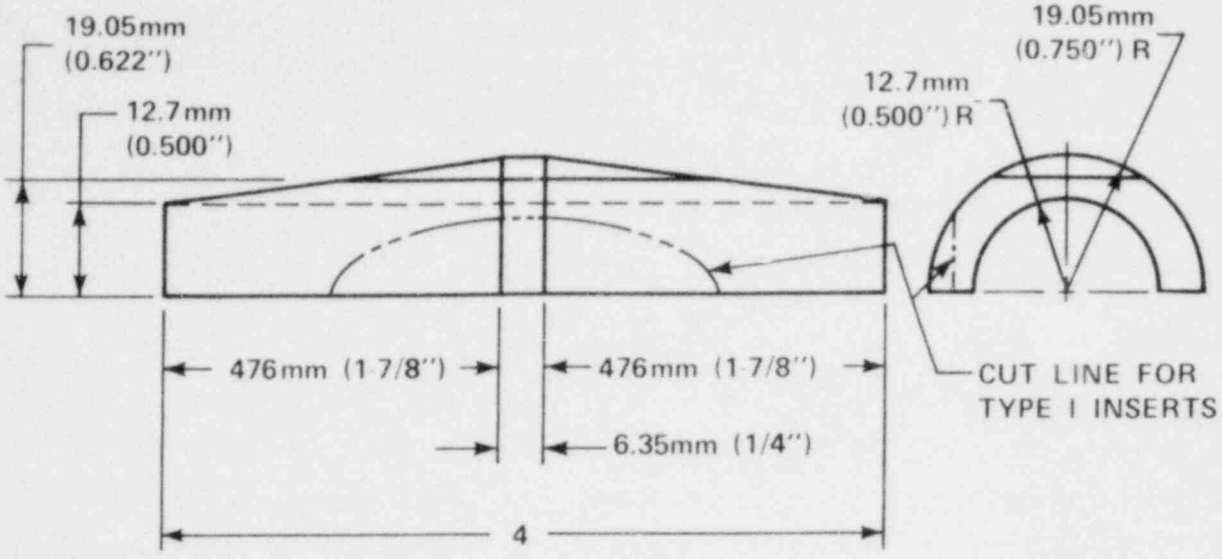

(A) NOMINAL DIMENSIONS OF SLEEVE BLOCKAGE INSERTS

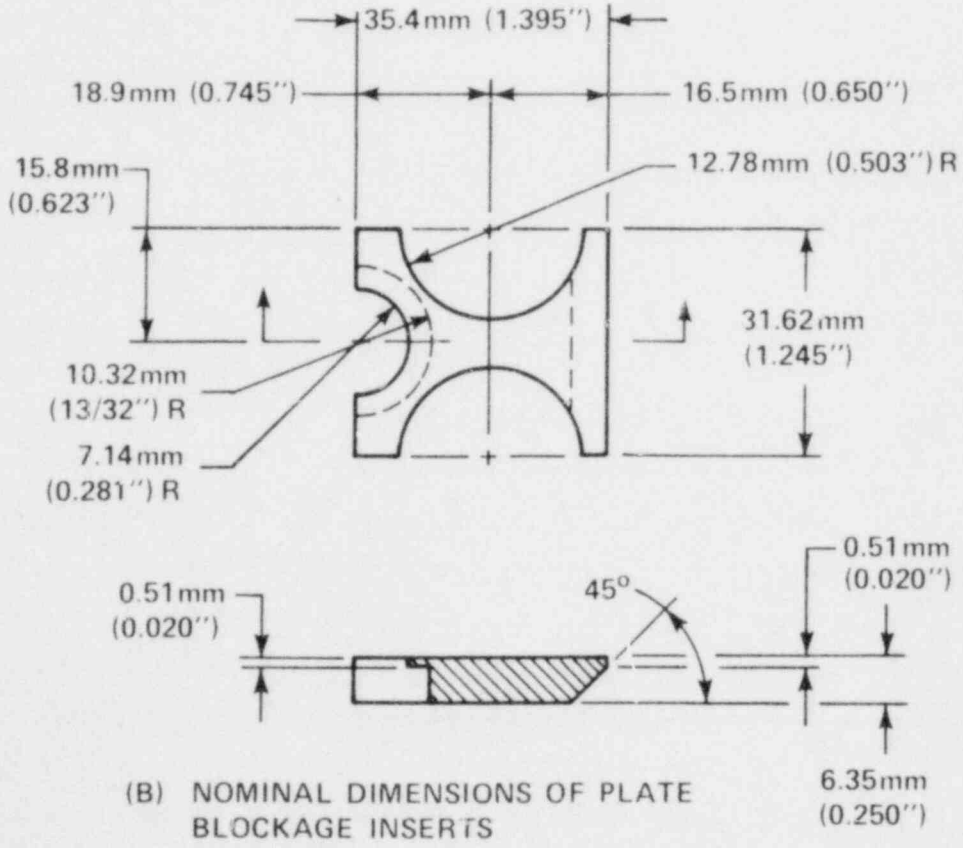

(B) NOMINAL DIMENSIONS OF PLATE BLOCKAGE INSERTS

Figure A-3. Sleeve and Plate Blockage Insert Dimensions

the plate and sleeve blockages were modeled using a combination of subchannel area reduction and blockage loss coefficients. The approximations of the physical blockages are shown in figure A-4 for all three blockage configurations. An unrecoverable blockage pressure loss was also included by the use of a subchannel loss coefficient. BNWL found that for the sleeve blockage, the local subchannel form loss factor was quite small, 0.03 to 0.12, for the different smooth entry sleeve blockage channels; the plate form loss factor was larger, typically 0.73 to 0.76.

COBRA calculations were performed with and without these form factors; it was found that the area reduction model was the major mechanism for providing forced flow diversion from the blocked subchannels. The primary purpose of the blockage loss coefficients was to account for the unrecoverable pressure loss. Therefore, BNWL feels that blockage loss coefficients used by themselves without the proper area variation model will not yield accurate subchannel flow redistributions in a blocked assembly.

Sample comparisons of the COBRA predictions for different blockage geometries are shown in figures A-5 through A-7. Inputs for COBRA simulation of this system are given in table A-3. In these figures, simulated results with and without the K factor (loss coefficient) for blockage are also compared. With the exception of a flat plate, it can be seen that the effect of the blockage loss coefficient is not significant, and the flow redistribution effect is not strongly influenced by the value of K_i. An estimate of the uncertainty in the flow subchannel data is indicated in figures A-5 through A-7. This uncertainty value was derived by BNWL and is a result of having the average flow values. As the figures indicate, the COBRA predictions agree quite well with the data.

The mixing parameter, β, was also varied in the four-channel simulation and was assigned a maximum value at the point of maximum blockage. Two others values of β were examined to determine the importance of this parameter. In the first case, β was assumed to have a constant value of 0.02 (typical of clean rod bundles) over the entire length of the model. This produced identical velocity distributions at the inlet, but the velocity distribution downstream of the inlet changed by approximately 7 percent. The calculated pressure loss was also observed to change by 3 percent. The other model assumed a constant β of 0.12 over the entire length. This produced velocity and pressure distributions downstream of the blockage that deviated by less than 5 percent from those computed

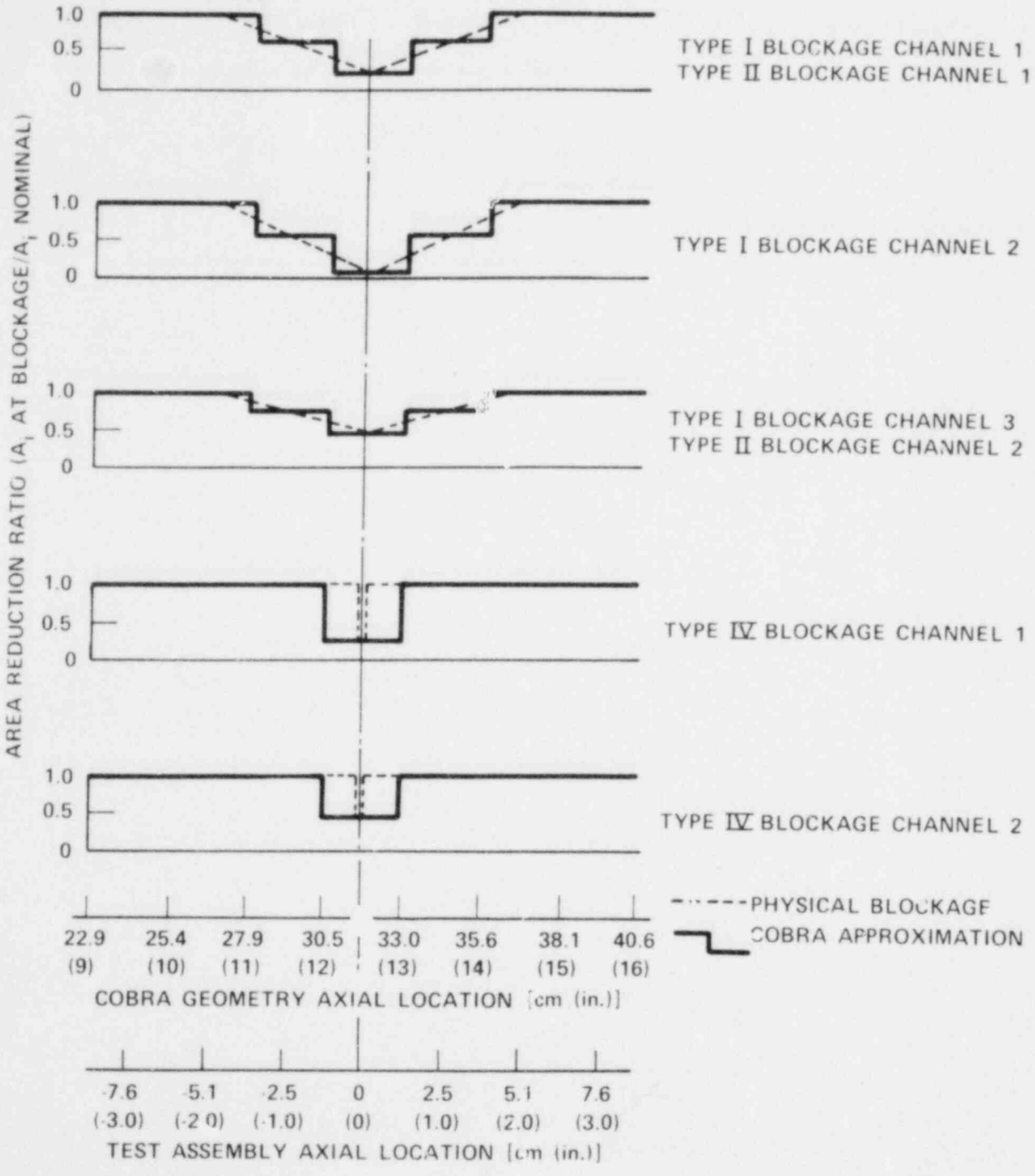

Figure A-4. Subchannel Area Reduction To Model Blockages

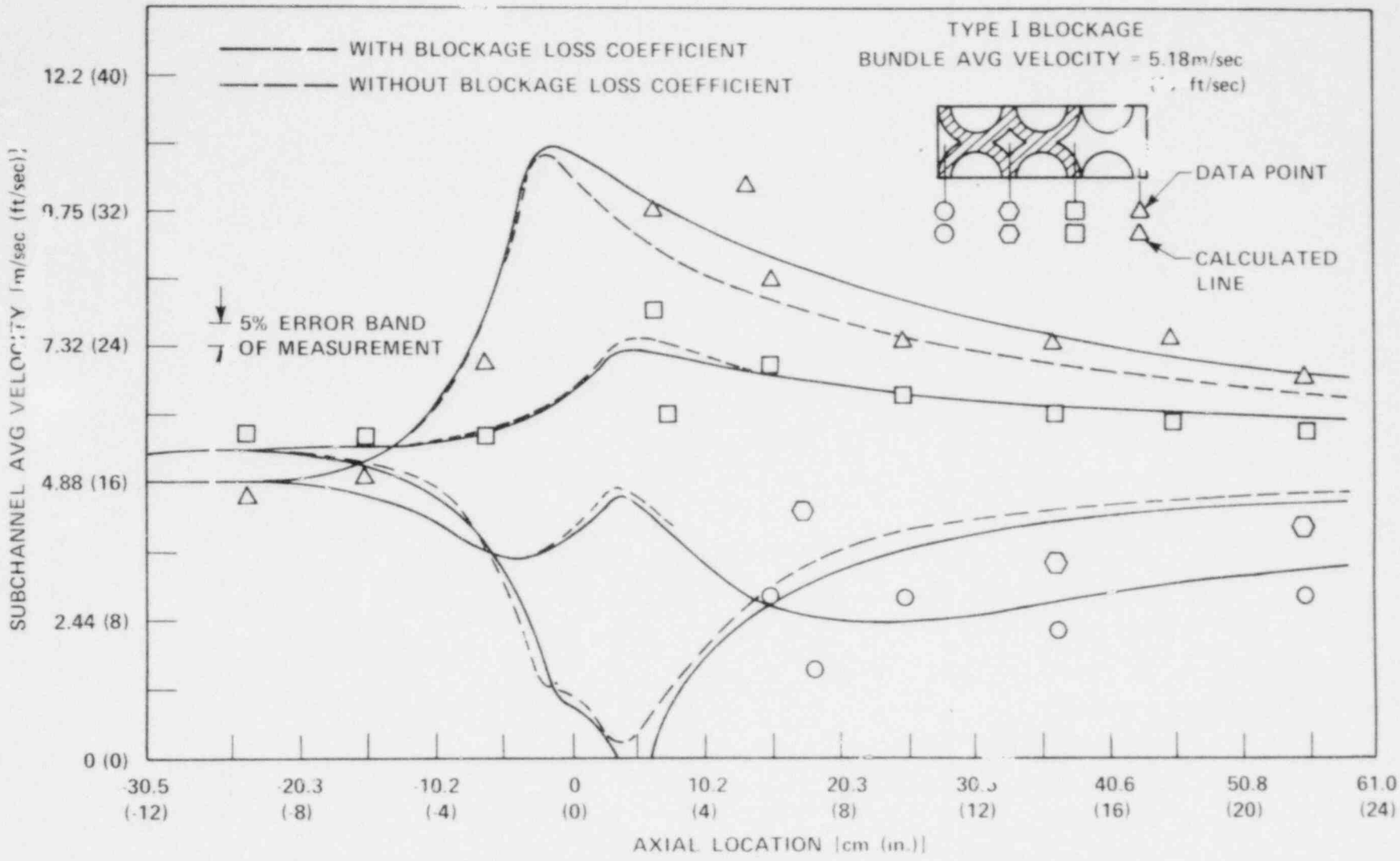

Figure A-5. Comparison of Experimental Flow Rate Estimates With Prediction of COBRA-IIIC Program for Type I Sleeve Blockage

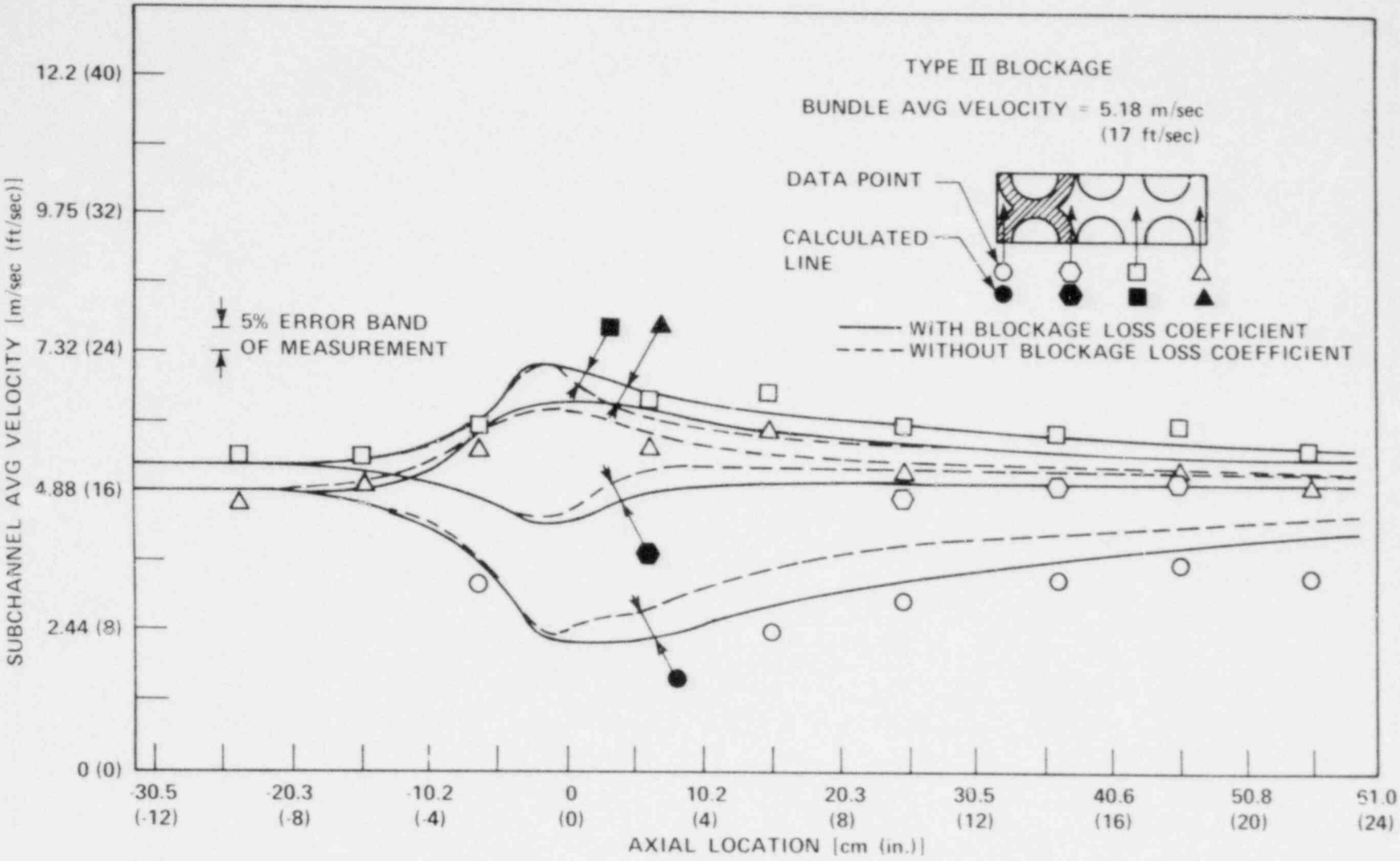

Figure A-6. Comparison of Experimental Flow Rate Estimates With Prediction of COBRA-IIIC Program for Type II Sleeve Blockage

16,047-44

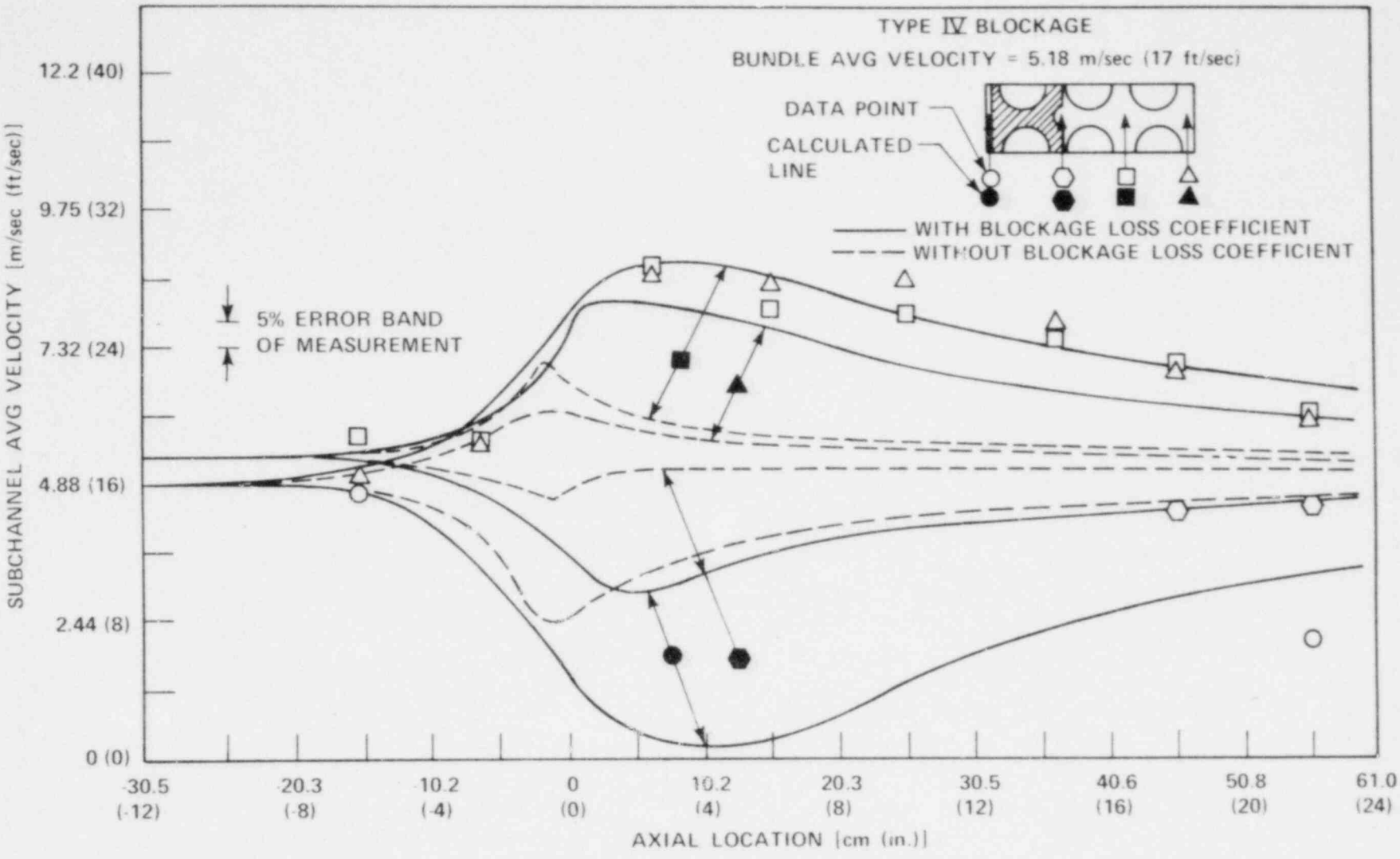

Figure A-7. Comparison of Experimental Flow Rate Estimates With Prediction of COBRA-IIIC Program for Type IV Plate Blockage

16,047-45

TABLE A-3

COBRA INPUTS FOR FOUR-CHANNEL FLOW

Crossflow resistance	K_{ij}	0.15
Transverse momentum	S/ℓ	0.25
Turbulent momentum factor	ft	1.0
Bare rod friction factor	f	$0.225\ Re^{-0.22}$ (internal subchannel)
		$0.217\ Re^{-0.2}$ (wall subchannel)
Subchannel blockage loss coefficient	K	0.08 type I blockage
		0.1 type II blockage
		0.75 type IV blockage
Turbulent mixing coefficient	β	0.02 - 0.1 (function of Z) types I and IV blockage
		0.02 - 0.05 (function of Z) type II blockage

using the reference profile. Therefore, the uncertainty of β does not change the flow redistribution results significantly, and sufficient data do exist that a proper value can be chosen for FLECHT SEASET which will result in a minimum uncertainty in the flow redistribution.

Additional flow blockage studies were performed by BNWL in a 7x7 bundle[1,2] using both air and water (separately). The test assembly cross section with a blockage cluster at the center of the bundle is shown in figure A-8. The details of blockage with pertinent dimensions are shown in figure A-9. Flow area reductions of 70 and 90 percent could be attained in the center four subchannels. The 70- and 90-percent severities correspond to area reductions of 35 and 45 percent in the subchannels adjacent to the sides of the cluster and 17 and 22 percent in the subchannels next to the corners of the blockage, respectively. Air and water flows in local subchannels were measured using a laser-doppler anemometer (LDA) technique.

For COBRA simulation, a full-length, 1/8-symmetrical cross section of the bundle was modeled (figure A-10). COBRA input parameters for the water flow test simulation are given in table A-4. The same model was used for both the air flow test and the water flow test; only the operational temperature and fluid properties were changed. The same technique of area reduction was used to model the blockage in these tests as in the BNWL-1771 1x4 subchannel tests. Sample comparisons of the subchannel velocities predicted by COBRA-IIIC and measured in the experiment are shown in figures A-11 through A-14.

The agreement between COBRA predictions and the data is quite good, typically within 10 percent. It should be noted that uncertainty based on the mean velocity data is approximately 10 percent.[3] The data uncertainty is a result of making the point velocity measurements with the LDA and developing a subchannel averaging technique such that the mean velocity in the subchannel can be compared

---

1. Creer, J. M., et al., "Effects of Sleeve Blockages on Axial Velocity and Intensity of Turbulence in an Unheated 7 x 7 Rod Bundle," BNWL-1965, January 1976.

2. Creer, J. M., and Bates, J. M., "Effects of Sleeve Blockages on Air Velocity Distributions In an Unheated 7 x 7 Rod Bundle," BNWL-1975, January 1976.

3. Telephone conversation with J. M. Creer, June 23, 1978.

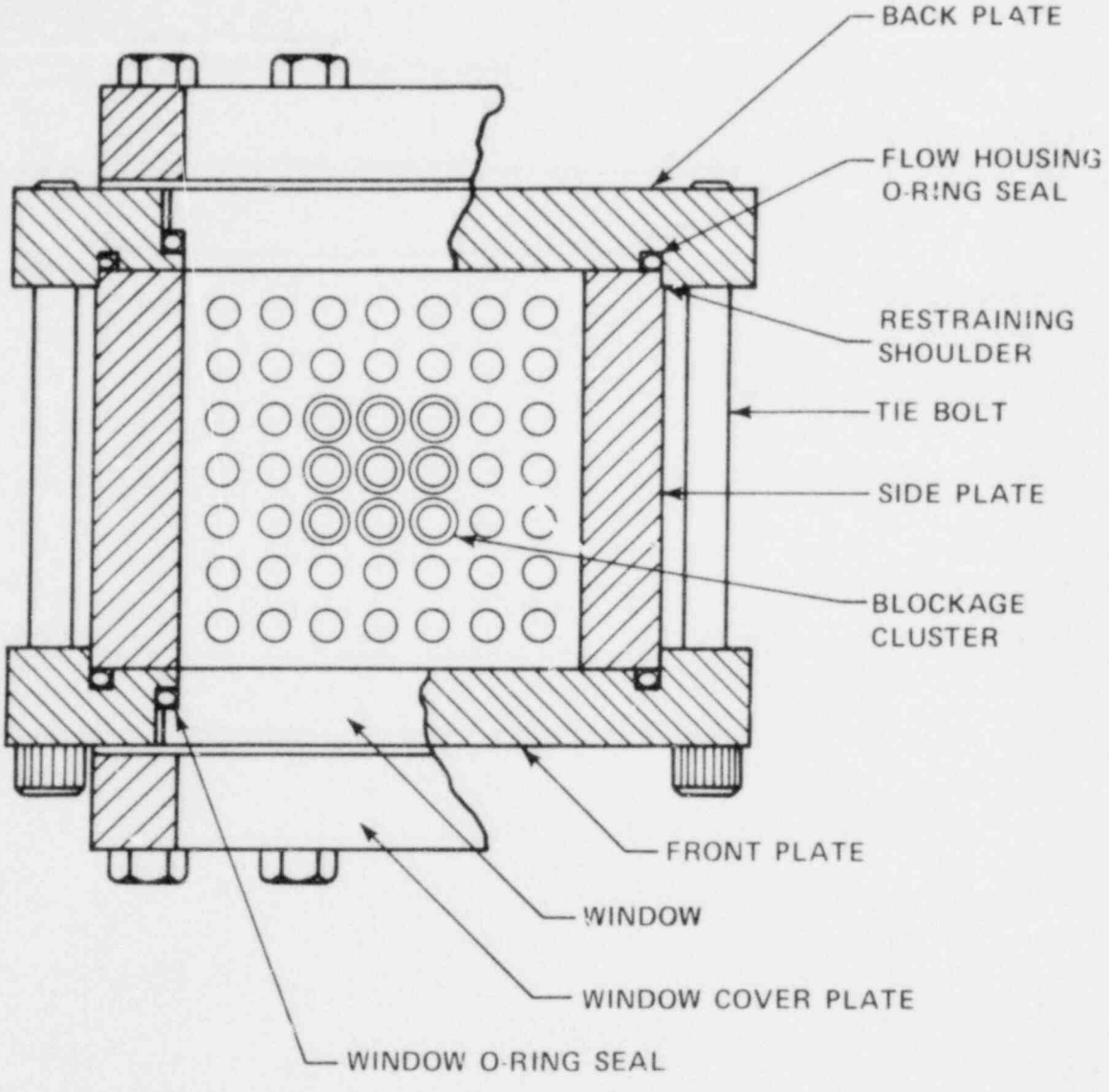

Figure A-8. Test Assembly Cross Section at Blockage Axial Centerline

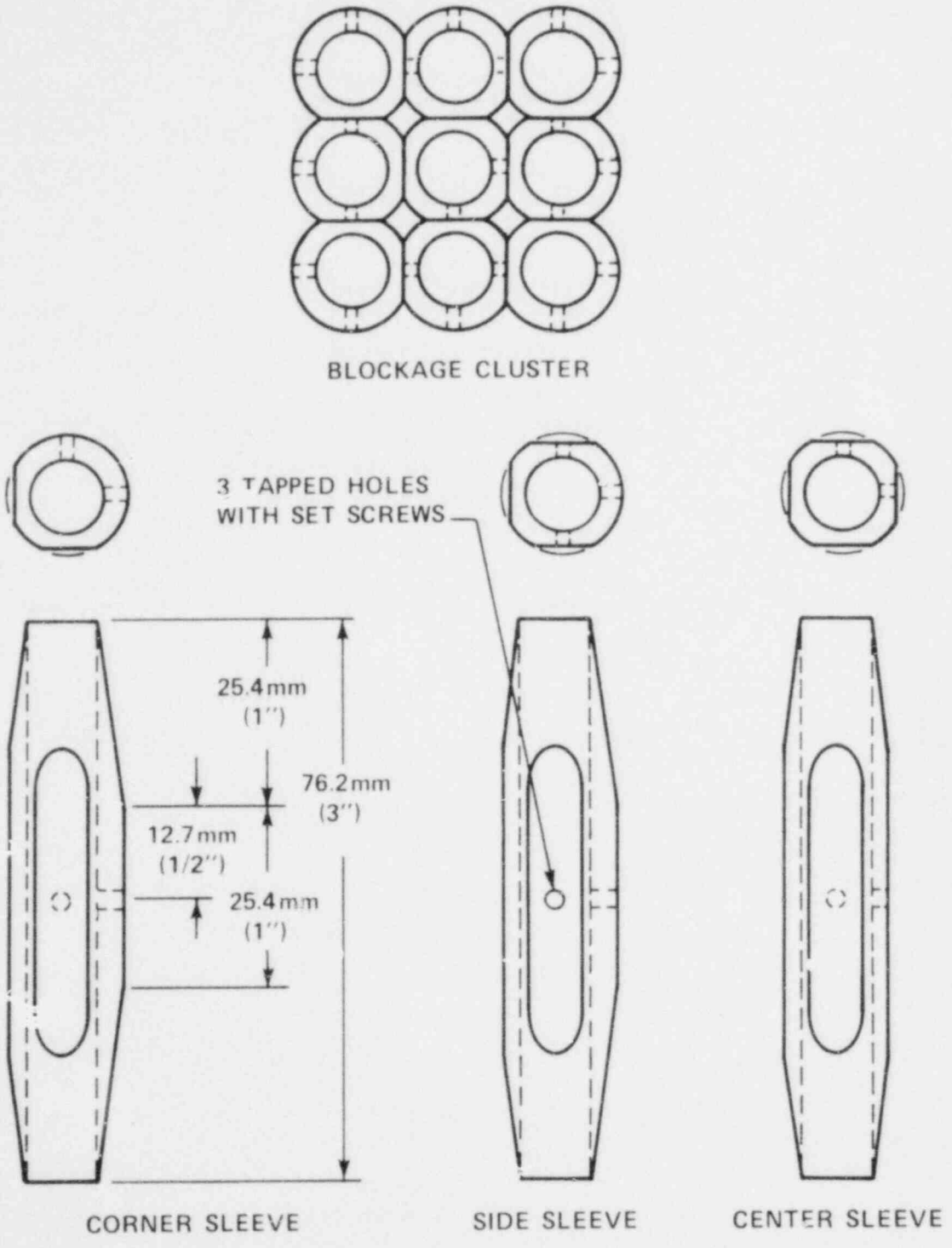

Figure A-9. Flow Blockage Sleeves

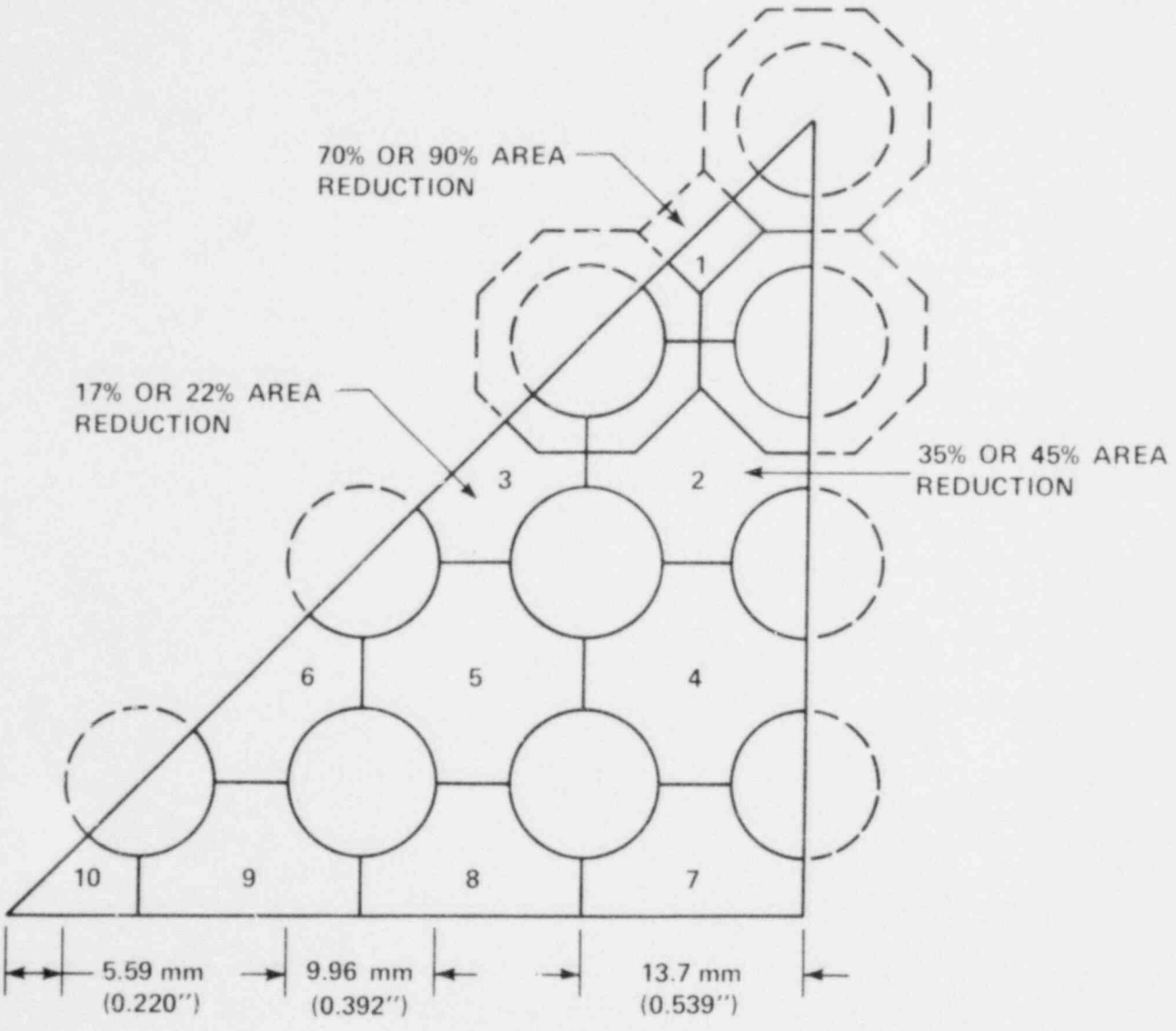

Figure A-10. COBRA Geometry Model

TABLE A-4

COBRA INPUT PARAMETERS (BNWL 7x7 BUNDLE)

Parameter	COBRA Symbol	Value	
		70%	90%
Crossflow resistance	K_{ij}	0.02	0.02
Transverse momentum	S/ℓ	0.25	0.25
Turbulent momentum factor	ft	1.0	1.0
Bare rod friction factor	f	$0.34\ (Re)^{-0.25}$	$0.34\ (Re)^{-0.25}$
Subchannel spacer loss coefficient	K_{s1}	1.14	1.14
Subchannel blockage loss coefficient	K_{s2}		
For subchannel 1		0.5	0.5
For subchannel 2		0.0	0.05
For other subchannels		0.0	0.0
Model length [m (in.)]		1.0 (40)	1.0 (40)
Calculation increment [cm (in.)]	Δz	1.27 (0.5)	1.27 (0.5)
Total transient time (sec)	t	0.0	2.0
Turbulent mixing coefficient	β	0.02	0.02
Temperature [°C (°F)]	T	29.4 (85.0)	29.4 (85.0)

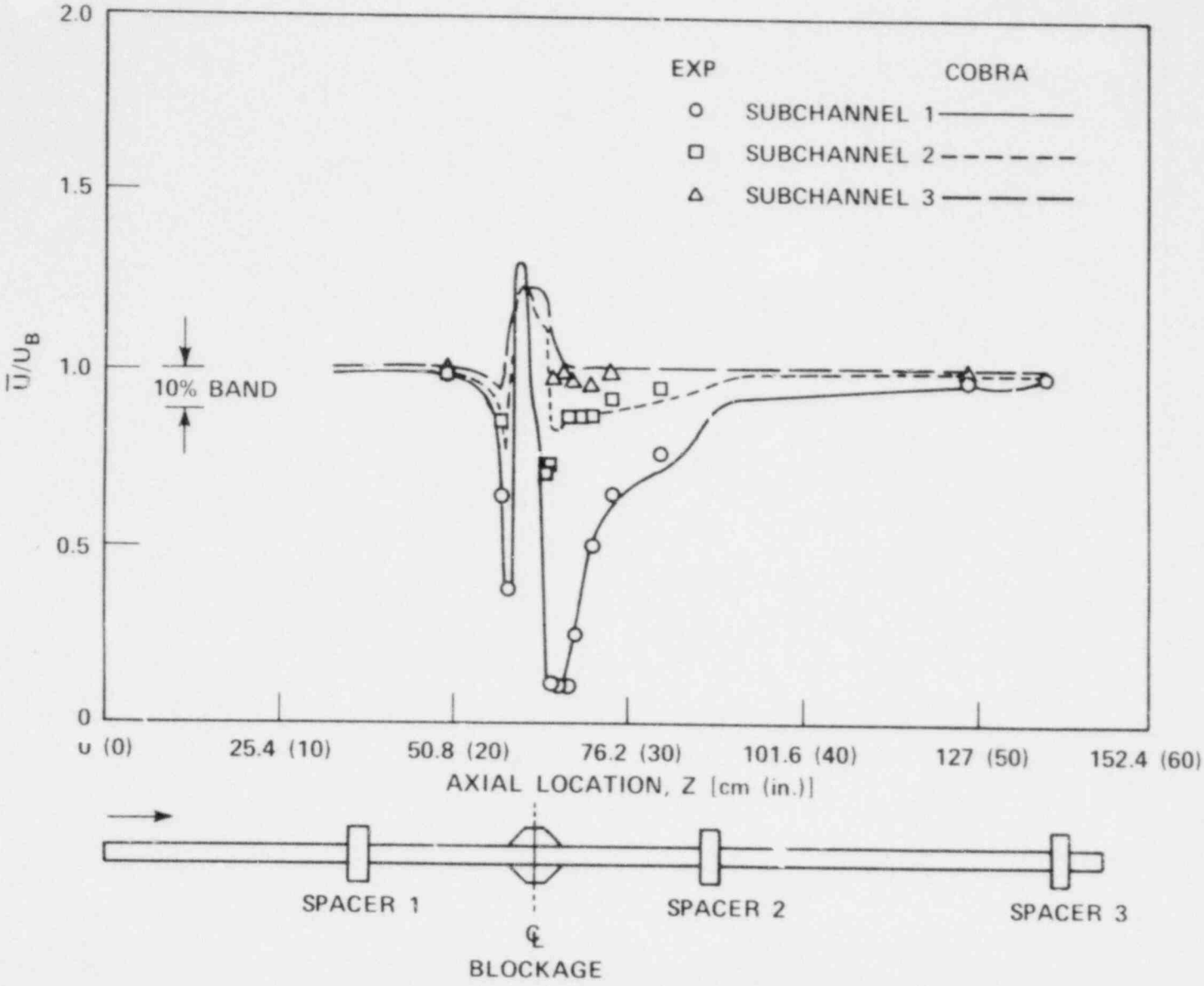

Figure A-11. COBRA Velocity Predictions in Subchannels 1, 2, and 3 With 90-Percent Blockage, U_B = 5.7 ft/sec Water Flow

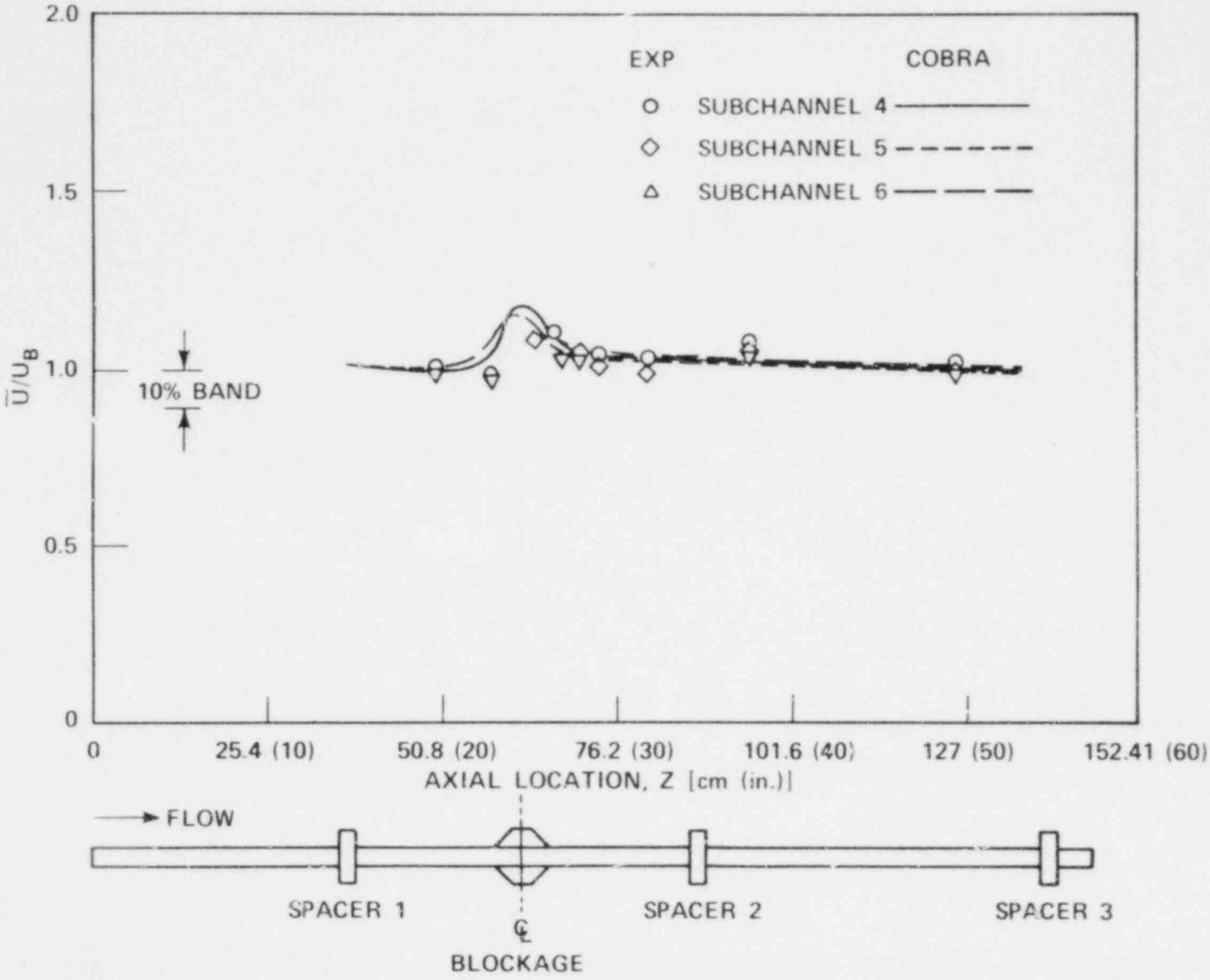

Figure A-12. COBRA Velocity Predictions in Subchannels 4, 5, and 6 With 90-Percent Blockage U_B = 5.7 ft/sec Water Flow

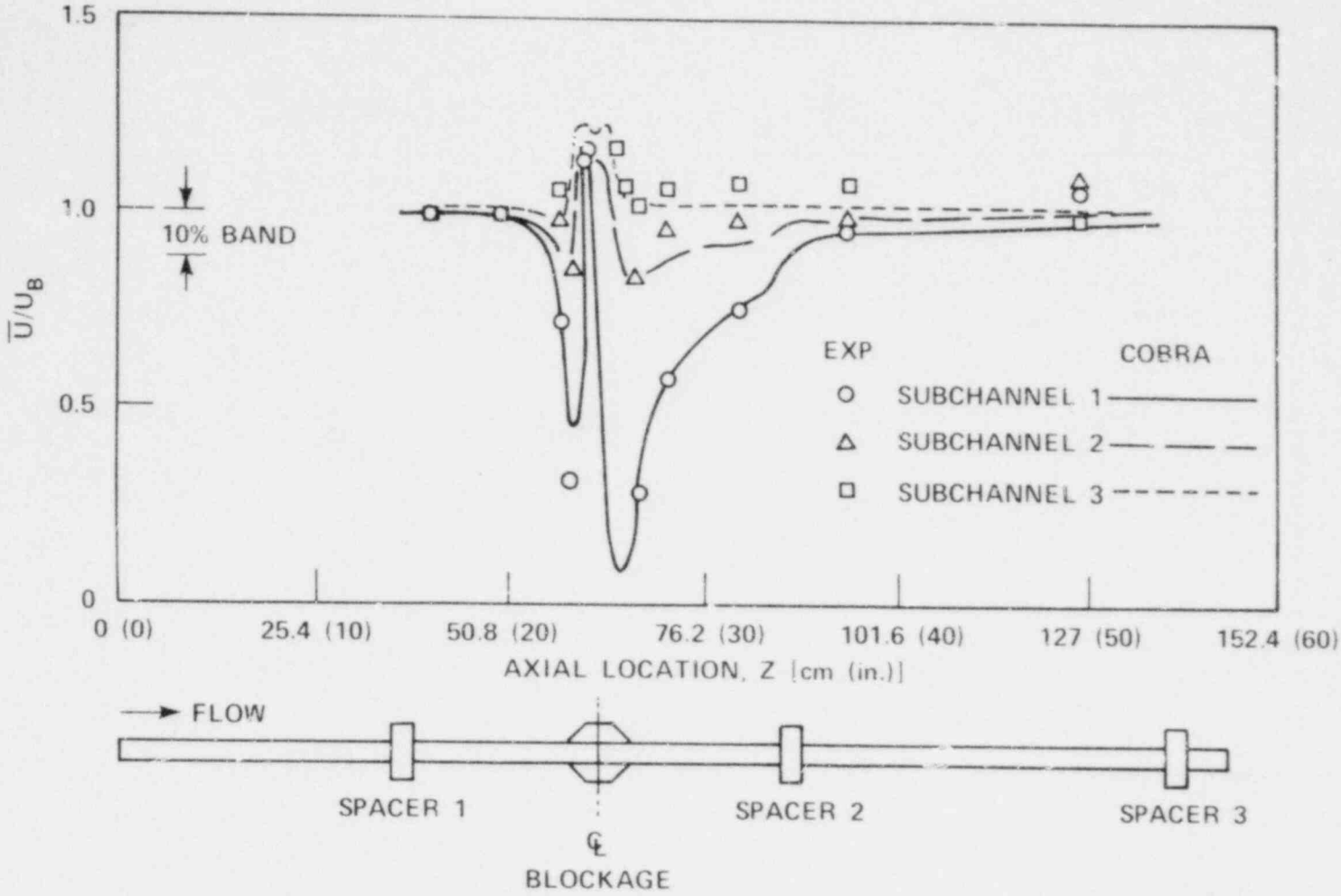

Figure A-13. COBRA Velocity Predictions in Blocked Subchannels 1, 2, and 3 With 90-Percent Blockage, U_B = 38 ft/sec Axial Flow

16,047-51

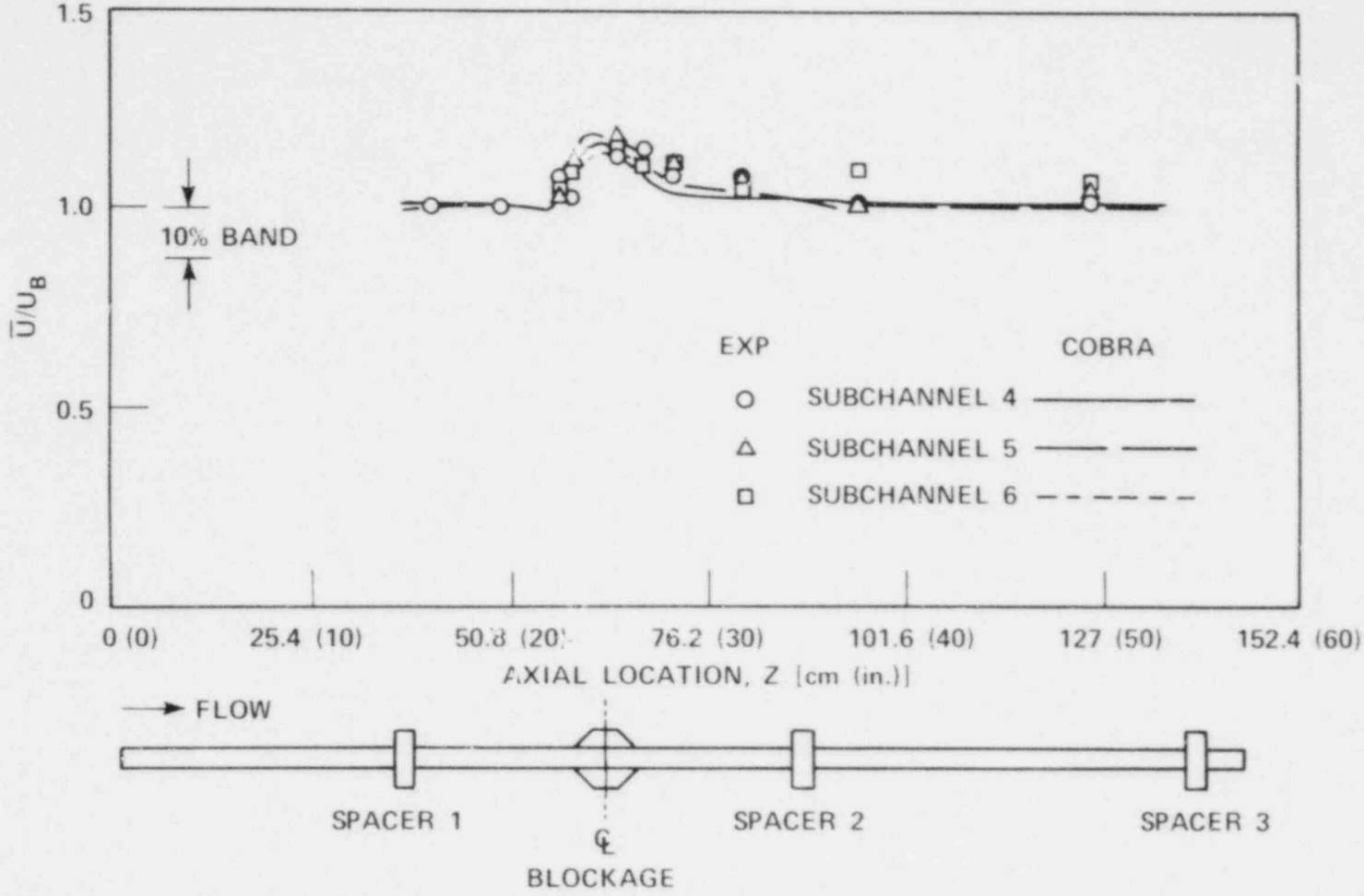

Figure A-14. COBRA Velocity Predictions in Unblocked Subchannels 4, 5, and 6 With 90-Percent Blockage, U_B = 38 ft/sec Air Flow

16,047-52

to the COBRA predictions. Considering the data uncertainty, the agreement between the COBRA predictions and the data is quite good.

The input parameters used in COBRA for the 7x7 blockage study and the 1x4 subchannel blockage study can also be compared (tables A-3 and A-4). The crossflow resistances are different, the axial friction factor relationships are somewhat different, and the mixing coefficient, β, is also different. In spite of these changes, the calculated flow distribution predicted by COBRA agrees very well with the data. The friction factor correlations are different, but all of them are effectively close to the Blassius equation. Blockage loss coefficients for sleeve types are small in comparison to the grid loss coefficients and thus affect flow redistribution minimally. This confirms BNWL's feeling that the primary variable is the blockage area variation, which is an input quantity into the code. All the other effects are second order.

BNWL further tested the COBRA code[1] by simulating the mass flow distribution in two adjacent open-lattice 14x14 rod bundles, as reported by Chelemer, et al.[2] Several tests were run with different inlet mass flows in each bundle to simulate a partially (67 percent/33 percent) or completely (100 percent/0 percent) blocked inlet to one of the rod bundles. This system was lumped into a strip of 29 channels, 14 for each bundle and one channel representing the region between them, for the simulation using COBRA-IV-I. Computed velocity profiles are compared with the 67 percent/33 percent inlet flow distribution results in figure A-15. Again, the agreement between COBRA results and the experimental data is excellent.

Based on the above comparisons, it appears that the COBRA-IIIC or COBRA-IV subchannel code will predict the local subchannel velocities for single-phase flow, and its application should be suitable for the FLECHT SEASET flow blockage program.

---

1. Stewart, C. W., et al., "COBRA-IV: The Model and the Method," BNWL-2214, July 1977.

2. Chelemer, H., et al., "THINC-IV: An Improved Program for Thermal-Hydraulic Analysis of Rod Bundle Cores," WCAP-7956, June 1973.

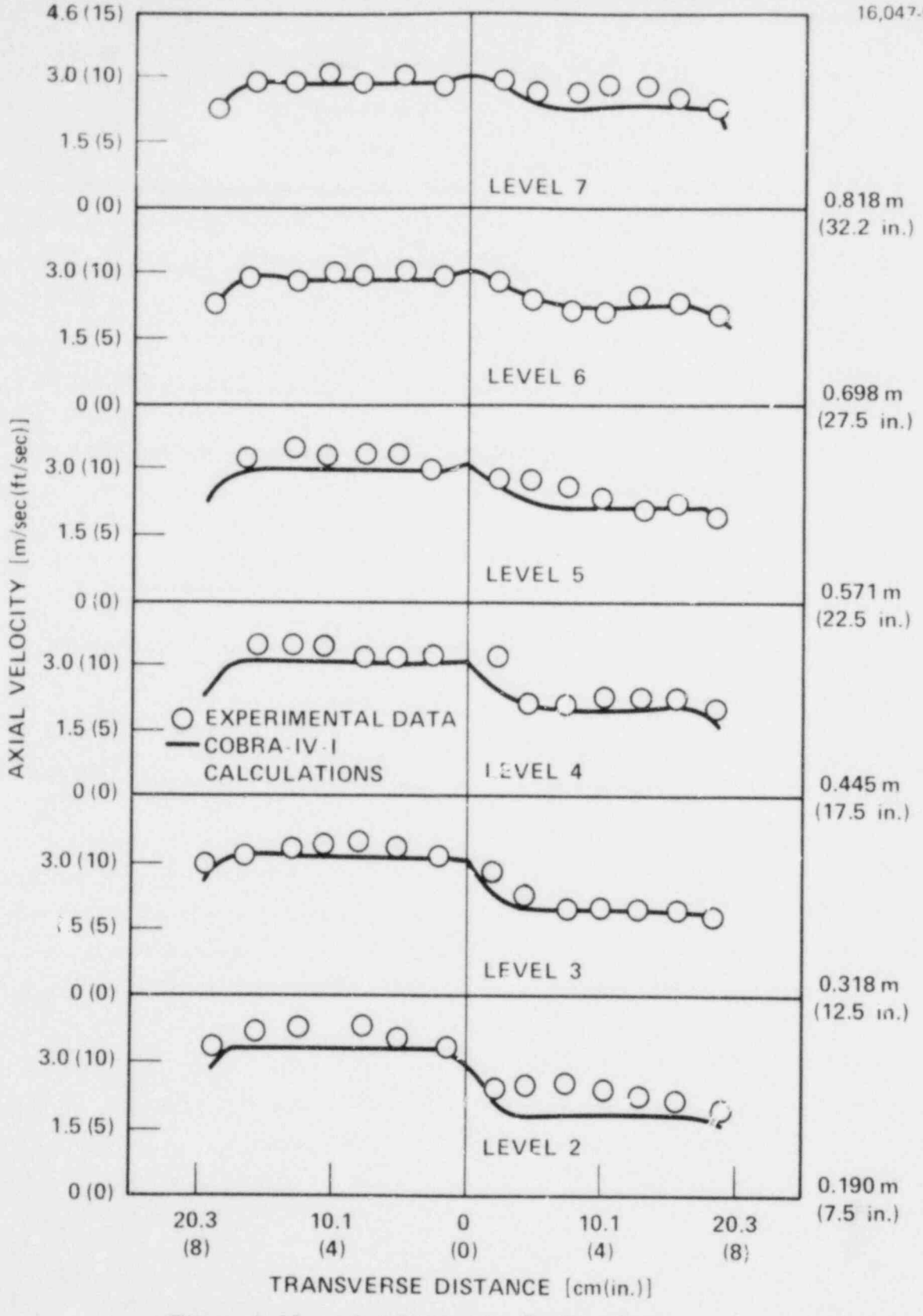

Figure A-15. Axial Velocity Profiles for Westinghouse Flow Blockage Data

APPENDIX B
COMPARISON OF THEORETICAL FLOW SEPARATION LENGTH WITH EXPERIMENTAL DATA

Equation (4-1), in paraqraph 4-5, was developed to predict the flow reattachment length after the flow separation at backward step flows. The equation is given as

$$\chi = 6.3\ h$$

where χ is the reattachment distance from the step and h is the height of the step.

In this appendix, available experimental results are compared with the predictions by equation (4-1) to establish the validity of this equation.

Chang[1] quoted the work of Tani, et al.,[2] which dealt with a fluid flow along a backward-facing step (figure B-1). Their results of stream line mean velocity, turbulence intensity, and turbulent shear stress behind the step are presented in figure B-2.

It can be seen that the reattachment distance (χ/h) is about 6.8; this agrees fairly well with the calculated value of 6.3 from equation (4-1). Chang also reviewed studies on a diffuser and found that the diverging angle of 14 degrees does not give flow separation. This diverging angle is not much different from the theoretical jet expansion angle.

Krall and Sparrow[3] studied turbulent heat transfer downstream of the orifice and found the reattachment distances shown in table B-1. They also showed that

---

1. Chang, P. K., Separation of Flow, 1st edition, New York, Pergamon Press, 1970.
2. Tani, I., et al., "Experimental Investigation of Flow Separation Associated With Step or Groove," Tokyo University, Aeronautical Research Institute, Report 364, April 1961.
3. Krall, K. M., and Sparrow, E. M., "Turbulent Heat Transfer in the Separated, Reattached, and Redevelopment Regions of a Circular Tube," Trans. Am. Soc. Mech. Engrs. 88, Series C, 131-136 (1966).

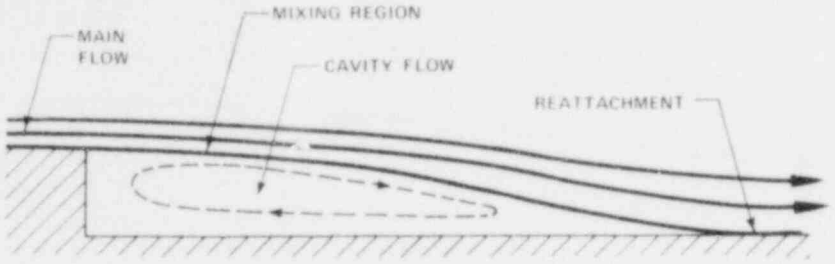

Figure B-1. Separated Flow Model Over a Backward-Facing Step

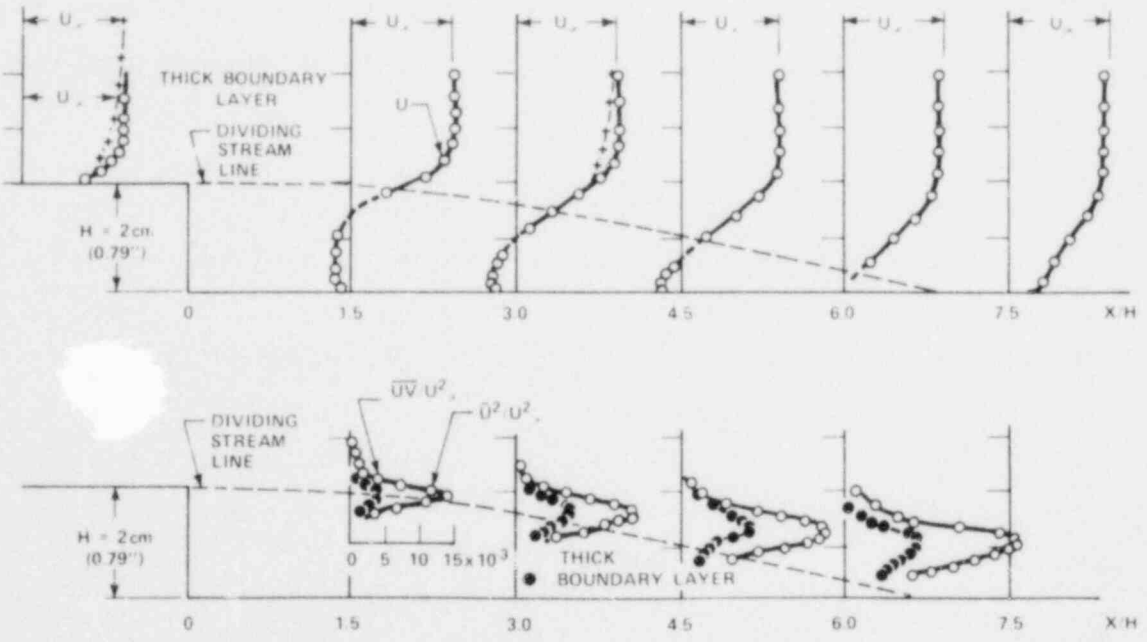

Figure B-2. Distribution of Streamwise Mean Velocity, Turbulence Intensity, and Turbulent Shear Stress Behind a Backward-Facing Step ($h = 2cm$, $U_\infty = 28$ m/sec)

TABLE B-1

REATTACHMENT DISTANCE RESULTS OF
KRALL AND SPARROW VERSUS ESTIMATIONS

TEST GEOMETRY: CIRCULAR TUBE
WITH ORIFICE

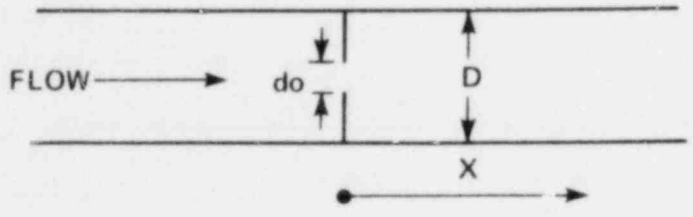

do/D	X/D	
	Measured	Estimated
1/2	1.5 - 1.8	1.6
2/3	1.3	1.1
1/4	2.0 - 2.3	2.4
1/3	1.7 - 2.3	2.1

the reattachment distance is a very weak function of the Reynolds number. An example of their results is shown in figure B-3. The maximum heat transfer points in this figure are considered to be the flow reattachment points. In the same table, the calculated reattachment distances based on equation (4-1) are compared. Generally the agreements between measurements and estimations are good.

Filetti and Kays[1] examined the sudden expansion effects on a backward step flow. They used rectangular cross-sectional tests and observed nonsymmetric flow separation with a long and a short stall. Their findings about reattachment locations are summarized in table B-2, which gives both short and long stall distances. Figure B-4 shows an example of their results. Calculated distances are again compared in the table; the estimates are midvalues of the long and short stall distances. They also observed that the Reynolds number does not affect the reattachment location.

Zemanick and Dougall[2] also studied local heat transfer downstream of abrupt circular channel expansion and found the reattachment points. Their results are summarized in table B-3. Again, the estimated values of reattachment length compared well to the measured ones.

Bishop, et al.,[3] reviewed hydrodynamic characteristics of a wake behind a fuel assembly local flow blockage. Their results are summarized in table B-4; the values of L/h are fairly comparable to the calculated value of 6.3.

---

1. Filetti, E. G., and Kays, W. M., "Heat Transfer in Separated, Reattached, and Redevelopment Regions Behind a Double Step at Entrance to a Flat Duct," Trans. Am. Soc. Mech. Engrs. 89, Series C, 163-168 (1967).

2. Zemanick, P. P., and Dougall, R. S., "Local Heat Transfer Downstream of Abrupt Circular Channel Expansion," Trans. Am. Soc. Mech. Engrs. 92, Series C, 53-60 (1970).

3. Bishop, A. A., et al., "Hydrodynamic Characteristics of a Wake Behind a Fuel Assembly Local Flow Blockage," Trans. Amer. Nucl. Soc. 14, 748-749 (1971).

Roidt and Tang[1] found essentially same results in their air flow experiments in a simulated LMFBR seven-rod bundle.

Therefore, it is concluded that the flow reattachment distance predicted by equation (4-1) is a good approximation of real reattachment distance.

---

1. Roidt, R. M., and Tang, Y. S., "Air Flow Experiments on a Simulated LMFBR Seven-Rod Bundle, Part II, Measurements of Velocities Downstream of Blocked Subchannels," Scientific Paper 72-7E9-MIXIN-P1, January 1972 (Westinghouse Research Laboratories, Pittsburgh, PA).

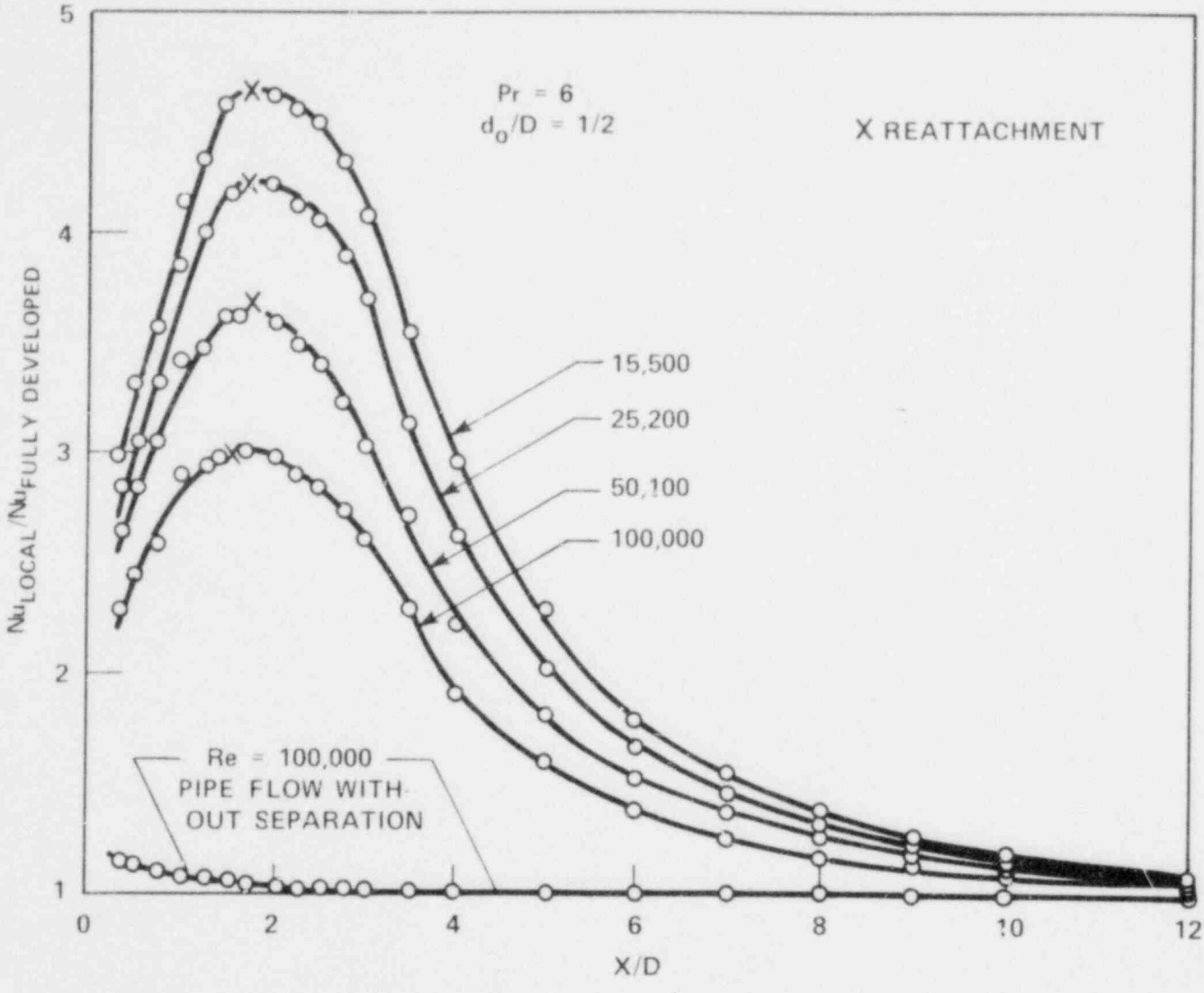

Figure B-3. Reattachment Results of Krall and Sparrow

TABLE B-2

REATTACHMENT DISTANCE RESULTS OF
FILETTI AND KAYS VERSUS ESTIMATIONS

TEST GEOMETRY: BACKWARD-FACING STEP WITH
RECTANGULAR CROSS SECTION

W/Wo	X/D		
	Measured		Estimated
	Long Stall	Short Stall	
1.125	1.4-1.7	0.6	0.84
2.1	1.9-2.4	0.7	1.1

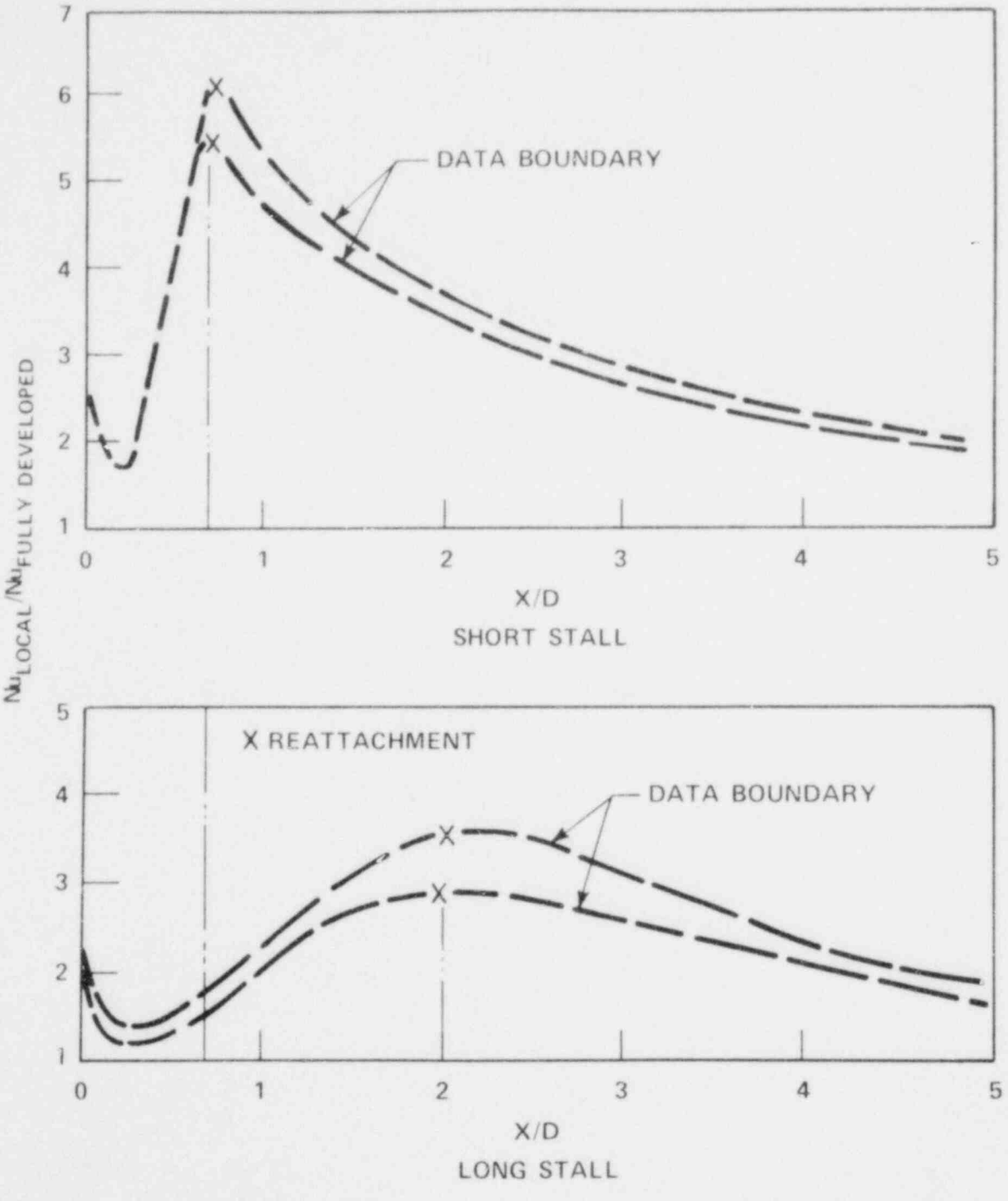

Figure B-4. Reattachment Results of Filetti and Kays

TABLE B-3

REATTACHMENT DISTANCE RESULTS OF
ZEMANICK AND DOUGALL VERSUS ESTIMATIONS

TEST GEOMETRY: CIRCULAR TUBE EXPANSION

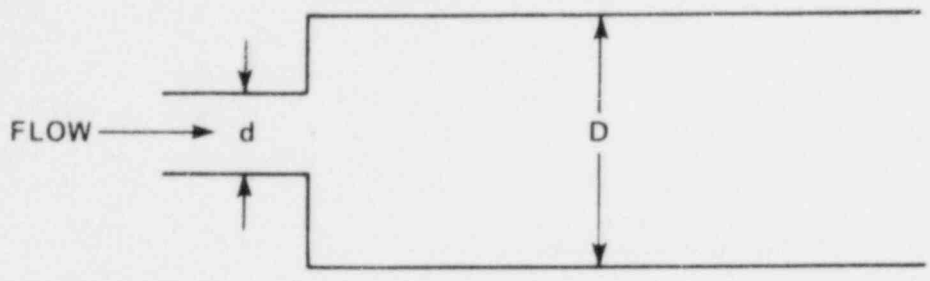

d/D	Reattachment Location	
	Measured	Estimated
0.43	6-9	6.3
0.54	5-8	6.3
0.82	7	6.3

TABLE B-4

LENGTH OF WAKE DOWNSTREAM OF A LOCAL FLOW BLOCKAGE FOR DIFFERENT GEOMETRIES AND BOUNDARY CONDITIONS

Case	a	b	h	L/h
Isolated circular disk normal to flow (sharp-edged) three-dimensional flow	Finite	o	Finite	5.2
Isolated disk normal to flow (non-sharp-edged) three-dimensional flow	Finite	Finite	Finite	-
Isolated rectangular (sharp-edged) two-dimensional flow	∞	o	Finite	4.6

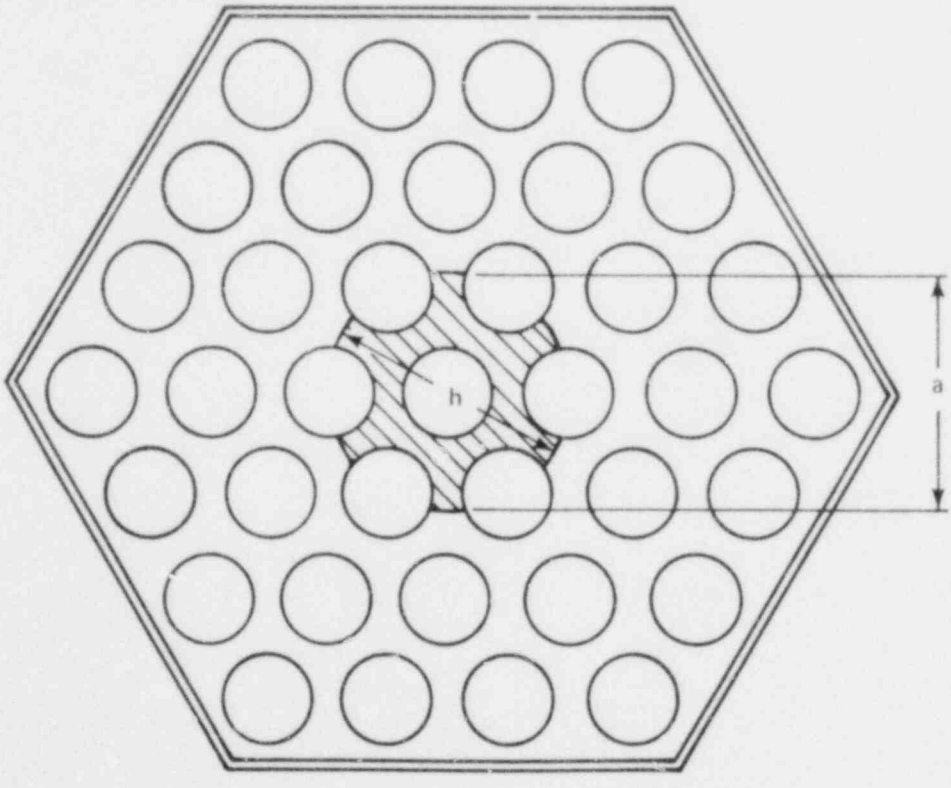

Note: The wake length L and the blockage height b are dimensions perpendicular to the plane of the paper.

APPENDIX C
DESCRIPTION OF COFARR PROGRAM

C-1. GENERAL

This program executes the procedure described in paragraph 4-11 to determine sleeve locations on rods. Further, the program can calculate subchannel flow area blockage, given sleeve strain information. Program variables and subroutines are explained in this appendix. Schematic flow charts for the routines are provided in figures C-1 through C-7.

C-2. MAIN PROGRAM

The main program handles inputs/outputs and coordinates subroutines, as follows:

M:	Number of rods
NCH:	Number of channels
REST:	Logical to note whether there is restriction in sleeve assignment (as in 21-rod) or not
ABL:	Maximum blockage effected by a single sleeve (in^2)
L:	Number of axial increments
TSIG:	Standard deviation of local temperature fluctuation
TAV(I):	Mean temperature (T) Must ensure $T_{max} - 6\sigma < T_{min}$
MCHAN(I,J):	Channel numbers which are affected by I-th rod J=1-4 Must ensure $B_{MCHAN(I,1)} \geq B_{MCHAN(I,2)} \geq B_{MCHAN(I,3)} \geq B_{MCHAN(I,4)}$
MM:	Number of axial increments affected by single sleeve (odd number)
BLOCK(I,J)	Blockage at J-th channel by I-th increment of sleeve Ensure BLOCK(I,1) $\geq$ BLOCK(I,2) $\geq$ BLOCK(I,3) $\geq$ BLOCK(I,4)
ZO:	Lowest height of the concerned section of rod
TAREA:	Nominal total coolant flow area (in^2)

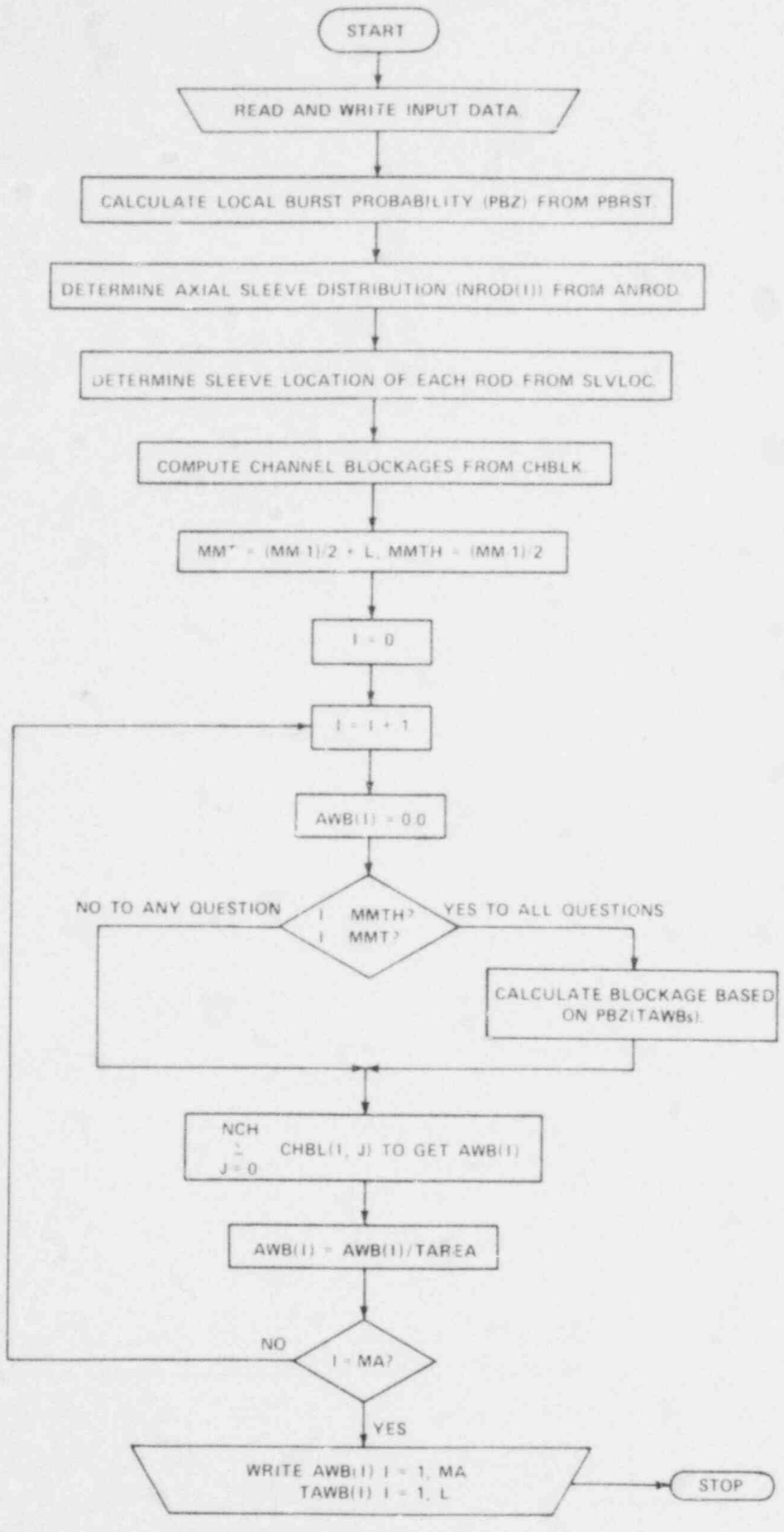

Figure C-1. Flow Chart of Main Program

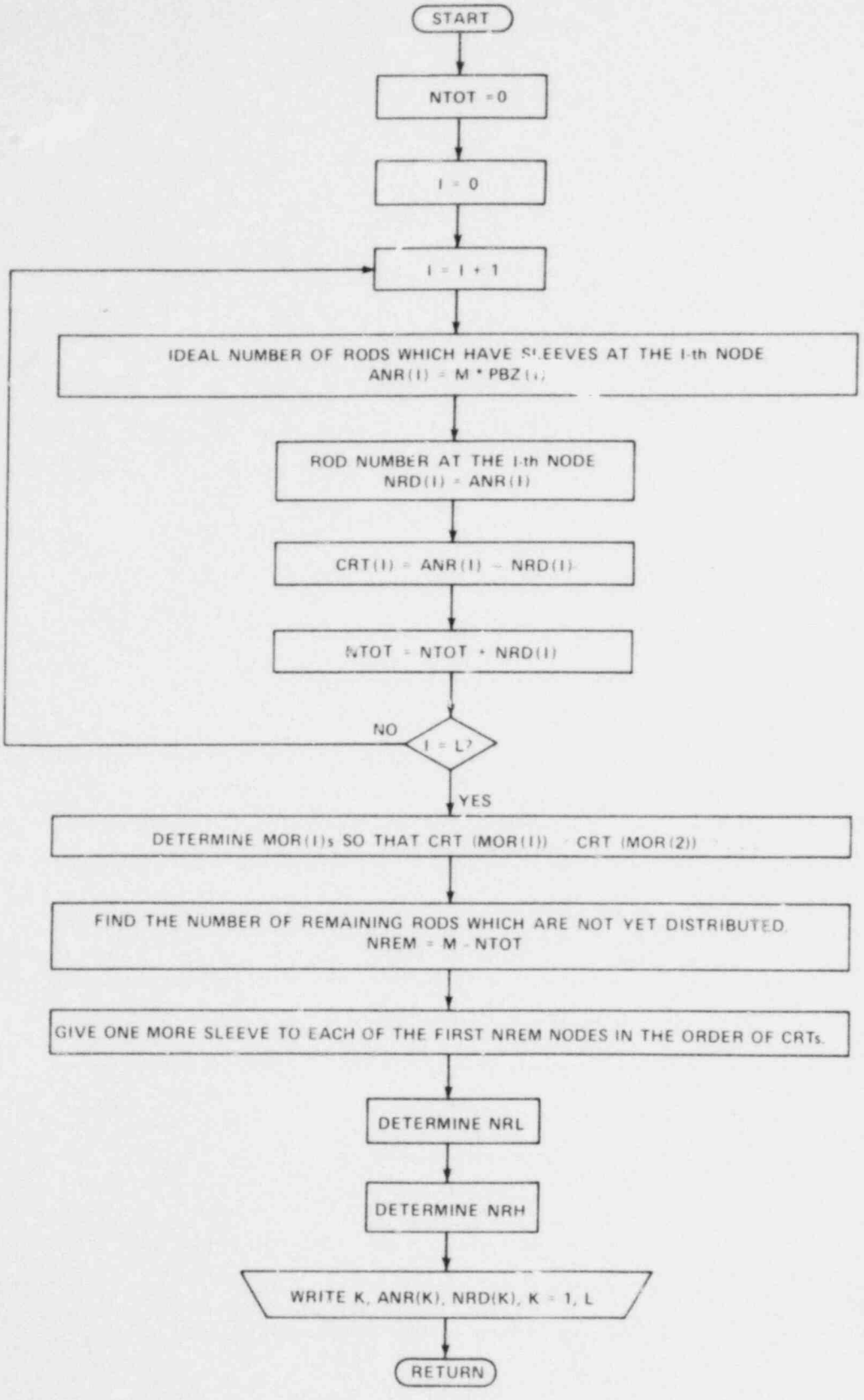

Figure C-2. ANROD Flow Chart

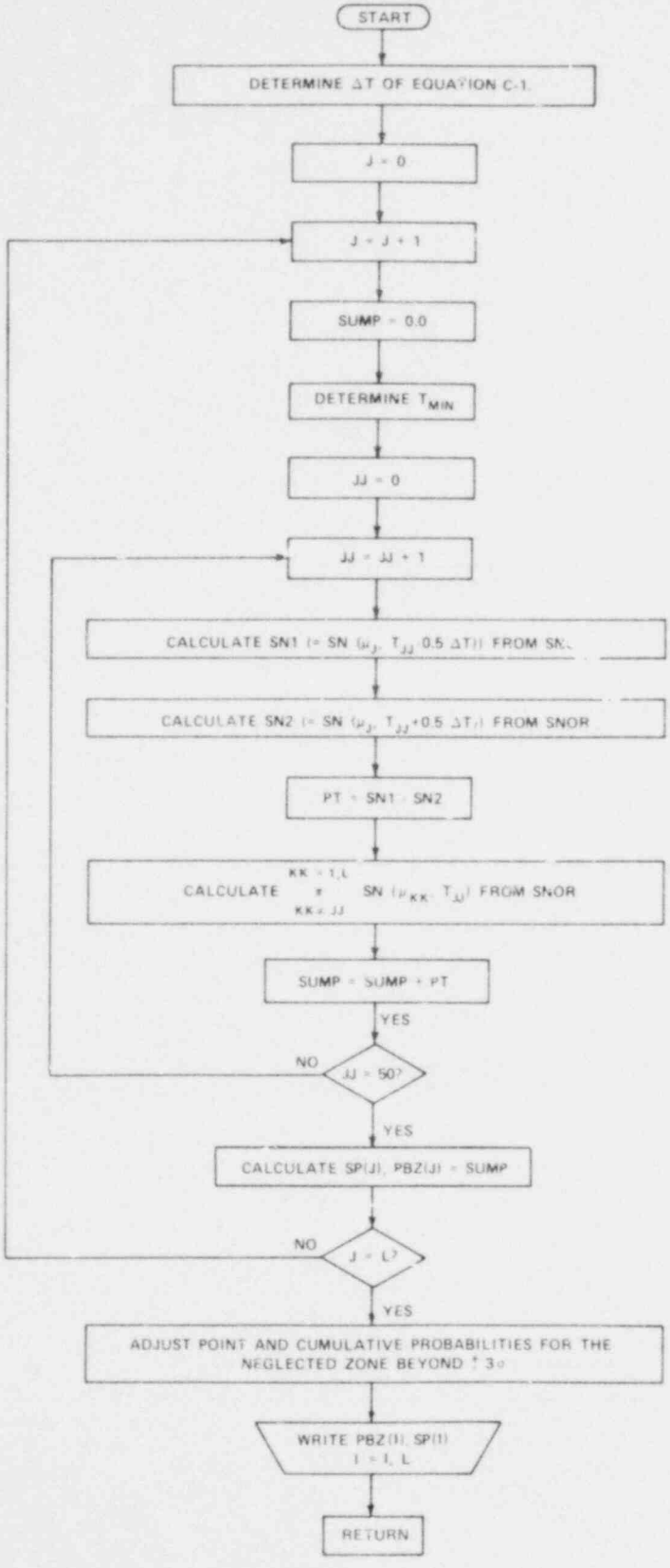

Figure C-3. PBRST Flow Chart

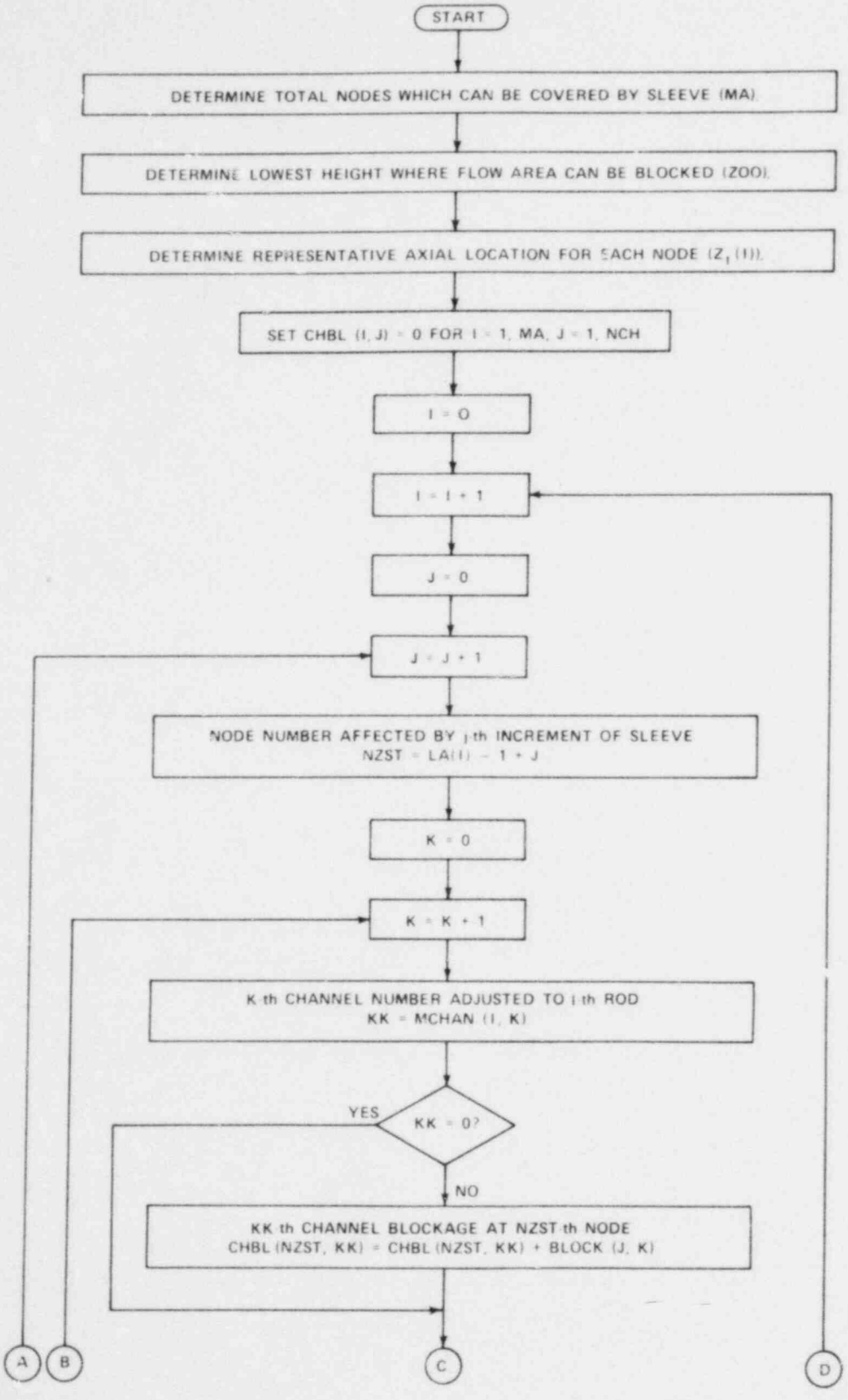

Figure C-4. CHBLK Flow Chart (sheet 1 of 2)

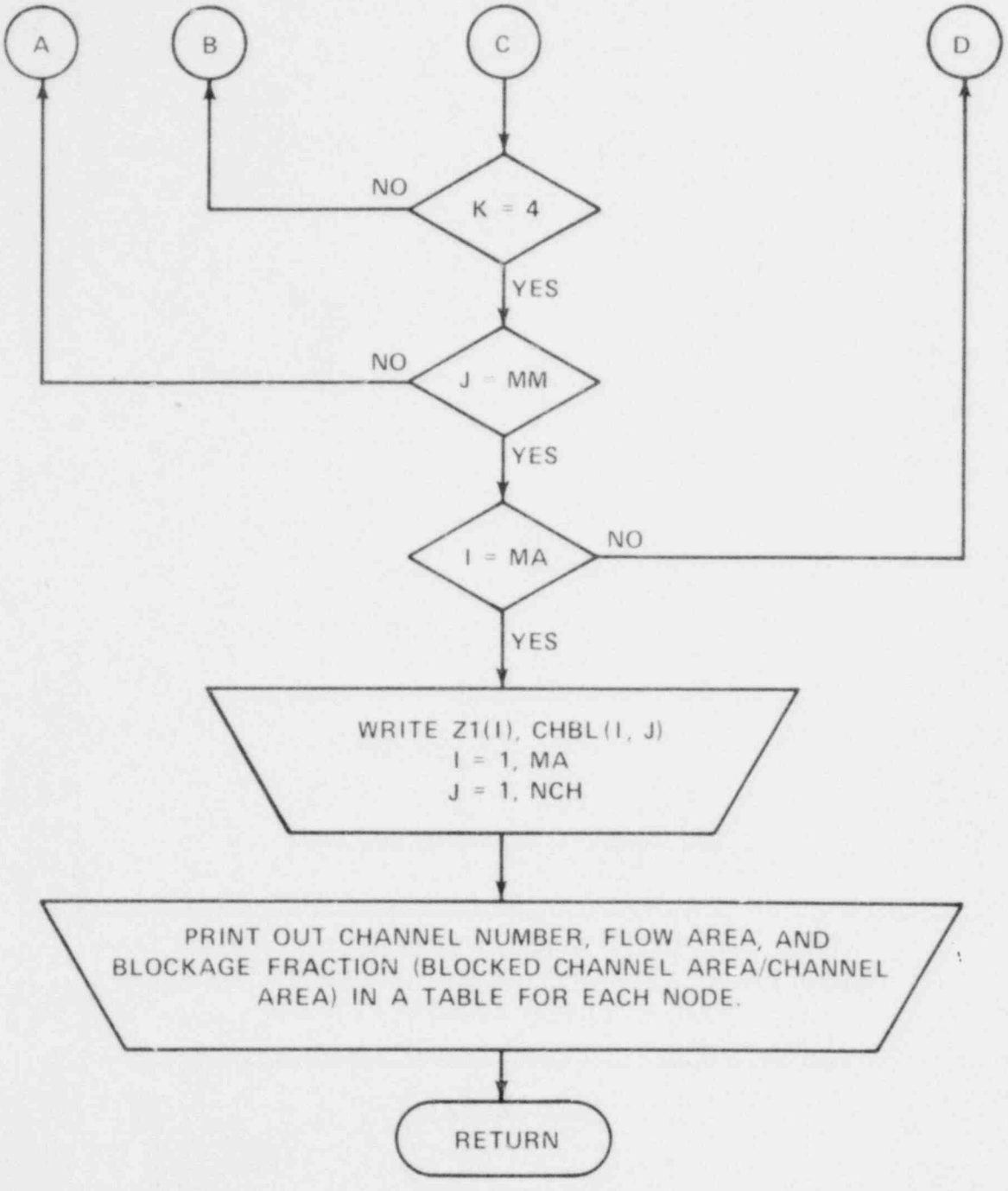

Figure C-4. CHBLK Flow Chart (sheet 2 of 2)

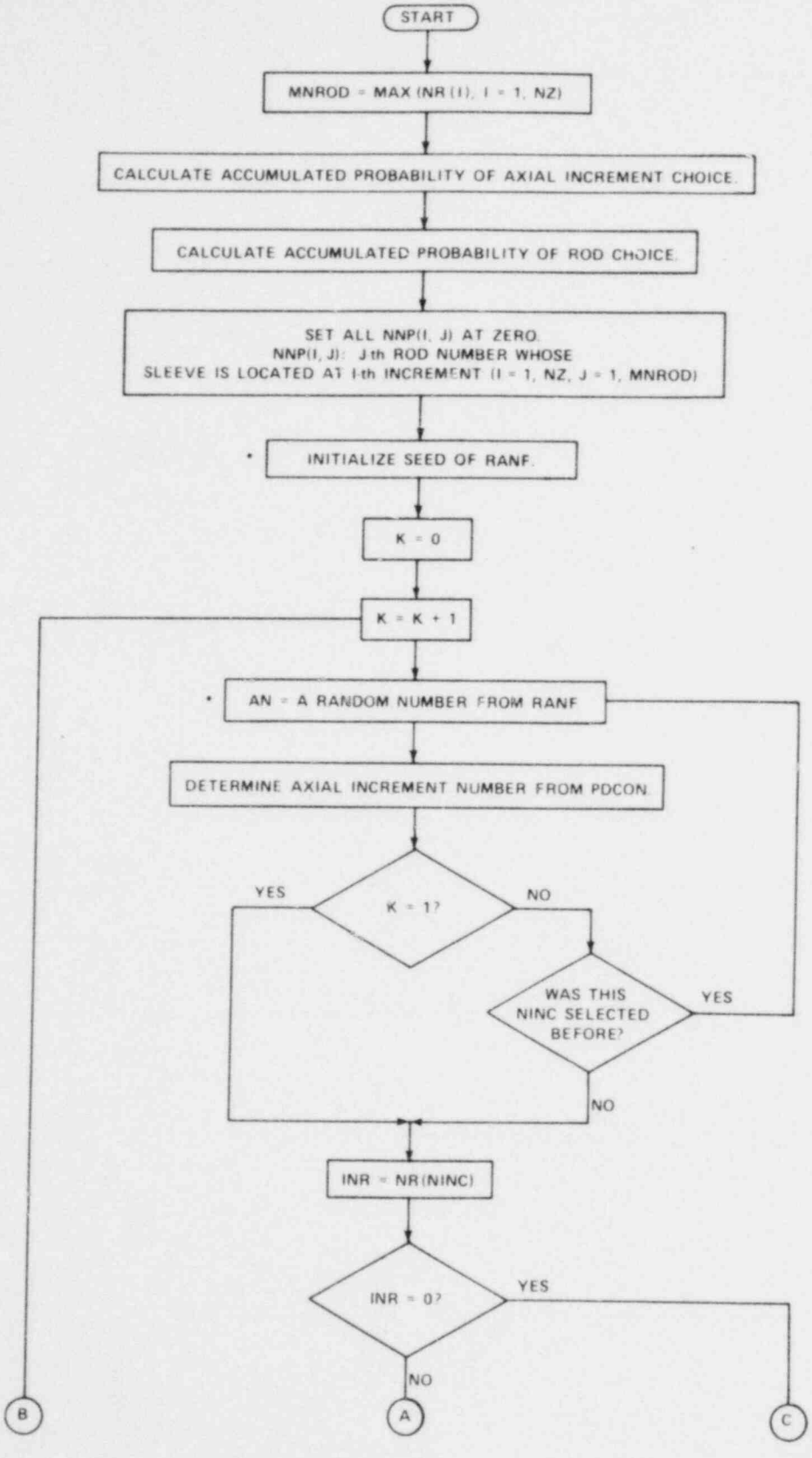

Figure C-5. SL VLOC Flow Chart (sheet 1 of 3)

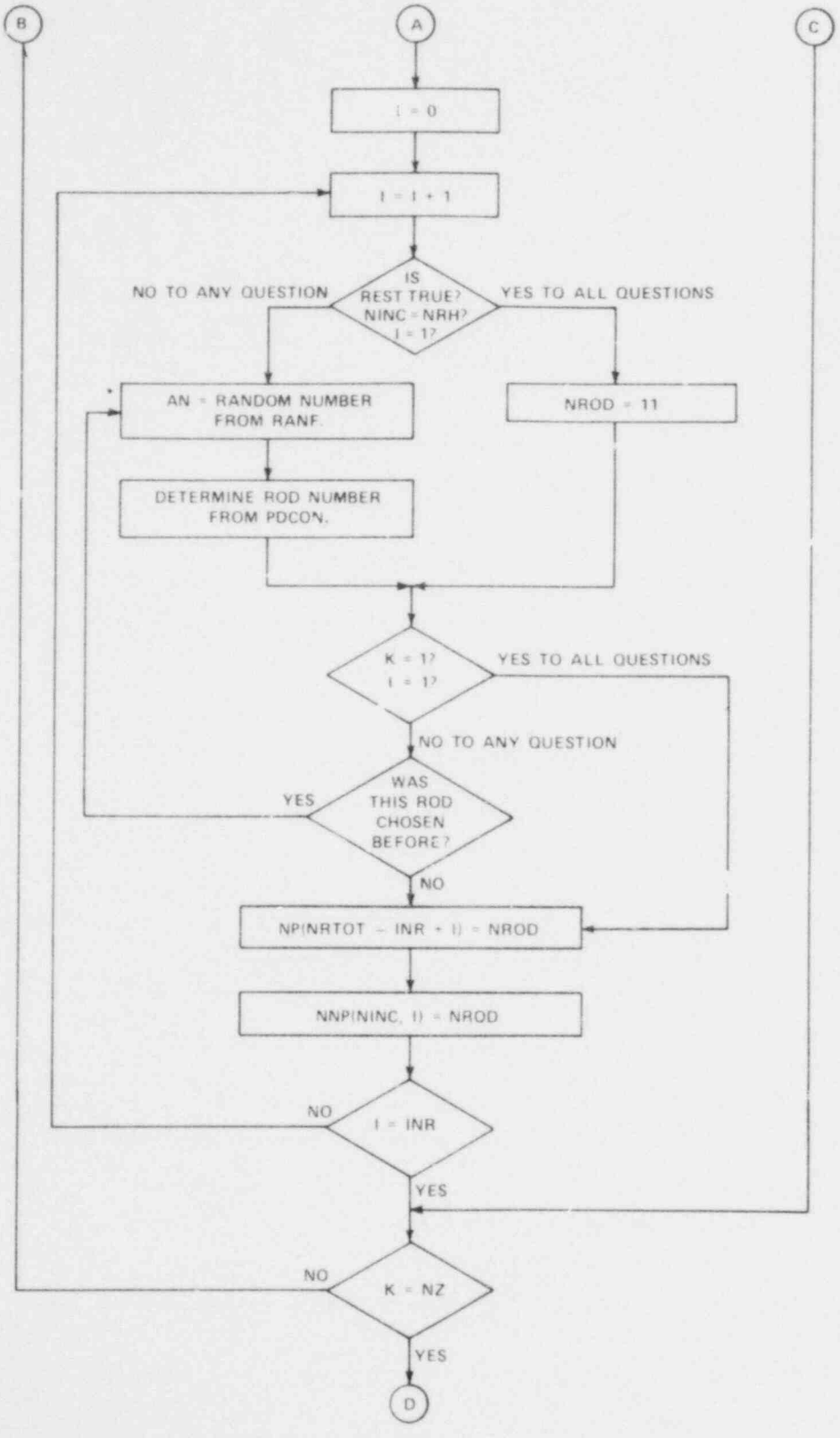

Figure C-5. SL VLOC Flow Chart (sheet 2 of 3)

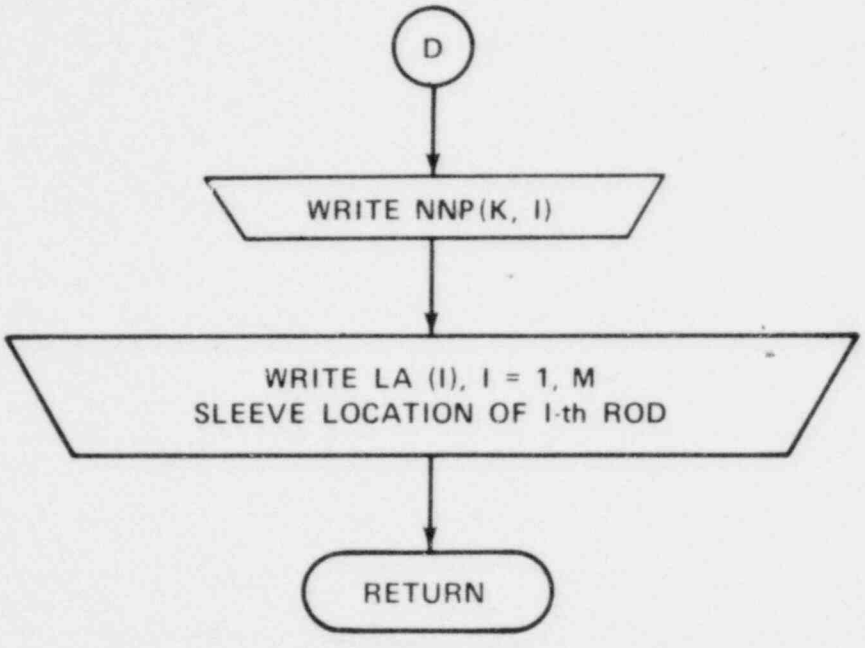

*RANF IS A SYSTEM INTRINSIC FUNCTION OF CDC 7600.
ANY RANDOM NUMBER GENERATOR CAN REPLACE RANF.

Figure C-5. SLVLOC Flow Chart (sheet 3 of 3)

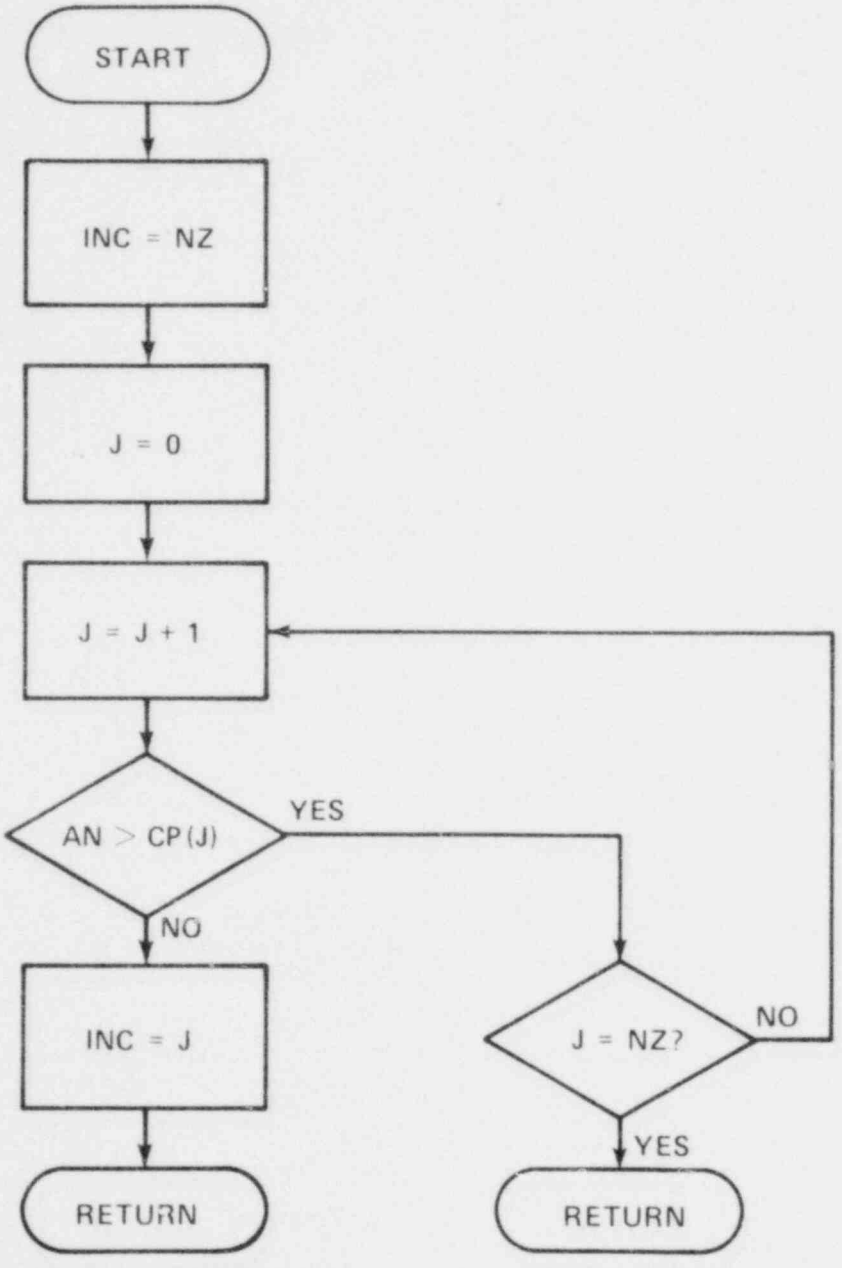

Figure C-6. PDCON Flow Chart

C-3. SUBROUTINE ANROD

This subroutine determines axial sleeve distribution, as follows:

PBZ:	Probability distribution provided by PBRST (input)
L:	See main program.
M:	See main program.
NRD(I):	Number of rods which have sleeves at I-th increment
NRL:	Lowest increment which has sleeves on it
NRH:	Highest increment which has sleeves on it

C-4. SUBROUTINE PBRST

This routine determines the probability of burst using a discrete version of equation (4-2):

$$P_i = \sum_{T_{min}}^{T_{max}} \left\{ \left[SN(\mu_i, T + 0.5\,\Delta T) - SN(\mu_i, T - 0.5\,\Delta T) \right] \cdot \prod_{\substack{j=1,L \\ j=i}} SN(\mu_j, T) \right\}$$

where

$$SN(\mu_i, T) = \int_0^T \frac{1}{\sqrt{2\pi}\,\sigma} \exp \frac{-(\mu_i - t)^2}{2\sigma^2}\, dt \qquad (C\text{-}1)$$

L:	See main program.
TSIG:	See main program.
TAV:	See main program.
PBZ:	Probability distribution (output)

C-5. SUBROUTINE SNOR

This routine evaluates error functions, as follows:[1]

$$TM = \int_{T}^{\infty} \frac{1}{\sqrt{2\pi}} e^{\frac{-t^2}{2}} \, dt$$

$$TP = \int_{-\infty}^{T} \frac{1}{\sqrt{2\pi}} e^{\frac{-t^2}{2}} \, dt$$

TT:	2TP-1
Q:	Convergence criterion
H:	Last term in the series
N:	Number of series terms used in the evaluation of the integrals

C-6. SUBROUTINE CHBLK

This calculates channel-wise blockage at every increment, as follows:

LA, M, L, NCH, MM, BLOCK, MCHAN, ZO, ZINT: See previous routines.

MA:	Total axial increment which can have area reduction
	MA = L + MM - 1
CHBL(I,J):	Blockage in J-th channel at I-th increment
IC(I):	Channel number
AREA(I):	Channel area
X(J):	CHBL(I,J)/AREA(J)

C-7. SUBROUTINE SLVLOC

This routine determines sleeve location on each rod, as follows:

NR(I):	Number of rods which have sleeves at I-th increment (input)
LA(I):	Sleeve location of I-th rod (output)

1. A flow chart of this program is not provided here. Any program for error function can serve the purpose.

M:	Total number of rods (input)
NZ:	Number of axial increments (input)
REST:	Logical (same as COFARR) (input)
NRL, NRH:	See ANROD (inputs)

C-8. SUBROUTINE PDCON

This routine converts a uniform probability to specified (by cumulative probability curve) probability distributions, as follows:

CP(I):	Cumulative probability at I-th increment (input)
NZ:	Number of axial increments (input)
AN:	Random number (input)
INC:	See figure C-7 (output).

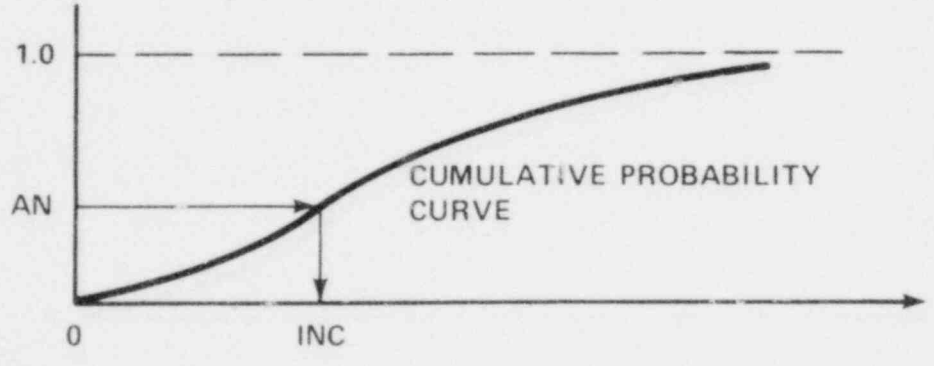

Figure C-7. Definition of INC

APPENDIX D
COFARR LISTING AND SAMPLE OUTPUT

A list and sample output from the COFARR program is reproduced on the following pages.

```
      PROGRAM CJFARR(INPUT,OUTPUT,TAPE5=INPUT,TAPE6=OUTPUT)
      LOGICAL REST
      DIMENSION TAV8(45),AV8(45),CHBL(45,120)
      DIMENSION BLOCK(15,4),MCHAN(70,4)
      DIMENSION TAV(30),PBZ(30),NROD(30),LA(30)
      READ(5,25) REST,M,NCH,L,MM,TSIG,ABL,ZO,ZINT,TAREA
   25 FORMAT(L10,4I5,5F10.4)
      READ(5,28) (TAV(I),I=1,L)
   28 FORMAT(7F10.4)
      WRITE(6,30) REST,M,NCH,L,MM,TSIG,ABL,ZO,ZINT,TAREA
   30 FORMAT( 2X , 5HREST= , L5 , / ,
     *        2X , 5HM=     , I5 , / ,
     *        2X , 5HNCH=   , I5 , / ,
     *        2X , 5HL=     , I5 , / ,
     *        2X , 5HMM=    , I5 , / ,
     *        2X , 5HTSIG=  , F10.4 , / ,
     *        2X , 5HABL=   , F10.4 , / ,
     *        2X , 5HZO=    , F10.4 , / ,
     *        2X , 5HZINT=  , F10.4 , / ,
     *        2X , 5HTARA=  , F10.4 , /)
      WRITE(6,31) (TAV(I),I=1,L)
   31 FORMAT(5X, *MEAN TEMPERATURES*/(10X,10F10.1))
      WRITE(6,115)
  115 FORMAT(//12X,*ROD* , 29X, * CHANNEL * ,/)
      DO 40 I=1,MM
      READ(5,110) (MCHAN(I,J),J=1,4)
      WRITE(6,112) I,(MCHAN(I,J),J=1,4)
   40 CONTINUE
  112 FORMAT(10X,I5,10X,4I10)
  110 FORMAT(4I10)
      WRITE(6,125)
  125 FORMAT(//12X,*SLEEVE INCREMENT * ,13X,16HBLOCKAGE (IN**2) ,/)
      DO 50 I=1,MM
      READ(5,28) (BLOCK(I,J),J=1,4)
      WRITE(6,128) I,(BLOCK(I,J),J=1,4)
   50 CONTINUE
  128 FORMAT(15X,I5,10X,4F10.3)
      CALL PBRST(L,TSIG,TAV,PBZ)
      CALL ANROD(PBZ,L,M,NROD,NRL,NRH)
      CALL SLVLOC(NROD,LA,M,L,REST,NRL,NRH)
      CALL CHBLK(LA,M,L,NCH,MM,BLOCK,MCHAN,ZO,ZINT,CHBL,MA)
      MTT=0
      MMT=(MM-1)/2+L
      MMTH=(MM-1)/2
```

```
                      DO 90 I=1,MA
                      AWB(I)=0.0
                      IF(I.GT.MMTH.AND.I.LE.MMT) GO TO 81
                      GO TO 82
                   81 CONTINUE
                      MTT=MTT+1
                      TAWB(MTT)=ABL*PBZ(MTT) *FLOAT(M)/TAREA
                   82 CONTINUE
                      DO 80 J=1,NCH
                      AWB(I)=AWB(I)+CHBL(I,J)
                   80 CONTINUE
                      AWB(I)=AWB(I)/TAREA
                   90 CONTINUE
                      WRITE(6,19)
                      WRITE(6,21) ( AWB(I),I=1,MA)
                      WRITE(6,20)
                      WRITE(6,21) (TAWB(I),I=1,L )
                   19 FORMAT(// , *   AXIAL BLOCKAGE DISTRIBUTION BASED ON THE CALCULATE
                     *D SLEEVE DISTRIBUTION* , / )
                   20 FORMAT( // , *   AXIAL BLOCKAGE DISTRIBUTION BASED ON PROBABILITY
                     *DISTRIBUTION* , / )
                   21 FORMAT(10F10.4)
                      STOP
                      END
```

SYMBOLIC REFERENCE MAP (R=2)

ENTRY POINTS

46	COFARR	1

DEF LINE REFERENCES

VARIABLES SN TYPE RELOCATION

550	ABL	REAL		REFS	10	51	DEFINED	6	
641	AWB	REAL	ARRAY	REFS	3	54	56	59	
				DEFINED	46	54	56		
13346	BLOCK	REAL	ARRAY	REFS	4	35	41		
				DEFINED	34				
716	CHBL	REAL	ARRAY	REFS	3	41	54		
554	I	INTEGER		REFS	8	21	26	2*27	34
				2*35	46	2*47	3*54	2*56	59
				61	DEFINED	8	21	25	33

```
      SUBROUTINE ANROD(PBZ,L ,M    ,NRD,NRL,NRH)
      DIMENSION PBZ(30),ANR(30),NRD(30),CRT(30),MOR(30)
      NTOT=0
      DO 10 I=1,L
      ANR(I)=       M     *PBZ(I)
      NRD(I)=ANR(I)
      CRT(I)=ANR(I)-       NRD(I)
   10 NTOT=NTOT+NRD(I)
      DO 20 I=1,L
      CRTO=CRT(1)
      DO 30 J=1,L
      CRTO=AMAX1(CRT(J),CRTO)
      IF(CRTO.EQ.CRT(J)) KK=J
   30 CONTINUE
      MOR(I)=KK
      CRT(KK)=0.0
   20 CONTINUE
      NREM=M    -NTOT
      DO 40 I=1,NREM
      JJ=MOR(I)
      NRD(JJ)=NRD(JJ)+1
   40 CONTINUE
      DO 50 I=1,L
   50 IF(NRD(I).NE.0) GO TO 55
   55 NRL=I
      DO 60 J=1,L
      K=L +1-J
   60 IF(NRD(K).NE.0) GO TO 65
   65 NRH=K
      WRITE(6,455)
  455 FORMAT(//,1X,2(18X,*Z*,16X,*ANR*, 9X,*NRD*)/)
      WRITE(6,450) (K,ANR(K),NRD(K),K=1,L )
  450 FORMAT(2(10X,I10,10X,F10.4,I10))
      RETURN
      END
```

SYMBOLIC REFERENCE MAP (R=2)

```
      SUBROUTINE SLVLOC(NR,LA,M,NZ,REST,NRL,NRH)
      LOGICAL REST
      DIMENSION LA(30)
      DIMENSION  NNP(30,70),NNA(30),NR(30),NP(70),CPZ(30),CPR(70)
      MNROD=0
      DO 42 I=1,NZ
      MNROD=MAXO(NR(I),MNROD)
   42 CONTINUE
      DO 45 I=1,NZ
   45 CPZ(I)=FLOAT(I)/FLOAT(NZ)
      DO 46 I=1,M
   46 CPR(I)=FLOAT(I)/FLOAT(M)
      DO 55 I=1,NZ
      DO 55 J=1,MNROD
      NNP(I,J)=0
   55 CONTINUE
      CALL RANSET(AN)
      NRTOT=0
      DO 110  K=1,NZ
  115 AN = RANF(AN)
      CALL PDCON(CPZ,NINC,NZ,AN)
      IF(K.EQ.1) GO TO 125
      K1=K-1
      DO 120 J=1,K1
      IF(NINC.EQ.NNA(J)) GO TO 115
  120 CONTINUE
  125 NNA(K)=NINC
      INR=NR(NINC)
      IF(INR.EQ.0) GO TO 110
      NRTOT=NRTOT +INR
      DO 210 I=1,INR
      IF(REST.AND.NINC.EQ.NRH.AND.I.EQ.1) GO TO 217
  215 AN = RANF(AN)
      CALL PDCON(CPR,NROD,M,AN)
      GO TO 218
  217 NROD=11
  218 CONTINUE
      IF(K.EQ.1.AND.I.EQ.1) GO TO 225
      NREF=NRTOT-INR+I-1
      DO 220 J=1,NREF
      IF(NROD.EQ.NP(J)) GO TO 215
      IF(REST.AND.NROD.EQ.11.AND.NINC.NE.NRH) GO TO 215
  220 CONTINUE
  225 NP(NRTOT-INR+I)=NROD
```

```
                NNP(NINC,I)=NROD
            210 CONTINUE
            110 CONTINUE
                WRITE(6,539)
            539 FORMAT( // , T10 , *INCREMENT* , T35 , *ROD* , / )
                DO 310 K=1,NZ
                WRITE(6,510) K, (NNP(K,I),I=1,MNROD)
            310 CONTINUE
            510 FORMAT(13X,I2,5X,15I5/(20X,15I5))
                WRITE(6,64)
             64 FORMAT( // , T21 , *SLEEVE   LOCATIONS* , // T18 , *ROD* ,
               *   T36 , *INCREMENT* , / )
                DO 30 I=1,M
                DO 40 J=1,NZ
                DO 40 K=1,MNROD
                IF(NNP(J,K).EQ.I) GO TO 50
             40 CONTINUE
             50 LA(I)=J
                WRITE(6,65) I, LA(I)
             65 FORMAT(10X,I10,10X,I10)
             30 CONTINUE
                RETURN
                END
```


SYMBOLIC REFERENCE MAP (R=2)

ENTRY POINTS		DEF LINE	REFERENCES
3	SLVLOC	1	66

VARIABLES		SN TYPE		RELOCATION						
320	AN	REAL			REFS	17	20	21	33	34
					DEFINED	20	33			
4616	CPR	REAL	ARRAY		REFS	4	34	DEFINED	12	
4560	CPZ	REAL	ARRAY		REFS	4	21	DEFINED	10	
316	I	INTEGER			REFS	7	2*10	2*42	15	32
						38	39	44	45	51	60
						62	2*63	DEFINED	6	9	11
						13	31	51	57		
325	INR	INTEGER			REFS	29	30	31	39	44
					DEFINED	28				

```
      1               SUBROUTINE PDCON(CP,INC,NZ,AN)
                      DIMENSION CP(100)
                      INC=NZ
                      DO 15 J=1,NZ
      5               IF(AN.GT.CP(J)) GO TO 15
                      INC=J
                      RETURN
                   15 CONTINUE
                      RETURN
     10               END
```

```
       SYMBOLIC REFERENCE MAP (R=2)

ENTRY POINTS      DEF LINE     REFERENCES
    3  PDCON            1          7          9

VARIABLES     SN  TYPE              RELOCATION
    0  AN         REAL                    F.P.        REFS          5    DEFINED         1
    0  CP         REAL          ARRAY     F.P.        REFS          2          5    DEFINED         1
    0  INC        INTEGER                 F.P.      DEFINED         1          3          6
   31  J          INTEGER                           REFS            5          6    DEFINED         4
    0  NZ         INTEGER                 F.P.        REFS          3          4    DEFINED         1

STATEMENT LABELS              DEF LINE   REFERENCES
   26  15                           8          4          5

LOOPS  LABEL     INDEX      FROM-TO     LENGTH     PROPERTIES
   21  15      * J             4 8         108

STATISTICS
  PROGRAM LENGTH                  428       34
          030008 SCM USED
```

```
      SUBROUTINE PBRST(L,TSIG,TAV,PBZ)
      DIMENSION TAV(30),SP(30),PBZ(30)
      DT = 6.0 * TSIG / 50.0
      DO 100 J = 1,L
      SUMP = 0.0
      T = TAV(J) - 3.0 * TSIG
      DO 70 JJ = 1,50
      T = T + DT
      T1 = T - 0.5 * DT
      TT = ( TAV(J) - T1) / TSIG
      CALL SNOR( TT , 0. , SN1 , XX , XY , XZ , NN )
      TT = ( TAV (J) - T1+ DT )/TSIG
      CALL SNOR( TT , 0. , SN2 , XX , XY , XZ , NN )
      PT = SN1 - SN2
      DO 60 KK = 1,L
      IF( KK .EQ. JJ ) GO TO 60
      TT = ( TAV(KK) - T ) / TSIG
      CALL SNOR( TT , 0. , SN , XX , XY , XZ , NN )
      PT = PT * SN
   60 CONTINUE
   70 SUMP = SUMP + PT
      IF( J .EQ. 1 ) SP(J) = SUMP
      IF( J .GT. 1 ) SP(J) = SP(J-1) + SUMP
      PBZ(J)=SUMP
  100 CONTINUE
      DO 90 J = 1,L
      PBZ(J)=PBZ(J)/SP(L)
   90 SP(J) = SP(J) / SP(L)
      WRITE(6,107)
  107 FORMAT(//19X,*Z*,16X,*PBZ*,12X,*SP*,/)
      WRITE(6,105) (J, PBZ(J),SP(J),J=1,L)
  105 FORMAT(10X,I10,10X,F10.4,5X,F10.4)
       RETURN
      END
```

SYMBOLIC REFERENCE MAP (R=2)

ENTRY POINTS	DEF LINE	REFERENCES
3 PBRST	1	33

```
      SUBROUTINE SNOR(T,Q,TM,TP,IT,H,N)                                 SNOR
      IF(T.GE.10.) GO TO 20                                             SNOR
      IF(Q.LE.10.) Q=1.0E-14                                            SNOR
      H=1.                                                              SNOR
      N=1                                                               SNOR
      AN=1.                                                             SNOR
      SUM=1.                                                            SNOR
      PROD=1.                                                           SNOR
      X=AMIN1(T,5.)                                                     SNOR
      X=-.5*X**2                                                        SNOR
   10 CONTINUE                                                          SNOR
      ADH=X**N/PROD                                                     SNOR
      ADT=ADH/(AN+AN+1.)                                                SNOR
      N=N+1                                                             SNOR
      AN=AN+1.                                                          SNOR
      PROD=PROD*AN                                                      SNOR
       SUM=SUM+ADT                                                      SNOR
      H=H+ADH                                                           SNOR
      IF(ABS(ADH).GT.ABS(Q*H) ) GO TO 10                                SNOR
      TM=.5-.398942*SUM*T                                               SNOR
      IF(T.LE.5.) GO TO 15                                              SNOR
      F=2.-.2*T                                                         SNOR
      TM=F*TM                                                           SNOR
      H=F*H                                                             SNOR
   15 CONTINUE                                                          SNOR
      TP=1.-TM                                                          SNOR
      IT=TP+TP-1.                                                       SNOR
      H=.398942*H                                                       SNOR
      GO TO 30                                                          SNOR
   20 TP=1.                                                             SNOR
      TM=0.                                                             SNOR
      IT=1.                                                             SNOR
      H=0.                                                              SNOR
   30 RETURN                                                            SNOR
      END                                                               SNOR
```

SYMBOLIC REFERENCE MAP (R=2)

```
      SUBROUTINE CHBLK(LA,M,L,NCH,MM,BLOCK,MCHAN,ZO,ZINT,CHBL,MA)
      DIMENSION LA(30),BLOCK(15,4),MCHAN(70,4),CHBL(45,12)
      DIMENSION NZS(70,15),Z1(45)
      DIMENSION IFMT(3,4) , IC(32) , AREA(32)
      DIMENSION X(32)
      DATA IFMT / 10H(1H+,33X,4 , 10H(4X,I2,3X) , 104)          ,
     *            10H(1H+,33X,4 , 10H(2X,F6.4,1 , 10HX))       ,
     *            10H(1H+,24X,6 , 10H(4X,I2,3X) , 104)         ,
     *            10H(1H+,24X,6 , 10H(2X,F6.4,1 , 10HX))          /
      DATA AREA / .039 , 2*.104 , 2*.039 , .077 , 2*.136 , .077 ,
     * .039 , .104 , 4*.136 , 2*.104 , 4*.136 , .104 , .039 , .077 ,
     *  2*.136 , .077 , 2*.039 , 2*.104 , .039    /
      MA=L+MM-1
      ZOO=ZO-ZINT*((MM-1)/2)
      DO 110 I=1,MA
      II=2*I-1
      Z1(I)=ZOO+ZINT*FLOAT(II)/2.
      DO 110 J=1,NCH
  110 CHBL(I,J)=0.0
      DO 113 I=1,M
      DO 112 J=1,MM
      NZST=LA(I)-1+J
      DO 111 K=1,4
      KK=MCHAN(I,K)
      IF(KK.EQ.0) GO TO 111
      CHBL(NZST,KK)=CHBL(NZST,KK)+BLOCK(J,K)
  111 CONTINUE
  112 CONTINUE
  113 CONTINUE
      WRITE(6,149)
  149 FORMAT( // , T10 , *Z(IN)* , T50,24HBLOCKAGE(I,J)  ( IN**2 ) ,//)
      DO 115 I=1,MA
  115 WRITE(6,150) Z1(I),(CHBL(I,J),J=1,NCH)
  150 FORMAT(5X,F10.4,5X,8F10.4,/(20X,8F10.4))
      IC(1) = 1
      DO 30 I = 2,NCH
   30 IC(I) = IC(I-1) + 1
      DO 10 MG=1,MA
      DO 35 I = 1,NCH
   35 X(I)=CHBL(MG,I)/AREA(I)
      WRITE(6,11) Z1(MG)
   11 FORMAT( 1H1 , /// , T10 , *Z=* , F7.2 , T20 , *(IN)* , /// )
      NL = 1
      NH = -2
```

```
      DO 12 N = 1,6
      IF( N .LT. 6 ) NH = NH + 6
      IF( N .EQ. 6 ) NH = NH + 4
      WRITE(6,13)
   13 FORMAT( 25X , 55( 1H* ) )
      WRITE(6,14)
      WRITE(6,14)
   14 FORMAT( 25X , 7(9H*        ) )
      IF( N .EQ. 1 .OR. N .EQ. 6 ) GO TO 20
      I1 = 3
      I2 = 4
      GO TO 21
   20 I1 = 1
      I2 = 2
   21 CONTINUE
      WRITE(6,IFMT(1,I1)) ( IC(I) , I=NL,NH )
      WRITE(6,14)
      WRITE(6,IFMT(1,I2)) ( AREA(I) , I=NL,NH )
      WRITE(6,14)
      WRITE(6,IFMT(1,I2)) ( X(I) , I=NL,NH )
      WRITE(6,14)
      NL = NH + 1
   12 CONTINUE
      WRITE(6,13)
   10 CONTINUE
      RETURN
      END
```

SYMBOLIC REFERENCE MAP (R=2)

ENTRY POINTS		DEF LINE	REFERENCES
3	CHBLK	1	70

VARIABLES	SN	TYPE	RELOCATION								
2572	AREA	REAL	ARRAY		REFS	4	40	62			
					DEFINED	10					
0	BLOCK	REAL	ARRAY	F.P.	REFS	2	26	DEFINED	1		
0	CHBL	REAL	ARRAY	F.P.	REFS	2	26	33	40		
					DEFINED	1	19	26			
373	I	INTEGER			REFS	16	17	19	22	24	

```
SYSACCT
  SYSACCT      32271   08.IO.      25411
                       FORSYS.     27061
REST.    T
M.      21
NCH.    32
L.      20
MM.      3
TSIG.   12.0000
ABL.     .0932
ZO.     60.5000
ZINT.    1.0000
TARA.    3.0820

 MEAN TEMPERATURES
      1678.0   1688.0   1697.0   1706.0   1713.0   1720.0   1727.0   1732.0   1736.0   1737.0
      1741.0   1738.0   1735.0   1721.0   1712.0   1705.0   1701.0   1698.0   1693.0   1684.0
```

ROD	CHANNEL			
1	1	2	6	7
2	2	3	7	8
3	3	4	8	9
4	5	6	11	12
5	6	7	12	13
6	7	8	13	14
7	8	9	14	15
8	9	10	15	16
9	11	12	17	18
10	12	13	18	19
11	13	14	19	20
12	14	15	20	21
13	15	16	21	22
14	17	18	23	24
15	18	19	24	25
16	19	20	25	26
17	20	21	26	27
18	21	22	27	28
19	24	25	29	30
20	25	26	30	31
21	26	27	31	32

SLEEVE INCREMENT	BLOCKAGE (IN**2)			
1	.005	.006	.006	.005
2	.021	.021	.021	.021
3	.006	.006	.006	.005

Z	PBZ	SP
1	.0000	.0000
2	.0000	.0000
3	.0000	.0000
4	.0002	.0002
5	.0022	.0025
6	.0118	.0143
7	.0418	.0561
8	.0865	.1426
9	.1418	.2844
10	.1586	.4430
11	.2378	.6808
12	.1767	.8575
13	.1262	.9837
14	.0144	.9981
15	.0017	.9998
16	.0001	1.0000
17	.0000	1.0000
18	.0000	1.0000
19	.0000	1.0000
20	.0000	1.0000

Z	ANR	NRD	Z	ANR	NRD
1	.0000	0	2	.0000	0
3	.0000	0	4	.0046	0
5	.0470	0	6	.2480	0
7	.8776	1	8	1.8174	2
9	2.9780	3	10	3.3311	3
11	4.9937	5	12	3.7097	4
13	2.6505	3	14	.3032	0
15	.0354	0	16	.0031	0
17	.0005	0	18	.0001	0
19	.0000	0	20	.0000	0

INCREMENT ROD

1	0	0	0	0	0
2	0	0	0	0	0
3	0	0	0	0	0
4	0	0	0	0	0
5	0	0	0	0	0
6	0	0	0	0	0
7	17	0	0	0	0
8	4	15	0	0	0
9	3	7	20	0	0
10	9	8	6	0	0
11	14	12	5	2	10
12	18	19	1	16	0
13	11	13	21	0	0
14	0	0	0	0	0
15	0	0	0	0	0
16	0	0	0	0	0
17	0	0	0	0	0
18	0	0	0	0	0
19	0	0	0	0	0
20	0	0	0	0	0

SLEEVE LOCATIONS

ROD	INCREMENT
1	12
2	11
3	9
4	8
5	11
6	10
7	9
8	10
9	10
10	11
11	13
12	11
13	13
14	11
15	8
16	12
17	7
18	12
19	12
20	9
21	13

Z(IN)	BLOCKAGE(I,J) (IN**2)							
60.0000	0.0000	0.0000	0.0000	0.0000	0.0000	0.0000	0.0000	0.0000
	0.0000	0.0000	0.0000	0.0000	0.0000	0.0000	0.0000	0.0000
	0.0000	0.0000	0.0000	0.0000	0.0000	0.0000	0.0000	0.0000
	0.0000	0.0000	0.0000	0.0000	0.0000	0.0000	0.0000	0.0000
61.0000	0.0000	0.0000	0.0000	0.0000	0.0000	0.0000	0.0000	0.0000
	0.0000	0.0000	0.0000	0.0000	0.0000	0.0000	0.0000	0.0000
	0.0000	0.0000	0.0000	0.0000	0.0000	0.0000	0.0000	0.0000
	0.0000	0.0000	0.0000	0.0000	0.0000	0.0000	0.0000	0.0000
62.0000	0.0000	0.0000	0.0000	0.0000	0.0000	0.0000	0.0000	0.0000
	0.0000	0.0000	0.0000	0.0000	0.0000	0.0000	0.0000	0.0000
	0.0000	0.0000	0.0000	0.0000	0.0000	0.0000	0.0000	0.0000
	0.0000	0.0000	0.0000	0.0000	0.0000	0.0000	0.0000	0.0000
63.0000	0.0000	0.0000	0.0000	0.0000	0.0000	0.0000	0.0000	0.0000
	0.0000	0.0000	0.0000	0.0000	0.0000	0.0000	0.0000	0.0000
	0.0000	0.0000	0.0000	0.0000	0.0000	0.0000	0.0000	0.0000
	0.0000	0.0000	0.0000	0.0000	0.0000	0.0000	0.0000	0.0000
64.0000	0.0000	0.0000	0.0000	0.0000	0.0000	0.0000	0.0000	0.0000
	0.0000	0.0000	0.0000	0.0000	0.0000	0.0000	0.0000	0.0000
	0.0000	0.0000	0.0000	0.0000	0.0000	0.0000	0.0000	0.0000
	0.0000	0.0000	0.0000	0.0000	0.0000	0.0000	0.0000	0.0000
65.0000	0.0000	0.0000	0.0000	0.0000	0.0000	0.0000	0.0000	0.0000
	0.0000	0.0000	0.0000	0.0000	0.0000	0.0000	0.0000	0.0000
	0.0000	0.0000	0.0000	0.0000	0.0000	0.0000	0.0000	0.0000
	0.0000	0.0000	0.0000	0.0000	0.0000	0.0000	0.0000	0.0000
66.0000	0.0000	0.0000	0.0000	0.0000	0.0000	0.0000	0.0000	0.0000
	0.0000	0.0000	0.0000	0.0000	0.0000	0.0000	0.0000	0.0000
	0.0000	0.0000	0.0000	.0063	.0063	0.0000	0.0000	0.0000
	0.0000	.0063	.0063	0.0000	0.0000	0.0000	0.0000	0.0000
67.0000	0.0000	0.0000	0.0000	0.0000	.0063	.0063	0.0000	0.0000
	0.0000	0.0000	.0063	.0063	0.0000	0.0000	0.0000	0.0000
	0.0000	.0063	.0063	.0210	.0210	0.0000	0.0000	.0063
	.0063	.0210	.0210	0.0000	0.0000	0.0000	0.0000	0.0000
68.0000	0.0000	0.0000	.0063	.0063	.0210	.0210	0.0000	.0126
	.0126	0.0000	.0210	.0210	0.0000	.0063	.0063	0.0000
	0.0000	.0210	.0210	.0063	.0063	0.0000	0.0000	.0210
	.0273	.0126	.0063	0.0000	0.0000	.0063	.0063	0.0000
69.0000	0.0000	0.0000	.0210	.0210	.0063	.0063	.0063	.0463
	.0463	.0063	.0126	.0126	.0063	.0273	.0273	.0063
	.0063	.0126	.0063	0.0000	0.0000	0.0000	0.0000	.0063
	.0273	.0210	0.0000	0.0000	0.0000	.0210	.0210	0.0000
70.0000	0.0000	.0063	.0126	.0063	0.0000	.0063	.0336	.0394
	.0336	.0210	.0210	.0336	.0336	.0336	.0336	.0210

	.0273	.0336	.0063	.0063	.0063	0.0000	.0063	.0063
	.0063	.0063	0.0000	0.0000	0.0000	.0063	.0063	0.0000
71.0000	.0063	.0273	.0210	0.0000	0.0000	.0273	.0546	.0273
	.0063	.0063	.0063	.0483	.0483	.0273	.0273	.0063
	.0273	.0483	.0273	.0273	.0273	.0063	.0210	.0273
	.0126	.0063	.0063	.0063	.0063	.0063	0.0000	0.0000
72.0000	.0210	.0273	.0063	0.0000	0.0000	.0273	.0336	.0063
	0.0000	0.0000	0.0000	.0126	.0189	.0126	.0126	.0063
	.0063	.0126	.0336	.0336	.0336	.0273	.0063	.0273
	.0420	.0273	.0273	.0210	.0210	.0210	.0063	.0063
73.0000	.0063	.0063	0.0000	0.0000	0.0000	.0063	.0063	0.0000
	0.0000	0.0000	0.0000	0.0000	.0210	.0210	.0210	.0210
	0.0000	0.0000	.0273	.0273	.0273	.0273	0.0000	.0063
	.0126	.0273	.0273	.0063	.0063	.0063	.0210	.0210
74.0000	0.0000	0.0000	0.0000	0.0000	0.0000	0.0000	0.0000	0.0000
	0.0000	0.0000	0.0000	0.0000	.0063	.0063	.0063	.0063
	0.0000	0.0000	.0063	.0063	.0063	.0063	0.0000	0.0000
	0.0000	.0063	.0063	0.0000	0.0000	0.0000	.0063	.0063
75.0000	0.0000	0.0000	0.0000	0.0000	0.0000	0.0000	0.0000	0.0000
	0.0000	0.0000	0.0000	0.0000	0.0000	0.0000	0.0000	0.0000
	0.0000	0.0000	0.0000	0.0000	0.0000	0.0000	0.0000	0.0000
	0.0000	0.0000	0.0000	0.0000	0.0000	0.0000	0.0000	0.0000
76.0000	0.0000	0.0000	0.0000	0.0000	0.0000	0.0000	0.0000	0.0000
	0.0000	0.0000	0.0000	0.0000	0.0000	0.0000	0.0000	0.0000
	0.0000	0.0000	0.0000	0.0000	0.0000	0.0000	0.0000	0.0000
	0.0000	0.0000	0.0000	0.0000	0.0000	0.0000	0.0000	0.0000
77.0000	0.0000	0.0000	0.0000	0.0000	0.0000	0.0000	0.0000	0.0000
	0.0000	0.0000	0.0000	0.0000	0.0000	0.0000	0.0000	0.0000
	0.0000	0.0000	0.0000	0.0000	0.0000	0.0000	0.0000	0.0000
	0.0000	0.0000	0.0000	0.0000	0.0000	0.0000	0.0000	0.0000
78.0000	0.0000	0.0000	0.0000	0.0000	0.0000	0.0000	0.0000	0.0000
	0.0000	0.0000	0.0000	0.0000	0.0000	0.0000	0.0000	0.0000
	0.0000	0.0000	0.0000	0.0000	0.0000	0.0000	0.0000	0.0000
	0.0000	0.0000	0.0000	0.0000	0.0000	0.0000	0.0000	0.0000
79.0000	0.0000	0.0000	0.0000	0.0000	0.0000	0.0000	0.0000	0.0000
	0.0000	0.0000	0.0000	0.0000	0.0000	0.0000	0.0000	0.0000
	0.0000	0.0000	0.0000	0.0000	0.0000	0.0000	0.0000	0.0000
	0.0000	0.0000	0.0000	0.0000	0.0000	0.0000	0.0000	0.0000
80.0000	0.0000	0.0000	0.0000	0.0000	0.0000	0.0000	0.0000	0.0000
	0.0000	0.0000	0.0000	0.0000	0.0000	0.0000	0.0000	0.0000
	0.0000	0.0000	0.0000	0.0000	0.0000	0.0000	0.0000	0.0000
	0.0000	0.0000	0.0000	0.0000	0.0000	0.0000	0.0000	0.0000
81.0000	0.0000	0.0000	0.0000	0.0000	0.0000	0.0000	0.0000	0.0000
	0.0000	0.0000	0.0000	0.0000	0.0000	0.0000	0.0000	0.0000
	0.0000	0.0000	0.0000	0.0000	0.0000	0.0000	0.0000	0.0000
	0.0000	0.0000	0.0000	0.0000	0.0000	0.0000	0.0000	0.0000

Z= 66.00 (IN)

	1 .0390 0.0000	2 .1040 0.0000	3 .1040 0.0000	4 .0390 0.0000	
5 .0390 0.0000	6 .0770 0.0000	7 .1360 0.0000	8 .1360 0.0000	9 .0770 0.0000	10 .0390 0.0000
11 .1040 0.0000	12 .1360 0.0000	13 .1360 0.0000	14 .1360 0.0000	15 .1360 0.0000	16 .1040 0.0000
17 .1040 0.0000	18 .1360 0.0000	19 .1360 0.0000	20 .1360 .0463	21 .1360 .0463	22 .1040 0.0000
23 .0390 0.0000	24 .0770 0.0000	25 .1360 0.0000	26 .1360 .0463	27 .0770 .0818	28 .0390 0.0000
	29 .0390 0.0000	30 .1040 0.0000	31 .1040 0.0000	32 .0390 0.0000	

Z= 67.00 (IN)

	1 .0390 0.0000	2 .1040 0.0000	3 .1040 0.0000	4 .0390 0.0000	
5 .0390 .1615	6 .0770 .0818	7 .1360 0.0000	8 .1360 0.0000	9 .0770 0.0000	10 .0390 0.0000
11 .1040 .0606	12 .1360 .0463	13 .1360 0.0000	14 .1360 0.0000	15 .1360 0.0000	16 .1040 0.0000
17 .1040 0.0000	18 .1360 .0463	19 .1360 .0463	20 .1360 .1544	21 .1360 .1544	22 .1040 0.0000
23 .0390 0.0000	24 .0770 .0818	25 .1360 .0463	26 .1360 .1544	27 .0770 .2727	28 .0390 0.0000
	29 .0390 0.0000	30 .1040 0.0000	31 .1040 0.0000	32 .0390 0.0000	

Z= 68.00 (IN)

	1	2	3	4		
	.0390	.1040	.1040	.0390		
	0.0000	0.0000	.0606	.1515		
5	6	7	8	9	10	
.0390	.0770	.1360	.1360	.0770	.0390	
.5385	.2727	0.0000	.0926	.1635	0.0000	
11	12	13	14	15	16	
.1040	.1360	.1360	.1360	.1360	.1040	
.2019	.1544	0.0000	.0463	.0463	0.0000	
17	18	19	20	21	22	
.1040	.1360	.1360	.1360	.1360	.1040	
0.0000	.1544	.1544	.0463	.0463	0.0000	
23	24	25	26	27	28	
.0390	.0770	.1360	.1360	.0770	.0390	
0.0000	.2727	.2007	.0926	.0818	0.0000	
	29	30	31	32		
	.0390	.1040	.1040	.0390		
	0.0000	.0606	.0606	0.0000		

Z= 69.00 (IN)

	1	2	3	4	
	.0390	.1040	.1040	.0390	
	0.0000	0.0000	.2019	.5385	
5	6	7	8	9	10
.0390	.0770	.1360	.1360	.0770	.0390
.1615	.0818	.0463	.3551	.6273	.1615
11	12	13	14	15	16
.1040	.1360	.1360	.1360	.1360	.1040
.1212	.0926	.0463	.2007	.2007	.0606
17	18	19	20	21	22
.1040	.1360	.1360	.1360	.1360	.1040
.0606	.0926	.0463	0.0000	0.0000	0.0000
23	24	25	26	27	28
.0390	.0770	.1360	.1360	.0770	.0390
0.0000	.0818	.2007	.1544	0.0000	0.0000
	29	30	31	32	
	.0390	.1040	.1040	.0390	
	0.0000	.2019	.2019	0.0000	

Z= 70.00 (IN)

	1 .0390 0.0000	2 .1040 .0606	3 .1040 .1212	4 .0390 .1515	
5 .0390 0.0000	6 .0770 .0818	7 .1360 .2471	8 .1360 .2934	9 .0770 .4364	10 .0390 .5385
11 .1040 .2019	12 .1360 .2471	13 .1360 .2471	14 .1360 .2471	15 .1360 .2471	16 .1040 .2019
17 .1040 .2625	18 .1360 .2471	19 .1360 .0463	20 .1360 .0463	21 .1360 .0463	22 .1040 0.0000
23 .0390 .1515	24 .0770 .0818	25 .1360 .0463	26 .1360 .0463	27 .0770 0.0000	28 .0390 0.0000
	29 .0390 0.0000	30 .1040 .0606	31 .1040 .0606	32 .0390 0.0000	

Z= 71.00 (IN)

	1	2	3	4	
	.0390	.1040	.1040	.0390	
	.1615	.2625	.2019	0.0000	
5	6	7	8	9	10
.0390	.0770	.1360	.1360	.0770	.0390
0.0000	.3545	.4015	.2007	.0818	.1615
11	12	13	14	15	16
.1040	.1360	.1360	.1360	.1360	.1040
.0606	.3551	.3551	.2007	.2007	.0606
17	18	19	20	21	22
.1040	.1360	.1360	.1360	.1360	.1040
.2625	.3551	.2007	.2007	.2007	.0606
23	24	25	26	27	28
.0390	.0770	.1360	.1360	.0770	.0390
.5385	.3545	.0926	.0463	.0818	.1615
	29	30	31	32	
	.0390	.1040	.1040	.0390	
	.1615	.0606	0.0000	0.0000	

Z= 72.00 (IN)

	1	2	3	4		
	.0390	.1040	.1040	.0390		
	.5385	.2625	.0606	0.0000		
5	6	7	8	9	10	
.0390	.0770	.1360	.1360	.0770	.0390	
0.0000	.3545	.2471	.0463	0.0000	0.0000	
11	12	13	14	15	16	
.1040	.1360	.1360	.1360	.1360	.1040	
0.0000	.0926	.1390	.0926	.0926	.0606	
17	18	19	20	21	22	
.1040	.1360	.1360	.1360	.1360	.1040	
.0606	.0926	.2471	.2471	.2471	.2625	
23	24	25	26	27	28	
.0390	.0770	.1360	.1360	.0770	.0390	
.1615	.3545	.3088	.2007	.3545	.5385	
	29	30	31	32		
	.0390	.1040	.1040	.0390		
	.5385	.2019	.0606	.1615		

Z= 73.00 (IN)

	1	2	3	4		
	.0390	.1040	.1040	.0390		
	.1515	.0606	0.0000	0.0000		
5	6	7	8	9	10	
.0390	.0770	.1360	.1360	.0770	.0390	
0.0000	.0818	.0463	0.0000	0.0000	0.0000	
11	12	13	14	15	16	
.1040	.1360	.1360	.1360	.1360	.1040	
0.0000	0.0000	.1544	.1544	.1544	.2019	
17	18	19	20	21	22	
.1040	.1360	.1360	.1360	.1360	.1040	
0.0000	0.0000	.2007	.2007	.2007	.2625	
23	24	25	26	27	28	
.0390	.0770	.1360	.1360	.0770	.0390	
0.0000	.0818	.0926	.2007	.3345	.1615	
	29	30	31	32		
	.0390	.1040	.1040	.0390		
	.1615	.0606	.2019	.5385		

Z= 74.00 (IN)

	1	2	3	4	
	.0390	.1040	.1040	.0390	
	0.0000	0.0000	0.0000	0.0000	
5	6	7	8	9	10
.0390	.0770	.1360	.1360	.0770	.0390
0.0000	0.0000	0.0000	0.0000	0.0000	0.0000
11	12	13	14	15	16
.1040	.1360	.1360	.1360	.1360	.1040
0.0000	0.0000	.0463	.0463	.0463	.0606
17	18	19	20	21	22
.1040	.1360	.1360	.1360	.1360	.1040
0.0000	0.0000	.0463	.0463	.0463	.0606
23	24	25	26	27	28
.0390	.0770	.1360	.1360	.0770	.0390
0.0000	0.0000	0.0000	.0463	.0818	0.0000
	29	30	31	32	
	.0390	.1040	.1040	.0390	
	0.0000	0.0000	.0606	.1515	

AXIAL BLOCKAGE DISTRIBUTION BASED ON THE CALCULATED SLEEVE DISTRIBUTION

0.0000	0.0000	0.0000	0.0000	0.0000	0.0000	.0082	.0436	.0872	.1226
.1472	.1935	.1744	.1145	.0245	0.0000	0.0000	0.0000	0.0000	0.0000
0.0000	0.0000								

AXIAL BLOCKAGE DISTRIBUTION BASED ON PROBABILITY DISTRIBUTION

.0000	.0000	.0000	.0001	.0014	.0075	.0255	.0550	.0901	.1007
.1510	.1122	.0802	.0092	.0011	.0001	.0000	.0000	.0000	.0000

APPENDIX E
VENDOR INPUTS AND COMMENTS

E-1. GENERAL

Westinghouse requested that the three other PWR fuel vendors (Babcock & Wilcox, Combustion Engineering, and Exxon) provide relevant information to calculate a roncoplanar blockage distribution. To date they have provided the mean temperature distribution at the time of burst and some comments on the flow blockage task. The letters from the three vendors are attached at the end of this appendix. Burman and Olson[1] have already analyzed an expected local temperature fluctuation for a Westinghouse plant with a 15 x 15 fuel assembly.

E-2. MEAN TEMPERATURE

Westinghouse calculated a mean temperature distribution at the time of burst (figure E-1) by analyzing a LOCA using a proprietary code. Burst was calculated to occur at the end of blowdown. Babcock & Wilcox[2] calculated an axial temperature distribution for its plant (15 x 15 fuel) for a 0.794 m^2 (8.55 ft^2) double-ended cold leg break. Babcock & Wilcox also analyzed a plant with 17 x 17 fuel for the same accident case. The results are shown in figures E-2 and E-3. Clad rupture was calculated to occur during blowdown. Combustion Engineering[3] analyzed its 16 x 16 fuel assembly for a worst-temperature distribution using LOCA licensing analysis codes and input data. The result is shown in figure E-4. Exxon[4] also

---

1. Burman, D. L., and Olson, C. A., "Temperature and Cladding Burst Distributions in a PWR Core During LOCA," presented at The Specialists' Meeting on the Behaviour of Water Reactor Fuel Elements Under Accident Conditions, Spatind (Nord-Torpa), Norway, September 13-16, 1976.

2. Personal communication from J. J. Cudlin, Babcock & Wilcox, to H. W. Massie, Jr., Westinghouse, April 5, 1978.

3. Personal communication from J. H. Holderness, Combustion Engineering, to H. W. Massie, Jr., Westinghouse, April 11, 1978.

4. Personal communication from R. E. Collingham, Exxon Nuclear, to M. W. Hodges, USNRC, August 3, 1978.

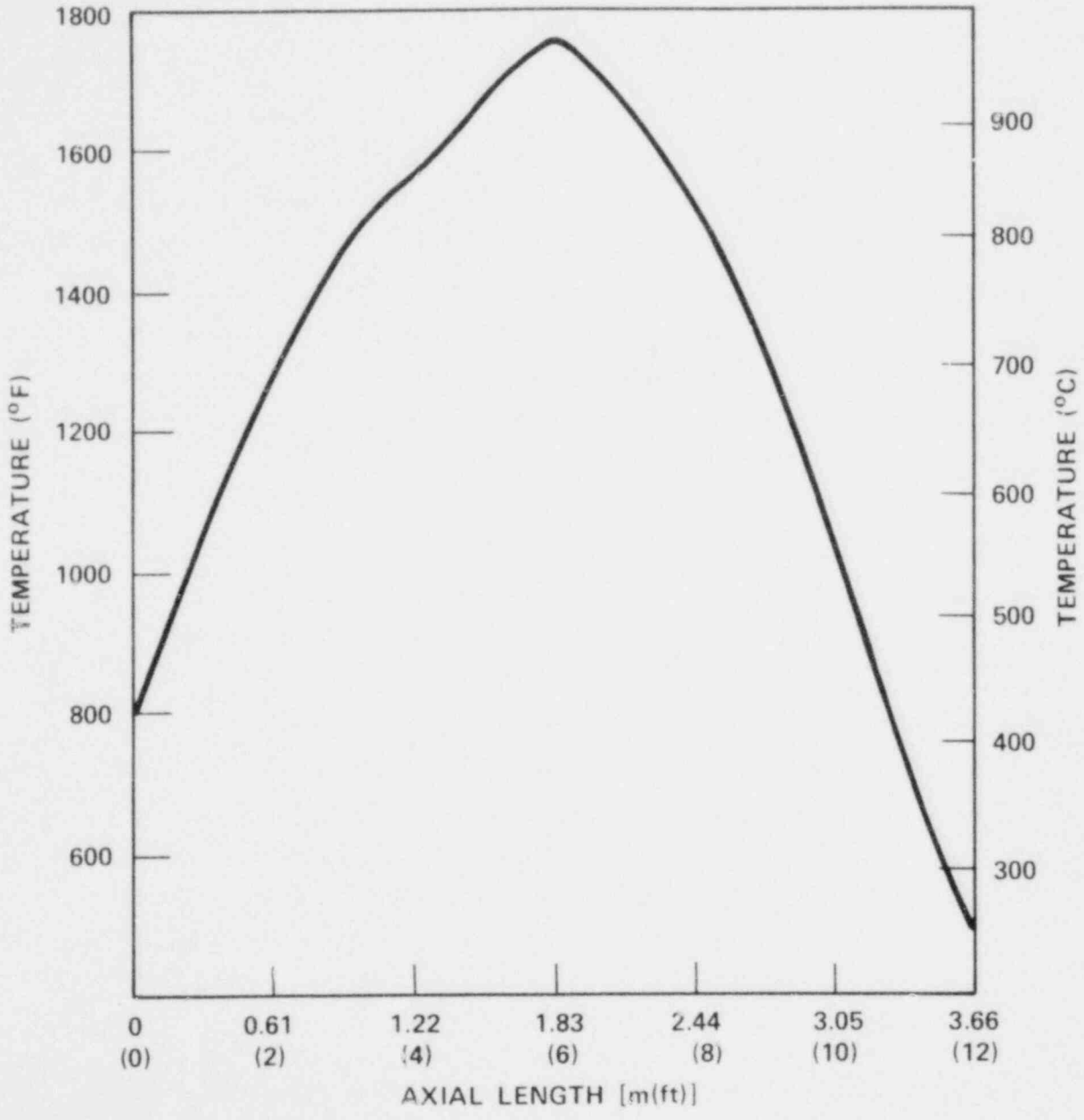

Figure E-1. Westinghouse Mean Temperature Distribution

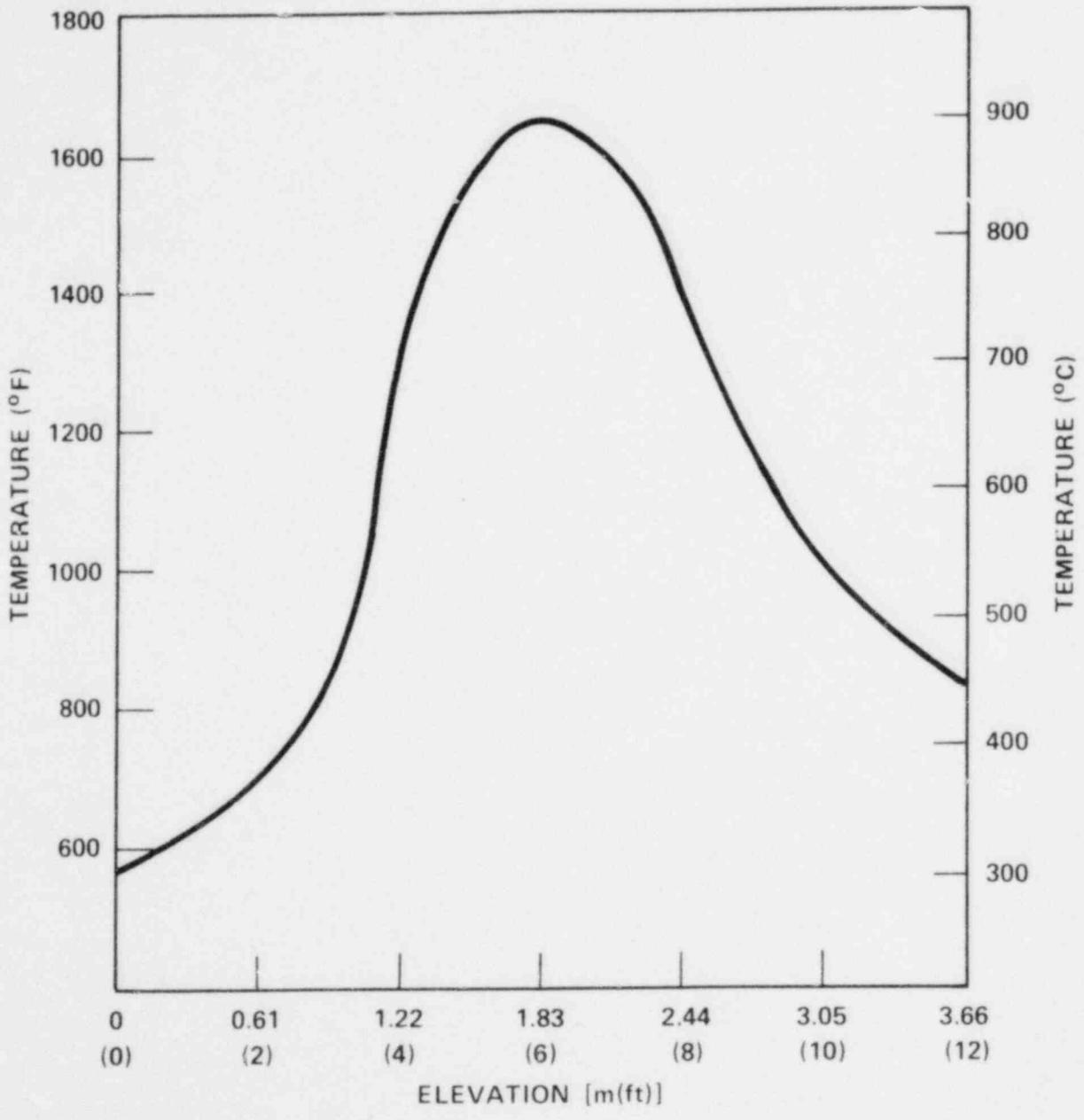

Figure E-2. Babcock & Wilcox Mean Temperature Distribution (15 x 15)

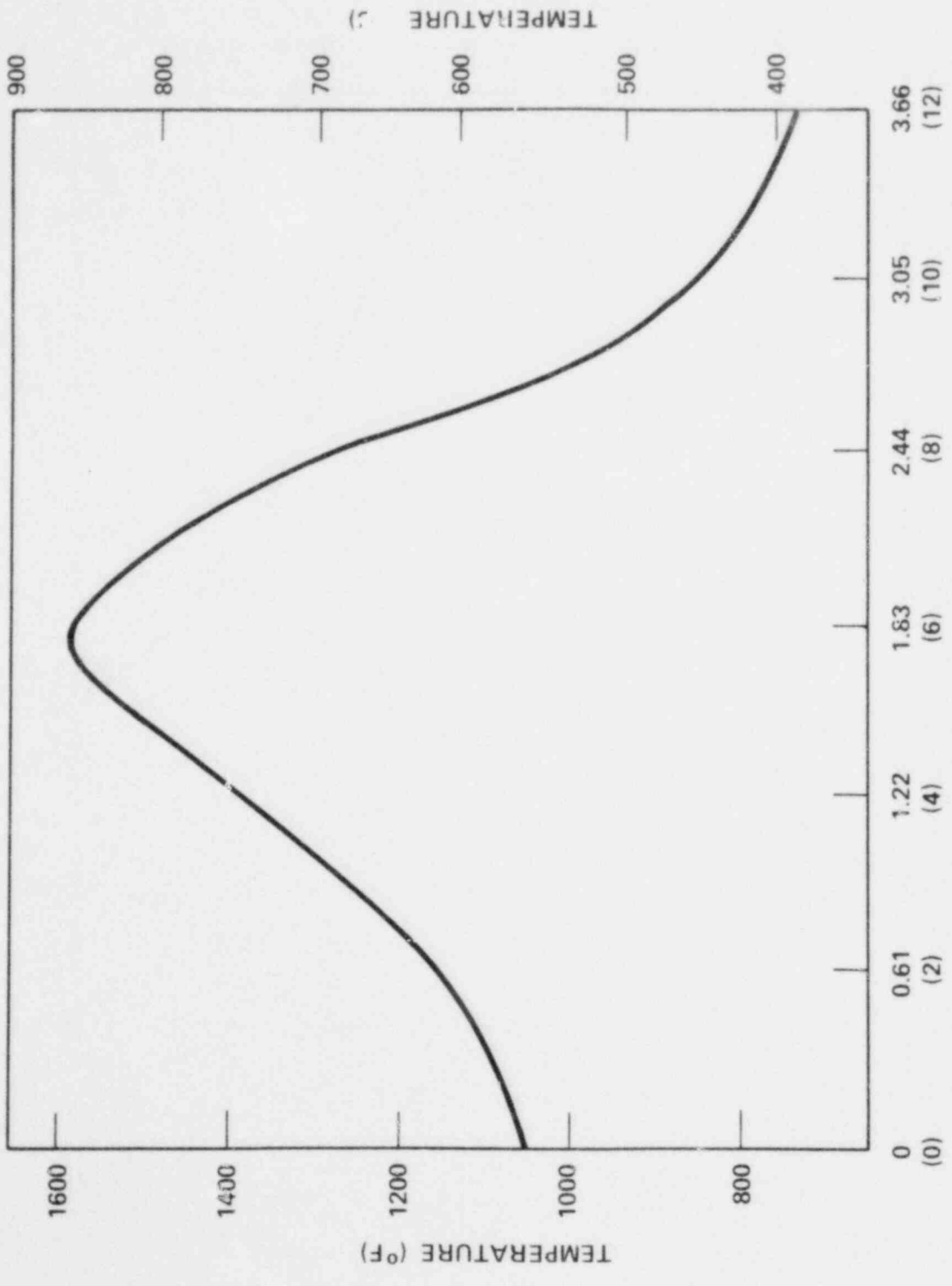

Figure E-3. Babcock & Wilcox Mean Temperature Distribution (17 x 17)

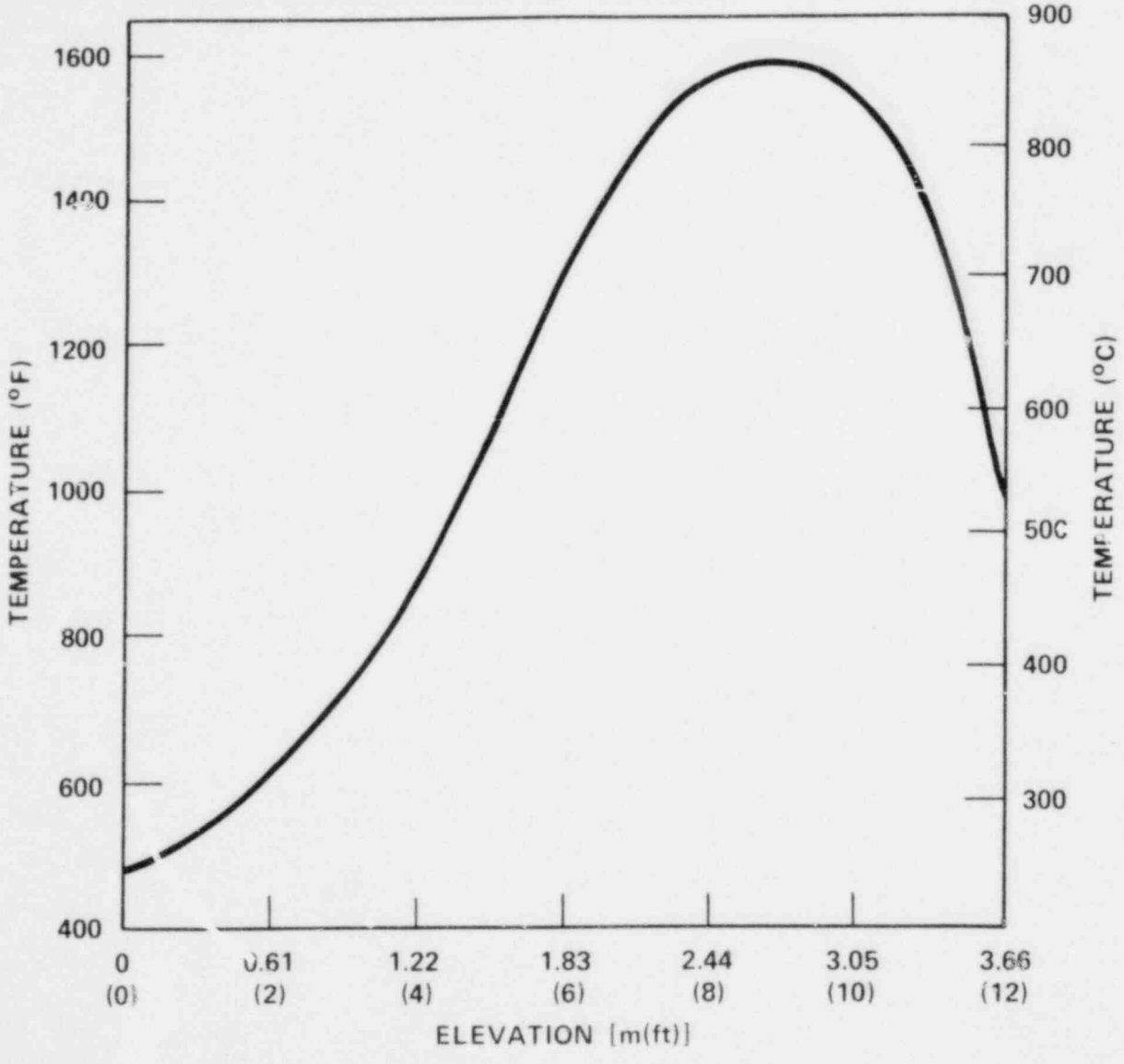

Figure E-4. Combustion Engincering Mean Temperature Distribution

used its WREM ECCS model to get a mean temperature distribution for a 15 x 15 fuel assembly at the time of rod rupture. The axial temperature profile of the hot rod in the hot channel at the time of its rupture is shown in figure E-5. Comparisons of the available mean temperature data reveal that Westinghouse and Babcock & Wilcox plants are expected to have most peaked axial temperature distributions. Combustion Engineering and Exxon have flatter distributions.

E-3. TEMPERATURE UNCERTAINTY

Local temperature can be divided into two components, as follows:

$$T_{local} = \bar{T}_{local} + T'_{local}$$

where $\bar{T}_{local}$ and T'_{local} are the mean and variation of local temperature, respectively. The mean temperature is obtained from the axial mean temperature distribution. The local temperature variation depends on several in-pile conditions and manufacturing effects, as discussed in section 3. Burman and Olson analyzed these effects, assuming that the temperature uncertainty is normally distributed. Their results are given here.

Manufacturing quality assurance records were reviewed to determine the realistic distribution for pellet parameters which would have an effect on local temperature variation, such as enrichment (negligible), initial density, sintering characteristics, diameter, and surface roughness. The variations thus obtained were input into Westinghouse standard design codes to determine their effect on operating temperature. Perturbation studies using the LOCTA-4 program were analyzed to determine the effect of small variations in initial power and temperature on the clad temperature at the time of burst, for cases in which burst occurred during refill. The initial temperature distributions were then modified to account for these effects. The resulting responses were statistically combined to obtain the overall temperature uncertainty just prior to the accident due to manufacturing variables. The resulting standard deviation in temperature was found to be approximately $9.8^{o}C$ ($17.6^{o}F$).

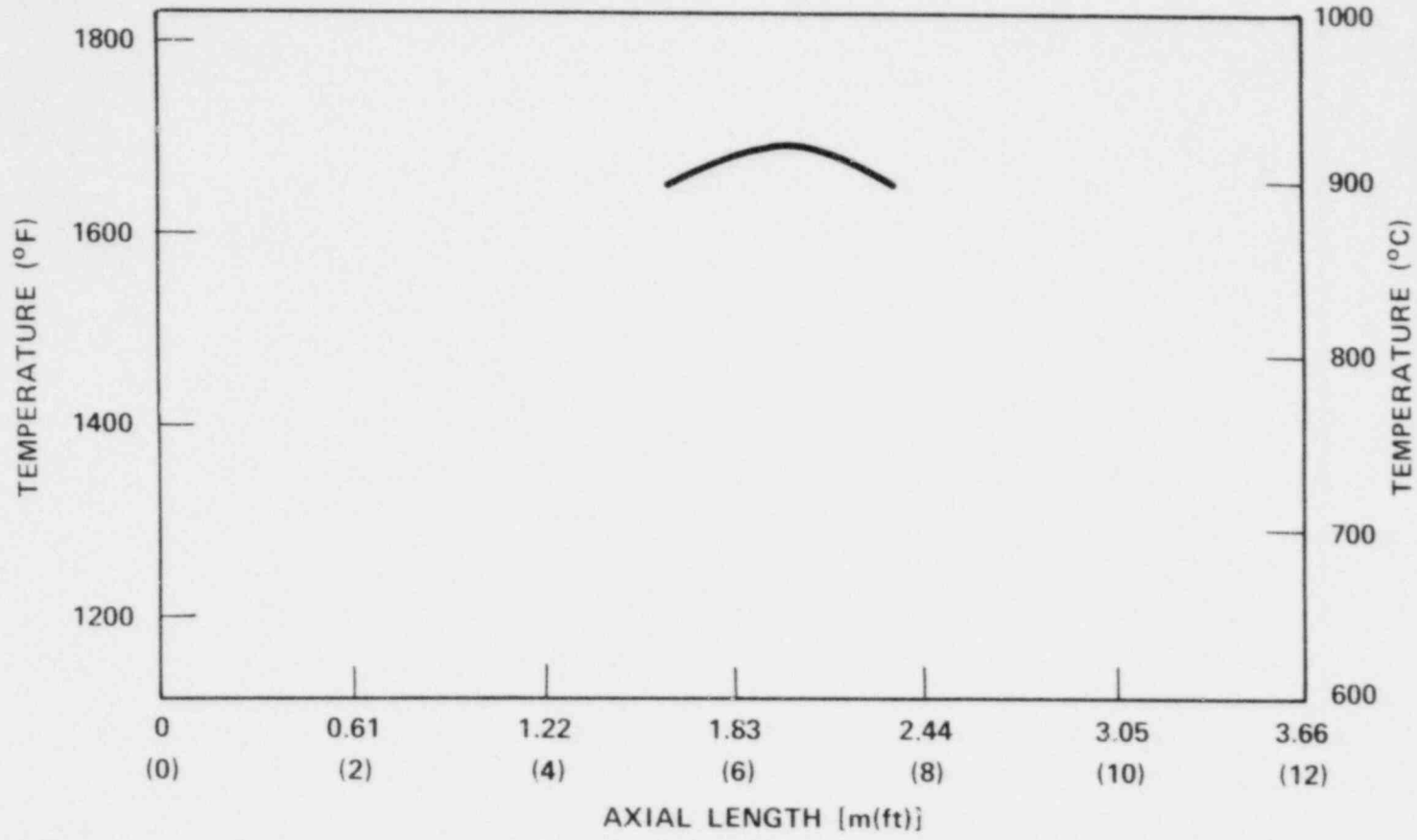

Figure E-5. Exxon Mean Temperature Distribution

Of the various uncertainties in pellet temperature due to in-pile effects, only the standard deviation in pellet temperature due to pellet offset was analyzed. Using a finite difference program, the effect of pellet eccentricity on pellet average temperature during normal operation was calculated, assuming various degrees of pellet clad eccentricity. The resulting temperature distribution was convoluted with that arising from manufacturing variables and the convoluted sum corrected to account for the temperature variability at burst time for a given temperature variability at power. This variation was determined to be 9.1°C (16.4°F). When statistically combined with the uncertainties due to manufacturing variables, the total standard deviation in local temperature becomes 13.4°C (24°C) at the time of blowdown or 6.7°C (12°F) at the time of burst.

It should be noted that, as the time increases after LOCA, the uncertainty decreases. The temperature uncertainty data have not been provided by the other vendors.

Babcock & Wilcox

Power Generation Group

P.O. Box 1260, Lynchburg, Va. 24505
Telephone: (804) 384-5111

RECEIVED
APR 07 1978
STRATEGIC
PROGRAM MANAGEMENT

April 5, 1978

Mr. H. W. Massie, Jr.
FLECHT-SEASET Project Engineer
Strategic Program Management
Westinghouse Electric Corporation
PWR Systems Division
Box 355
Pittsburgh, Pa. 15230

Dear Mr. Massie:

Enclosed please find plots of the information you requested regarding fuel cladding axial temperature distribution immediately prior to rupture. Figure 1 shows the axial variation in clad average temperature for a 15x15 hot assembly prior to mid-blowdown rupture. The data were produced for a 177 FA plant at 6 ft LOCA limit peak subject to an 8.55 ft^2 double-ended break at the pump discharge. Data for the same accident conditions based upon analysis for a 205 FA plant with 17x17 fuel are presented in Figure 2. In that case, the rupture was predicted to occur shortly after the end of blowdown.

I hope that this information is sufficient to contribute to your test design. Please feel free to contact me should you require clarification or further information.

Sincerely yours,

Joseph J. Cudlin

J. J. Cudlin

JJC/bm

enclosure

C-E Power Systems
Combustion Engineering, Inc.
1000 Prospect Hill Road
Windsor, Connecticut 06095

Tel. 203/688-1911
Telex 99297

C-E POWER SYSTEMS

April 11, 1978

Mr. H. W. Massie, Jr.
FLECHT-SEASET Project Engineer
Westinghouse Electric Corporation
P.O. Box 355
Pittsburgh, Pennsylvania 15230

Dear Mr. Massie:

This letter is in response to your March 28, 1978 request for information to be used as input to a statistical blockage calculation for the FLECHT-SEASET program. Attached is an axial mean temperature distribution which is representative of that calculated to occur in a LOCA licensing analysis for a Combustion Engineering 16x16 fuel assembly plant, at a time just prior to clad rupture. It should be noted that this is a worst case temperature distribution, computed with LOCA licensing analysis codes and input data.

You also stated your intention to define the local strain distribution using data from the ORNL MRBT program single rod test series. The α-phase rupture strains observed in these tests are significantly lower than those observed in the GFK single rod tests (1), or in the ORNL MRBT program multi-rod test series (2). Since the FLECHT-SEASET data will have potential application to licensing analyses, the program should examine a range of blockages greater than that which would result from considering the ORNL MRBT single rod tests alone. We therefore recommend that the data in references 1 and 2 be included in the definition of the local strain distribution.

Sincerely,

James H. Holderness

James H. Holderness
ECCS Analysis

JHH:jdg
Attach.

References:

1. F. Erbacher, handout for Fifth Water Reactor Safety Research Information Meeting, National Bureau of Standards, Gaithersburg, Maryland, November 11, 1977.

2. R. H. Chapman, handout for Zircaloy Cladding Review Group Meeting, Silver Spring, Maryland, January 18, 1978.

EXXON NUCLEAR COMPANY, Inc.

2101 Horn Rapids Road
P. O. Box 130, Richland, Washington 99352
Phone: (509) 943-8100 Telex: 32-6353

RECEIVED
AUG 15 1978
STRATEGIC
PROGRAM MANAGEMENT

August 3, 1978
REC-78-22

Mr. M. W. Hodges
US Nuclear Regulatory Comm.
Washington, D. C. 20555

Dear Wayne:

In a telephone call on July 18, 1978, Herb Massie (FLECHT-SEASET Project Engineer) requested that Exxon Nuclear Company supply an axial temperature profile representative of that calculated in ENC LOCA analyses at time of rod rupture; of particular interest is the profile in the average rod in the hot assembly at the time of its rupture.

He indicated that a bounding profile would be developed from the ENC profile and the profiles already supplied by the other PWR fuel manufacturers. This bounding profile is to be used in a statistical analysis to develop the blockage configuration for the NRC sponsored SEASET blockage reflood tests.

The attached figure is a representative axial temperature profile of the hot rod in the hot assembly at time of its rupture. The axial profile of the average rod is not available; however, it is anticipated that the axial profile in the average rod at the time of rupture would be similar to that shown in the attached figure.

I expect the attached figure will satisfy the request; please call if additional information is needed.

Sincerely,

Dr. R. E. Collingham, Manager
Systems Model Development

REC:tw

✓ c: Herb Massie
P. O Box 355
Pittsburgh, Pennsylvania 15310

K. H. Sun
3412 Hillview Ave
Palo Alto, California 94303

EXXON NUCLEAR COMPANY, Inc.

2101 Horn Rapids Road
P. O. Box 130, Richland, Washington 99352
Phone: (509) 943-8100 Telex: 32-6353

April 19, 1978
REC-78-08

RECEIVED
APR 25 1978
STRATEGIC
PROGRAM MANAGEMENT

Mr. H. W. Massie, Jr.
FLECHT-SEASET Project Engineer
Westinghouse Electric Corporation
Box 355
Pittsburgh, Pennsylvania 15310

Dear Mr. Massie:

Subject: INFORMATION FOR FLECHT-SEASET BLOCKAGE CALCULATIONS

In order to define the blockage configuration for the FLECHT-SEASET reflood heat transfer program, you requested in your letter of March 28, 1978 that Exxon Nuclear Company (ENC) provide you with statistical information on fuel temperature, fuel properties and rod rupture strain from the ENC ECCS flow blockage model.

Since the present ENC flow blockage model is not based on statistical temperature variation due to fuel property variations, the information you requested is not available. However, to aid you in the design of your flow blockage tests, the following guidance is provided based on open literature information (original ORNL MRBTS).

- Blockage fractions from 23 to 80% should be considered.
- The axial distribution of the assembly blockage can be enveloped by a 6-inch peak length with 3-inch linear tails as shown in the attached Figure.

Your letter indicated that the issue of coplaner versus noncoplaner blockage had not been resolved. Our recommendation is that both coplaner and noncoplaner blockages be tested and the coplaner blockage be 60 to 70% in magnitude with an axial distribution based on the attached Figure.

If we can provide additional assistance to guide you in your test planning and design, please let me know.

Sincerely,

R. E. Collingham, Manager
Systems Model Development

REC:mld

cc: K. H. Sun - EPRI
M. W. Hodges - NRC

Attachment

Attachment to
REC-78-08

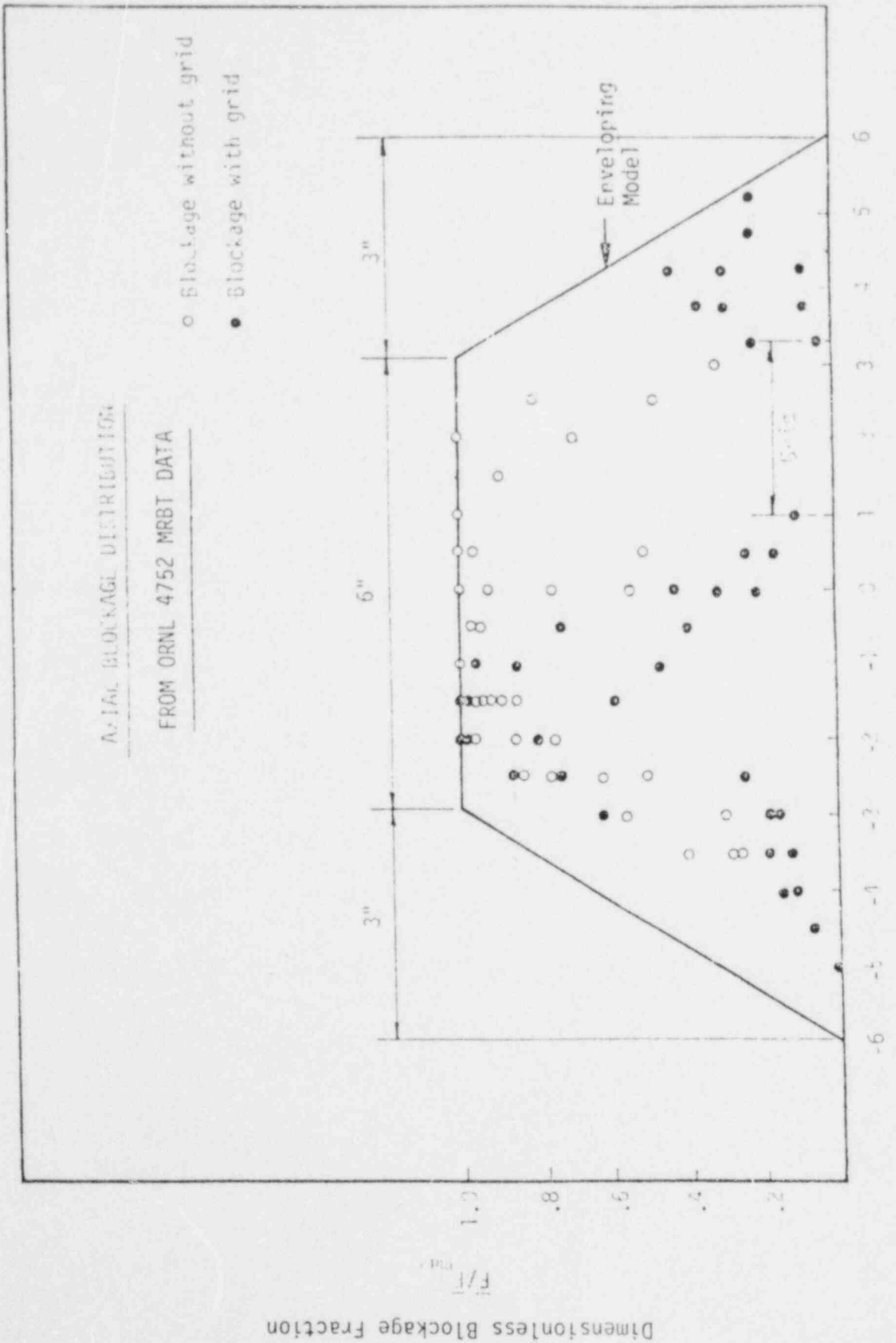

APPENDIX F
WORK SCOPE

The following describes the work scope and objectives of the 21-rod bundle flow blockage task (Task 3.2.2).

F-1. OBJECTIVE

The objective is to obtain, evaluate, and analyze thermal hydraulic data from a test program using 21-rod bundles to determine the effects of flow blockage geometry variation on the reflood heat transfer. The resultant data and analyses would then be used to guide the selection of a blockage shape for use in the large blocked bundle task (Task 3.2.3), and to develop an analytical or experimental method for use in analyzing the blocked bundle heat transfer data.

F-2. SCOPE

The scope of this program is as follows:

(1) Prepare a task plan per section 4 of the contract work scope,[1] including rationale for the choice of blockage geometries to be tested.

(2) Design, procure, and construct a test facility to provide hydraulic and heat transfer data.

(3) Design and procure CRG heater rods with a cosine axial power profile.

(4) Design and procure blockage sleeves and develop a method of attaching them to the heater rods. Conduct prototype heater rod testing with a blockage sleeve to verify sleeve attachment method and heater rod integrity as related to the blockage sleeve.

---

1. Conway, C. E., et al., "PWR FLECHT Separate Effects and Systems Effects Test (SEASET) Program Plan," NRC/EPRI/Westinghouse-1, December 1977, appendix B.

(5) Perform system calibration, instrumentation calibration, facility checkout, and facility shakedown tests.

(6) Perform tests for each blockage configuration in the sequence: hydraulic test, single-phase heat transfer test, and reflooding test.

(7) Review and validate test data.

(8) Reduce data to obtain loss coefficients for blockage and grids and friction factor for the bundle, heater rod temperature, rod heat flux, rod heater transfer coefficients, vapor temperatures, bundle inlet flows, bundle vapor exit flows, bundle liquid exit flows, bundle pressure drop data, and test section housing and piping temperatures.

(9) Analyze and evaluate data to obtain hydraulic and heat transfer comparisons between the unblocked reference data and the blockage data. The comparisons will define the effects of different blockage shapes and distributions for different tests and conditions, to separate hydraulic and heat transfer effects. Analyze data to obtain bundle-averaged fluid conditions such as vapor temperatures, liquid flows, vapor flows, and void fraction at several axial positions, where applicable.

(10) Process and store transducer data on computer tapes.

(11) Prepare a data report per section 4.0 of the contract work scope. In addition, data packages of selected data from each test configuration will be supplied to the PMG members and their consultants during the test period.

(12) Develop an analytical or experimental method which can be used to analyze blockage heat transfer data. For the calculation of the thermal-hydraulic quantities, existing computer codes (such as COBRA) will be used.

(13) Provide analysis of the data such that the blockage shape can be selected for the large bundle task (Task 3.2.3).

(14) Prepare a data analysis and evaluation report per section 4.0 of the contract work scope.

APPENDIX G
FACILITY DRAWINGS

Drawings applicable to the 21-rod flow blockage task are listed in table G-1. Those drawings not included in sections 6 and 7 are reproduced on the following pages.

TABLE G-1

LIST OF DRAWINGS FOR FLOW BLOCKAGE TASK
TEST FACILITY

Drawing No.	Sub	Sheets	Title
1541E68 (figure 6-1)	1	1	FLECHT SEASET 21-Rod Bundle Flow Diagram
1460E65 (figure 6-2)	1	1	FLECHT SEASET 21-Rod Test Housing Assembly
1453E60 (figure 6-3)	1	1	FLECHT SEASET 21-Rod Bundle Test - Low Mass Housing Detail
1460E39 (figure 6-5)	1	1	FLECHT SEASET 21-Rod Bundle Heater Rods
1460E76 (figure 6-6)	1	3	FLECHT SEASET 21-Rod Bundle Loop Piping
1460E40 (figure 7-7)	1	1	FLECHT SEASET 21-Rod Bundle Forced Reflood Instrumentation Schematic
1460E41 (figure 7-8)	1	1	FLECHT SEASET 21-Rod Bundle Gravity Reflood Instrumentation Schematic
1453E62 (figure G-1)	2	1	FLECHT SEASET 21-Rod Bundle Upper and Lower Plenum Detail and Assembly
1460E48 (figure G-2)	2	1	FLECHT SEASET 21-Rod Test Bundle Strongback and Assembly Fixture
8764D69 (figure G-3)	2	1	FLECHT SEASET 21-Rod Bundle Upper and Lower Seal Plate
1446E87 (figure G-4)	1	1	FLECHT SEASET 21-Rod Bundle Grid Assembly and Details
1460E50 (figure G-5)	1	1	FLECHT SEASET 21-Rod Test Instrumentation Components
1460E63 (figure G-6)	2	1	21-Rod FLECHT SEASET 21-Rod Test Bundle Assembly
9556D10 (figure G-7)	1	2	FLECHT SEASET 21-Rod Test Filler Strip

TABLE G-1 (cont)

LIST OF DRAWINGS FOR FLOW BLOCKAGE TASK
TEST FACILITY

Drawing No.	Sub	Sheets	Title
1680C97 (figure G-8)	5	1	FLECHT SEASET 21-Rod Bundle O-Ring Sleeves
1460E59 (figure G-9)	1	1	FLECHT SEASET 21-Rod Test Details
1684C06 (figure G-10)	1	1	FLECHT SEASET 21-Rod Test Flow Blockage Sleeve
9553D26 (figure G-11)	1	1	FLECHT SEASET 21-Rod Test Nonconcentric Flow Blockage Sleeve

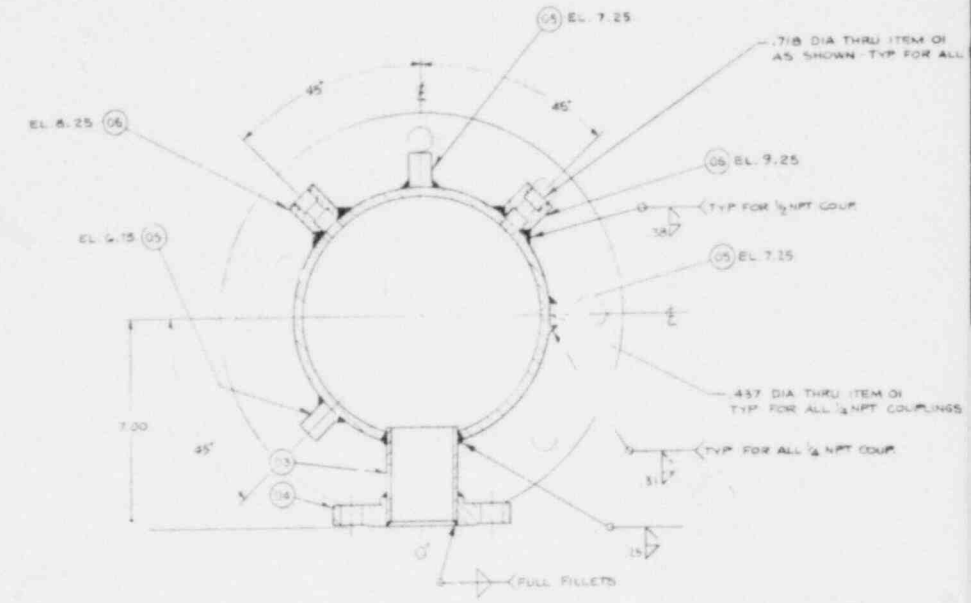

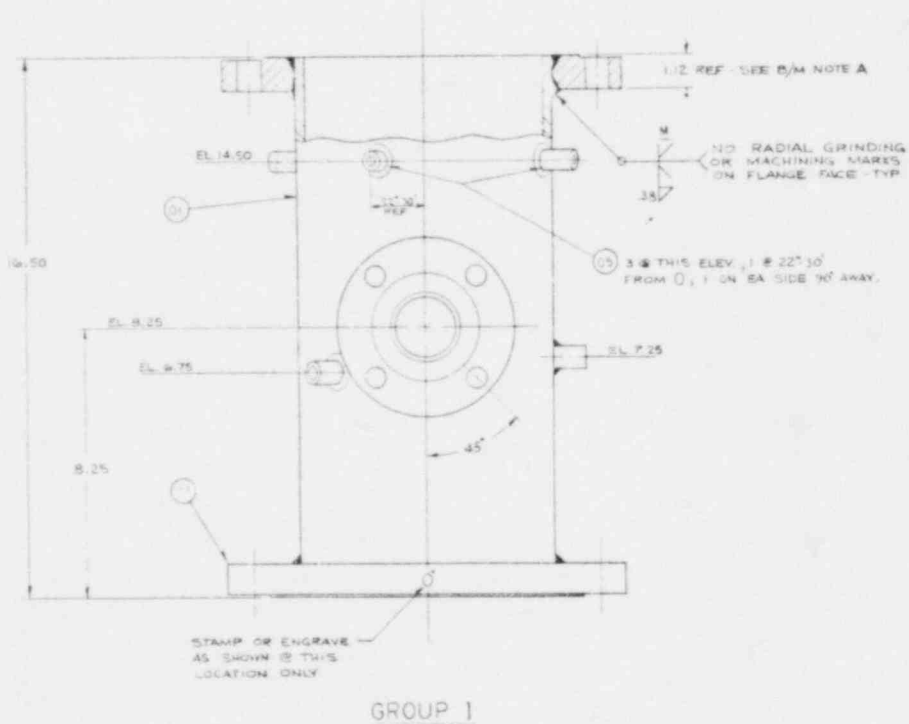

GROUP 1

UPPER PLENUM

BILL OF MATERIAL							
ITEM	QTY	PART NAME	[illegible]	MATERIAL	NO. PER GROUP		
					01	02	03
01		PIPE, 6" SCH 40		SA 106 GR B	1	1	
02	A	FLANGE, 6" 150 LB SLIP ON		A 105 GR II	2	4	
03		PIPE, 2" SCH 40		SA 106 GR B	1	1	
04		FLANGE, 2" 150 LB SLIP ON		A 105 GR II	1	1	
05		¼ NPT COUPLING 6000#		SA 105	4	1	
06		½ NPT COUPLING 6000#		SA 105	2		

A REMOVE HUB BEFORE MACHINING WELD PREP

NOTES:
1-DESIGN, FABRICATE, TEST & STAMP PER SECT I OF THE ASME BOILER & PRESSURE VESSEL CODE.
2-DESIGN PRESSURE 100 PSIG @ 700°F
3-WELD PER W PROC SPEC 82127-2V (ALL WELDS FULL PENETRATION EXCEPT ITEM 04)

½ NPT COUPLINGS

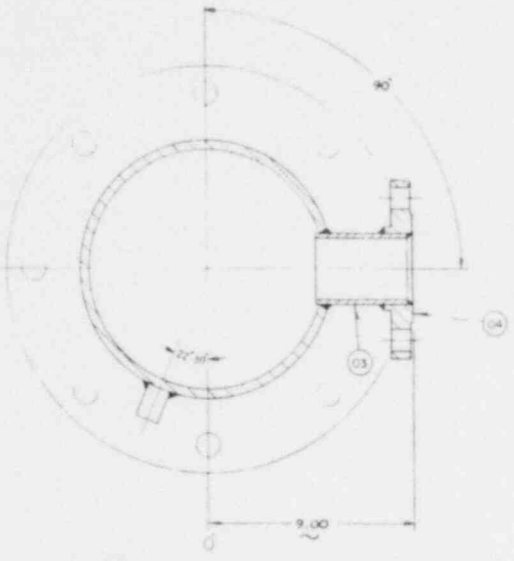

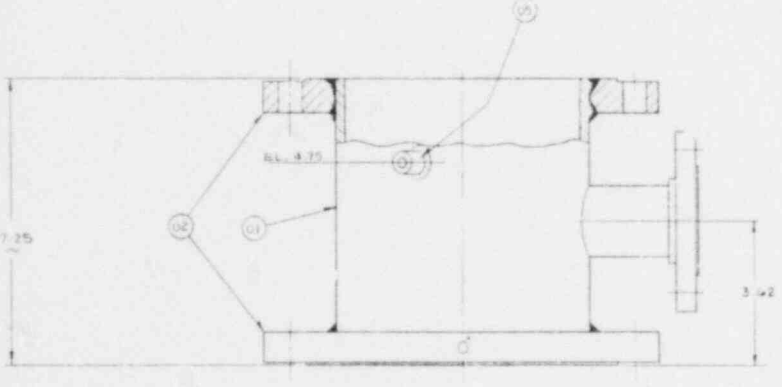

GROUP 2

LOWER PLENUM

(OTHERWISE SAME AS GROUP 1)

Figure G-1. FLECHT SEASET 21-Rod Bundle Test Plenums (Drawing No. 1453E62)

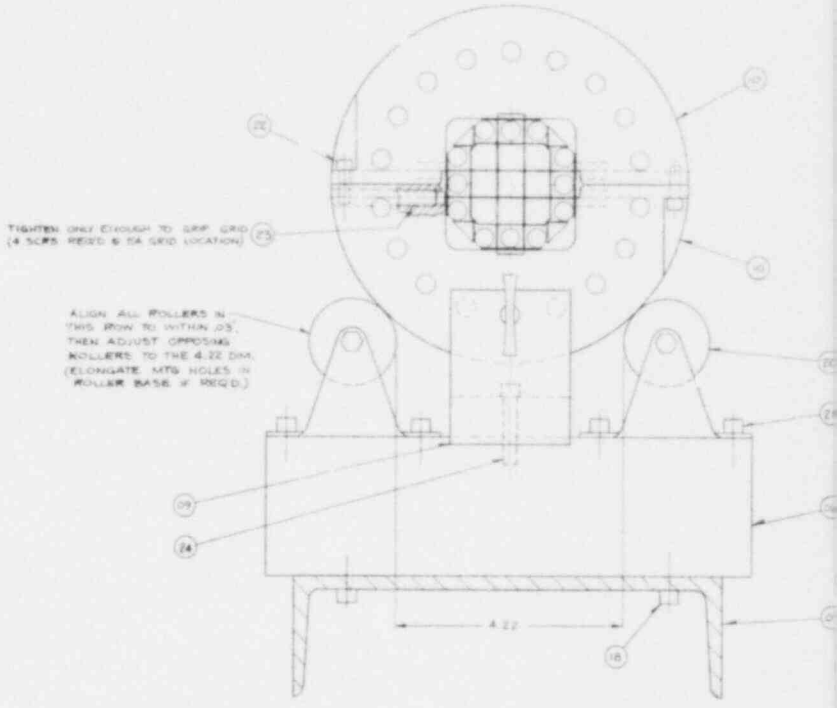

VIEW B B

TYP 8 PLACES

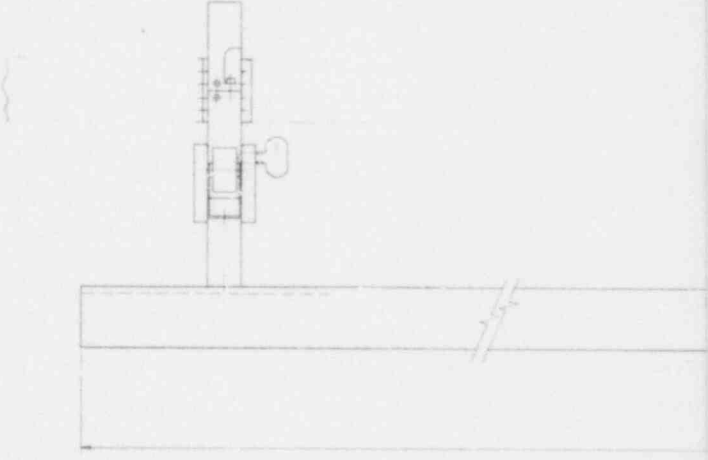

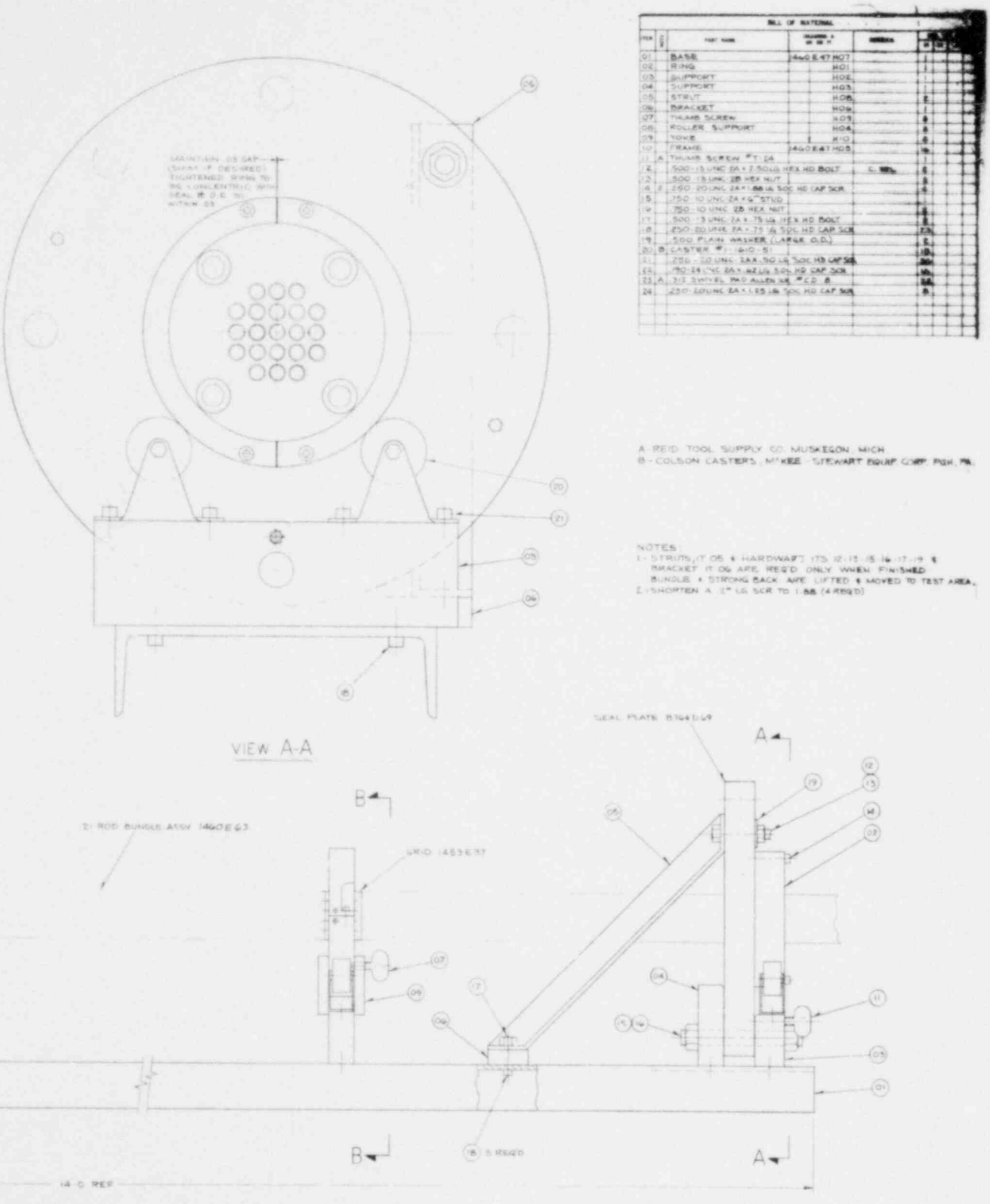

Figure G-2. FLECHT SEASET 21-Rod Test Bundle Strongback and Assembly Fixture (Drawing No. 1460E48)

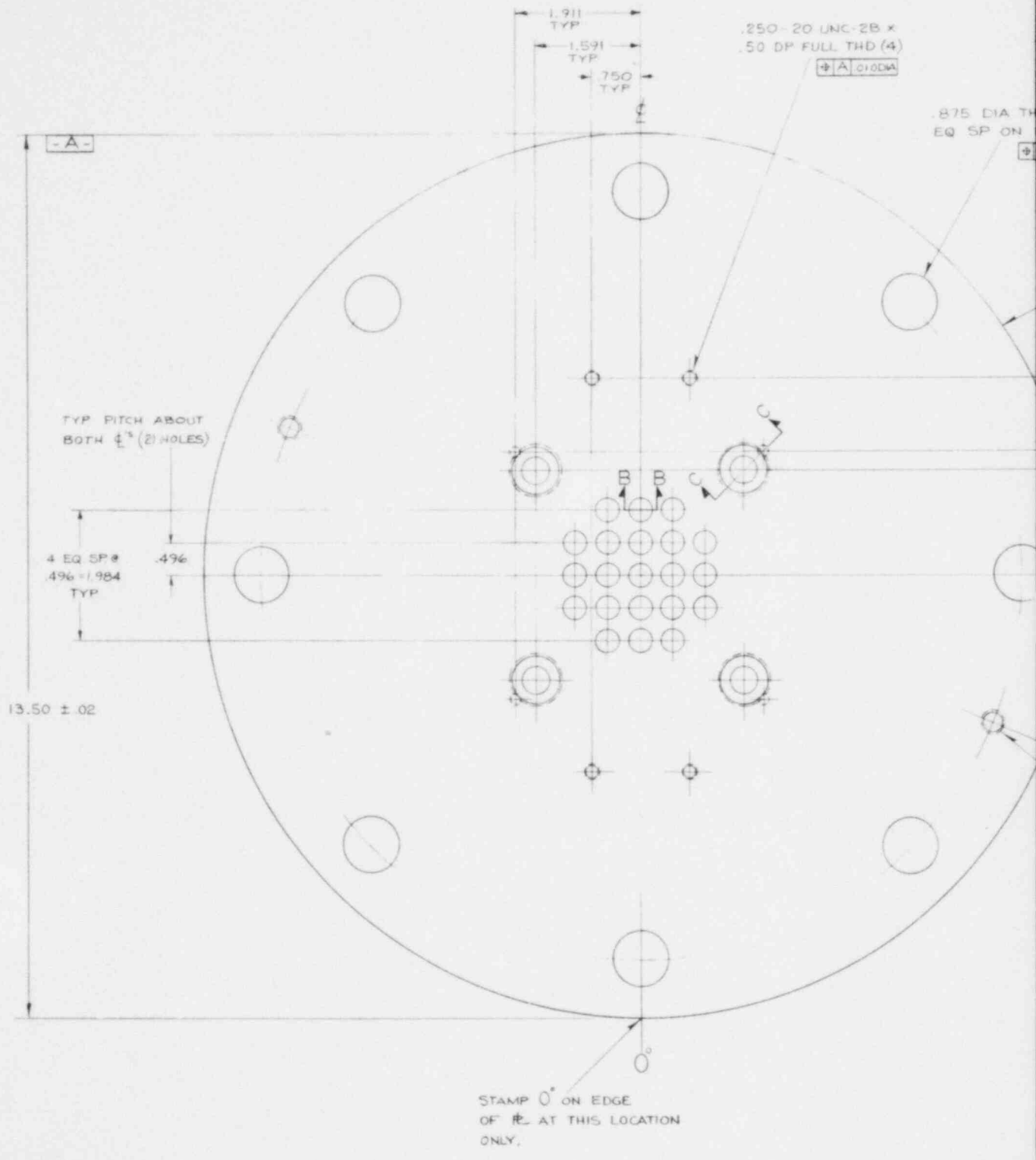
1.911
TYP
1.591
TYP
.750
TYP
.250 - 20 UNC-2B x
.50 DP FULL THD (4)
⌖ A 0.1 DIA
.875 DIA TH
EQ SP ON
- A -
TYP PITCH ABOUT
BOTH ℄'S (21 HOLES)
4 EQ SP @
.496 = 1.984
TYP
.496
13.50 ± .02
B B
C
C
0°
STAMP 0° ON EDGE
OF ℄ AT THIS LOCATION
ONLY.

BILL OF MATERIAL								
ITEM	NOTE	PART NAME	DRAWING & GR OR IT	MATERIAL	REQ. PER GROUP			
					01	02	03	04
01		SEAL PLATE		ASTM 240 304	1			

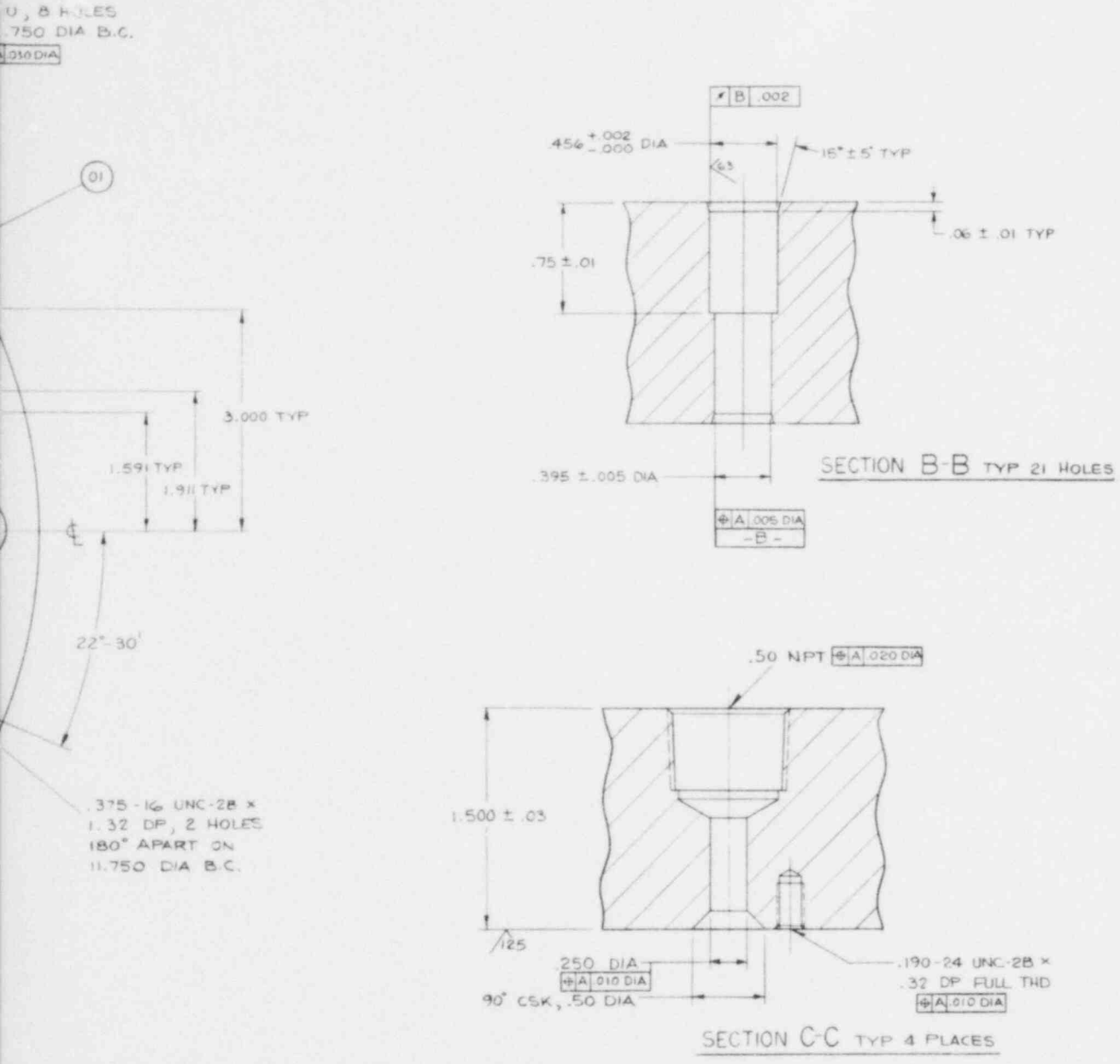

Figure G-3. FLECHT SEASET 21-Rod Bundle Upper and Lower Seal Plate (Drawing No. 8764D69)

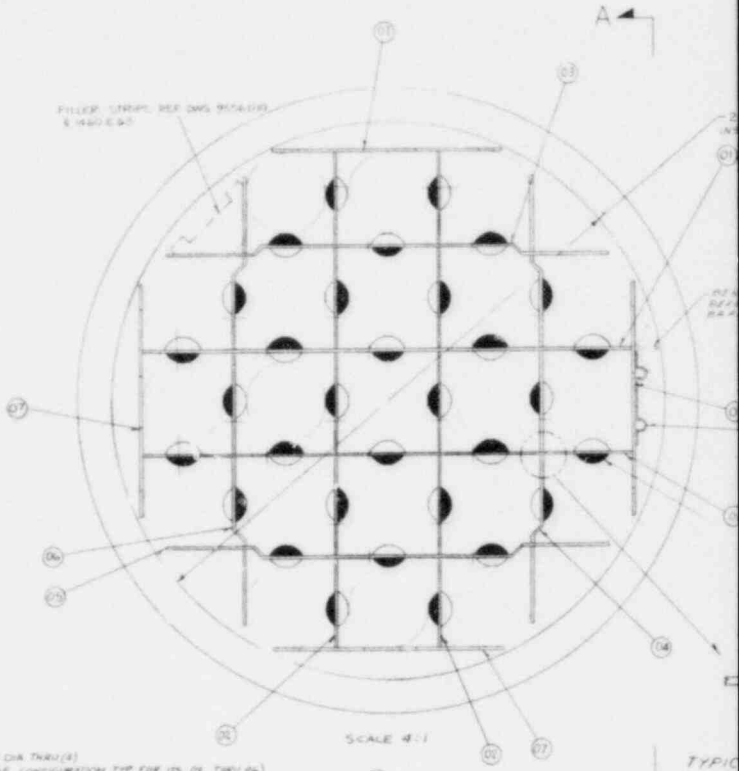
A
FILLER STRIP, SEE DWG 9974010
SCALE 4:1

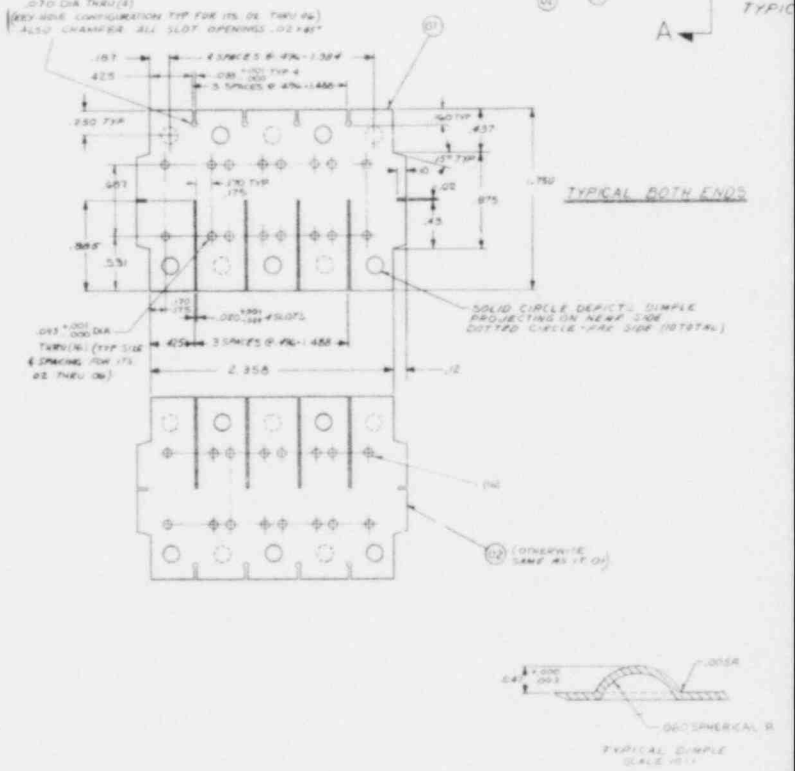
A
TYPIC
TYPICAL BOTH ENDS
SOLID CIRCLE DEPICTS DIMPLE PROJECTING ON NEAR SIDE
DOTTED CIRCLE FAR SIDE (TOTAL)
(OTHERWISE SAME AS 17.01)
TYPICAL DIMPLE
SCALE 10:1

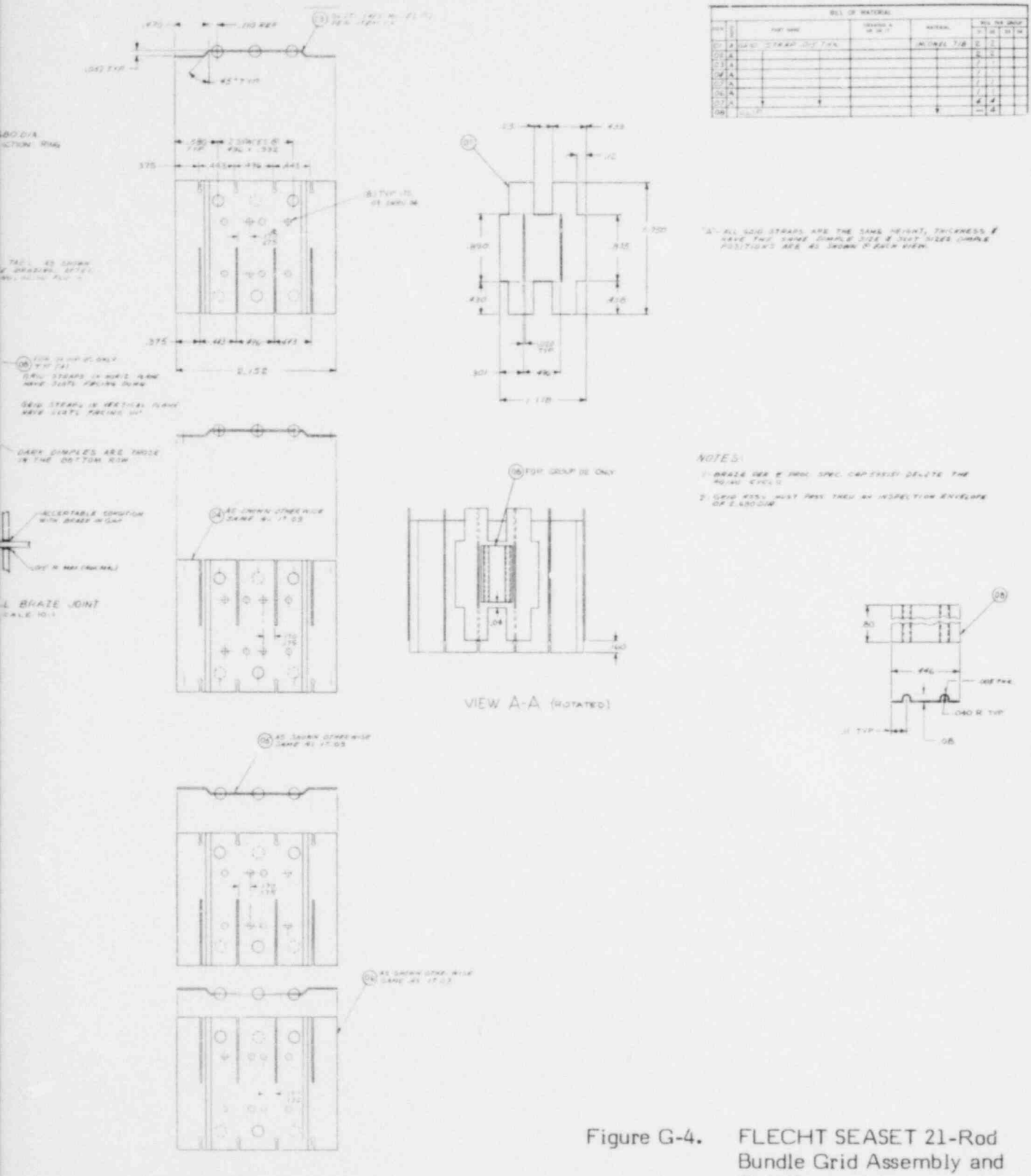

Figure G-4. FLECHT SEASET 21-Rod Bundle Grid Assembly and Details (Drawing No. 1446E87)

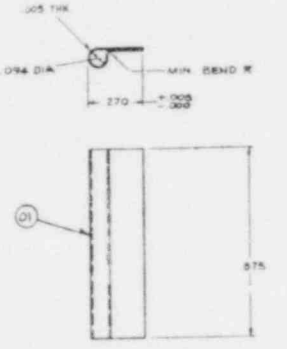

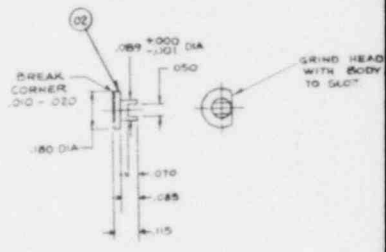

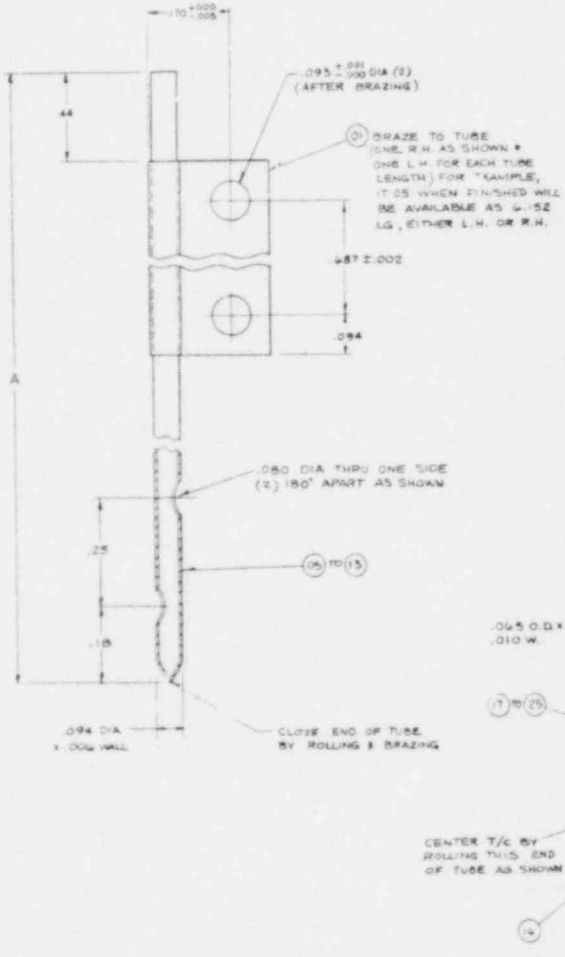

ITEM	A
05	6.15
06	4.15
07	7.15
08	5.15
09	7.90
10	3.15
11	9.75
12	8.75
13	6.75

ITEM	B
17	5.62
18	3.62
19	6.62
20	4.62
21	7.37
22	2.62
23	9.22
24	8.22
25	6.22

AT FINAL ASSY, IT. 05 & 17 TOGETHER; IT. 06 & 18, 07 &

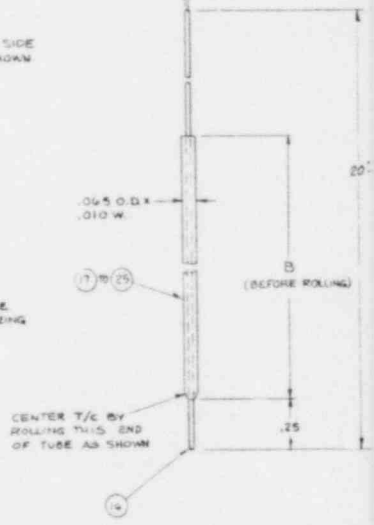

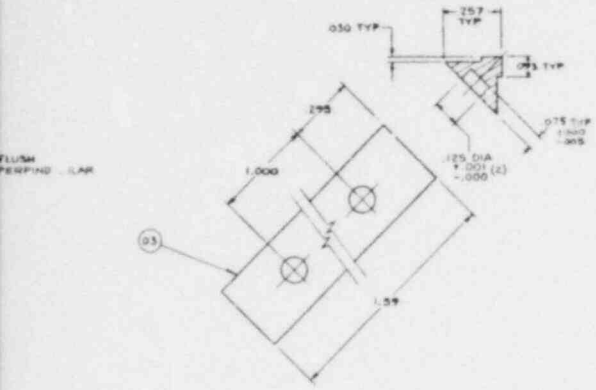

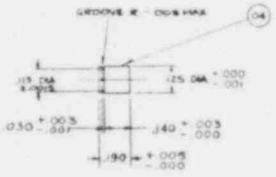

BILL OF MATERIAL

ITEM	QTY	PART NAME	MATERIAL	BILL OF MATERIAL GROUP 13	20	21	24
-		CLIP	304 SST				
02		RIVET					
03		FILLER STRIP SUPPT					
04		FILLER STRIP SUPPT PIN					
05		PROBE HOLDER L H, R H					
06							
07							
08							
09							
10							
11							
12							
13		PROBE HOLDER L H - R H	304 SST				
14	A	TEFLON SEAL (HALF)					
15	A	SEAL COMP. (HALF)					
16	B	T/C .020 DIA x 20' CHROMEL-ALUMEL	304 SST UN-SPD				
17		SLEEVE	304 SST				
18							
19							
20							
21							
22							
23							
24							
25		SLEEVE	304 SST				

A - ITEM 14 & 15 ARE COMPONENTS OF CONAX FITTING NO. SPG-100 MODIFY AS SHOWN.
B - C. S. GORDON CO.

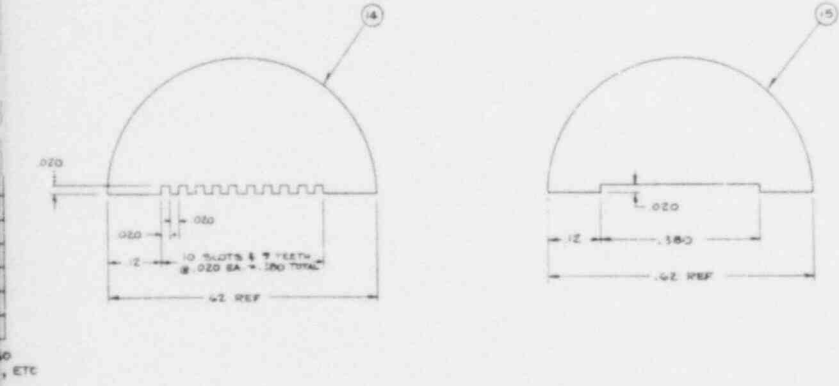

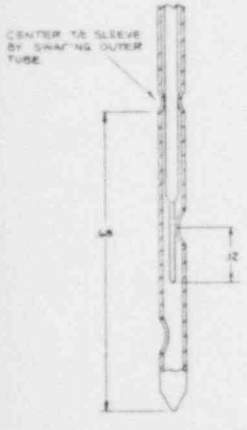

PROBE HOLDER & T/C ASSY

Figure G-5. FLECHT SEASET 21-Rod Test Instrumentation Components (Drawing No. 1460E50)

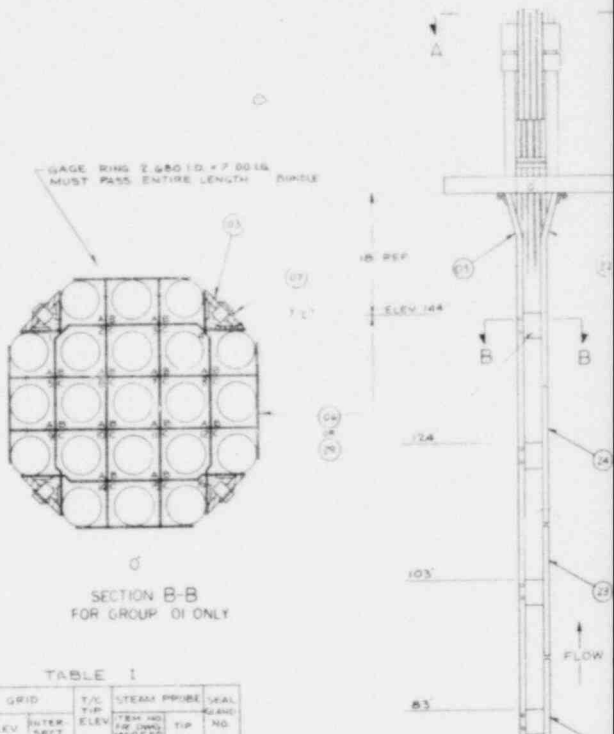

SECTION B-B
FOR GROUP 01 ONLY

TABLE 1

GRID		T/C TIP ELEV	STEAM PROBE		SEAL GLAND NO.
ELEV	INTER-SECT		ITEM NO. FOR (2MW) (4MW) (6 MW)	TIP	
144	6B	138	09-LH	UP	1
124	11B	132	11-RH	DN	3
	4B	120	06-LH	UP	1
	7C	120	06-LH	UP	3
103	5A	111	11-LH	DN	1
	10A	111	11-RH	DN	4
	9B	96	07-RH	UP	4
	8C	96	07-LH	UP	2
	10C	96	07-LH	UP	4
83	5A	90	12-RH	DN	1
	7A	90	12-RH	DN	2
	10C	90	12-RH	DN	4
	4B	78	08-LH	UP	1
	11B	73	08-LH	UP	3
	9B	78	08-LH	UP	4
	7C	74	09-RH	UP	2
62	6A	67	13-LH	DN	1
	8B	67	13-RH	DN	2
	9B	67	13-LH	DN	4
	11B	67	13-LH	DN	3
	SPEL	67	13-RH	DN	3
	10B	59	10-LH	UP	4
	15B	59	10-LH	UP	3
41	10A	48	12-LH	DN	4
	15A	48	12-LH	DN	3
	9B	38	10-RH	UP	4

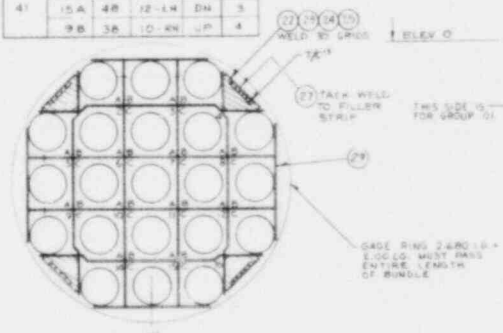

SECTION B-B
FOR GROUP 02 ONLY

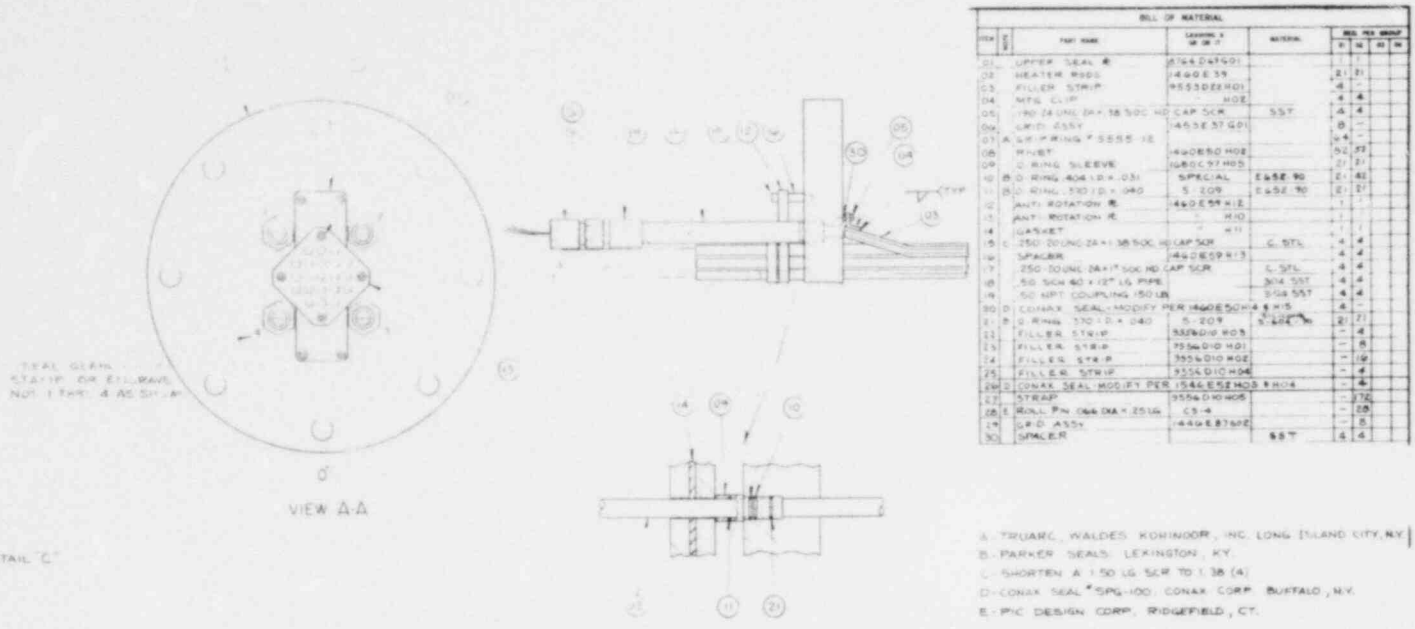

BILL OF MATERIAL

ITEM	QTY	PART NAME	DRAWING # OR SPEC #	MATERIAL	REQ. PER GROUP			
					21	37	43	54
01		UPPER SEAL A	1464D47G01		1	1		
02		HEATER RODS	1460E39		21	21		
03		FILLER STRIP	9553DEEH01		4	-		
04		MTG. CLIP	- H02		4	4		
05		1/80-24 UNC-2A x .38 SOC. HD. CAP SCR.		SST	4	4		
06		GRID ASSY	1463E37G01		8	-		
07	A	GRIP RING 9555-12			4	-		
08		RIVET	1460E50 H02		52	37		
09		O RING SLEEVE	1460C97 H05		21	21		
10	B	O RING .406 I.D. x .051	SPECIAL	E652-90	21	42		
11	B	O RING .370 I.D. x .040	S-209	E652-90	21	21		
12		ANTI-ROTATION PL	1460E59 H12		1			
13		ANT. ROTATION PL	- H10		1			
14		GASKET	- H11		1	1		
15	C	.250-20 UNC-2A x .38 SOC. HD. CAP SCR		C. STL	4	4		
16		SPACER	1460E59 H13		4	4		
17		.250-30 UNF-2A x 1" SOC. HD. CAP SCR.		C. STL	4	4		
18		.50 SCH 40 x 12" LG PIPE		304 SST	4	4		
19		.50 NPT COUPLING 150 LB		304 SST	4	4		
20	D	CONAX SEAL-MODIFY PER 1460E50 H04 & H15			4			
21	B	O RING .370 I.D. x .040	S-209	E652-90	21	21		
22		FILLER STRIP	9556D10 H03		-	4		
23		FILLER STRIP	9556D10 H01		-	8		
24		FILLER STRIP	9556D10 H02		-	10		
25		FILLER STRIP	9556D10 H04		-	4		
26	D	CONAX SEAL MODIFY PER 1546E52 H03 & H04			-	4		
27		STRAP	9556D10 H05		-	376		
28	E	ROLL PIN .066 DIA x .251G	C5-4		-	28		
29		GRID ASSY	1449E87G02		-	8		
30		SPACER		SST	4	4		

A - TRUARC, WALDES KOHINOOR, INC. LONG ISLAND CITY, N.Y.
B - PARKER SEALS, LEXINGTON, KY.
C - SHORTEN A 1.50 LG SCR TO 1.38 (4)
D - CONAX SEAL "SPG-100" CONAX CORP. BUFFALO, N.Y.
E - PIC DESIGN CORP. RIDGEFIELD, CT.

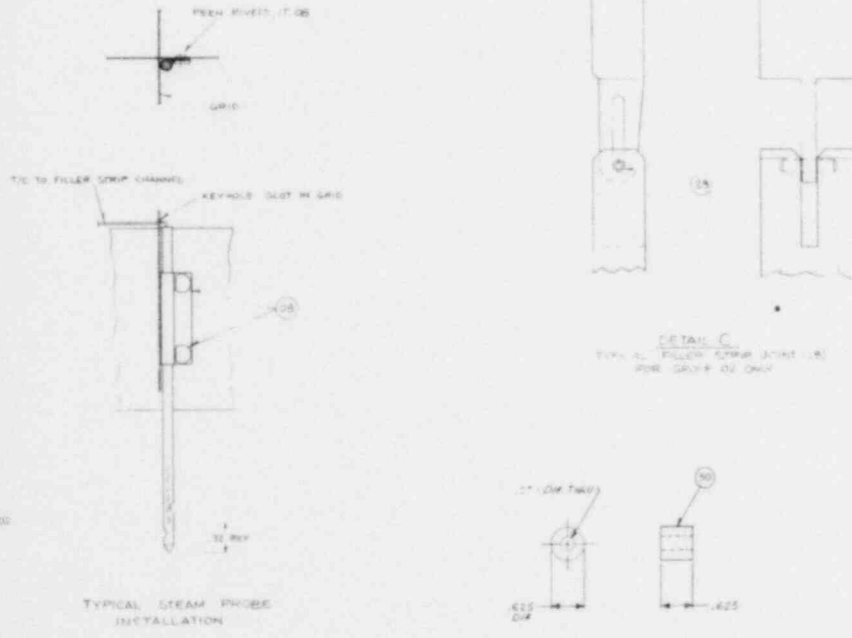

Figure G-6. FLECHT SEASET 21-Rod Test Bundle Assembly (Drawing No. 1460E63)

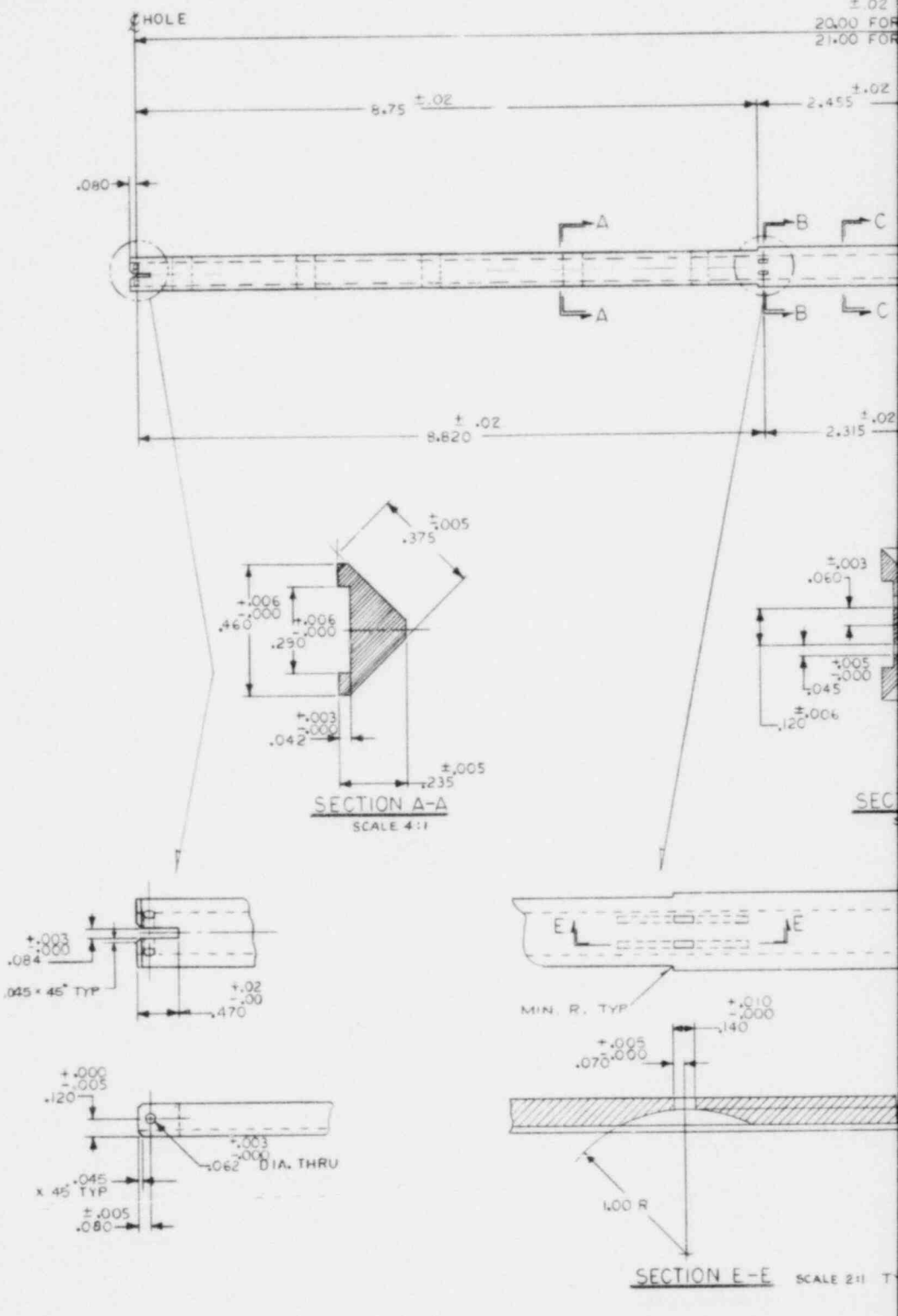
HOLE
20.00 FOR
21.00 FOR
8.75 ±.02
2.455 ±.02
.080
A
B
C
8.820 ±.02
2.315 ±.02
.375 ±.005
.460 +.006 -.000
.290 +.006 -.000
.042 +.003 -.000
.235 ±.005
SECTION A-A
SCALE 4:1
.060 ±.003
.045 +.005 -.000
.120 ±.006
.084 +.003 -.000
.045 x 45° TYP
.470 +.02 -.00
.120 +.000 -.005
.062 +.003 -.000 DIA. THRU
x 45° TYP .045
.080 ±.005
E
MIN. R. TYP
.140 +.010 -.000
.070 +.005 -.000
1.00 R
SECTION E-E
SCALE 2:1

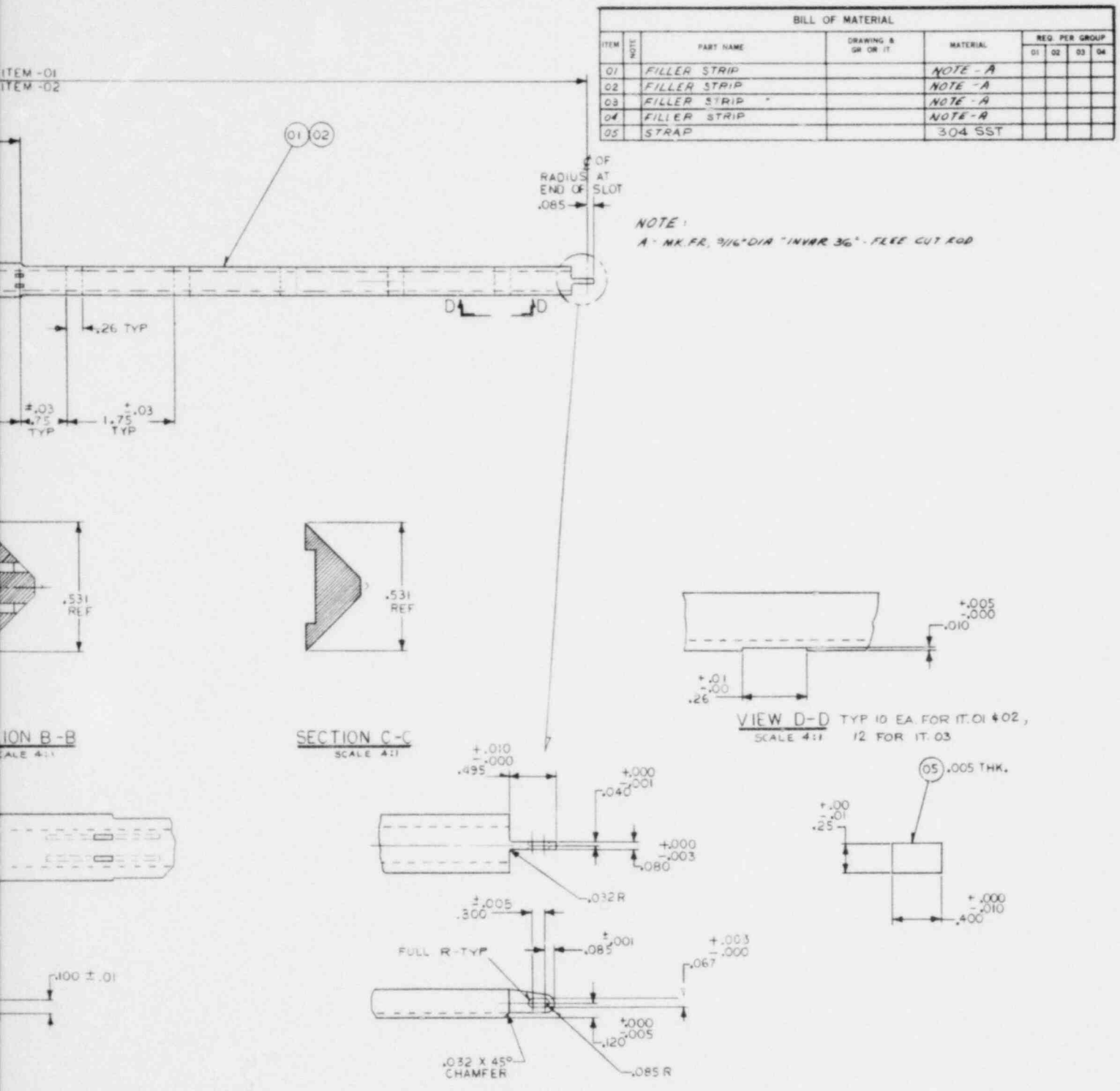

Figure G-7. FLECHT SEASET 21-Rod Test Filler Strip (sheet 1 of 2) (Drawing No. 9556D10)

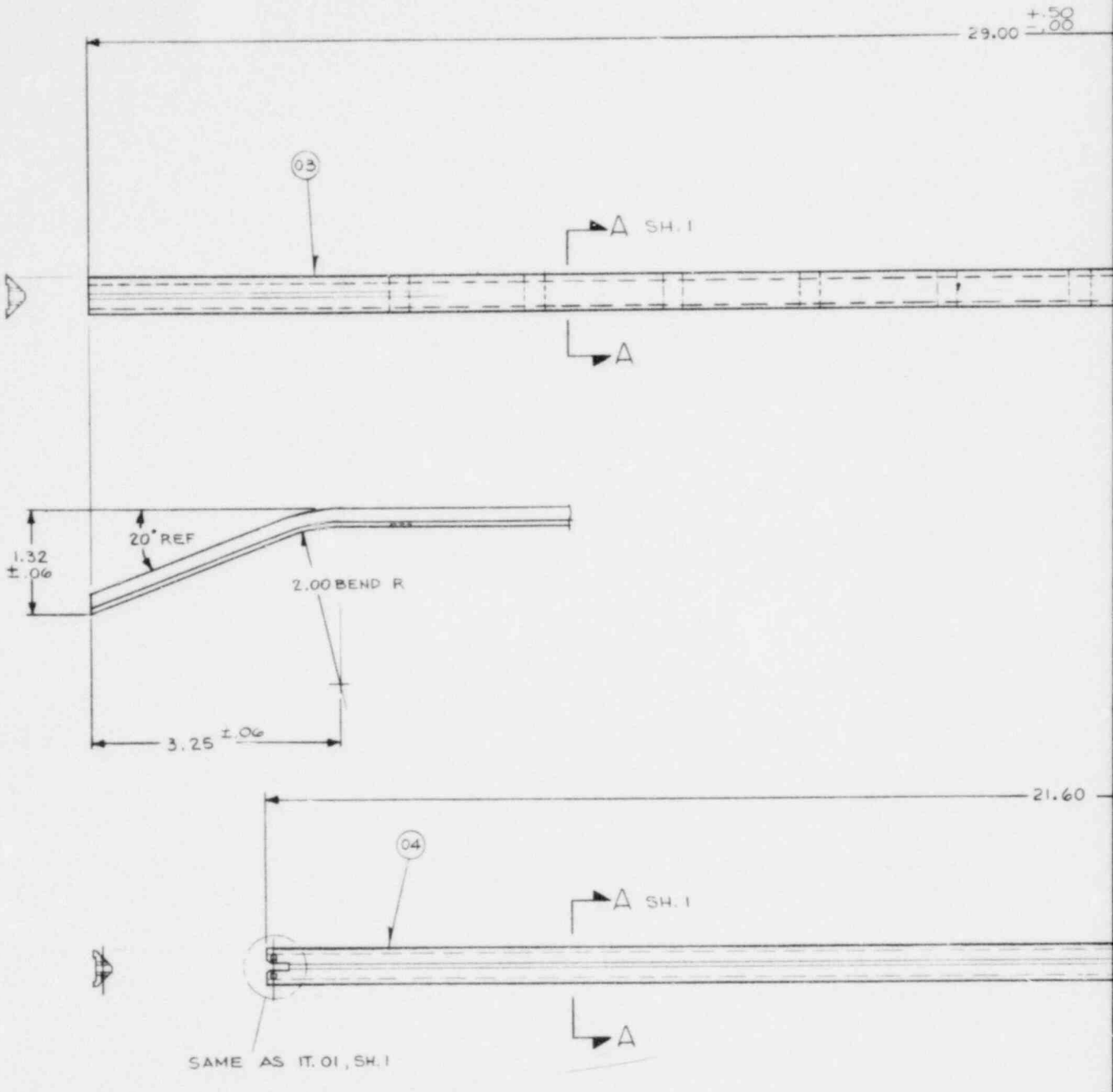
29.00 +.58 -.08
03
A SH. 1
A
1.32 ±.06
20° REF
2.00 BEND R
3.25 ±.06
21.60
04
A SH. 1
A
SAME AS IT. 01, SH. 1

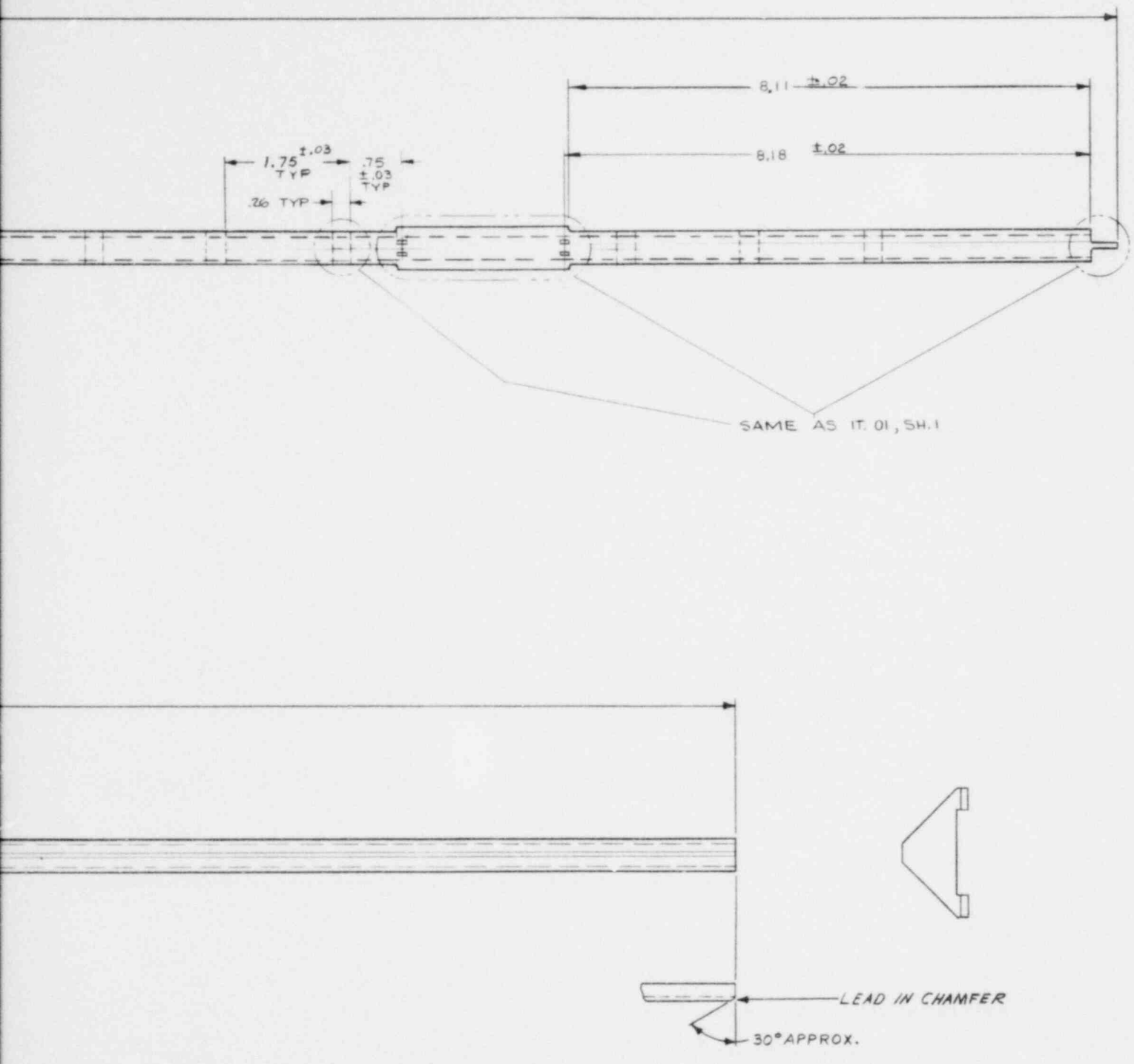

Figure G-7. FLECHT SEASET 21-Rod Test Filler Strip (sheet 2 of 2) (Drawing No. 9556D10)

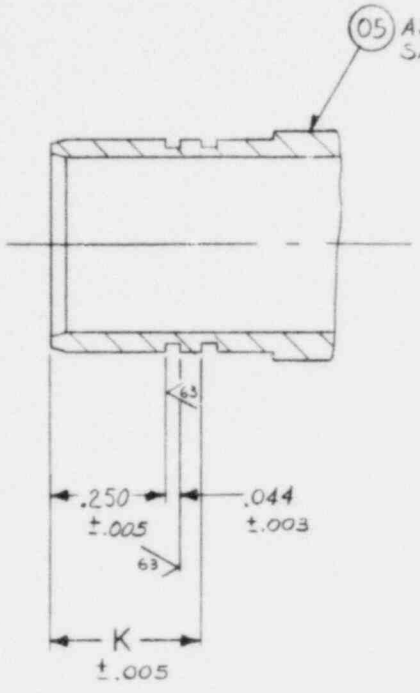

ITEM	B	C	D	E	F
01	.500	.975	.451	.410	.38
02	.625	1.100	.451	.410	.38
03	.625	1.100	.351	.310	.28
04	.625	1.100	.451	.410	.37
05	.625	1.100	.451	.410	.38

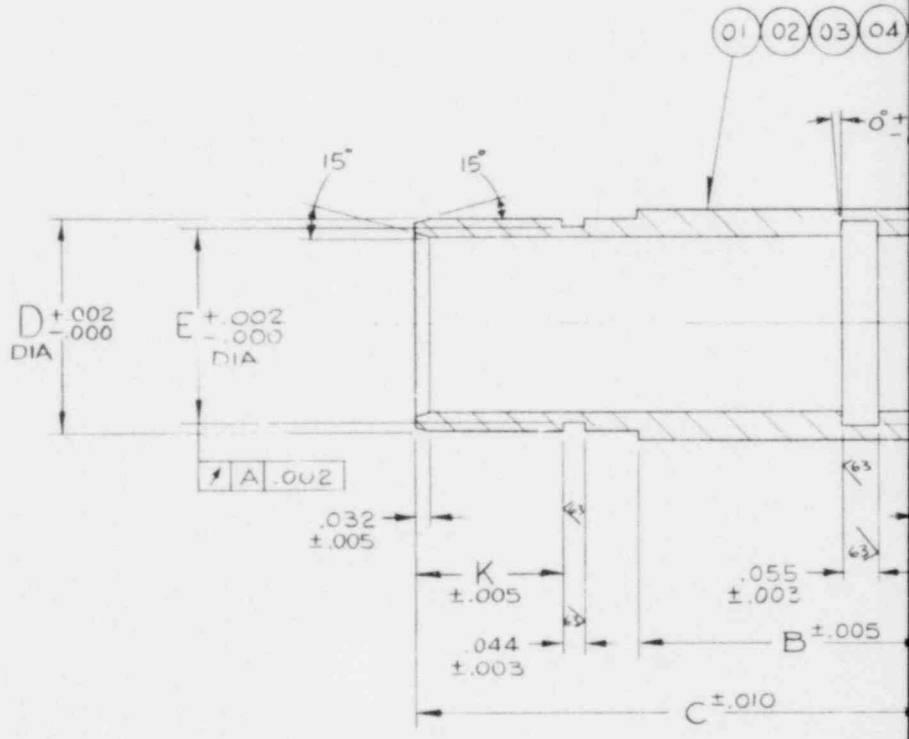

BILL OF MATERIAL								
ITEM	NOTE	PART NAME	DRAWING & GR OR IT.	MATERIAL	REQ. PER GROUP			
					01	02	03	04
01	A	SLEEVE			1			
02	A	SLEEVE			1			
03	A	SLEEVE			1			
04	A	SLEEVE			1			
05	A	SLEEVE			1			

	G	H	J	K
	.435	.485	.100	.325
	.435	.485	.250	.325
	.335	.385	.100	.325
7	.435	.485	.250	.250
0	.435	.485	.250	.325

A - MATERIAL - BERYLLIUM COPPER, BERYLCO 33-25, WILLIAMS & CO.

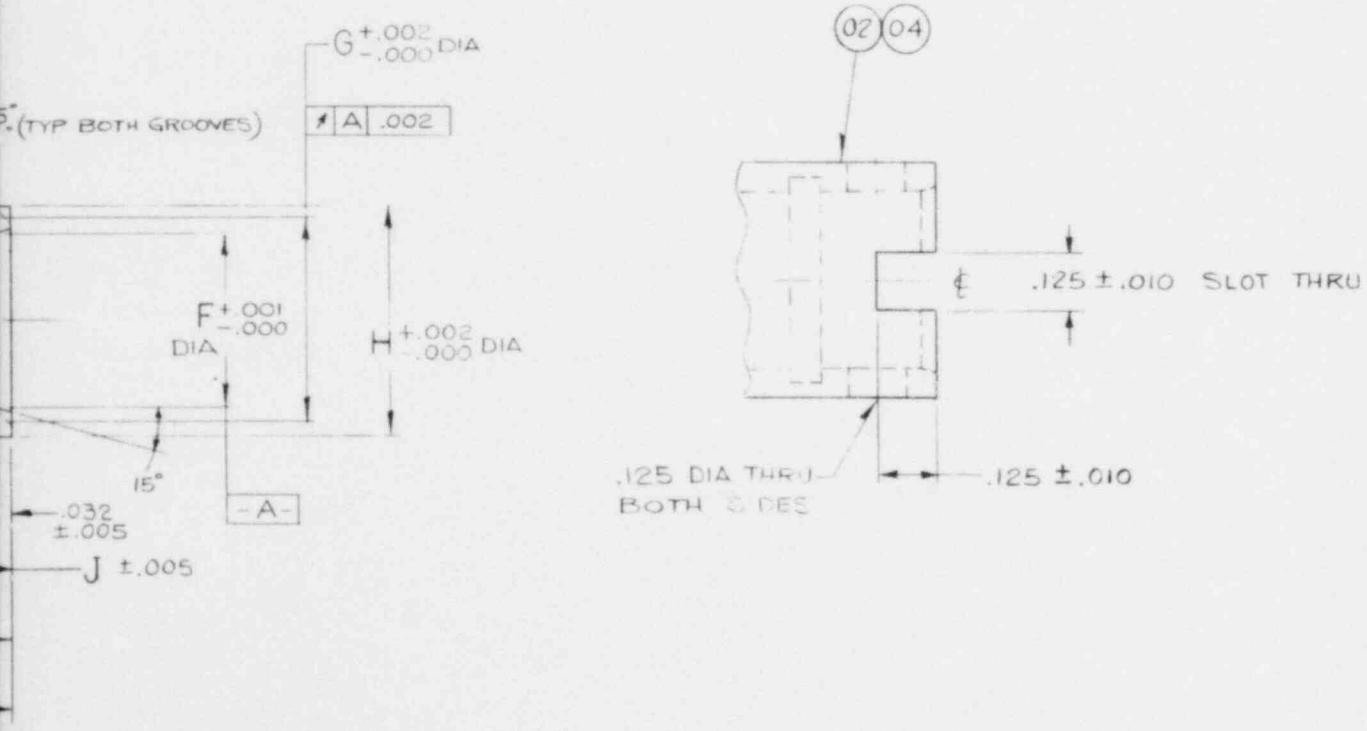

Figure G-8. FLECHT SEASET O-Ring Sleeves (Drawing No. 1680C97)

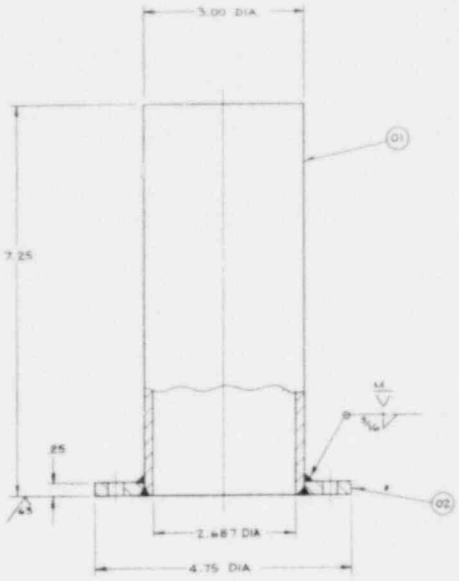

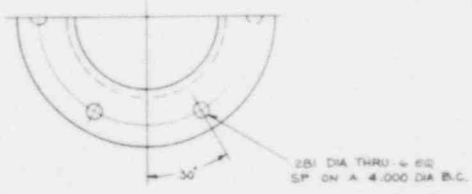

GROUP 1
UPPER EXTENSION

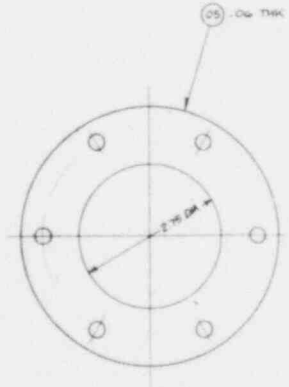

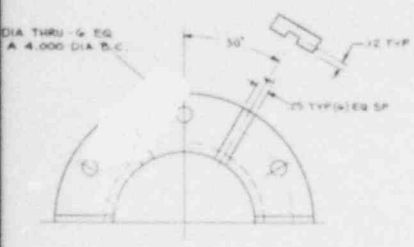

BILL OF MATERIAL

ITEM	QTY	PART NAME	DRAWING # OR SPEC #	MATERIAL	REQ PER GROUP 01	02	03	04
01		CYLINDER		304 SST	1			
02		BASE		"	1			
03		CYLINDER		"		1		
04		BASE		"		1		
05		GASKET		DURABLA	1			
06		FLANGE		304 SST			1	
07		PIPE 1" SCH 40		"			1	
08		GUTTER		INCONEL			2	
09		COVER		304 SST			1	
10		ANTI-ROTATION IR		C STL				1
11	A	GASKET		NEOPRENE				1
12		ANTI-ROTATION IR		C STL				1
13		SPACER (FR STL TUBING)		C STL				4

* DUROMETER - MED/HARD

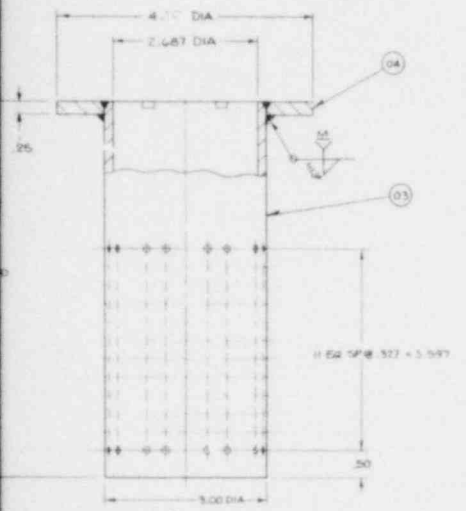

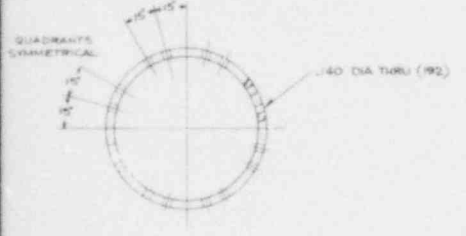

GROUP 2
LOWER EXTENSION

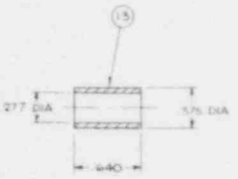

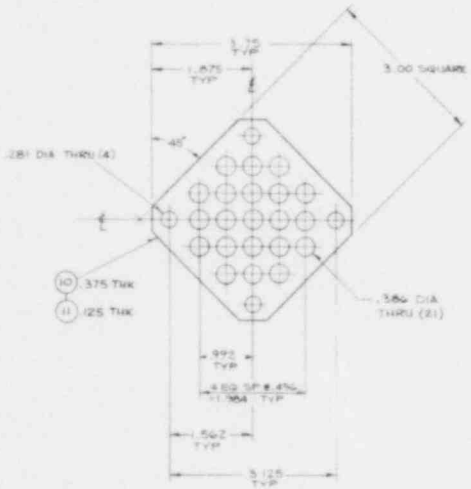

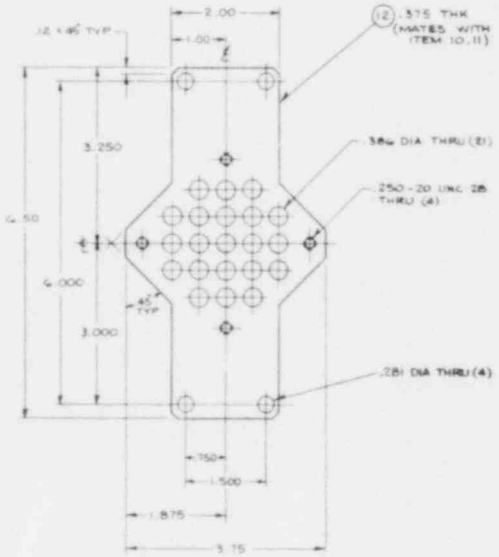

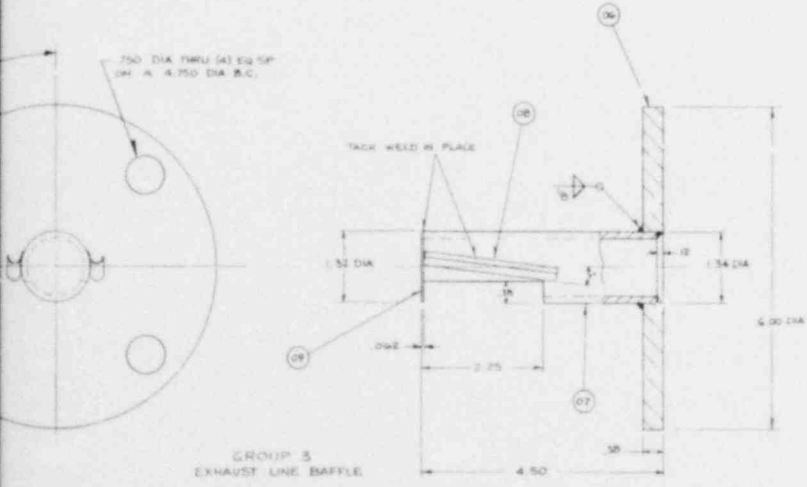

GROUP 3
EXHAUST LINE BAFFLE

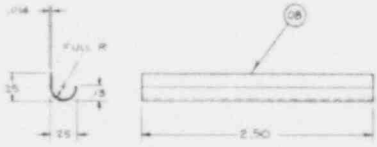

Figure G-9. FLECHT SEASET 21-Rod Test Details (Drawing No. 1460E59)

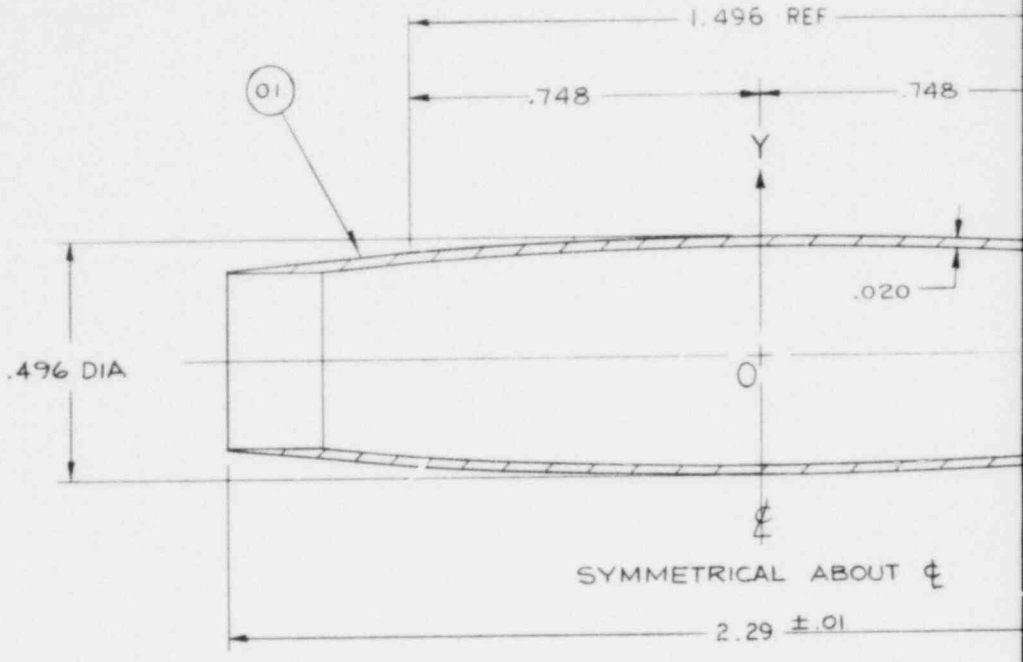

FU

DIM. O-X	DIM. O-Y
0	.248
.10	.247
.20	.246
.30	.243
.40	.240
.50	.236
.60	.231
.70	.226
.748	.224

BILL OF MATERIAL						
ITEM	NOTE	PART NAME	DRAWING & GR OR IT	MATERIAL	REQ 01	REQ 02
01	A	SLEEVE			1	

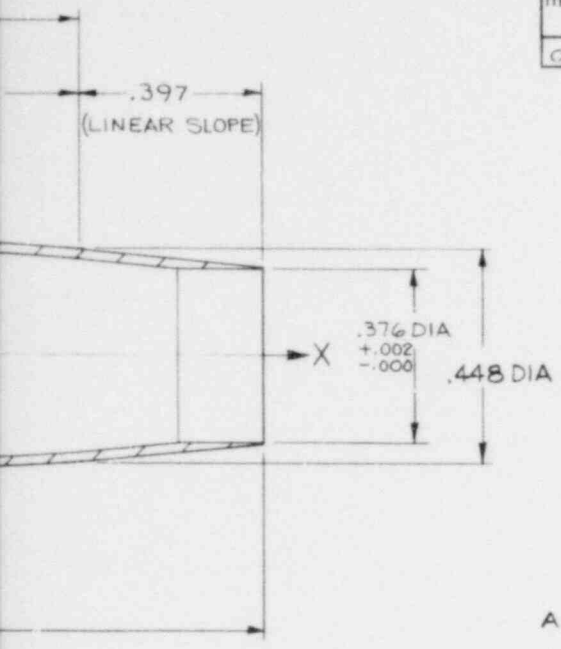

A - MAKE FR 300 SERIES SST

FORMULA : $-.748 < X < .748$
$Y = .024 \cos 120.3X + .224$

L SIZE

Figure G-10. FLECHT SEASET 21-Rod Test Flow Blockage Sleeve (Drawing No. 1684C06)

SYMMETRIC

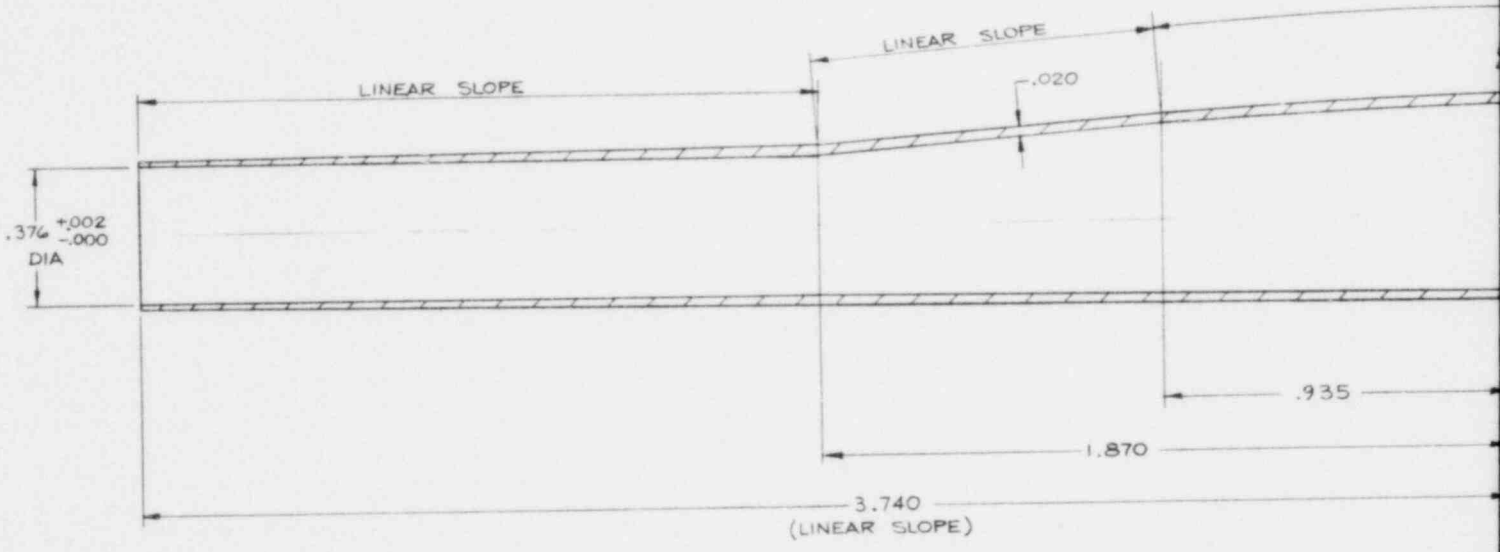

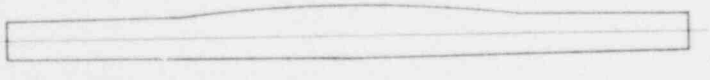

ACTUAL SIZE

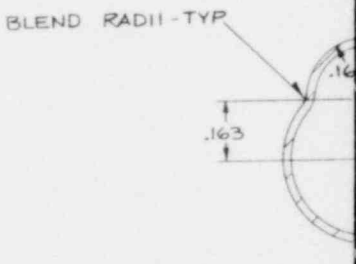

BILL OF MATERIAL								
ITEM	NOTE	PART NAME	DRAWING & GR OR IT.	MATERIAL	REQ. PER GROUP			
					01	02	03	04
01	A	SLEEVE			1			

A - MAKE FR 300 SERIES SST

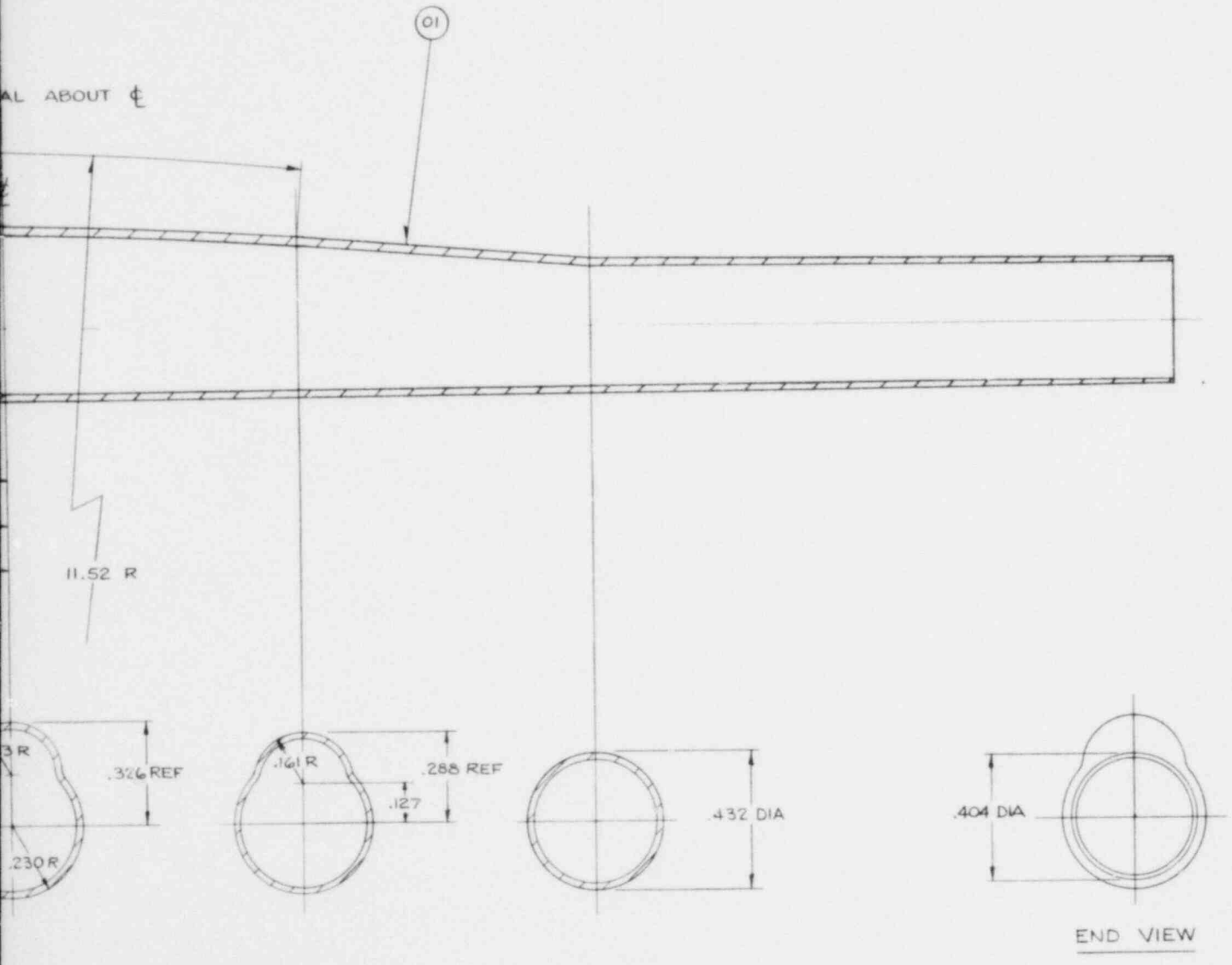

Figure G-11. FLECHT SEASET 21-Rod Test Nonconcentric Flow Blockage Sleeve (Drawing No. 9553D26)

APPENDIX H
BUNDLE INSTRUMENTATION PLAN

The bundle instrumentation plan includes specifications for the location of the heater rod thermocouples, steam probes, and blockage sleeve thermocouples for the first three bundle configurations. The basis for this plan was described briefly in paragraph 7-3; however, a more detailed description is provided herein.

The number of heater rod thermocouples was limited to eight per rod. These thermocouples are generally placed symmetrically around the rod no less than 45 degrees apart, so that the effect of the thermocouple leads on the rod heat release is minimized. The heater rods are designed such that the thermocouple leads do not pass through the high-temperature zone and introduce temperature errors. For those rods with eight leads coming out one end of the rod, the thermocouples are 45 degrees apart; for those rods with four leads coming out each end of the rod, the thermocouples are 90 degrees apart. The thermocouples were oriented in the bundle toward the subchannel such that the effect of the subchannel flow rather than the effect of an adjacent rod could be measured.

The outer row of 12 rods in the bundle is considered as a boundary condition for the inner 3x3 array of nine rods. Thermocouples for these nine rods were distributed axially based somewhat on the distribution established for the unblocked bundle, to obtain data for quench front progression, high-power zone, high-temperature zone, and blockage zone. Of the 72 thermocouples associated with these nine rods, nine thermocouples at the 0.30 m, 0.61 m, 0.99 m, 1.22 m, 1.52 m, 1.70 m, 3.35 m, and 3.51 m (12 in., 24 in., 39 in., 48 in., 60 in., 67 in., 132 in., and 138 in.) elevations are utilized to determine the progression of the quench front from the bottom and top of the bundle; 15 thermocouples at the 2.18 m, 2.44 m, 2.59 m, 2.82 m, and 3.05 m (86 in., 96 in., 102 in., 111 in., and 120 in.) elevations are utilized to determine the location of peak clad temperature; 29 thermocouples at the 1.78 m, 1.80 m, 1.83 m, 1.88 m, 1.91 m, 1.93 m, 1.96 m, 1.98 m, 2.13 m, and 2.29 m (70 in., 71 in., 72 in., 75.25 in., 76 in., 77 in., 78 in., 84 in., and 90 in.) elevations are utilized to determine the effect of flow blockage on heat transfer; and the remaining 19 thermocouples at the 1.78 m,

1.80 m, 1.83 m, 1.88 m, 1.91 m, 1.93 m, 1.96 m, and 1.98 m (70 in., 71 in., 72 in., 74 in., 75.25 in., 76 in., 77 in., and 78 in.) elevations are utilized to determine the temperature in the high-power zone.

The 29 thermocouples which are utilized to determine the effects of flow blockage were placed axially and radially, based on the assumption that symmetry exists between the four subchannels created by the 3x3 rod array. Based on this assumption, it will be possible to "map" the heater rod temperature for four rods of a given subchannel as a function of elevation. Relative to the heater rod diameter of 9.49 mm (0.374 in.) and the sleeve length of 6d, heater rod thermocouples are located within $\pm$1d, -3.7d, +4.3d, +6.3d, + 9d and $\pm$11.7d of the ends of the sleeve, with the sleeve centered at 1.84 m (72.5 in.).

For the 29 thermocouples used to determine the flow blockage effects, at least two heater rod thermocouples per elevation were oriented toward the same subchannel. This "instrumented" subchannel was subsequently rotated among the four available subchannels from an elevation of 1.78 m (70 in.) to an elevation of 2.29 m (90 in.). For four of these ten elevations, 1.88 m, 1.93 m, 2.13 m, and 2.29 m (74 in., 76 in., 84 in., and 90 in.), two subchannels are instrumented with the heater rod thermocouples to evaluate the assumption of symmetry. Also, for two of these elevations, 1.88 m and 1.93 m (74 in. and 76 in.), the subchannel is instrumented with three heater rod thermocouples. Thus, out of a possible 32 heater rod thermocouples[1] for evaluating the effect of flow blockage in the four subchannels created by the 3x3 rod array, 29 thermocouples have been utilized. The remaining three thermocouples are used at the 0.30 m, 3.35 m, and 3.51 m (12 in., 132 in., and 138 in.) elevations for detecting the progression of the quench fronts.

The outer row of 12 rods was instrumented axially based generally on the distribution established for the inner 3x3 array of nine rods. Approximately half the 96 thermocouples associated with these 12 rods was assigned to the high-power/blockage zone from 1.78 m (70 in.) to 2.29 m (90 in.). The remaining half of the 96 thermocouples was split approximately equally between measurement of the quench front progression and measurement of the high-temperature zone.

1. Eight thermocouples on the center rod, two each on the four corner rods, and four each on the four remaining rods

The number of steam probe thermocouple leads and blockage sleeve thermocouple leads which can be accommodated in the four fillers of the 21-rod bundle is currently believed to be limited to 40.

The axial distribution of the steam probes is based somewhat on the distribution established for the unblocked bundle. Approximately two-thirds of the 26 steam probes (a total of 15) have been placed in the four subchannels created by the inner 3x3 array of nine rods. The remaining third of the steam probes was placed in the outside subchannels to evaluate radial temperature gradients and cold housing effects. Eleven steam probes have been placed immediately upstream and downstream of the flow blockage zone, from 1.70 m (67 in.) to 1.98 m (78 in.), to determine the axial and radial effects of blockage on the steam temperature. Of these 11 steam probes, six have been placed in a subchannel where at least one heater rod thermocouple is facing. Symmetry of steam temperature measurements in the inner four subchannels can be checked at three elevations, 1.70 m, 1.98 m, and 2.29 m (67 in., 78 in., and 90 in.), utilizing the steam probes in two diametrically opposed subchannels per elevation.

The quantity of sleeve thermocouples was based mainly on the assumption that 40 thermocouple leads could be run through the fillers of the rod bundle, as previously discussed. Since 26 of the 40 thermocouples are associated with the steam probes, a maximum of 14 blockage sleeve thermocouples can be placed in the bundle. Therefore, a thermocouple was placed on each blockage sleeve corresponding to a heater rod thermocouple at the 1.88 m (74 in.) elevation, with the exception of a corner rod where the heater rod thermocouple was facing the filler. Each blockage sleeve thermocouple was oriented azimuthally such that it would be adjacent to the respective heater rod thermocouple.

Sufficient computer space and electrical hookups are provided for a total of 252 bundle thermocouple channels. Of these 252 channels, 108 channels are allocated to thermocouples exiting the bottom of the bundle and 144 are allocated to those exiting the top of the bundle. At present, a maximum of 207 channels have been planned for the second bundle configuration, which has a blockage sleeve on all 21 rods. Therefore, 45 additional bundle thermocouple channels could be utilized for future bundle configurations. These additional channels could be utilized for heater rod thermocouples, blockage sleeve thermocouples, or steam probes, or a combination thereof.

Additional heater rod thermocouples would require a heater rod design capable of handling more than the present eight thermocouples. Additional blockage sleeve thermocouples and steam probes would require a bundle filler design capable of handling more than the present 10 thermocouples.

Figure H-1 is a diagram of a bundle cross section, showing the radial distribution of heater rod groups and the reference axis for thermocouple azimuthal orientation. Figure H-2 shows the axial distribution of steam probes and grids to which the steam probes will be attached. The locations of heater rod thermocouples (radial and azimuthal) and steam probes (radial) are shown in figures H-3 through H-26. In these figures, the number inside the heater rod signifies the heater rod group number (2b, 2, 4b, 13b, 14, and so forth). A solid circle on the outside surface of a heater rod signifies azimuthal orientation of the thermocouple, and SP signifies the subchannel in which the steam probe is located.

Figure H-27 shows the azimuthal orientation of blockage sleeve thermocouples for the second configuration (all rods blocked); figure H-28 shows the azimuthal orientation of blockage sleeve thermocouples for the third configuration (nine rods blocked).

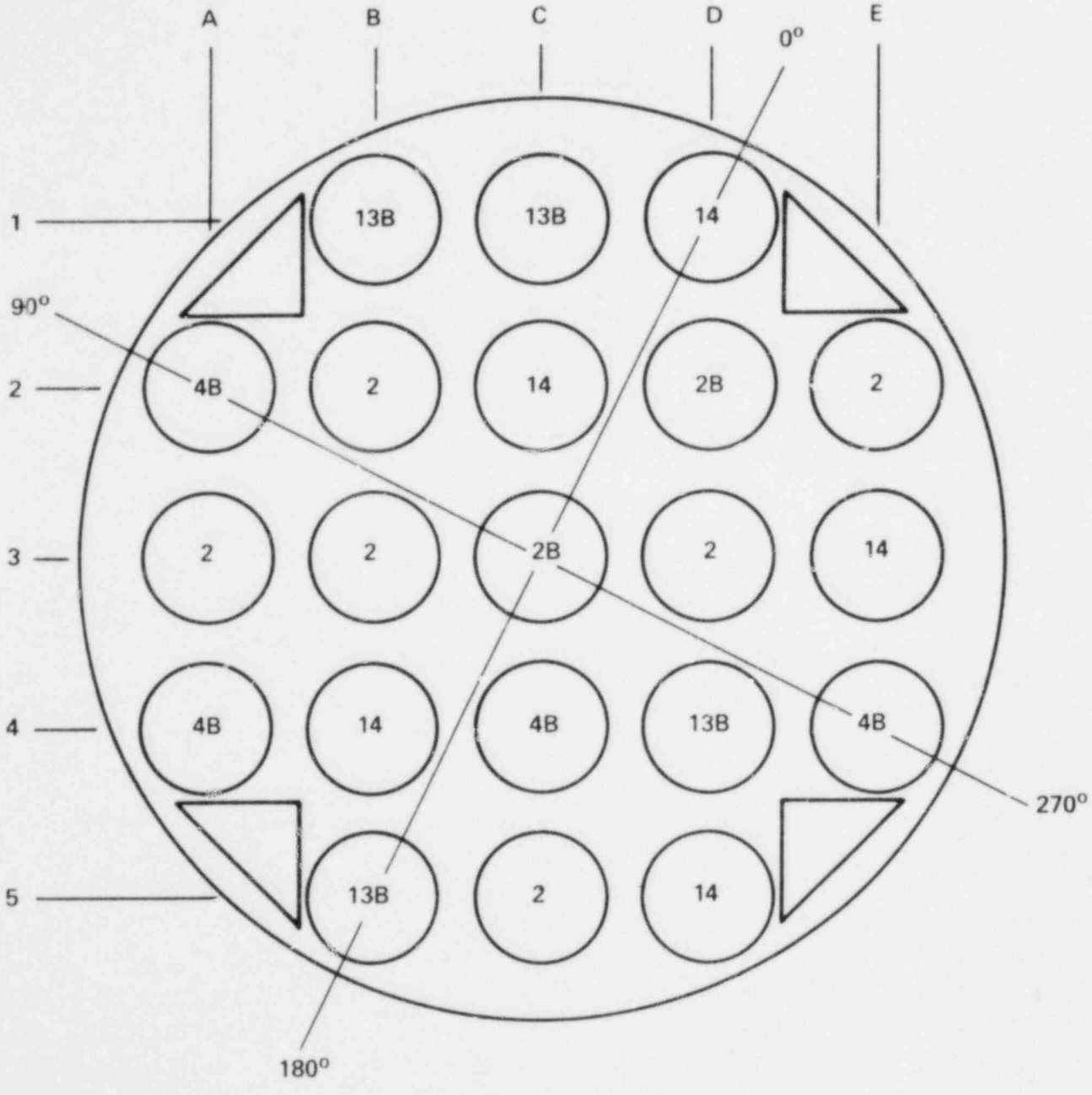

Figure H-1. Radial Distribution of Heater Rods

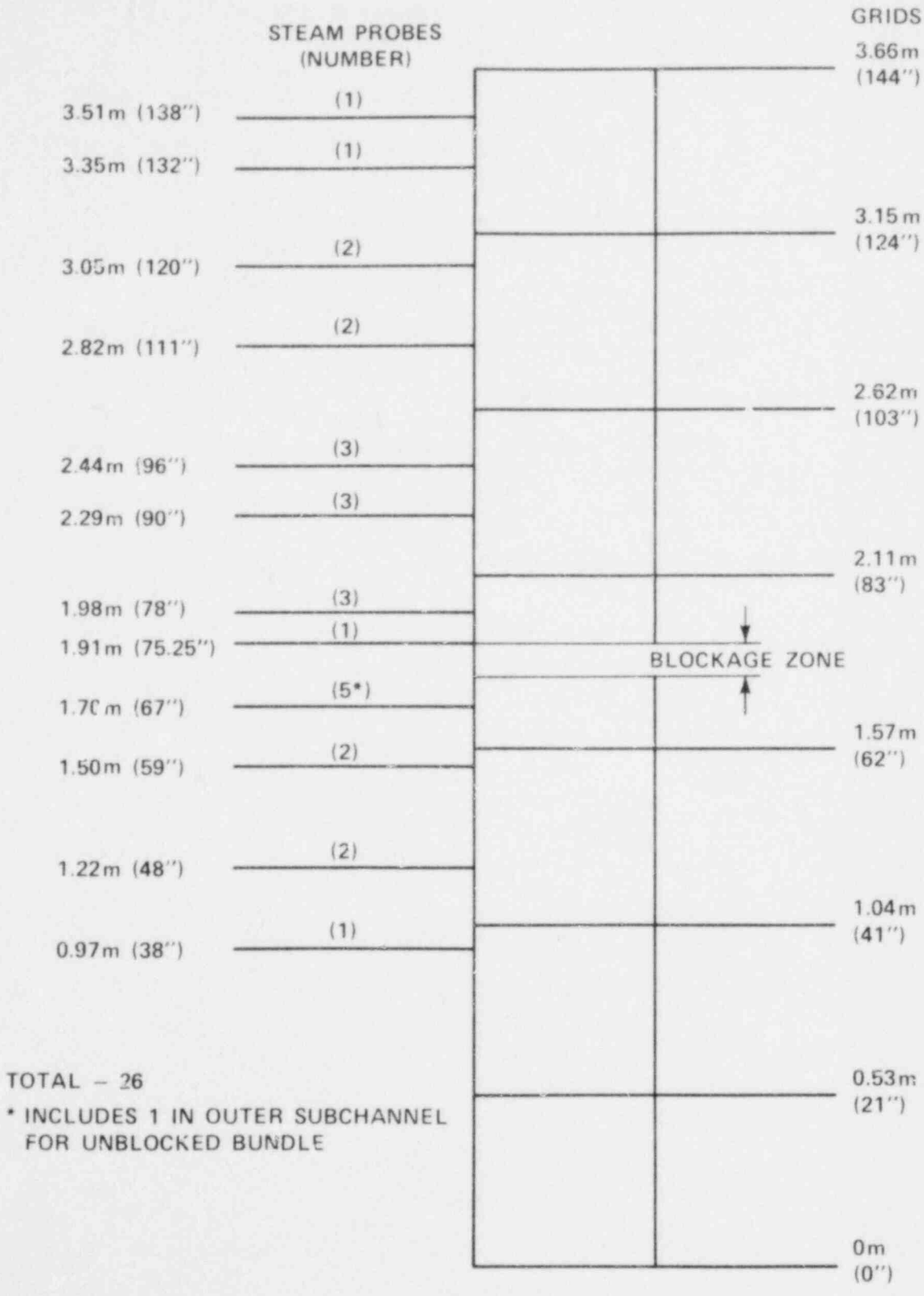

Figure H-2. Steam Probe and Grid Elevations

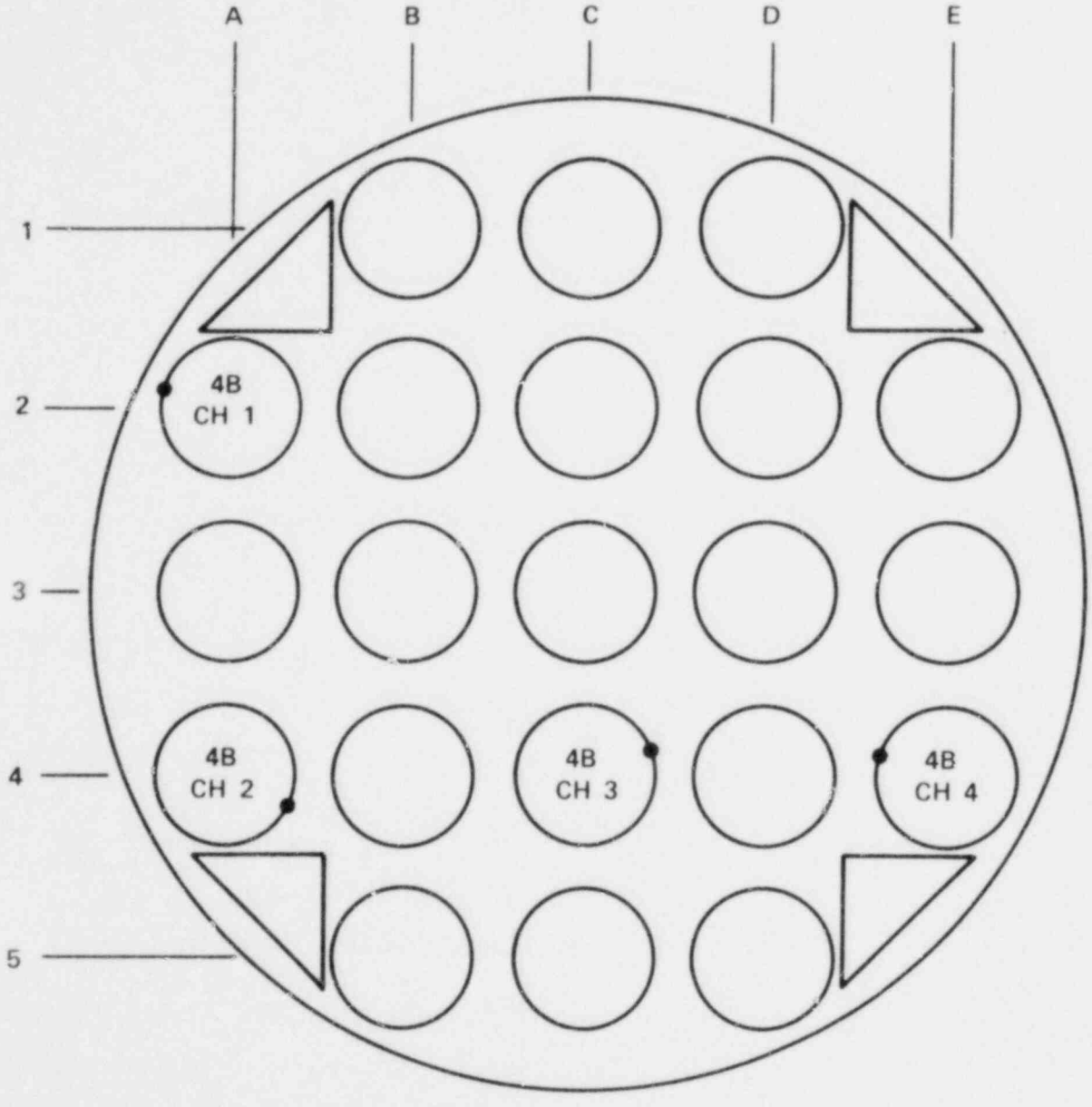

Figure H-3. Thermocouple and Steam Probe Locations - 0.305 m (12 in.) Elevation

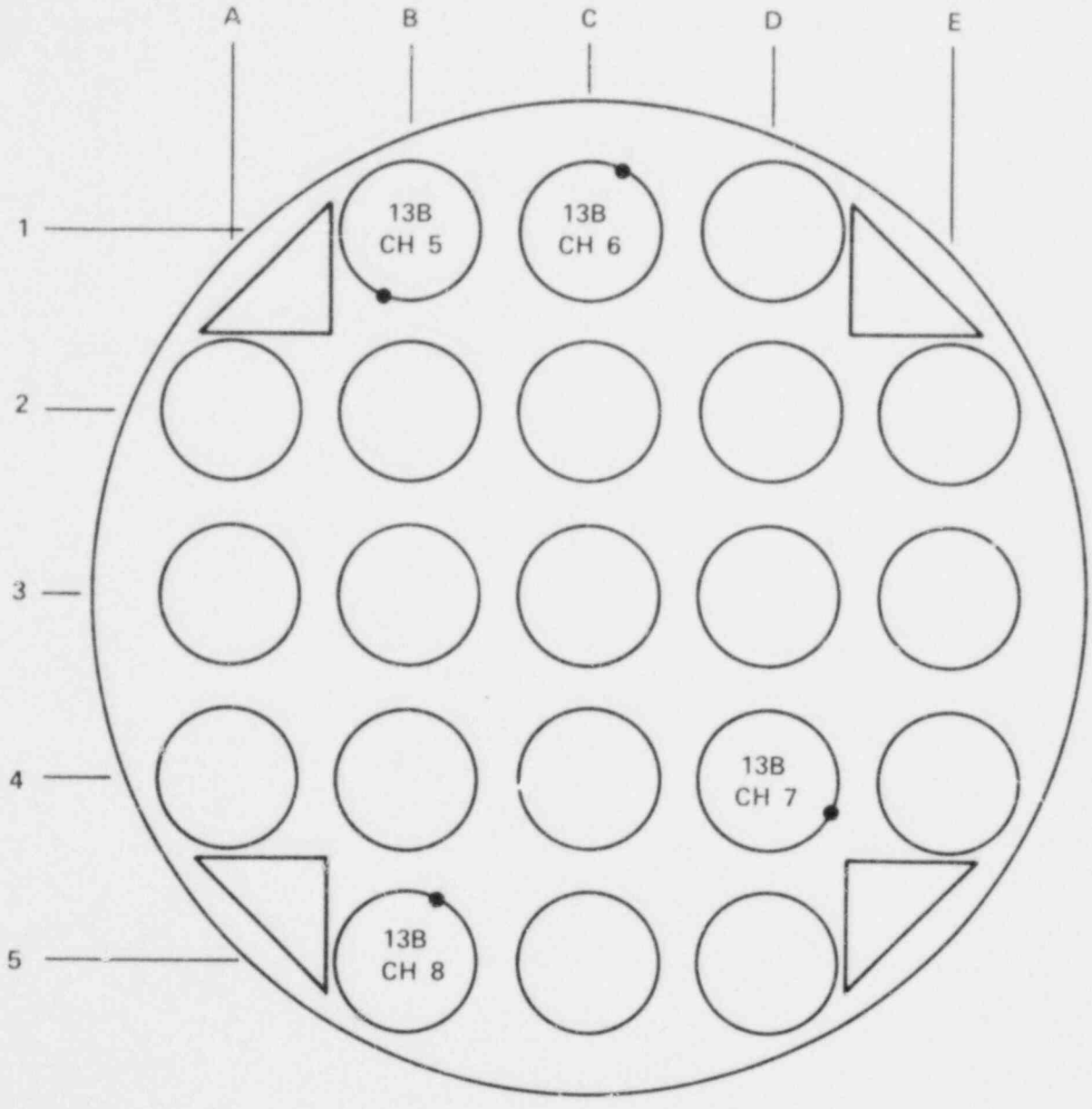

Figure H-4. Thermocouple and Steam Probe Locations - 0.610 m (24 in.) Elevation

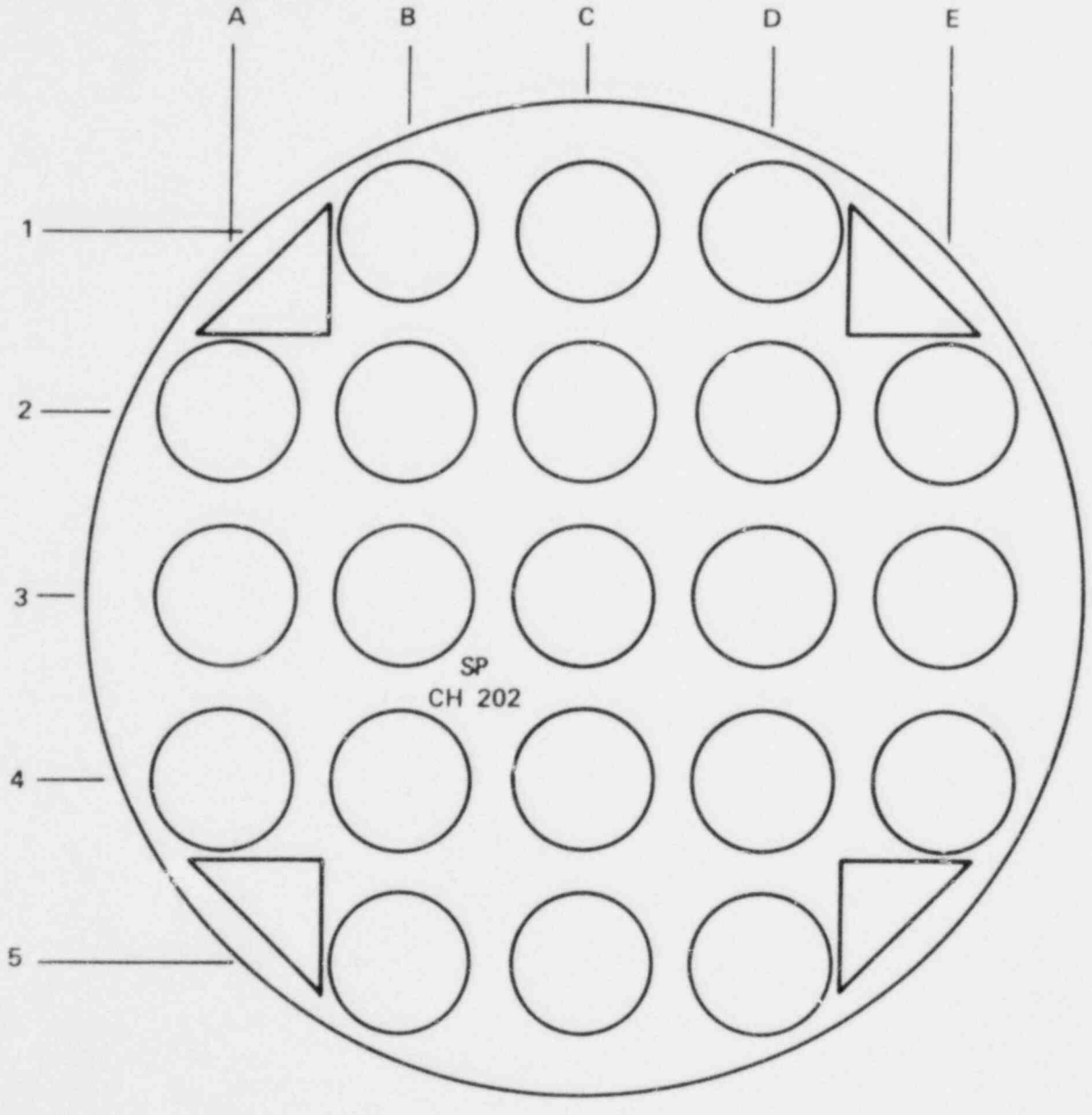

Figure H-5. Thermocouple and Steam Probe Locations - 0.965 m (38 in.) Elevation

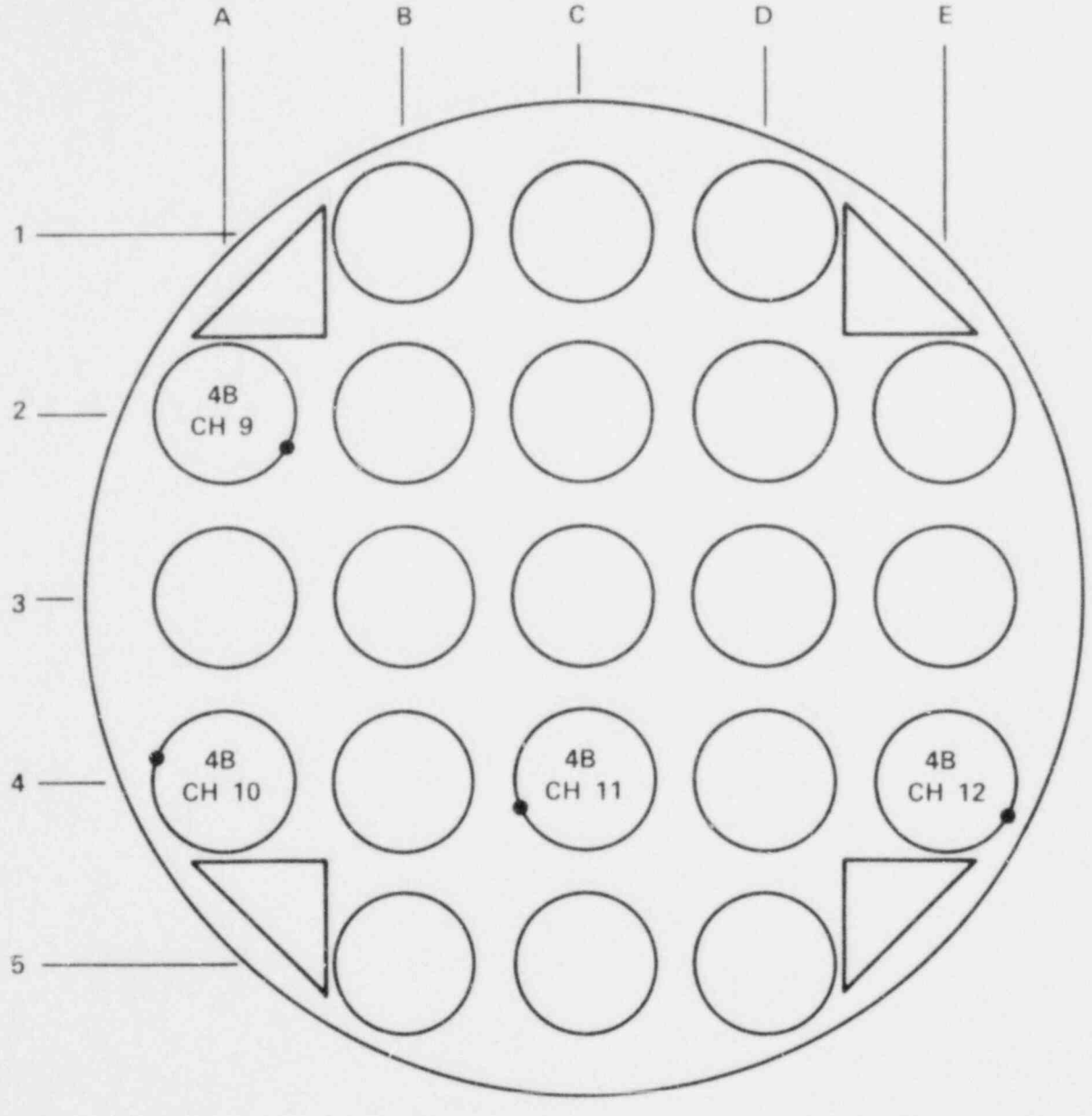

Figure H-6. Thermocouple and Steam Probe Locations - 0.991 m (39 in.) Elevation

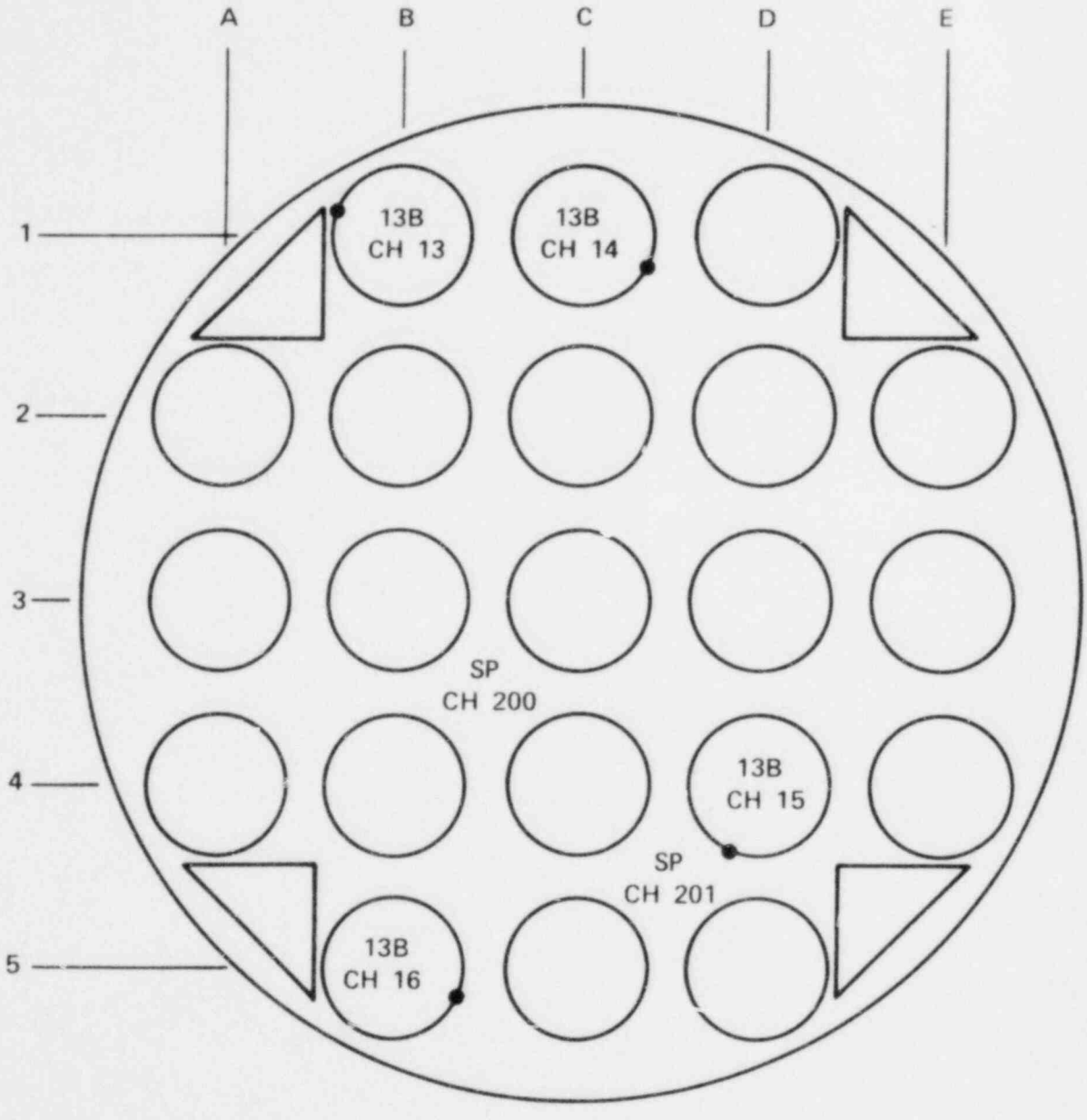

Figure H-7. Thermocouple and Steam Probe Locations - 1.22 m (48 in.) Elevation

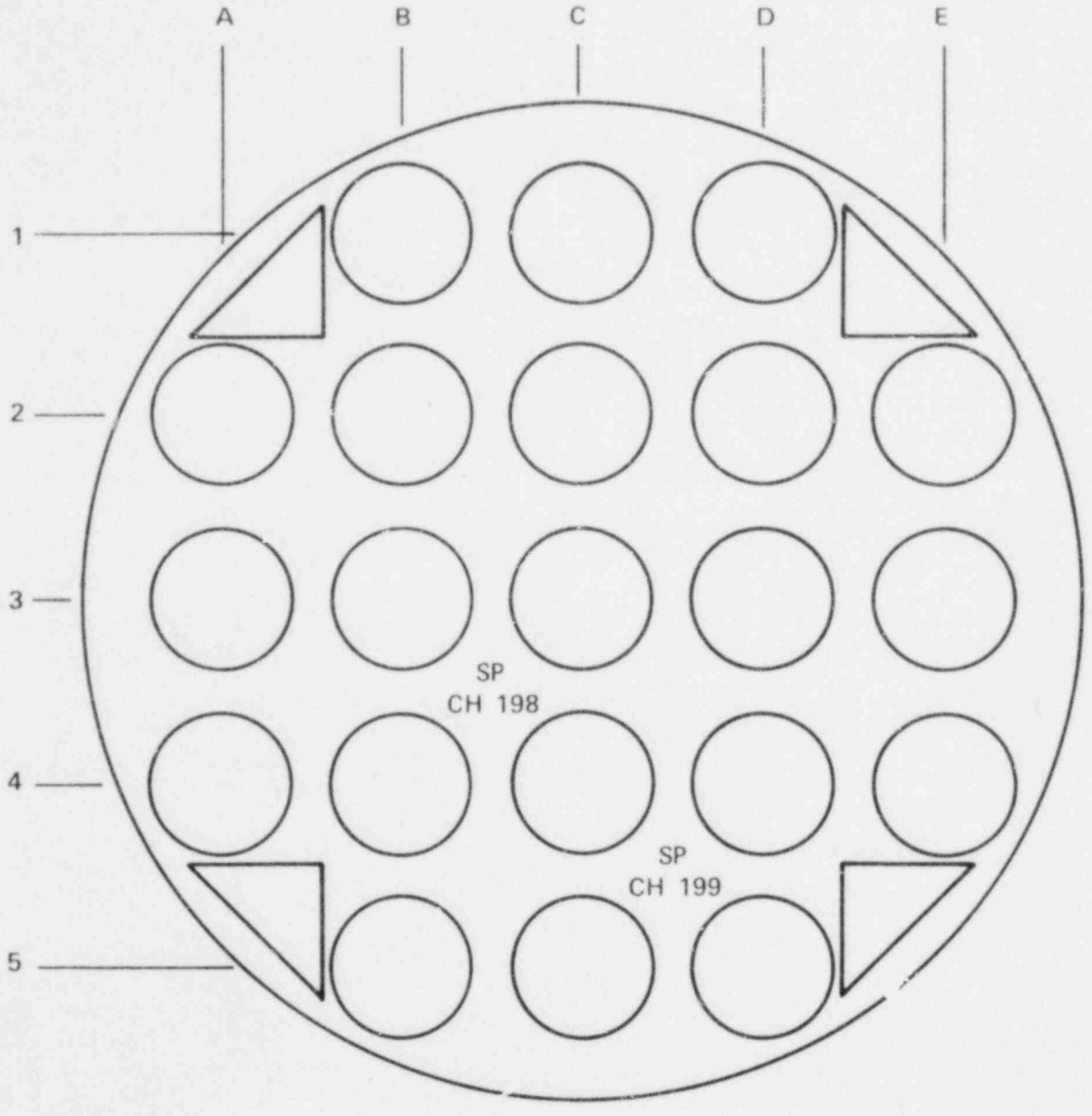

Figure H-8. Thermocouple and Steam Probe Locations - 1.50 m (59 in.) Elevation

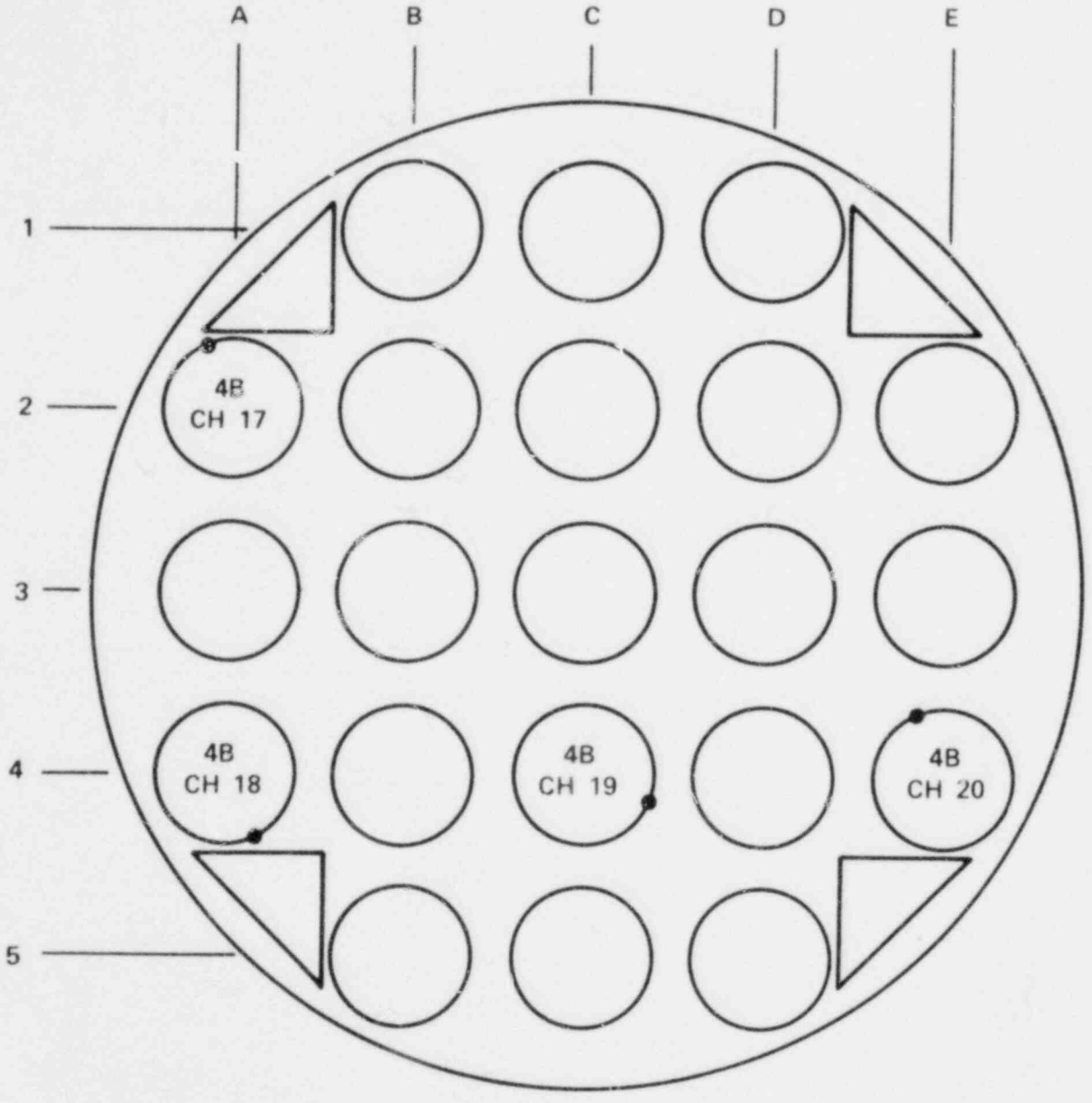

Figure H-9. Thermocouple and Steam Probe Locations - 1.52 m (60 in.) Elevation

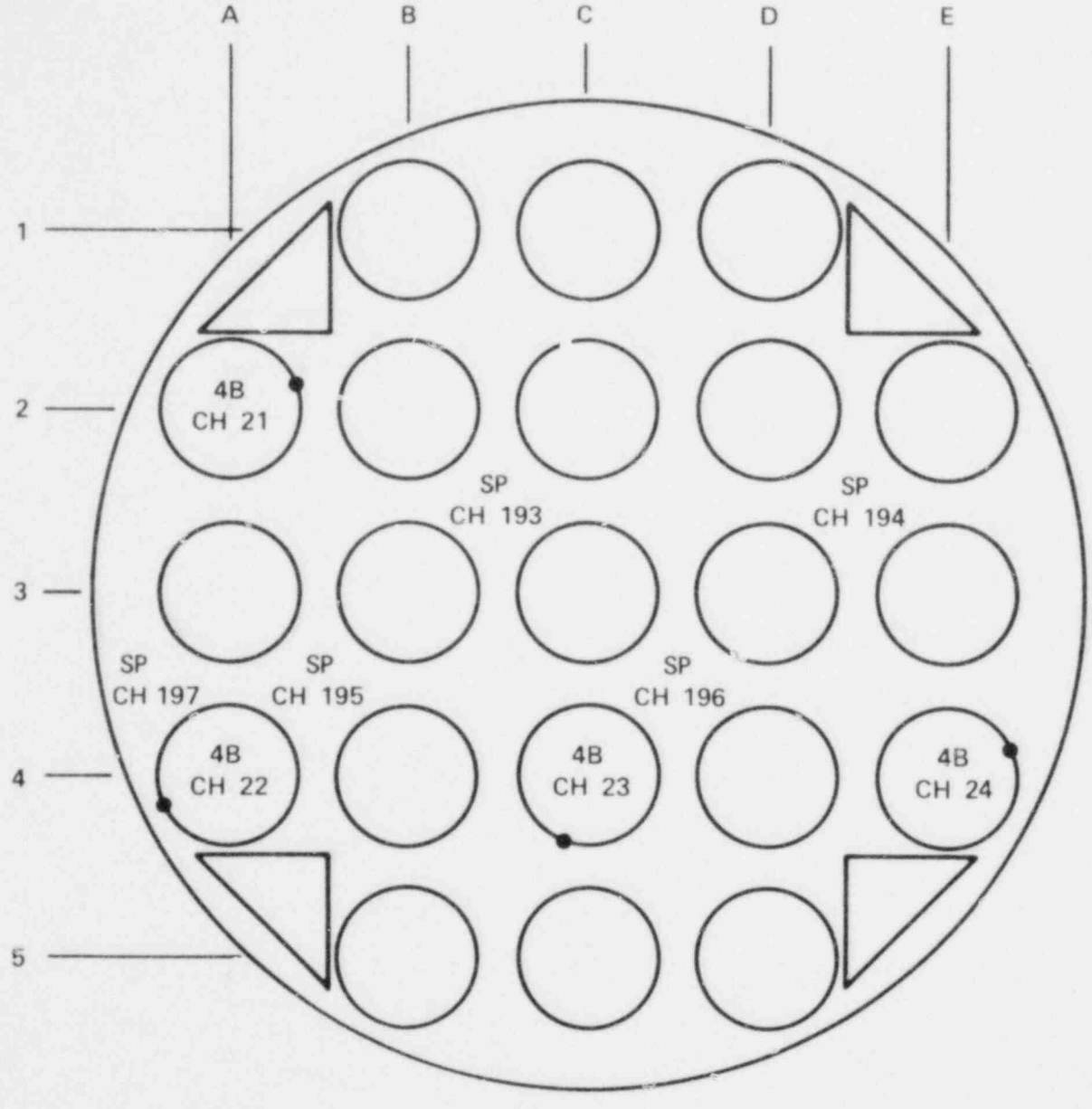

Figure H-10. Thermocouple and Steam Probe Locations - 1.70 m (67 in.) Elevation

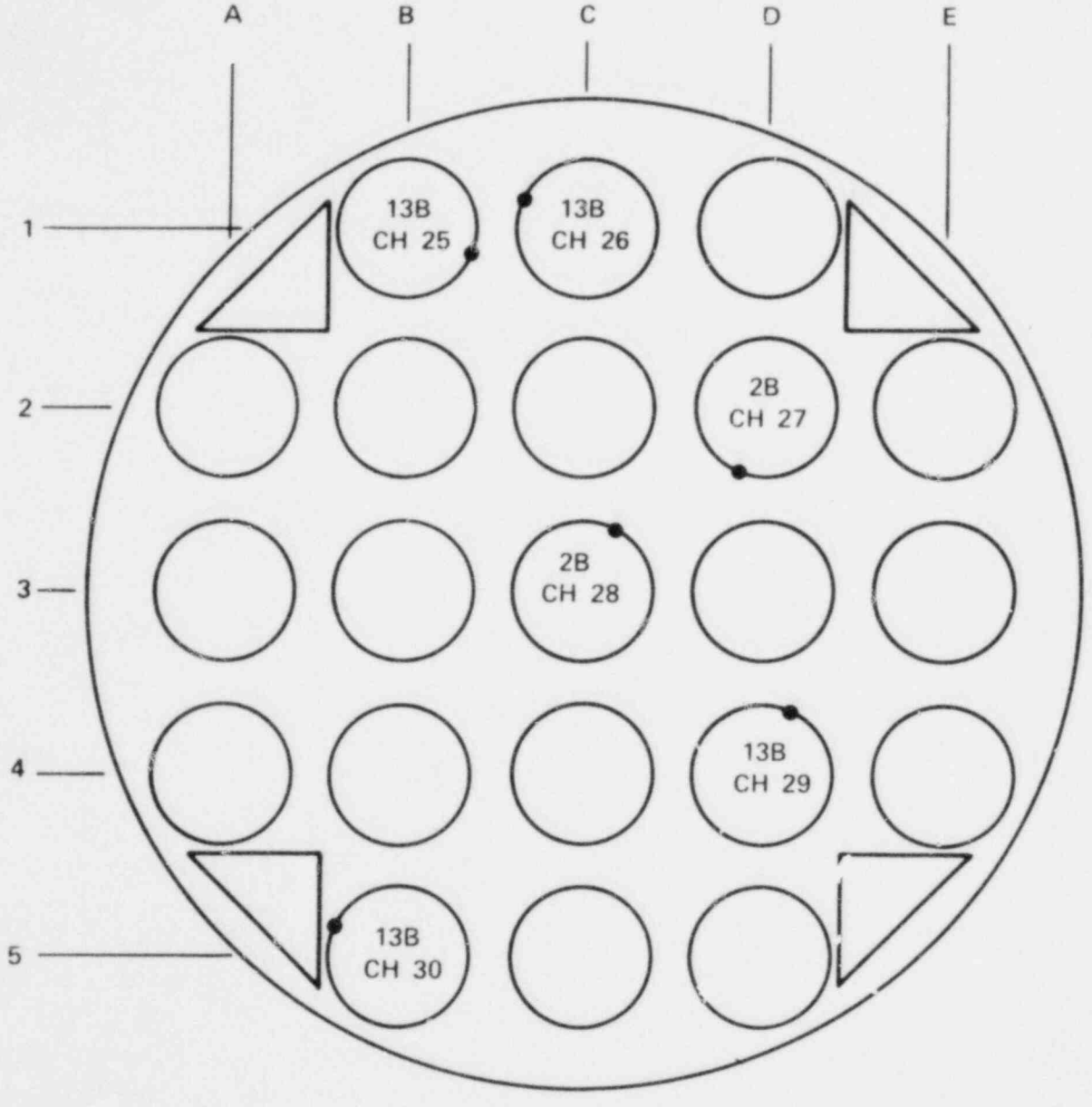

Figure H-11. Thermocouple and Steam Probe Locations - 1.78 m (70 in.) Elevation

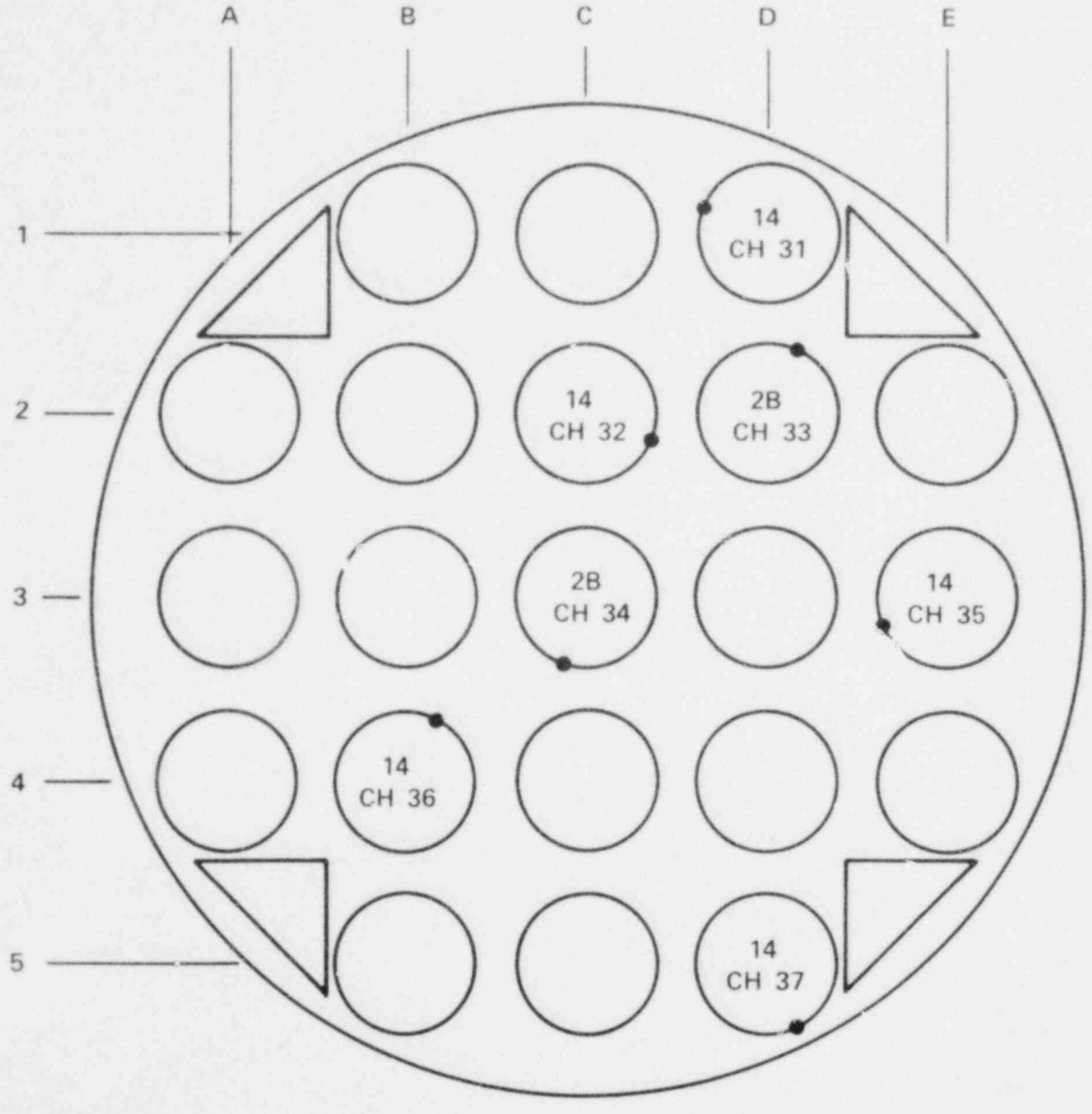

Figure H-12. Thermocouple and Steam Probe Locations - 1.80 m (71 in.) Elevation

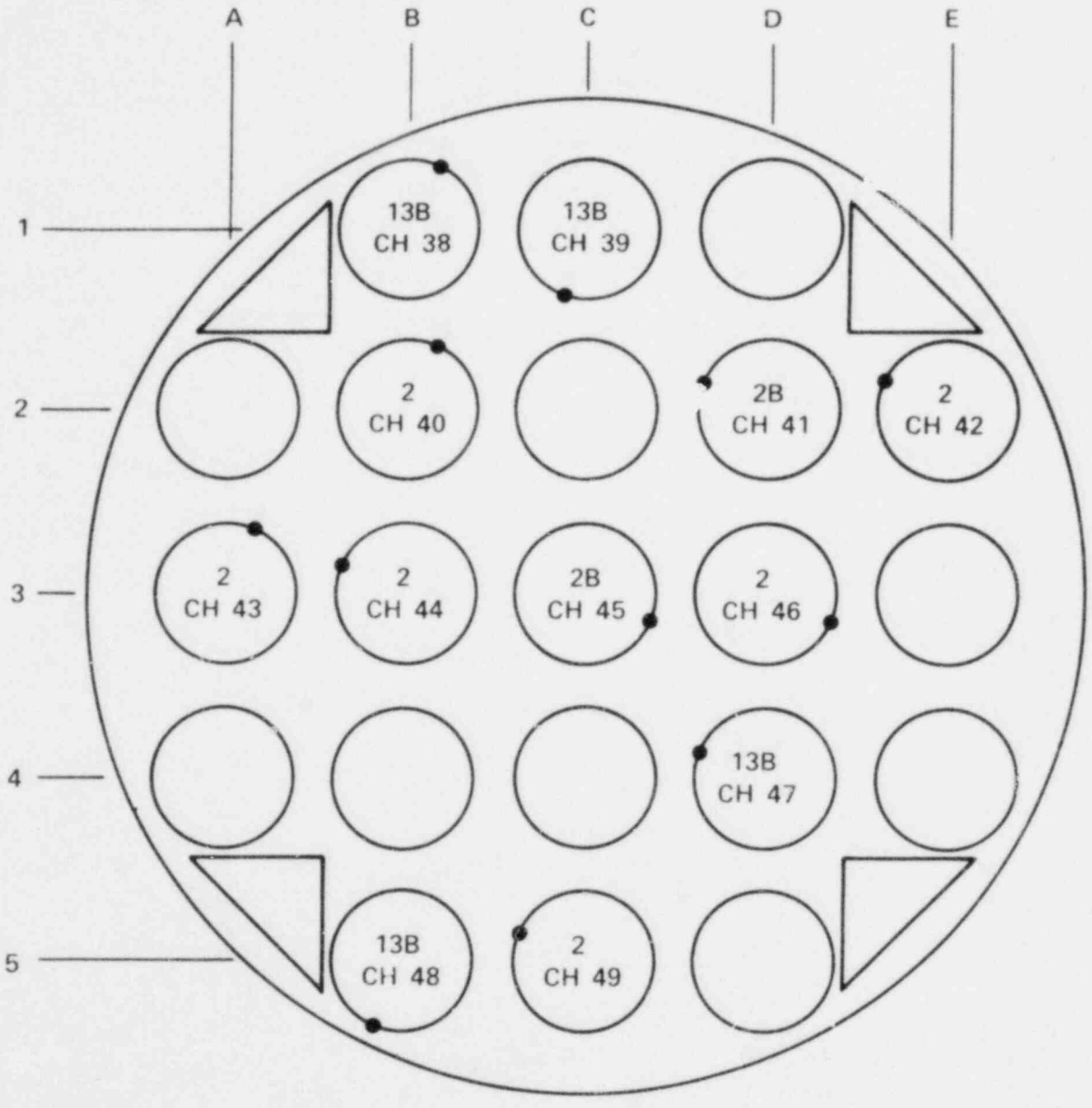

Figure H-13. Thermocouple and Steam Probe Locations - 1.83 m (72 in.) Elevation

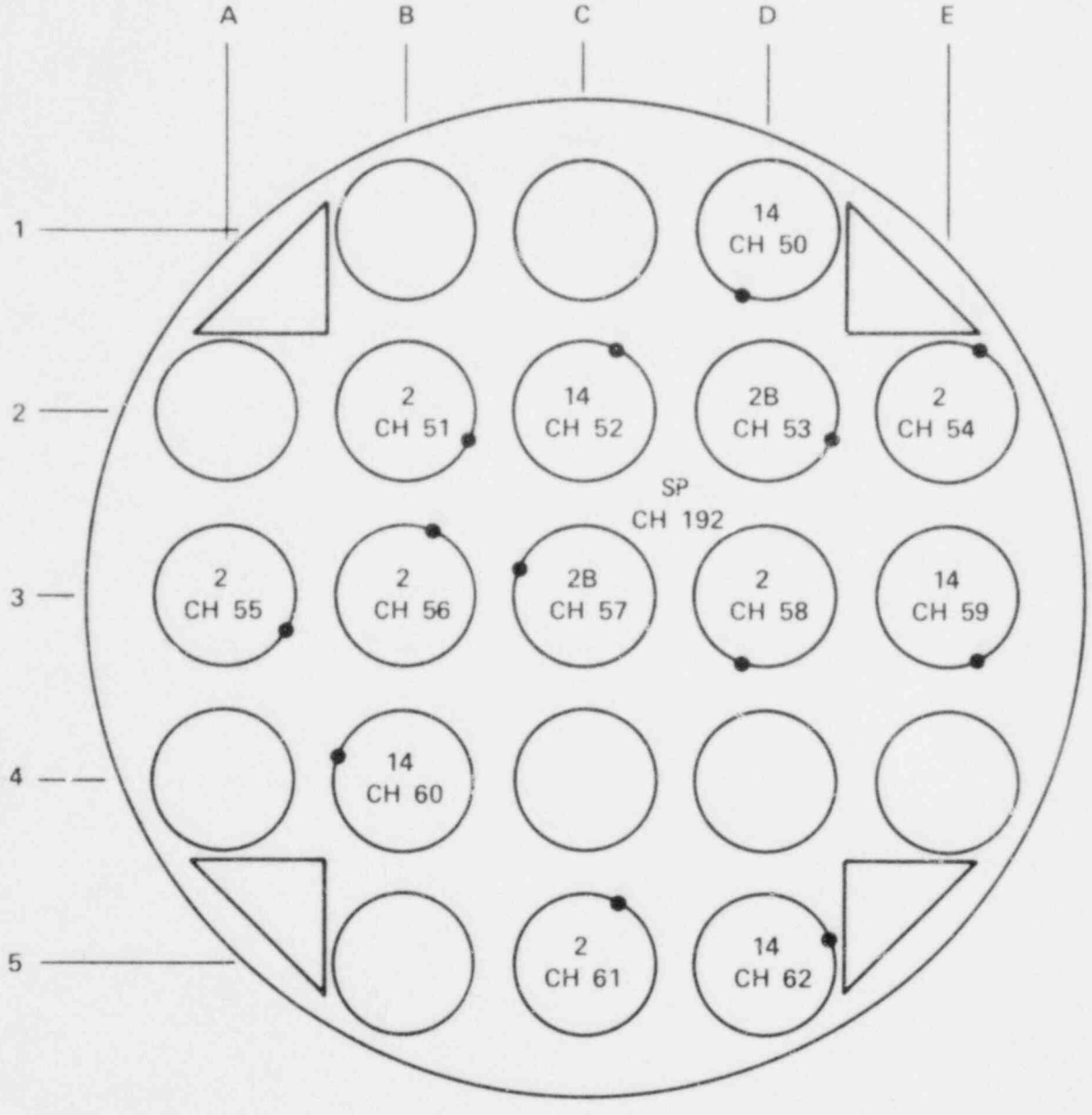

Figure H-14. Thermocouple and Steam Probe Locations - 1.88 m (74 in.) Elevation

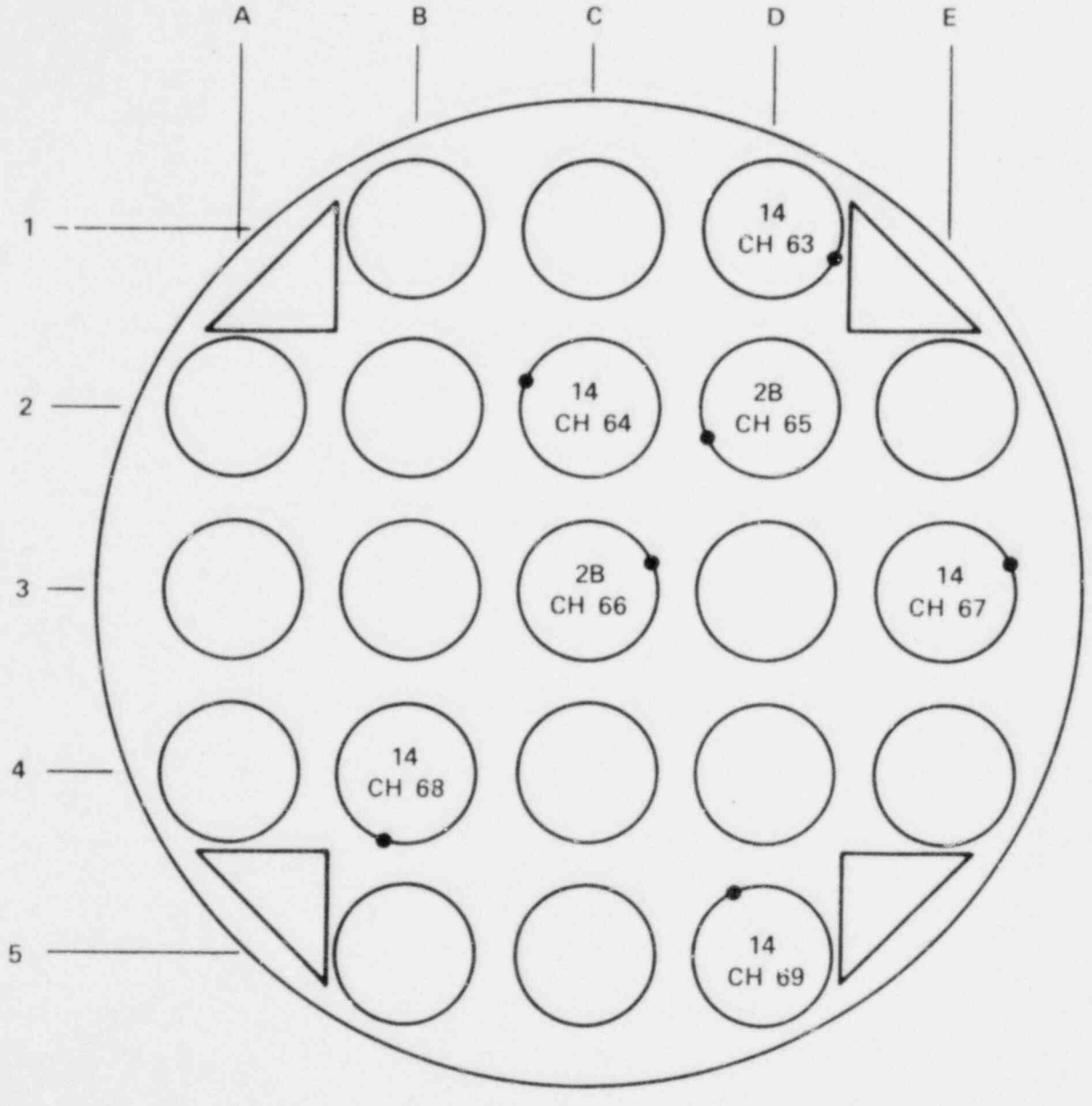

Figure H-15. Thermocouple and Steam Probe Locations - 1.91 m (75.25 in.) Elevation

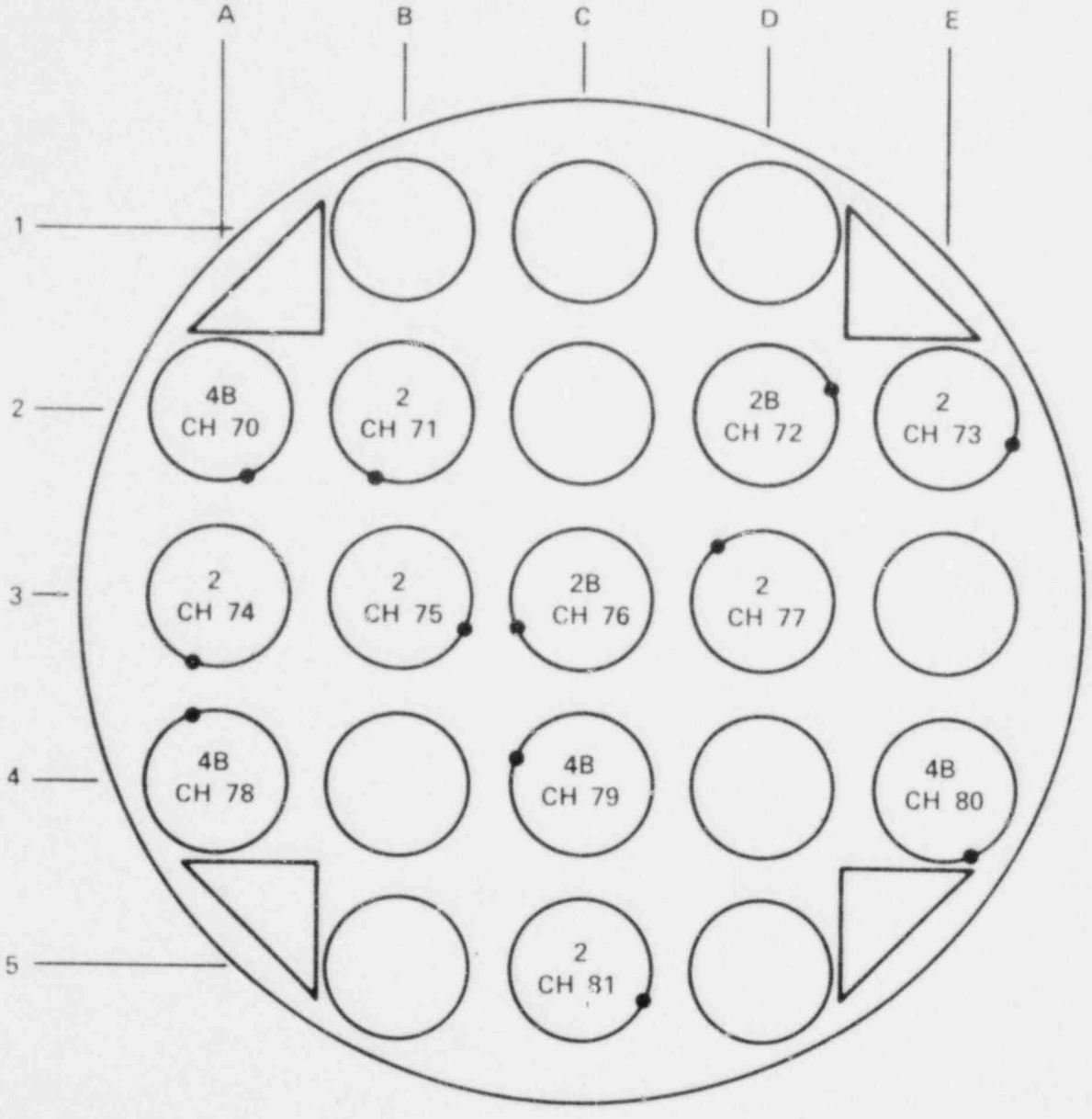

Figure H-16. Thermocouple and Steam Probe Locations - 1.93 m (76 in.) Elevation

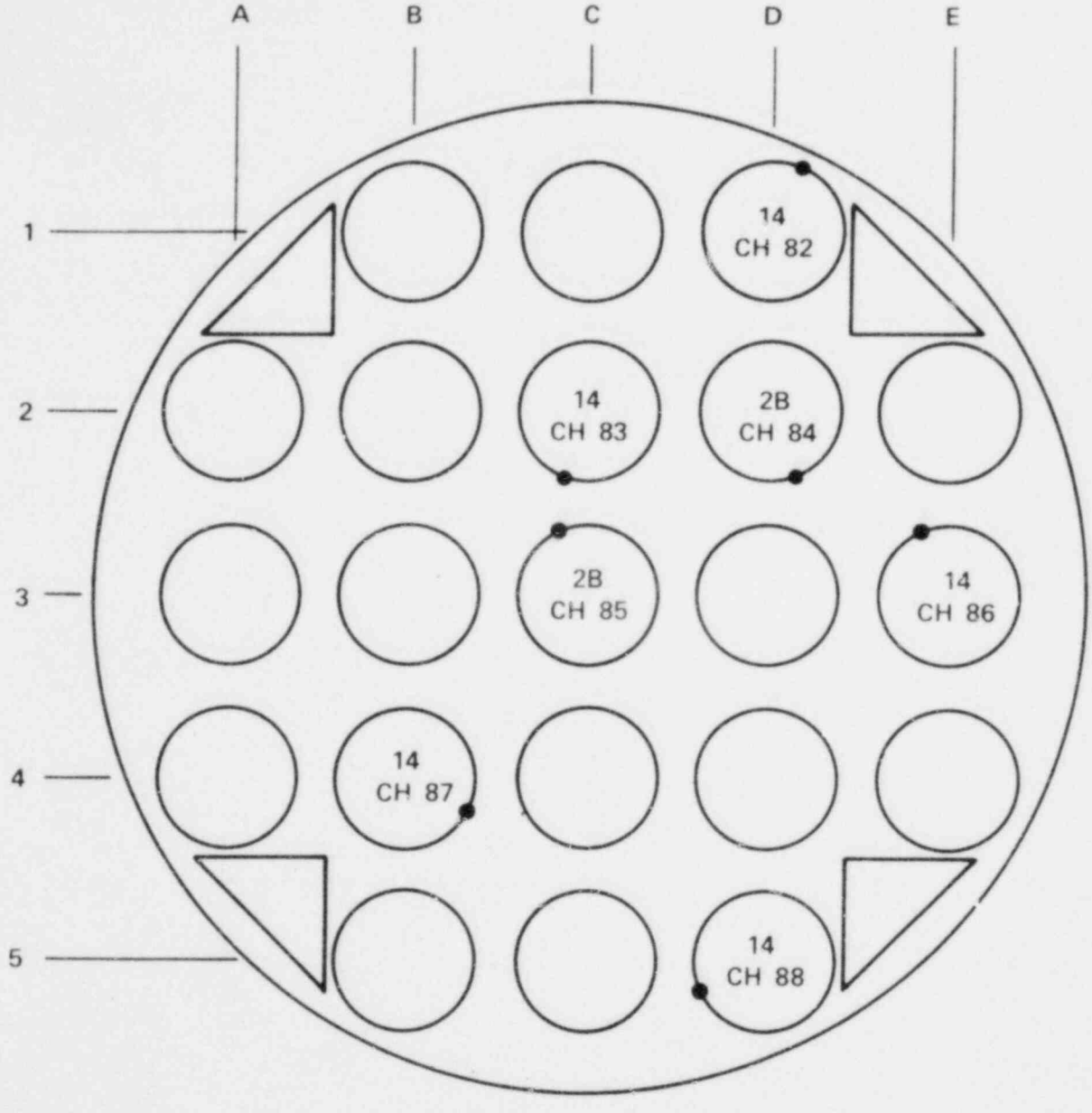

Figure H-17. Thermocouple and Steam Probe Locations - 1.96 m (77 in.) Elevation

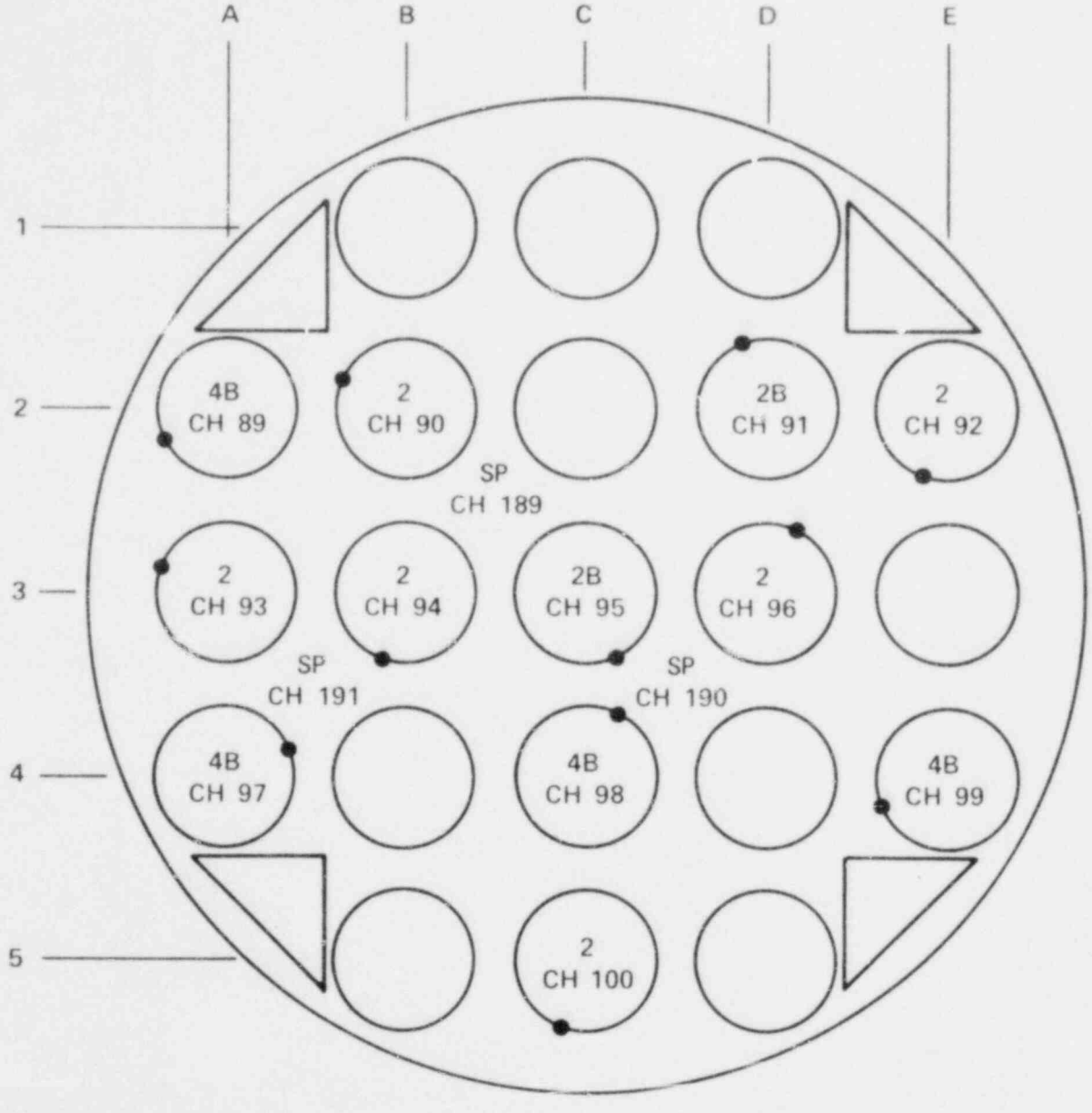

Figure H-18. Thermocouple and Steam Probe Locations - 1.98 m (78 in.) Elevation

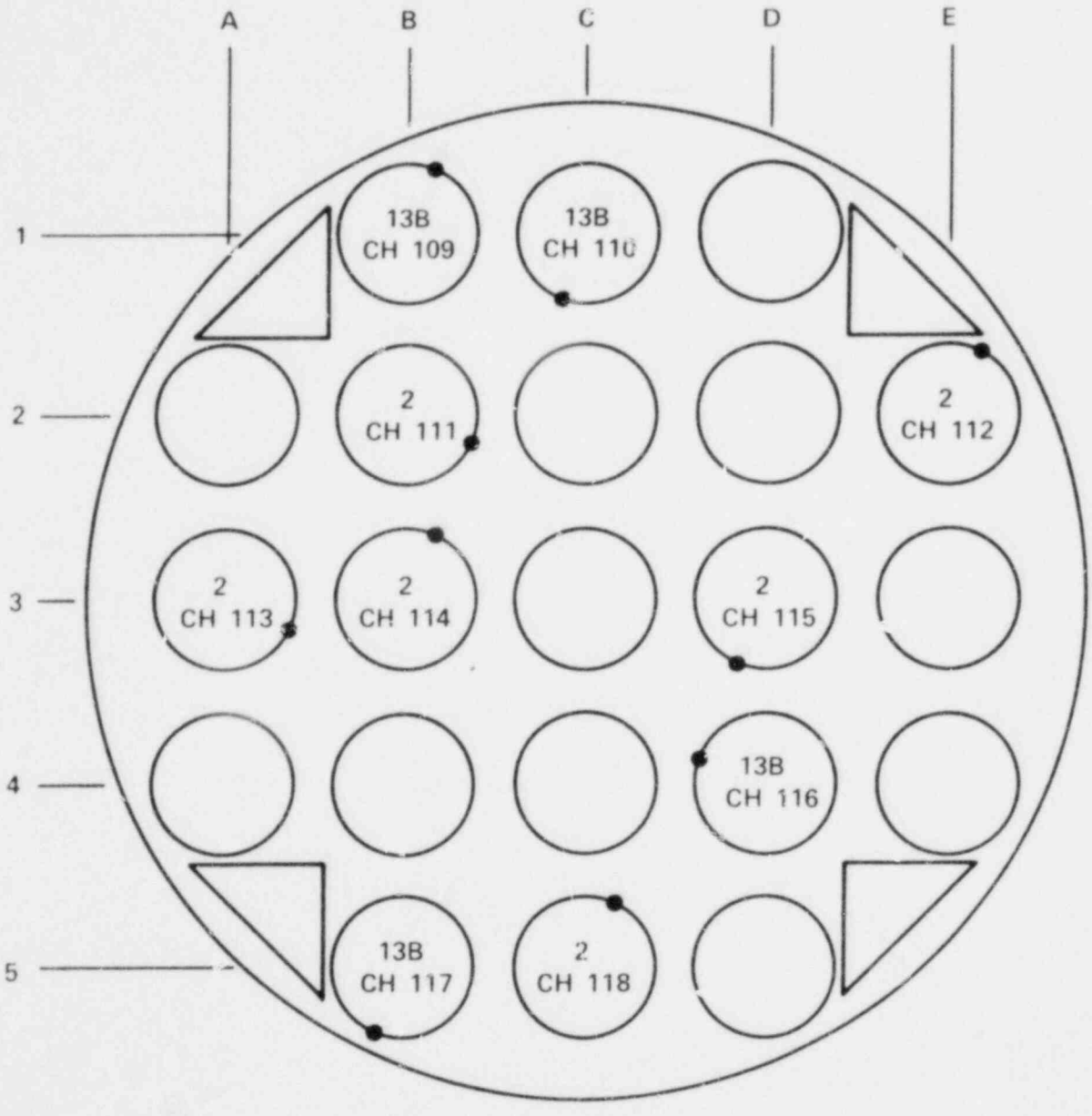

Figure H-19. Thermocouple and Steam Probe Locations - 2.13 m (84 in.) Elevation

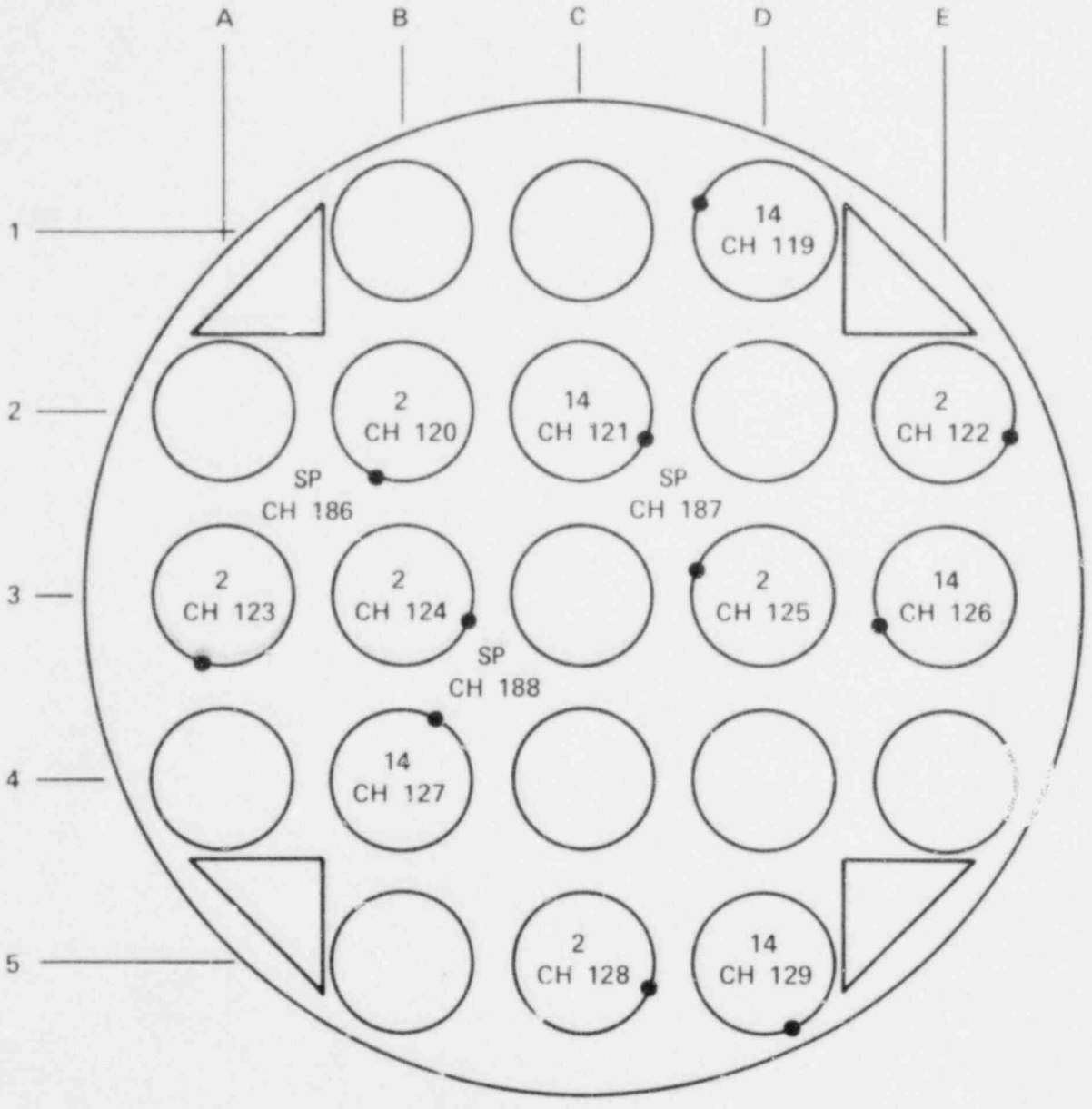

Figure H-20. Thermocouple and Steam Probe Locations - 2.29 m (90 in.) Elevation

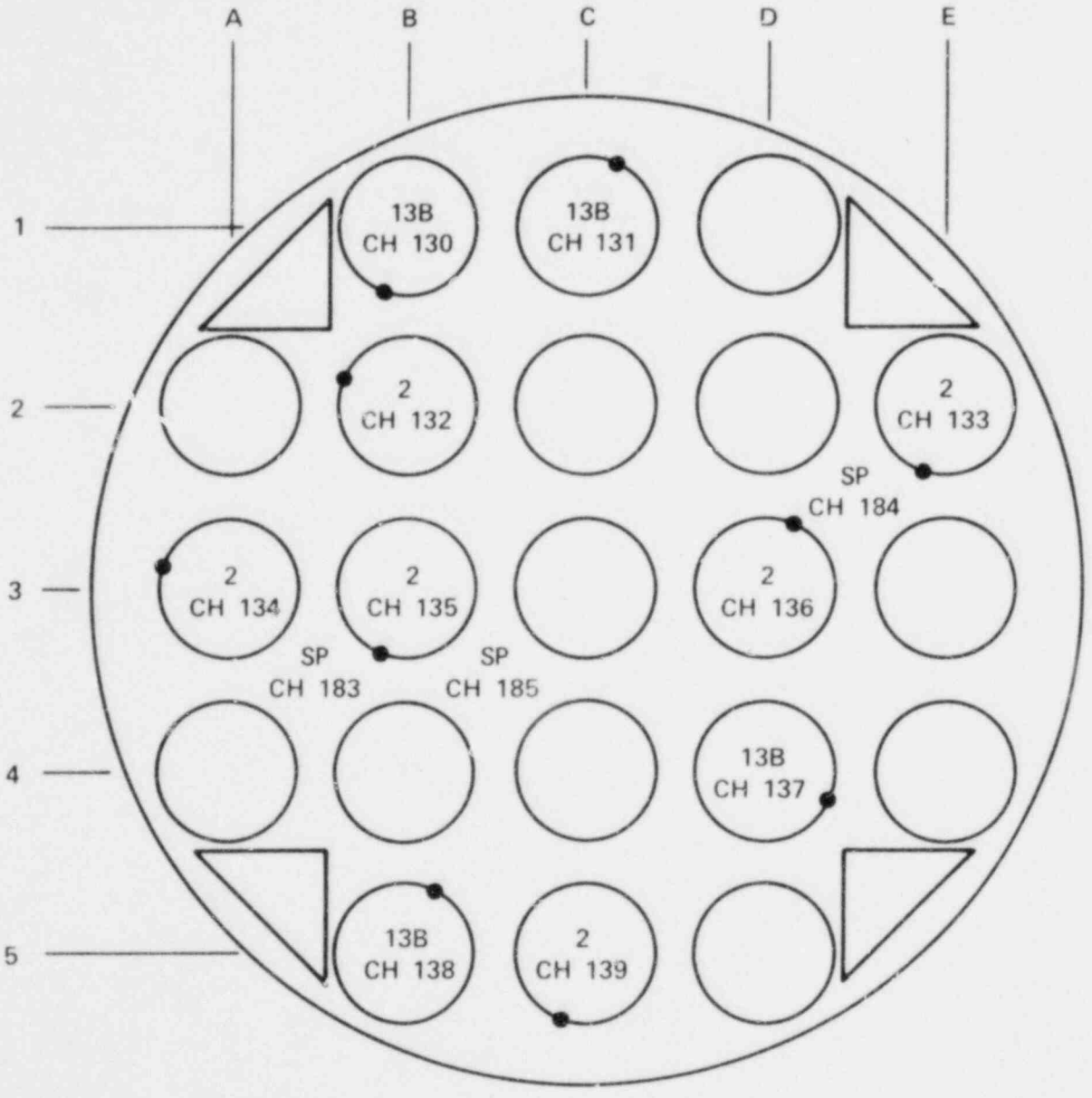

Figure H-21. Thermocouple and Steam Probe Locations - 2.44 m (96 in.) Elevation

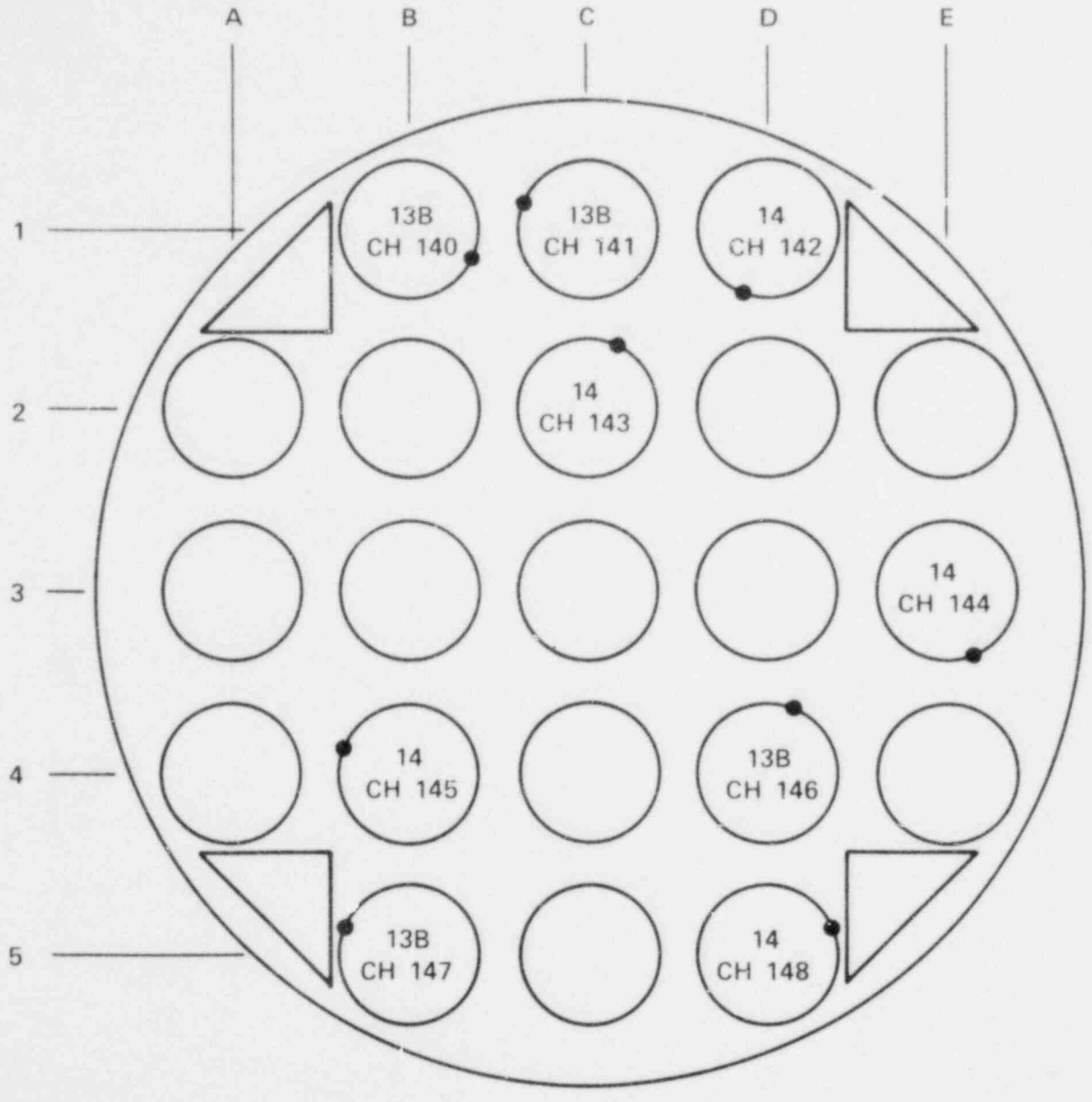

Figure H-22. Thermocouple and Steam Probe Locations - 2.59 m (102 in.) Elevation

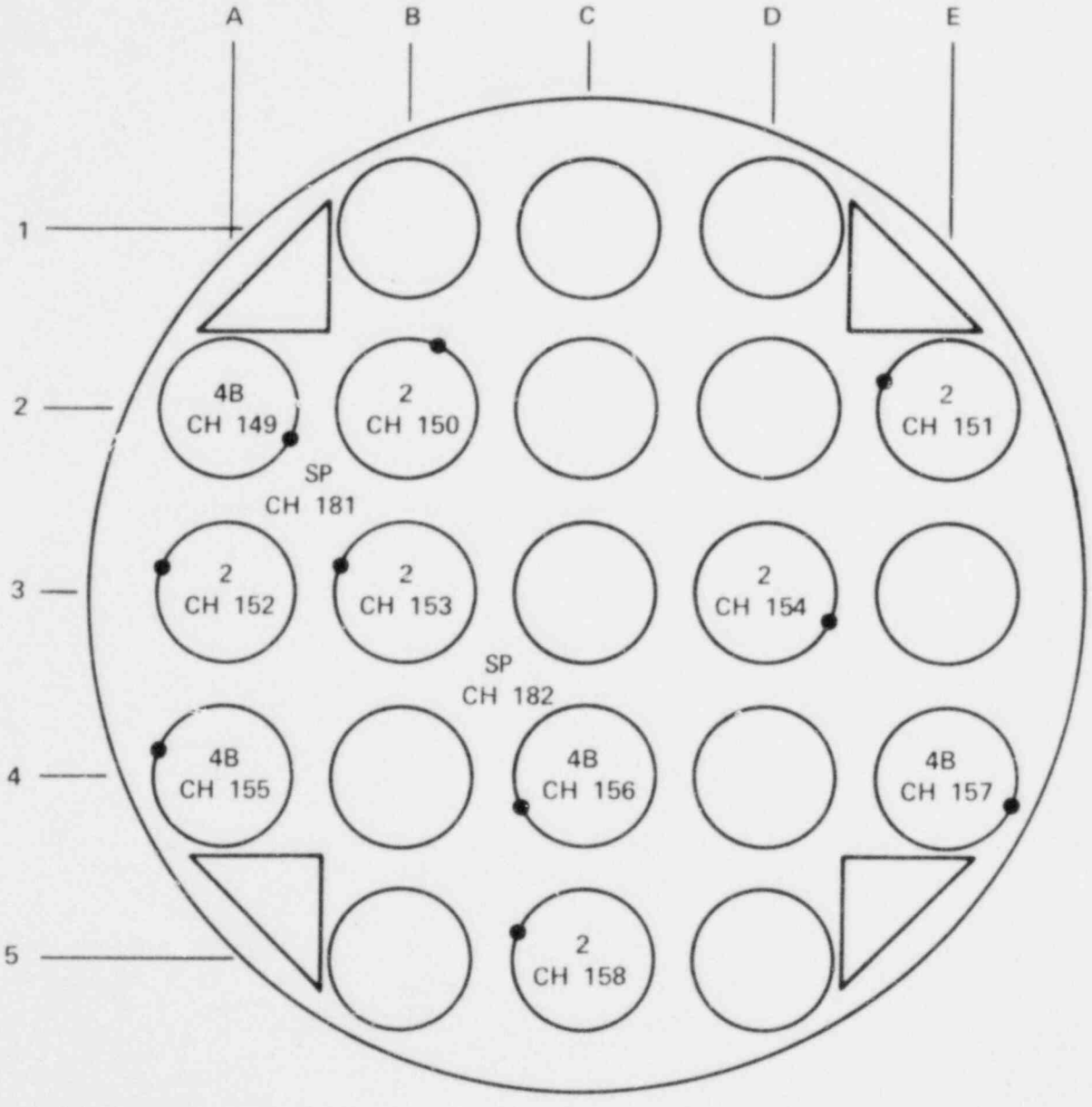

Figure H-23. Thermocouple and Steam Probe Locations - 2.82 m (111 in.) Elevation

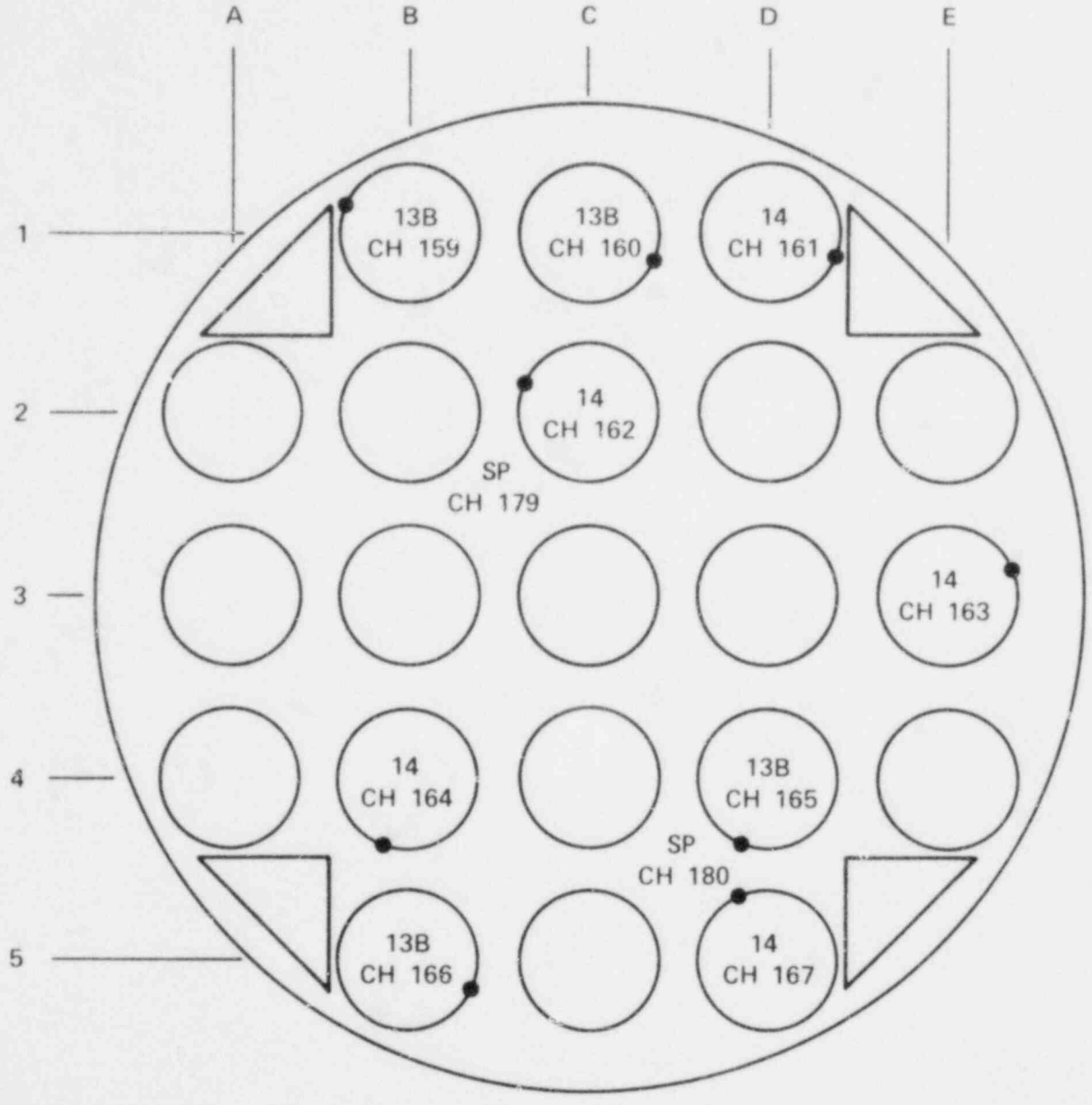

Figure H-24. Thermocouple and Steam Probe Locations - 3.05 m (120 in.) Elevation

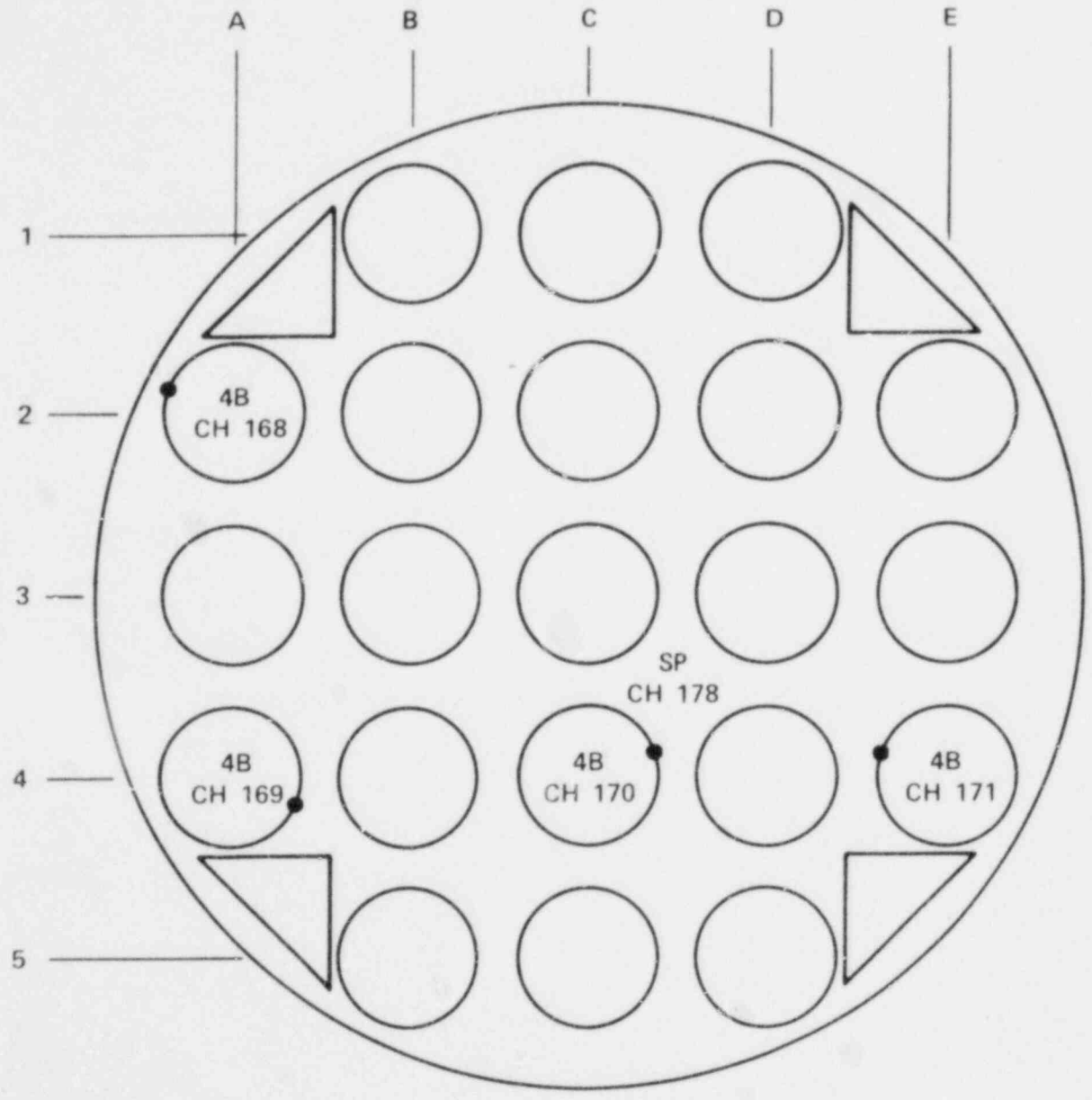

Figure H-25. Thermocouple and Steam Probe Locations - 3.35 m (132 in.) Elevation

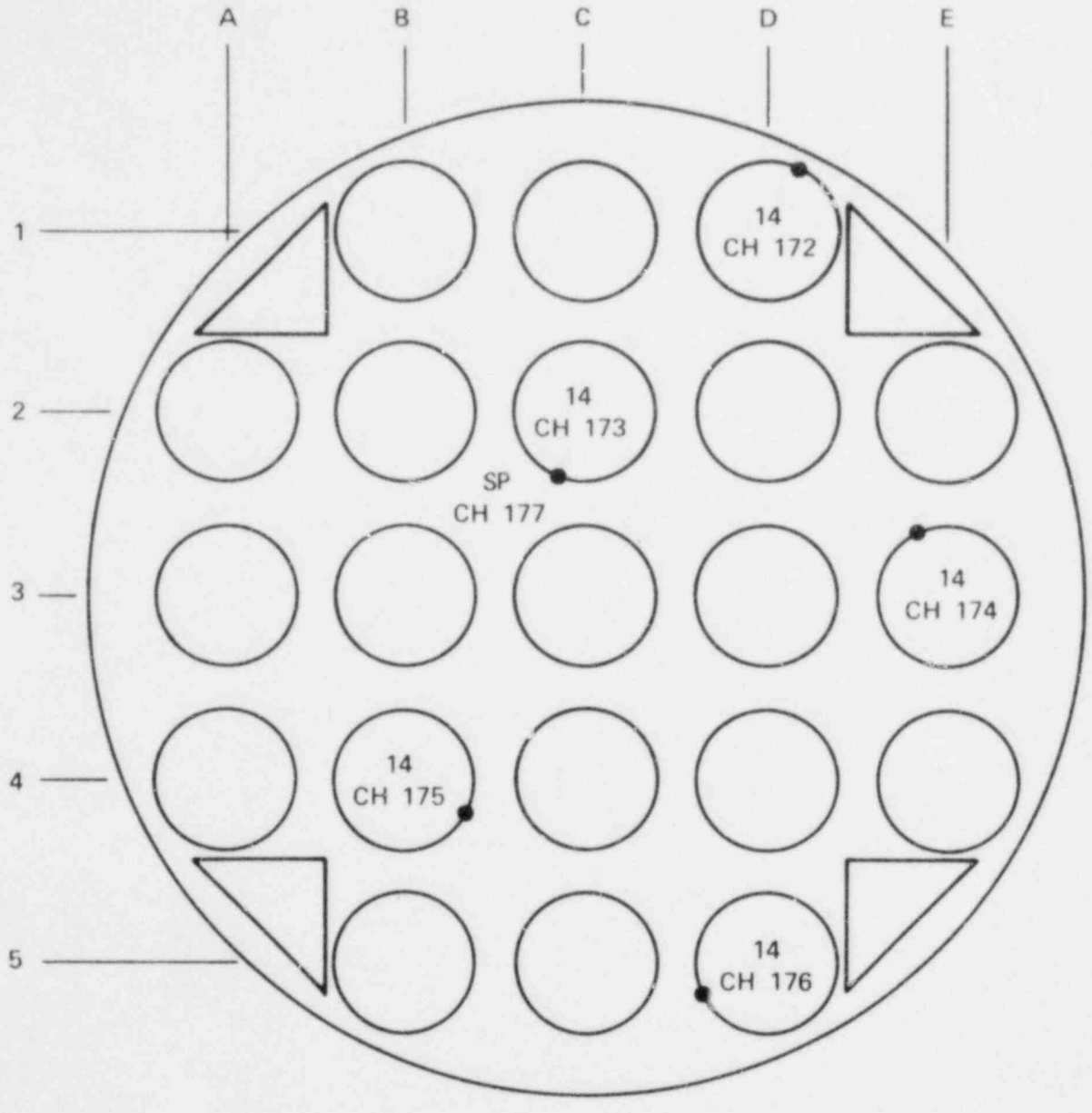

Figure H-26. Thermocouple and Steam Probe Locations - 3.51 m (138 in.) Elevation

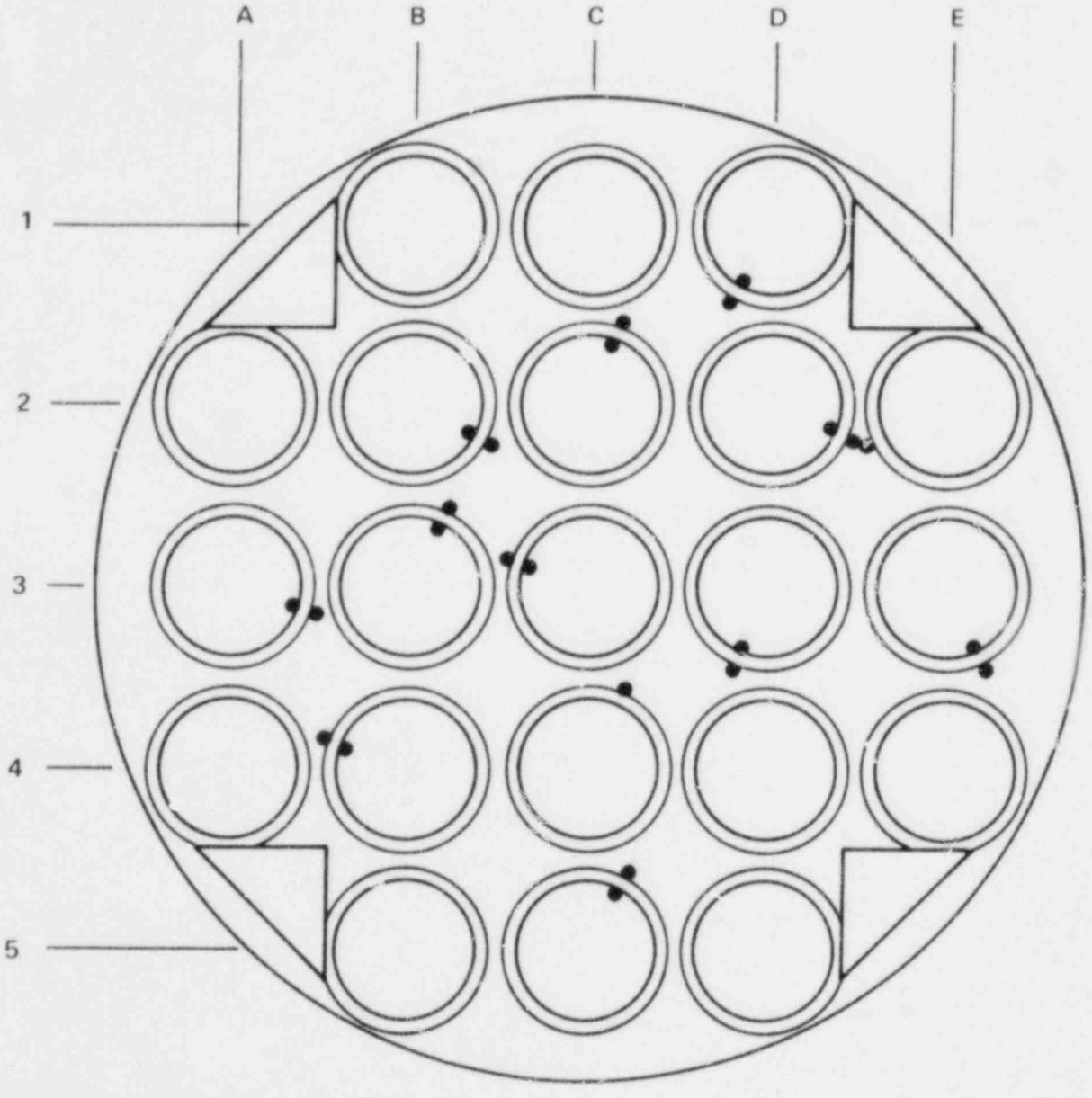

Figure H-27. Thermocouple Azimuthal Orientation for Second Configuration (All Rods Blocked)

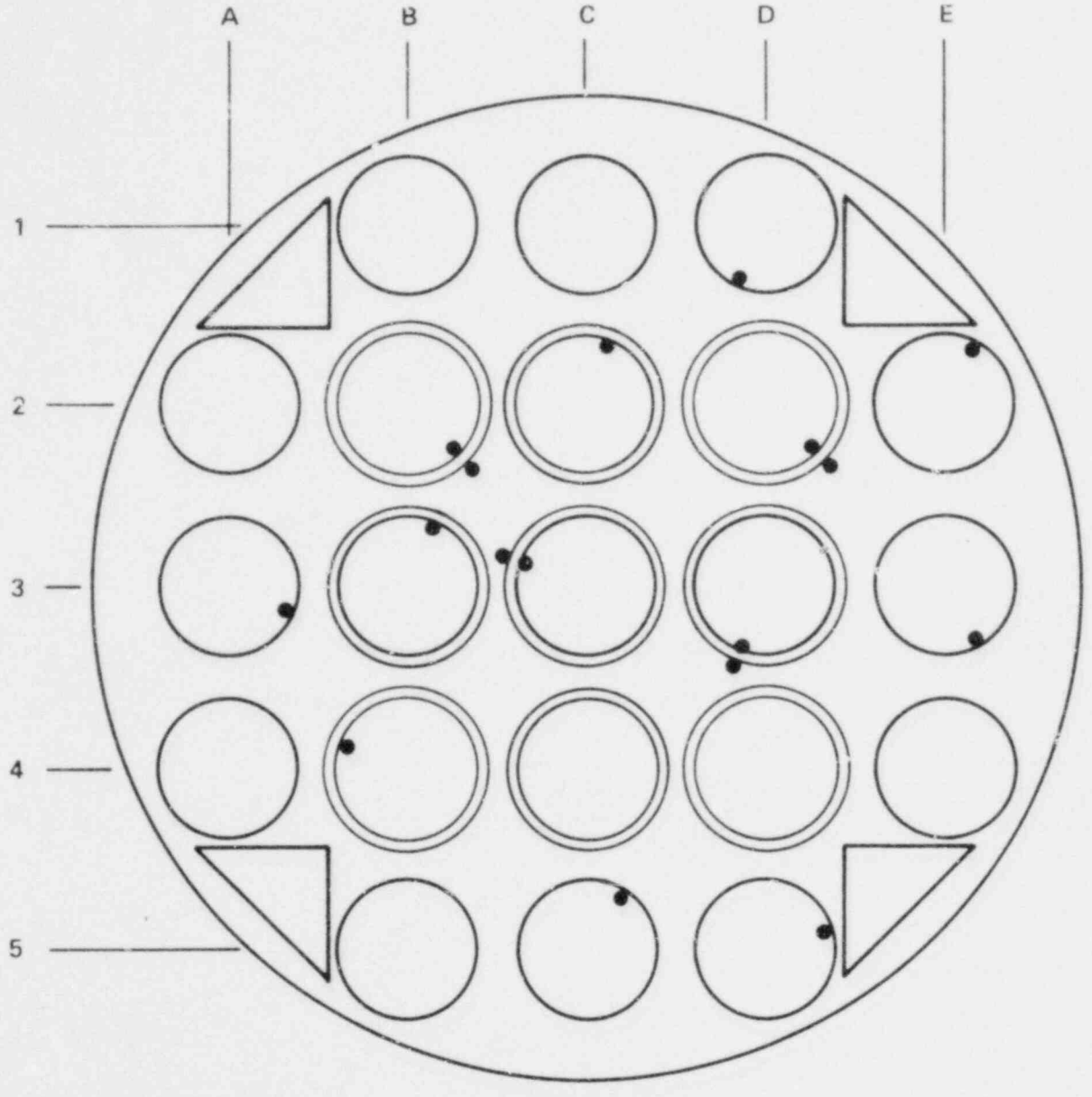

Figure H-28. Thermocouple Azimuthal Orientation for Third Configuration (Nine Rods Blocked)

APPENDIX I
CALCULATIONAL MODEL OF STEAM PROBE

The design of the 21-rod bundle steam probe, as briefly described in paragraph 7-4 of this report, was based on the calculational models discussed herein. The first discussion concerns the hydraulic model utilized to determine the flow through the steam probe; the second deals with the heat transfer model utilized to determine the "true" steam temperature.

A new type of steam probe was required for the 21-rod bundle task because of the lack of thimble tubes typically utilized, as in the unblocked bundle task,[1] for measuring superheated steam temperature in a nonequilibrium mixture.

The same general principle was applied in designing the steam probe for the 21-rod bundle as in design of the unblocked bundle probe. The principle is to shield the thermocouple from the heater rods, and separate the steam from the nonequilibrium mixture by providing a torturous flow path. The significant difference between the unblocked bundle steam probe and 21-rod bundle steam probe is that the former aspirates to atmospheric pressure, thereby providing a significant pressure drop for flow through the probe; the latter depends on a frictional pressure drop across the steam probe length as the driving force for steam flow.

A 0.51 mm (0.020 in.) thermocouple was selected as the minimum size appropriate for this high-temperature application. The thermocouple junction was placed midway between the two diametrically opposed flow holes, to minimize the inside frictional losses associated with an annulus, and to provide maximum radiation shielding and protection from water droplets. The following schematic diagram of the steam probe shows the parameters involved in this hydraulic model:

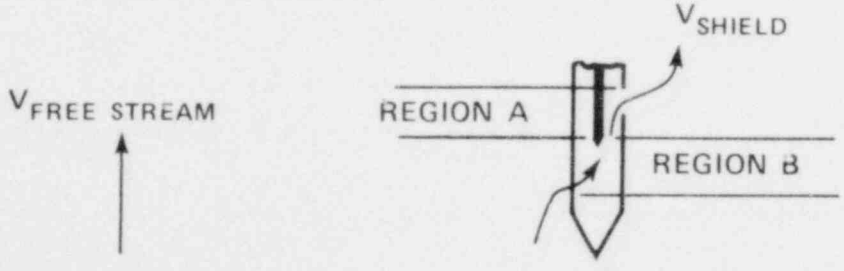

1. Hochreiter, L. E., et al., "PWR FLECHT SEASET Unblocked Bundle, Forced and Gravity Reflood Task: Task Plan Report," NRC/EPRI/Westinghouse-3, March 1978.

In parallel flow paths, the pressure drops across both flow paths are equal:

$$\Delta P_{\text{free steam}} = \Delta P_{\text{shield}}$$

where

$$\Delta P_{\text{free steam}} = \left(\frac{f_f L}{D_f}\right)\left(\frac{\rho V^2_{\text{free steam}}}{2\, g_c}\right)$$

$$\Delta P_{\text{shield}} = \Delta P_{\text{region A}} + \Delta P_{\text{region B}}$$

$$\Delta P_{\text{region A}} = \left(K_{SA} + \frac{f_{SA} L/2}{D_{SA}}\right)\left(\frac{\rho V^2_{SA}}{2 g_c}\right)$$

$$\Delta P_{\text{region B}} = \left(K_{SB} + \frac{f_{SB} L/2}{D_{SB}}\right)\left(\frac{\rho V^2_{SB}}{2 g_c}\right)$$

Therefore, assuming constant density,

$$\frac{f_f L}{D_f} V^2_{\text{free steam}} = \left(K_{SA} + \frac{f_{SA} L/2}{D_{SA}}\right) V^2_{SA} + \left(K_{SB} + \frac{f_{SB} L/2}{D_{SB}}\right) V^2_{SB} \qquad \text{(I-1)}$$

where

f	=	friction factor = 64/Re
D_f	=	hydraulic diameter of bundle = 0.00832 m (0.0273 ft)
K_{SA}	=	shield exit pressure loss coefficient = 1.0 (maximum)
K_{SB}	=	shield entrance pressure loss coefficient = 0.5 (maximum)
D_{SA}	=	hydraulic diameter of region A = D_S - 0.51 mm (0.020 in.)
D_{SB}	=	hydraulic diameter of region B = D_S
D_S	=	inside diameter of shield

The steam velocity in the free steam was assumed to be 12.2 m/sec (40 ft/sec).[1,2] By applying the continuity equation,

$$V_{SA}A_{SA} = V_{SB}A_{SB}$$

equation (I-1) can be solved for the maximum velocity, V_{SA}, in the shield. The results of this calculation are shown in figure I-1 for various shield inside diameters. The axial spacing between the diametrically opposed flow holes, L, was varied at values of 0.635 and 2.54 cm (0.25 and 1.0 in.). A calculation was also performed which neglected the frictional losses within the steam probe, thereby accounting for only the entrance and exit losses. This calculation resulted in a velocity of 1.55 m/sec (5.1 ft/sec) for a 0.635 cm (0.25 in.) spacing between flow holes and 3.11 m/sec (10.2 ft/sec) for a 2.54 cm (1.0 in.) spacing. However, when the frictional losses were accounted for, the shield velocity was found to be fairly independent of the axial spacing between flow holes at the small inside shield diameters. The difference in shield velocity between the two spacings increased as the shield diameter increased, but the subchannel flow blockage also increased, as shown in figure I-1. Therefore, to minimize the subchannel blockage at approximately 5 percent, an outside shield diameter of 0.24 cm (0.094 in.) was selected, with an inside diameter of 0.21 cm (0.082 in.)

The velocity through the shield could fall, inherent upon the assumptions regarding frictional losses, between 0.55 m/sec (1.8 ft/sec) and 1.55 m/sec (5.1 ft/sec) for a spacing of 0.635 cm (0.25 in.), and between 0.64 m/sec (2.1 ft/sec) and 3.11 m/sec (10.2 ft/sec) for a spacing of 2.54 cm (1.0 in.). It is believed that, in the case of the 2.54 cm (1.0 in) spacing, some frictional losses will be present which will provide a velocity lower than the upper bound velocity of 3.11 m/sec (10.2 ft/sec). Since the difference between the velocities for the two spacings is only 15 percent when friction is accounted for, a spacing of 0.635 cm (0.25 in.) between flow holes was selected because of greater uncertainty associated with the 2.54 cm (1.0 in.) spacing pressure loss model. The lower bound velocity of 0.55 m/sec (1.8 ft/sec) was

1. Lilly, G.P., et al., "PWR FLECHT Cosine Low Flooding Rate Test Series Evaluation Report," WCAP-8838, March 1977.

2. Lilly, G. P., et al., "PWR FLECHT Skewed Profile Low Flooding Rate Test Series Evaluation Report," WCAP-9183, November 1977.

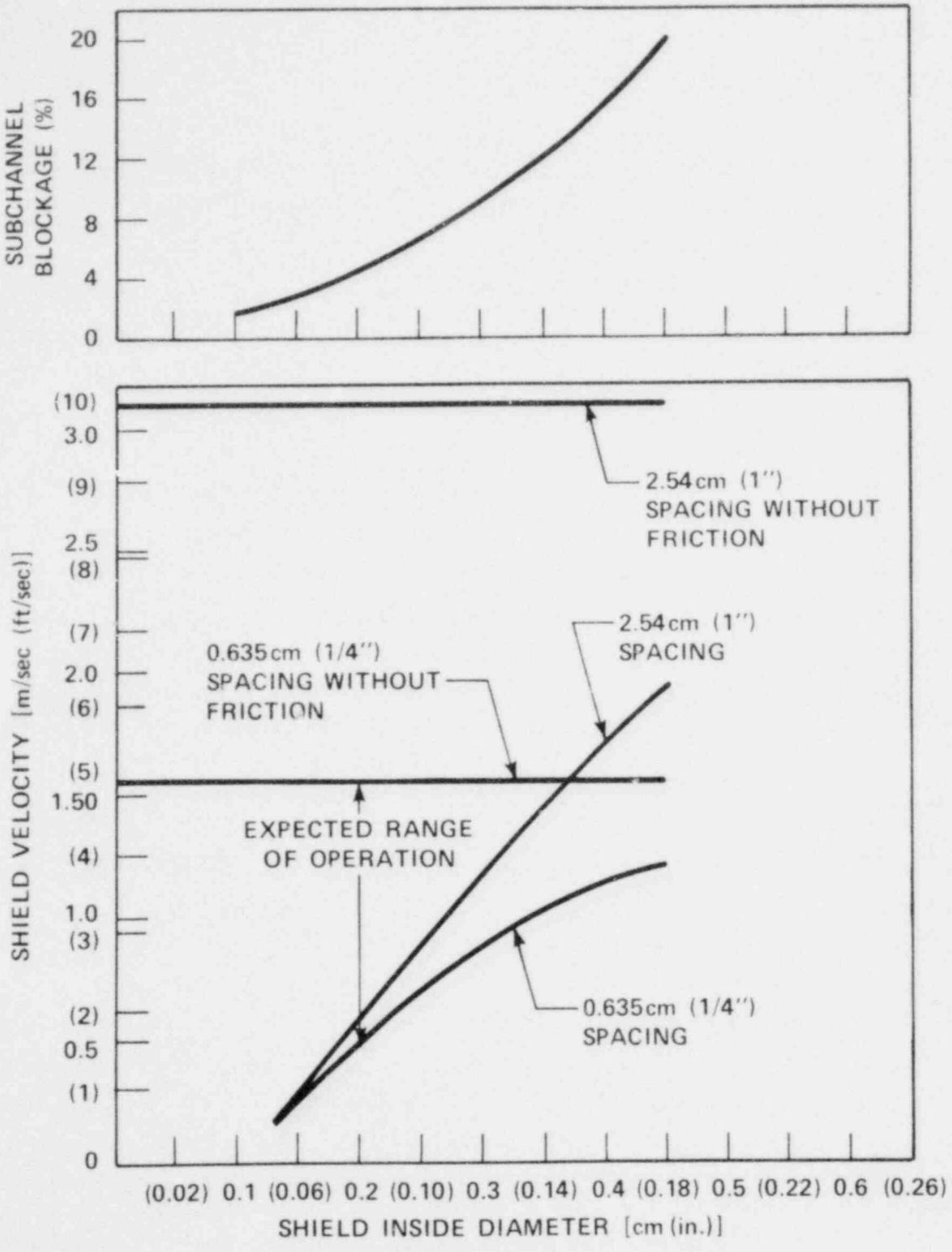

Figure I-1. Maximum Shield Velocity Versus Shield Inside Diameter

chosen to be utilized in the subsequent heat transfer calculation, thereby providing a high estimate of the temperature measurement error. It should be noted that the free steam velocity utilized in this analysis represents a low estimate and that an increase in this velocity will also increase the velocity through the shield.

As reported in appendix K, the steam probe with the 0.51 mm (0.020 in.) diameter thermocouple was tested in a single-rod reflood facility. The steam probe did not survive the desired number of thermal cycles; therefore the diameter of the thermocouple was increased to 0.81 mm (0.032 in.). The preceding calculation was performed utilizing the 0.81 mm (0.032 in.) diameter thermocouple, and it was found that the velocity through the probe was reduced from 0.55 m/sec (1.8 ft/sec) to 0.41 m/sec (1.33 ft/sec).

The temperature measured by the thermocouple within the steam probe will be adversely affected by the radiation heat transfer from the surrounding high-temperature heater rods. A sufficient steam flow through the probe is required to "cool" the thermocouple to the temperature of the steam. The following calculation was performed to determine the cooling effectiveness of the steam flow, as previously determined.

An energy balance[1] on the shield yields the following heat flow equation:

$$\dot{q}_{\substack{\text{shield to steam} \\ \text{by convection}}} + \dot{q}_{\substack{\text{shield to thermocouple} \\ \text{by radiation}}} = \dot{q}_{\substack{\text{rod to shield} \\ \text{by radiation}}}$$

An energy balance[1] on the thermocouple junction, which is assumed to be at the same temperature as the thermocouple sheath, yields the following:

$$\dot{q}_{\substack{\text{thermocouple junction to steam} \\ \text{by convection}}} = \dot{q}_{\substack{\text{shield to thermocouple junction} \\ \text{by radiation}}}$$

1. Steady-state conditions are assumed in this calculation, because of the slow response of the system during reflood.

The previous five terms are defined as follows:

$$\dot{q}_{\text{shield to steam by convection}} = h\,(T_{\text{shield}} - T_{\text{steam}})$$

where $h = \left[(hA)_{\text{outside}} + (hA)_{\text{inside}}\right]$ shield to steam

$$\dot{q}_{\text{shield to thermocouple by radiation}} = \frac{A_{T/C}\,\sigma\,(T_{SH}^4 - T_{T/C}^4)}{\left(\frac{1 - \varepsilon_{SH}}{\varepsilon_{SH}}\right)\left(\frac{A_{T/C}}{A_{SH}}\right) + \frac{1}{\varepsilon_{T/C}}}$$

$$\dot{q}_{\text{rod to shield by radiation}} = A_{SH}\,\varepsilon_{SH}\,\sigma\,(T_R^4 - T_{SH}^4)$$

since $A_{SH} << A_{rod}$.

$$\dot{q}_{\text{thermocouple junction to steam by radiation}} = \bar{h}_{\text{thermocouple junction to steam}}\,A_{T/C\ \text{junction}}\,(T_{T/C} - T_{STM})$$

$$\dot{q}_{\text{shield to thermocouple junction by radiation}} = A_{T/C\ \text{junction}}\,\sigma\,\varepsilon_{T/C}\,(T_{SH}^4 - T_{T/C}^4)$$

The outside film coefficient for the shield was determined by the following correlation for laminar flow over a plane surface:[1]

$$\bar{h}_{\text{shield to steam}} = \frac{K}{L}\,(0.664\,Re_L^{1/2}\,Pr^{1/3})$$

1. Chapman, A. J., Heat Transfer, 3rd edition, Macmillan, New York, 1974.

The inside film coefficient for the shield was determined by the following correlation[1] for laminar flow inside a cylindrical pipe:

$$h_{\substack{\text{shield to}\\ \text{steam}}} = \frac{K}{D} 1.86 \left(Re\ Pr \frac{D}{L} \right)^{1/3}$$

The thermocouple junction was assumed to be a sphere in an open flow stream; therefore the film coefficient was determined by the following correlation:[2]

$$h_{\substack{\text{thermocouple junction}\\ \text{to steam}}} = \frac{K}{D} (2 + 0.03\ Pr^{0.33} Re^{0.59} + 0.35\ Pr^{0.356} Re^{0.58})$$

The respective heat transfer areas are as follows:

-- Shield outside area - 4.75×10^{-5} m^2 (5.11×10^{-4} ft^2)
-- Shield inside area - 4.15×10^{-5} m^2 (4.47×10^{-4} ft^2)
-- Thermocouple junction area - 4.05×10^{-7} m^2 (4.36×10^{-6} ft^2)
-- Thermocouple sheath area - 5.88×10^{-6} m^2 (6.33×10^{-5} ft^2)

The steam properties were assumed constant at a temperature of 760°C (1400°F). The emissivities of the shield and the thermocouple were assumed to be 0.8.[3]

The following equations (in metric units) were developed from the preceding energy balances and respective correlations:

$$T_{SH} + 1.61 \times 10^{-11} (T_{SH} + 273)^4 = T_{T/C} + 8.34 \times 10^{-11} (T_{T/C} + 273)^4 + 7.79 \times 10^{-11} (T_R + 273)^4$$

$$T_{STM} = T_{T/C} - 7.35 \times 10^{-11} \left[(T_{SH} + 273)^4 - (T_{T/C} + 273) \right]^4$$

1. Chapman, A. J., Heat Transfer, 3rd edition, Macmillan, New York, 1974.
2. Kutateladze, S. S., Fundamentals of Heat Transfer, 2nd edition, Academic Press, New York, 1963.
3. McAdams, W. H., Heat Transmission, 3rd edition, McGraw-Hill, New York, 1954.

In English engineering units, the above equations are

$$T_{SH} + 2.76 \times 10^{-11} (T_{SH} + 460)^4 = T_{T/C} + 1.43 \times 10^{-11} (T_{T/C} + 460)^4 + 1.336 \times 10^{-11} (T_R + 460)^4$$

$$T_{STM} = T_{T/C} - 1.26 \times 10^{-11} \left[(T_{SH} + 460)^4 - (T_{T/C} + 460)^4 \right]$$

The above equations contain four unknown temperatures: shield, thermocouple, rod, and steam. Therefore, rod temperatures of 982°C (1800°F), 1093°C (2000°F), and 1204°C (2200°F) were assumed, as well as various thermocouple and shield temperatures, to satisfy the above equations. The ratios of the thermocouple temperature to the steam temperature for the three rod temperatures are shown in figure I-2 as a function of the steam temperature. As shown by this figure, relatively small errors, 3 percent and less, are introduced in this steam temperature measurement technique for the expected range of operation.(1) The error in the temperature measurement is increased by approximately 1 percent for an increase of 0.1 in the emissivity of both the shield and the thermocouple, and similarly, is decreased approximately 1 percent for a decrease of 0.1 in the emissivity. The error in the temperature measurement is rather insensitive to the film coefficient. A ± 50-percent change in the film coefficient results in approximately a ∓ 1.5-percent change in the temperature measurement error.

The preceding calculations were also performed for the steam probe with the 0.81 mm (0.032 in.) diameter thermocouple. The respective equations (in metric units) are shown below:

$$T_{SH} + 2.212 \times 10^{-11} (T_{SH} + 273)^4 = T_{T/C} + 14.12 \times 10^{-11} (T_{T/C} + 273)^4 + 7.99 \times 10^{-11} (T_R + 273)^4$$

$$T_{STM} = T_{T/C} - 7.35 \times 10^{-11} \left[(T_{SH} + 273)^4 - (T_{T/C} + 273)^4 \right]$$

1. Rosal, E. R., et al., "FLECHT Low Flooding Rate Skewed Test Series Data Report," WCAP-9108, May 1977.

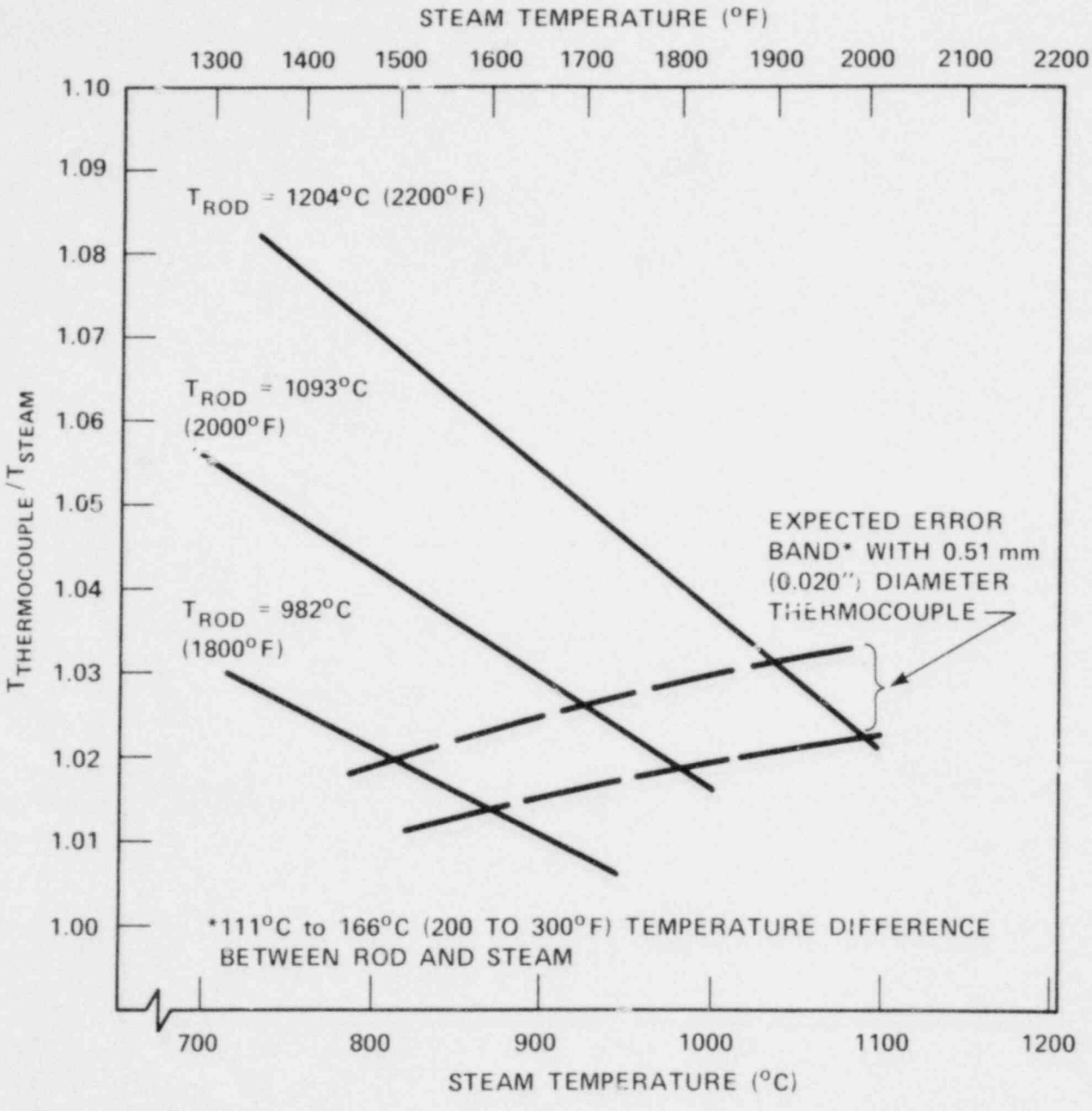

Figure I-2. Steam Probe Measurement Error With 0.51 mm (0.020 in.) Diameter Thermocouple

In English engineering units, the above equations are

$$T_{SH} + 3.792 \times 10^{-11} (T_{SH} + 460)^4 = T_{T/C} + 2.421 \times 10^{-11} (T_{T/C} + 460)^4 + 1.372 \times 10^{-11} (T_R + 460)^4$$

$$T_{STM} = T_{T/C} - 1.26 \times 10^{-11} \left[(T_{SH} + 460)^4 - (T_{T/C} + 460)^4 \right]$$

The results of the calculation for the 0.81 mm (0.032 in.) thermocouple are presented in figure I-3.

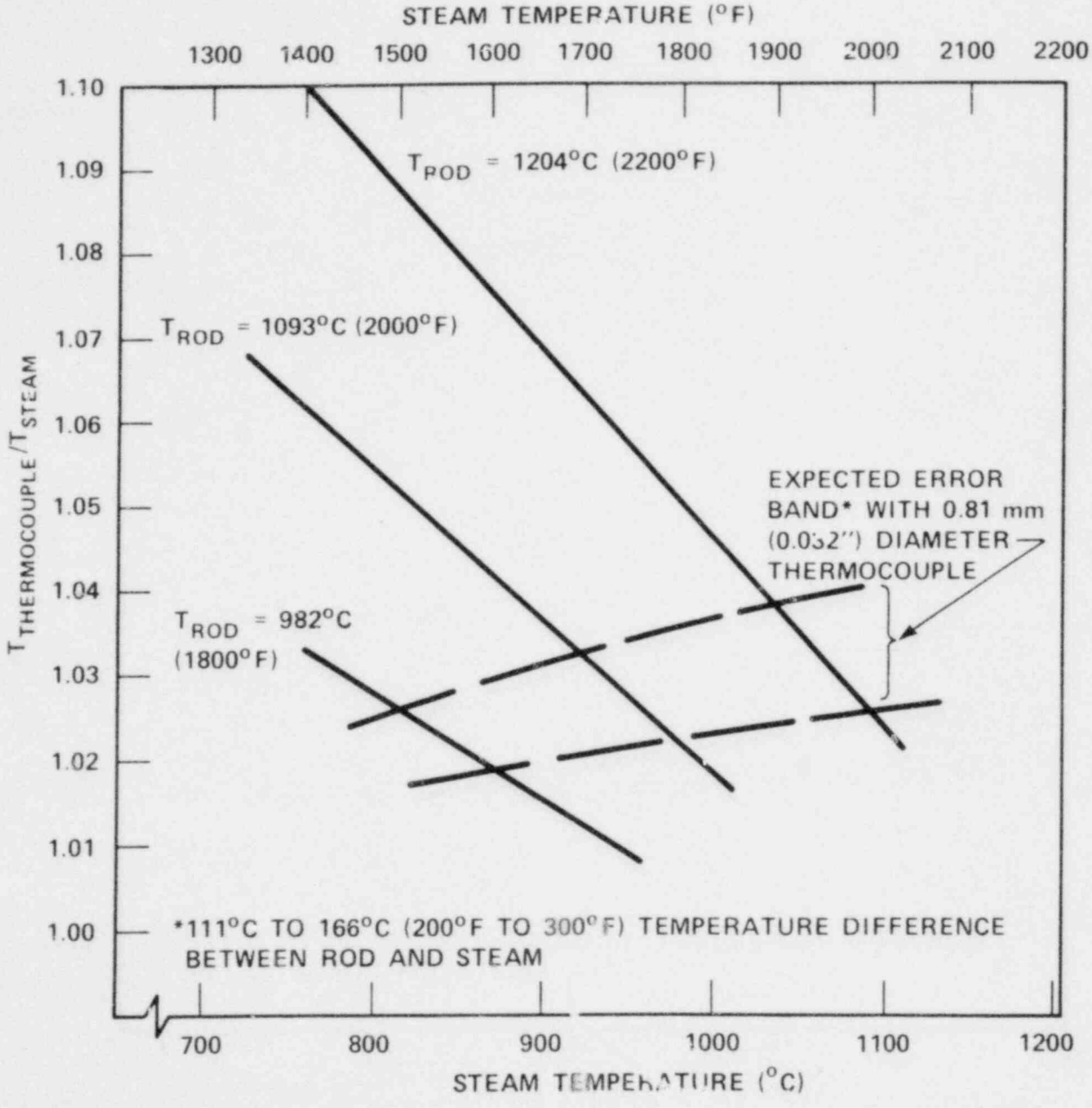

Figure I-3. Steam Probe Measurement Error With 0.81 mm (0.032 in.) Diameter Thermocouple

APPENDIX J
BLOCKAGE SLEEVE EFFECT ON HEATER ROD TEMPERATURE

The effect of the blockage sleeve on the heater rod has been investigated utilizing the TAP-A computer program.[1] The TAP-A program, for computing transient and steady-state temperature distributions, can solve problems in multidimensional systems having arbitrary geometric configurations, boundary conditions, initial conditions, and physical properties.

This investigation was undertaken to determine the change in the heater rod temperature with addition of the blockage sleeve. It was felt that the blockage sleeve could insulate the heater rod from the coolant, and therefore provide extreme heater rod temperatures to the point of rod burnout.

Two computer models were subsequently set up, as described below:

- 0.950 cm (0.374 in.) OD heater rod

- As above, with 1.25 cm (0.492 in.) OD blockage sleeve made of 0.061 cm (0.024 in.) thick stainless steel

For the blocked rod, simultaneous radiation and conduction heat transfer was provided in the 0.089 cm (0.035 in.) steam gap between the rod and the sleeve. The same initial and boundary conditions were applied to both rods, as listed below:

- 2.3 kw/m (0.70 kw/ft) constant power generation

- 100°C (212°F) ambient temperature

- 822°C (1620°F) average clad temperature

The material properties were held constant (independent of temperature) at the following conservative values:

1. Pierce, B. L., and Stumpf, H. J., "TAP-A: A Program for Computing Transient or Steady-State Temperature Distributions," WANL-TME-1872, December 1969.

-- Steam thermal conductivity - 0.093 W/m-^{o}C (0.054 Btu/hr-ft-^{o}F)

-- Stainless steel thermal conductivity - 24.6 W/m-^{o}C (14.2 Btu/hr-ft-^{o}F)
Stainless steel heat capacity - 4.90×10^{6} J/m^{3}-^{o}C (73.1 Btu/ft^{3}-^{o}F)
Stainless steel emissivity - 0.5

-- Boron nitride thermal conductivity - 24.9 W/m-^{o}C (14.4 Btu/hr-ft-^{o}F)
Boron nitride heat capacity - 3.64×10^{6} J/m^{3}-^{o}C (54.6 Btu/ft^{3}-^{o}F)

The results of the steady-state analysis are shown in figure J-1. The heater temperatures for the unblocked rod and for the blocked rod both with and without radiation heat transfer in the gap are shown as a function of the outside film coefficient. Also shown are the results of a similar calculation performed for EPRI,[1] which generally show the same trends. The temperature response of the unblocked rod in both calculations is exactly the same. The calculations for EPRI base the thermal resistance on the sleeve outside radius, thereby providing greater thermal resistance and higher temperatures. As the film coefficient increases, the heater temperature decreases for all cases, as would be expected. The blockage sleeve provides for a lower heater temperature on the blocked rod as compared to the unblocked rod for film coefficients below approximately 68 W/m^{2}-^{o}C (12 Btu/hr-ft^{2}-^{o}F). However, as the film coefficient increases, the unblocked rod heater temperature is lower than that for the blocked rod. This behavior is attributed to the thermal resistance associated with a cylindical element.

The heat transfer from the clad surface can written as

$$\frac{q}{2\pi K \ell (T_c - T_f)} = \frac{1}{\ell n (R_o/R) + (K/h_o R)/(R_o/R)}$$

where the gap resistance and sleeve resistance are reflected in the first term of the denominator and the film resistance is reflected by the second term.

The heat transfer relationship above reveals that when the thickness of the blockage sleeve is varied, the first and second terms of the denominator on the right-hand side vary inversely. The variation in the first term, which is related to the conductive resistance of the sleeve, is logarithmic; the variation in the second term, which is

1. Memo from K. H. Sun, EPRI, to L. E. Hochreiter, Westinghouse, FLECHT SEASET Heater Rod Considerations, by R. Eichhorn, August 28, 1978.

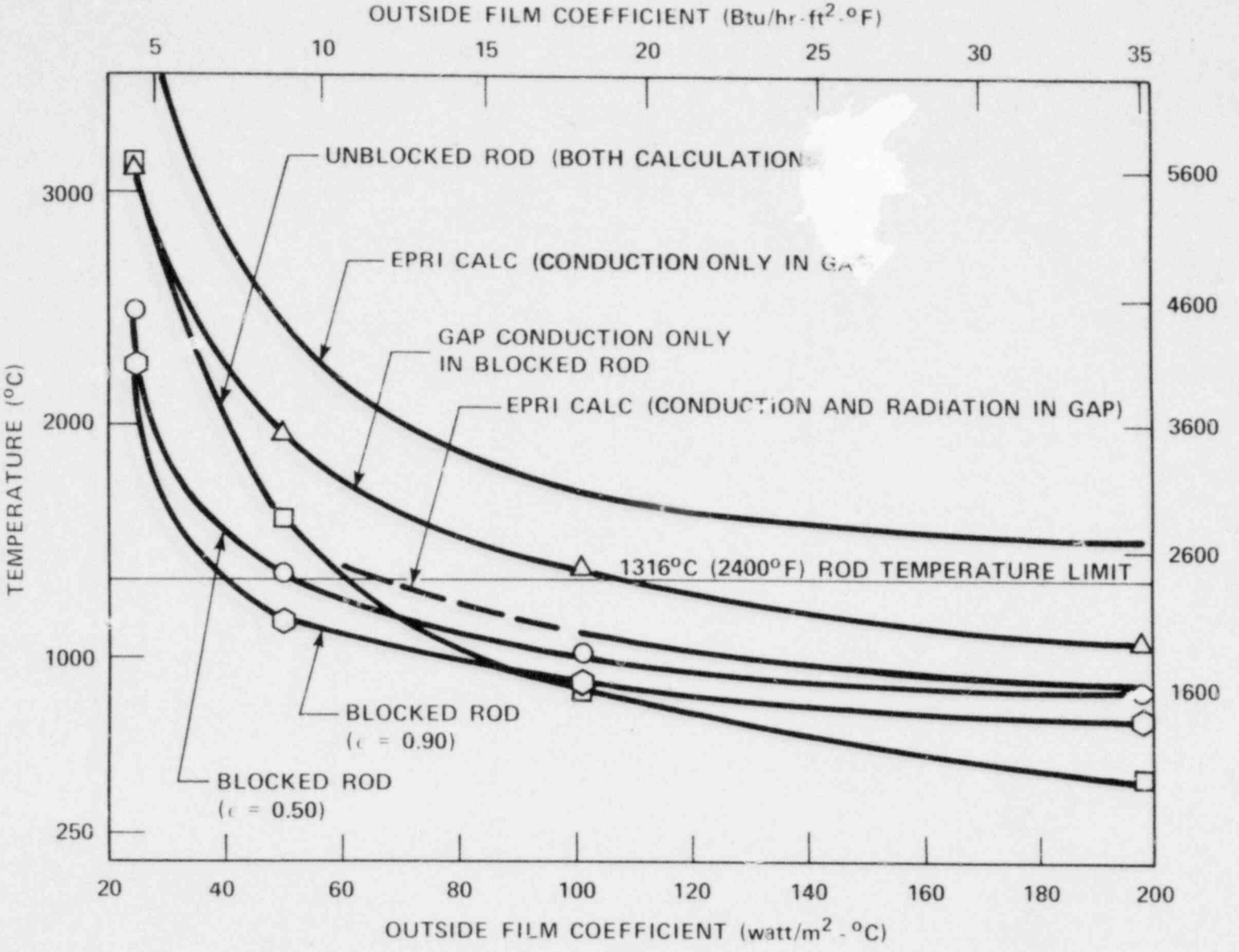

Figure J-1. Steady-State Heater Rod Clad Temperature as a Function of Outside Film Coefficient

16,047-103

related to the outside convective resistance, is hyperbolic. Thus the sum of the two terms assures a minimum value for the blockage sleeve thermal resistance at the so-called critical radius: This, in turn, provides for the maximum rate of heat transfer and minimum temperature. The critical radius, which is determined by setting the first derivative of the heat transfer rate with respect to radius equal to zero, is

$$R_c = K/h_o$$

The above relationship shows that the critical radius is dependent on the thermal conductivity of the blockage sleeve material and the outside film coefficient.

Essentially, the blockage sleeve being added to the heater rod provides for better heat transfer capability than the outside film coefficient when the film coefficient is low. Thus there is a reduction in the heater temperature. As the outside film coefficient increases, the blockage sleeve restricts heat transfer and therefore the heater temperature is increased.

A transient calculation utilizing a film coefficient typical of a FLECHT reflooding test is shown in figure J-2 for both the unblocked rod and the blocked rod. As the film coefficient increases to approximately 68 W/m^2-^oC (12 Btu/hr-ft^2-^oF), the heater temperature for each case "turns around" and the unblocked rod temperature is lower than that for the blocked rod, both of which are much lower than the 1316^oC (2400^oF) maximum temperature limit for the rod.

When radiation is neglected in the steam gap between the heater rod and the blockage sleeve, energy is transfered by conduction, which results in a substantial increase in the heater temperature (figure J-1). However, it is felt that radiation will be the dominant mode of heat transfer in the steam gap.

In conclusion, sufficient instrumentation[1] will be provided on the blockage sleeve, on the heater rod at the location of the blockage sleeve, and on the heater rod immediately upstream and downstream of the blockage sleeve not only to evaluate the heat transfer in the blockage zone but also to protect the rods from burnout.

1. See paragraphs 7-3 and 7-5.

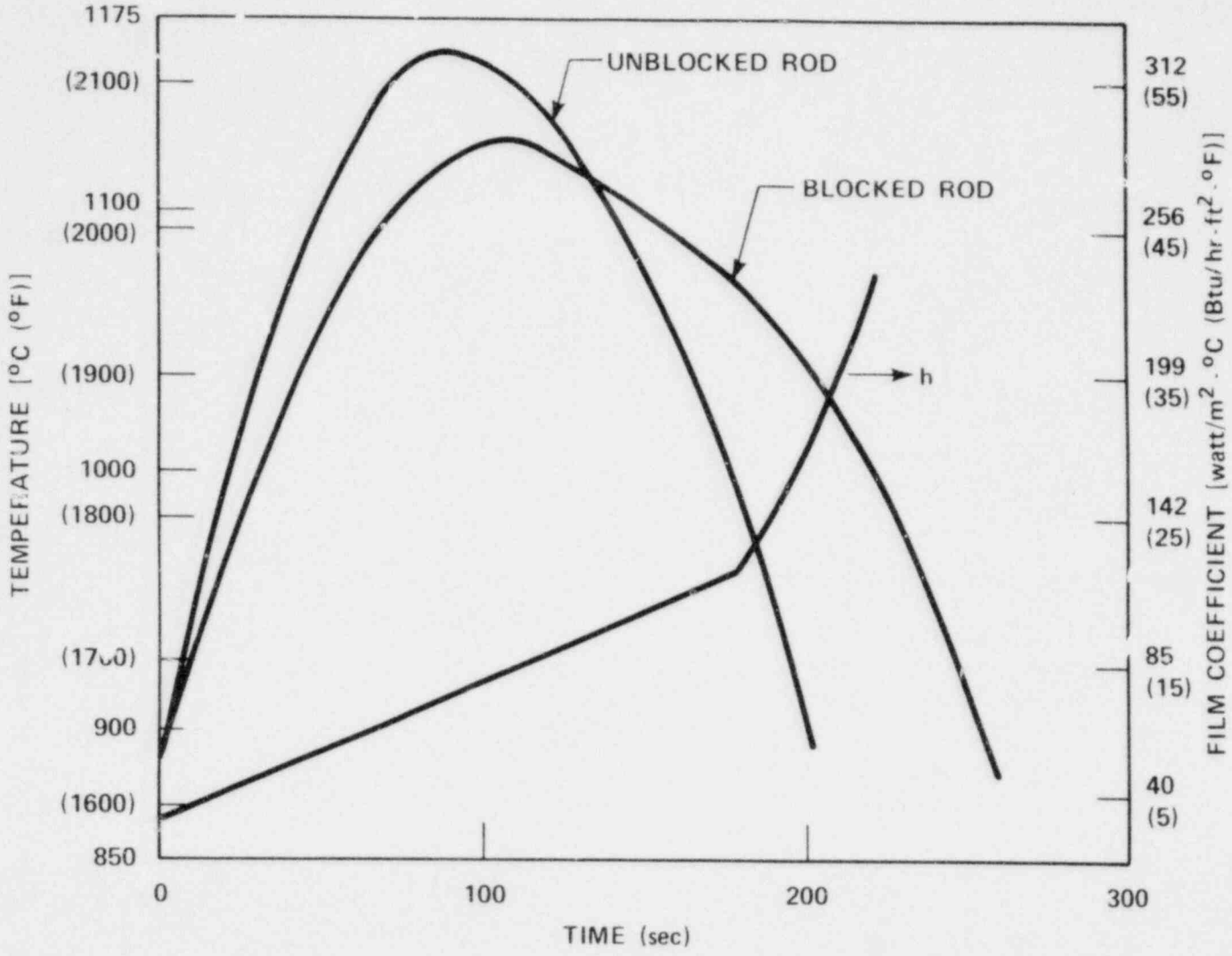

Figure J-2. Transient Heater Rod Clad Temperature for Unblocked and Blocked Rods

APPENDIX K
BLOCKAGE SLEEVE ATTACHMENT AND INSTRUMENTATION TEST

The instrumented blockage sleeve and steam probe were placed in the single-rod test facility to evaluate the following:

- Blockage sleeve attachment technique
- Blockage sleeve instrumentation
- Steam probe attachment technique
- Steam probe instrumentation

Two blockage sleeves were attached by two different methods to an instrumented heater rod at the 1.88 m and 2.29 m (74 in. and 90 in.) elevations. The sleeves were of a design different from that specified in section 4; they were much shorter and of a higher strain. The sleeve at the 1.88 m (74 in.) elevation was spot-welded to the rod at four locations around the periphery downstream edge of the sleeve. (This is readily seen in a pretest photograph, figure K-1). The sleeve at the 2.29 m (90 in.) elevation was not attached directly to the rod, but was simply held in place by drilling a 3.18 mm (0.125 in.) diameter hole in the downstream side of the sleeve [3.18 mm (0.125 in.) from the end] and placing a spot-weld on the rod through the hole in the sleeve. (This is readily seen in pretest and posttest photographs, figures K-2 and K-3, respectively).

Each of the blockage sleeves was instrumented with a 0.51 mm (0.020 in.) stainless steel sheathed, ungrounded, type K chromel-alumel thermocouple. The thermocouple was attached to the sleeve as shown in figure K-4. A hole was drilled in the sleeve at the point of maximum strain and the thermocouple junction was brazed into this hole. The thermocouple lead was run in the gap between the rod and the sleeve. A 1.02 mm (0.040 in.) OD stainless steel hollow tube was brazed to the upstream side of the sleeve and the thermocouple lead was run through this hollow tube to provide protection and strength for a distance of approximately 30 cm (12 in.). (This is shown in a preassembly photograph, figure K-5.) The thermocouple leads were subsequently wrapped around the 3.18 mm (0.125 in.) diameter grid support rods. It should be noted that, because of the size of the blockage sleeve

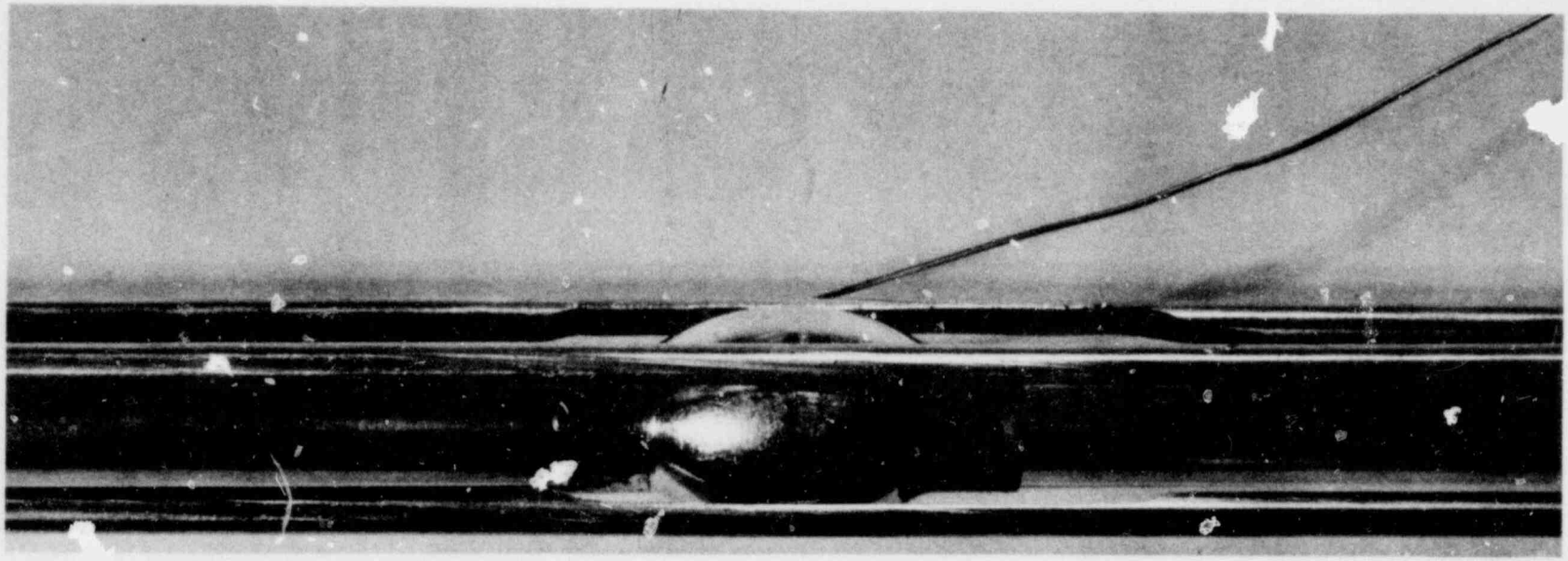

Figure K-1. Blockage Sleeve at 1.88 m (74 in.) Elevation (Pretest)

16,047-111

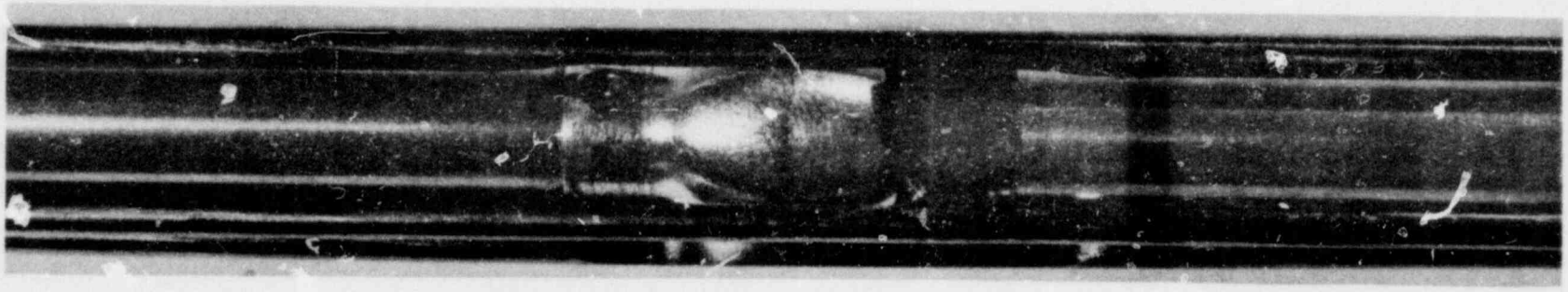

Figure K-2. Blockage Sleeve at 2.29 m (90 in.) Elevation (Pretest)

16,047-110

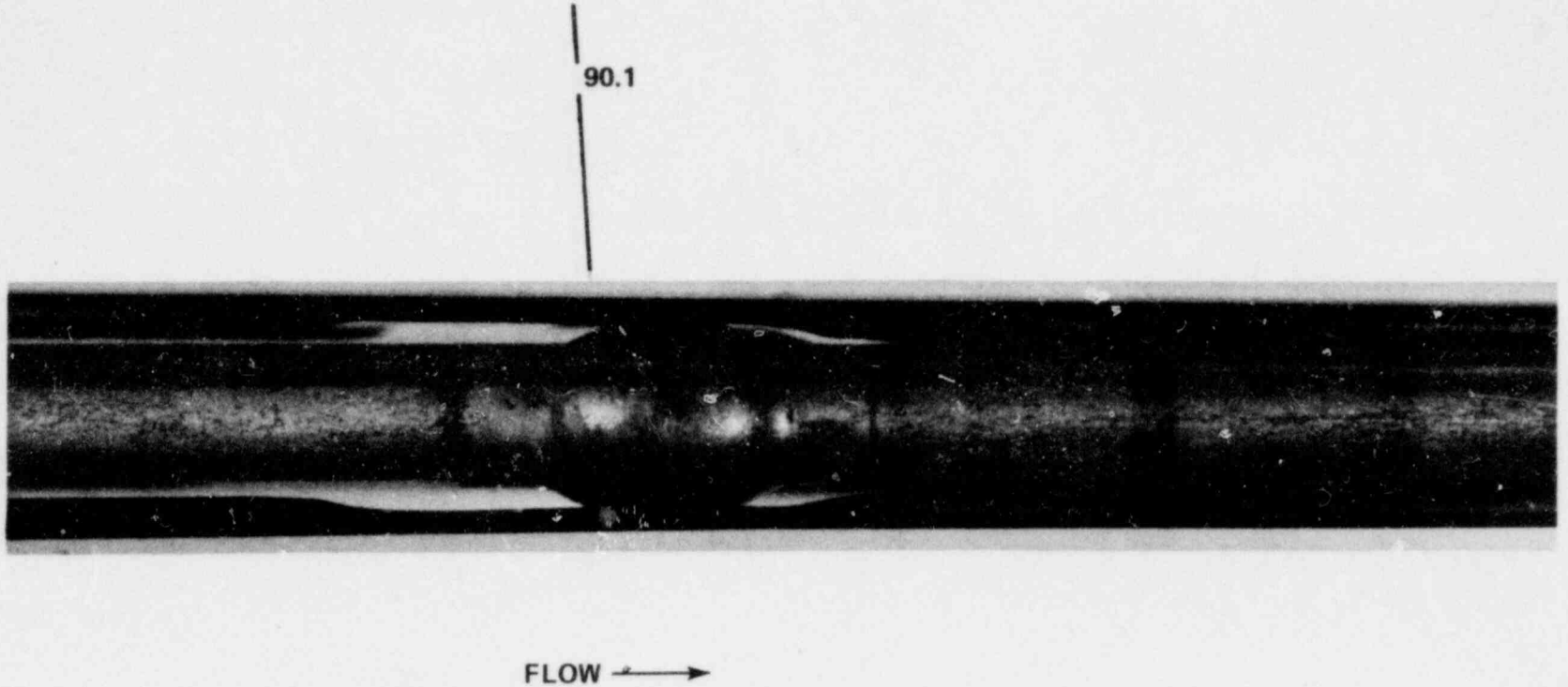

Figure K-3. Blockage Sleeve at 2.29 m (90 in.) Elevation (Posttest)

16,047-112

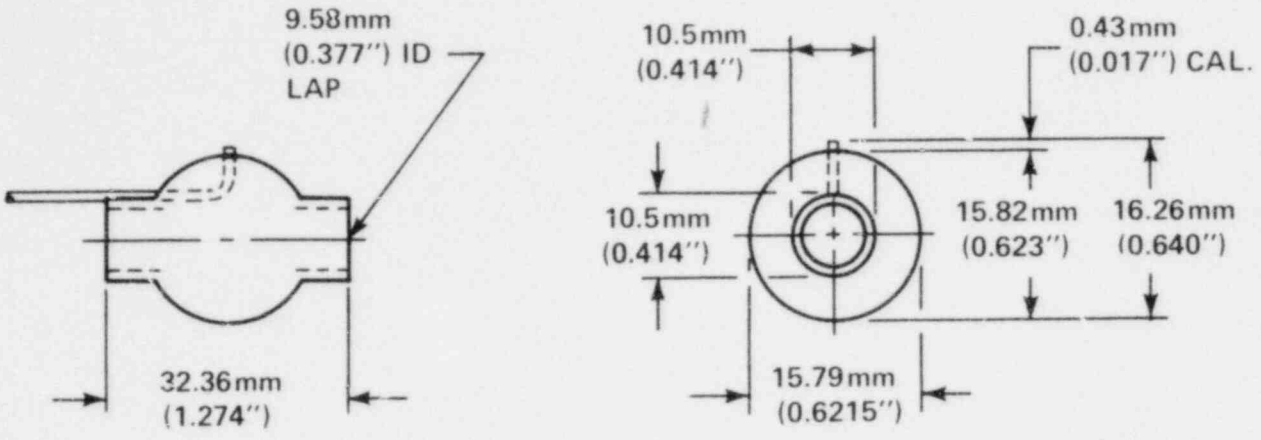

SLEEVE WITH 3.175mm (1/8") DIA HOLE

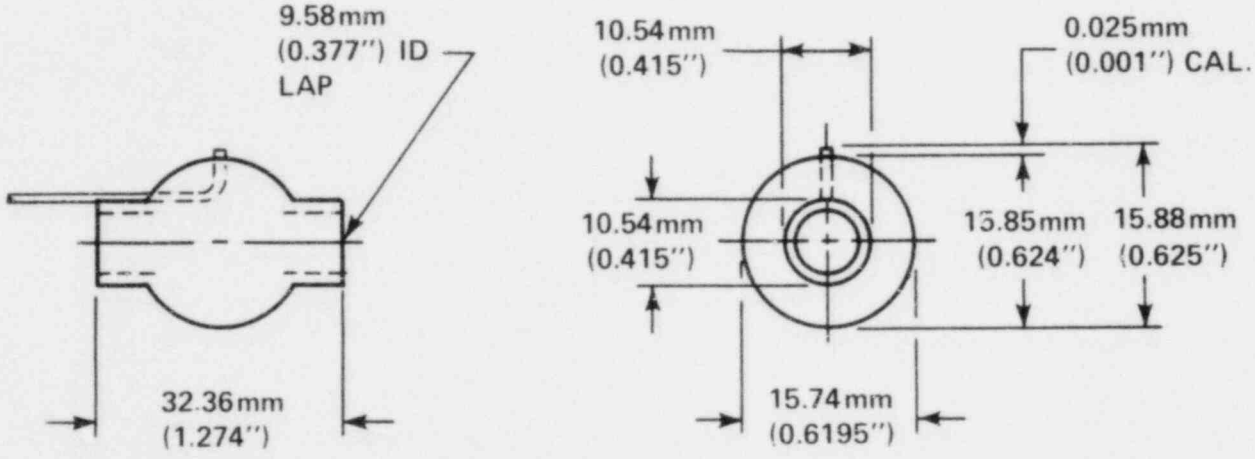

SLEEVE WITHOUT 3.175mm (1/8") DIA HOLE

Figure K-4. Thermocouple Installation in Sleeve

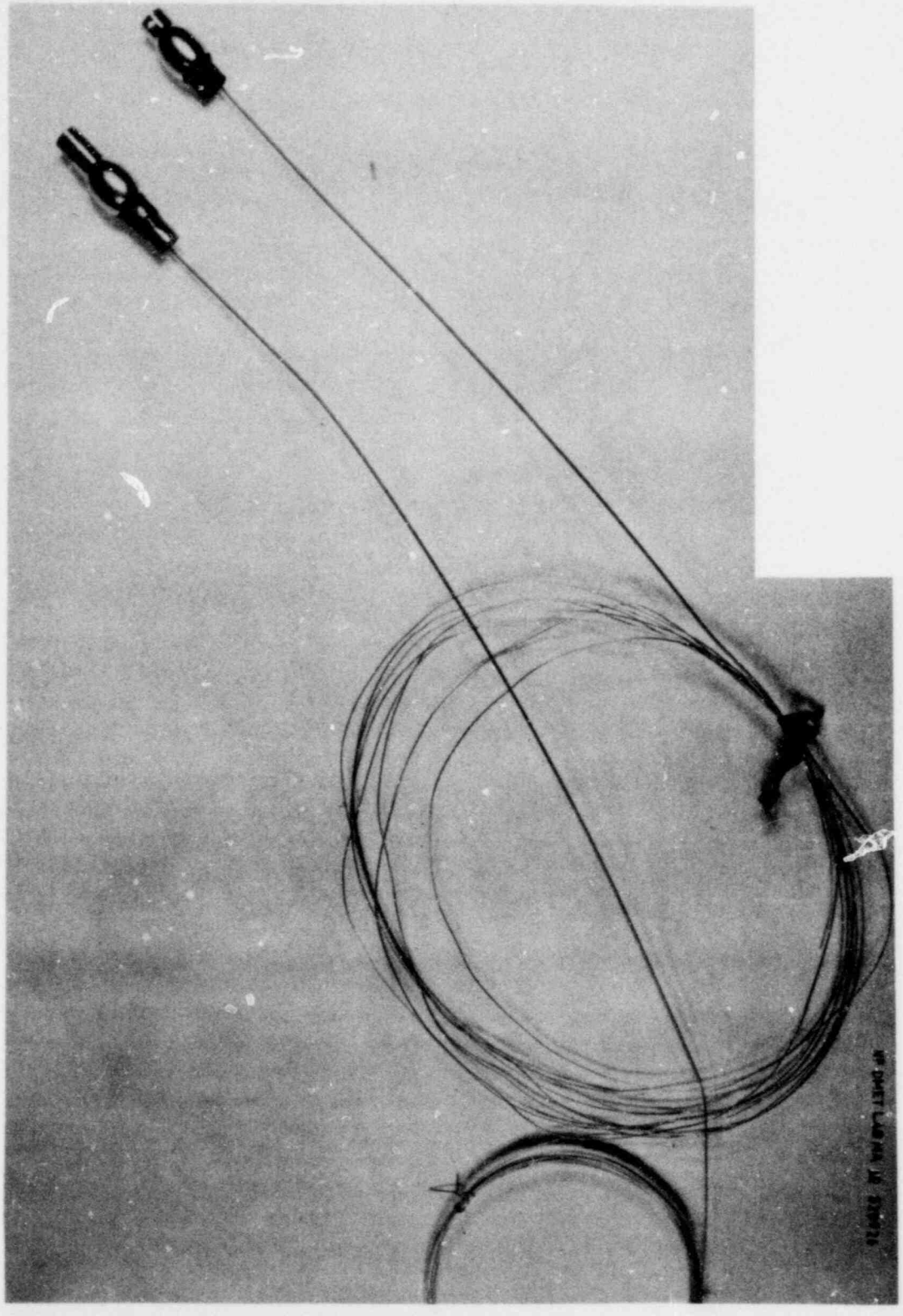

Figure K-5. Instrumented Blockage Sleeve (Preassembly)

utilized in these tests, which is larger in outside diameter than the prototypical sleeve to be used in the bundle tests, the 3.18 mm (0.125 in.) diameter support rods had to be cut back, as shown in Figure K-6.

The steam probe was attached to the 2.11 m (83 in.) elevation grid with the sensing holes located at 2.01 m (79 in.), as shown in the preassembly and pretest photographs (figures K-7 and K-8). The thermocouple used in the steam probe was the same as that used in the blockage sleeve.

All of the instrumentation (steam probe, blockage sleeve and heater rod thermocouples) leads were brought out the bottom of the test section. In this manner, the steam probe thermocouple lead and the 2.29 m (90 in.) elevation blockage sleeve thermocouple lead "crossed over" the 1.88 m (74 in.) elevation blockage sleeve.

The test was performed under the following nominal conditions:

Number of Cycles	Initial Clad Temperature [$^{o}C(^{o}F)$]	Flooding Rate [m/sec(in./sec)]
1-2	538 (1000)	0.038 (1.5)
3-12	1093 (2000)	0.038 (1.5)
13-22	1093 (2000)	0.020 (0.8)

The power was applied to the heater rod during an adiabatic heatup period at a rate of 2.3 kw/m (0.7 kw/ft)[1] until the initial clad temperature was reached. The power was then reduced to a rate of 1.8 kw/m (0.55 kw/ft) and flooding was initiated. After 180 seconds of constant flooding, the power was reduced to 1.4 kw/m (0.42 kw/ft) until all thermocouples had quenched, at which time the power was turned off.

The results from the single-rod sleeve attachment and instrumentation test are summarized below:

- The blockage sleeve thermocouple at the 2.29 m (90 in.) elevation failed after the first two temperature cycles.

1. Peak rod power at the 1.83 m (72 in.) elevation

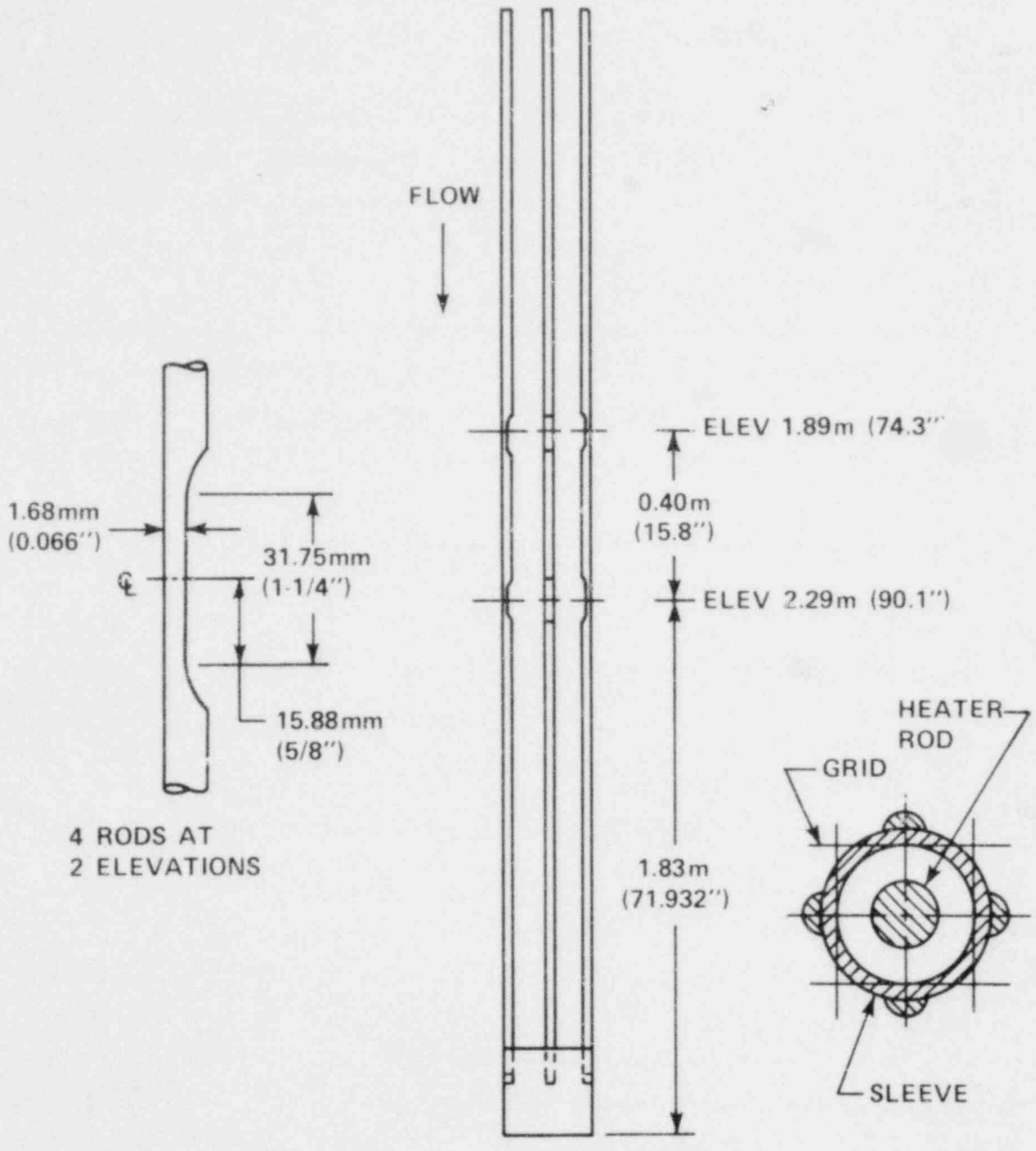

Figure K-6. Support Rod Cut-Back

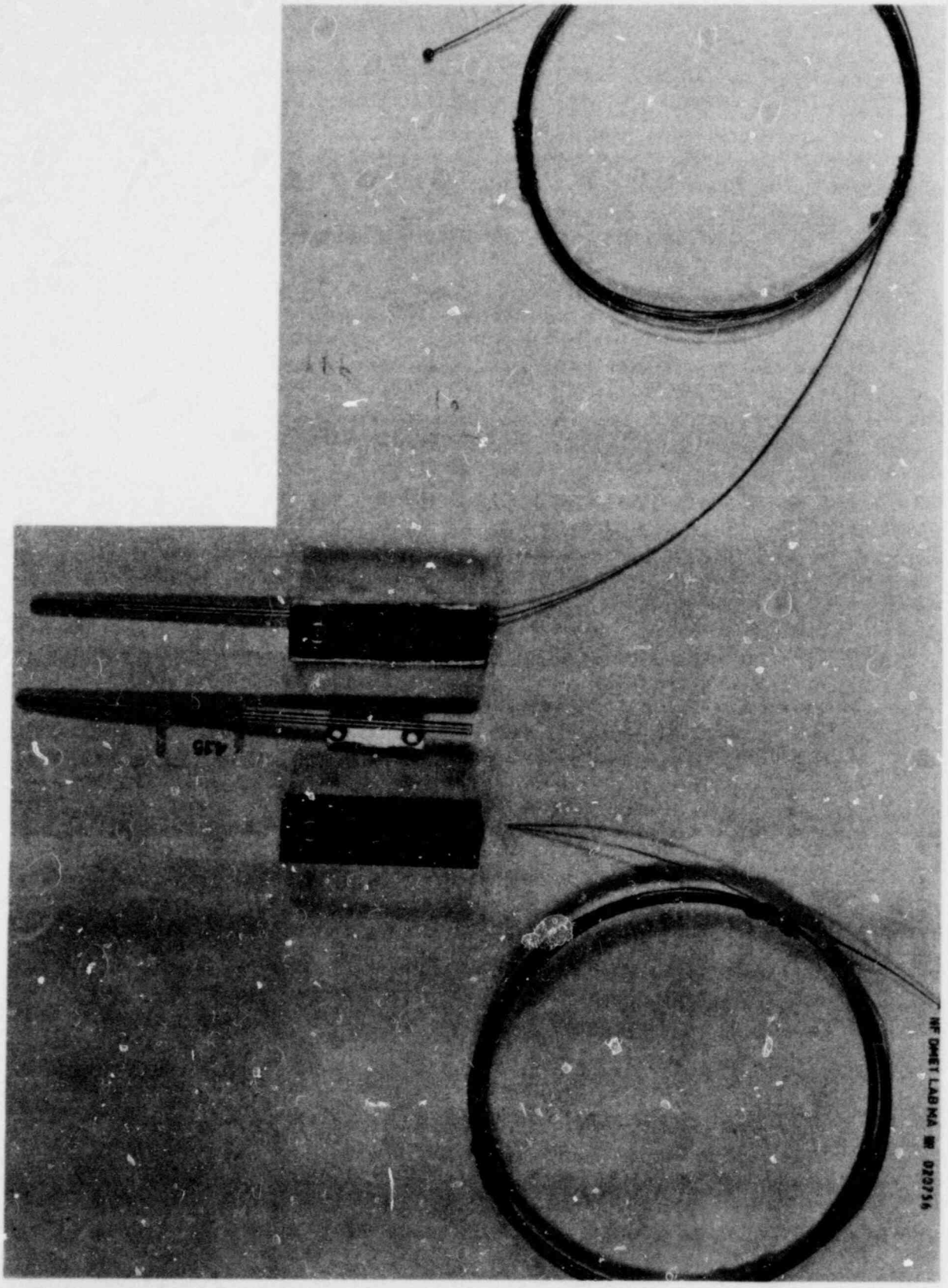

Figure K-7. Steam Probe (Preassembly)

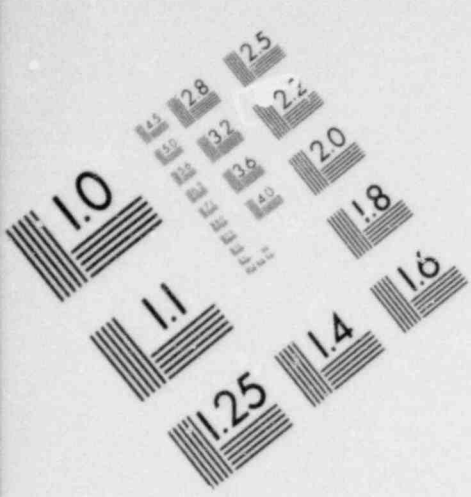

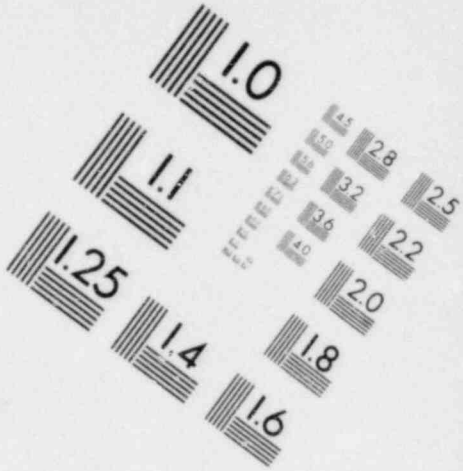

IMAGE EVALUATION
TEST TARGET (MT-3)

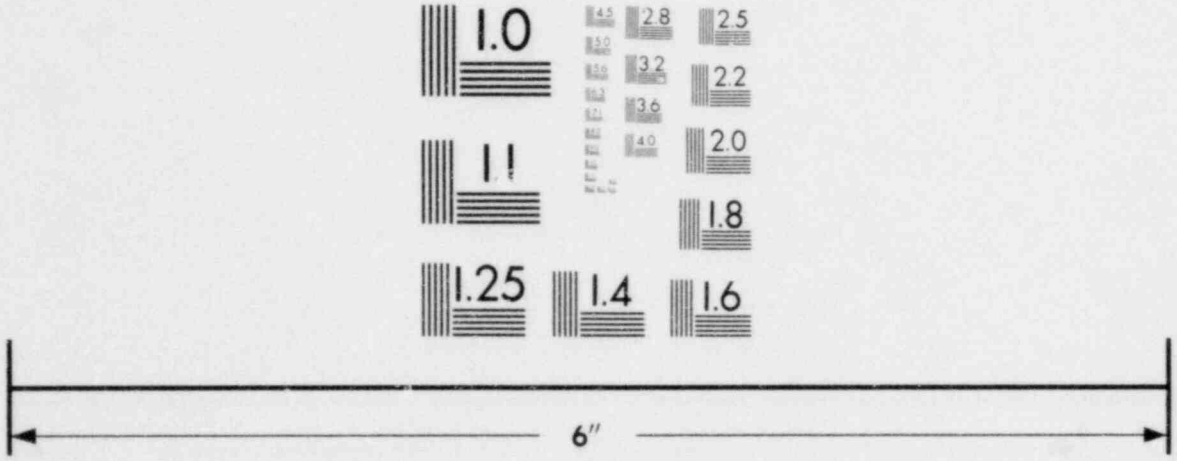

MICROCOPY RESOLUTION TEST CHART

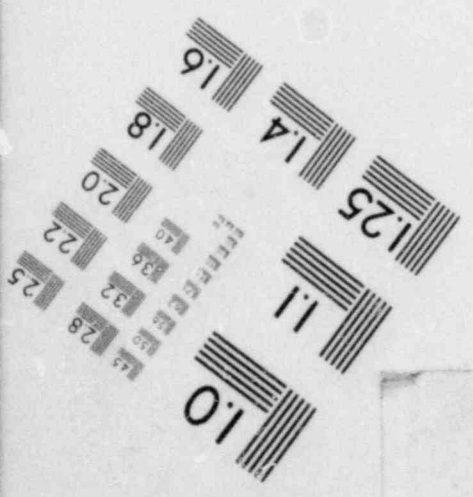

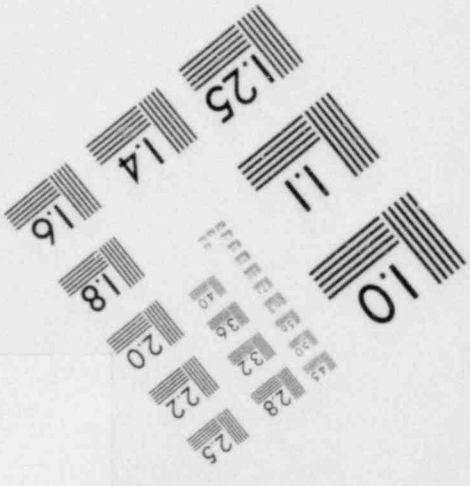

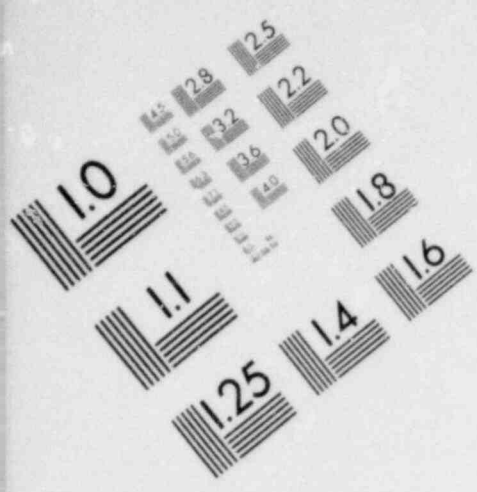

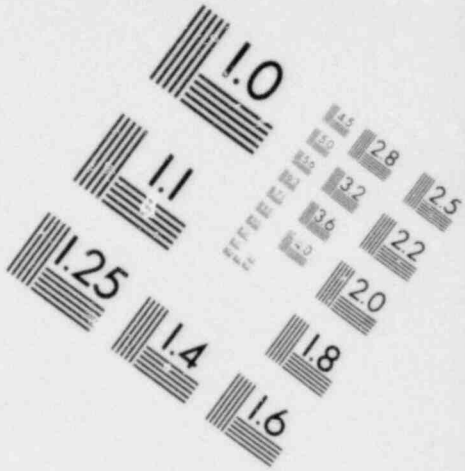

IMAGE EVALUATION
TEST TARGET (MT-3)

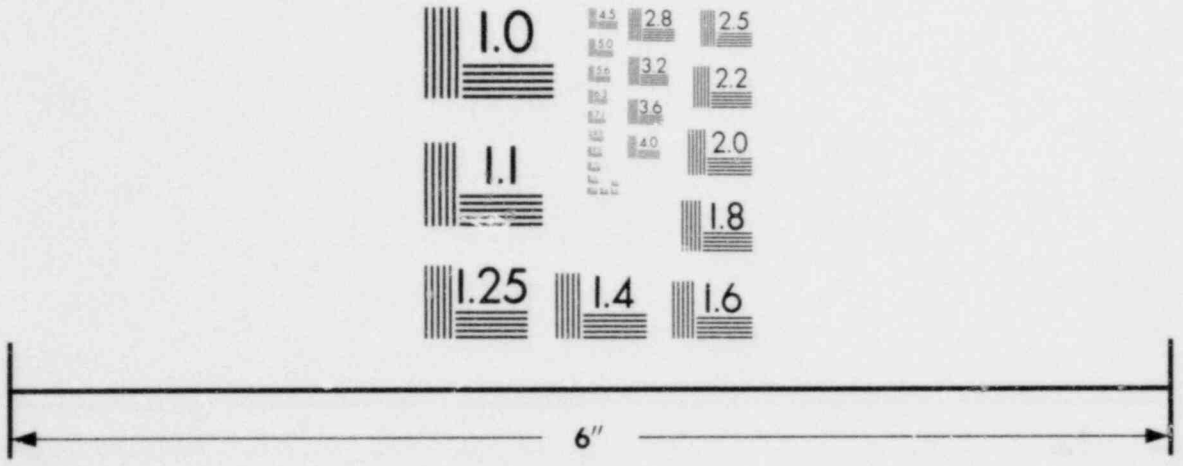

MICROCOPY RESOLUTION TEST CHART

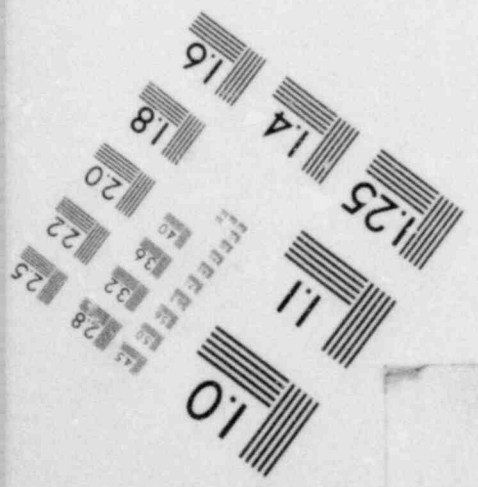

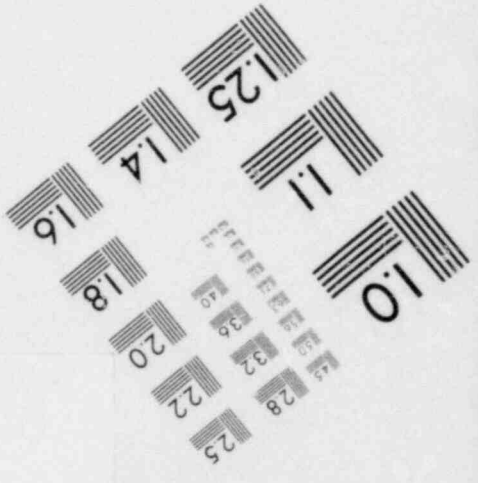

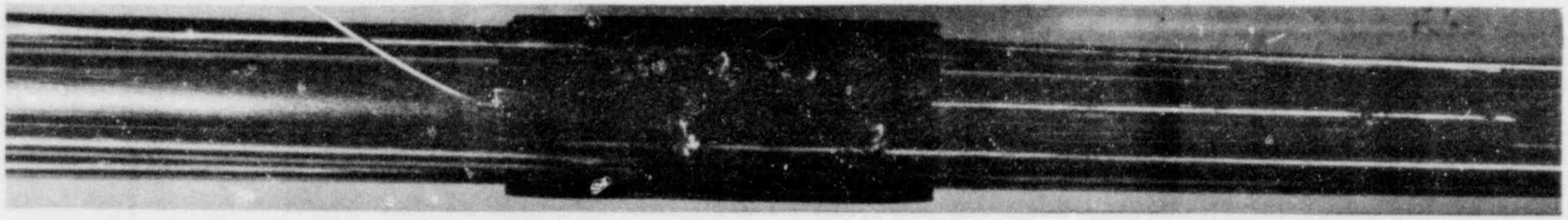

FLOW

79.0

Figure K-8. Steam Probe (Pretest)

16,047-117

-- The steam probe at the 2.01 m (79 in.) elevation failed after a total of 10 cycles. Prior to failure, the steam probe provided consistent temperature data from cycle to cycle, as shown in figures K-9 through K-11.

-- The blockage sleeve thermocouple at the 1.88 m (74 in.) elevation failed after a total of 14 cycles. Prior to failure, the thermocouple provided consistent temperature data from cycle to cycle, as shown in figures K-12 through K-14.

-- The heater rod was subjected to a total of 15 cycles without thermocouple or rod failure. The test was terminated after 15 cycles to inspect and examine the instrumentation.

-- After disassembly of the test section, the blockage sleeves and steam probe were found to be securely attached to the rod and grid, respectively.

Close examination of the heater rod, blockage sleeves, steam probe, and instrumentation after disassembly led to the following observations:

-- The 0.51 mm (0.020 in.) thermocouple lead from the 2.29 m (90 in.) elevation blockage sleeve was burned in two where the lead came into physical contact with the sleeve at the 1.88 m (74 in.) elevation. This is shown in a posttest photograph (figure K-15) taken of the 1.88 m (74 in.) elevation blockage sleeve after disassembly.

-- The thermocouples in the two sleeves and the one in the steam probe were checked for continuity after being removed from the heater rod.

The thermocouple in the sleeve at the 2.29 m (90 in.) elevation was found to be open. It was not possible to determine at what location the thermocouple opened, since the leads could not be exposed. However, the thermocouple junction in the sleeve at the 1.88 m (74 in.) elevation as well as the thermocouple junction in the steam probe at the 2.01 m (79 in.) elevation were found to be intact.

These two thermocouples were then rechecked by heating the tips with a microtorch; they remained intact.

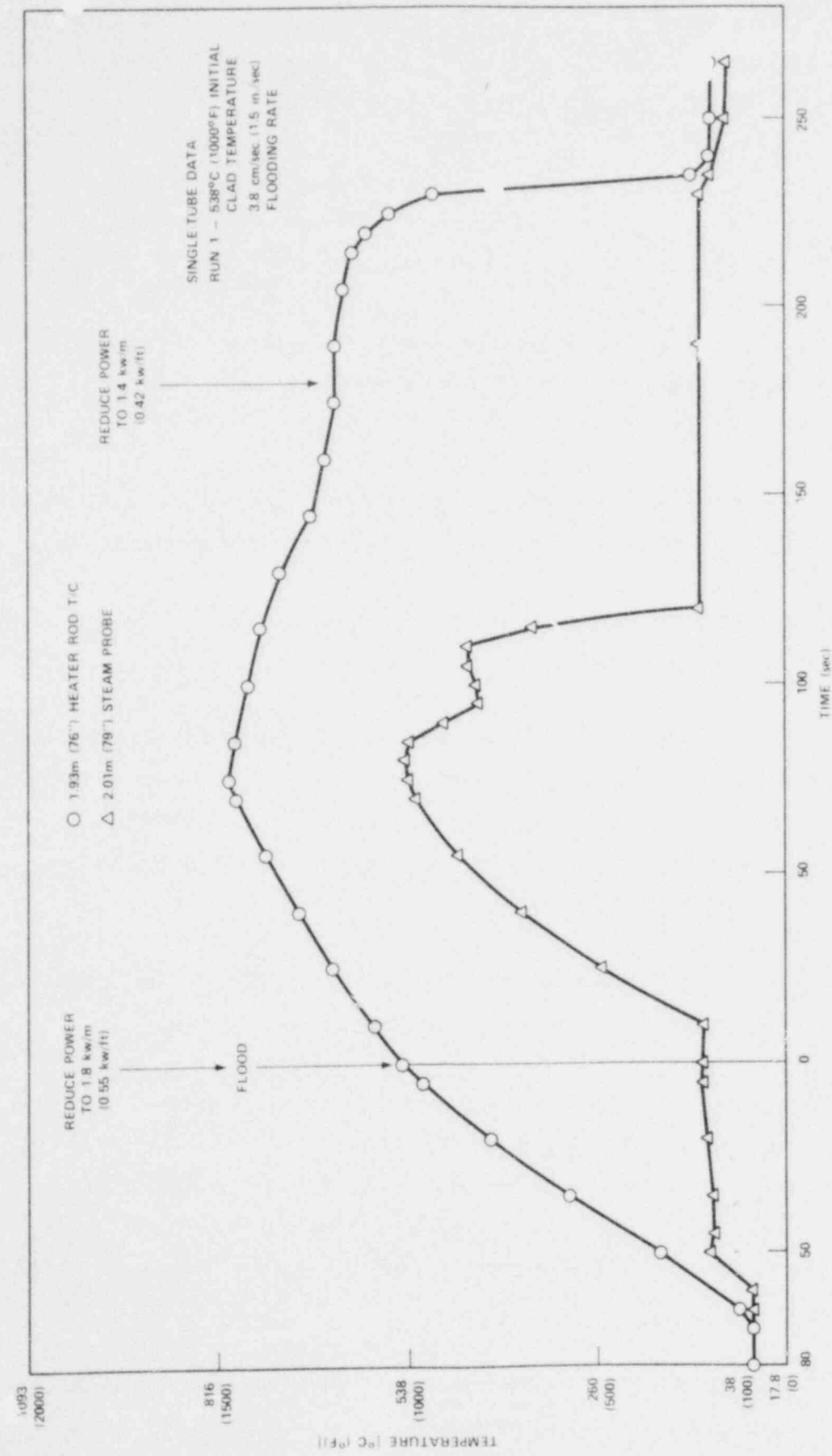

Figure K-9. Single-Rod Test Steam Probe Data, Run 1

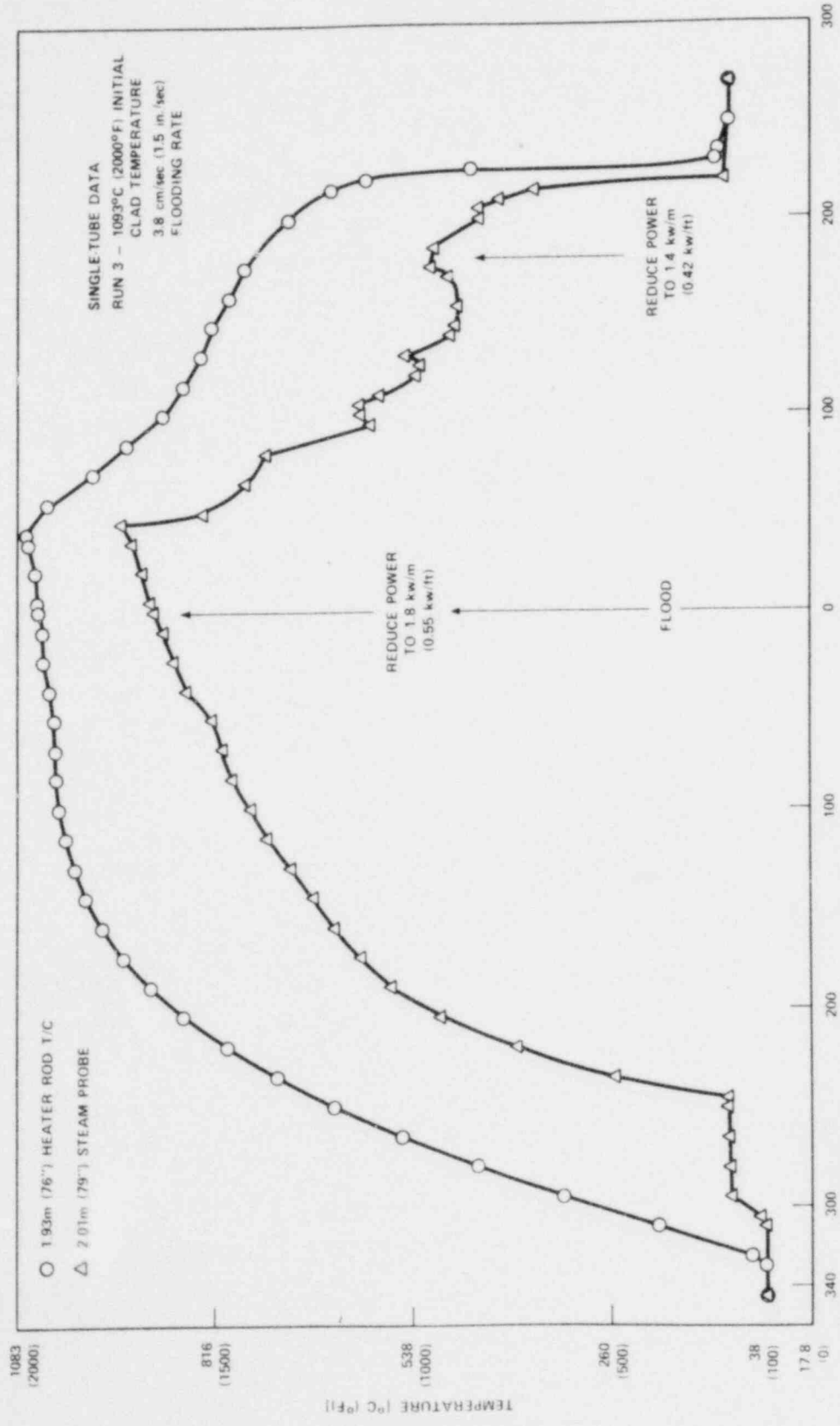

Figure K-10. Single-Rod Test Steam Probe Data, Run 3

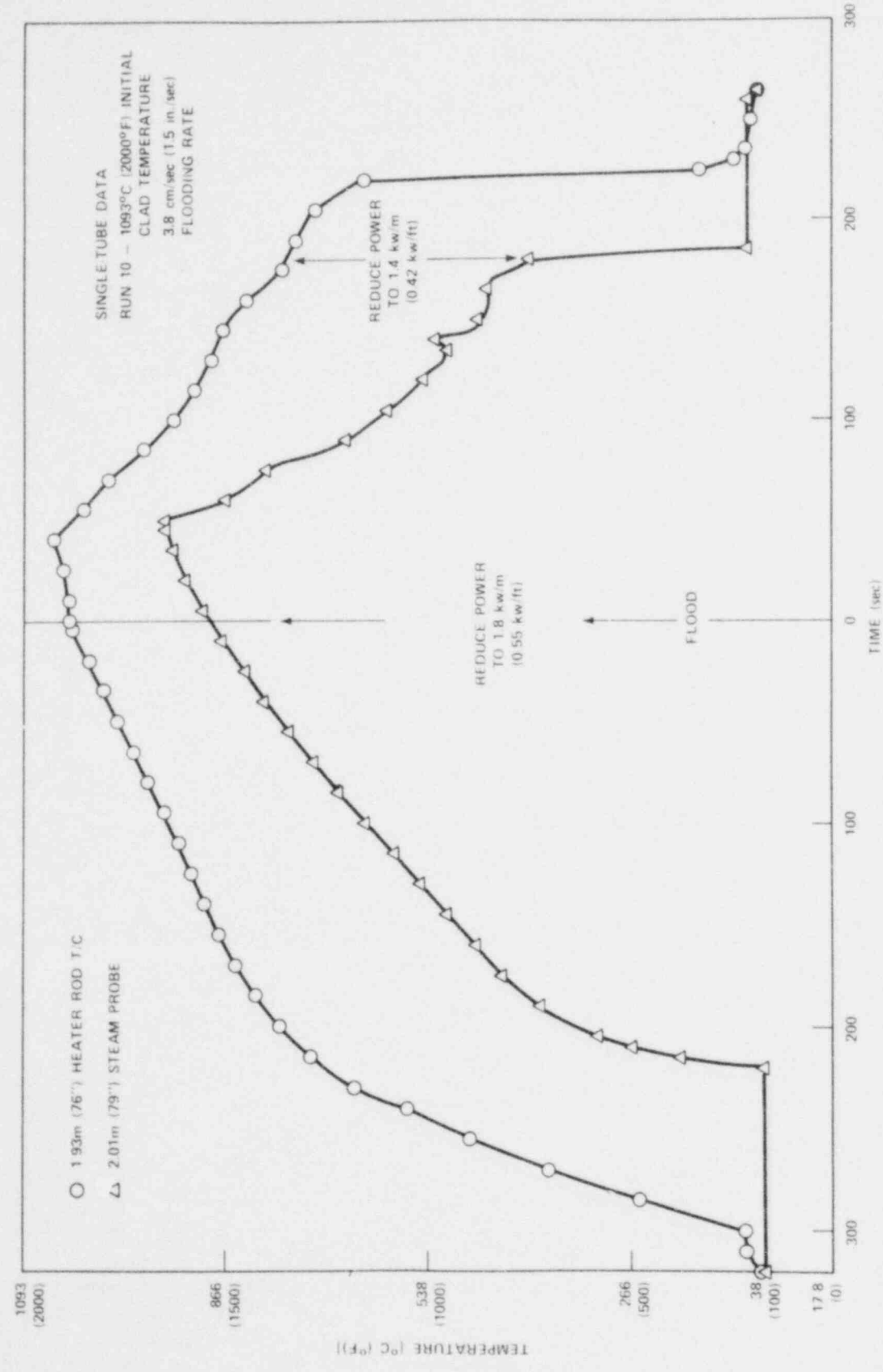

Figure K-11. Single-Rod Test Steam Probe Data, Run 10

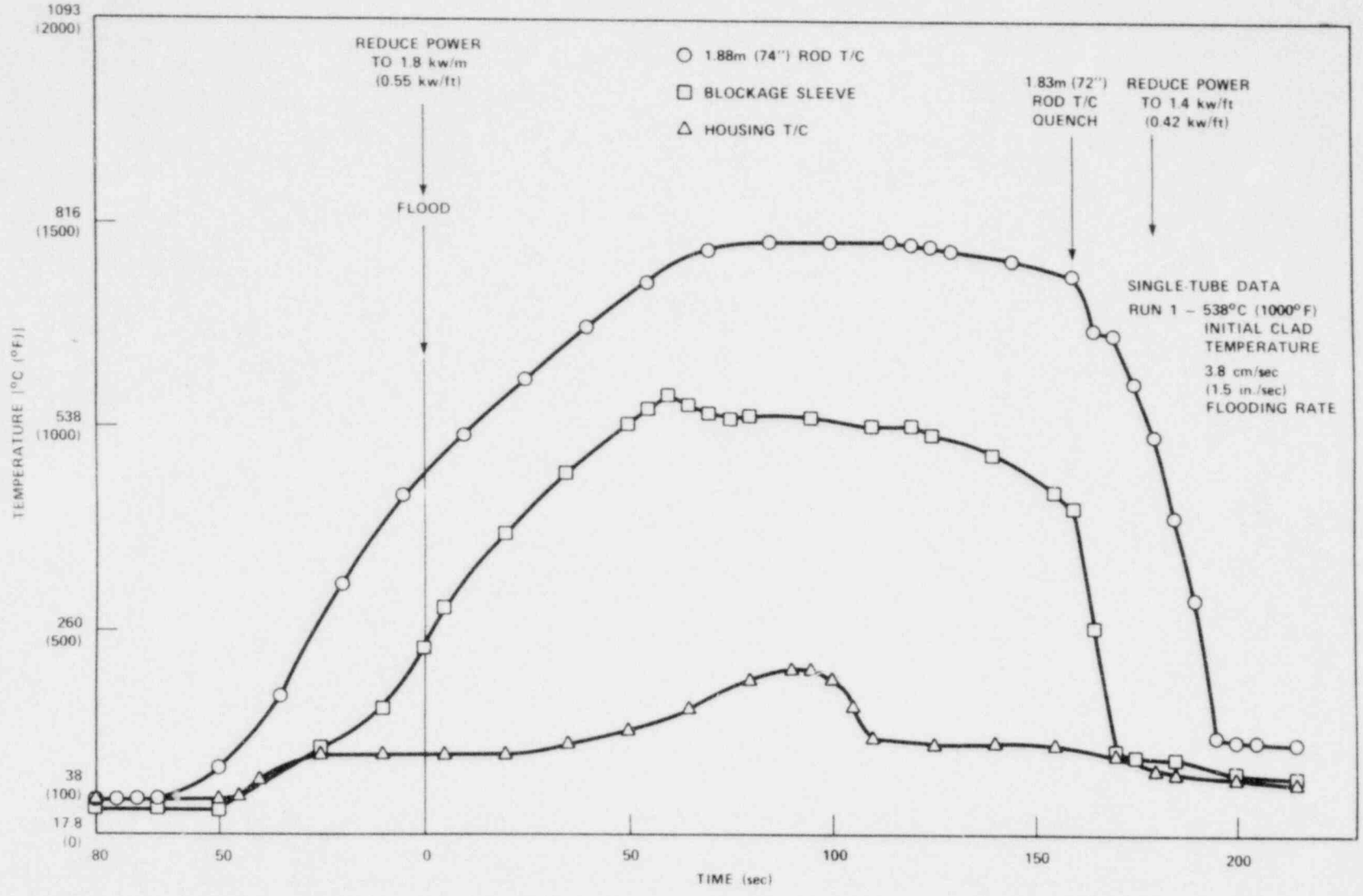

Figure K-12. Single-Rod Test Blockage Sleeve Data, 1.88 m (74 in.) Elevation, Run 1

16,047-10

Figure K-13. Single-Rod Test Blockage Sleeve Data, 1.88 m (74 in.) Elevation, Run 3

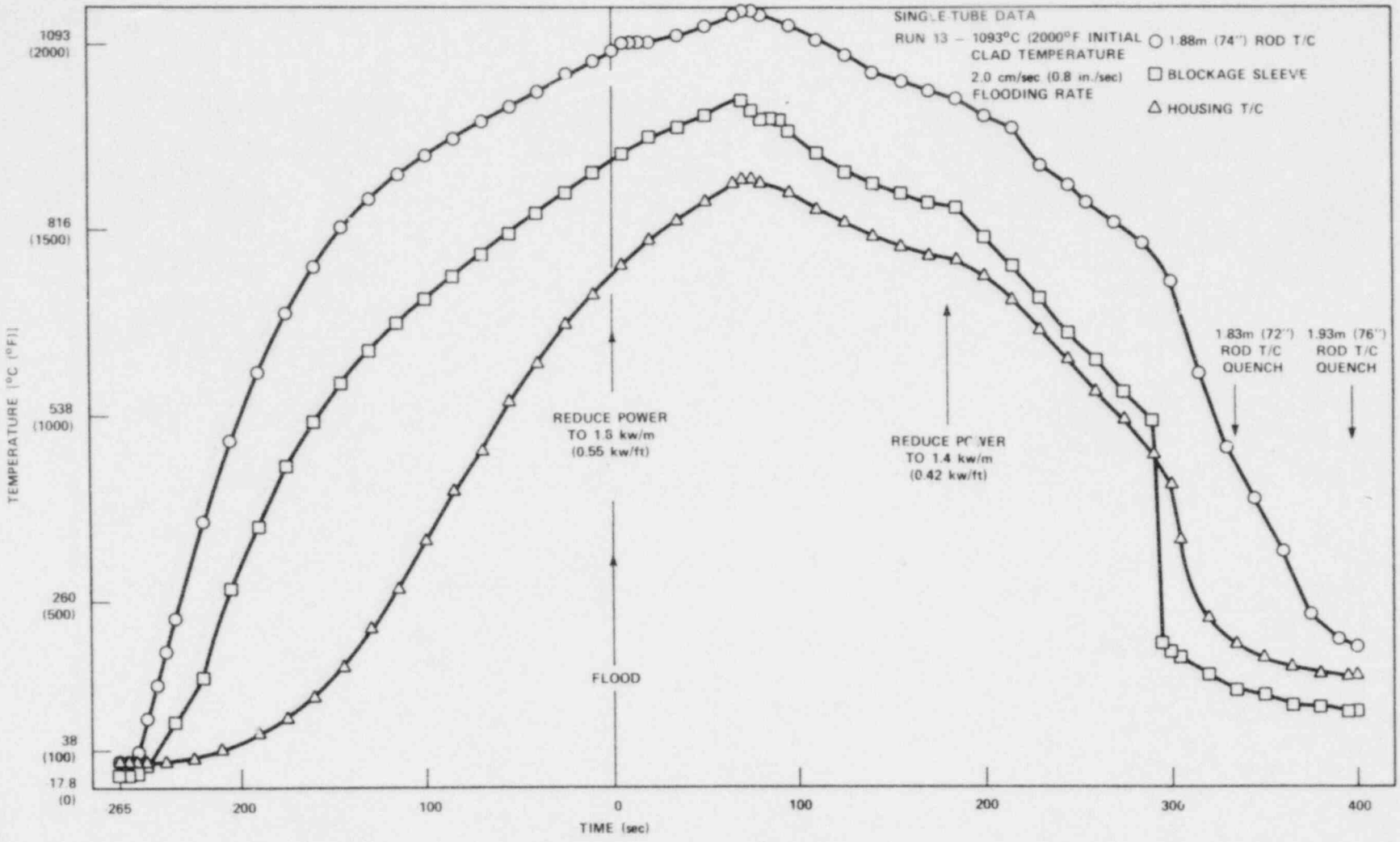

Figure K-14. Single-Rod Test Blockage Sleeve Data, 1.88 m (74 in.) Elevation, Run 13

16,047-12

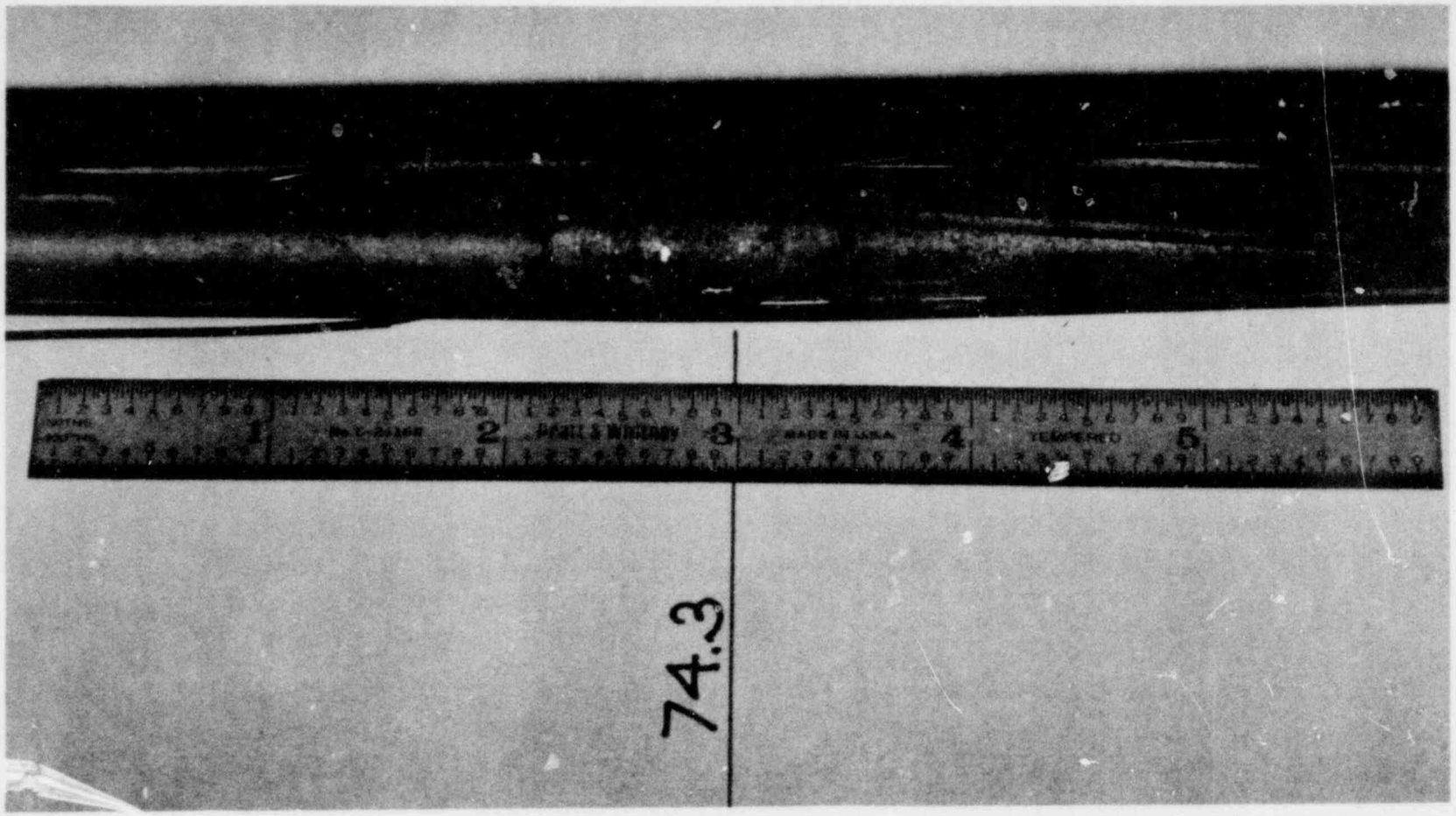

Figure K-15. Blockage Sleeve at 1.88 m (74 in.) Elevation (Posttest)

The lead of the steam probe was then locally heated along its length and an intermittent break[1] was found in the lead approximately 10 cm (4 in.) down from the point where the lead exits the grid. The steam probe and thermocouple lead are shown in a posttest photograph (figure K-16). The break in the thermocouple lead at 10 cm (4 in.) from the top of the grid is attributed to either the lead touching the heater rod and subsequently burning, or a stretching of the lead because of thermal expansion of the rod.

The 1.02 mm (0.040 in.) OD support tube which enclosed the lead for the 1.88 m (74 in.) elevation blockage sleeve thermocouple was also locally heated along its length; no break in the lead was found. It is presumed that the break occurred along the unsupported and unprotected length of the thermocouple lead because of the lead contacting the hot rod.

-- The heater rod did not take a permanent set as a result of this test, and the length and outside diameter did not change.

-- The heater rod moved freely through the bottom O-ring plug and did not bow significantly.

-- The expansion of the heater rod was restricted (perhaps by the sleeve contacting the support rods) during testing; this forced the rod axially out of the clamp at the top end of the housing by 6.98 mm (0.275 in.) (figure K-17).

-- The two sleeves were removed from the heater rod easily with insignificant effect on the heater rod surface.

-- The rod was readily cleaned of scale deposits and the rod color was as shown in figure K-18.

-- One of the 3.18 mm (0.125 in.) diameter support rods moved to within 1.14 mm (0.045 in.) of the steam probe (figure K-19).

---

1. Secondary junction where the two thermocouple wires are not insulated from each other

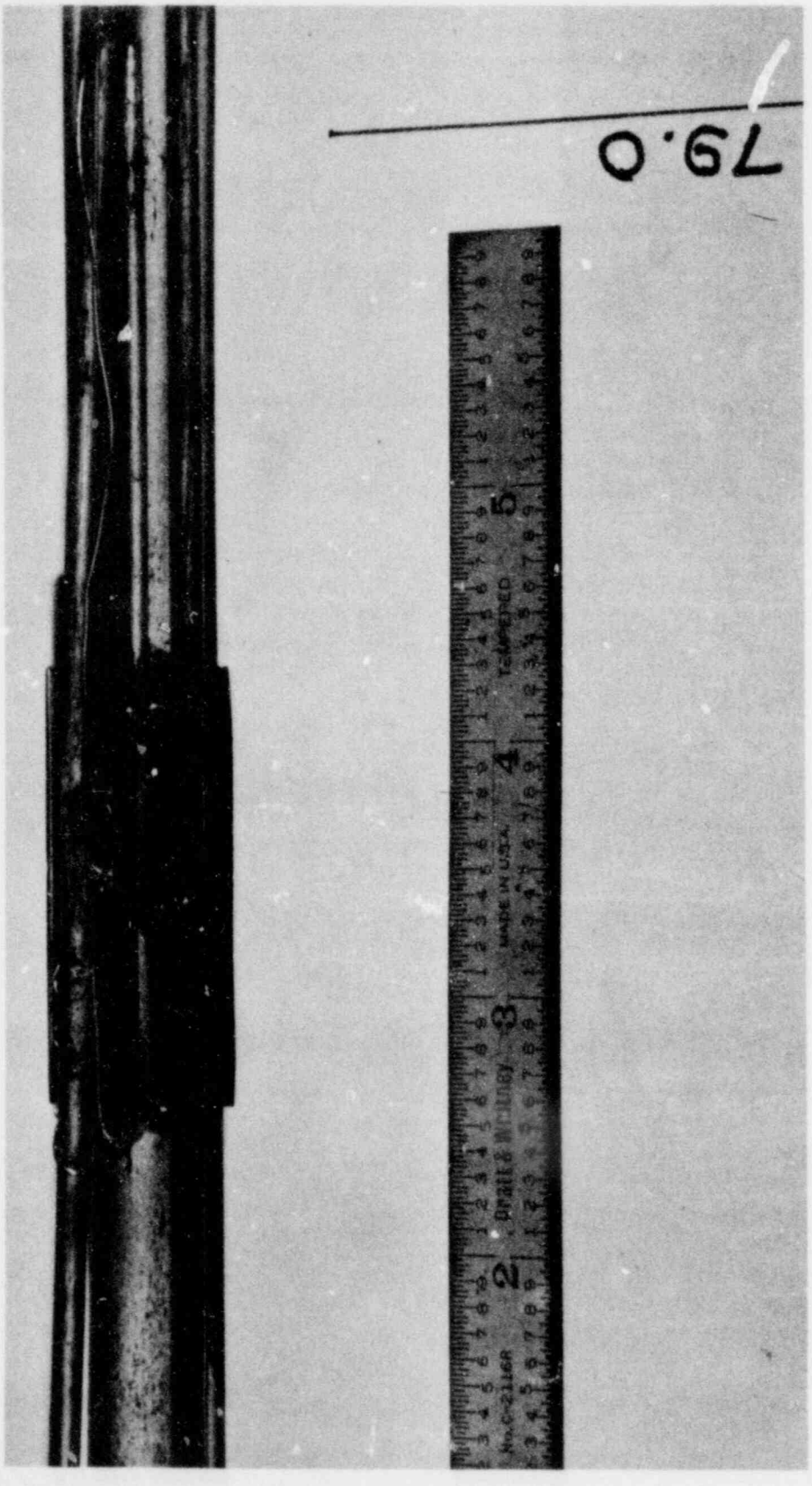

Figure K-16. Steam Probe (Posttest)

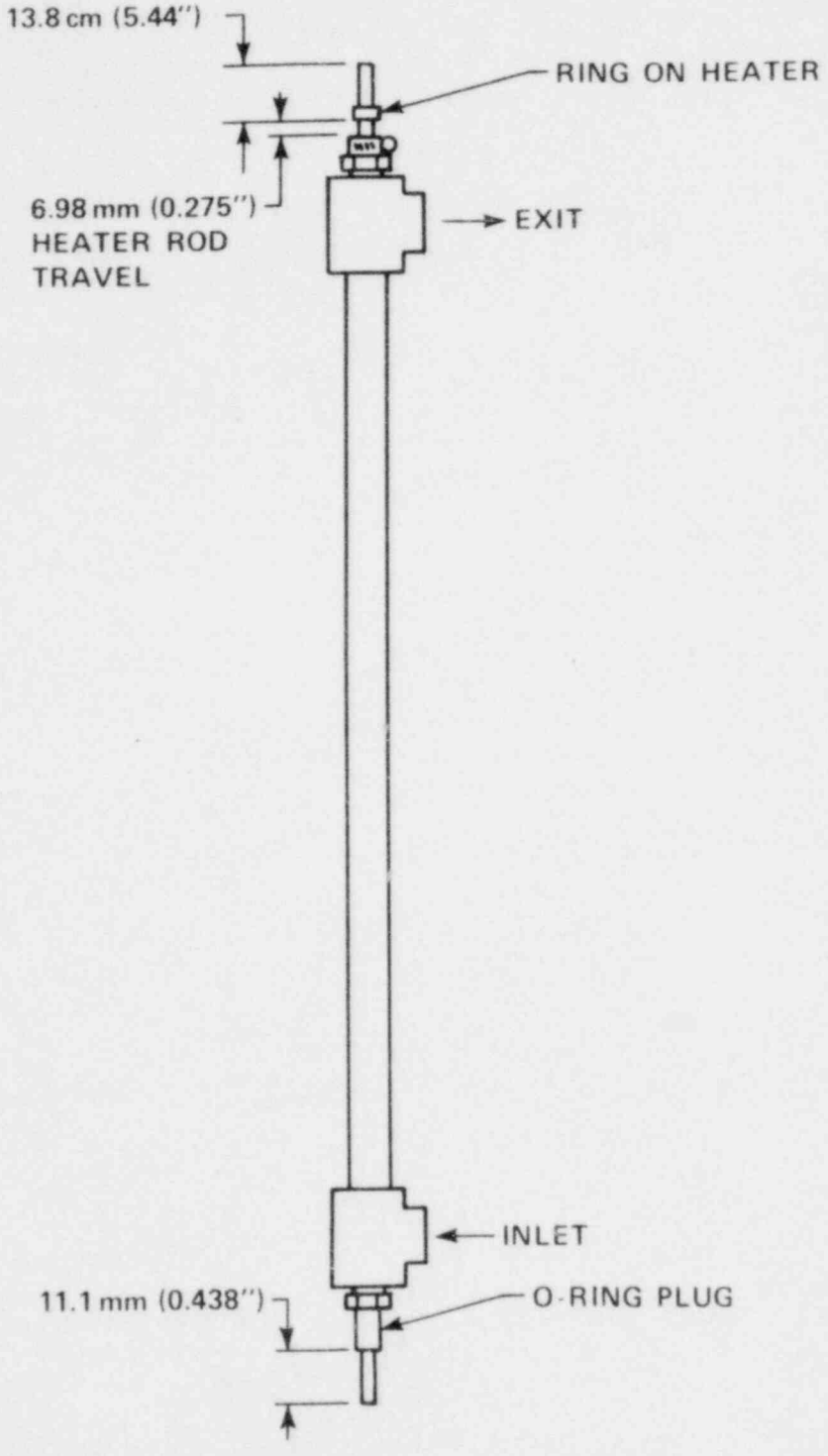

Figure K-17. Heater Rod in Housing Before Disassembly

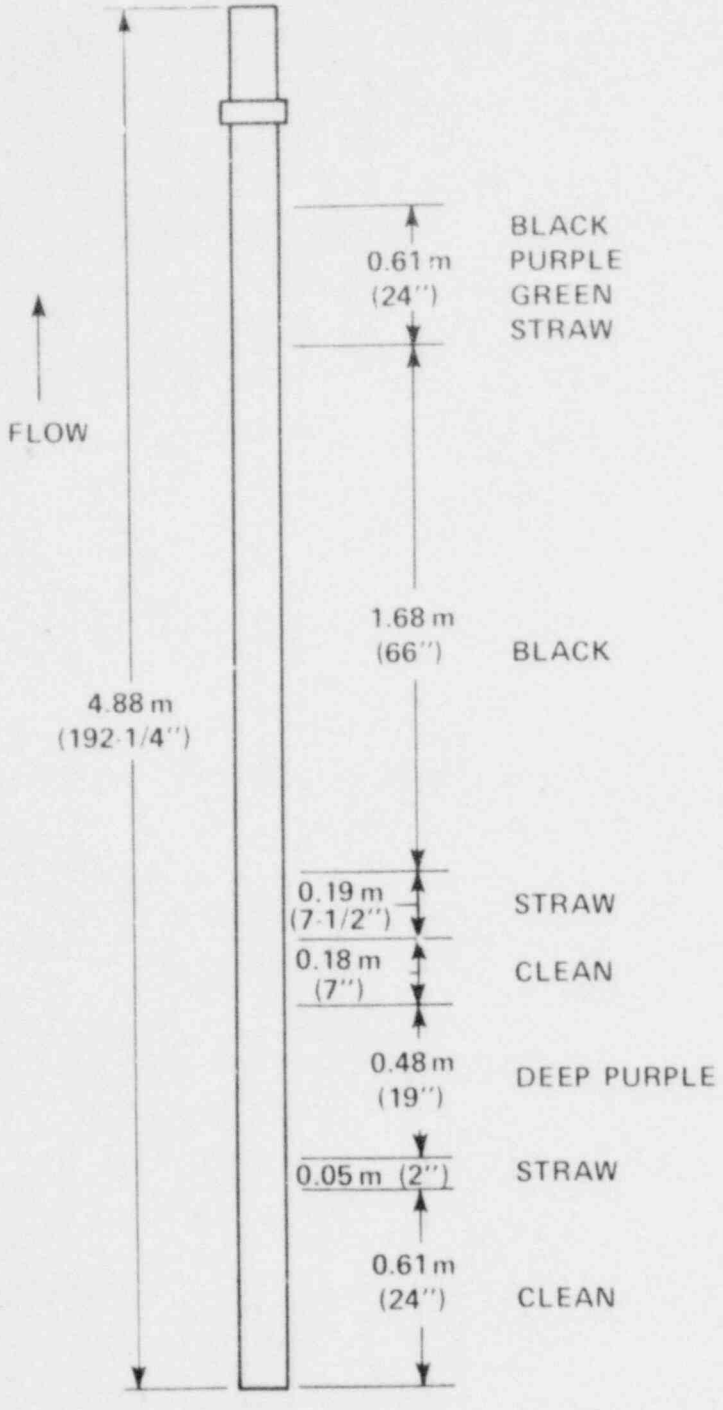

Figure K-18. Heat Flux Shape Indication by Color

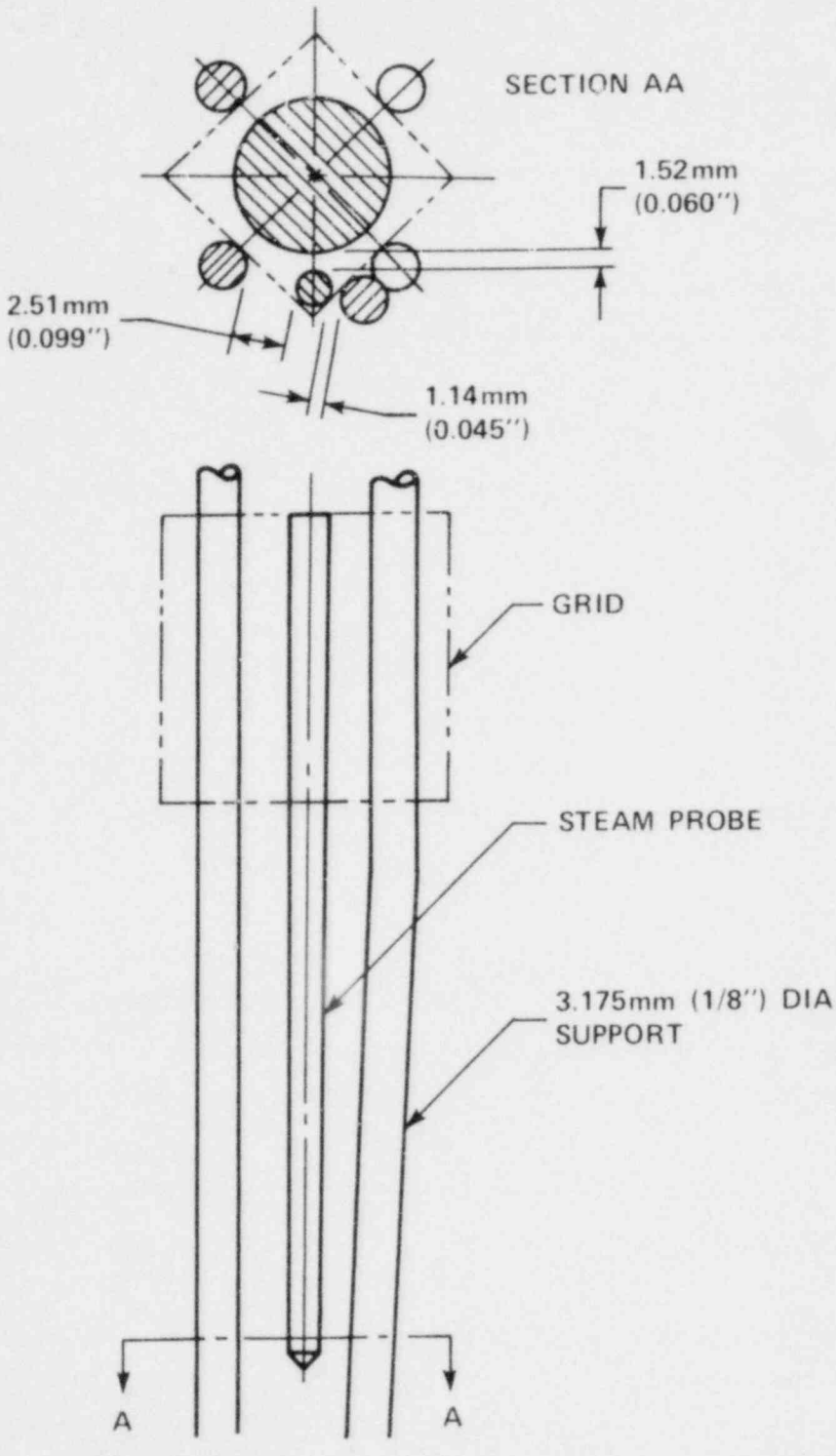

Figure K-19. Steam Probe Position After Test

The following conclusions have been drawn from the examination of the sleeves and instrumentation, and analysis of the data:

-- Both methods of attaching the blockage sleeves to the heater rod are acceptable; however, the method of spot-welding the rod through the hole in the sleeve is preferable, since it is easier to remove the sleeve and clean the rod surface.

-- The blockage sleeve instrumentation and steam probe will not survive the entire matrix of 17 valid tests currently proposed for the bundle. The temperature data for the thermocouples were analyzed based on the integral of the temperature-time curve when the heater rod temperature was above 538°C (1000°F). Predictions were also made to determine the rod bundle integral of the temperature-time curve needed to complete all tests proposed in the test matrix (except for the three steam cooling tests). The steam probe survived 1.28×10^6 °C-sec (2.31×10^6 °F-sec), the 1.88 m (74 in.) elevation blockage sleeve thermocouple survived 2.02×10^6 °C-sec (3.63×10^6 °F-sec), and the heater rod was subjected to 2.24×10^6 °C-sec (4.03×10^6 °F-sec). To complete 14 valid tests out of the 17 proposed matrix tests, the thermocouples in the sleeve and steam probe would have to survive 1.91×10^6 °C-sec (3.44×10^6 °F-sec).

It is believed that the failure mode of the thermocouples is attributable to the physical contact of the 0.51 mm (0.020 in.) thermocouple sheath with either the heater rod or the grid support rods, with the consequential breakdown of the insulation material within the thermocouple sheath.

The following recommendations are made based on the preceding test results, observations, and conclusions:

-- The thermocouple size for both the blockage sleeve and steam probe should be increased from 0.51 mm (0.020 in.) to approximately 0.81 mm (0.032 in.) to minimize burning of the sheath and insulation when contact with a heater rod occurs.

-- The thermocouple sheath material should be changed from stainless steel to Inconel to provide additional strength at elevated temperatures.

-- Another single-rod test should be performed with the prototypical blockage sleeve instrumented as recommended above, including a steam probe. This test would verify the recommended design changes and would ensure the longevity of the bundle instrumentation. [Another test was performed which showed that the 0.81 mm (0.032 in.) Inconel-sheathed blockage sleeve thermocouple performed satisfactorily. The thermocouple lead was routed downstream of the blockage sleeve in the flow subchannel with no effect on the heater rod or blockage sleeve thermal response.]

APPENDIX L
FLECHT SEASET RUN SPECIFICATION AND VALIDATION SHEET

RUN NO. _____ FACILITY ENGINEERING _____

DATE _____ SAFEGUARDS DEVELOPMENT _____

I. HEATER ROD POWER

	Parameter	Specified Value	Actual Value
1.	Initial peak linear power	_____ kw/ft ± 1%	_____ kw/ft
2.	Initial power	_____ kw ± 1%	_____ kw

Note: The power decay should also be ± 1% of specified.

II. INJECTION FLOW

		Specified		Actual	
1.	Injection rate	Rate	Duration	Rate	Duration
	Step 1	_____ gpm	_____ sec	_____ gpm	_____ sec
	Step 2	_____ gpm	_____ sec	_____ gpm	_____ sec
2.	Coolant supply temperature	_____ ^{o}F ± 5^{o}F		_____ ^{o}F	
3.	Initial temperature of coolant injection line	_____ ^{o}F ± 10^{o}F		_____ ^{o}F	
4.	Initial temperature of coolant in lower plenum	_____ ^{o}F ± 10^{o}F		_____ ^{o}F	

III. INITIAL TEST SECTION PRESSURE _____psia ± 5% _____psia

Note: The test section pressure should not vary by more than 1 psia during the test run, except for the first 20 seconds after flood.

IV. HOUSING TEMPERATURES AT FLOOD(1)

1.	2 ft elevation	_____°F
2.	4 ft elevation	_____°F
3.	5 ft elevation	_____°F
4.	6 ft elevation	_____°F
5.	7 ft elevation	_____°F
6.	9 ft elevation	_____°F
7.	11 ft elevation	_____°F

V. LOOP PIPING AND COMPONENT TEMPERATURES

1.	Lower plenum	_____°F ± 10°F	_____°F
2.	Upper plenum	_____°F ± 20°F	_____°F
3.	Carryover tank	_____°F ± 20°F	_____°F
4.	Steam separator	_____°F ± 20°F	_____°F
5.	Steam separator collection tank	_____°F ± 20°F	_____°F
6.	Exhaust pipe		
	a) Upstream of separator	_____°F ± 20°F	_____°F
	b) Downstream of separator	_____°F ± 20°F	_____°F

Note: Temperature should be an average of working thermocouples, but each thermocouple should be within limits.

---

1. Location E, figure 7-6 (Drawing 1460E40)

VI. DACPF INITIALIZATION

1.	Maximum acceptable temperature	_____ ^{o}F
2.	Maximum test time	_____ sec
3.	Slow scan time	_____ sec
4.	Flood temperature	_____ ^{o}F
5.	Power decay delay	_____ sec
6.	Delta T time	_____ sec
7.	Termination temperature	_____ ^{o}F
8.	Defective temperature	_____ ^{o}F

VII. DRPF INITIALIZATION

1.	Maximum power	_____ kw/ft
2.	Sink temperature	_____ ^{o}F

VIII. SPECIAL COMMENTS ON RUN CONDITIONS

IX. CONDITIONS CAUSING RUN TERMINATION

X. CONDITIONS CAUSING RUN TO BE INVALID

XI. INSTRUMENTATION FAILURES

XII. GENERAL COMMENTS ON TEST RUN

XIII. PRELIMINARY RESULTS

1. Hottest thermocouple channel at turnaround

Thermocouple Elevation	Initial Temperature at Flood	Maximum Temperature	Flood Time	Turnaround Time	Quench Time
____ft	____°F	____°F	____sec	____sec	____sec

2. Drained water weights

Carryover tank	____lbm	at ____°F
Steam separator and collection tank	____lbm	at ____°F
Exhaust steam probe tank No. 1	____lbm	at ____°F
Exhaust steam probe tank No. 2	____lbm	at ____°F
Exhaust steam probe tank No. 3	____lbm	at ____°F
Test section	____lbm	at ____°F

XIV. HEATER ELEMENT INSULATION RESISTANCE CHECK

Heater No.	Prior to Test	Posttest

APPENDIX M
DATA REDUCTION AND ANALYSIS COMPUTER PROGRAMS

M-1. GENERAL

This appendix contains details of the various computer programs which will be used to reduce and analyze the test data from this task. The flow logic diagram for the data reduction methods, shown in figures 9-1 and 9-2, is repeated here as figures M-1 and M-2. Each code is discussed in detail below.

M-2. FVALID PROGRAM

The program FVALID provides a printout for the test run specification and validation sheet (appendix L). The validation sheet is a specific listing of the data recorded by the PDP 11/20 computer during a test, 1 second before flooding. The listing of these data is used to compare specified values and actual values for the following quantities:

-- Heater rod power
-- Injection flow
-- Initial test section pressure
-- Flow housing temperature
-- Loop piping and component temperatures

This information is used to determine run validity.

M-3. FLOOK PROGRAM

The FLOOK program permits the examination of selected analog/digital data from a FLECHT run. Data are taken directly from the disk file on the PDP 11/20 and printed in engineering units. Ten channels may be examined in one pass.

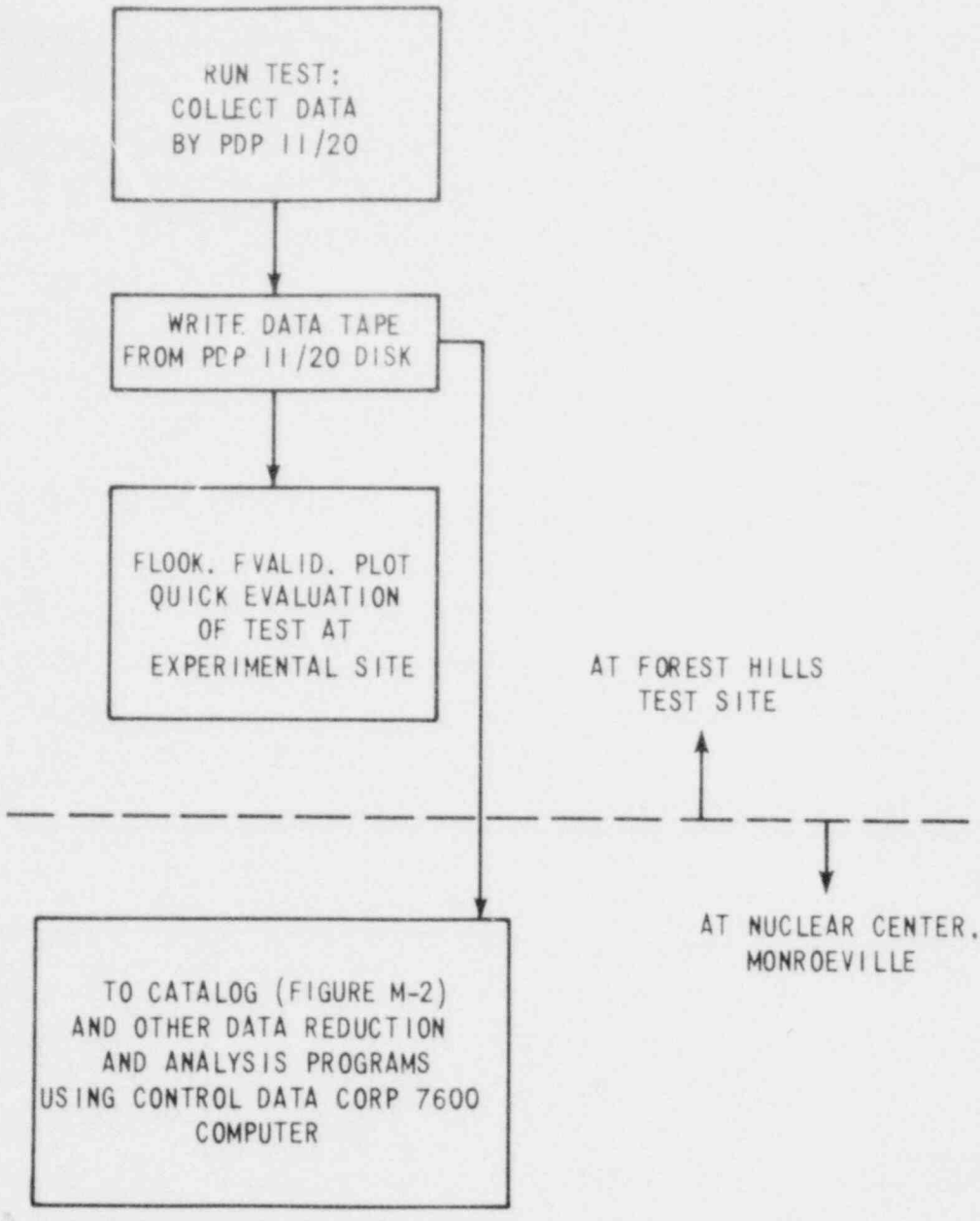

Figure M-1. Flow Logic of Computer Codes

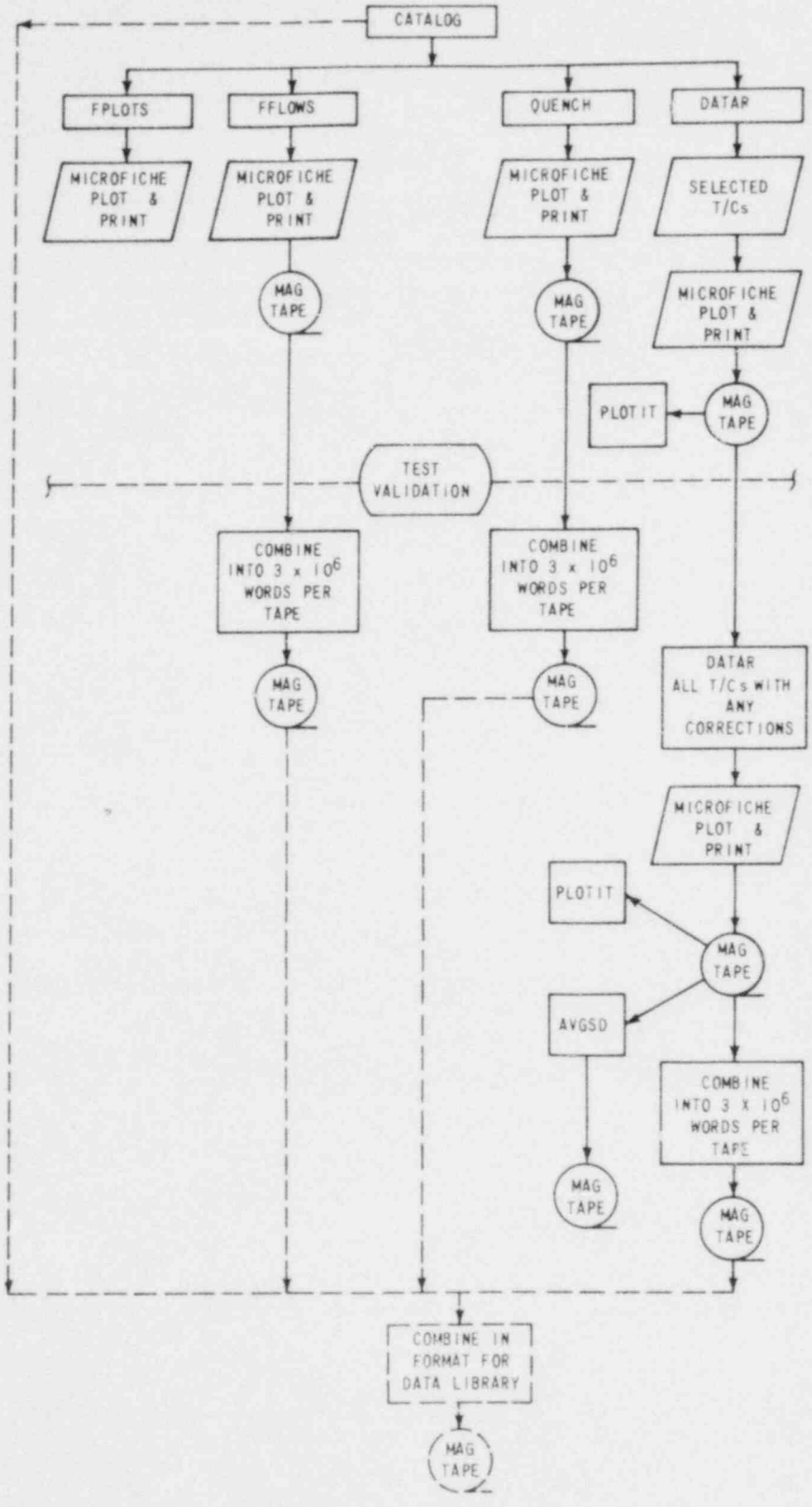

Figure M-2. FLECHT SEASET Data Reduction Flow Chart

M-4. PLOT PROGRAM

PLOT is a program which manipulates data that have been stored on the disk such that the necessary conversion, scaling, and formatting of data for the PLOT-10 package is accomplished. PLOT information is entered thrcugh the Tektronix 4010, which specifies the graphic fun tions to be performed. A dialog exists between the operator and computer in a question/answer format. Once the dialog has been completed, a "Y" response to the "Run" command will cause plotting of the desired data. This information is also used in the da' ı validation procedure.

M-5. CATALOG PROGRAM

CATALOG is the common name for two programs linked in series: FASTDRP and MAKEBIN. The purpose of CATALOG is to reduce data recorded at the test site to a form that is compatible with the Control Data Corporation (CDC) 7600 system at the Westinghouse Nuclear Center.

FASTDRP takes input from the PDP-11/20 system and converts it to the 60-bit-per-word CDC system. These data are then stored in updated form.

MAKEBIN, using the updated tape, corrects the appropriate channels for instrument shift. The data are then written in a compact form enabling 10 runs to be stored on each tape. (That is, each 60-bit word is converted into 30-bit words, and then two 30-bit words are stored per 60-bit word.)

The output is as follows:

-- Raw data in updated form

-- Calibration file

-- Time array (1 sec -- 0.5 sec -- 1 sec)

-- Bad channel list

-- Data from each of 309 channels

M-6. FPLOT PROGRAM

FPLOT is a code that presents FLECHT data in tabular and graphic form, using engineering units.

FPLOT has several options for graphical output, as follows:

-- Plot any or all data with a predetermined scale or one that is supplied as test conditions warrant

-- Plot any portion of a transient

-- Multiplot up to four curves

Input to this code consists of data from all channels connected to the computer for a given test.

M-7. QUENCH PROGRAM

The QUENCH program determines key quantities associated with heatup and quenching of the heater rod bundle in the FLECHT facility. The quantities determined from QUENCH are heatup rates, initial temperature, turnaround temperature, turnaround time, quench time, and quench temperature. Statistical computations are performed for each quantity to determine maximum, minimum, mean, and standard deviation.

Standard criteria are used to determine rod quench time and temperature. These criteria reduce the possibility of error and the injection of an individual's judgment into the computations. The criteria for heater rod quench are as follows:

-- A slope greater than $10^{o}C$/sec ($50^{o}F$/sec) and a temperature greater than $149^{o}C$ ($300^{o}F$). A larger value of slope tends to call any thermocouple noise a quench and a smaller slope tends to miss the quench altogether.

-- If the first criterion is not satisfied the first time the thermocouple reaches saturation temperature.

The PDP 11/20 computer records data from the initiation of heatup sequence, during which the bundle is pulsed, on through reflood. The time scale is shifted such that time = 0 sec corresponds to the beginning of reflood. The heatup period prior to reflood is then rescaled with negative times. The QUENCH program linearly interpolates temperature data to determine the rod initial temperature at time = 0.

In most cases rods do not start to heat up at the same time the computer starts to scan channels. In these cases a time and temperature at the beginning of heatup is calculated. It is assumed that heatup begins when the first 1.1°C (2°F) difference is seen between any two consecutive scans of thermocouples. Heatup rates are found by calculating an average time and temperature over a given time increment. This heatup rate in degrees per second can be used to determine if the correct power is being supplied to the bundle through an energy balance calculation. A more detailed explanation of the QUENCH criteria and assumptions is contained in WCAP-8651[1] and WCAP-9108.[2] For each valid thermocouple measurement, the output from QUENCH is as follows:

-- Heatup rates

-- Initial temperature

-- Turnaround temperature

-- Turnaround time

-- Quench time

-- Quench temperature

---

1. Rosal, E. R., et al., "FLECHT Low Flooding Rate Cosine Test Series Data Report," WCAP-8651, December 1975.

2. Rosal, E. R., et al., "FLECHT Low Flooding Rate Skewed Test Series Data Report," WCAP-9108, May 1977.

M-8. FFLOWS PROGRAM

The program FFLOWS calculates mass flow rate and mass storage for the FLECHT test section and accompanying loop components. A calculation of the fraction of inlet mass leaving the bundle is performed based on two criteria: (1) mass stored in the test section and (2) mass leaving the test section. An overall system mass balance is performed to account for system losses.

This mass balance takes into account the total mass stored in the test section, the total mass leaving the test loop, and the total mass remaining in the loop after the test. The steam probe collection tanks, upper plenum, and steam separator tank account for the mass remaining after the test. This sum is compared with the total measured mass (M) injected to obtain a mass balance. That is

$$\Delta M = \frac{\Sigma M_{injected} - \left(\Sigma M_{\substack{stored\ in \\ bundle}} + \Sigma M_{out} + \Sigma M_{\substack{stored\ in \\ loop}} \right)}{\Sigma M_{injected}}$$

The total mass injected is taken from the inlet turbine meter data. The collected liquid is calculated from the liquid collection tank differential pressure cells assuming saturated liquid conditions. The steam flow is calculated from the orifice meter differential cell using the measured steam temperature and local pressure to obtain a steam density. Mass stored in the test section is calculated from the 0-3.66 m (0-12 ft) differential pressure cell after a correction has been made for frictional pressure drop.

Calculations are also performed to find the average void fraction using the measured pressure drop over each 0.3 m (1 ft) section of the bundle. The measured pressure drop consists of three effects: elevation head, frictional pressure drop, and acceleration drop due to vapor generation. That is,

$$\Delta P_{measured} = \Delta P_{elevation} + \Delta P_{acceleration} + \Delta P_{friction}$$

WCAP-8238[1] and WCAP-9108[2] contain detailed descriptions of the frictional pressure drop, measured pressure drop, and void fraction calculations.

Output from FFLOWS is presented both in tabular and graphical form. The following is a list of output quantities from FFLOWS:

-- Two-phase pressure drop

-- Void fraction

-- Two-phase density

-- Two-phase mass storage

-- Two-phase frictional pressure drop

-- Overall pressure drop 0-3.66 m (0-12 ft)

-- Overall mass storage 0-3.66 m (0-12 ft)

-- Mass difference

-- Mass in upper plenum

-- Accumulator mass loss

-- Mass injected into bundle (total and rate)

-- Mass stored in bundle (total and rate)

-- Mass out of bundle (total and rate)

-- Mass difference (total and rate)

---

1. Blaisdell, J. A., et al., "PWR FLECHT SET Phase A Report," WCAP-8238, December 1973.

2. Rosal, E. R., et al., "FLECHT Low Flooding Rate Skewed Test Series Data Report," WCAP-9108, May 1977.

-- Carryout fraction (total and rate)

-- Test section mass (total and rate)

-- Carryover tank mass (total and rate)[1]

-- Steam separator mass (total and rate)

-- Exhaust orifice mass (total and rate)

-- Overall mass balance

-- Lower bound quality

-- Upper bound quality

M-9. DATAR PROGRAM

The purpose of the DATAR program is to calculate the heat transfer coefficient and wall heat flux for heater rods in the FLECHT SEASET facility from temperature data (as read from the CATALOG tape), as-built heater rod dimensions, and an inverse conduction mathematical model. The DATAR code consists of 13 overlays, to reduce the computer field length required for code execution. These overlays consist of the following:

-- The main program overlay, together with those subroutines necessary to calculate film coefficients

-- The overlay which controls the reading and checking of input data, both from cards and from tape

-- The overlay which checks for restart and, if present, properly positions input and output files and sets internal values

---

1. Based on both mass stored and mass out

-- The overlay which reads input information from the main data tape header and calculates several internal values based on this information.

-- The overlay which checks cards input consistency and echoes the information to printed output.

-- The overlay which echoes data tape leader information to printed output

-- The overlay which reads iunput from cards and performs miscellaneous operations on the data

The program provides it sown dynamic field length management, resulting in minimum operating expense

With the exception of plotting, the main program controls the flow of all input and output data read and generated by the program. A typical DATAR program is conducted using the following steps:

(1) Calculate heater rod material radial node positions based on as-built radii and power step interval information. Note that the code performs one-dimensional calculations in the radial direction only. Axial conduction is ignored.

(2) Calculate appropriate time values for each data point produced. The calibration file values are read by means of a call to the second overlay.

(3) Enter heater information on the output tape (run number, number of data scans, and the like). Read data tapes and position correctly. Calculate bundle power. The sink temperature is assumed to be the saturation temperature corresponding to the specified pressure for the test.

(4) Read temperature data for a rod thermocouple from the main data tape and miscellaneous information for that thermocouple (such as bundle position and axial and radial power factors) from a secondary data tape.

(5) Determine if a thermocouple is good. This is true if its channel number is not included in the bad channel list and the first temperature is greater than

65.6°C (150°F). If these two criteria are not met, a short entry is made on the output tape and data from the next channel are read.

(6) Calculate rod temperature profiles, surface heat flux, and heat transfer coefficients by successively calling data reduction subroutines in the model. The number of future temperatures used is determined by the shape of the temperature-versus-time curve at the next time. This number is constrained to be between 1 and 3, and may be different from the previous value by no more than 1.

(7) Enter data results of calculations performed in step (6) on output. Plot clad temperature and heat transfer coefficient using a call to the third overlay.

(8) Repeat steps (4) through (7) for all bundle thermocouple channels and terminate data reduction.

DATAR uses four principal subroutines. The function of each of these is as follows:

(1) To calculate the coefficient matrix (solution-to-simultaneous equation set)

(2) To calculate the temperatures and surface heat flux given the coefficient matrix

(3) To invert the tridiagonal coefficient matrix

(4) To smooth surface heat flux and heat transfer coefficient over a 10-second time window

Several other subroutines perform miscellaneous calculations, such as material property evaluation and data interpolation.

M-10. AVGSD PROGRAM

AVGSD is a statistical program used to evaluate the large volume of data produced by DATAR. Calculations are performed to obtain a time-dependent mean; one standard deviation, maximum, and minimum for the measured temperature;

calculated surface temperature; heat flux; and heat transfer coefficient. This calculation is performed at each elevation for which valid data exist. In addition, at each elevation the data are grouped into power zones. Input to this program consists of the output tape from DATAR.

The quantities below are output from AVGSD in both graphical and tabular form for measured temperature, heat flux, and heat transfer coefficients:

-- Time

-- Group (a given set of heater rod thermocouples at an elevation)

-- Average

-- Standard deviation

-- Maximum

-- Channel number from which maximum value came

-- Minimum

-- Channel number from which minimum value came

M-11. ALLTURN PROGRAM

ALLTURN computes heat transfer coefficients based on distance above the quench front. This is accomplished in two ways: (1) using reduced experimental data output from the QUENCH and DATAR programs and (2) using a FLECHT-type empirical correlation based on run conditions.

When DATAR results are reduced, thermocouples within an inner rod array are used for a uniform radial power distribution. When the power is a FLECHT radial distribution only, the high-power (1.1 power factor) rods within the same array are used to eliminate any effects caused by the housing. At each time of interest, a quench elevation is determined from the QUENCH code output. The difference

between this elevation and the elevation of interest is the distance above the quench front. Average heat transfer coefficients at each time and elevation are calculated. These experimental results are compared with predicted heat transfer coefficients calculated by a trial correlation. A detailed description of this correlation and comparisons are contained in WCAP-9183.[1]

M-12. FLEMB PROGRAM

FLEMB performs a mass and energy balance on the FLECHT bundle. Input is taken from DATAR, FFLOWS, and CATALOG output tapes. FLEMB consists of a main program and two principal subroutines. The main program controls the input, the output, and the user-selected method by which local mass flow, local quality, and local enthalpy are calculated. The local mass options are as follows:

-- Without mass storage above quench front based on mass stored in the bundle

-- Without mass storage above quench front based on mass out of the bundle

-- With mass storage above quench front based on mass stored in the bundle

-- With mass storage above quench front based on mass out of the bundle

The basic equation for calculating the local mass flow at any differential pressure cell location i corresponding to 0.305, 0.610, 0.914, . . . 3.66 m (1, 2, 3, . . . 12 ft) is

$$\dot{m}_i = \dot{m}_{i-1} - \frac{d}{dt}\left(m_{\text{stored } i-1,\, i}\right)$$

Local enthalpy options are as follows:

-- Without mass and energy storage above quench front

-- With mass and energy storage above quench front

---

1. Lilly, G. P., et al., "PWR FLECHT Skewed Profile Low Flooding Rate Test Series Evaluation Report," WCAP-9183, November 1977.

The basic equation for calculating local quality is

$$h(z) = xh_v(z) + (1-x)h_f(z)$$

where h(z) is the local enthalpy [refer to equation (M-1) below].

Local vapor temperatures supplied by the steam probes are used to calculate a local nonequilibrium quality.

A detailed description and examples of code output are contained in WCAP-9183.[1]

The functions of the two subroutines are as follows:

-- To integrate heat flux data to find the heat release from the quench front to the 3.66 m (12 ft) elevation. The basic form of the equation is

$$m_{\text{bundle exit}}\left(h_{\text{bundle exit}} - h(z)\right) = \int_{z}^{\text{bundle exit}} Q'dz \qquad \text{(M-1)}$$

where Q' = bundle heat release rate per foot

-- To extract needed data from input and arrange it into the form needed by the program

Calculations within FLEMB are based on the following assumptions:

-- Quasi-steady state

-- Liquid at saturation temperature

-- Negligible stored energy within a low-mass housing

---

1. Lilly, G. P., et al., "PWR FLECHT Skewed Profile Low Flooding Rate Test Series Evaluation Report," WCAP-9183, November 1977.

Output from FLEMB is in tabular and graphical form as follows:

-- Mass flow rate

-- Enthalpy

-- Local quality

-- Equilibrium quality

-- Vapor temperature

-- Rod wall temperature

-- Local Reynolds number

-- Void fraction

-- Hot rod heat flux

-- Radiation heat flux

-- Nusselt number

-- Total integrated heat flow

-- Net heat flow to drops

M-13. HEAT-II PROGRAM

HEAT-II calculates the heat transfer to the entrained liquid droplets and the steam, using the method of Sun, et al.,[1] along with a dynamic droplet model[2] developed in the FLECHT program.

---

1. Sun, K. H., et al., "Calculations of Combined Radiation and Convection Heat Transfer in Rod Bundles Under Emergency Cooling Conditions," Trans. Amer. Soc. Mech. Engrs. 98, Series C, 414-416 (1976).
2. Lilly, G. P., et al., "PWR FLECHT Skewed Profile Low Flooding Rate Test Series Evaluation Report," WCAP-9183, November 1977.

Input to HEAT-II is generated by the FLEMB program. This input includes mass flow rates, quality, steam temperature, wall temperature, and hot rod heat flux. When appropriate, a linear interpolation model is used to obtain the desired data. The calculations within HEAT-II are based on the following assumptions:

-- Quasi-steady state

-- Constant system pressure

-- Liquid at saturation conditions

-- Positive droplet velocity and acceleration

-- Slip (or void fraction) given at quench front

A typical run contains the following steps:

(1) Calculate initial drop size.

(2) Calculate slip and droplet volumetric density.

(3) Determine the effect of initial void on slip.

(4) Calculate the radiation to vapor and drops using the method of Sun, et al.

Output from HEAT-II contains the following quantities:

-- Droplet diameter

-- Droplet number density

-- Droplet velocity

-- Droplet Reynolds number

-- Droplet Weber number

-- Vapor velocity

-- Slip ratio

-- Void fraction

-- Rod heat flux

-- Wall-to-vapor radiation heat flux

-- Wall-to-droplet radiation heat flux

-- Surface-to-surface radiation heat flux

-- Wall-to-vapor convection heat flux

-- Heater rod wall-to-vapor heat transfer coefficient

-- Vapor Nusselt number

-- Quality

-- Heater rod wall temperature

-- Steam temperature

NRC/EPRI/WESTINGHOUSE REPORT NO. 5
EXTERNAL DISTRIBUTION

Dr. L. S. Tong, Assistant Director
Water Reactor Safety Research
Division of Reactor Safety Research
U.S. Nuclear Regulatory Commission
Washington, DC 20555

Dr. H. Sullivan
Division of Reactor Safety Research
U. S. Nuclear Regulatory Commission
Washington, DC 20555

A. L. M. Hon
Separate Effects Research Branch
U. S. Nuclear Regulatory Commission
Washington, DC 20555

K. V. Morton, Chief
Research Contracts Branch
Division of Contracts
U. S. Nuclear Regulatory Commission
Washington, DC 20555

D. E. Solberg
U. S. Nuclear Regulatory Commission
Washington, DC 20555

Mr. Wayne Hodges
U. S. Nuclear Regulatory Commission
DSS
Washington, DC 20555

Dr. J. H. Holderness
Combustion Engineering, Inc.
Nuclear Power Department
P. O. Box 500
Windsor, CT 06095

Dr. D. A. Powers
U. S. Nuclear Regulatory Commission
DSS
Washington, DC 20555

Dr. B. Bingham
Babcock & Wilcox Company
P. O. Box 1206
Lynchburg, VA 24505

Mr. W. Kayser
Exxon Nuclear
2101 Horn Rapids Road
Richland, WA 99352

Mr. G. E. Wilson (TSB)
EG&G Idaho, Inc.
P. O. Box 1625
Idaho Falls, ID 83401

J. A. Dearien
EG&G Idaho, Inc.
P. O. Box 1625
Idaho Falls, ID 83401

P. North
EG&G Idaho, Inc.
P. O. Box 1625
Idaho Falls, ID 83401

Mr. G. Sozzi
General Electric Co.
175 Curtner Avenue
San Jose, CA 95125

Dr. P. Griffith
Dept. of Mechanical Engineering
MIT
Cambridge, MA 02139

Dr. P. A. Lottes
Argonne National Laboratory
9700 South Cass Avenue
Argonne, IL 60439

Mr. R. Jensen
Intermountain Technology
Box 1604
Idaho Falls, ID 83401

Mr. F. D. Lang
Energy Incorporated
P. O. Box 763
Idaho Falls, ID 83401

Dr. J. Chen
Lehigh University
Dept. of Mechanical Engineering
Bethlehem, PA 18015

Dr. K. H. Sun (5 copies)
Nuclear Power Division
Electric Power Research Institute
P. O. Box 10412
Palo Alto, CA 94303

Dr. J. J. Cudlin
Power Generation Group
Babcock & Wilcox
P. O. Box 1260
Lynchburg, VA 24505

Mr. J. Longo, Jr.
Combustion Engineering
P. O. Box 500
Windsor, CT 06095

Mr. Ken Moore
Energy, Inc.
P. O. Box 736
Idaho Falls, ID 83401

Dr. K. P. Galbraith
Nuclear Safety Engineering
Exxon Nuclear Company
2101 Horn Rapids Road
Richland, WA 99352

Dr. J. A. Block
Creare Inc.
Hanover, NH 03755

Dr. W. Hancox
Whiteshell Nuclear Laboratory
Atomic Energy of Canada
Pinawa, Manitoba
Canada ROE 1LO

Dr. R. E. Henry
Argonne National Laboratory
9700 South Cass Avenue
Argonne, IL 60439

Professor T. Theofanous
Department of Nuclear Energy
Purdue University
West Lafayette, IN 47907

Professor I. Catton
Dept. of Chemical, Nuclear, and
Thermal Engineering
University of California
Los Angeles, CA 90024

Dr. Max W. Carbon
Nuclear Engineering Department
The University of Wisconsin
Madison, WI 53706

Professor R. A. Seban
Dept. of Mechanical Engineering
University of California
Berkeley, CA 94720

Professor W. Y. Chon
Dept. of Engineering Science,
Aerospace Engineering, and
Nuclear Engineering
State University of New York
Buffalo, NY 14214

Dr. R. R. Gay
Nuclear Engineering Department
Rensselaer Polytechnic Institute
Troy, NY 12181

Dr. Owen Jones
Brookhaven National Laboratory
Building 820
Upton, NY 11973

Professor E. V. McAssey, Jr.
Dept. of Mechanical Engineering
Villanova University
Villanova, PA 19085

Professor S. C. Yao
Dept. of Mechanical Engineering
Carnegie-Mellon University
Pittsburgh, PA 15213

Dr. S. J. Board
CEGB
Berkeley Nuclear Laboratory
Berkeley
Gloucestershire, England

Dr. M. S. Plessel
California Institute of Technology
Pasadena, CA 91109

Dr. S. Levy
S. Levy, Inc.
1901 S. Bascom Ave. Suite 275
Campbell, CA 95008

Dr. D. A. Prelewicz
NUS Corporation
4 Research Place
Rockville, MD 20850

Professor A. Tapucu
Ecole Polytechnique,
Universite de Montreal
Institut de Genie Nucleaire
Casier Postale 6079
Succursal "A,"
Montreal, Quebec H3C 3A7

Ms. Nora Schofield
EG&G Idaho, Inc.
P. O. Box 1625
Idaho Falls, ID 83401

for NRC (360 copies)
Distribution Services Branch
Nuclear Regulatory Commission
7920 Norfolk Avenue
Bethesda, MD 20555